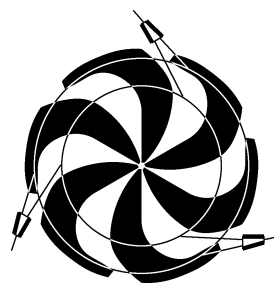


TRIUMF



ANNUAL REPORT SCIENTIFIC ACTIVITIES 2003

ISSN 1492-417X

**CANADA'S NATIONAL LABORATORY
FOR PARTICLE AND NUCLEAR PHYSICS**

OPERATED AS A JOINT VENTURE

MEMBERS:

THE UNIVERSITY OF ALBERTA
THE UNIVERSITY OF BRITISH COLUMBIA
CARLETON UNIVERSITY
SIMON FRASER UNIVERSITY
THE UNIVERSITY OF VICTORIA

ASSOCIATE MEMBERS:

THE UNIVERSITY OF GUELPH
THE UNIVERSITY OF MANITOBA
McMASTER UNIVERSITY
L'UNIVERSITÉ DE MONTRÉAL
QUEEN'S UNIVERSITY
THE UNIVERSITY OF REGINA
THE UNIVERSITY OF TORONTO

UNDER A CONTRIBUTION FROM THE
NATIONAL RESEARCH COUNCIL OF CANADA

DECEMBER 2004

TRIUMF

ISSN 1492-417X

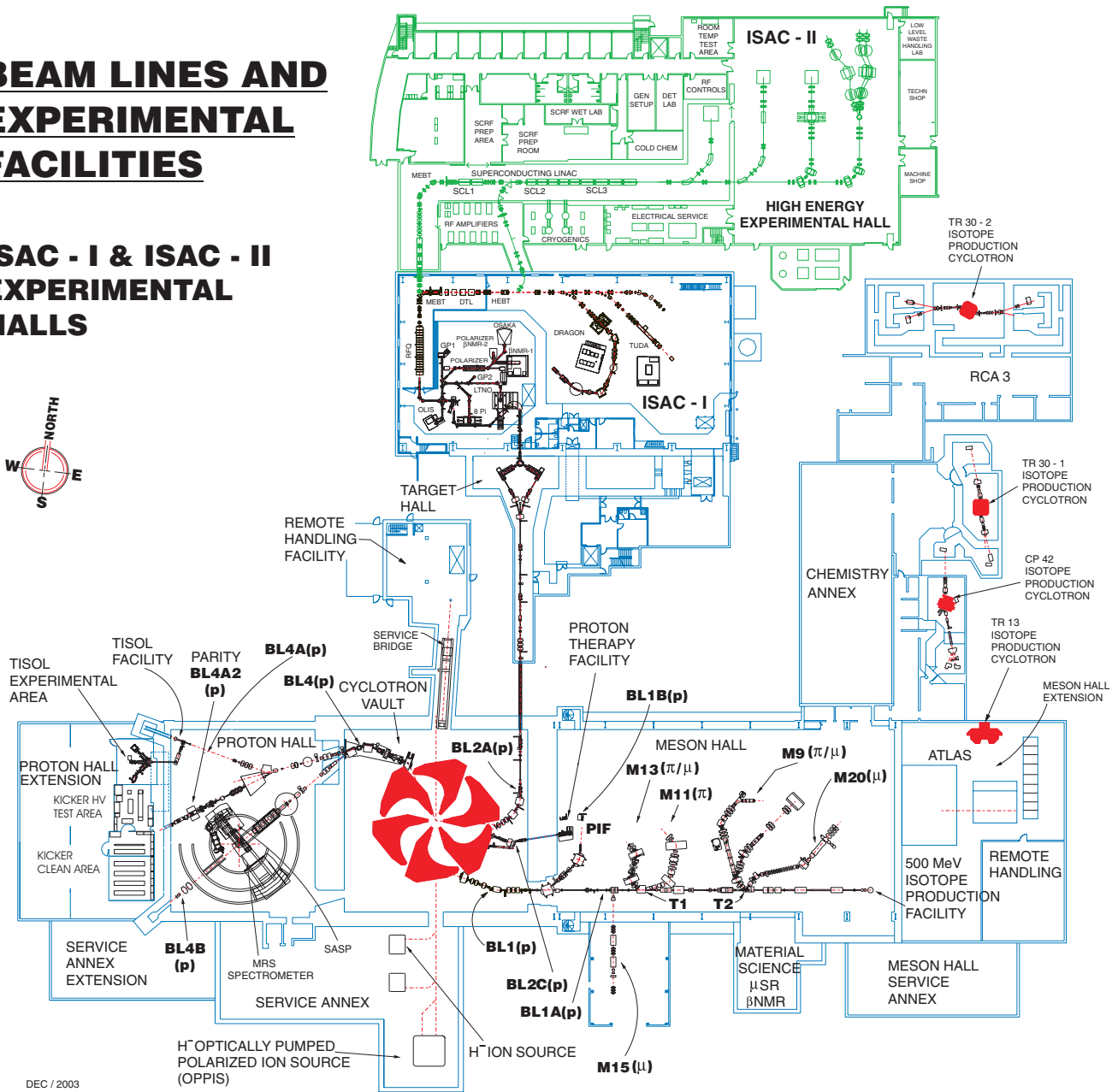
ANNUAL REPORT SCIENTIFIC ACTIVITIES 2003

Postal Address:

TRIUMF
Publications Office
4004 Wesbrook Mall
Vancouver, BC V6T 2A3
Canada

<http://www.triumf.ca/annrep>

ISAC - I & ISAC - II EXPERIMENTAL HALLS



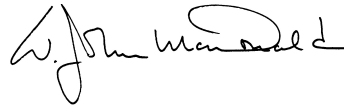
The contributions on individual experiments in this report are outlines intended to demonstrate the extent of scientific activity at TRIUMF during the past year. The outlines are not publications and often contain preliminary results not intended, or not yet ready, for publication. Material from these reports should not be reproduced or quoted without permission from the authors.

FOREWORD

The year 2003 was one of major accomplishments for TRIUMF. I take special pleasure on behalf of the Board of Management in congratulating Dr. Shotter and every one of the dedicated TRIUMF staff whose hard work and exceptional talent contributed to making it so. The opening of the ISAC-II building was a significant milestone as was the completion of 52 warm quadrupole magnets for CERN. I also wish to acknowledge the contributions of the researchers from Canadian Universities and TRIUMF whose talent and drive have resulted in an unprecedented level of peer reviewed funding for TRIUMF related research in 2003. Equally important to the high quality of the science program has been the contribution of many visitors from abroad.

Of particular note this year was the completion of an excellent Five Year Plan for the period 2005–2010. The effort of TRIUMF Management, members of the planning committee along with TRIUMF users groups and staff all helped to ensure the plan would be both exciting and realistic. The reaction of the National Research Council's peer review committee and of ACOT reflected their very positive reaction to the plan.

2003 was also a year of growth. The Board was pleased to welcome the University of Guelph as an associate member, in keeping with its increasing involvement with TRIUMF. This represents an important step in the realization of TRIUMF's role as Canada's National Laboratory for Particle and Nuclear Physics.

A handwritten signature in black ink, appearing to read 'W.J. McDonald', with a stylized, cursive script.

W.J. McDonald
Chair, Board of Management

TRIUMF was established in 1968 as a laboratory operated by the University of Alberta, the University of British Columbia, Simon Fraser University and the University of Victoria under a contribution agreement from the National Research Council of Canada. The initial consortium has been expanded to include Carleton University as a full member, and the University of Guelph, the University of Manitoba, McMaster University, the Université de Montréal, Queen's University, the University of Regina, and the University of Toronto as associate members. The facility is operated for all Canadian as well as foreign users.

The experimental program is based on a cyclotron which is capable of producing four simultaneous beams of protons, two of which are individually variable in energy from 180–520 MeV, the third from 472–510 MeV, and the fourth between 70 and 110 MeV. The potential for high beam currents – 100 μA at 500 MeV to 300 μA at 400 MeV – qualified this machine as a “meson factory”. The third high intensity beam line feeds the new isotope production facility, ISAC, which started operation in 1998 and qualifies as a second generation radioactive beam facility.

Fields of research include basic science, such as particle physics, nuclear physics, nuclear astrophysics, and condensed matter research, as well as life sciences based primarily on isotope research. There is also a biomedical research facility which uses protons for treatment of ocular melanomae. TRIUMF is providing the Canadian contribution to the Large Hadron Collider at CERN and TRIUMF resources are also available to support the Canadian subatomic program at other laboratories.

The ground for the main facility, located on the UBC campus, was broken in 1970. Assembly of the cyclotron started in 1971. The machine produced its first full-energy beam in 1974 and its full current in 1977.

The laboratory employs approximately 325 staff at the main site in Vancouver and 19 based at the participating universities. The number of university scientists, graduate students and support staff associated with the present scientific program is about 625.

CONTENTS

INTRODUCTION	1
SCIENCE DIVISION	3
Introduction and Overview	3
Particle Physics	5
(Expt. 614) TWIST – the TRIUMF weak interaction symmetry test	5
(ATLAS) The ATLAS Experiment at the LHC	10
(ATLAS) The ATLAS Endcap Signal Feedthroughs	13
(BNL 787/949/KOPIO) Measurement of $K \rightarrow \pi\nu\bar{\nu}$ and other rare decays	15
(FINUDA) Hypernuclear Physics with FINUDA at LNF Frascati	18
(HERMES) The HERMES Experiment	19
(J-PARC) T2K long baseline neutrino experiment	23
(SNO) Sudbury Neutrino Observatory	26
(TJNAF 00-006) Measurement of the flavour singlet form factors of the proton (G^0)	26
(TJNAF 02-020) Q_{weak}^p : a search for new physics at the TeV scale via a measurement of the proton’s weak charge	33
Nuclear Physics	40
(Expt. 715) Weak interaction symmetries in β^+ decay of optically trapped $^{37,38}\text{mK}$	40
(Expt. 744) A kinematically complete study of $\pi^- p \rightarrow e^+ e^- n$	44
(Expt. 766) The ortho-para transition rate in muonic molecular hydrogen	45
(Expt. 778) Pion proton cross sections in the Coulomb-nuclear interference region	47
(Expt. 823) Pure Fermi decay in medium mass nuclei	48
(Expt. 824) Further measurement of the rate of the $^{21}\text{Na}(p,\gamma)^{22}\text{Mg}$ reaction	49
(Expt. 838) Double radiative capture on pionic hydrogen	52
(Expt. 862) Analyzing powers in the $\vec{p}(\pi,\pi\pi)$ reactions with CHAOS	54
(Expt. 863) Ground state magnetic moments of $^{75,77,79}\text{Ga}$ (LTNO)	54
(Expt. 864) Measurement of the two-photon capture mode of the pionic deuterium atom	55
(Expt. 871) Meson and quark effects in nuclear β decay of ^{20}Na	56
(Expt. 875) MuScat: muon scattering in low Z materials for muon cooling studies	61
(Expt. 880) Ortho-para effect of muon catalyzed fusion in solid deuterium	64
(Expt. 893) The hyperfine field of Rb in Fe, Ni and Co (LTNO at ISAC)	65
(Expt. 909) Isospin symmetry breaking in superallowed Fermi β -decays	67
(Expt. 920) Nuclear charge radii and moments of short lived neutron deficient lanthanum and other rare earth isotopes	68
(Expt. 921) High- K isomers in the mass 180 region	69
(Expt. 927) ($^3\text{He},p$) as an alternative to resonant elastic scattering	70
(Expt. 928) Level structure of ^{21}Mg : nuclear and astrophysical implications	72
(Expt. 929) Toward radon electric dipole moment measurements at ISAC	72
(Expt. 947) Evaluation of the competition between single-step and multi-step γ decay in the $^{12}\text{C}(^{12}\text{C},\gamma)$ reaction	73
(Expt. 948) Proton and neutron radiation effects in silicon-on-insulator and bulk-silicon devices	74
(Expt. 952) A new measurement of $^{12}\text{C}(\alpha,\gamma)^{16}\text{O}$ reaction	76
(Expt. 955) Study of the β -decay of ^{32}Na	77
(Expt. 964) A study of the partial and total cross sections of the $^8\text{Li}(\alpha,n)^{11}\text{B}$ at astrophysically relevant energies	79
(Expt. 967) Beta decay branching ratio of ^{21}Na	79
(Expt. 968) Ortho-para effect of muon catalyzed fusion in liquid deuterium; R&D of fusion neutron detection	80
(8π) Halo neutrons and the β -decay of ^{11}Li	82
(LANSCÉ NPDGamma) Measurement of the parity-violating gamma asymmetry A_γ in the capture of polarized cold neutrons by para-hydrogen, $\vec{n} + p \rightarrow d + \gamma$	83
Molecular and Materials Science	88
(Expt. 768) Generalized FFLO state and anomaly of flux line lattice state in novel superconductors	88

(Expt. 842)	Mu-substituted free radicals in sub- and supercritical water	89
(Expt. 847)	Electron-doped high- T_c superconductors	91
(Expt. 851)	μ^+ SR in ruthenate and cuprate superconductors	92
(Expt. 852)	Magnetic phases in geometrically frustrated rare earth pyrochlores	93
(Expt. 865)	Electronic structure and diffusion kinetics of Mu in group III nitrides and related wide-gap semiconductors	95
(Expt. 883)	Muoniated methyl and associated free radicals	96
(Expt. 895)	Vortex structure and magnetism of electron-doped cuprate superconductors	97
(Expt. 914/835)	Zero-field μ SR in Bi2212 and Bi2201 searching for effects related to pseudo-gap	99
(Expt. 915)	Muonium in semiconductor alloys	100
(Expt. 916)	QLCR of diamagnetic muonium states in GaP	101
(Expt. 917)	Correlation between magnetism and transport properties of thermoelectric oxides	103
(Expt. 918/950)	High field study of La_2CuO_4 based superconductors / High field study of Zn doped/Eu doped/overdoped systems	105
(Expt. 931)	Magnetic properties of $\text{M}[\text{Au}(\text{CN})_2]_2 \cdot (\text{H}_2\text{O})_2$ ($\text{M} = \text{Cu}, \text{Ni}$) coordination polymers	105
(Expt. 938)	Muonium formation and ionization in semiconductors and insulators	107
(Expt. 939)	Guest-host interactions and Hfcs of Mu-alkyl radicals in zeolites	108
(Expt. 941)	Investigation of spin statics and dynamics in the transition metal oxides $\text{Sr}_2\text{CaReO}_6$ and $\text{Li}_2\text{Mn}_2\text{O}_4$	109
(Expt. 943)	Muonium formation and reactivity in sub- and supercritical carbon dioxide	111
(Expt. 944)	Muonium in silicon carbide	113
(Expt. 949)	μ SR study of magnetic order in high- T_c superconductors under high pressure	114
(Expt. 951)	Magnetism and flux line lattice structure of oxychloride superconductors	115
(Expt. 953)	Spin dynamics and quantum coherence in molecular magnets	116
(Expt. 960)	Hydrogen (Mu) defects in II-VI chalcogenides	118
(Expt. 965)	Investigation of spin dynamics in the new dipolar spin ice $\text{Ho}_2\text{Ru}_2\text{O}_7$	119
(Expt. 974)	Unconventional superconductivity in $\text{Na}_x\text{CoO}_2 \cdot 1.3 \text{H}_2\text{O}$ and proximity to an ordered phase	120
(Expt. 975)	Magnetism and superconductivity in $\text{Na}_x\text{CoO}_2 \cdot y\text{H}_2\text{O}$ and related cobalt oxides	122
Life Sciences		125
Introduction		125
(Expt. LS0)	PET facilities	125
(Expt. LS3)	Synthesis of radiopharmaceuticals for positron emission tomography	126
(Expt. LS4)	Targets for radioisotope production	127
(Expt. LS8)	Radiotracers	128
(Expt. LS33)	Evaluation and improvement of a dual head coincidence camera	129
(Expt. LS35)	Development of ^{18}F labelled nitroimidazole PET imaging agents for tissue hypoxia	129
(Expt. LS39/LS44)	Positron emission profiling (PEP) for pulp and paper fluid dynamic studies / Development of a high-speed formation (areal density) measurement system for paper	130
(Expt. LS42)	Configuration modelling and image reconstruction studies on a depth encoding research tomograph	131
(Expt. LS50)	Antisense imaging nucleic acids for Parkinson's disease	131
(Expt. LS51)	Auger therapy for prostate cancer	131
(Expt. LS53)	Synthesis of $^{99\text{m}}\text{Tc}$ and $^{186,188}\text{Re}$ sugar derivatives	132
(Expt. LS56)	Synthesis of radiolabelled nucleotides and oligonucleotides	132
(Expt. LS57)	Quantitative imaging with the Concorde microPET	132
(Expt. LS69)	<i>In-vivo</i> studies on regulation of dopamine turnover using a Parkinson's disease rat model and a microPET	134
(Expt. LS70)	Quantification of high resolution brain imaging	134
Theoretical Program		136
Introduction		136
Nuclear Structure and Reactions		136
Nuclear Astrophysics, Cosmology		138
Lattice QCD		139

Effective Field Theories and Chiral Perturbation Theory	140
Few-Body and Medium Energy Processes	141
Particle Physics	142
Miscellaneous	144
Experimental Facilities	145
Proton Irradiation Facility	145
Proton Therapy Facility	146
μ SR User Facility	147
Cryogenic Targets	151
Computing Services	151
Data Acquisition Systems	157
Detector Facility	159
Experimental Support	161
GEANT4	161
Scientific Services	162
The DRAGON Facility	165
8π Spectrometer	167
TIGRESS	168
Status of the TITAN System	171
R&D for the Time Projection Chamber for the International Linear Collider	175
Linear Collider TPC Development	178
CYCLOTRON OPERATIONS DIVISION	181
Introduction	181
Beam Production	182
Winter Shutdown	186
Beam Schedule 103	187
Fall Mini-Shutdown	188
Beam Schedule 104	188
Beam Development	189
Cyclotron Beam Development	189
ISIS Beam Dynamics Development	190
BL1 Beam Dynamics Development	191
Radio Frequency Systems	191
RF Operation	191
RF Refurbishing	193
RF Support	193
Radio Frequency Controls	194
Probes and Diagnostics Mechanical MRO	194
Probes MRO	194
Monitor MRO	194
ISAC Diagnostics	194
Cyclotron Vacuum and Cryogenics	194
Beam Line Vacuum	195
Vacuum and Cryogenics Support	195
ISIS	195
Primary Beam Lines	196
Beam Line 2C	197
Prompt Radiation Hazard	198
Safety-Critical Devices	198
Controls	198
CCS Facilities	199
Secondary Beam Lines	200
Other Systems	200

Operational Services	200
Remote Handling	200
Magnet Power Supplies	201
Electrical Services	201
Mechanical Services	203
ISAC DIVISION	204
Introduction	204
ISAC Operations	204
ISAC Targets	217
ZrC Target Material	217
Increased ^{11}Li Production from Ta	217
^{26}gAl Beam Development	218
High Power Target Development	219
ISAC Ion Sources	220
ECRIS-1 Tests	220
Charge State Booster (CSB)	222
Resonant Ionization Laser Ion Source (TRILIS)	223
ISAC Polarizer	224
Remote Handling/Target Hall Facilities	225
Modules	225
Remote Handling	225
ISAC Controls	225
New Systems	225
Functionality Enhancements	226
System Support	226
Development Support	227
Commissioning and Operation	227
Vacuum	227
ISAC-I	227
Vacuum/Cryogenics, ISAC-II	228
Liquid Helium and Liquid Nitrogen	228
ISAC-I RF Systems	228
RFQ	228
Bunch Rotator	228
MEBT Rebuncher	228
DTL	229
HEBT High Beta Buncher	230
Phase Measuring System	230
RF Controls	230
ISAC-II Transfer Line 35 MHz Buncher	230
Beam Dynamics	231
LTNO Optics	231
GUIs	231
ISAC Diagnostics	231
Experimental Support	232
ISAC-I Conventional Facilities and Infrastructure	232
Mechanical Services	232
Electrical Services	232
ISAC Planning	233
ISAC-I	233
ISAC-II	233
Experimental Facilities	234

Contract Administration	234
Personnel Resources	234
ISAC-II Conventional Facilities and Infrastructure	238
ISAC-II S-Bend HEBT	238
ISAC-II Accelerator Development	239
Hardware and Development	239
RF Systems Ancillaries	239
Progress in ISAC-II Cryogenics	242
ISAC Beam Dynamics	243
Operating the DTL Above 1.5 MeV/u	243
ISAC-II HEBT	244
ISAC-II Cryogenic System	244
Refrigeration System	244
Cryomodules	245
ACCELERATOR TECHNOLOGY DIVISION	246
Introduction	246
Beam Dynamics	246
J-PARC Collaboration	246
Muon Acceleration in an FFAG	248
Magnets	249
Magnet Measurements	249
Kickers	250
Mechanical Engineering	252
ISAC-I	252
ISAC-II	252
Engineering – Other	253
Engineering – Victoria	254
Engineering – Carleton	255
Planning	256
ISAC	256
Shutdown Activities	257
Design Office	257
Machine Shop	258
Building Program	258
Electronics Services	259
Overview	259
Site Communications	259
Technical Support	259
PC Support/Desktop Services	259
Electronics Repair Shop	259
Electronics Shop	260
Experimental and Target Technical Support	260
High Level Software Support	260
Electronics Development	260
ISAC Support	260
CERN	261
Engineering Support	261
Experiment Support	261
Secondary Channel Support	261
New Hardware Designs	261
Infrastructure	261

CERN COLLABORATION	262
Introduction	262
Beam Dynamics	262
Beam Optics and Collimation	262
Coherent Beam-Beam Effects in the LHC	263
Controls and Instrumentation	264
LHC Orbit System Components	264
Magnet Development	264
Kicker Magnets	265
RCPS	265
PFN	265
Thyratron Switch Tanks	266
Shipping Container	267
TECHNOLOGY TRANSFER DIVISION	268
Introduction	268
Technology Transfer	268
Applied Technology Group	268
500 MeV Isotope Production Facility	268
CP42 Facility	268
TR30-1 Facility	268
TR30-2 Facility	269
ATG Development Projects	269
Radioisotope Processing (MDS Nordion)	269
ADMINISTRATION DIVISION	271
Introduction	271
Human Resources and Administration	271
Environmental Health and Safety	271
Licensing	271
Personnel Dosimetry	272
Occupational Health and Safety	272
Training	272
Interlocks and Monitoring	273
Administration Computing and Communications	273
Management Information Systems	273
Public Web Services	273
Telephones	273
TRIUMF Outreach Program	273
High School Teacher Programs	274
TRIUMF/ISCBC High School Fellowship	274
Future Directions	274
CONFERENCES, WORKSHOPS AND MEETINGS	275
ORGANIZATION	282
APPENDICES	
A. Publications	286
B. Seminars	307
C. Users Groups	310
D. Experiment Proposals	311
E. Life Sciences Project Proposals	329

INTRODUCTION

TRIUMF, one of Canada's premier international scientific institutions, is a national institution serving the needs of university scientists from across Canada. It is supported by a renewable five-year federal government financial contribution channeled through the National Research Council. The current funding cycle covers the period 2000–2005. During the period up to the end of 2003, many of the challenges identified for this five-year funding cycle have been successfully met. Highlights include the development of ISAC as the world's leading exotic-isotope production facility, and, based on Canadian know-how, the design and construction of advanced equipment for the world's largest scientific project, the Large Hadron Collider (LHC), based at CERN in Geneva.

During this report year, 2003, the ISAC program reached an important milestone with the completion of the ISAC-II building, which was formally opened in June by the Premier of British Columbia, the Hon. Gordon Campbell. A number of other prominent provincial ministers as well as several hundred guests attended the opening ceremony. The ISAC science program received a significant boost by the commissioning of a major piece of equipment, the 8π spectrometer, which from startup is proving an exceptional tool to probe the properties of the exotic nuclei produced at TRIUMF. Other tools being developed include TITAN, TRIUMF's Ion Trap facility for atomic and nuclear science, which will probe the limits of existence of nuclei, and TIGRESS, the TRIUMF-ISAC Gamma-Ray Escape Suppressed Spectrometer, which will be used to probe the structure of exotic nuclei. All these projects involve many physicists from across Canada and around the world.

Another major milestone during the year was the completion of the construction and delivery of 52 warm quadrupole magnets for the LHC at CERN. Due to the very exacting specification of these magnets, producing the magnets was a real challenge, and it is a tribute to TRIUMF and ALSTOM staff in Tracy, Quebec that the magnets were delivered to CERN on time and on budget. During the year good progress has been made in the construction of the hadronic endcap modules, which are part of the Canadian contribution to the ATLAS detector of the LHC. Commissioning of these modules is on schedule to take place in 2004. Interesting results continued to emerge from the deep inelastic experiment HERMES at the DESY laboratory. Significant efforts were made during the year to prepare for new experiments concerning rare K decay (KOPIO at Brookhaven National Laboratory), neutrino oscillations (T2K at J-PARC), and measurement of flavour

singlet form factors of the proton (G_0 at the Thomas Jefferson National Accelerator Facility).

The μ SR program has been part of TRIUMF's scientific portfolio for many years. Each year exciting new work continues to flow from this program that is relevant to fundamental physics, materials science, chemistry and nuclear physics. For such a wide field it is difficult to pick examples, but perhaps the work identifying a new test of quantum electrodynamics concerning the behaviour of the muon under extremely high electric and magnet fields, and the use of muons to help understand industrial catalysts, shows just how wide the field has become.

The life sciences program took a major leap forward with the delivery of new PET scanners. One of these scanners, the High Resolution Research Tomograph, will enable the human brain to be probed to a higher level of precision than ever before. The other scanner, the MicroPET, is a small animal scanner that will expand the collaborative network using PET for *in-vivo* biochemical studies and will include oncology as well as the established collaboration with the neuroscience community.

TRIUMF has a number of commercial licensees for its technologies that range from life sciences to environmental protection techniques. According to the latest statistics from the Association of University Technology Managers (AUTM), TRIUMF ranks second in Canada in terms of Gross Licence Income received as a percentage of Total Sponsored Research. A good example of this technology transfer is that during the year MDS Nordion commissioned their third small commercial cyclotron at the TRIUMF site. This TR30 machine is based on a TRIUMF design and built by a local company, Advanced Cyclotron Systems Inc.; some of the work was subcontracted to another TRIUMF licensee, Dehnel Consulting Ltd., of Nelson, B.C. With the addition of this third cyclotron, MDS Nordion will supply about 50,000 medical patient doses per week, in Canada and around the world, from the TRIUMF site.

Another example of where TRIUMF expertise has been vital to an outside organization is the strong collaboration that has been established with the B.C. Cancer Agency to set up a new Centre of Excellence in Functional Imaging.

The new TRIUMF Outreach Program is in its second full year of operation. New initiatives such as the Teacher Internship Program continue to attract interest among high school teachers, with a dozen teachers from all over British Columbia waiting to take part.

The last two years, 2002 and 2003, have seen the

Canadian scientific community collaborate with TRIUMF staff to develop a scientific plan for the next funding cycle, 2005–2010. The main features of this plan are completion of the ISAC facility to ensure it firmly establishes and maintains world leadership; an increase in the capabilities of the μ SR facility for materials science and chemistry; increased capacity for radioisotope production for the life sciences program in order to, among other things, take optimal advantage of two new PET scanners; and to make strong Canadian contributions to some exciting projects at other national laboratories around the world. The plan identifies TRIUMF as the Canadian centre for the world computing grid network that will handle the vast data outflow from the ATLAS experiment at CERN's LHC. Among other activities, the plan identifies important Canadian contributions to the rare K -decay experiment at Brookhaven in the USA, and to an experiment

in Japan which is a natural extension of the highly successful and visible Canadian program at SNO, located in Sudbury, Ontario. Technology transfer and outreach activities are important components of the plan.

The plan was reviewed during the year by panels of internationally renowned scientists and was given their very strong support. It is an ambitious plan but it is a realistic one, building on TRIUMF's past and present record of achievement. It will deliver first-rate science at an internationally competitive cost in a timely and efficient manner, and will ensure for the Canadian Government, and therefore the taxpayer, the highest return on their previous investment in TRIUMF. The plan is under active consideration by the Federal Government and, if accepted, the plan will ensure that the Canadian scientific community using TRIUMF will continue to be competitive at the highest international levels.



A. Shotter,
Director

SCIENCE DIVISION

INTRODUCTION AND OVERVIEW

2003 will be remembered as a year of intense activity, both in the current experimental program and in the shaping of TRIUMF's future through the development of the next five-year plan and the review of TRIUMF by a National Research Council (NRC) appointed international peer-review committee.

In the science program, a strong push for ISAC beams has resulted in a significant growth in publications and invited talks. ISAC science is getting on the mass shell. This is also coupled with two major investments by the Natural Sciences and Engineering Research Council (NSERC) which funded two new instruments: TITAN for ISAC-I and TIGRESS, mainly for ISAC-II. This is a testimony to the quality of the science, the quality of the team behind these projects, and the recognition of the potential of ISAC as the world's most advanced radioactive beam facility.

The challenge for the ISAC team is to produce and deliver intense or rare beams that users request. The operation of ISAC is extremely complex as nothing is routine nor easy and the potential disasters numerous. But, 2003 has seen new beams being delivered – the first major nuclear astrophysics experiment with DRAGON produced final publications and two Ph.D. theses.

The β -NMR team moved towards physics data-taking after a series of commissioning runs.

The 8π detector was improved with additional scintillator detectors and this allowed for coincidence β - γ correlation studies. New information was collected on the ^{11}Li decay using the Doppler broadened γ transition to infer the neutron emission energy. New isomeric states were searched for in the Lu isotopes; a new collinear laser spectroscopy group is starting a program of systematic studies of neutron deficient La isotopes. High precision data were obtained on the vector transition and small branches identified in the decay of $^{38\text{m}}\text{K}$.

Amongst many other results, this shows that the nuclear physics community is now recognizing the opportunities offered by ISAC.

In the particle physics program, a major milestone was reached with the completion of a major contract to provide warm quadrupole magnets for the Large Hadron Collider (LHC), the completion of the endcap calorimeter modules for the ATLAS experiment at the LHC, and the beginning of their assembly and installation in the cryostats at CERN. These investments will be leading to exciting physics by 2007 when the LHC

will turn on, and the next five-year plan will be aimed at positioning TRIUMF as a major ATLAS hub for the benefit of Canadian scientists.

A new experiment is being developed to search for the neutrino oscillation evidence with muon neutrinos to be produced at J-PARC. An international collaboration was formed and the Japanese government formally approved the experiment in December with a funding of US \$156 million. This will present Canadians with a golden opportunity in science by 2008.

Locally, despite the tragic loss in May of a most valuable team member, J.A. Macdonald, the TWIST experiment made considerable progress towards a 10^{-3} precision determination of the Michel parameters which characterize the angular and energy distribution of positrons from surface muon decays.

Strong support has been received from the Theory group and their enthusiastic contingent of research associates.

Most of the available beam time in the meson hall is devoted to μSR studies of materials. Beam time is distributed amongst four main lines of research:

- studies of muonium as an isotope of hydrogen in semiconductors;
- studies of magnetic materials like frustrated magnets, spin-ice systems, molecular magnets, etc.;
- studies of superconductivity and phase diagrams of novel superconductors, and
- muonium chemistry with two main topics – studies of supercritical water and CO_2 , studies of zeolite structures and associated chemical reactions.

The Life Sciences program has been dominated this year by the commissioning of two new PET tomographs funded through the Canadian Foundation for Innovation (CFI). These instruments have generated considerable interest in the community and more demands for specialized tracers are being made from the PET isotope production group.

In 2003, the Laboratory of Advanced Detector Development, also funded by CFI, started to take shape with the hiring of support personnel and the start of equipment purchases.

But the overall activities of the Science Division (and of TRIUMF as a whole) were focused on producing the next five-year plan for TRIUMF and in presenting a strong portfolio of achievements at the NRC International Review of TRIUMF which took place

in September. A strong positive endorsement of TRI-UMF's performance was achieved, thanks to a dedi-

cated, competent and hard working staff. We are all grateful for the support of our personnel.

PARTICLE PHYSICS

Experiment 614

TWIST – the TRIUMF weak interaction symmetry test

(B. Shin, TRIUMF)

TWIST is an experiment to measure the muon decay spectrum, to extract precise values of the decay (Michel) parameters, ρ , δ , and ξ [Michel, Proc. Phys. Soc. **A63**, 514 (1950)]. If the results differ from the standard model (SM) prediction [Fetscher and Gerber in *Advanced Series in Directions in High Energy Physics*, ed. P. Langacker (World Scientific, Singapore, 1995) v.14, p.657], the deviations indicate contributions from physics beyond the SM. The goal of TWIST is to simultaneously determine these decay parameters with experimental precision better than 10^{-3} , to eventually achieve approximately a tenfold improvement over the existing precision, shown in Table I along with theoretical SM predictions. When this goal is met, it will set new limits on the right-handed coupling of the muon in a model independent way, as well as squeeze the parameter space for certain classes of extensions to the SM.

The TWIST collaboration began to collect data in late 2002. During that first running period, measurements were made with the goal of providing an initial measurement of the ρ and δ parameters, as well as investigating systematic dependences and sensitivities to many different experimental variables.

Following the collection of about 6×10^9 events during that time, the simulation and various analysis codes, including the newly developed blind analysis code, were tested and validated in 2003. The availability of the WestGrid facility has enabled us to compare high statistics analyses of combinations of many experimental and Monte Carlo (MC) data sets. Comparisons of the GEANT3-based MC program currently in use with GEANT4 have begun in the year, and a more detailed study is continuing.

We have also improved the functionality and reliability of the M13 beam line, established an improved beam tune, and extended the region of the spectrometer magnetic field map. As a result of analysis of the 2002 data where the muon stopping target was $125 \mu\text{m}$

Table I. Theoretical and measured values of the muon decay parameters.

	SM(V-A)	PDG current value
ρ	3/4	0.7518 ± 0.0026
η	0	-0.007 ± 0.013
δ	3/4	$0.7486 \pm 0.0026 \pm 0.0028$
$\mathcal{P}_\mu \xi$	1	$1.0027 \pm 0.0079 \pm 0.0030$

mylar, the target was changed to a $71 \mu\text{m}$, 99.99% pure Al foil.

Brief description of the TWIST spectrometer

The spectrometer is designed to measure simultaneously ρ , δ , and $\mathcal{P}_\mu \xi$, where \mathcal{P}_μ is the muon polarization at the time of decay. The expected precision is such that the result will be about one order of magnitude better than the currently available best results, limited by systematic effects. Muons are stopped in a thin target at the centre of a stack of 56 low-mass, high-precision planar wire chambers in a uniform solenoidal field of 2 T. Each detector plane has a thickness of only about 5×10^{-5} radiation lengths, an important feature of the TWIST detector. The stack is shown in Fig. 1. Different types of wire chamber detector planes are employed and compared in Table II.

PCs serve to identify the primary characteristics of an event and to identify the times of each track with respect to a simple thin scintillator event trigger. The four PC planes at each of the upstream and downstream ends of the stack identify decay positrons as well as beam positrons. The four PC planes surrounding the stopping target (PC(t) in Table II) define the end of the incoming muon track. DCs use a much slower gas to achieve better position resolution. Their function is to determine precisely the coordinates of the decay positron path.

Table II. Description of DC, PC and target PC (PC(t)) chambers.

	DC	PC	PC(t)
Planes	44	8	4
Wires/plane	80	160	48
Wire spacing	4 mm	2 mm	2 mm
Gas	DME	CF ₄ / iso-C ₄ H ₁₀	CF ₄ / iso-C ₄ H ₁₀

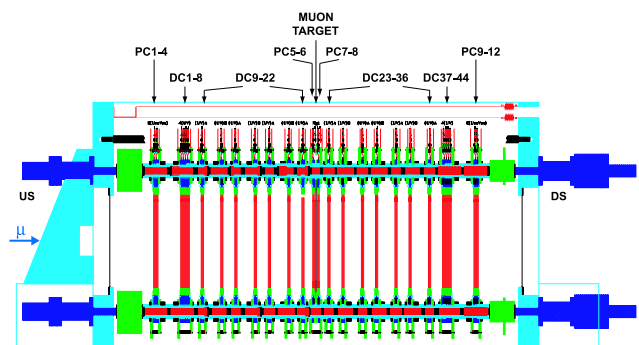


Fig. 1. Side view of the TWIST spectrometer detector stack.

The M13 beam

The M13 beam is a source of surface positive muons (μ^+), having a high degree of polarization in a direction opposite to the muon momentum ($\mathcal{P}_\mu \sim -1.0$) at production. However, the polarization at the stopping target is less than at the source, from real or apparent reductions due to known effects such as beam size and divergence, scattering from the materials along the beam line, and the fringe field of the spectrometer.

The most challenging measurement is $\mathcal{P}_\mu \xi$, for which the absolute polarization \mathcal{P}_μ of the muons at the time of decay must be known precisely. Most importantly, deviations from $\mathcal{P}_\mu = -1.0$ must be quantified in terms of systematic corrections. However, the possibility of an unknown source of small depolarization exists, so that a measurement of $\mathcal{P}_\mu \xi$ which is less than one might have to be interpreted as a lower limit.

Most depolarization effects related to beam transport can be minimized by using a small momentum acceptance, beam divergence and beam size. During 2003, these have been measured as a function of the beam line element settings (beam tune) using a movable slit and fast wire chambers, and a new tune has been established. For frequent monitoring of the beam size and divergence, a time expansion chamber (TEC) has been designed and constructed, and is being tested.

The stability and reproducibility of the beam line magnet power supplies was previously improved by installing precision direct current transformers. Plans were made for a further upgrade with installation of a new vacuum isolation valve at the first focus point of the beam line as well as a removable window valve to prevent radioactive residual gases from migrating from a graphite production target to the end of M13 and disrupting the TWIST detectors. The Be production target which has so far been used can then be replaced by a graphite target to improve beam characteristics. The solenoid field has been mapped to the position of the last quadrupole of the beam line, so that the fringe field depolarization can be estimated precisely.

Progress in software and analysis

Tracking decay positrons Tracking of decay positrons is very demanding for TWIST because of the low tolerance for biases from reconstruction errors. Consequently a great deal of effort has been allocated to optimization of tracking.

1. Crosstalk removal: Although it is not a substantial source of chamber noise, crosstalk is removed prior to event classification using primarily the time width of the chamber hit signals and the existence of a coincident generating signal.
2. Event classification: Temporal and spatial properties of the hits allow the classification of events.

For example, a muon as the trigger particle can readily be distinguished from a beam positron trigger, while decay positrons following the muon are also easily recognized. Subsequently, many types of problematic events can be identified without bias.

3. Pattern recognition: Drift chamber hits are sorted into temporal groups for which initial helix parameters are calculated from the positions of clusters of wire hits. Two independent routines have been written and compared, both statistically and by visual event screening. At present, reconstruction failures are at the 1% level.
4. Delta identification: Once hits are assigned to tracks, associated low energy tracks (deltas) can be identified and removed. Delta identification is a very important validation of the simulation, because we rely on the simulation to account for deltas produced below our detection threshold. Comparisons show that the number of deltas removed from the data is consistent with simulation.
5. Tracking: A least squares procedure is used to fit to the wire centres of the hits using the “narrow windows” method, which also resolves most left-right ambiguities. Drift time fits to overcome limitations of the wire centre fits (especially the granularity of the detector resolution function) were implemented. Multiple scattering (MS), which occurs mainly at the detector plane positions, is significant in the TWIST detector, especially for high angle tracks. To account for MS, kinks are introduced in the fitting function at the positions of the detector planes.

The detector plane spacing of the inner DCs in TWIST causes the circle radius of some events to be undefined. However, for these difficult cases, the outer 8 DCs can be utilized since their plane spacing is much smaller. All wires in these planes were instrumented in the last year and are now used in tracking.

There are several key tracking software development projects in progress which include: replacement of the uniform field by non-uniform fields, introduction of the variation of the resolution with distance from the wire in place of an averaged resolution function currently in use, and using a maximum likelihood fitter.

Calibrations Several calibration procedures have been refined. Calibration of the relative TDC times can now be done both with straight and helical tracks, and the accuracy of the energy calibration has been improved. The fitting of 120 MeV pion tracks in zero magnetic field has been complemented with the use

of decay positron helices for determining translational and rotational alignments of chamber planes.

Simulation Improvements this year include the incorporation of a realistic distribution of charge clusters produced by ionization in the chambers, leading to reasonable simulation of the observed spatial resolution. Detector translational and rotational (mis)alignments have been included in the simulation. The phase space of the M13 beams used in 2002 was characterized this year and included as input. Additionally we have carried out a series of comparisons between the GEANT3 and GEANT4 packages to explore differences which might affect our results.

Computer cluster and grid computing Much of the development and testing of our analysis software has been accomplished using a local cluster of some 30 computers. In November, TWIST became a beta-tester of the WestGrid cluster of 1008 processors at UBC, allowing full scale simulation and data analysis. Submission scripts had to be revised significantly to conform with WestGrid disk storage architecture, while instabilities in the storage and queuing systems added additional complications. Nevertheless, access to this powerful system permitted generation and analysis of 15 Tbytes of simulation data, and analysis of much of both the 2002 and 2003 data sets (about 2.5 Tbytes). Twelve separate analyses were performed on a “standard” data set to study various analysis-dependent systematics.

Extraction of decay parameters and blind analysis

To extract decay parameters from the experimental energy and angle spectrum of decay positrons, there are two possible approaches: one is de-convoluting the measured spectrum to allow for direct comparison with the theoretical prediction, and the other is convoluting the theoretical shape with the detector response function and comparing to the experimental spectrum. The de-convolution method requires a precise knowledge of detector response function without which its application is impractical. The convolution, on the other hand, can be calculated directly by the MC simulation program without the explicit knowledge of detector response, but with a theoretical formula containing specific values of decay parameters.

To perform a fit for unknown values of decay parameters, TWIST has developed a technique which uses an expansion of the convoluted spectrum in deviations of the parameters from the values used as MC input. Assuming that the measured spectrum results from small deviations in the input values of decay parameters, the measured spectrum can be expressed near those values of the parameters by Taylor expansion up to the first order term, which is exact since the Michel form of the spectrum is linear in param-

eters ρ , η , ξ , and $\xi\delta$. Thus the measured spectrum is the sum of the MC spectrum assuming the input values, plus MC-generated derivative spectra multiplied by the differences between the input and measured parameters. The input values of the decay parameters are chosen randomly and are hidden, and only the deviations from the MC input values, not the decay parameters themselves, are given by the fit results. Experimenters remain “blind” to the parameters until the final result is determined. The MC simulated spectrum and the derivative distributions are obtained from *reconstructed* MC events; since TWIST uses the same reconstruction program for MC as for real data, any distortions introduced by the reconstruction software cancel exactly. The uncertainties come from how well the simulation recreates the real detector and the physics processes taking place.

During 2003 TWIST implemented and tested all parts of the blind analysis software chain, from the “black box” spectrum generator to the fitter. The tools have been checked with simulations and are now being used for fitting of experimental distributions. The system is also being applied to the estimation of biases and systematic effects.

Verification of simulation precision

TWIST results depend on the inherent and inevitable biases of experimental variables and analysis software. To minimize these biases, the physics content and implementation of the simulation can be compared with real data which are not sensitive to the decay distribution parameters. For this purpose the TWIST detector can be used for different kinds of verifications. A few that have so far been explored with the detector are listed here.

1. Muon stopping distribution: The muon range spread near the target will influence the energy calibration as well as muon depolarization. With external degradation of muon energy, the muon stopping distribution can be moved into the upstream half of the detector stack. Comparison of the stopping positions with simulated data tests the simulation of the energy loss as well as sensitivity of the observed range to small changes in the muon beam settings.

2. Response function and positron energy loss: Since the detector stack is made of two mirror-symmetric independent positron spectrometers, real decay positron tracks can be measured twice, once in each half of the stack, by arranging for muons to stop near either the entrance or exit of the spectrometer. Measurement of the difference of momentum and angle between the two halves, for both real data and simulated data, will show any weakness of the positron simulation and test not only how well the response function is reproduced but also how well the simulation

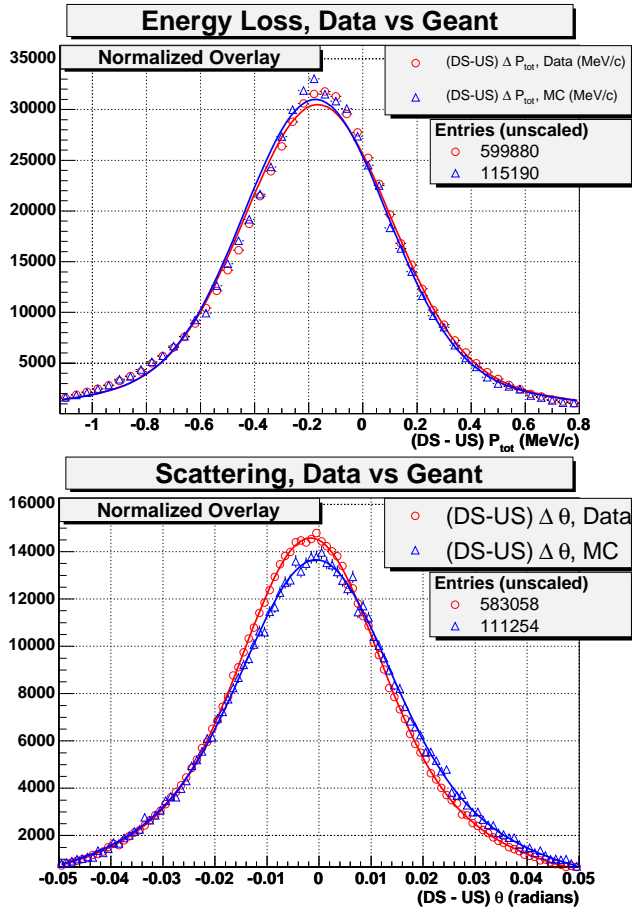


Fig. 2. Preliminary comparison of data and MC for decay positron tracks originating from muons stopping near the entrance to the stack. Top shows energy loss, and bottom shows multiple scattering. Circles are for data, and triangles for MC. The curves are simple two-component Gaussian fits, which are shown for comparison purposes only.

handles energy loss and multiple scattering of positrons in our fiducial range. Data taken with the stopping Al target in 2003 have been compared with simulation. A very preliminary result is shown in Fig. 2. The top graphs show that energy loss of less than 200 keV between the two halves is well reproduced by the simulation, while the Gaussian curves do not reproduce the shapes properly for either data or simulation. The bottom graph shows some disagreement with the simulation, which may be related to incomplete alignment of detector modules in the reconstruction program; a similar comparison for 2002 data, where a more complete alignment procedure was completed, does not show the difference.

3. Material asymmetries: If the simulation does not accurately generate secondary charged particles from positrons passing through and exiting the detector, there is a potential for bias in the decay parameters extracted from the comparison of real data with MC. This is most obvious in the angular distribution, since

the number of secondaries produced varies approximately as $1/\cos(\theta)$. The beam entrance assembly of scintillators, vacuum tubes, flanges and windows, etc. is potentially a significant source of secondaries. To estimate how well the simulation reproduces these, comparisons of real data (with and without a disk of thickness 6.3 mm Al at the exit of the stack) with simulations show noticeable differences near $\cos(\theta) \approx 0.3$ as shown in Fig. 3. This is the most obvious weakness in the simulation, and efforts to identify its source are under way.

Tests and evaluations of systematic effects

TWIST accumulated several data sets in 2002, each large enough to determine ρ and δ with statistical precisions of about 10^{-3} . Two of these sets were accumulated in preferred conditions, i.e. optimum setting of experimental conditions at the time. Some fourteen other such sets were taken in which an experimental variable was modified or changed significantly beyond the normal control and/or monitoring range, so that the influence of each variable on the extracted Michel decay parameters could be studied. The altered variables included, among others, the solenoid field, the trigger (muon) rate, the μ stopping position, the field of the second bending dipole magnet in the beam line, the upstream/downstream material asymmetry, the voltages on the detectors, and the μ polarization. Some portions of these data sets were taken at different atmospheric pressures and temperatures so that systematic sensitivity to these environmental variables could be studied. Several small data sets were taken to add further information on the energy calibration and detector material thicknesses versus that in the MC simulation.

In 2003, some of the measurements described above have been repeated with a new M13 beam tune and a with an Al stopping target replacing the graphite-coated mylar target used in earlier runs. The high purity metal stopping target appears to reduce depolarization of the stopping muons, which could otherwise severely limit the sensitivity to the more fundamental effects on $\mathcal{P}_\mu \xi$ which TWIST hopes to explore. The usefulness of analogue information from the PCs near the the stopping target was also studied.

Examples of preliminary results

Two approximately equivalent experimental data sets (which we call Set A and Set B) were taken in 2002 with our preferred set of experimental variables. An initial WestGrid analysis of each one was compared with an identical analysis of a simulated spectrum plus derivative spectra using the blind analysis procedures. All three distributions were subjected to an independent end-point energy calibration, and the calibrated

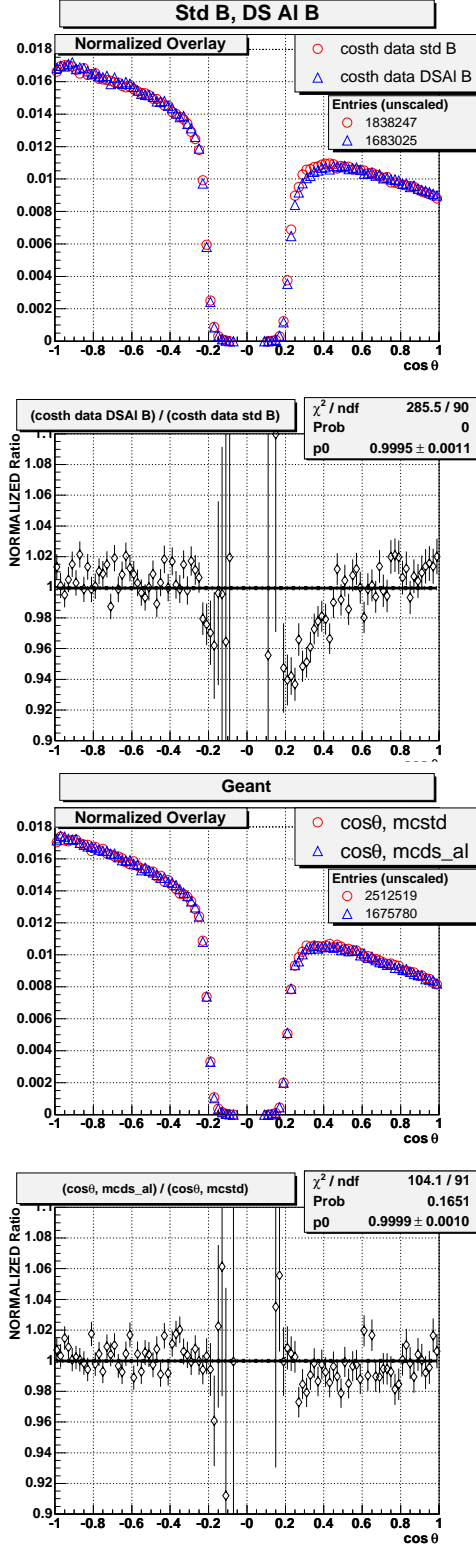


Fig. 3. Effect of the addition of a 6.3 mm thick Al plate at the DS exit of the detector stack, for data (upper two plots) and in the simulation (lower two plots). In both cases, one plot compares histograms where both have been scaled to a common number of entries (normalized overlay), while the other shows the differences by plotting the ratio of the normalized distributions.

data were binned in two dimensions. Within the very conservative fiducial range of $20 \leq p_e \leq 50$ MeV, and $0.54 \leq |\cos(\theta)| \leq 0.80$, the simulated base spectrum had about 1.4×10^7 events, while each experimental data set had about 1.0×10^7 events. The preliminary fit results shown in Table III were obtained. Improvements to these initial fits are continuing, with increased statistical precision of the simulations. A study of the optimum form and extent of the fiducial regions is also under way to determine a suitable compromise between sensitivity and statistics vs. systematic uncertainties.

Figure 4 shows plots of normalized residuals of the differences between the experimental and the MC data for momentum and $\cos(\theta)$ from fit results for Set A.

Table III. Preliminary results of blind analysis fits of simulated data to two experimental data sets. The values are differences from hidden decay parameters used by the simulation.

	Set A	Set B
$\Delta\rho(10^{-3})$	-12.7 ± 2.6	-14.2 ± 2.6
$\Delta\eta(10^{-1})$	-1.0 ± 1.4	-0.8 ± 1.4
$\Delta\mathcal{P}_\mu\xi(10^{-3})$	62.0 ± 2.6	61.8 ± 2.6
$\Delta\delta(10^{-3})$	-10.8 ± 1.4	-12.5 ± 1.4
χ^2/dof	1449/1556	1557/1556

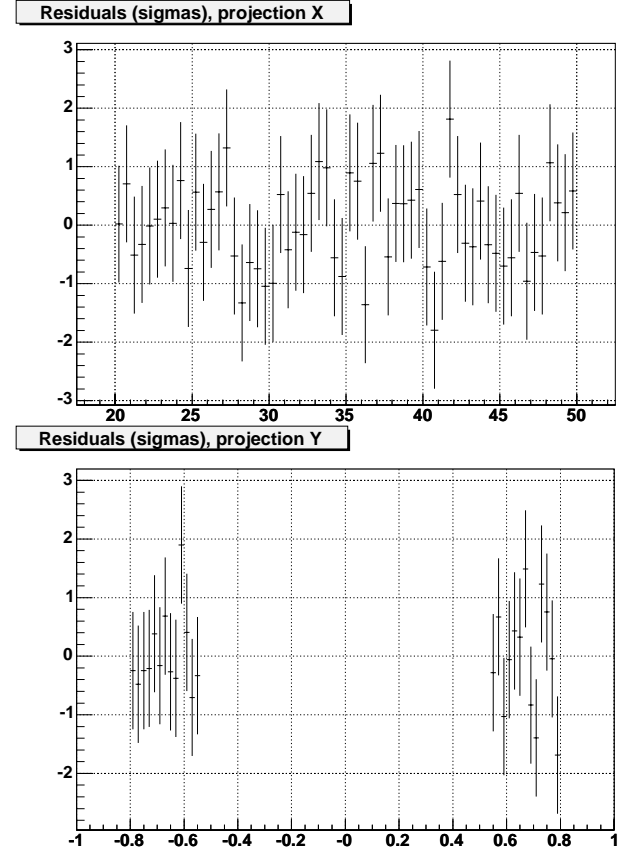


Fig. 4. Differences of experimental and simulated data in terms of normalized residuals of the two-dimensional fit, shown as projections in momentum (top) and $\cos(\theta)$ (bottom).

While the fit values, taken independently, are not particularly meaningful due to the hidden values of the simulated decay parameters, there is good agreement between the two experimental sets for all four parameters. The fit quality is very satisfactory. The statistical uncertainties, while not yet below the level of 10^{-3} , are close enough that we can say with confidence that we have enough experimental data to exceed this goal. The gains will come from an increase in simulation statistics, an expansion of the fiducial region, and a combination determined *a priori* of results of data sets taken under different conditions.

Summary

TWIST has achieved substantial progress in 2003. Problems which have been encountered either have been or are in the process of being solved. Data obtained so far appear to give the information necessary to provide ρ and δ at a precision of 10^{-3} . The WestGrid system satisfies our computing needs for this goal. Event reconstruction, data simulation, and fitting procedures are becoming mature and have passed many tests. The blind analysis procedure is proving to be extremely valuable for fitting of data to simulated distributions, and for evaluation of systematic effects between different data sets or different simulations in terms of precisely extracted values of decay parameters. Improvements to the muon beam, as well as our ability to control and measure it, are also continuing. All indications so far are that the goals of the experiment will be achieved, i.e. to attain at least an order of magnitude improvement in the existing uncertainties for ρ , δ , and $\mathcal{P}_\mu\xi$.

The ATLAS Experiment at the LHC (C. Oram, TRIUMF)

As described in detail in the 1996 Annual Report, ATLAS is building a general purpose pp detector which is designed to exploit the full discovery potential of the Large Hadron Collider (LHC) at CERN. The TRIUMF group is responsible for the management and engineering of the hadronic endcap (HEC) calorimeters, and the feedthroughs for the endcap cryostats. For the HEC, this year has seen the insertion of the two wheels of the first endcap into their cryostat, and the assembly of the two wheels for the second (and final) endcap. The wheel assembly and cryostat insertion at CERN is led by a TRIUMF staff member.

Physics goals

The present theoretical understanding of elementary particles is in the context of the standard model. It is a remarkably successful model, providing predictions which have been consistently confirmed by experiments for over two decades. Its agreement with experimental

results, to enormous accuracy in some cases, makes it the most accurately verified model in science. Of the many elementary particles contained in the standard model, only the Higgs remains to be discovered. The central goal of ATLAS is the search for the Higgs particle.

There are good theoretical reasons to believe that the discovery of the Higgs will at least contain hints at, and more likely direct evidence of, what lies beyond the standard model. If the Higgs is composite, its existence requires as yet unknown ultra-strong forces. If it is elementary, it would be the only spinless particle to be discovered so far. There is a theoretical “naturalness” problem for the masses of spinless particles. In the standard model, which is a highly nonlinear dynamical system, the elementary particles tend to take on the heaviest of all possible mass scales, which in such a model are at inaccessible energies and inconsistent with other requirements of the model. All other particles discovered thus far have natural mechanisms, such as gauge and chiral symmetries, for protecting their masses so that they can lie in the observable range. For the Higgs particle, there is no such symmetry in the present model. The only theoretical scenarios which leave the Higgs particle light enough to observe are hypothetical ones, either technicolour or supersymmetry, both radical departures from the present structure of the standard model. If the Higgs is observed at the LHC, one of these scenarios should be seen at the same time.

Particle theory has progressed enormously over the last few decades with many appealing scenarios for physics beyond the standard model. The most likely of these is supersymmetry and the boldest of these is superstring theory. These theories are intimately related and are both radical ideas which promise a new conceptual framework for understanding elementary particles. Though far from being complete theories at present, there are superstring models which resemble the standard model in their low energy limit. These models have a great appeal as they contain a unification of fundamental forces which includes gravity. They have already had substantial impact on gravitational physics where, for example, in addition to the long sought reconciliation of gravity with quantum mechanics, they have been used to derive a fundamental understanding of black hole thermodynamics. Superstring theory is still in its infancy, but progress has been dramatic and the promise of great things to come has captured the imagination of a substantial fraction of the world’s theoretical particle physicists.

The present theoretical view is that the conventional grand unification of the strong, weak and electromagnetic forces can only work in the supersymmet-

ric extension of the standard model. In that model, the grand unified energy scale is only two decades below the Planck scale, the ultimate energy where space-time itself has quantum fluctuations. It is not out of the realm of imagination that, at energy scales where supersymmetry would be observed, evidence for an ultimate theory of everything, or at least everything that can exist once space-time is formed, is within human grasp.

Experiments at the LHC, where the ATLAS detector will take data, will probe the energy region where the Higgs particle, possibly supersymmetry, or other structures will be visible. This will be the first experimental probe of an energy region in many years where fundamentally new physics is expected to occur. There is every reason to believe that the results will be among the most dramatic ever.

Basic ATLAS design considerations

The most prominent issue for the LHC is the quest for the origin of the spontaneous symmetry-breaking mechanism in the electroweak sector of the standard model. This is related to one of the most fundamental questions of physics: What is the origin of the different particle masses? New direct experimental insight is required to answer this question.

One of the possible manifestations of the spontaneous symmetry-breaking mechanism could be the existence of a standard model Higgs boson (H), or of a family of Higgs particles (H^\pm , h , H and A) when considering the minimal supersymmetric extension of the standard model (MSSM). The Higgs search is therefore used as a first benchmark for the detector optimization. For the SM Higgs, the detector has to be sensitive to the following processes ($\ell = e$ or μ) in order to cover the full mass range above the discovery limit set by the final LEP operation in the fall of 2000:

$H \rightarrow b\bar{b}$ from WH , ZH and $t\bar{t}H$ using a ℓ^\pm and b -tagging,
mass range $80 < m_H < 100$ GeV;

$H \rightarrow \gamma\gamma$
mass range $90 < m_H < 150$ GeV;

$H \rightarrow WW^* \rightarrow \ell^\pm \nu \ell^\pm \nu$
mass range $150 < m_H < 200$ GeV;

$H \rightarrow ZZ^* \rightarrow 4\ell^\pm$
mass range $130 \text{ GeV} < m_H < 2m_Z$;

$H \rightarrow ZZ \rightarrow 4\ell^\pm, 2\ell^\pm + 2\nu$
mass range $m_H > 2m_Z$;

$H \rightarrow WW, ZZ \rightarrow l^\pm \nu + 2 \text{ jets}, 2\ell^\pm + 2 \text{ jets}$
from WW, ZZ fusion using tagging of forward jets for m_H up to about 1 TeV.

In addition to signatures similar to these, the MSSM Higgs searches also require sensitivity to processes such as:

$$\begin{aligned} A \rightarrow \tau^+ \tau^- &\rightarrow e\mu + \nu\text{'s} \\ &\rightarrow \ell^\pm + \text{hadrons} + \nu\text{'s}; \\ H^\pm \rightarrow \tau^\pm \nu &\text{ from } t\bar{t} \rightarrow H^\pm W^\mp b\bar{b} \text{ and} \\ &\rightarrow 2 \text{ jets using a } \ell^\pm \text{ tag and } b\text{-tagging.} \end{aligned}$$

The observable cross sections for most of these processes are small over a large part of the mass range to be explored at the LHC. Hence it is important to operate at high luminosity, and to maximize the detectable rates above backgrounds by high-resolution measurements of electrons, photons, and muons.

Figure 5 shows the estimated signal significance for the standard model Higgs discovery in ATLAS over the presently theoretically favoured region: 100–200 GeV/ c^2 . From 100–190 GeV/ c^2 , the most significant discovery channels are where the Higgs is produced by vector boson fusion [see Asai *et al.*, “Prospects for the search for a standard model Higgs boson in ATLAS using vector boson fusion”, ATLAS Note SN-ATLAS-2003-24]. While the cross section for production is lower in these channels, the ability to cleanly tag the Higgs production by forward jets that enter the endcap calorimeters more than compensates, yielding superior signal to noise in these channels. The need to use the endcap calorimeters for this tag, puts a premium on obtaining an early robust calibration for the calorimeters over the entire angular range.

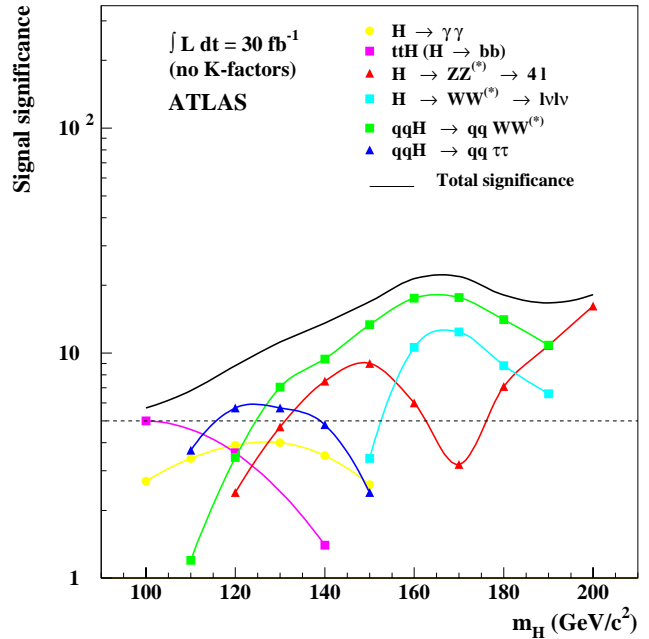


Fig. 5. ATLAS sensitivity for the discovery of a standard model Higgs boson for an integrated luminosity of 30 fb $^{-1}$. The signal significances are plotted for individual channels, as well as for the combination of all channels.

Canada's participation in ATLAS

The Canadian group consists of about 35 grant eligible physicists from TRIUMF, University of Alberta, Carleton University, Simon Fraser University, University of British Columbia, Université de Montréal, University of Toronto, University of Victoria, and York University. We are strongly involved in three construction projects centred around detecting hadrons in the endcap region: the hadronic endcap project, the hadronic portion of the forward calorimeter project, and the pipeline electronics for calorimetry. In addition, we are committed as part of our common project contribution to providing the feedthroughs for the two endcap cryostats. TRIUMF is directly involved in all of these projects, and in the physics simulations.

The hadronic endcap project

The hadronic endcap (HEC) calorimeter is a liquid argon sampling calorimeter with copper absorbers [ATLAS Collab., ATLAS Liquid Argon Technical Design Report (1996)]. A concise overview of this design was provided in the 1996 TRIUMF Annual Report. An artist's impression of a module can be seen in Fig. 6. Four detector systems sit in each endcap cryostat: nearest the interaction region is the presampler, followed by the electromagnetic endcap (EMEC) and the HEC. At the inner diameter around the beam pipe is the forward calorimeter (FCAL).

Hadronic endcap module production and testing

By the end of 2002 we had constructed all the modules, and tested 120 of the 132 modules that constitute the

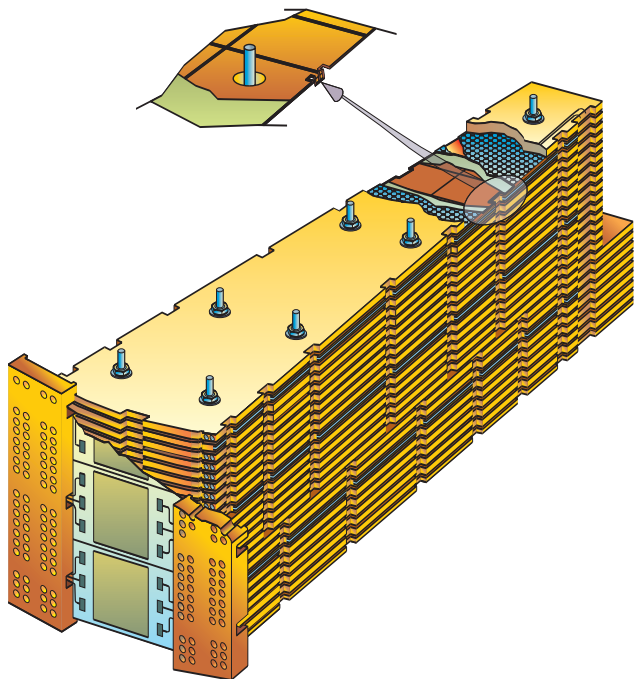


Fig. 6. Artist's impression of a hadronic endcap module.

two HEC endcaps in ATLAS. During 2003 the final 12 modules were successfully tested, bringing to an end the era of module production.

Test beam measurements of the hadronic endcap modules This year we were preparing for the joint test of the three calorimeters in the endcap, scheduled for beam in 2004. During 2003, 16 purpose built small “inner radius” HEC modules were constructed in the HEC Russian Institutes, with full involvement of TRIUMF in design, materials procurement, and management. An engineering run of the test beam set-up is scheduled for February, 2004, with beam runs in the spring and fall of 2004. This test will use pre-existing EMEC and FCAL modules, along with these “inner radius” HEC modules.

In the summer of 2002, the combined performance of the HEC and EMEC series production modules was successfully tested in the H6 beam line at CERN. The H6 beam line provides beams from 20 to 180 GeV. During 2003 these data were successfully analyzed and a NIM article is presently in the final stages of preparation. This is an important step for the group as these measurements form the basis of the calibration of the calorimeter system as it will be used at LHC beam startup.

Wheel assembly at CERN A HEC wheel is formed from 32 modules. There are two wheels at each end of ATLAS, so we must assemble 128 modules into four wheels. The equipment for the wheel assembly is a Canadian responsibility. The four wheels and the two wheels of the EM calorimeter, which go into the same cryostat, are assembled in the horizontal orientation. Hence each wheel, which weighs about 90 tonnes, must be taken from its assembly table, rotated to the vertical and moved to the cryostat. This rotation and translation of equipment is also a Canadian responsibility. The engineering was undertaken by a collaboration between Alberta and TRIUMF personnel. The production of the equipment was by Canadian industry. This year saw the rotation of the first EM calorimeter wheel, and the successful insertion of the EM and HEC wheels into the cryostat, thus completing the first cryostat for the three large wheels (see Fig. 7). The two HEC wheels which will go into the second cryostat, have been assembled during 2003, and one of them rotated into the vertical.

The cold test of the first cryostat is scheduled for the summer of 2004, and the second cryostat should be filled by early 2005.

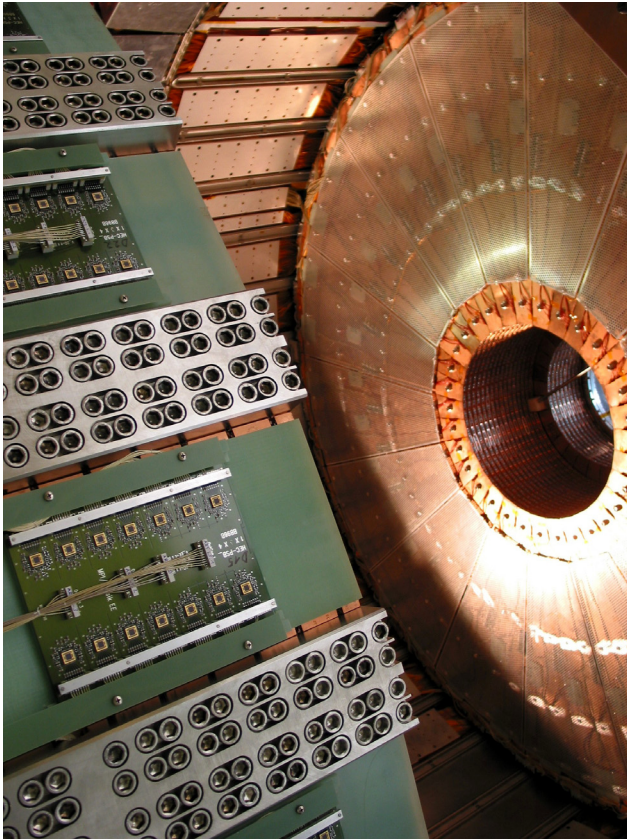


Fig. 7. The second HEC wheel being inserted into the first endcap cryostat.

The ATLAS Endcap Signal Feedthroughs (M. Lefebvre, Victoria)

As described in detail in the 1996 Annual Report, ATLAS is building a multi-purpose *pp* detector which is designed to exploit the full discovery potential of the Large Hadron Collider (LHC) at CERN. The TRIUMF group is responsible for the engineering of the hadronic endcap calorimeter (HEC), and contributes to the production of high density cryogenic signal feedthroughs for both endcap cryostats. The feedthroughs are critical to the success of ATLAS. They have been built and tested at the University of Victoria by TRIUMF and Victoria staff. The endcap signal feedthroughs have been installed on the two endcap cryostats between December, 2002 and September, 2003. The ATLAS endcap signal feedthrough project was covered in detail in the 2001 TRIUMF Annual Report. This final endcap signal feedthrough project report focuses on the 2003 activities.

Reviews

A Canadian involvement in the endcap signal feedthroughs was already proposed in 1995. From the \$12.2 M NSERC Major Installation Grant awarded to ATLAS in the 1997–98 competition, over \$4 M was allocated to the endcap signal feedthrough project. The

most recent status report was presented at the last NSERC ATLAS Review, held at TRIUMF on November 5, 2003.

Overview of the project

The ATLAS liquid argon calorimetry is composed of a barrel section and two endcap sections. Each endcap cryostat contains an electromagnetic calorimeter, two wheels of one HEC, and a forward calorimeter. The calorimeter signal and calibration lines are routed to the outside of each endcap cryostat via 25 feedthrough assemblies arranged approximately equally spaced in azimuth. The low voltage needed to operate the endcap hadronic calorimeter preamplifiers, which are located in the cold, are also supplied via the signal feedthroughs as well as various monitoring lines.

The design is based on gold plated conductive pins insulated and sealed by glass inserts in a stainless steel carrier. The carriers are then welded into the cold and ambient (temperature) flanges. A total of 1920 signal and calibration lines per feedthrough assembly is required in the chosen design. Figure 8 shows an overview drawing of one endcap signal feedthrough. The ambient and cold flanges are connected by a bellows to

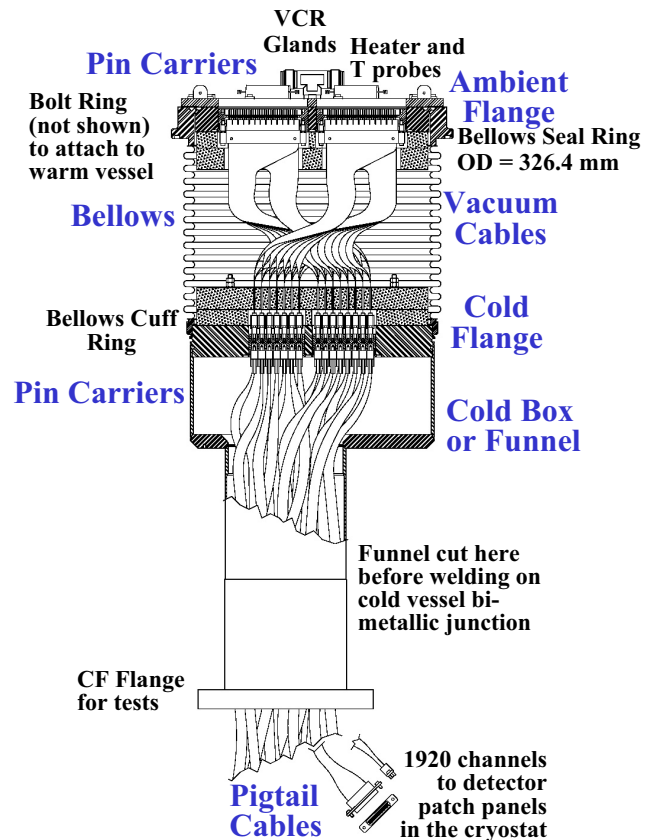


Fig. 8. Overview drawing of one endcap signal feedthrough, identifying its most important components.

isolate the feedthrough vacuum from the cryostat inter-vessel vacuum. The cold flange is attached to a transition piece, known as a funnel, which is welded to the cryostat via a bi-metallic joint. The electrical signals are brought from the calorimeter to the cold flange by coaxial kapton cables; these are called pigtail cables. Cables located in the vacuum between the cold and the ambient flange, i.e. inside the bellows, carry the signals through the cryostat wall; these are called vacuum cables. For each endcap, four feedthrough assemblies also carry the low voltage for the HEC preamplifiers.

Assembly and installation

A total of 50 feedthrough assemblies plus 5 spares has been produced following a detailed assembly procedure, quality plan and quality assurance plan. These include the description of the testing of components from their arrival in Victoria through the completion of feedthrough units. Complete material traceability is ensured through the use of detailed traveller sheets. The funnel and cold flange of each feedthrough assembly are part of the cryostat pressure vessel. An officially licensed company has done the welding and extensive testing to conform to accepted welding code.

The shipment of feedthrough assemblies to CERN was done by air freight. The last shipment was completed in January, 2003. Upon arrival at CERN, each feedthrough assembly was subjected to an ambient temperature leak test and a basic electrical test. We are responsible for these tests, the last of which were performed in June, 2003.

The installation of the feedthrough assemblies on the cryostat was a delicate and complex operation. Although the feedthrough installation is not a Canadian responsibility, our group actively assisted during the operation. The installation of the feedthrough assemblies on the first endcap cryostat started on December 2, 2002 and ended on January 4, 2003 (see Fig. 9).



Fig. 9. Paul Poffenberger (front, Victoria) during feedthrough installation on the first ATLAS endcap cryostat.

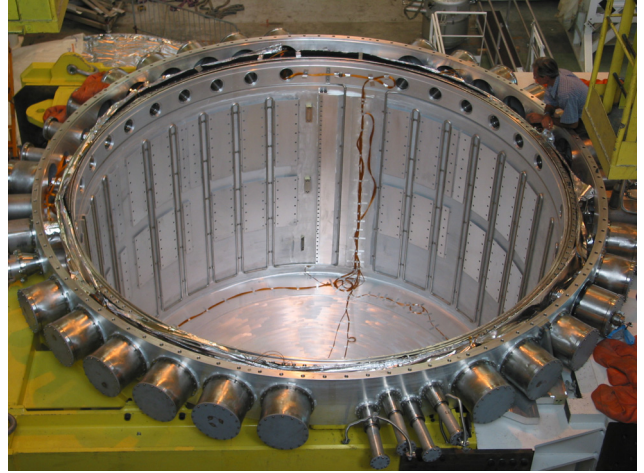


Fig. 10. Second ATLAS endcap cryostat with its cover removed, before feedthrough installation, CERN June 26, 2003.



Fig. 11. Paul Birney (TRIUMF) and Ken Sexton (BNL) during feedthrough installation on the second ATLAS endcap cryostat.

Installation on the second cryostat (see Fig. 10) started on July 23, 2003 and ended on September 26, 2003 (see Fig. 11).

Members of our team manually connected the so-called warm cables that join the outside of the ambient flange to the electronics crate baseplane; each baseplane and corresponding pedestal are associated with two feedthroughs (see Fig. 12). Given the softness of the pins, this was a particularly delicate operation. Each feedthrough assembly, once welded on the cryostat, was also electrically tested (see Fig. 13). Results of these tests will form part of the ATLAS detector database.

A paper describing the ATLAS LAr signal feedthroughs is being written in collaboration with our colleagues from Brookhaven National Laboratory (who produced the barrel signal feedthroughs), and will be submitted to Review of Scientific Instruments in 2004.

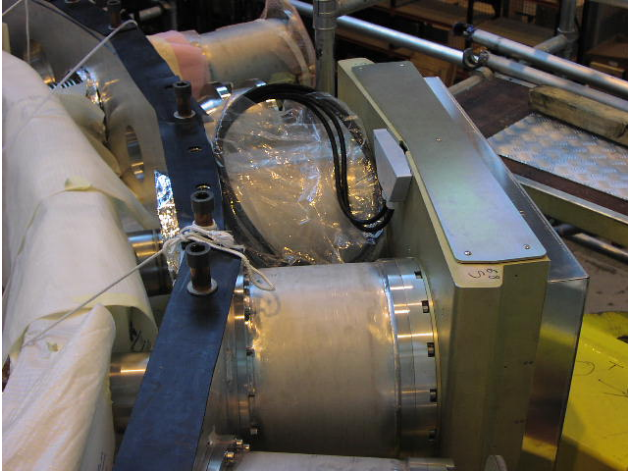


Fig. 12. View of the first mounted pedestal on the first cryostat.



Fig. 13. Fiona Holness (Victoria) performing electrical tests on feedthroughs recently welded on an ATLAS endcap cryostat.

Other tasks in 2004 will include finalizing the inventory, the storage of spare parts, the interfacing of electrical test results with the ATLAS database, the decommissioning of the feedthrough production equipment, and the maintenance of readiness for repairs until the endcap cryostats are in operation in the ATLAS cavern.

BNL 787/949/KOPIO

Measurement of $K \rightarrow \pi\nu\bar{\nu}$ and other rare decays

(D. Bryman, UBC)

The rare kaon decays $K^+ \rightarrow \pi^+\nu\bar{\nu}$ and $K_L^0 \rightarrow \pi^0\nu\bar{\nu}$ offer unique opportunities to scrutinize higher order phenomena associated with quark mixing and charge-parity (CP) non-invariance. Experiment 787 at Brookhaven National Laboratory (BNL) discovered initial evidence for $K^+ \rightarrow \pi^+\nu\bar{\nu}$ decay based on the observation of two clean events [Adler *et al.*, Phys. Rev.

Lett. **88**, 041803 (2002); *ibid.*, Phys. Rev. Lett. **84**, 3768 (2000); *ibid.*, Phys. Rev. Lett. **79**, 2204 (1997)]. The branching ratio indicated by E787 data is consistent with the standard model (SM) expectation. However, to fully explore the possibility of new physics or to make a precise measurement of the t-d quark coupling $|V_{td}|$, E949 is scoped to obtain a single event sensitivity of $B(K^+ \rightarrow \pi^+\nu\bar{\nu}) = (8-14) \times 10^{-12}$, roughly an order of magnitude below the SM prediction. In order to reach this sensitivity, upgrades to the E787 detector system were made and E949 commenced $K^+ \rightarrow \pi^+\nu\bar{\nu}$ data acquisition in 2002. With the completion of E949, the possibility of an inconsistency with the SM prediction of $B(K^+ \rightarrow \pi^+\nu\bar{\nu})$ will be fully explored or the important top-down quark mixing parameter will be determined to a precision 15–30% if the SM expectation is confirmed.

Despite an enormous worldwide effort and significant progress in B physics, it has become evident that the K sector can yield the single most incisive measurement in the study of direct CP violation through a measurement of the branching ratio for $K_L^0 \rightarrow \pi^0\nu\bar{\nu}$ ($B(K_L^0 \rightarrow \pi^0\nu\bar{\nu})$). In the context of the SM, $B(K_L^0 \rightarrow \pi^0\nu\bar{\nu})$ is a unique quantity which directly measures the common area of the CKM unitarity triangles, i.e. the physical parameter that characterizes all CP violation phenomena or, alternately, the height of the triangle. Measurements of both $B(K_L^0 \rightarrow \pi^0\nu\bar{\nu})$ and $B(K^+ \rightarrow \pi^+\nu\bar{\nu})$ will allow the unitarity triangle to be precisely reconstructed from K decay information alone. Thus, a complete picture of standard model CP violation in the K system will result and a comparison with comparably precise measurements anticipated from the B sector will be enabled.

The challenges of measuring $B(K_L^0 \rightarrow \pi^0\nu\bar{\nu})$, expected to occur at 3×10^{-11} , have been taken up by the KOPIO collaboration at BNL. KOPIO employs a low energy, time structured K_L^0 beam to allow determination of the incident kaon momentum. The goal of KOPIO is to discover the reaction $K_L^0 \rightarrow \pi^0\nu\bar{\nu}$ and obtain a sample of at least 40 events with a signal to background ratio greater than 2:1. This will yield a statistical uncertainty in the measurement of the area of the CKM unitarity triangle of less than 10%. Capital construction for KOPIO is presently planned to begin in 2005.

E787/949

The decay $K^+ \rightarrow \pi^+\nu\bar{\nu}$ had been sought since the early 1960s as an indication of the existence of flavour changing neutral currents. E949 grew out of the successful precursor experiment, E787, which took data from 1995–98 and improved the sensitivity to $K^+ \rightarrow \pi^+\nu\bar{\nu}$ by four orders of magnitude beyond previous attempts. E787 discovered the first two $K^+ \rightarrow \pi^+\nu\bar{\nu}$

events as well as several other important rare K decays and performed many non-SM searches.

The result for E787 data, based on two observed events and the expected background levels, was $B(K^+ \rightarrow \pi^+ \nu \bar{\nu}) = 1.57^{+1.75}_{-0.82} \times 10^{-10}$. This result is consistent with the SM prediction. Even with low statistics, the E787 result already impacts limits on SM quark mixing and CP violation parameters, as well as possibilities for new physics as illustrated by D'Ambrosio and Isidori [hep-ph/0112135 (2002)].

Progress has also been made to access the region below the $K_{\pi 2}$ peak. Analysis of two E787 data sets (1996–97) has been completed. Combining the results, one event was found with an expected background of 2 ± 1 events giving a limit $B(K^+ \rightarrow \pi^+ \nu \bar{\nu}) < 2 \times 10^{-9}$ (90% CL) [Adler *et al.*, Phys. Lett. **B537**, 211 (2002)]. Since the lower region of phase space is more sensitive to new types of physics arising from scalar and tensor interactions, new limits have been derived on such couplings as well as new limits on processes like

$K^+ \rightarrow \pi^+ X$. Substantial improvements will be made in E949.

E949 was based on incremental upgrades to the techniques and technology of E787. A drawing of the E787 detector upgraded for E949 is shown in Fig. 14. With the approved E949 running time of 6000 hours (about 60 weeks), the expected single event sensitivity for $K^+ \rightarrow \pi^+ \nu \bar{\nu}$ is 1.7×10^{-11} . Combined with the E787 data, the sensitivity will be 1.4×10^{-11} with 0.7 expected background events. With the added acceptance from the region below the $K^+ \rightarrow \pi^+ \pi^0$ peak, the sensitivity may reach 7.6×10^{-12} . We would therefore expect to see 7 to 13 events if the branching ratio is equal to the central SM value.

E949 had a short initial running period in 2002 in which approximately 2×10^{12} kaons were stopped (roughly one third of the number collected by E787). Problems with high voltage breakdown in the electro-magneto-static separators forced E949 to run with a larger pion contamination and with 50% fewer kaons

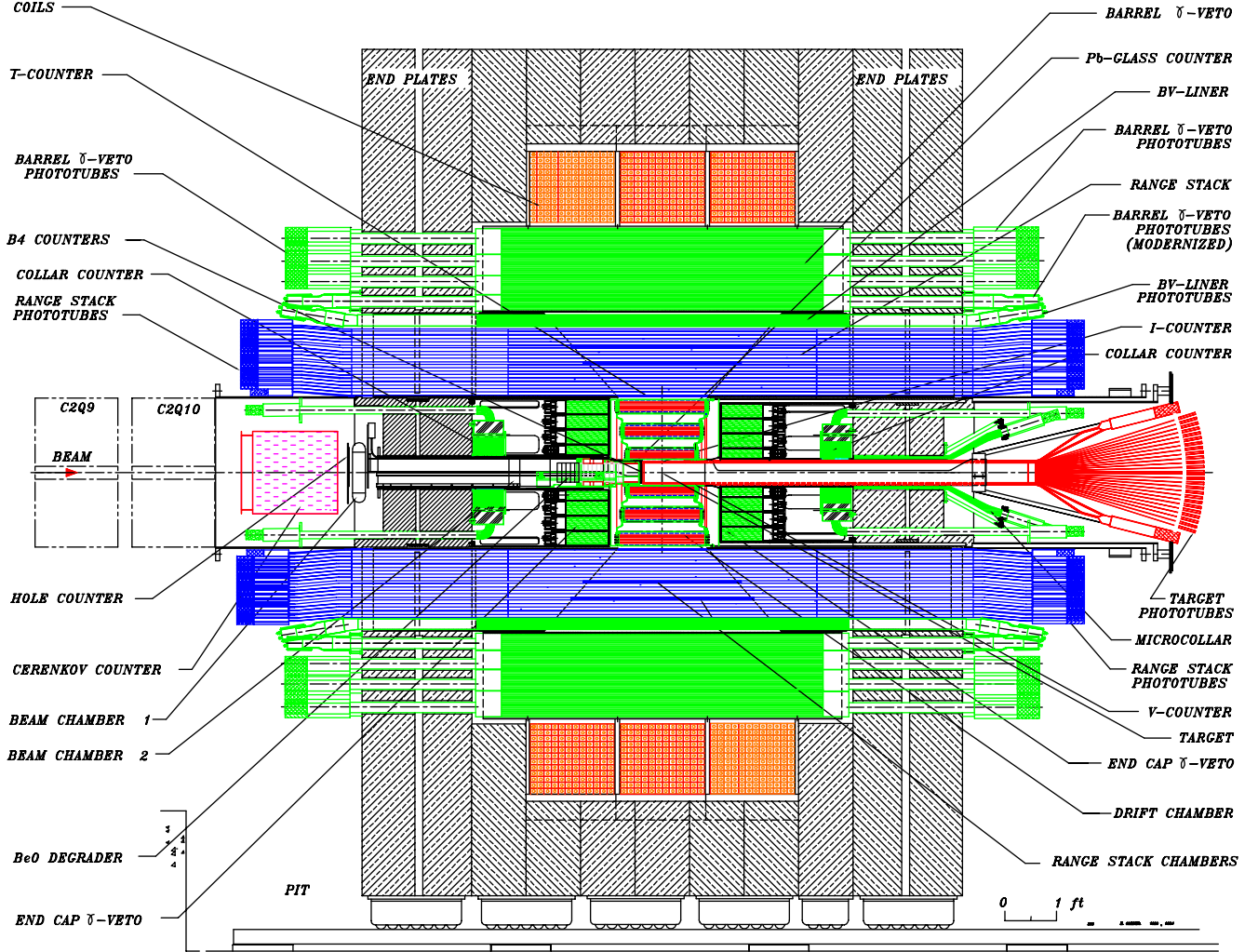


Fig. 14. The E949 detector.

per proton. The primary motor generator set for the AGS had been damaged, necessitating the use of the backup set, which required running at the reduced duty factor of 41% and with lowered primary proton beam momentum. These problems will be corrected before future running of E949.

In spite of these difficulties the projected improvements for E949 were confirmed. The analysis of the 2002 data was completed during 2003 at TRIUMF with assistance from BNL and Japan and results are expected to be published in early 2004.

KOPIO R&D

Overview The goal of KOPIO is to observe and definitively measure the rate of the decay $K_L^0 \rightarrow \pi^0 \nu \bar{\nu}$. We aim to unambiguously detect a large sample of events so that η , the SM CP violation parameter, can be determined to 15% accuracy with minimal contributions from background or systematic effects. Like E787/E949, KOPIO has built-in redundancies and a reasonable level of contingency to meet the goal of a successful measurement.

In the KOPIO experiment, a 500 μ sr solid angle neutral beam is extracted at 45° to produce a “soft” K_L spectrum peaked at 0.65 GeV/ c ; kaons in the range from about 0.5 GeV/ c to 1.3 GeV/ c will be used. Downstream of the final beam collimator is a 3.5 m long decay region which is surrounded by the main detector. The decay region is surrounded by an efficient Pb/scintillator photon detector which serves to veto photons and charged particles. In the forward detection region the primary photon detector system consists of two sections: a fine grained preradiator (PR) in which the photons are converted and the first e^+/e^- pair is tracked, followed by an 18 X_0 calorimeter in which the remaining energy of the photon shower is measured. The preradiator consists of 64 0.03 X_0 layers, each with plastic scintillator, metal converter and dual-coordinate drift chambers. The preradiator, which has a total effective thickness of 2 X_0 , functions to measure the photon positions and directions accurately in order to allow reconstruction of the K_L decay vertex while also contributing to the achievement of sufficient energy resolution. The calorimeter is constructed using Pb/scintillator layers. In the barrel and upstream regions, a Pb/scintillating combination will also be used to obtain high veto efficiency. Downstream of the main π^0 detector, a beam hole photon counter (“beam catcher”) consists of Čerenkov detectors designed to be insensitive to neutrons.

Preradiator project The requirements of the preradiator include a photon angular resolution of approximately 25 mr, a photon conversion efficiency of about 0.7 (2.0 X_0), a good measurement of the deposited en-

ergy and as short as possible linear extent so as to limit shower size at the calorimeter. The principle employed is to measure the positions and angles of the first e^+e^- pair following photon conversion in a series of thin converter/detector modules. Each PR module consists of an inactive converter material, a dual-coordinate drift chamber (anode wires and cathode strips CSC) and a scintillator.

A stack of 5 small (8 cm \times 15 cm) KOPIO chambers has been constructed and is under test. Two medium size KOPIO chambers (30 cm \times 30 cm) are operational for electronics development and specification and cosmic ray measurements. Initial measurements gave the expected level of performance of full efficiency and good position resolution. The maximum drift was measured to be 70 ns with full efficiency. Position resolution was found to be $\sigma = 200 \mu$ m for both anodes and cathodes which is more than adequate for KOPIO. Two other chambers with full scale (2 m) in one dimension (anode or cathode) are under development. The anode version was completed and is undergoing test measurements with prototype electronics. These will be used primarily for final electronics development and testing. The final prototype level will be a full size pre-production model of eight chamber layers.

Front end chamber electronics systems for both the anodes (including HV distribution) and cathodes have been tested on the development chambers. Multiple channel boards are being constructed. Designs have been developed for the receiver and processor boards at TRIUMF. Montreal has responsibility for the cathode digitizer/processor boards (which are also being spun off for other applications such as TIGRESS at TRIUMF). The anode processor board is under design at TRIUMF. An engineer at TRIUMF (paid by the US KOPIO collaboration) is dedicated to this work. Tests of the tracking and energy measurement performance in test beams at TRIUMF and BNL LEGS using pre-production electronics are planned.

During the past year, we have been working with a local company, CELCO (Surrey, BC) to develop the extruded scintillator for the KOPIO preradiator which will be read out with 1 mm dia. wavelength shifter fibre (wls). To achieve the light output, uniform hole diameters for the wls fibre, and the mechanical tolerances that are required for KOPIO, we have done several exploratory runs producing scintillator. The CELCO product has comparable light output to other commercial extruded scintillators. In addition, we have developed a new design for the preradiator’s external veto detector along with assembly plans for the preradiator modules. To test the mechanical strength of the preradiator modules, we are performing finite element analysis studies of the proposed structure and a me-

chanical design model of a module is presently under construction. We will use the model to make stress and stability measurements which will be compared with the simulation studies.

Considerable infrastructure for the KOPIO project is being supplied by the CFI-supported LADD project. CFI approved the final budget in July and ordering of equipment has begun. This will be a boon to the design and construction of the KOPIO preradiator mechanical and electronic systems.

Beam studies Particle beam simulations for KOPIO are in progress at TRIUMF. The very short kaon bunches required are produced by extracting 0.15 ns (RMS) long proton bunches with 40 ns separation. Beams of this type, but not quality, became feasible at the AGS in 1997 with the development of a micro-bunched slow extracted beam which relies on the technique of squeezing the debunched beam through the gap between empty rf buckets that are centred near the extraction radius. The betatron tune depends on the longitudinal momentum; and chromatic extraction is effected by a 1/3-integer transverse resonance driven by sextupoles. The micro-bunches have high momenta and are preferentially extracted.

Along with new graphical and analysis software for displaying and processing the output, a computer program, LONG1D-SLEX, that combines rf manipulations and longitudinal tracking with the slow extraction transverse dynamics, was written to study the micro-bunching process. At first the program was used in support of experiments at the AGS with a 20 kV 93 MHz cavity yielding proton bunches of 0.3 ns length and 11 ns spacing. The 40 ns bunch spacing for KOPIO and the 0.15 ns bunch length at the lower frequency (25 MHz) is somewhat more challenging; a solution that makes economical use of rf voltage is required. The computer program was used to study an innovation in which a higher harmonic cavity is used to distort and stretch the rf buckets. The presently favoured scheme uses a 3 s magnet cycle, the natural chromaticity, and fundamental and anti-phased fourth harmonic cavities each with 150 kV. Currently missing from the simulations are the influence of collective effects due to wake fields.

In addition to simulating the primary beam, we have also been studying the neutral beam to insure that the beam halo of neutrons is manageable. The collimator system for the neutral beam was re-examined by studying a number of different geometries to minimize the neutron halo in the kaon decay region, especially in the vertical plane. A consensus was reached for a new geometry, which is now being used to study other aspects of the neutral kaon beam. For instance, a sweeping magnet system is being considered to sweep

away charged particles in the beginning of the beam. A downstream magnet is intended to eliminate the charged kaons, produced by neutral kaons in the collimators. These studies are continuing in collaboration with colleagues at BNL and Yale.

Hypernuclear Physics with FINUDA at LNF Frascati

(A. Olin, P. Amaudruz, TRIUMF; G. Beer, Victoria)

Following the long-delayed operation of the DAFNE Phi Factory at the Laboratory for Nuclear Science (LNF) at Frascati, several milestones were recently achieved in research programs with Canadian participation. After completion of successful DEAR kaonic hydrogen X-ray measurements soon to be published, the FINUDA spectrometer was rolled into the electron-positron interaction zone shared with DEAR. The scheduled engineering test run of the FINUDA detector was begun in late fall and will be continued as a data-acquisition run until spring, 2004 if it is established that both detector and accelerator are functioning well. Some years ago, TRIUMF scientists constructed and beam-tested sixteen large low mass planar wire chambers essential to the tracking, as well as participating in the construction and installation of over 2000 straw tubes and their gas distribution system. Both these components have functioned satisfactorily, despite the long delay in the scheduled start of data acquisition. A preliminary announcement in the CERN Courier summarizes the situation at the end of 2003.

The first results from the FINUDA experiment at INFN's Frascati National Laboratory show that the detector is performing well and is in good shape for its future studies of hypernuclear physics. At the XLII International Winter Meeting on Nuclear Physics in Bormio, Italy, at the end of January, the FINUDA team presented data on the performance of the detector, as well as preliminary observations of the formation of hypernuclei and their decay spectra.

The FINUDA detector was installed at the DAFNE Phi Factory in Frascati in the spring. The experiment makes use of the low-energy negative kaons emitted in the decays of the ϕ particles created in DAFNE. The decays produce an almost monochromatic beam of K^- with an energy of about 16 MeV. These low-energy K^- can come to a stop in thin targets and interact with nuclei via a strangeness-exchange reaction, where the strangeness of the kaon is transferred to a nucleus in which a neutron (containing udd quarks) becomes a lambda particle (uds).

The use of thin targets means that the FINUDA experiment can make the most of its intrinsic momentum resolution in order to provide high-resolution measurements of hypernuclear energy levels. In addition, the

apparatus is designed to detect charged and neutral particles with large angular coverage and high statistics. The experiment can also measure spectra from different targets at the same time, so reducing the number of possible systematic errors.

Once the commissioning of FINUDA was complete in October, data-taking could begin with a set of targets of different nuclei – ${}^6\text{Li}$, ${}^7\text{Li}$, ${}^{12}\text{C}$, ${}^{27}\text{Al}$ and ${}^{51}\text{V}$ – that were chosen to allow a variety of simultaneous studies of the formation and decay of hypernuclei. The targets form an octagon surrounding the interaction region, where the K^- are produced in the decay of ϕ particles to K^+K^- pairs. Within the target array, thin slabs of scintillator detect the highly ionizing low-energy kaons. Hypernuclear-formation events are selected by a trigger that picks out K^+K^- pairs accompanied by a fast particle (a pion) coming from the interaction of the K^- in a target.

The data indicate a momentum resolution, $\Delta p/p$ of 1.1% full width at half maximum (FWHM), corresponding to a resolution of approximately 2.5 MeV on hypernuclear energy levels. This value should improve after final calibration and detector alignment. The indications are that during its first phase of data-taking FINUDA should collect about 3×10^5 useful events per target – which is enough for some high-resolution spectroscopy on the various nuclei. The ${}^{12}\text{C}$ spectra are already comparable in quality to the best results from KEK.

The HERMES Experiment

(C.A. Miller, S. Yen, TRIUMF; M.C. Vetterli, SFU/TRIUMF; M.G. Vinciter, Alberta)

The HERMES experiment was designed to comprehensively study the spin structure of the nucleon. It has been running at the HERA electron accelerator at the DESY laboratory in Hamburg, Germany since 1995, measuring spin asymmetries for deeply inelastic electron scattering (DIS). The combination of a polarized high energy electron beam in a storage ring with undiluted polarized atomic gas targets is unique in this field, and has important experimental advantages. Furthermore, the spectrometer detecting the scattered electrons also has substantial acceptance and the capability to identify all types of hadrons produced in coincidence.

This was a pivotal year for the HERMES collaboration. A letter was submitted [Airapetian *et al.*, Phys. Rev. Lett. (in press)] reporting a key result distilled from all of the data recorded with longitudinally polarized hydrogen and deuterium targets from 1996 to 2000. This fulfills a primary original goal of the experiment – the determination of the polarizations of the quarks of various flavours (u , d , \bar{u} , \bar{d} and s) rela-

tive to the spin direction of the nucleon, independent of any assumptions about their inter-relationship. The Canadian group played a major role in the analysis, and drafted the paper. In an important step in a new direction, the collaboration released a preliminary result constituting the first single-spin azimuthal asymmetries measured with a transversely polarized target. These data shed first light on the path towards the determination of the unknown transversity quark distribution. They are presented here, followed by one other highlight from the year’s new results.

Transversity

The relativistic motion of partons inside the proton can be interpreted in a frame in which the proton is moving with “infinite” momentum, where the parton motion transverse to this direction is effectively frozen. Nucleon structure can then be investigated through measurements of parton distributions in x , the dimensionless Bjorken scaling variable representing the longitudinal momentum fraction of the proton carried by the parton. After averaging over intrinsic transverse quark momentum p_T , for each quark flavour three fundamental distributions in x can be interpreted as probability densities. Two of these have already been experimentally explored in some detail – the spin-independent density $q(x)$, and the helicity density $\Delta q(x) \equiv q^{\vec{\uparrow}}(x) - q^{\vec{\downarrow}}(x)$ reflecting the probability of finding the helicity of the quark to be the same as that of the target nucleon. Viewed in the same helicity basis, the third distribution known as transversity, δq or alternatively h_1^q , is related to a forward scattering amplitude involving helicity-flip ($N^{\rightarrow}q^{\leftarrow} \rightarrow N^{\leftarrow}q^{\rightarrow}$) and has no probabilistic interpretation. However, it is a probability density in a basis of transverse spin eigenstates: $\delta q = q^{\uparrow\uparrow} - q^{\uparrow\downarrow}$. The transversity and helicity densities differ only because quarks probed with sufficient spatial resolution (or sufficiently hard scattering) move relativistically, in which regime boosts and rotations don’t commute.

Transversity has thus far remained unmeasured because it is chiral-odd, and hard interactions conserve chirality. However, it may be probed by a process involving some additional chiral-odd structure. If a hadron produced from the struck quark is detected in addition to the scattered lepton in semi-inclusive measurements, the distribution of the hadrons in the azimuthal angle ϕ about the virtual photon direction relative to the lepton scattering plane (see Fig. 15) can be sensitive to the transverse polarization of the struck quark. The fragmentation function H_1^\perp describing this dependence is indeed chiral-odd, and also odd under naive time reversal (T-odd). Known as the Collins

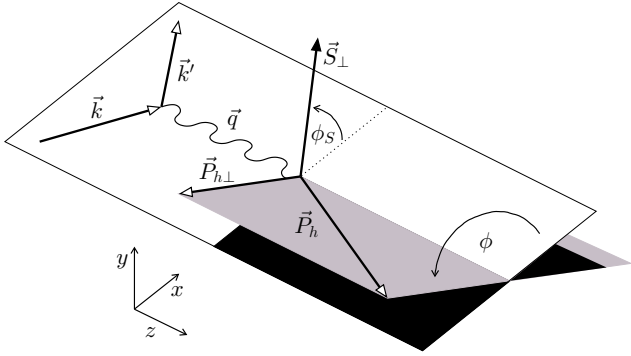


Fig. 15. The definitions of the azimuthal angles of the hadron production plane and the target spin axis.

function, it represents the interference of two amplitudes with different imaginary parts that can account for single-spin asymmetries in the ϕ distribution. Such asymmetries involving longitudinal target polarization have already been observed in pion electroproduction by HERMES. Theoretical interpretation of those data in terms of transversity-related distributions, as well as recent theoretical calculations, suggests that the Collins function has a substantial magnitude, thereby implying that measurements employing transverse target polarization can constrain transversity itself. HERMES has now released preliminary results for the first such measurements.

Azimuthal asymmetries measured with transverse target polarization can also provide another completely different window on non-perturbative QCD. It was realized over a decade ago that such asymmetries might arise from correlations between the transverse polarization of the target nucleon and the intrinsic transverse momentum of quarks. A vestige of that quark transverse momentum can survive both the photo-absorption and the ordinary fragmentation process and influence the transverse momenta of the produced hadrons, and hence their azimuthal distributions. Recently this idea has found a new reformulation “near to the heart” of non-perturbative QCD. It was realized that single-spin asymmetries that can be attributed to p_T -dependent parton distributions, such as the “Sivers function” f_{1T}^\perp describing the correlation of p_T with target polarization, can also be understood in terms of a final-state interaction (FSI) via a soft gluon. This FSI is a model for a gauge link that is necessary to restore colour gauge invariance. A key point is that the FSI offers a mechanism to create the interference of amplitudes that is associated with the T-odd nature of the Sivers function, which was once believed to forbid its existence. A closely-related chiral-odd partner h_1^\perp of the chiral-even Sivers function was found to provide an explanation for the substantial observed $\cos 2\phi$ dependence of unpolarized Drell-Yan cross sections. The

Sivers function itself is predicted to create Drell-Yan single-spin asymmetries, but there it is predicted to have the opposite sign to its appearance in DIS, due to the fundamental time reversal symmetry of QCD. This prediction of perturbative QCD needs to be tested experimentally.

Single-spin azimuthal asymmetries arising from the Collins and Sivers mechanisms both have a $\sin \phi$ behaviour when the target is polarized along the lepton beam axis, as was the case for all previously published DIS data. However, the additional degree of freedom representing the azimuthal angle ϕ_S of the axis of transverse target polarization results in distinctive signatures $-\sin(\phi - \phi_S)$ for the Sivers mechanism, and $\sin(\phi + \phi_S)$ for the Collins mechanism. Only the Collins mechanism is sensitive to the orientation of the lepton scattering plane because it depends on the acquisition in the fragmentation process of transverse momentum k_T by the struck quark orthogonal to its transverse polarization, *after* its spin component in the lepton scattering plane has been flipped by the photo-absorption. On the other hand, the Sivers effect arises through the struck quark “remembering” the p_T that it had in the target. In either case, the struck quark transverse momentum tends to be inherited by a leading hadron that may “contain” this quark. Hence the hadron transverse momentum component $p_{h\perp}$ orthogonal to the virtual photon direction is correlated with k_T (p_T) in the case of the Collins (Sivers) effect.

In the analysis reported here, the cross section asymmetry in the target polarization is extracted as a two-dimensional distribution in ϕ versus ϕ_S , which is then fitted with a sum of contributions from the above two sinusoidal dependences. This simultaneous extraction of both the Collins and Sivers Fourier components was shown by detailed Monte Carlo simulations to avoid cross-contamination, even when they have very different magnitudes in the context of a limited detector acceptance.

The extracted Collins and Sivers asymmetries averaged over the experimental acceptance are shown in Table IV for production of π^+ and π^- mesons. The statistical precision is limited because these data were recorded in the fall of 2002 and the first two months of 2003, when the HERA beam delivery was

Table IV. Collins and Sivers virtual-photon asymmetries averaged over the experimental acceptance, which is defined in part by the ranges $0.023 < x < 0.4$ and $0.2 < z < 0.7$. The uncertainties given for each value are statistical and systematic.

	A_C^h (Collins)	A_S^h (Sivers)
π^+	$0.021 \pm 0.007 \pm 0.018$	$0.017 \pm 0.004 \pm 0.012$
π^-	$-0.038 \pm 0.008 \pm 0.022$	$0.002 \pm 0.005 \pm 0.014$

seriously hampered by backgrounds in the two collider detectors (which have since been cured). Many more data have since been recorded, and this will continue until mid-2005. The selected ranges in x and z are $0.023 < x < 0.4$ and $0.2 < z < 0.7$, and the corresponding mean values of kinematic parameters are $\langle x \rangle = 0.09$, $\langle y \rangle = 0.54$, $\langle Q^2 \rangle = 2.41 \text{ GeV}^2$, $\langle z \rangle = 0.36$ and $\langle P_{h\perp} \rangle = 0.41 \text{ GeV}$. Here z is the fraction of the virtual photon energy carried by the detected hadron. The dependences of the asymmetries on x and z are shown in Figs. 16 and 17. No corrections were applied for the effects of instrumental smearing or acceptance, the latter of which was found to be negligible in Monte Carlo simulations.

The averaged Collins asymmetry is positive for π^+ and negative for π^- , by about three standard deviations. This can be expected if the transversity densities resemble the helicity densities to the extent that δu is positive and δd is negative and smaller in magnitude, as models predict. However, the magnitude of the π^- asymmetry appears to be at least as large as that for π^+ . The left part of Fig. 16 shows that this trend becomes more apparent as the magnitudes of these transverse asymmetries increase at larger x where valence quarks tend to dominate, as did the longitudinal asymmetries previously measured by HERMES. However, the large negative π^- asymmetries might be considered unexpected as neither quark flavour dominates π^- production like the u quark dominates π^+ , and one expects $|\delta d| < |\delta u|$ in analogy with $|\Delta d| < |\Delta u|$. This expectation is reflected in model predictions based on the interpretation of those longitudinal

asymmetries. This failure of those predictions could be due to the neglect of the Sivers mechanism, the contribution of sea quarks or disfavoured Collins fragmentation. On the other hand, the dependence of the Collins asymmetries on z shown in the right part of Fig. 16 are not so inconsistent with theoretical predictions that they should increase with increasing z .

An interpretation of the acceptance-averaged asymmetries in the quark-parton model indicates that the disfavoured (e.g. up quark to π^-) Collins fragmentation function has the opposite sign to the favoured one (e.g. up quark to π^+), and probably has a substantial magnitude. This represents the first information about the flavour dependence of the Collins function. Work by others is now under way to extract the Collins functions from Belle e^+e^- data. This information will help to extract information about transversity from the HERMES data now being recorded.

The averaged Sivers asymmetries are significantly positive for π^+ (by four standard deviations for π^+), which constitutes the first evidence for a T-odd parton distribution function appearing in leptonproduction. The π^- Sivers asymmetries are consistent with zero. Some theoretical predictions for the Sivers function f_{1T}^\perp have recently emerged. Since the π^+ asymmetries should be dominated by up quarks, the positive tendency implies a positive value for the Sivers function of this flavour, which already disfavours some theoretical models. The fragmentation function believed to combine with this quark distribution is the familiar spin-independent $D_1(z)$, which also appears in the unpolarized cross section constituting the denominator

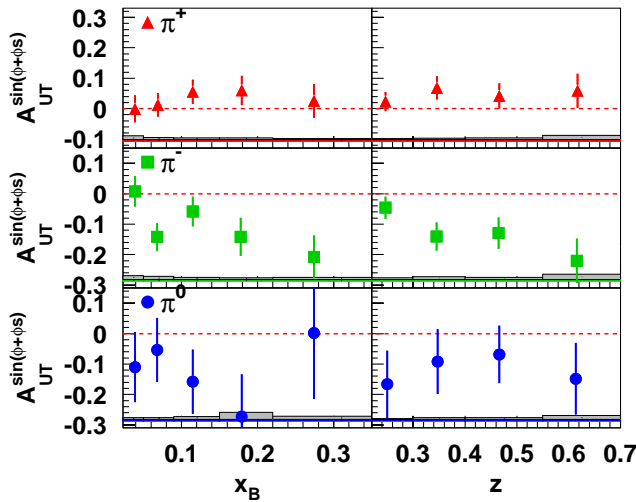


Fig. 16. Collins asymmetries for electroproduction of pions as labelled, as a function of x and z . The error bars represent the statistical uncertainties, while the lower band represents a possible interpretive uncertainty from diffractive vector meson production. In addition, there is a common overall scale uncertainty in the asymmetries that is 8% of the central value in each bin.

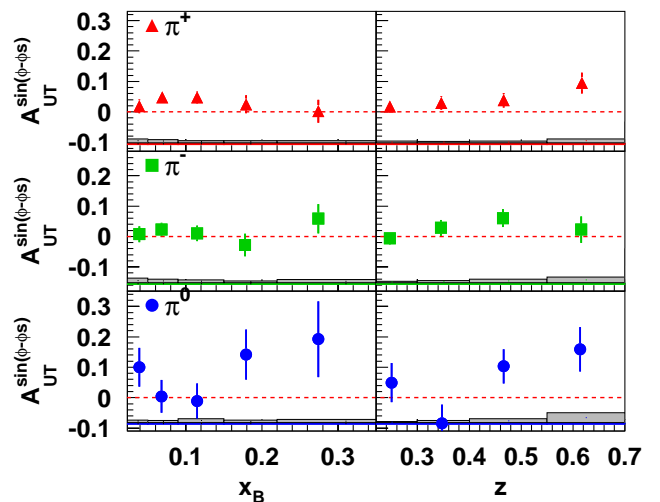


Fig. 17. Sivers asymmetries for electroproduction of pions as labelled, as a function of x and z . The uncertainties are shown as in Fig. 16.

of the asymmetry. Hence the Sivers asymmetries should depend only weakly on z , whereas the π^+ and π^0 data shown in Fig. 17 may have a surprising tendency to be more prominent at large z . The fact that the relevant fragmentation functions are known in this case implies that it will be possible to extract the Sivers distribution functions from the data now being recorded. Future Drell-Yan measurements in a polarized proton collider will be able to determine if the Sivers functions have the expected opposite sign in that process.

The pentaquark

For several years prior to 2003, the field of baryon spectroscopy had been relatively inactive. The Particle Data Group dropped their discussion on exotic baryon searches after 1988. However, starting even in the early days of QCD in the 1970's, there had been various theoretical predictions that resonances based on five-quark configurations could be narrow enough to be detectable. In 1997, calculations in the chiral quark soliton model predicted a narrow $uudd\bar{s}$ state at 1540 MeV, unbound by only 100 MeV with respect to its only strong decay channel to NK . Such a state would have “manifestly exotic” quantum numbers in the sense that its value of $+1$ for strangeness rules out a three-quark configuration. The first evidence for such a state appeared in 2003 as a narrow peak at $1540 \pm 10(\text{syst})$ MeV in the K^- missing mass spectrum for the $\gamma n \rightarrow K^+ K^- n$ exclusive reaction on ^{12}C [Nakano *et al.*, Phys. Rev. Lett. **91**, 012002 (2003)]. This decay mode uniquely identifies a $S=+1$ resonance, now known as the Θ^+ . Confirmation came quickly from a series of experiments, with the observation of sharp peaks in nK^+ and pK_s^0 invariant mass spectra near 1540 MeV, in each case with a width limited by the experimental resolution. Taken together, these results, all based on data previously recorded for other purposes, were heralded as the discovery of the first manifestly exotic hadron in the 40 years since the Ω^- .

HERMES made significant contributions to this set of data. Further evidence for the pentaquark resonance was detected as a peak in the proton- K_s^0 invariant mass spectrum in quasi-real photoproduction on deuterium. The good mass resolution of the HERMES spectrometer with well-understood systematics provided more restrictive information related to the mass and isospin of the resonance than did previous publications. Figure 18 shows the pK_s^0 mass spectrum, compared with a fit based on a model for the background that incorporates a simulation of the non-resonant background together with fitted peaks for known Σ^{*+} resonances. The mass of $1528 \pm 2.6(\text{stat}) \pm 2.1(\text{syst})$ MeV resulting

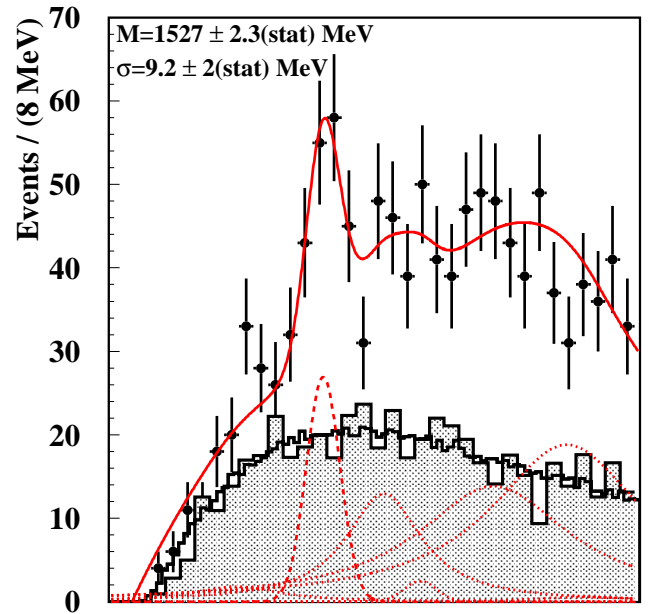


Fig. 18. Distribution in invariant mass of the $p\pi^+\pi^-$ system. The experimental data are represented by the filled circles with statistical error bars, while the fitted smooth curves result in the indicated position and σ width of the peak of interest. A PYTHIA6 Monte Carlo simulation is represented by the gray shaded histogram, a mixed-event background model normalized to the PYTHIA6 simulation is represented by the fine-binned histogram, and the fitted curve includes in addition a Gaussian fitted to the peak of interest and Breit-Wigner peaks with the positions and widths of various known Σ^{*+} resonances but with free amplitudes.

from the fit was the most precise value at the time, and constituted a departure from the earlier reports, which had clustered around 1540 MeV. However, mass values subsequently reported by other experiments have also tended to fall below 1530 MeV. Another contribution was the first indication of a finite width of the resonance after accounting for instrumental resolution. The ZEUS Collaboration has since also reported such an indication.

There has been theoretical speculation that the small width of the Θ could be understood if it were a member of an isospin multiplet, whose decay violated isospin conservation. HERMES contributed strong evidence that the Θ^+ is an isosinglet. Figure 19 shows distributions in pK^\pm invariant mass. While the $\Lambda(1520)$ appears where expected in the pK^- spectrum, the pK^+ spectrum shows no sign of a Θ^{++} , in spite of the acceptance being about 30 times larger for this decay than for pK_s^0 .

The ongoing HERMES program

DESY has promised beam for HERMES until at least the end of 2006, probably until mid-2007. The present HERMES running plan is to continue until mid-2005 on the transversely-polarized hydrogen

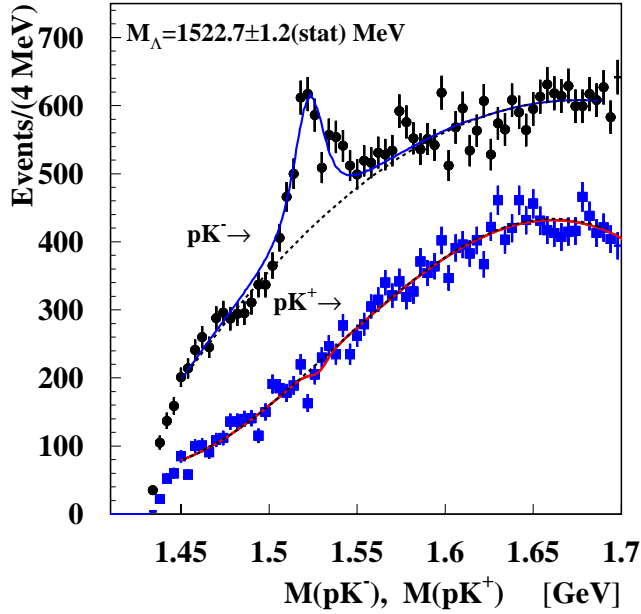


Fig. 19. Spectra of invariant mass M_{pK^-} (top) and M_{pK^+} (bottom). A clear peak is seen for the $\Lambda(1520)$ in the M_{pK^-} invariant mass distribution. However, no peak structure is seen for the hypothetical Θ^{++} in the M_{pK^+} invariant mass distribution near 1.53 GeV.

target to complete the first measurement of quark transversity in the proton. Meanwhile, HERMES is assembling a new recoil detector to surround the target cell and detect the recoiling intact target nucleon from hard exclusive processes, in order to guarantee their exclusivity. This fully funded €1.4 M project is scheduled to be ready for two years of running on high density unpolarized targets in 2005/7. This will yield the first really high quality data on asymmetries in both beam spin and charge for DVCS, the process that holds the most promise to shed light on the orbital angular momentum of partons.

HERMES collaborators in 2003: G. Gavrilov, J. Lu, C.A. Miller, S. Yen (TRIUMF); M.V. Vetterli (SFU/TRIUMF); M.G. Vincet (Alberta); K. Garrow (Alberta/SFU); J. Wendland (SFU).

J-PARC

T2K long baseline neutrino experiment

(A. Konaka, TRIUMF)

Introduction

Convincing evidence for neutrino oscillations has recently been obtained in measurements of both solar and atmospheric neutrino interactions by the Super-Kamiokande and SNO collaborations. The KamLAND experiment independently confirmed the solar neutrino oscillation effect using reactor neutrinos. It determined the mass difference Δm_{12}^2 and the mixing angle θ_{12} to be consistent with the large mixing angle (LMA) solution. The K2K experiment observed oscillations

of accelerator-produced muon neutrinos, in agreement with the observation of oscillation of atmospheric muon neutrinos at the 99% confidence level using neutrinos from an accelerator beam at KEK. K2K has started to see an indication of the energy dependence of the oscillations.

The next step is an accelerator-based long baseline experiment to determine the remaining parameters of the lepton mixing matrix: the first to third generation mixing angle θ_{13} and the CP -violating phase, δ_{CP} . The most promising avenue for measuring these parameters is to study $\nu_{\mu} \rightarrow \nu_e$ oscillations using so-called “superbeams” – high intensity neutrino beams derived from the decays of pions. The large statistics provided by a superbeam will also greatly improve the precision with which the mixing parameters Δm_{23}^2 and θ_{23} can be measured. A number of initiatives are being considered worldwide to address this physics. The most advanced program is the J-PARC (Japan Proton Accelerator Research Complex) to Super-Kamiokande (SK) experiment (see Fig. 20). This neutrino project, which is called T2K (Tokai to Kamioka), submitted a letter of intent (LOI) signed by 155 physicists from 12 countries to the J-PARC office in January, 2003. Twenty scientists from Canada signed this LOI. J-PARC has been under construction since April, 2001. Funding for the neutrino beam line was approved by the Japanese government in December, 2003, and the first T2K international collaboration meeting will be held in January, 2004. An NSERC grant for an R&D of T2K near detector has been awarded to the Canadian T2K collaboration (TRIUMF, UBC, UVic, Alberta, Toronto and York).

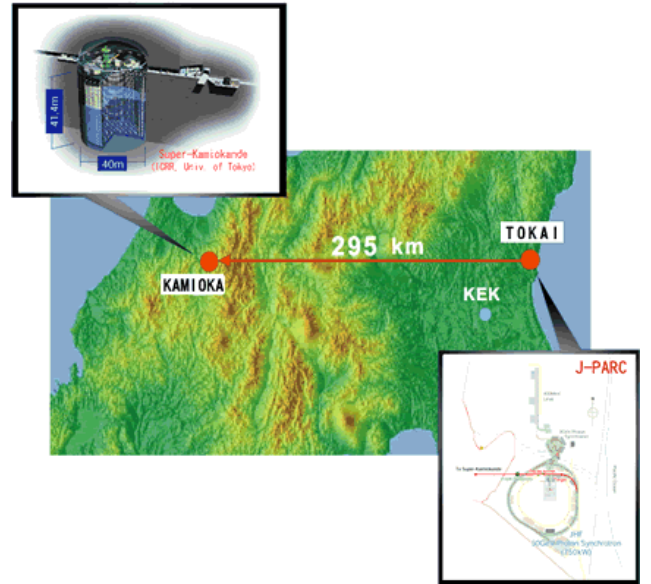


Fig. 20. A neutrino beam produced at J-PARC will be sent to the Super-Kamiokande detector located 295 km away.

Canadians have been involved from the beginning of the T2K project and have made a number of important contributions to the physics, including the off-axis concept, the ν_e appearance analysis, and a study of the prospects for measuring CP violation. Canadians have also made important contributions to the accelerator design, including studies of the beam transport using combined function superconducting magnets and a dual abort/extraction kicker concept. A JHF(J-PARC) neutrino workshop was held in February when eight J-PARC facility construction members visited TRIUMF. An R&D collaboration between TRIUMF and KEK on the J-PARC project was discussed. Contributions to J-PARC's accelerator and neutrino beam line components are proposed for the next TRIUMF 5 year plan. In June, some of the Canadian T2K members joined the K2K experiment, which is an ongoing long baseline neutrino experiment from KEK to Super-Kamiokande. K2K is an ideal prototype experiment for the T2K project, providing a test bed in which to develop equipment and methods that will later be adapted to T2K.

The T2K project

Overview The J-PARC accelerator is a 50 GeV proton synchrotron currently under construction, and will begin operation in 2008. It will be the first MW class machine (0.75 MW) in this energy range. The construction of the neutrino beam line was funded by the Japanese government in December, and the beam line commissioning is expected in January, 2009. The far detector already exists, namely the well-understood 50 kton water Čerenkov Super-Kamiokande (SK) detector. The experiment uses a narrow-band neutrino beam whose energy is tuned to the oscillation maximum (0.5–1.0 GeV) given the distance from J-PARC to SK (295 km). The technique which has been adopted is to aim the neutrino beam 2–3° away from the detector (off-axis beam). This idea was originated by a Canadian group in connection with BNL proposal E889. This method provides a larger ν_μ flux and a smaller ν_e contamination than other methods for producing narrow-band beams. The neutrino energy will be reconstructed through the two body quasi-elastic (QE) scattering reaction, $\nu n \rightarrow l^- p$. The T2K neutrino energy of 0.5–1.0 GeV is ideal, because the cross section is dominated by the QE scattering. A new fine-grained detector of several tonnes will be placed 280 m from the production target to provide measurements of the neutrino beam flux.

Precision measurement of the oscillation pattern

The oscillation pattern of the ν_μ disappearance is measured precisely as a function of the reconstructed neutrino energy.

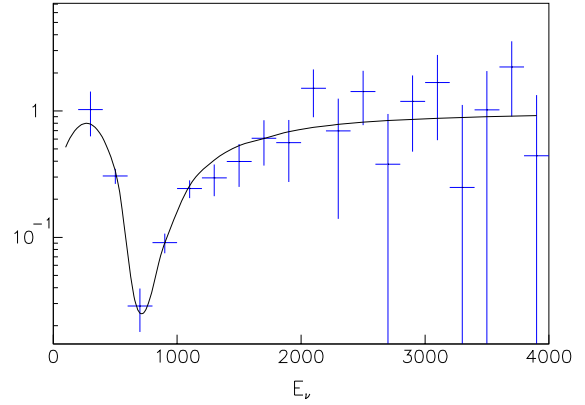


Fig. 21. The ratio of the measured neutrino energy spectrum to the expected one without neutrino oscillation, as a function of neutrino energy in MeV, after subtracting non-QE events.

Figure 21 shows the ratio of the measured neutrino energy spectrum to the expected one without neutrino oscillation. The position and the depth of the dip in this ratio provide Δm_{23}^2 and $\sin^2 2\theta_{23}$, respectively. The goal of the experiment is to achieve an order of magnitude improvement in precision of the ν_μ disappearance parameters: $\delta(\Delta m_{23}^2) \sim 0.01$ and $\delta(\sin^2 2\theta_{23}) \sim 1 \times 10^{-4}$ eV². Deviation of the pattern from the neutrino oscillation prediction would indicate new physics beyond the MNS matrix, such as sterile neutrinos, extra dimensions, or new leptonic flavour changing neutral current interactions. Comparison of Δm_{23}^2 and $\sin^2 2\theta_{23}$ between ν_μ and $\bar{\nu}_\mu$ provides a precise test of CPT conservation in neutrino oscillation. The neutral current to charged current ratio (NC/CC), similar to what is studied by SNO for the solar ν_e disappearance, provides a sensitive test of the sterile neutrinos hypothesis.

$\nu_\mu \rightarrow \nu_e$ appearance: θ_{13} The $\nu_\mu \rightarrow \nu_e$ appearance channel is sensitive to the first to third generation lepton mixing angle θ_{13} . Figure 22 shows the

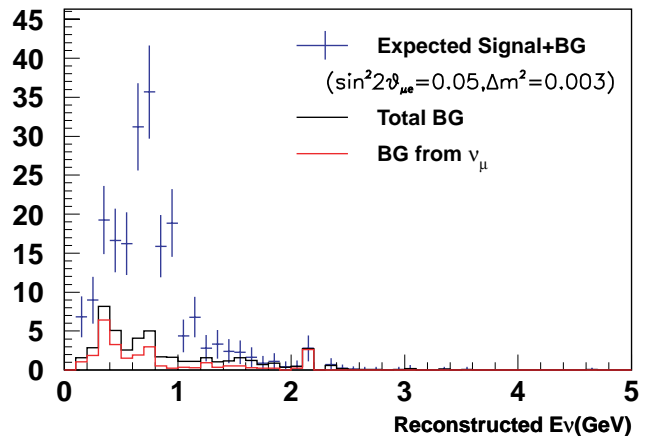


Fig. 22. Reconstructed electron neutrino energy distributions for 5 years' exposure assuming θ_{13} is at the current reactor (CHOOZ) limit.

reconstructed electron neutrino energy spectrum assuming θ_{13} is at the current reactor (CHOOZ) limit. A clean reconstructed ν_e energy peak is expected at the oscillation maximum. If θ_{13} is small, a 90% C.L. upper limit of $\sin^2 2\theta_{13} = 0.006$ ($\sin^2 2\theta_{\mu e} = 0.003$) can be achieved, which is a factor of 20 improvement over the reactor limit.

Accelerator and beam line contributions to J-PARC

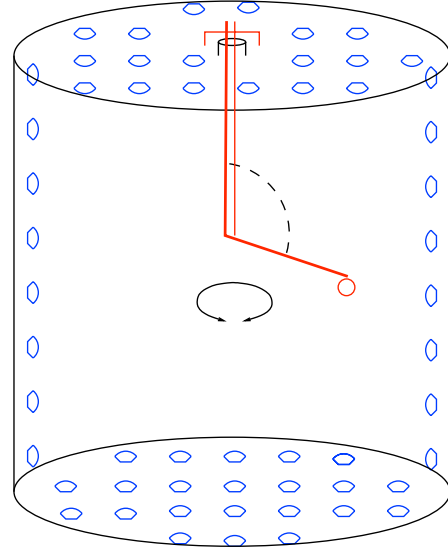
High-intensity proton accelerators have long been the dream of many accelerator and particle physicists and are attracting renewed interest as sources of neutrino super-beams. A megawatt class accelerator like J-PARC will have to overcome new problems in handling unprecedented beam power. Expected Canadian contributions target the elements that are the most critical in controlling beam losses, namely the beam dynamics and damper system in the main ring, the extraction kicker magnet, beam diagnostic systems in the proton transport line, and the shielding and remote handling of the target station. All of these are areas where TRIUMF has world-leading expertise.

Detector R&D for the T2K project

There are three sets of detectors in T2K: the muon monitor in the beam dump, the fine-grained calorimeter at the 280 m near site, and the Super-Kamiokande water Čerenkov detector at the 295 km far site. The Canadian group is interested in the 280 m fine-grained calorimeter, optical calibration for the water Čerenkov detectors, and diamond sensors for the muon monitor.

Fine-grained calorimeter A fine-grained calorimeter is the optimum near (280 m) detector for T2K because the ability to measure the energies and directions of both the outgoing muon and the recoil proton will give a strong kinematic selection on the quasi-free scattering process that will dominate the cross section at the ~ 700 MeV neutrino energy of this experiment, and allow the reconstruction of the incident neutrino energy and direction. This near detector is key to understanding the systematic uncertainty in the θ_{13} and θ_{23} measurements through detailed understanding of the neutrino flux and interactions at intermediate energies. Since there is a lack of data about neutrino interactions in the 1 GeV region, it provides interesting physics by itself. It also provides important information about backgrounds to the proton decay search, which will be performed concurrently by the far detector. The technology we have been studying is based on a water-soluble scintillator which is read out by wavelength-shifting fibres and photosensors. Photomultipliers, avalanche photodiodes, and silicon photomultipliers are being examined as photosensor candidates.

Strawman Manipulator Design



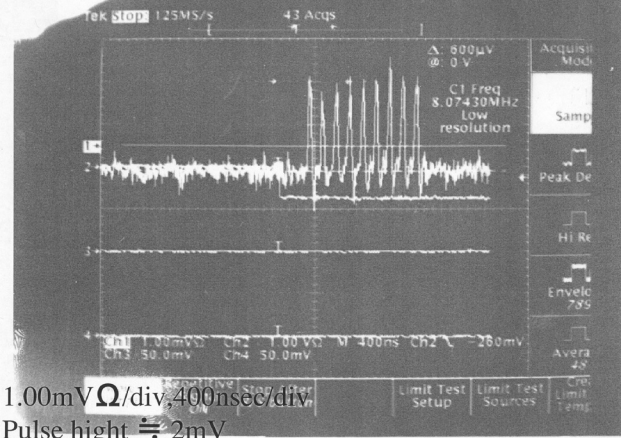
Name “Canadarm” already taken ... Calibarm???

Fig. 23. A schematic view of a deployable manipulator arm for optical calibration of the K2K near water Čerenkov detector.

Optical calibration of the water Čerenkov detectors Optical calibrations play a critical role in the T2K experiment. The systematic uncertainty on the rejection of the main π^0 background in the $\nu_\mu \rightarrow \nu_e$ appearance is determined by the knowledge of the optical properties of the water Čerenkov detector. The main systematic uncertainty in the ν_μ disappearance mode comes from the fiducial volume and the energy scale, in which optical calibrations again play the main role. Sophisticated optical calibration tools, namely an isotropic laser ball, manipulator system, and analysis procedure, have been developed by the SNO collaboration. The Canadian group participates in the K2K 1 kton water Čerenkov group and is designing a manipulator system for its optical calibration (Fig. 23).

Diamond sensors for the muon monitor Muons in the beam dump provide spill-by-spill information about the hadronic beam. In order to separate muons from hadronic showers in the beam dump, it is proposed to detect delayed Michel electrons from stopped muons decaying in the beam dump. Diamond sensors are of particular interest because of their radiation hardness and fast response, enabling the detection of Michel electrons. They may also be useful for monitoring the beam halo in the primary beam line. A diamond sensor has been installed behind the K2K beam dump in the fall, and a clear muon signal has been observed (Fig. 24).

With HV 300V



There are 9 bunches

Fig. 24. Diamond signal observed behind the K2K beam dump. The 9 micro-bunch structure of the beam spill is clearly observed.

Sudbury Neutrino Observatory

(R. Helmer, TRIUMF)

Data-taking in the salt phase of SNO was completed in the past year. During this phase, detection of neutral current (NC) interactions was enhanced by the addition of 2 tons of salt (sodium chloride) to the heavy water. Neutrons from the break-up of the deuterons were detected by observing the gamma cascade following neutron capture on chlorine. The Q-value for capture on chlorine is higher than for capture on deuterium; hence there is better energy separation between these signals and those from the competing charged current (CC) reaction. The gamma cascade also implies that signals from capture on chlorine will be more isotropic than for either capture on deuterium or charged current interactions; the latter two both have only a single associated gamma. It was possible to take advantage of the isotropy to extract the neutral current interaction rate independently of assumptions about the shape of the energy spectrum.

Results based on the first 254.2 live days of data have been submitted for publication [Ahmed *et al.* (SNO collaboration), submitted to Phys. Rev. Lett., nucl-ex/0309004]. Only the distributions of isotropy, cosine of the event direction relative to the vector from the sun, and radius within the detector (to limit backgrounds) were used to extract the total numbers of CC, elastic scattering (ES), NC, and external-source neutron events. The equivalent ^8B fluxes for the CC, ES and NC reactions were found to be (in units of $10^6\text{cm}^{-2}\text{s}^{-1}$):

$$\phi_{\text{CC}}^{\text{SNO}} = 1.59_{-0.07}^{+0.08}(\text{stat})_{-0.08}^{+0.06}(\text{syst})$$

$$\phi_{\text{ES}}^{\text{SNO}} = 2.21_{-0.26}^{+0.31}(\text{stat}) \pm 0.10(\text{syst})$$

$$\phi_{\text{NC}}^{\text{SNO}} = 5.21 \pm 0.27(\text{stat}) \pm 0.38(\text{syst}).$$

$\phi_{\text{NC}}^{\text{SNO}}$ gives the total flux of active neutrinos and is consistent with solar model calculations.

These results were combined with day and night energy spectra obtained during the pure heavy water phase of the experiment, and results from other solar neutrino experiments and KamLAND, to place constraints on allowed neutrino mixing parameters. The best fit point occurs for $\delta m^2 = 7.1_{-0.3}^{+1.0} \times 10^{-5}\text{eV}^2$ and $\theta = 32.5_{-1.6}^{+1.7}$ degrees. The new SNO result has further restricted the allowed LMA region and disfavors maximal mixing by 5.4σ .

With the completion of the salt phase, SNO has entered the third, and final, phase of the experiment. Discrete ^3He proportional counters have been placed in the heavy water volume to provide a third, independent measurement of the neutral current interaction. Insertion of these detectors required removal of the glove box originally supplied by TRIUMF (see TRIUMF Annual Report, 1996) to aid in the deployment of calibration sources. To increase the utility of the box, one new side with extra access ports was designed and fabricated at TRIUMF. The original side was removed and the new side welded on using local shops in Kingston.

TJNAF Experiment 00-006

Measurement of the flavour singlet form factors of the proton (G_0)

(W.T.H. van Oers, Manitoba)

The detailed structure of the nucleon at low energies is not well understood within the framework of quark and gluon degrees of freedom. For example, relatively little is known about the importance of the sea quarks at these energies. The G_0 experiment will measure two proton ground state matrix elements which are sensitive to point-like strange quarks and hence to the quark-antiquark sea in the proton. The matrix elements of interest are the elastic scattering vector weak neutral current charge and magnetic form factors, G_E^Z and G_M^Z , respectively. These can be extracted from a set of parity-violating electron-proton scattering measurements. If one assumes a relationship between the proton and neutron structure in that the proton and neutron differ only by the interchange of up and down quarks, i.e. isospin symmetry, the strange quark (as well as the up and down quark) contribution to the charge and magnetic form factors of the nucleon can be determined. This would result from taking appropriate linear combinations of the weak neutral form factors and their electromagnetic counterparts.

Determinations of both the charge and magnetic strange quark form factors are of fundamental interest, as these would constitute the first direct evidence

of the quark sea in low energy observables. It is the objective of the $G0$ experiment to determine these contributions to the proton form factors at the few per cent level. Observations at high energy suggest that the strange quarks carry about half as much momentum as the up and down quarks in the sea. It is important to determine both the role of the quark sea and the relevance of strange quarks at low energy where there are voids in understanding the theory of the strong interaction (quantum chromodynamics, QCD). Even if the strange quark contributions do not amount to the level of sensitivity of the experiment, upper limit determinations at this level are as valuable as non-zero results. The matrix elements, G_E^Z and G_M^Z , are also relevant to discussions of the Ellis-Jaffe sum rule and the pion-nucleon sigma term; there is uncertainty in both of these about the strange quark contributions. The $G0$ experiment will allow the determination of the strange contributions to the proton charge and magnetic form factors in a much more straightforward manner than is possible with regard to the corresponding observables in the above two deduced relations.

In the $G0$ experiment, which is being carried out in Hall C at the Thomas Jefferson National Accelerator Facility (TJNAF), parity-violating longitudinal analyzing powers will be measured in electron-proton scattering in the range $0.1 \leq Q^2 \leq 1.0 \text{ GeV}^2$ at both forward and backward angles. The longitudinal analyzing power is defined as

$$A_z = (1/P) \frac{[\sigma^+(\theta) - \sigma^-(\theta)]}{[\sigma^+(\theta) + \sigma^-(\theta)]}$$

where P is the polarization of the incident electron beam and the $+$ and $-$ signs indicate the helicity state. Making pairs of measurements at forward and backward angles will allow the separation of G_E^Z and G_M^Z . Predicted longitudinal analyzing powers range from about $(-3 \text{ to } 35) \times 10^{-6}$; the goal is to measure the longitudinal analyzing powers with statistical uncertainties of $\Delta A/A = 5\%$ and systematic uncertainties related to helicity correlated effects of $\Delta A/A \leq 2.5 \times 10^{-7}$.

The heart of the $G0$ detection system is a spectrometer which consists of an eight-sector toroidal magnet, with an array of scintillation detectors located at the focal surface of each octant and, for the backward angle mode, arrays of scintillation and Čerenkov detectors located near the magnet cryostat-exit window of each octant. In the first phase of the experiment, longitudinal analyzing powers will be measured concurrently at several values of the momentum transfer in the range $0.1 \leq Q^2 \leq 1.0 \text{ GeV}^2$. It must be realized that the length of the experiment is in part governed by making rather elaborate control measurements to determine

the corrections that have to be made to the measured asymmetries and to assess systematic errors. In the second phase of the experiment each subsequent backward angle analyzing power measurement would require from one half to one month of running time. The results of the SAMPLE experiment at the MIT-Bates Laboratory have shown the importance of measuring the axial form factor corrections, since these may be quite different from the theoretical predictions. Therefore, companion measurements of quasi-elastic scattering from deuterium will also be made at the backward angles. With these measurements, the effective axial current of the nucleon will also be determined. This current includes effects from the effective axial coupling of the photon to the nucleon or anapole moment, which are relevant also in other processes, e.g. parity violating Moller scattering and atomic parity violation.

The $G0$ collaboration

The $G0$ experiment is being carried out in Hall C at TJNAF by a collaboration of scientists from Canada, France, Georgia, and the United States, with funding provided through NSERC (Canada), IN2P3 (France), and DOE/NSF (US).

Following the completion of many critical milestones, this past year also saw the completion of a very successful commissioning run for the first phase forward angle mode of the $G0$ experiment. Preliminary analysis of the data taken under much less than ideal conditions for the experiment exhibits great promise. Considerable progress has also been made in the design, prototyping, and fabrication of critical components for the second phase backward angle mode of the experiment, in particular with the cryostat exit detectors, the aerogel Čerenkov detectors, and the support structure for these. The Canadian contributions to these efforts have been significant. Below follows an enumeration of the various Canadian contributions to the $G0$ experiment. The three components mentioned above as well as other aspects of the $G0$ experiment are described in some detail below.

Canadian contributions

The Canadian members of the $G0$ collaboration, based at the Universities of Manitoba, Northern British Columbia, and TRIUMF, have been asked to:

- (1) Develop and produce specialized photomultiplier tube bases for the focal plane detector arrays;
- (2) Design, build, and commission an automated magnetic field measuring (magnetic verification) apparatus complete with its own data acquisition system;
- (3) Prototype and fabricate the cryostat exit detector arrays for the backward angle measurements;

- (4) Prototype and fabricate (together with the Grenoble group) the aerogel Čerenkov arrays for background rejection in the backward angle measurements;
- (5) Design the support structure for the aerogel Čerenkov and cryostat exit detector arrays;
- (6) Coordinate the implementation of TJNAF built beam monitors and control apparatus with TRIUMF built parity electronics.

Much progress has been made in the design and construction of the various subsystems listed above, many of which are now already in operation.

Photomultiplier tube bases and magnetic verification system

The photomultiplier tube bases and magnetic verification system have been described in some detail in last year's Annual Report. Both of these construction projects have been successfully completed and the hardware is currently in operation or has already been successfully operated.

Cryostat exit detectors

For the backward angle second phase of the $G\theta$ experiment, the addition of a second array of scintillation detectors, located near the spectrometer cryostat exit windows, will be required in order to separate the elastic and inelastically scattered electrons. The geometry of these cryostat exit detector (CED) arrays (see Fig. 25) has been studied in detail and a reference design was completed. With the resident expertise at TRIUMF in producing high quality scintillation detectors and lightguides, the Canadian subgroup was asked to play the lead role in the prototyping and production of the CEDs. A set of prototype CEDs

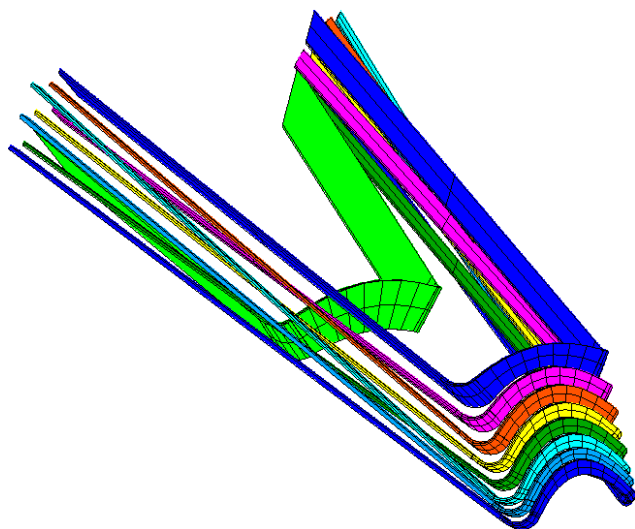


Fig. 25. Layout of a cryostat exit detector (CED) array for a single octant.

was built at TRIUMF and delivered to the $G\theta$ collaboration for studies with cosmic rays. Results from these studies showed that the reference design and the prototype detectors met the specification requirements for these arrays. Production of a full set of dummy CED prototypes was then completed at TRIUMF, to aid in the design of the CED support structure. After finalizing the CED design, construction of the production versions of the CED arrays took place in 2001. Fabrication of the CED scintillators for all 8 octants was completed and delivery made to TJNAF, and fabrication of the special helical-bent lightguides began in 2002. In order to achieve the unique helical bend required in the $G\theta$ back angle geometry, customized bending jigs were designed and constructed at TRIUMF and tested on a first set of prototype CED lightguides. Production of a full set of lightguides for the first CED octant was completed and delivery made to TJNAF in 2003, where they are undergoing further tests. Production of the remaining lightguides is nearing completion and they will be delivered to TJNAF in early 2004. The CEDs will also make use of the same types of photomultiplier tubes and specialized TRIUMF/ $G\theta$ bases as the focal plane detectors.

Aerogel Čerenkov detectors

Monte Carlo simulation results have shown that backgrounds from negative pions will be problematic for the second phase backward angle measurements involving the deuterium target. The $G\theta$ simulation subgroup has focused on characterizing this π^- background and providing options regarding the design of an additional set of detectors to reject the background pions. The $G\theta$ Canadian and French (Grenoble) subgroups have been asked to jointly undertake the prototyping and construction of this crucial set of detectors, which will be made up of an array of aerogel Čerenkov counters. Much effort has gone into the design of this detector array and a conceptual design (see Fig. 26) was evolved into a first prototype at TRIUMF.

Prototype tests using the TRIUMF pion beam (M11) were carried out in December, 2001, but were hampered by the fact that there was insufficient aerogel to fully load the detector, which led to inconclusive results. This situation was rectified in early 2002 (with the loan of some sample aerogel from Caltech), and further tests using cosmic rays were carried out at TRIUMF over the spring and summer of 2002. Issues that have been studied include: the optimal choice and configuration of reflective material within the light diffusion box; the choice of photomultiplier tube (PMT) and base; the best procedure to establish a hit (summed signal vs. multiplicity); characterization

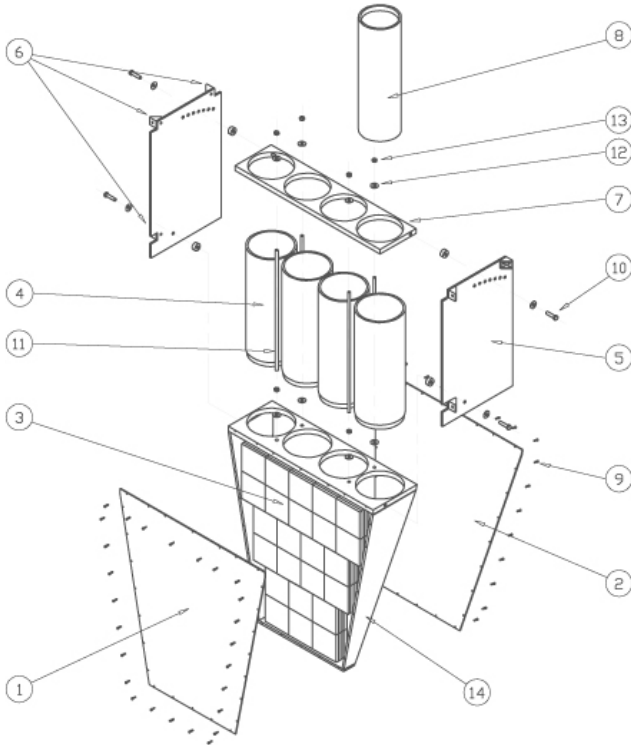


Fig. 26. Conceptual layout of the aerogel Čerenkov detector.

of the diffusion box response by Monte Carlo simulations; magnetic shield requirements; radiation shielding requirements; and optimization of the solid angle of the detector.

In the tests with cosmic rays, different PMTs were examined in the detector box and the Photonis XP4572B was chosen. Millipore paper was chosen as the diffuse reflector in the box. Most of the inner surfaces of the box were lined initially with an underlayer of Tyvek and one layer of millipore. Later, a second layer of millipore was added. The collars around the PMTs were also lined with millipore. Another issue, related to the inactive region of the photocathode around the PMT front face, was studied in detail. A reflective cone was designed to cover this region and to redirect the light toward the active portion of the PMT photocathode. Different reflective materials on this cone were tested, including an experimental reflective (dichroic) film from 3M. Although results with the dichroic reflector were initially encouraging, it was later demonstrated that good quality (thicker) aluminized mylar resulted in comparable or even slightly better detector efficiencies. Measurements were made at different positions: (i) near the PMTs, (ii) at the centre of the box, and (iii) far from the PMTs. Studies of light propagation in the diffusion box were also carried out using the programs LITRANI, GEANT4, and a simple Monte Carlo.

During this past year, tests with the prototype Čerenkov detector were carried out using both cosmic rays and the M9 and M11 beam lines at TRIUMF. With our last funding increment, we were finally able to purchase the full amount of aerogel needed to fully implement the four Canadian octants of the Čerenkov counter array. Most of this aerogel is now at Jefferson Lab, but a sufficient amount was received at TRIUMF to allow us to extend our tests. Over the summer, the sample aerogel in our prototype detector was replaced with the production aerogel, and the photon yield (and, thus, the detector efficiencies) immediately improved. Average yields of approximately 6.5 photoelectrons were observed for measurements made at the centre of the diffusion box. (With the earlier sample aerogel, which had many cracks, the average yield was closer to 5 photoelectrons, at the centre of the box.) Further tests using the TRIUMF secondary beams in M11 were carried out in late summer. After some initial problems related to magnetic shielding were resolved, very encouraging results were obtained using the electron and muon beams. Average yields of approximately 12, 8, and 6 photoelectrons were observed for measurements made at the near, centre, and far ends of the diffusion box (see Fig. 27). Furthermore, the position-dependent efficiencies were relatively flat, even at higher thresholds. At a threshold cut of 2.5 photoelectrons, the electron efficiency remained above 90% at all 3 measurement positions (see Fig. 28).

Based on the results with the first prototype, a second iteration design has been completed and will be used for the production version of the Čerenkov detector. Construction is scheduled to begin in early 2004 and further in-beam tests will be performed using the muon/pion beam lines at TRIUMF.

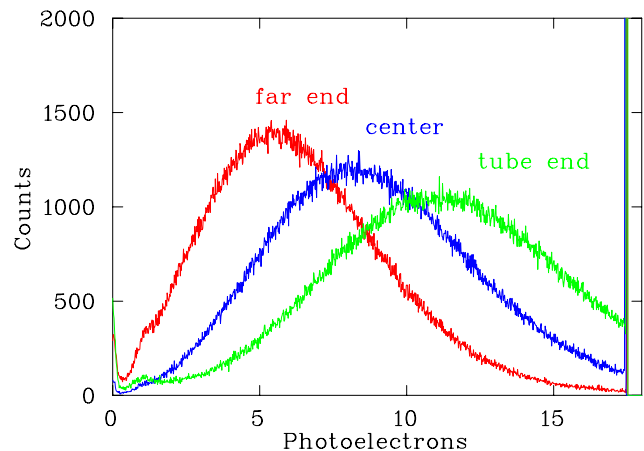


Fig. 27. Photoelectron yields for the prototype Čerenkov detector as a function of beam position.

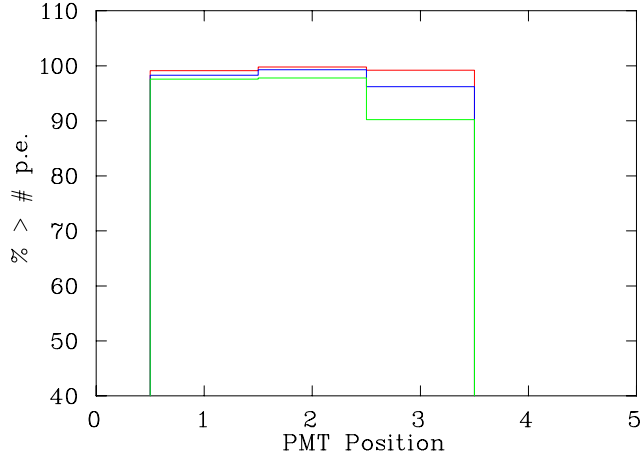


Fig. 28. Measured electron efficiencies for the prototype Čerenkov detector as a function of beam position.

Back angle support structure

Considerable effort has gone into the engineering design of a support structure for the $G\emptyset$ Čerenkov and CED arrays. Although the Canadian subgroup was initially responsible only for the design of the Čerenkov support structure, it was soon realized that the CED support structure would be closely coupled to the former due to the physical proximity of the two detector subsystems. As such, an integrated design for the two detector subsystems was pursued. The support structure centres around the use of prefabricated aluminum extrusions from Bosch because of their strength, versatility, and relatively low costs. A series of detailed finite-element analysis studies was carried out at TRIUMF, using the program ANSYS, to identify potential problems and to optimize the strength and cost of the support structure. The design consists of a second Ferris wheel type support structure, which will couple to the existing FPD support structure (also a Ferris wheel type design) and to the linear rails on the existing $G\emptyset$ detector platform. A conceptual illustration of the $G\emptyset$ backward angle configuration is shown in Fig. 29, with the superconducting magnet, the 3 detector arrays (FPD, CED, Čerenkov) in each of the 8 sectors, and their respective support structures.

Over the spring, the parts for a single octant of the support structure were procured and this subsystem was successfully assembled at TJNAF (see Fig. 30). As various components of the backward angle detectors arrived at TJNAF over the summer, work began on a test assembly of one octant of the backward angle system. Both the Canadian and French groups have supplied a mock-up Čerenkov detector for test mounting in the support structure frame. Both Čerenkov mock-ups have been test fitted and will mount as required to meet nominal design specifications. Concurrent with this work, test-fitting of the CED scintillators, lightguides, and PMTs also began. An assembly

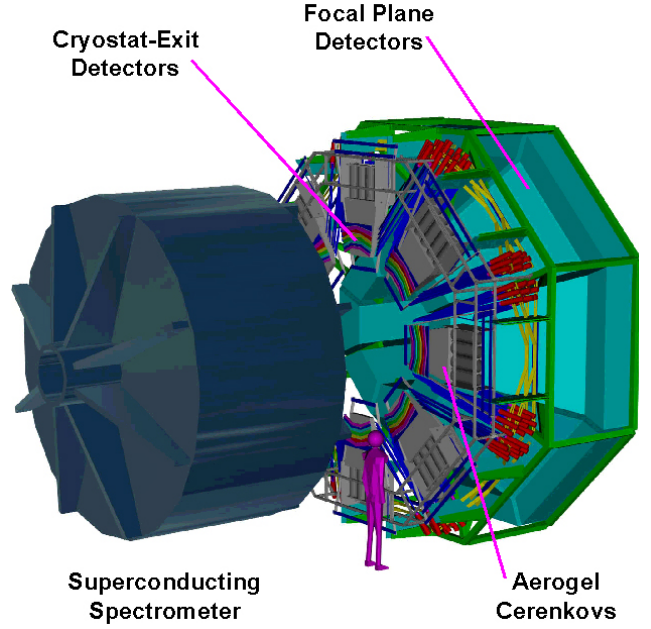


Fig. 29. Conceptual layout of the $G\emptyset$ backward angle configuration.



Fig. 30. A single octant of the back angle detector support structure.

to locate and hold the CED scintillators was designed and built. This assembly was constructed from a structural foam material, Rohacell-71, which is light-weight ($\approx 71 \text{ g/cm}^3$) and is easily machinable. Presently, work is under way to complete the optical and mechanical coupling of the CED scintillators to their respective lightguides. Once assembly of this first octant is successfully completed, a first set of tests using cosmic rays will be carried out at TJNAF to characterize these detectors and to help identify potential problems.

Beam line monitors

The success of the $G\theta$ experiment will be closely linked to the precise measurement and control of the electron beam properties. To make the subtle, refined asymmetry measurement of 1 ppm or better, the beam properties must be held within tight constraints. In pursuit of this, the beam position must be measured to better than $25\ \mu\text{m}$ per 33 ms time window and the beam current to 40 ppm during the same 33 ms time window. To accomplish this, $G\theta$ uses two sets of XYQ microwave cavity monitors. These monitors require precision electronics designed and built by TJ-NAF and TRIUMF. Specifically, the position monitors produce a voltage signal based on position for the X and Y cavities, and a current proportional voltage signal for the current cavity. The voltage is amplified by dedicated amplifiers designed specifically for the dynamic range of the cavities expected during the course of the $G\theta$ experiment. The output from these amplifiers is fed into the TRIUMF precision voltage to frequency converters and thence into the $G\theta$ DAQ scalars.

One set of these XYQ cavities is installed approximately 30 m upstream of the $G\theta$ target. The second set of XYQ cavities is installed on the $G\theta$ diagnostic girder immediately before the target. Also on this girder are a pair of standard stripline beam position monitors, a pair of super-harp wire scanners, and an optical transmission view. The combination of these monitors will allow a beam position measurement of better than $10\ \mu\text{m}$ per helicity window and an angle measurement of better than $0.5\ \mu\text{rad}$.

In addition to measuring and tightly controlling the beam properties, there will also be a need to determine the false asymmetries contributed by the beam parameters of position, angle, and current on target. Knowledge of the false-asymmetries is required in order to extract the physics asymmetries and its associated uncertainties. The false asymmetries are given by

$$A_f = \sum \frac{\partial Y}{\partial X_i} \Delta X_i$$

where ∂Y is the change in the detector yield, ∂X_i is the change in the i^{th} beam parameter, and ΔX_i is the helicity correlated asymmetry per quartet. To calculate these false asymmetries, the sensitivities $\frac{\partial Y}{\partial X_i}$ must be measured. To accomplish this, deliberate and controlled beam modulation is introduced. This is accomplished by sending a dc current to beam steering magnets far upstream from the $G\theta$ target. The steering magnet positions are chosen to minimize $x - y$ motion coupling at the target. By modulating a specific beam parameter, $\{X, Y, \Theta_x, \Theta_y, E\}$, and noting the detector yield response, $\partial Y / \partial X_i$ can then be extracted. These slopes will be measured at the beginning of each

data run while the helicity asymmetry will be measured continuously throughout the run. This modulation system has been tested with beam and works as expected. Shown in Figs. 31 and 32 are plots of the beam displacements resulting from modulation of the upstream steering coil.

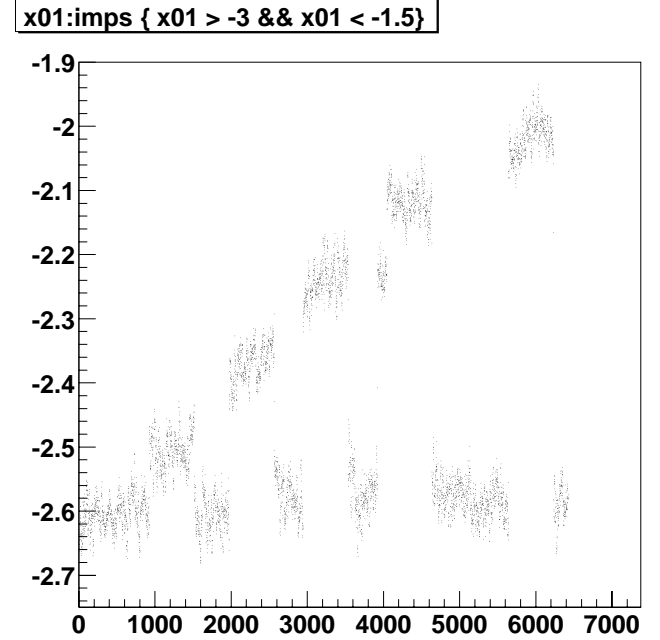


Fig. 31. Beam displacement resulting from modulation of upstream steering coils. The vertical axis gives a measure of the beam position (in mm) and the vertical axis is in units of time (macro pulse signal).

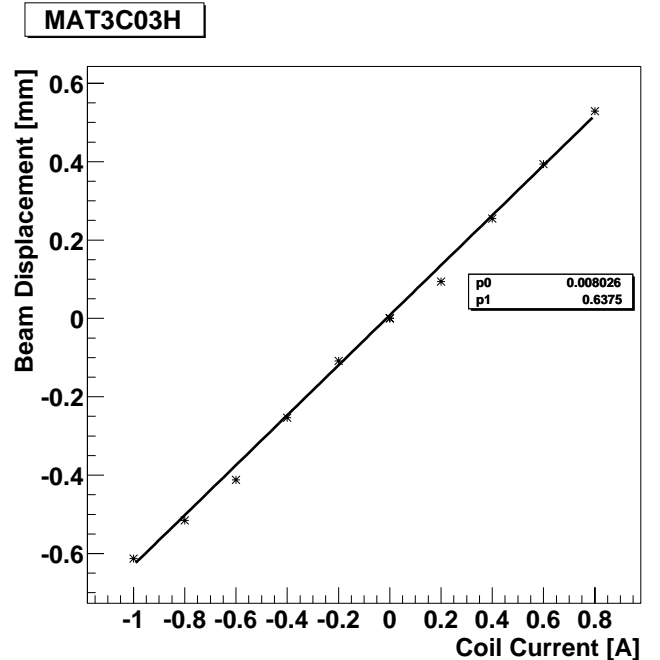


Fig. 32. Beam displacement as a function of steering coil excitation.

This modulation control system is being developed by members of the Canadian subgroup, and was tested in the $G0$ commissioning run during the fall and winter, 2002. Further developments of this system have included general beam/detector diagnostic software which allows for searches on the detector-magnet system asymmetry null coordinates, otherwise known as the sweet spot.

The 2002–2003 commissioning runs

The $G0$ experiment ran in forward angle mode from October, 2002 to January, 2003. During this period and the development period starting in August, TRIUMF, University of Manitoba and UNBC personnel staffed a total of approximately 17 person-weeks of shifts.

The equipment used is shown in Fig. 33. One can see the liquid hydrogen target service module, the 8-sector toroidal superconducting spectrometer magnet (SMS), and the focal plane detector array. During the engineering run, the magnet, target, detectors, electronics, DAQ, and software were commissioned and are operational. The principle of the forward angle measurement is shown in Fig. 34. Recoil protons at $\theta \sim 62^\circ - 68^\circ$ (corresponding to electrons at $15^\circ - 5^\circ$) are focused on the detector array in contours of constant Q^2 .

Magnet (SMS) Initial manufacturing defects in the magnet were repaired in early 2002. Initially, the magnet was only run to 4500 A, but the full design current of 5000 A was reached on December 18, 2002 and this current was used for the rest of the December running period and in January, 2003.

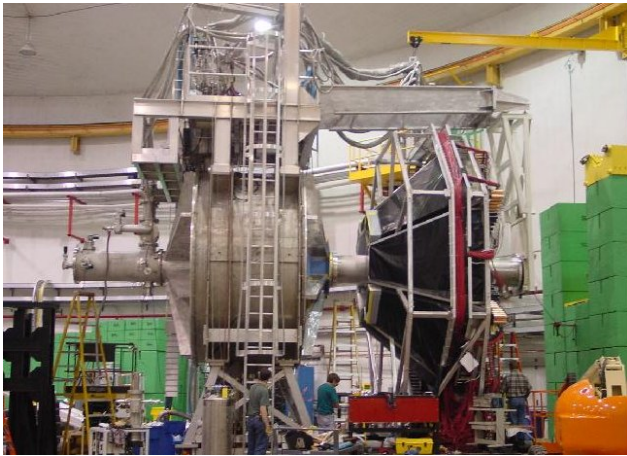


Fig. 33. Apparatus being prepared for the 2002–2003 engineering run. From left to right are the liquid hydrogen target service module, the 8-sector toroidal superconducting spectrometer magnet, and the detector array.

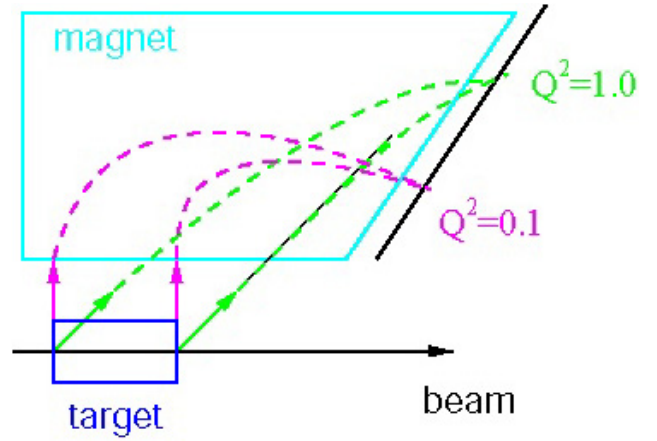


Fig. 34. A schematic of the $G0$ forward-angle configuration tested in the 2002–2003 engineering run. Recoil protons are focused on the detector array in contours of constant Q^2 .

LH₂ target The $G0$ liquid hydrogen target is a 200 mm long, 6 l target. It operates at 1.7 atm and 19 K and is designed to handle 500 W without boiling. The liquid is circulated at 5.9 l/s. The target was tested at full 40 μA $G0$ beam and worked well. Figure 35 shows the $G0$ asymmetry width as a function of raster size. By reducing the raster to a very small size, it was possible to see the effects of the onset of target boiling. At the normal operating raster size there was no indication of target boiling and density fluctuations are negligible.

As discussed in more detail later, there was evidence that the downstream target window was contributing inelastic background. The target cell has been modified to reduce this background. As well, an insertable thick window has been added as a diagnostic tool.

$G0$ beam: $G0$ requires an unusual beam time structure with 32 ns between pulses. This dictates operation at 31 MHz, 1/16 the usual 499 MHz with 2 ns between pulses. To reach the desired $G0$ beam current of 40 μA , much higher charge must be in each bunch than would normally be the case, putting special demands on the ion source and on beam optics in the injector.

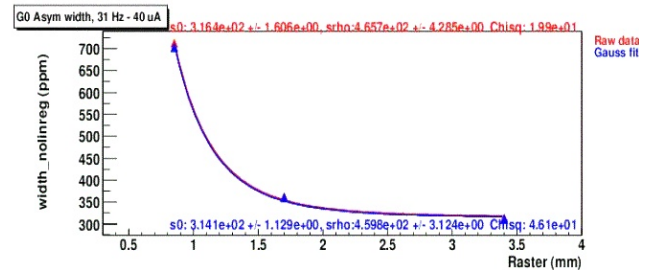


Fig. 35. The $G0$ asymmetry width in ppm as a function of the raster size in mm. Normal operation is at the right-hand end of the plot, far from any indication of target boiling.

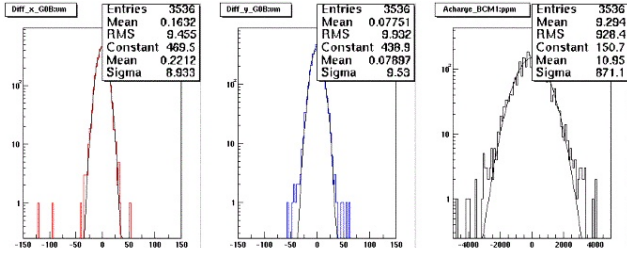


Fig. 36. Helicity-correlated beam properties measured in the 2002–2003 engineering run. From left to right, the panels show the change in x -position, y -position and beam current on helicity flip. The centroids are consistent with zero and the peak widths are $\sigma_{\Delta x} = 9 \mu\text{m}$, $\sigma_{\Delta y} = 10 \mu\text{m}$, $\sigma_{A_z} = 870 \text{ ppm}$.

A $40 \mu\text{A}$ beam with most of the desired $G\theta$ properties was delivered in January, but the beam was not as stable as required, and work is continuing. Helicity correlated variations in beam properties may be reduced by use of feedback systems, some of which were tested in the 2002–2003 engineering run. In general the charge feedback system worked well, but the position feedback did not. Figure 36 shows an example of the helicity correlated position and intensity measured during the run. The goal of the beam development program is to have helicity correlated beam position differences $<20 \text{ nm}$ averaged over a 700 hour run.

Detectors and electronics For each octant, the focal plane detectors are arranged in 16 pairs of arc-shaped scintillators, each arc following a curve of constant Q^2 . Front-back coincidences eliminate neutrals. All detectors, electronics and data acquisition were tested and worked well. It was found, however, that there was an unexpectedly large low energy background which was below the discriminator threshold but which increased the anode currents in the photomultiplier tubes. Shielding around the beam line has now been modified to reduce this background and the gains of the affected photomultiplier tubes have been reduced to further decrease their anode currents.

In the forward angle configuration, time of flight is used to separate the desired elastically scattered protons from pions and inelastic protons. Figure 37 shows a time-of-flight spectrum from one of the focal plane detectors (detector 8). The pion peak is cleanly separated from the elastic peak, but a tail of the inelastic proton peak extends under the elastic proton peak. This causes a dilution of the asymmetry which must be corrected for. Simulations suggest that the inelastic peak contains important contributions from the downstream target window. As mentioned in the target section, the target cell has been modified to reduce this background.

Asymmetry data In January the experiment was able to take some asymmetry data at $40 \mu\text{A}$ beam

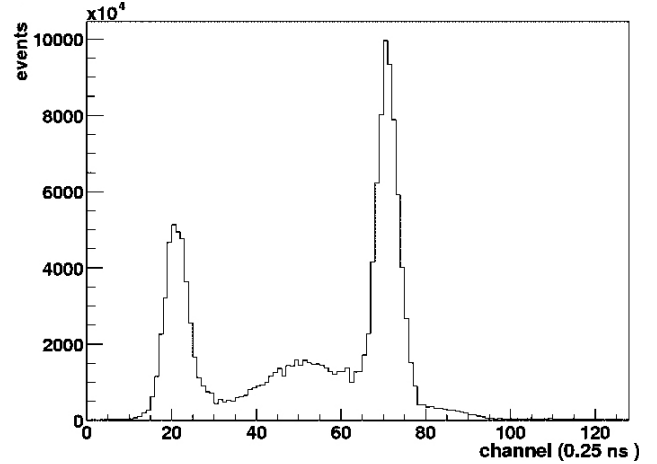


Fig. 37. A time-of-flight spectrum taken from one focal plane detector (detector 8). From left to right the peaks are pions, inelastic protons and elastic protons. The asymmetry measured for the elastic peak must be corrected for dilution by the tail of the inelastic peak.

current. Although only 51 hours of data were accumulated, clear negative value was already evident.

Future In late 2003, a second commissioning/engineering run commenced and will continue into early 2004. Upon completion of this run, the forward angle production running will begin, with 700 hours of good data expected. Back angle production running is planned for 2004–2006.

Canadian subgroup of the $G\theta$ collaboration: J. Birchall, W.R. Falk, M. Froese, Z. Ke, L. Lee, S.A. Page, W.D. Ramsay, A. Rauf, G. Rutledge, M.J. Steeds, W.T.H. van Oers (Manitoba); E. Korkmaz, T. Porcelli (UNBC); C.A. Davis (TRIUMF).

TJNAF Experiment 02-020

Q_{weak}^p : a search for new physics at the TeV scale via a measurement of the proton's weak charge (*J. Birchall, W.R. Falk, L. Lee, S.A. Page, W.D. Ramsay, W.T.H. van Oers, Manitoba; E. Korkmaz, T. Porcelli, UNBC; J. Doornbos, TRIUMF*)

Introduction

A major new initiative, the Q_{weak} experiment [TJNAF proposal E-02-020], is under rapid development at Thomas Jefferson National Accelerator Facility (Jefferson Lab), a premier electron scattering facility for nuclear and particle physics. The Q_{weak} experiment will measure the proton's weak charge to high precision, in turn providing a precise measurement of the weak mixing angle $\sin^2(\theta_W)$ at low energy, which can be compared to data from high energy collider experiments at LEP and SLC. The Q_{weak} experiment is moving forward on an aggressive construction schedule with the aim of installing equipment in Jefferson Lab's Hall C by 2007. One member of the Canadian

group (S.A. Page) is a Co-Spokesperson for the experiment, while another (W.T.H. van Oers) leads the team building the magnetic spectrometer, the coils of which are to be constructed with NSERC funds, under project management provided by TRIUMF.

Physics motivation

Precision tests continue to play a central role in elucidating the nature of the electroweak interaction. Existing experimental data provide impressive constraints both on the standard model and on proposed scenarios for extending it. Measurements at the Z^0 pole have constrained the weak mixing angle $\sin^2(\theta_W)$ to impressive precision at that energy scale. However, a precision experimental study of the evolution of the weak mixing angle to lower energies has not yet been successfully carried out. The standard model evolution predicts a shift of $\Delta \sin^2(\theta_W) = +0.007$ at low Q^2 with respect to the Z^0 pole best fit [Particle Data Group] value of 0.23113 ± 0.00015 (Fig. 38). This gives rise to a firm prediction of the proton's weak charge, $Q_{wp} = 1 - 4 \sin^2(\theta_W)$, based on the running of the weak mixing angle, corresponding to a 10σ effect in our experiment.

Figure 38 shows the standard model prediction in a particular scheme¹ for $\sin^2(\theta_W)$, together with

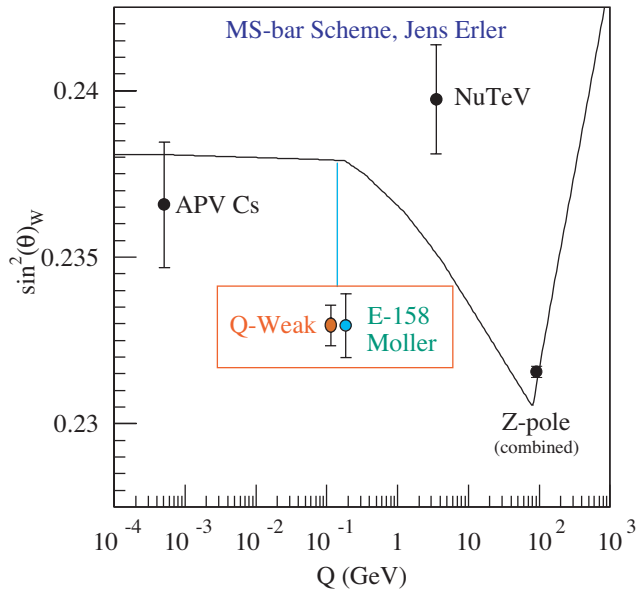


Fig. 38. Calculated running of the weak mixing angle in the standard model. Data points are from the atomic parity violation experiment on Cs, the NuTeV experiment, and from experiments at the Z^0 pole. Also shown are anticipated error bars for Q_{weak} and the Møller experiment at SLAC.

¹Note that $\sin^2(\theta_W)$ is not strictly an observable, but depends on what has been absorbed into the definition and what has been corrected for. Figure 38 shows a recent calculation by Erler, Kurylov and Ramsey-Musolf, details of which are given in Erler *et al.* [Phys. Rev. **D68**, 016006 (2003)].

²The interpretation of the APV result changes from agreement with the standard model to as much as a 2.6σ deviation *below* the predicted value, depending on what is included in the atomic theory calculations.

existing and proposed world data. As is seen from the figure, the very precise measurements near the Z^0 pole set the overall magnitude of the curve; to test its shape one needs precise measurements at other energies. Currently, there are only two other experiments which test the evolution of $\sin^2(\theta_W)$ to lower energy scales at a significant level – one in the Colorado atomic parity violation² (APV) experiment on cesium, and one from the NuTeV high energy neutrino-nucleus scattering experiment at Fermilab, showing a 3σ deviation *above* expectations. However, both of these results suffer from complications in theoretical interpretation which limit their physics impact. In contrast, the Q_{weak} experiment at Jefferson Lab will be performed with much smaller statistical and systematic errors, and has a much cleaner theoretical interpretation. The dominant hadronic effects that must be accounted for in extracting Q_{wp} from the data are contained in form factor contributions that can be sufficiently constrained by the current program of parity violating electron-proton scattering measurements under way at Jefferson Lab and elsewhere, without reliance on theoretical nucleon structure calculations.

M.J. Ramsey-Musolf, A. Kurylov and J. Erler have carried out an extensive review of theoretical uncertainties that affect the prediction of Q_{wp} itself, independent of nucleon structure contributions. Adding these uncertainties in quadrature gives a “theoretical” uncertainty of $\pm 1.9\%$ in Q_{wp} , as compared to the anticipated total uncertainty of $\pm 4\%$ for the Q_{weak} experiment.

We would like to emphasize that this new experiment is an essential element of a program of very sensitive low energy tests of the standard model that is complementary to other efforts under way or planned world wide. Erler, Kurylov and Ramsey-Musolf demonstrated that a measurement of Q_{wp} at the $\pm 4\%$ level probes new physics at energy scales up to 4.6 TeV [Erler *et al.*, Phys. Rev. **D68**, 016006 (2003)]. It should also be noted that the Q_{weak} experiment is complementary to an experiment under way at SLAC (E158) to measure the weak charge of the electron and infer the weak mixing angle from parity violating electron-electron (Møller) scattering, but which is currently not expected to reach a similar precision in $\sin^2(\theta_W)$.

The experiment

The Q_{weak} collaboration will carry out the first precision measurement of the proton's weak charge,

$Q_{wp} = 1 - 4 \sin^2(\theta_W)$ by measuring the parity violating asymmetry in elastic electron-proton scattering at very low momentum transfer:

$$A = (\sigma_+ - \sigma_-)/(\sigma_+ + \sigma_-) = Q^2 Q_{wp} + Q^4 B(Q^2)$$

where σ_+ and σ_- are cross sections for positive and negative helicity incident electrons, and $B(Q^2)$ is a hadronic form factor contribution. The results of earlier experiments in parity violating electron-proton scattering will be used to constrain hadronic corrections to the data. A 2200 hour measurement of the parity violating asymmetry in elastic electron-proton scattering at a momentum transfer of $Q^2 = 0.03 \text{ (GeV/c)}^2$ employing $180 \mu\text{A}$ of 80% polarized beam on a 35 cm liquid hydrogen target will determine the proton's weak charge with 4% combined statistical and systematic errors; this in turn implies a determination of $\sin^2(\theta_W)$ at the $\pm 0.3\%$ level at low energy. As a standalone measurement of $\sin^2(\theta_W)$, the Q_{weak} experiment is competitive with any channel measured in the recently completed SLD and LEP programs at the Z resonance.

A sketch showing the layout of the experiment is given in Fig. 39. A longitudinally polarized electron beam, a liquid hydrogen target, a room temperature toroidal magnetic spectrometer (QTOR), and a set of detectors for the scattered electrons at forward angles are the key elements of the experimental apparatus. The toroidal magnetic field will focus elastically scattered electrons onto a set of 8 rectangular quartz Čerenkov detectors coupled to photomultiplier tubes,

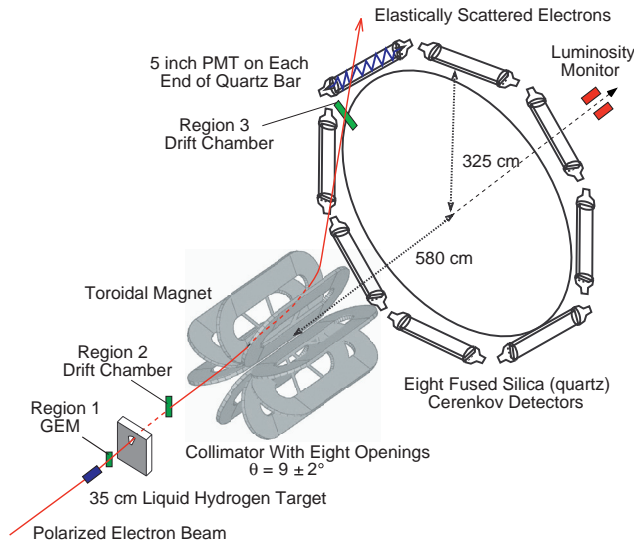


Fig. 39. Layout of the Q_{weak} experimental apparatus, showing the target, collimation, magnet coils and detectors for the eight identical octants of the spectrometer system. Incorporated in the apparatus is a tracking system to be used in ancillary measurements at very low beam current to map the Q^2 response of the detector system.

which will be read out in current mode to achieve the high statistical precision required for the measurements. A new high power cryotarget is under development for these measurements. The acceptance averaged asymmetry in our design is -0.3 ppm ; we will measure this asymmetry to $\pm 1.9\%$ statistical and $\pm 1.7\%$ systematic errors.

The main technical challenges result from the small expected asymmetry of approximately -0.3 ppm , and the required accuracy of $\pm 4\%$. The optimum kinematics corresponds to an incident beam energy of $E_0 = 1.165 \text{ GeV}$, scattered electron polar angles $\theta_e = 9.0 \pm 2.0^\circ$, and azimuthal detector acceptance as large as possible (8 electron detectors with acceptance $\Delta\phi_e = \pm 15^\circ$ each). Also, the high statistical precision required implies high beam current ($180 \mu\text{A}$), a long liquid hydrogen target (35 cm) and a large-acceptance detector operated in current mode. Radiation hardness, insensitivity to backgrounds, uniformity of response, and low intrinsic noise are criteria that are optimized by the choice of quartz Čerenkov bars for the main detectors.

It is essential to maximize the fraction of the detector signal (total light output in current mode) arising from the electrons of interest, and to calibrate both the dilution factor due to background and the detector-signal-weighted $\langle Q^2 \rangle$ in order to be able to extract a precise value for $\sin^2(\theta_W)$ from the measured asymmetry. This information will be extracted from ancillary measurements at low beam current, in which the quartz Čerenkov detectors are read out in pulse mode and individual particles are tracked through the spectrometer system using a set of wire chambers. The tracking system will be capable of mapping the $\langle Q^2 \rangle$ acceptance in two opposing octants simultaneously; chambers will be mounted on a rotatable wheel assembly so that the entire system can be mapped in 4 sequential measurements. A small “mini-toroid” magnet will be installed downstream of the first collimator to sweep low energy Møller electrons out of the acceptance of the middle tracking chambers (not shown in Fig. 39; this will not significantly affect the optics for the elastic electrons of interest for Q_{weak}). The front chambers are based on the CERN GEM design and will have a fast time response ($< 50 \text{ ns}$) and resolution of order $250 \mu\text{m}$. The chambers plus trigger scintillator system will be retracted during normal Q_{weak} data-taking at high current.

Systematic errors are minimized by construction of a symmetric apparatus, optimization of the target design and shielding, utilization of feedback loops in the electron source to null out helicity correlated beam excursions, careful attention to beam polarimetry, and by carrying out ancillary measurements to determine the system response to helicity correlated beam properties

and background terms. The electron beam polarization must be measured with an absolute uncertainty in the 1–2% range; at present this can be achieved in Hall C using an existing Møller polarimeter, which can only be operated at currents below 10 μA . A major effort to design and build a Compton polarimeter in Hall C at Jefferson Lab is under way as part of the laboratory's support of this and other experiments where precise beam polarimetry is an issue; the Compton polarimeter will provide a continuous on-line measurement of the beam polarization at full current (180 μA) which would otherwise not be achievable.

As noted earlier, the parity-violating asymmetry that we measure will contain contributions from nucleon structure form factors:

$$A = (\sigma_+ - \sigma_-)/(\sigma_+ + \sigma_-) = Q^2 Q_{\text{wp}} + Q^4 B(Q^2),$$

which can be re-expressed as:

$$A = A_{Q_{\text{wp}}} + A_{\text{eff}} + A_{\text{axial}} = -0.19 - 0.09 - 0.01 \text{ ppm},$$

where the first term involves the quantity of interest, the second term involves electromagnetic and strange nucleon form factors and reduces to $Q^4 B(Q^2)$ at low Q^2 , and the third term involves the eN axial form factor G_A^e .

The term A_{eff} can be constrained from the anticipated results of parity-violating electron scattering experiments that are either under way or planned over the next few years. Since these are performed at higher momentum transfers than Q_{weak} , the results must be extrapolated to the value of A_{eff} at our Q^2 . In our analysis, we consider the published uncertainty from the HAPPEX experiment [Aniol *et al.*, Phys. Lett. **B509**, 211 (2001)] together with the expected uncertainties from HAPPEXII [TJNAF E-99-115 (K.S. Kumar and D. Lhuillier, spokespersons)] and the forward angle running of $G0$ [TJNAF E-00-006 (D.H. Beck, spokesperson)]. For the extrapolation, we assume conventional dipole and Galster parametrizations for the electric and magnetic proton and neutron form factors. The fractional uncertainty in A_{eff} is $\pm 4.0\%$ at $Q^2 = 0.03 \text{ GeV}^2$; since A_{eff} contributes 40% to the parity violating asymmetry in our kinematics, this leads to a systematic uncertainty of 1.6% arising from our knowledge of nucleon form factors. The axial contribution, A_{axial} , depends on the eN axial-vector form factor G_A^e . The anticipated absolute error on the extrapolated value of G_A^e at $Q^2 = 0.03 \text{ GeV}^2$ will be ± 0.25 . Since this term makes a 5% contribution to the overall asymmetry, it contributes 1.2% to the systematic error in A . The quadrature sum of the two nucleon form factor errors is thus 2%.

The Q_{weak} magnetic spectrometer

A key component of the apparatus is a magnetic spectrometer QTOR, whose toroidal field will focus elastically scattered electrons onto a set of eight rectangular quartz Čerenkov detectors. The main requirement for the spectrometer is to provide a clean separation between elastic and inelastic electrons so that a detector system of reasonable size can be mounted at the focal plane to measure the elastic asymmetry with negligible contamination from inelastic scattering and other background processes. The axially symmetric acceptance in this geometry is very important because it reduces the sensitivity to a number of systematic error contributions.

The Q_{weak} magnetic spectrometer working group has designed a new resistive toroidal spectrometer with 8-fold symmetry to meet the needs of the experiment. The coil geometry has been optimized in a series of simulation studies using GEANT plus numerical integration over the conductor's current distributions to determine the magnetic field. The simplest and least expensive QTOR coil design that meets the needs of the Q_{weak} experiment is a simple racetrack structure with a layout shown in Fig. 40.

The QTOR magnet working group consists of scientists and engineers from the University of Manitoba, TRIUMF, MIT, Jefferson Lab, and Louisiana Technical University, led by W.T.H. van Oers (Manitoba). The Canadian group, via the University of Manitoba and TRIUMF, received funds in last year's NSERC competition to fabricate the 8 water-cooled conducting coils; the hollow copper conductor has been purchased by Jefferson Lab, which is also providing the power supply and services; the spectrometer support structure will be jointly engineered and built by MIT-Bates and Jefferson Lab.

With the conceptual design of the spectrometer essentially complete almost a year ago, our attention turned to further optics studies and simulation work to establish geometrical tolerances for coil fabrication and

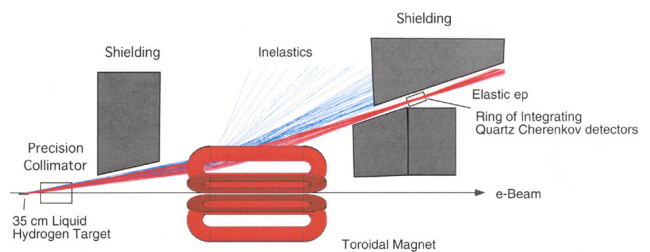


Fig. 40. Cutaway view of the experiment, showing the target, collimation, shielding, electron trajectories, and detectors for one of the eight identical octants of the spectrometer system. Elastically scattered electrons (red tracks) focus on the detectors while inelastically scattered electrons (blue tracks) are swept away by the toroidal magnetic field.

alignment. A GEANT Monte Carlo simulation package has been used to study the effects of coil misalignments on the Q^2 distribution at the focal plane as well as on the symmetry of the 8-octant system as required for systematic error reduction. Tolerances on the positioning of the QTOR magnet as a whole as well as on individual coils within the magnet have been set as a result of these studies.

A beam's eye view of the magnet, collimator, and detector systems is shown schematically in Fig. 41 with simulated GEANT events. Scattered electrons in the range $7\text{--}11^\circ$ are selected by a double collimator system. Photons project an image of the primary collimator onto a plane downstream at the magnet focus; inelastic electrons are deflected to larger angles, out of the acceptance of the detector bars. The nonideality of the 8-coil toroidal field leads to a distortion of the elastic event distribution at the focal plane, with drooping edges that we refer to as a “moustache”. The collimator shape plays a key role in defining the shape of the elastic event band accepted by the detectors, i.e. in “trimming the moustache”, which is important for minimizing the sensitivity to helicity-correlated beam motion, magnet alignment errors, and related systematic effects.

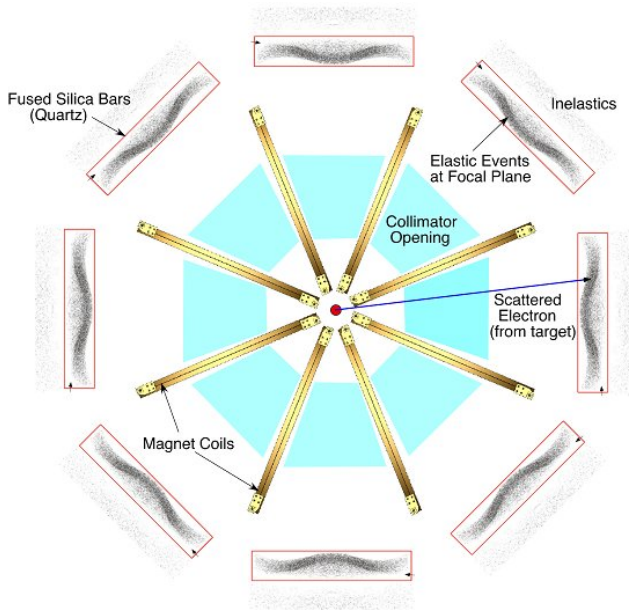


Fig. 41. Beam's eye view with simulated GEANT events. The magnet coils, primary collimator openings, and quartz detector bars are indicated. Elastic events are focused in θ and defocused in ϕ along the width and length of the detector bars, respectively. Inelastic events are deflected to larger angles, outside the detector boundaries.

Magnetic field verification

Acceptance tests of the assembled magnet of the QTOR spectrometer must guarantee that the desired Q^2 interval of the scattered electrons for each sector is properly focused on the quartz Čerenkov detectors. A magnetic field mapping apparatus, built by the Canadian group for the $G\theta$ experiment³, will be employed to map the QTOR spectrometer field. It is currently located at UIUC (Fig. 42); we will retrofit the field mapper and move it first to MIT-Bates and later to Jefferson Lab for mapping the QTOR spectrometer.

Much effort went into the design, construction and commissioning of the $G\theta$ field mapping system at TRIUMF, the University of Manitoba and the University of Northern BC. The system is capable of providing an absolute position determination of ± 0.2 mm, and a field determination of ± 0.2 G, in order to resolve a zero-crossing position to within ± 0.3 mm. The field mapping system consists of a programmable gantry with full 3D motion within a $(4 \times 4 \times 2)$ m³ volume, and a set of high precision Hall probes, thermocouples and clinometers (which measure tilt angle) mounted on the end of a probe boom on the gantry. Because the coils of the $G\theta$ magnet were completely encased in a cryogenic vacuum vessel, the field mapping had to determine the coil location by a very accurate measurement of the zero crossing of selected field components of the fringe field. Since the Q_{weak} magnet is open, the main magnetic field can be mapped directly. For the Q_{weak} mapping, new Hall probes with the appropriate dynamic range will be installed.

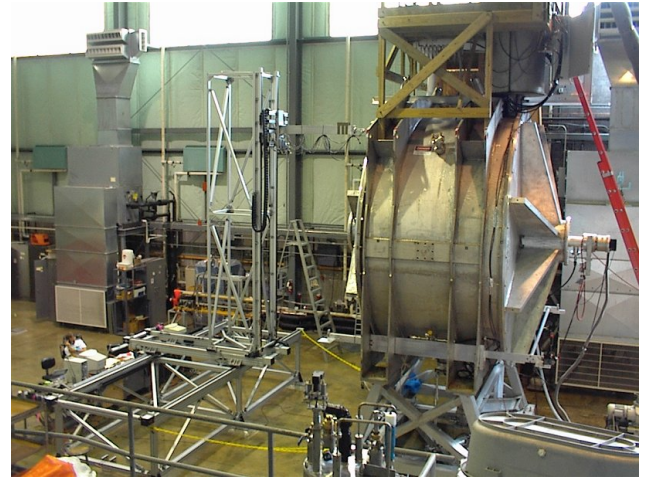


Fig. 42. Magnetic field mapper, on location at UIUC for mapping the $G\theta$ magnet.

³The $G\theta$ magnet is an 8-coil superconducting toroidal spectrometer of a similar size to QTOR. Magnetic field mapping for $G\theta$ posed a particular challenge since the coils were completely encased in a cryogenic vacuum vessel.

Simulation studies: systematic errors

The Canadian group's simulation effort builds on expertise gained from TRIUMF Expts. 497 (Measurement of parity violation in \vec{p} - p scattering at 221 MeV) and 704 (Measurement of charge symmetry breaking in $np \rightarrow d\pi^0$ close to threshold) as well as from the ongoing $G\theta$ experiment at Jefferson Laboratory. We are concentrating initially on the study of systematic errors that result from beam properties that change when electron beam helicity is reversed. Initial estimates that were made to set requirements on beam properties at the time of the experimental proposal were based on a simple geometrical model in which the acceptance of the detectors was set by the primary collimator. Systematic error estimates have now been made based on detailed Monte Carlo calculations that track electrons from the target, through the collimators and magnetic field to the detectors.

Helicity correlations in the beam parameters can lead to false parity asymmetries. The measured parity asymmetry, A_{meas} , is written in terms of the physics asymmetry, A_{phys} , in the following way for sufficiently small helicity correlations:

$$A_{\text{meas}} = A_{\text{phys}} + \sum_{i=1}^n \left(\frac{\partial A}{\partial S_i} \right) \delta S_i,$$

where beam parameter S_i changes on helicity reversal to $S_i^\pm = S_i \pm \delta S_i$. The detector sensitivities $\partial A / \partial S_i$ can be determined preferably by deliberate modulation of the relevant beam parameter or from natural variation of beam parameters. The helicity-correlated beam parameter differences, δS_i , are measured continuously during data-taking. The goal is to constrain systematic uncertainties from each source to be no more than the statistical uncertainty on the measurement of the parity asymmetry, i.e., no more than 6×10^{-9} , and that corrections should be accurate to 10%.

A perfectly symmetric detector system, magnet and collimator aligned precisely with the beam should be insensitive to small modulations of beam position on helicity flip. If the beam is moved away from this "position neutral axis", however, symmetry is broken and false parity-violating effects are seen. To study this, the Q^2 -weighted event rate, $N(x, y)$, seen by a Čerenkov bar is mapped out as a function of the position of the beam on target and of displacement of the magnetic field. It is then possible to estimate the false parity asymmetry due to beam motion on helicity flip and to set tolerances on the positioning of the magnet. Tolerances break down into dc properties, that is, average values for beam parameters, and helicity-correlated changes. A large beam raster size (4 mm in place of 2 mm) decreases the possibility of spurious results due

to bubbling of the target, so systematic errors were estimated for 4 mm and 2 mm rasters.

Likewise, the sensitivity to beam size modulation has been explored. The effects of the size modulation are diluted by the rastering if there is no correlation of the rastering with helicity. For a false asymmetry of 6×10^{-9} , the rastered beam should contain a size modulation no larger than about 2 nm. As the angle of incidence of the beam on target is changed, so the range of Q^2 accepted by the collimators changes and with it the event rate. There is in addition a variation of effective thickness of the target, but the effect is small compared with the variation of cross section and is, in any case, removed by normalization to the luminosity monitors. The systematic error requirement becomes $|\theta_0 \delta \theta_0| \leq 6.3 \times 10^{-6} \text{ mrad}^2$, corresponding to a dc offset of the angle of beam on target of about 60 μrad when $\delta \theta_0 = 100 \text{ nrad}$.

Spectrometer calibration efforts, Q^2 distribution and tracking

Through our heavy involvement in the design, construction, and field mapping of the QTOR magnetic spectrometer, the Canadian group plans to participate significantly in the spectrometer calibration and tracking effort of the collaboration. It should be noted that we must determine $\langle Q^2 \rangle$ to 1% to meet the goals of our experiment; since hadronic corrections to the asymmetry are proportional to Q^4 , we must also determine the Čerenkov-light-weighted average of this quantity in order to analyze the asymmetry data. It is clear that a thorough understanding of the spectrometer system and the shape of the light-weighted Q^2 distribution for elastic electrons at the focal plane is an essential ingredient to the success of this experiment. Work is proceeding on two fronts: simulations of the spectrometer tracking system and main detector response to predict the shape of the Q^2 observed distribution, and subsequent optimization of the calibration, alignment and tracking systems that will lead to measurements of this distribution under experimental conditions.

Experiment status

Following initial PAC approval in 2002 and a successful technical review in January, 2003, a funding package to support the equipment construction totalling approximately US\$3.4 M has been put in place, provided by Jefferson Lab, the US DOE, NSF, and NSERC, Canada. The experiment is on a fast track for construction and installation in Hall C at Jefferson Lab by 2007. Bids for construction of the magnetic spectrometer coils, which are the responsibility of the Canadian subgroup, will be solicited in early 2004, with initial assembly and field mapping planned to take place at MIT-Bates in 2005.

The Q_{weak} collaboration

The Q_{weak} collaboration consists of 51 scientists from 17 institutions. The principal Spokesperson is R.D. Carlini (Jefferson Lab) with Co-spokespersons J.D. Bowman (LANL), W.M. Finn (William and Mary), S. Kowalski (MIT), and S.A. Page (Manitoba). G.R. Smith (Jefferson Lab) is the Project Manager. Major stakeholders in the experiment are Jefferson Lab, who will provide the polarized beam, the target, the beam line instrumentation, and required shielding; Los Alamos National Lab, who lead the design and construction of the detector package and associated electronics; Louisiana Tech, who lead the effort in computer simulations and are building the forward GEM tracking detectors; MIT, who play a major role in the design and construction of the spectrometer support stand and the Compton polarimeter project, the Canadian collaboration (Manitoba, UNBC, TRIUMF) who are leading the magnetic spectrometer project, and a consortium of US university groups including The College of William and Mary, Louisiana Tech, and Virginia Polytechnic University, who have taken responsibility for the spectrometer calibration and particle tracking system. The major stakeholders are represented by an Institutional Council, which is the decision-making body regarding policy issues for the experiment. The

council holds regular meetings by telephone conference to monitor the status of institutional construction projects and contributions to the experiment. S.A. Page is currently serving as Chair of the Institutional Council.

List of Q_{weak} collaborators: M.J. Ramsey-Musolf, Caltech; D. Armstrong, T. Averett, W.M. Finn, K.H. Grimm, College of William and Mary; C. Keppel, Hampton University; R.D. Carlini, S. Chattopadhyay, R. Ent, D.J. Gaskell, A. Lung, D. Mack, S. Majewski, H. Mkrtchyan, M. Poelker, J. Roche, G.R. Smith, S. Wood, C. Zorn, Jefferson Lab; J.D. Bowman, G. Mitchell, S. Penttila, W.S. Wilburn, Los Alamos National Lab; T. Forest, K. Johnston, N. Simicevic, S. Wells, Louisiana Technical University; J.A. Dunne, Mississippi State University; S. Kowalski, R. Suleiman, S. Taylor, MIT; A.K. Opper, Ohio University; C.A. Davis, J. Doornbos, TRIUMF; J. Erler, Universidad Nacional Autonoma de Mexico; R. Jones, K. Joo, University of Connecticut; J. Birchall, W.R. Falk, L. Lee, S.A. Page, W.D. Ramsay, W.T.H. van Oers, University of Manitoba; F.W. Hersman, M. Holtrop, H. Zhu, University of New Hampshire; E. Korkmaz, T. Porcelli, University of Northern BC; C. Hagner, N. Morgan, M. Pitt, Virginia Polytechnic Institute. Experiment status: in preparation.

NUCLEAR PHYSICS

Experiment 715

Weak interaction symmetries in β^+ decay of optically trapped $^{37,38}\text{K}$

(D. Melconian, SFU; J.A. Behr, M.R. Pearson, TRIUMF; K.P. Jackson, TRIUMF/SFU)

We present here an update on our progress in testing the standard model using optically trapped ^{38}K and ^{37}K . The pure Fermi β^+ decay of ^{38}K is a sensitive probe of scalar contributions to the weak interaction, while the decay of polarized ^{37}K can be used to search for right-handed currents and time-reversal symmetry violating interactions. The background and experimental set-ups for these experiments have been described elsewhere [TRIUMF 2002 Annual Report, p.34], so we provide here only a brief report on recent progress.

Status on the scalar search

A great deal of progress has been made in accurately understanding all possible sources of systematic error, and their effect on our measurement of the $\beta^+ - \nu$ correlation parameter, $a_{\beta\nu}$. For example, by careful comparison of our three measurements of the electric field (fastest recoil TOF, fastest “wrong-way” recoil TOF, and photoionized atoms) we can now constrain our field nonlinearity to be less than 1.0 V/cm/cm and the resulting error in $a_{\beta\nu}$ to be <0.0011 . We can also constrain the angle dependence of the efficiency of the microchannel plate and assign an error of 0.0008 to this effect.

Our experiment can uniquely constrain one potential source of systematic error from the atomic physics. Dependence of the probability of electron shakeoff on the recoil ion energy has been demonstrated in ^6He β^- decay [Carlson *et al.*, Phys. Rev. **129**, 2220 (1963)]. A recent simple atomic physics calculation relates this effect to atomic oscillator strengths and suggests that it could be larger in β^+ decay [Scielzo *et al.*, Phys. Rev. **A68**, 022716 (2003)]. The recoil energy spectrum to lowest order is distorted by $(1 + sE_{\text{rec}})$. We are able to constrain this effect experimentally by fitting s and $a_{\beta\nu}$ simultaneously in our $\text{TOF}[E_\beta]$ fit for $\text{Ar}^{+1,+2,+3}$. We only include s in the Ar^{+1} spectrum because the model suggests that s for Ar^{+2} (or Ar^{+3}) would be 0.11 (or 0.05) the size of s for Ar^{+1} . We find $s = 0.007 \pm 0.017$, producing a change in $a_{\beta\nu}$ of 0.0002 ± 0.0020 . A similar simultaneous fit to Ar^{+1} using our reconstructed angular distribution gives consistent result and error (see Fig. 43). We can constrain s and $a_{\beta\nu}$ simultaneously because the greatest sensitivity to $a_{\beta\nu}$ is at the null in the angular distribution, and because we fit as a function of E_β . A fit to the total TOF spectrum summed over all E_β would be more strongly correlated to the

recoil momentum spectrum.

We have gone through our error budget in a similar fashion and have determined all systematic effects on $a_{\beta\nu}$. The plastic scintillator energy calibration is the one last source of systematic error we have yet to thoroughly define. Once this is done, the analysis will be completed. Alexandre Gorelov presented a preliminary result at the DNP03 meeting in Tucson: $\tilde{a}_{\beta\nu} \equiv a/(1 + b_F \Gamma m_e/E_\beta) = 0.9978 \pm 0.0030(\text{stat}) \pm 0.0045(\text{syst})$.

Polarized measurements

We continue to analyze the data set of our experiment on the decay of polarized ^{37}K taken in the fall of 2002. The results, described below, include an atomic measurement of the polarization and a 3% measurement of the neutrino asymmetry. We have also made very preliminary measurements of the D coefficient and an observable we call R_{slow} , which will require greater statistical accuracy to be competitive.

Our measurement cycle starts by accumulating and confining ≈ 2000 radioactive ($T_{1/2} = 1.23$ s) ^{37}K in a magneto-optic trap (MOT). The MOT provides a

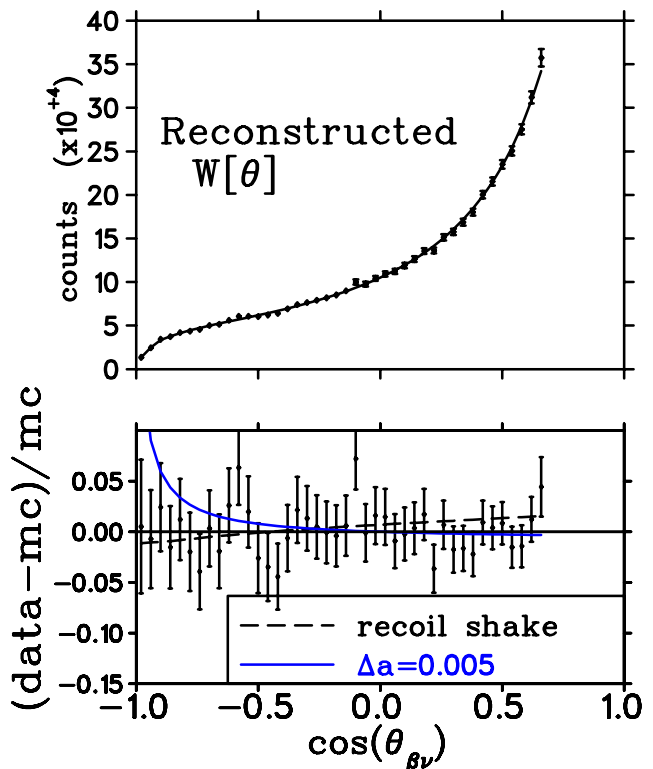


Fig. 43. Constraint of the recoil shake-off dependence on its momentum. The top plot shows the reconstructed angular distribution and comparison to a MC simulation. The lower plot shows the effect of a 0.5% change in $a_{\beta\nu}$ from the fit value, and the effect of a change in recoil shake-off dependence of $s = 0.03$ (the size predicted by Scielzo *et al.*). The functional dependence is quite different, so we can constrain both effects simultaneously.

nearly ideal source of atoms. They are well-localized in space ($\sim 1 \text{ mm}^3$) and are cold enough ($\sim 1 \text{ mK}$) to have a negligible contribution to the recoil momentum spread. The β^+ and daughter recoil freely escape the shallow trap with negligible perturbations to their momenta. We have shown from β asymmetry measurements that the MOT completely depolarizes the atoms, so we turn the MOT off and use optical pumping techniques to highly polarize the atoms. We make our nuclear measurement during the time the MOT is off, and so the cloud of atoms is expanding due to their small (yet finite) thermal motion. Therefore, we turn off the optical pumping after 1.4 ms and reactivate the MOT in order to re-trap atoms that have not decayed, and then we start the cycle again.

Atomic measurement of the polarization An important aspect of our polarized experiment is that we can measure the atom cloud polarization *in situ* and *non-destructively* using atomic techniques. We use a pulsed 355 nm laser which only photoionizes atoms from the excited $4P_{1/2}$ state. The resulting $^{37}\text{K}^+$ ions are collected by the electric field and detected by the MCP detector. The photoions not only serve to image the cloud of atoms, but also provide an extremely sensitive and clean measure of the excited state population, which is directly proportional to the fluorescence. This is a much cleaner method than looking for the fluorescence directly, because our geometry is optimized for particle (not light) collection efficiency, and we can use the TOF and position information to minimize and correct for the background from β decays.

Atoms that are fully polarized can no longer absorb the optical pumping light (because there is no higher $m_{F'}$ level to get excited to), so the degree to which the fluorescence vanishes is related to the polarization. This relationship has been modelled using the rate equations and we can fit the decay of the fluorescence as a function of the optical pumping time to deduce the polarization. This is shown in the left panel of Fig. 44. The background (dashed line) is determined from events which do not hit the MCP in the same place as the photoions. The right panel of Fig. 44 shows the χ^2 map for various values of the nuclear polarization input into the model. The results are consistent for σ^+ and σ^- light, and average to $\langle P \rangle = 0.965 \pm 0.004$. To account for the model dependence of the deduced polarization, we assign a systematic uncertainty of 1.5% so that the nuclear polarization is determined to be $P = (96.5 \pm 1.5)\%$.

Angular correlations: B_ν and D The β -telescope and MCP recoil detectors are very well understood from the in-depth analysis done in extracting our value of $\tilde{a}_{\beta\nu}$. Considering the kinematics of the decay of ^{37}K polarized perpendicular to the telescope-MCP

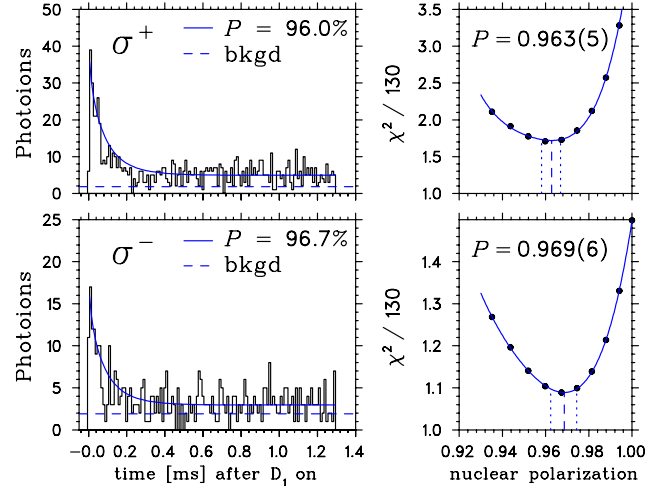


Fig. 44. Fit of the vanishing of the fluorescence for various values of the nuclear polarization for σ^\pm (left) and the χ^2 map (right) whose minima yield $\langle P_{\text{nuc}} \rangle = 0.966 \pm 0.015$.

detection axis, one can show that the recoil asymmetry, apparent as an asymmetry in the \hat{x} direction, is directly related to the neutrino asymmetry, B_ν . Thus using the polarization deduced from the photoion data and analyzing the position dependence of the clean β -Ar coincidences, we can measure B_ν . The data (points) and fit to a detailed MC simulation (line) of projections of the MCP position spectrum are shown in the top panel of Fig. 45. The bottom panel shows the asymmetries in \hat{x} (left) and \hat{y} (right), which are proportional to PB_ν and PD , respectively.

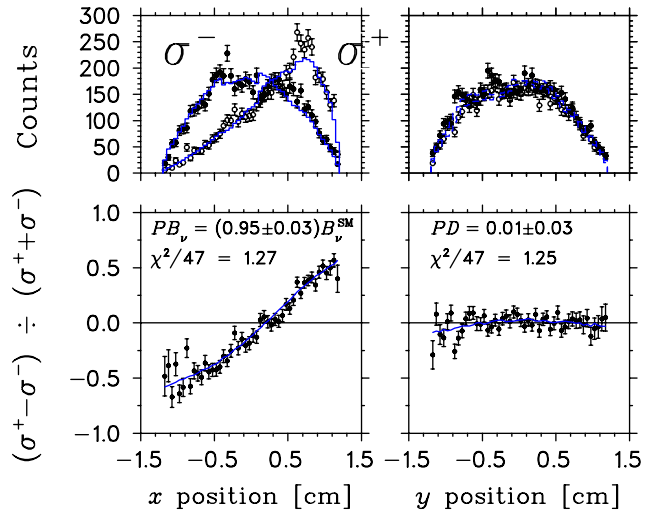


Fig. 45. MCP position spectra for β -Ar $^{+1}$ coincidences in the back-to-back geometry. The polarization axis is along \hat{x} and so the asymmetry along that direction is proportional to PB_ν . Shown is the data (points) and the fit to a MC simulation (solid line). A \hat{y} asymmetry would arise from the time-reversal violating D term; we do not see an asymmetry and so we limit D to be less than 0.04.

We obtain SM predictions for the correlation parameters based on the measured value of the ratio of matrix elements, $\lambda \equiv g_V M_F / g_A M_{GT} = -0.5754(16)$ [Hagberg, private communication; Ball, private communication]. The result of fitting the \hat{x} asymmetry and dividing out the measured nuclear polarization is $B_\nu = (0.986 \pm 0.029)$ $B_\nu^{\text{SM}} = -0.758 \pm 0.022$, with analysis on systematic effects ongoing (see below and Table V). Similarly, by fitting the \hat{y} asymmetry (or lack thereof), we can search for a non-zero D coefficient which violates time-reversal symmetry; final state effects which mimic T -violating interactions have been estimated [Holstein, Phys. Rev. **C5**, 1529 (1972)] and should be half as large as those in ^{19}Ne which measured $D < 1.6 \times 10^{-3}$ (90% CL) [Hallin *et al.*, Phys. Rev. Lett. **52**, 337 (1984)]. Our result, currently limited by statistics, is $D < 0.06$ (90% CL).

We have investigated a few of the larger systematic effects in the polarized experiment, the results of which are listed in Table V. The two most significant sources are from the atomic measurement of the polarization, and the position of the thermally expanding cloud of atoms. Upon turning off the magnetic field for trapping the atoms, the cloud centroid changes. This is difficult to characterize because the photoion techniques are effective on trapped atoms, but are relatively poor on the optically pumped atomic cloud. Instead we probe the polarized atom cloud position by varying its input to the MC and making χ^2 maps of the resulting fits to the projections in the top panel of Fig. 45. This gave an $\hat{x} - \hat{y}$ centroid with ± 0.5 mm uncertainty. The variation in the fit to PB_ν over this same range gives us the systematic uncertainty due to the cloud position: $\delta(PB_\nu) = \pm 0.012$. In the same manner, we estimate for each source listed in Table V the systematic uncertainty on our $B_\nu = -0.758$ measurement.

Our measurement of the ν asymmetry is in agreement with the standard model value of $B_\nu^{\text{SM}} = -0.7564(15)$ and so we interpret our result as a limit.

Table V. Error budget for the neutrino asymmetry measurement. We are still in the process of identifying additional systematic sources and assigning their systematic uncertainty.

Source of uncertainty	δB_ν
Statistical	0.022
Polarization	0.015
Direction of OP axis	0.002
Cloud $\hat{x} - \hat{y}$ position	0.012
Cloud size	0.003
MCP position efficiency	0.001
Others (in progress)	—
Systematic	~ 0.020
Total	~ 0.030

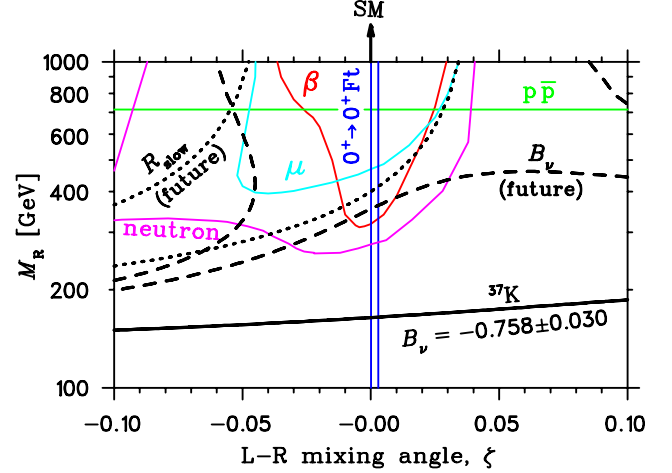


Fig. 46. 90% confidence level limits on the right-handed current parameters M_R and ζ in the manifest left-right symmetric model, including our ν asymmetry measurement. Also shown as dashed (dotted) lines are the limits obtained with measurements of B_ν (R_{slow}) with an accuracy of $\sigma = 0.001$.

A comparison of our 90% CL limit to other experiments that constrain right-handed currents in the manifest left-right symmetric models is given in Fig. 46. In the standard model, there is no right-handed boson, so these limits exclude regions of lower M_R and finite mixing angle, ζ . Our result excludes right-handed masses of $< 150 \text{ GeV}/c^2$. Shown as a dashed line is the limit one would obtain with a $\sigma_{B_\nu} = 0.001$ measurement in agreement with the SM.

As described in last year's Annual Report, we have added two phoswich β detectors along the optical pumping axis with the intent of measuring the β asymmetry. The β singles measurement was found to have unacceptably large backgrounds due to atoms implanting and depolarizing on the mirrors in front of the phoswiches. However, by requiring a recoil coincidence with the MCP, we obtain clean spectra of polarized atoms that decayed directly from the optically pumped cloud. The physics that can be extracted from such correlations is discussed below.

Angular correlations continued: R_{slow} The geometry of the phoswich and MCP detectors, depicted in Fig. 47, is such that fast Ar^+ recoil events are suppressed because the electric field of -810 V/cm is not large enough to significantly alter the ion trajectory, so recoils with large momenta along $-\hat{x}$ will miss the MCP. For slow recoils, however, the field is able to focus the ions within the active area of the MCP. In this way, the kinematics and geometry of these events help to pick out slow recoil events. In the purely back-to-back geometry depicted in Fig. 47, this translates to events where the β alone goes along \hat{x} into the phoswich, while the ν and recoil are both emitted in the opposite

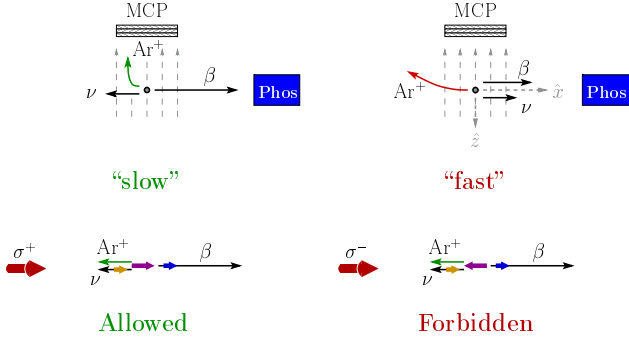


Fig. 47. Geometry (not to scale) and kinematics of phoswich-MCP coincidences. The top panel depicts how the experimental set-up and kinematics of the decay accept slow recoils, while fast Ar^+ will not fire the MCP. The bottom panel shows how angular momentum can only be conserved for the slow recoils if the initial nuclear spin is aligned with the β direction.

direction. In reality, however, the Ar^+ and ν are not constrained to be along $-\hat{x}$ and the differentiation of fast to slow recoils becomes less precise. We have shown that we can enhance selectivity of slow recoils based on the TOF. At the present time with current statistics this cut is not practical, however, this can be employed in the future when we have more events.

Continuing to consider the back-to-back geometry for simplicity, it is easy to show that helicity arguments require that, for a purely $V - A$ interaction, the initial nuclear spin of the ^{37}K must be aligned with the β direction. If it were opposite, the initial spin projection of $m_I = -I$ could not equal the sum of the final state spins: $m_{I'} + m_{\text{leptons}} = m_{I'} + 1 > m_I$. We therefore define a vanishing observable, R_{slow} , to be the ratio of phoswich-MCP coincidences with $\hat{i} \cdot \hat{p}_\beta = -1$ over $\hat{i} \cdot \hat{p}_\beta = +1$. We measure R_{slow} by looking at the \hat{x} -MCP asymmetry as per the B_ν measurement, except this time requiring that a β fired the phoswich detector instead of the (back-to-back) β -telescope.

Noting that the lepton spins are aligned in back-to-back decay, one can see that the Fermi component (i.e. where $a_{\beta\nu} = +1$) of this mixed F/GT decay is suppressed. To the extent that we measure only slow recoils, the Gamow-Teller part of the decay is singled out, making us much less sensitive to the value of λ . The dependence of R_{slow} on right-handed current (RHC) parameters goes like $(\delta + \zeta)^2$, where $\delta \equiv (M_L/M_R)^2$. This can be understood by considering how a $V + A$ interaction couples to left-handed neutrinos: 1) directly through a new right-handed boson exchange, or 2) weak eigenstate mixing of the left- and right-handed bosons. In the first case, the matrix element with a W_R exchange is suppressed relative to the W_L by the $1/M_W^2$ mass-dependence of the propagator, resulting in a M_L^2/M_R^2 dependence. For the second case, the mixing goes like $\sin \zeta$ which, for small admixtures, is linear

in ζ . The overall probability of having a right-handed current goes like the square of the sum of these two terms, namely $(\delta + \zeta)^2$.

The R_{slow} observable is therefore a sensitive probe of the RHC parameters and will depend only weakly on the accuracy of the measurement of λ . The drawback is in the number of events: there are approximately 4 times fewer events than our B_ν measurement due to kinematics and detector acceptances, and so R_{slow} is highly statistics limited. Our current data set yields a 10% measurement of the \hat{x}_{MCP} -asymmetry which translates into roughly similar limits as obtained by the 3% measurement of B_ν . We plan to continue analyzing this observable, in particular checking how much sensitivity can be gained by making the additional TOF cut to help pick slow recoil events.

These preliminary results are quite promising, and we expect to be able to make great improvements by resolving some simple detector problems and utilizing increased yield expected not only from ISAC, but also from the MBR laser upgrade described below.

Experiment 956 developments

Experiment 956, limits on tensor interactions from recoil singles spin asymmetry, has had experimental planning progress. This observable vanishes for Gamow-Teller transitions in the absence of tensor interactions, so our present level of polarization is more than good enough to make a competitive measurement.

We have realized that a coincidence between γ -ray and recoil will still produce a vanishing observable, but make the experiment cleaner as well as give the recoil momentum dependence. We are pursuing this with a plan to make a measurement in ^{80}Rb as an M.Sc. project.

Experiment 925 developments

Initial tests of Expt. 925, isospin mixing in ^{36}Ar from polarized observables in ^{36}K decay, form the bulk of Ofer Aviv's M.Sc. thesis, Tel Aviv University. Modelling of the rather complex recoil TOF spectrum to explore sensitivity to $a_{\beta\nu}$ is proceeding well. The higher-energy 9.8 MeV β^+ Q-value produces higher-momentum neutral recoils than ^{37}K , and the MCP detects them with good efficiency, a surprising result. Plans on completing the hyperfine splitting and quadrupole moment measurement are proceeding.

Off-line developments

We have moved the contents of the TRINAT off-line lab in the main office building to the on-line lab.

MOPA efficiency We have improved the output power from our tapered amplifier system by placing one of the frequency-shifting AOM's before it instead

of after it. There is still sufficient pump power to saturate the tapered amplifier.

MBR-110 upgrade After much effort, we were unable to adapt the lower-model MBR-PE ring laser to frequency lock it to a potassium line. The design, which replaces the 899-21 thick and thin etalons with a single higher-finesse etalon, requires very subtle control of that etalon with multiple feedback loops. We are commercially upgrading the unit to a full MBR-110. We can project that this will increase the number of trapped atoms by a factor of three.

CFORT On the polarization front, we are working to develop a circularly-polarized far-off resonance trap (CFORT) which promises extremely high polarizations because only the $M_F = F$ state is trapped and all others are repelled. It is expected that we can achieve >99.9% polarization. This type of trap was developed and loaded efficiently with Rb atoms by JILA [Miller *et al.*, Phys. Rev. **A66**, 023406 (2002)]. Adapting this to our requirements and to potassium atoms is the M.Sc. project of Erika Prime. A ring laser adapted from an existing standing-wave cavity will provide the light for the trap. We have characterized this laser to have very good spatial mode quality.

405 nm probe We hope to use the 405 nm laser to measure the magnetic sublevel populations directly by scanning our laser over the Zeeman-shifted transition frequencies. This is necessary to further calibrate the measurement of the vanishing of fluorescence to remove its model dependence, and also allow the measurement of the tensor alignment term in addition to the vector polarization. The 405 nm diode laser is presently limited by its frequency linewidth. In the meantime, we have measured the specific mass isotope shift of the potassium $5P_{1/2}$ state between stable ^{39}K and ^{41}K atoms. In the probing, we can distinguish between $4P$ and $5P$ populations because our 532 nm pulsed laser can only photoionize the latter. As part of this effort, we are measuring the absolute photoionization cross section of the $5P_{1/2}$ state as the senior thesis project of Lorraine Courneyea at UBC.

Photoionization If we are able to photoionize atoms directly from the ground state, we would be able to sensitively probe the cloud expansion once the MOT is off and the atoms are fully optically pumped. Presently the photoions vanish as the atoms polarize and so we have very weak statistics on the cloud parameters (size, position, temperature). Photoionization from the ground state, though destructive, could be used to image both the trapped *and* untrapped atoms.

Coherent population trapping Coherent population trapping is a subtle quantum mechanical interference effect in the laser-atom system that could in principle

limit polarization from optical pumping. Atoms can be stalled in a dark superposition of sublevels. Our work on creation and destruction of this effect in our apparatus has now been published [Gu *et al.*, Optics Comm. **220**, 365 (2003); *ibid.*, Phys. Rev. **A68**, 015804 (2003)].

Experiment 744

A kinematically complete study of $\pi^- p \rightarrow e^+ e^- n$

(M.A. Kovash, Kentucky)

TRIUMF Expt. 744 is a kinematically complete study of the inverse pion photoproduction reaction, $\pi^- p \rightarrow e^+ e^- n$. In the one photon exchange approximation this proceeds through the production and decay of a single virtual photon. In the low-energy region the amplitudes for the generalized process of charged pion photoproduction include the well-known contact Kroll-Ruderman interaction which is determined by gauge invariance at threshold, and which dominates the near-threshold region for real photons. An analogous set of diagrams also contributes to the yield of virtual photons in radiative pair production, although at values of $q^2 \neq 0$. A description of this process in terms of Feynman amplitudes then uses form factors to describe the coupling of the virtual photon to the hadrons. It is the Kroll-Ruderman term, through the combined requirements of gauge invariance and PCAC, which is sensitive to the nucleon axial and pseudoscalar form factors, G_A and G_P . Radiative pair production thus offers a *unique* opportunity to probe the axial structure of the nucleon at small time-like values of q^2 .

As in the case of pion electroproduction, the hadronic component of the cross section for radiative pair production is of the general form

$$\begin{aligned} \frac{d\sigma_{\gamma^*}}{d\Omega} &= \frac{d\sigma_T}{d\Omega} + |\epsilon| \frac{d\sigma_L}{d\Omega} + A\epsilon \cos(2\phi) \\ &+ B \sqrt{\frac{|\epsilon|(1+\epsilon)}{2}} \cos(\phi). \end{aligned}$$

The kinematic variables are the polar angle of the virtual photon, the azimuthal angle between the leptonic and hadronic planes, and the photon polarization. The various terms in this equation are the transverse and longitudinal cross sections, and the transverse-transverse and transverse-longitudinal interference cross sections. The ϕ and ϵ dependences shown in this equation can be exploited to experimentally determine the individual response functions. For example, the ϕ -averaged cross section contains only the longitudinal and transverse components, which are themselves individually determined via the usual Rosenbluth separation. Conversely, a harmonic analysis of the azimuthal dependence of the measured cross section allows one to determine

the transverse-transverse and longitudinal-transverse interference terms from the data. Of course, to do this decomposition requires knowledge of the variables $(\theta_\gamma, \phi_\gamma, \epsilon_\gamma)$ for each event.

We study the reaction $\pi^- p \rightarrow e^+ e^- n$ using the RMC pair spectrometer to detect the $e^+ e^-$ pairs. The pion beam enters the detector along the axial field lines (with $B = 2.4$ kG) and interacts with the liquid hydrogen target at the detector centre. The target is surrounded by an array of inner scintillators (A, A'), and the 12-segment C scintillator array. The $e^+ e^-$ pairs are tracked from the target through a dual-coordinate inner wire chamber (IWC) providing both z and azimuthal coordinates of the hits. The IWC is surrounded by a large-volume 4-layer drift chamber. Layers 1, 2 and 4 provide both x and y track coordinates. The wires in the third chamber have a 7° stereo angle with respect to the drift chamber axis, with which the z position of the track crossing can be determined. An outer layer of scintillators (D) is segmented into 16 sectors and provides a second component of the hardware trigger for $e^+ e^-$ events.

Study of the reaction $\pi^- p \rightarrow e^+ e^- n$ requires that both the electron and positron momentum vectors are determined at their point of origination in the target. From this information the five kinematic variables which characterize this 3-body final state can be determined: the photon mass, its polarization, and its polar angle of emission, as well as the angle between the $e^+ e^-$ plane and the plane containing the virtual photon and recoil neutron. The trajectories are individually recorded in the IWC and drift chambers. From these hit positions the tracking algorithm determines the magnitudes of the individual momenta and the coordinates of the centres of the helical trajectories.

During the summer we collected first production data for the capture in flight of 160 MeV/c pions in a liquid hydrogen target, using the RMC spectrometer to detect the $e^+ e^-$ pairs. For each event, the 3-momentum of each lepton was determined from the measured track direction and curvature, thus defining the energy, momentum and polarization of the virtual photon as well as its polar and azimuthal angles of emission. The large angular coverage of the RMC detector ($\Omega \sim 3\pi$) provides us with excellent acceptance for $e^+ e^-$ pairs emitted from photons produced at all angles.

Unfortunately, at about the mid-point of the data collection the power connections to the first quadrupole magnet on the M9A channel failed and the run had to be terminated. This equipment has been repaired and the final production run has been tentatively scheduled for the summer of 2004. In the meantime, the data from the 2003 run are being analyzed in Kentucky.

Experiment 766

The ortho-para transition rate in muonic molecular hydrogen

(D. Armstrong, College of William & Mary)

Muon capture has long been recognized as a useful probe of the semileptonic weak interaction. The elusive pseudoscalar coupling g_p for the proton, in particular, can be measured using μ^- capture. While the theoretical expectation for the value of g_p appears robust (chiral perturbation theory results match the older current algebra predictions), the experimental situation is not as clear. The two most recent and most precise measurements for the proton appear to disagree with each other significantly. The radiative muon capture (RMC) experiment (TRIUMF Expt. 452) [Wright *et al.*, Phys. Rev. **C57**, 373 (1998)] yields a much larger value for g_p than does the late-1970s measurement from Saclay [Bardin *et al.*, Phys. Lett. **104B**, 320 (1981)], which used ordinary, non-radiative muon capture (OMC). However, both experiments used liquid hydrogen targets, and their interpretation in terms of weak couplings requires knowledge of the relative population of the muonic atomic and molecular states. In particular, λ_{op} , the transition rate between the ortho and para states of the $p\mu p$ molecule needs to be known with precision. The extracted value of g_p is changed drastically (especially for the case of the OMC experiment) depending on the value of λ_{op} assumed – see Fig. 48.

The $p\mu p$ molecule is formed almost entirely in the (excited) ortho-molecular state, and can (if the muon doesn't itself decay, or get absorbed by the proton) decay to the para-molecular ground state. This decay rate (λ_{op}) is expected to be rather slow; the best

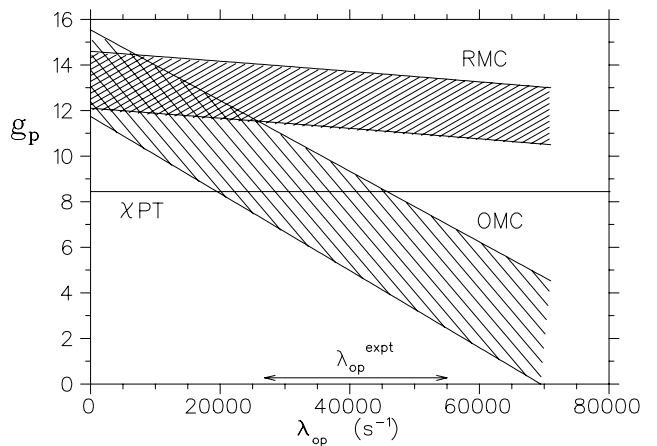


Fig. 48. The pseudoscalar coupling g_p from radiative (RMC) and ordinary (OMC) muon capture experiments vs. λ_{op} . The chiral perturbation theory (χ PT) prediction for g_p is indicated. The horizontal arrows indicate the single previous measurement of λ_{op} .

theoretical prediction $\lambda_{op} = (7.1 \pm 1.2) \times 10^4 \text{ s}^{-1}$ [Bakalov *et al.*, Nucl. Phys. **A384**, 302 (1982)] is not in good agreement with the only previous measurement which yielded [Bardin *et al.*, *op. cit.*] $\lambda_{op} = (4.1 \pm 1.4) \times 10^4 \text{ s}^{-1}$. Thus, a new measurement of λ_{op} is needed to resolve this dilemma.

Note that the RMC and OMC values could be reconciled if a sufficiently small value of λ_{op} is found (for example, they agree happily for $\lambda_{op} = 0$), however, this would imply serious problems with our theoretical understanding of g_p . Conversely, if λ_{op} is found to be significantly larger than the previous measurement, the RMC result would then be in reasonable agreement with theory for g_p , but doubt would be cast on the OMC result (OMC measurements previous to that of Bardin *et al.* had larger errors, and don't provide significant constraints on g_p).

Experimental technique

Our experiment accesses λ_{op} by measuring the time distribution of neutrons following μ^- capture in the target ($\mu^- + p \rightarrow \nu_\mu + n$). Due to the different combinations of hyperfine muonic atomic states that make up the ortho and para molecules, and the spin-dependence of the weak interaction, muon capture proceeds more rapidly from the ortho state ($\lambda_o \sim 600 \text{ s}^{-1}$) than the para state ($\lambda_p \sim 200 \text{ s}^{-1}$). Thus the time-dependence (relative to the arrival of the μ^- in the target) of the neutrons produced is not a simple exponential, but is modified by the ortho-para conversion. A fit to the time distribution allows λ_{op} to be extracted, and avoids the difficulty of determining the absolute neutron detection efficiency.

Five liquid scintillation detectors were used to detect the monoenergetic 5.2 MeV neutrons from μ^- capture on the proton. These detectors surrounded the liquid hydrogen target; the hydrogen is isotopically enriched protium to eliminate complications due to muon transfer to heavier isotopes. Plastic scintillators placed between the detectors and target allowed discrimination between neutrons and electrons from muon decay. Two independent levels of pulse-shape discrimination (PSD) in hardware and software were applied to separate neutrons from photons in the liquid scintillators. A pair of plastic scintillators in a telescope identified muons incident on the target.

The combination of TRIUMF's high duty factor and the use of multihit electronics allows us to avoid having to reject "pileup" muons. The arrival time was digitized for every muon arriving in a $32 \mu\text{s}$ window before the time of the neutron. Thus muon pileup causes a perfectly flat background to the time spectrum, and cannot cause a distortion to the time fit. Similarly, the (large) cyclotron-induced background of neutrons produced elsewhere than the target also creates a flat

background, since they are uncorrelated with a muon passing through the beam scintillators.

Data were taken in two periods (June and November, 1999) for a total of 3 weeks of beam. The analysis of these data is nearing completion.

Results

The only backgrounds that can produce anything other than a flat contribution to the time spectrum are 1) muon capture on the target walls, 2) muons that pass through the beam telescope but fail to enter the target, and 3) photons from the target that either sneak through the PSD or produce real neutrons through (γ, n) reactions. The target walls are made of Au and Ag so μ^- s stopped there are rapidly captured, thus the background is eliminated by a cut rejecting the first $\sim 500 \text{ ns}$ of the time spectrum. The second background (primarily muon capture in the final beam scintillator) was measured via empty-target runs and found to be manageable. The final background was measured by separate runs with a μ^+ beam. The primary source of photons from the target (aside from muonic X-rays, which are rejected via a prompt timing cut) is from bremsstrahlung of decay electrons, so the background remains the same for a μ^+ beam while the signal (muon capture) disappears. Again, the background was found to be small.

The 5.2 MeV neutron signal from a typical liquid scintillator is shown in Fig. 49. Electron rejection and PSD cuts have been applied, and an out-of-time background subtraction has been performed. The characteristic "box" shape of the liquid scintillator response to a monoenergetic neutron is clearly seen. The time distribution of events in the correct energy window is shown in Fig. 50, after the 500 ns wall-background cut

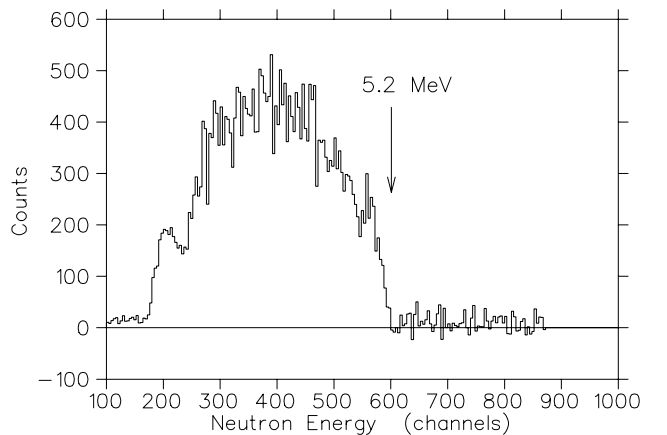


Fig. 49. Typical neutron energy spectrum, after neutron PSD cuts and subtraction of out-of-time background. The 5.2 MeV endpoint of the OMC neutron from hydrogen is indicated.

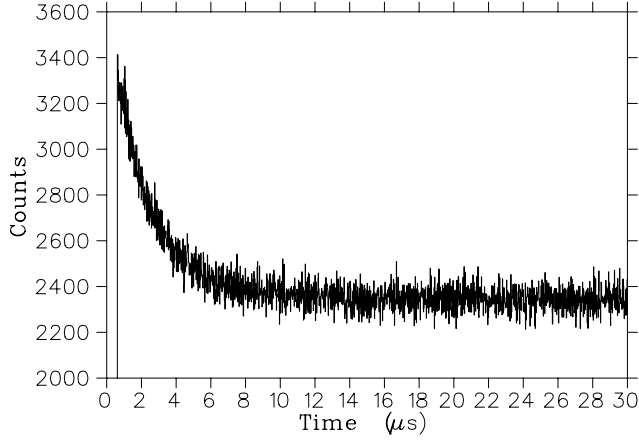


Fig. 50. Time spectrum of neutrons from μ^- capture on protium, after PSD, neutron energy, and wall-background cuts.

has been applied. The $\sim 2 \mu\text{s}$ lifetime hydrogen muon capture component is seen, superimposed on a time-independent background, as described above.

Figure 51 shows the neutron time spectrum after the flat background is subtracted. For clarity, the muon decay lifetime has been divided out. Clear evidence of the ortho-para transition is seen. The extracted value of λ_{op} is not quoted here, pending completion of careful checks of the systematic errors; final results should be available in a few months. All indications are that the result will be sufficiently precise to have a major impact in resolving the dilemma in our knowledge of the proton's pseudoscalar coupling.

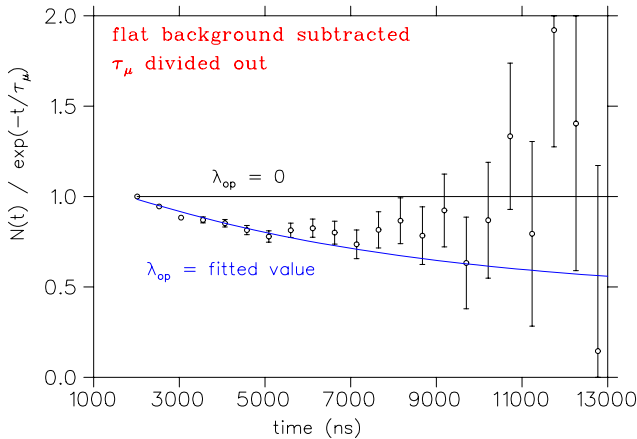


Fig. 51. Neutron time spectrum, with time-independent background subtracted, and the free muon lifetime divided out. A fit showing the functional form expected for a non-zero λ_{op} is shown, compared with the expectation for no ortho-para transfer.

Experiment 778

Pion proton cross sections in the Coulomb-nuclear interference region

(H. Denz, R. Meier, Tübingen; E.L. Mathie, Regina)

A number of quantities fundamental to the strong interaction, such as the πNN coupling constant and the sigma-term of the proton, may be extracted from pion nucleon phase shift analyses. The values of some of these quantities remain in dispute, due in part to the status of the πp database, in particular at low energies.

Cross section measurements at forward angles are typically problematic due to the overlap of scattered pions and muons arising from decays upstream. In addition the energy of recoil protons is such that they do not generally escape the target or survive out to the radius of detectors. Experiment 778 was specifically designed to determine differential cross sections of pion proton elastic scattering at low energies, in particular at small scattering angles in the so-called Coulomb-nuclear interference (CNI) region. This experiment is a complement to measurements of the πp analyzing power previously made in CHAOS Expt. 560, and recently in Expt. 862 (at higher energy).

This experiment received beam time in 1998 through 2000, using the CHAOS detector. In the interest of a well defined target thickness of high areal density protons, a planar liquid hydrogen target (developed at TRIUMF) was used. For each event, the incoming particle and the scattered pion were detected in CHAOS. The forward going proton, coincident with pions scattered to large angles, was also detected. In order to separate scattered pions at small angles from the beam halo of decay muons, forward going particles were tracked through the CHAOS wire chambers and then detected in an auxiliary detector array. A neural net, trained at each energy using multiple runs at different momenta with incident pion or muon triggers, was used to interpret the information from this array.

In total, data were taken for $\pi^\pm p$ differential cross sections at 8 energies between 15 and 67 MeV, in an angular range from 8° to 180° , with all of the low energy data obtained in M13 and the higher energy data obtained in M11. In earlier stages of the data analysis, the raw data (4.7 TB) were reduced by a factor of 10 by removing obvious decay events.

Enough disk space and computer power has been available at Tübingen to keep all of the remaining information for the M13 data sets on disk and to simultaneously analyze and simulate these data. In 2003 it became clear that the angular resolution was not sufficiently improved with tracking algorithms based upon GEANT to justify the factor of 10 penalty in analysis speed. A true 3D scattering angle determination was implemented. This is particularly important for

the forward angle results.

Studies of systematic effects, acceptance determinations and data analysis for the M13 data are virtually complete and final results for this important data set are expected in 2004. The simultaneous measurement of μp scattering with acceptances determined in the same Monte Carlo simulations gives an independent evaluation of the normalization uncertainty. Preliminary results from the analysis of the larger angle data show generally good agreement of the shape of angular distributions with current phase shift analyses at the higher measured energies, but deviate at very backward angles and low energies, more so for π^+p than for π^-p .

Experiment 823

Pure Fermi decay in medium mass nuclei

(G.C. Ball, TRIUMF)

Precise measurements of the intensities for superallowed Fermi $0^+ \rightarrow 0^+$ β -decays have provided a demanding test of the CVC hypothesis at the level of 3×10^{-4} and also led to a result in disagreement with unitarity (at the 98% confidence level) for the CKM matrix. Since this would have profound implications for the minimal standard model, it is essential to address possible “trivial” explanations for this apparent non-unitarity, such as uncertainties in the theoretical isospin symmetry-breaking correction. Uncertainties in the calculated Coulomb corrections can be studied by extending the precision β -decay measurements to heavier ($A \geq 62$, $T_z = 0$) odd-odd nuclei where these corrections are predicted to be much larger [Towner and Hardy, Phys. Rev. **C66**, 035501 (2002)]. The primary goal of the Expt. 823 experimental program is to measure the half-lives and branching ratios for the superallowed β -decay of these radioactive nuclei produced at ISAC. The early measurements have focused on ^{74}Rb (see 1999–2002 Annual Reports).

High precision measurement of the half-life of the superallowed β -emitter ^{62}Ga

A preliminary measurement of the half-life of ^{62}Ga , the first in the series of ($A \geq 62$, $T_z = 0$) odd-odd superallowed β -emitters, was carried out in the spring. A ^{62}Ga beam of $\sim 800/\text{s}$ was produced from the surface ion source using a ZrC target. Beam time was allotted near the end of the running period with this target for a preliminary half-life measurement for ^{62}Ga . By this time the target had deteriorated and the yield for the short-lived β -emitter ^{62}Ga had decreased by about a factor of 4. However, the yield was still sufficient to obtain a measurement of the half-life of ^{62}Ga with a precision of $\sim 0.16\%$. The experiment was carried out at GPS1 using the fast tape transport system. Details of this method have been described pre-

viously (see 1999 Annual Report). A total of 50 runs each with a statistical uncertainty of ~ 1.5 ms was obtained. The results are shown in Fig. 52. The long-lived (9.74 m) isobar ^{62}Cu was a significant contaminant that limited the precision of these measurements. The ratio of $^{62}\text{Ga}/^{62}\text{Cu}$ was increased by about a factor of two by operating the mass separator in high-resolution ($m/\Delta m \sim 5000$) mode. However, this also resulted in a decrease in the intensity of ^{62}Ga and therefore resulted in no real gain in the precision that could be achieved in a reasonable length of time. A preliminary analysis of these data gives a value of 116.10 ± 0.19 ms. This result is statistically consistent with all three previous measurements: 115.95 ± 0.30 ms [Alburger, Phys. Rev. **C18**, 1875 (1978)], 116.34 ± 0.35 ms [Davids *et al.*, Phys. Rev. **C19**, 1463 (1979)], and 115.84 ± 0.25 ms [Hyman *et al.*, Phys. Rev. **C68**, 015501 (2003)]. It should be possible to substantially improve the precision of the present measurement to the required precision of 0.05% once the ISAC laser ion source is operational.

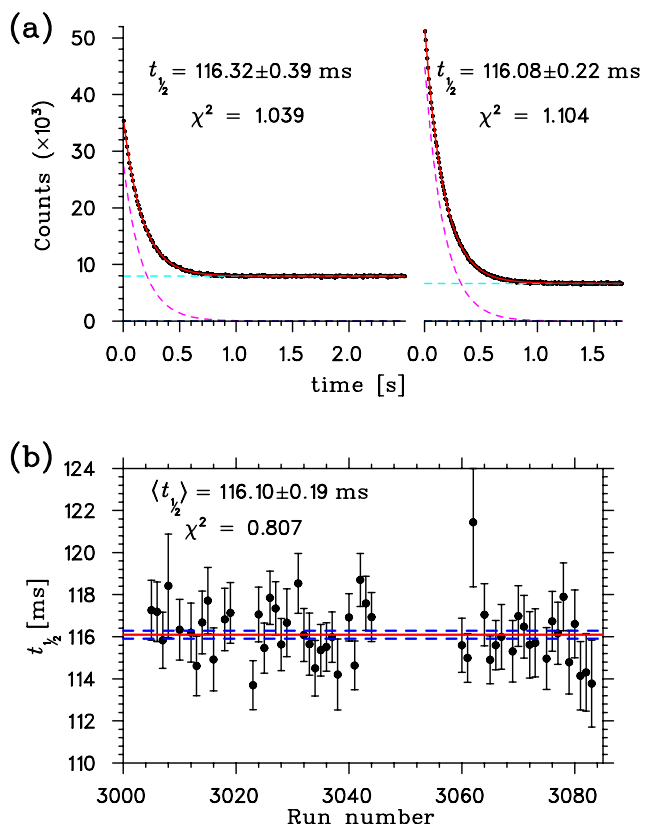


Fig. 52. a) Decay curves obtained for ^{62}Ga by summing and fitting the data obtained for all runs while operating the mass separator in low (left) and high (right) resolution modes; the long-lived background is ^{62}Cu and b) the half-life results obtained by fitting the data for each separately.

Measurement of the non-analogue $0^+ \rightarrow 0^+$ transition in $^{38\text{m}}\text{K}$

The determination of the transition strengths for non-analogue $0^+ \rightarrow 0^+$ decays provides a critical test of the model predictions for superallowed β -decays. In particular, they provide a direct measurement of the isospin-mixing component of the Coulomb correction. Recently, Towner and Hardy [*op. cit.*] have recalculated the nucleus-dependent corrections for the nine well-known superallowed β -emitters for several shell model effective interactions. The values of the square of the Fermi matrix element (δ_{C1}^1) to the first excited 0^+ state in $^{38\text{m}}\text{K}$ range from 0.062 to 0.186%.

An experiment designed to measure this weak decay branch was carried out in October, 2002. The fast tape transport system was used to collect and move the $^{38\text{m}}\text{K}$ samples out of the vacuum chamber and position them between two thin plastic scintillator paddles each backed by a Compton suppressed ($\sim 25\%$) HPGe detector from the 8π spectrometer. As a result, the sensitivity for detecting the 1209 keV γ -ray following the β -decay of $^{38\text{m}}\text{K}$ ($t_{1/2} = 0.925$ s) to the first excited 0_2^+ state in ^{38}Ar at 3377 keV was enhanced by the reduction in the background coming from the decay of the long-lived isobaric contaminant $^{38}\text{K}_{\text{gs}}$ ($t_{1/2} = 7.64$ min) which emits a 2168 keV γ -ray with a branching ratio of 99.8%. For more details see the 2002 Annual Report. The $^{38}\text{K}_{\text{gs}}$ contaminant was minimized by collecting the $^{38\text{m}}\text{K}$ samples for only 0.3 s. Unfortunately, with the ISAC TiC target used to produce the $^{38\text{m}}\text{K}$ beam, the yield of the short-lived $^{38\text{m}}\text{K}$ isomer was found to be two orders of magnitude smaller than the intensity of the long-lived $^{38}\text{K}_{\text{gs}}$. As a consequence, the ratio of the $^{38\text{m}}\text{K}/^{38}\text{K}_{\text{gs}}$ initial activities was only $\sim 4:1$ and no γ -ray peak was observed at 1209 keV. Nevertheless, from a preliminary analysis of these data the upper limit for the non-analogue $0^+ \rightarrow 0^+$ decay was found to be $<15\text{--}20$ ppm at the 90% confidence level, corresponding to $\delta_{C1}^1 < 0.22\text{--}0.29\%$.

This experiment will be repeated using the full 8π spectrometer and SCEPTAR which will give an increased β - γ coincidence efficiency of a factor of 10 and substantially improved Compton suppression since the HPGe detectors will be a factor of two further away from the source. In addition, a Ta production target operating at ≥ 40 μA will be used since recent yield measurements have shown that the ratio of beam intensities for $^{38}\text{K}_{\text{gs}}/^{38\text{m}}\text{K}$ is only $\sim 10:1$.

Experiment 824

Further measurement of the rate of the $^{21}\text{Na}(p, \gamma)^{22}\text{Mg}$ reaction

(J.M. D'Auria, SFU, for the DRAGON Collaboration)

While the main goal of Expt. 824 was completed in 2002, nevertheless, it was of interest to continue stud-

ies of the astrophysically important $^{21}\text{Na}(p, \gamma)^{22}\text{Mg}$ reaction. As described in some detail in the 2002 TRIUMF Annual Report, this reaction plays an important role in the production of the radionuclide, ^{22}Na . This isotope with a lifetime of 3.77 years, emits a γ -ray of 1.274 MeV, which should be observable by present gamma-ray telescopes. In the NeNa nuclear reaction cycle that occurs during an ONe novae stellar explosion, there should be sufficient ^{22}Na produced for such an observation according to present models of such explosive scenario. Knowledge of the various reactions, and in particular the $^{21}\text{Na}(p, \gamma)^{22}\text{Mg}$ reaction, that play a role in this cycle is quite important as this isotope has not yet been observed.

Beam time was provided in 2003 to allow a more complete study of the rate of this reaction over a wider stellar temperature range. In fact the DRAGON facility was used to study this reaction from $E_{\text{cm}} = 200$ to 1103 keV, a range covering both novae and a significant part of X-ray bursts in exploding stars. Figure 53 shows our present understanding of the levels of ^{22}Mg based primarily upon studies performed here and/or by the TRIUMF-DRAGON group elsewhere.

As was described previously, the experiment was carried out at ISAC using DRAGON. A beam of pure ^{21}Na ($q = 5^+$) with intensities up to 1×10^9 s^{-1} was delivered to the DRAGON hydrogen gas target (~ 4.6 torr). Incident beam energies were varied from ~ 215 keV/u to ~ 1.15 MeV/u to study directly radiative proton capture on states with $E_{\text{cm}} = 206$ keV to 1.101 MeV (see Fig. 53). As both the technique and some of these studies have been described in great detail elsewhere [Hutcheon *et al.*, Nucl. Instrum. Methods **A498**, 190 (2003); Bishop *et al.*, Phys. Rev. Lett. **90**, 162501 (2003); 2002 TRIUMF Annual Report; D'Auria *et al.* (submitted to Phys. Rev.)], only some of the results will be presented in this report.

Displayed in Fig. 54 are the ion energies observed with the DSSSD (double sided silicon strip detector) located at the focal plane of DRAGON. The incident ^{22}Na beam energy into the gas target was set to excite the level resonance at $E_{\text{cm}} = 738$ keV. This is a single spectra and switching on a coincidence with the prompt reaction gammas indicated that the few events above channel 2100 were due to beam pulses (leaky beam) transmitted through the separator. A total of 216 ^{22}Mg recoil events was observed for a total integrated beam on target of $1.67 \pm 0.07 \times 10^{12}$. The resulting thick target yield is $3.18 \pm 0.21_{\text{stat}} \pm 0.29_{\text{syst}} \times 10^{-10}$ per incident ^{21}Na ion, corresponding to a resonance strength, $\omega\gamma$, for the $E_{\text{cm}} = 738$ keV state in ^{22}Mg of $219 \pm 15_{\text{stat}} \pm 20_{\text{syst}}$ meV. The measured stopping cross section of ^{21}Na energies was determined as $8.74 \pm 0.39 \times 10^{-14}$ $\text{eV}/(\text{atom}/\text{cm}^2)$.

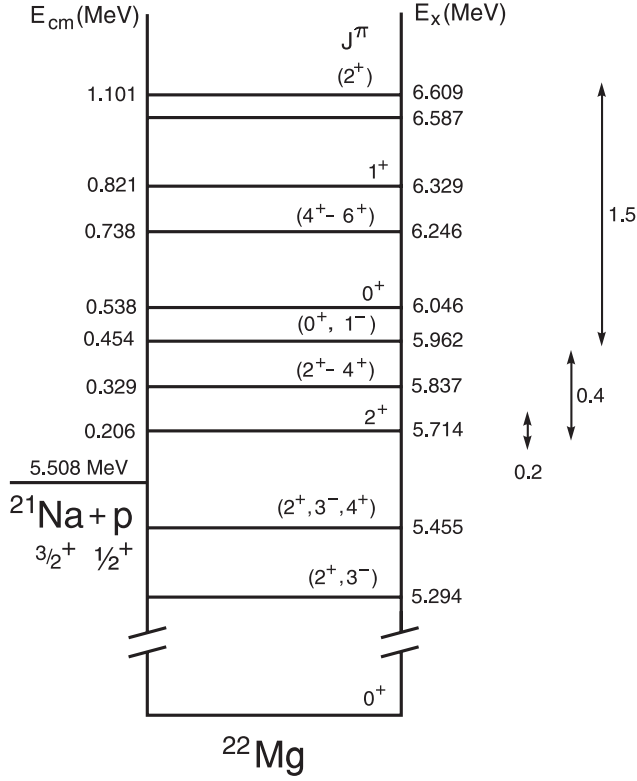


Fig. 53. Level scheme of ^{22}Mg in energy region for states of astrophysical interest.

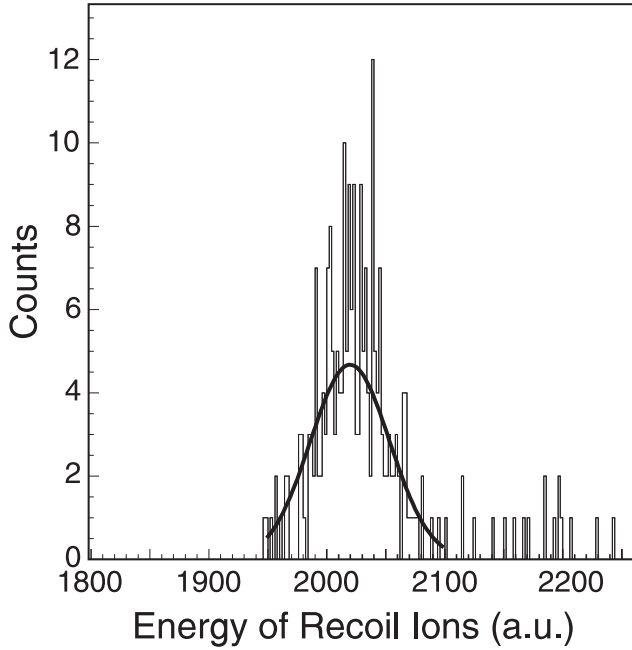


Fig. 54. DSSSD singles data for the ^{22}Mg resonance level at $E_{\text{cm}} = 738$ keV. The events above channel 2100 are from “leaky beam” events.

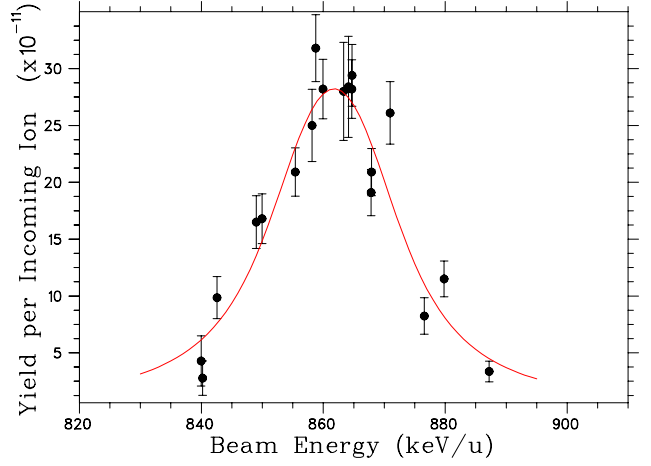


Fig. 55. Measured yield of ^{22}Mg recoils as a function of beam energy for the level resonance at $E_{\text{cm}} = 821$ keV.

The resonance at $E_{\text{cm}} = 821$ keV was studied over a range of 20 keV above and below the resonance energy. Data were analyzed in singles mode as the EMS provided suppression by a factor of $\sim 10^{11}$ of the ^{21}Na beam with respect to the recoiling reaction products. The experimental yield curve obtained for this resonance is displayed in Fig. 55 along with a least-squares fit of the thick target yield function for a wide resonance to the data. While E_{beam} , dE/dx and ΔE were measured, E_{cm} , Γ , and $\omega\gamma$ were set as free parameters in the fit. The error bars are statistical and were convoluted with an $\sim 0.2\%$ error due to the uncertainty in the incoming beam energy. To deduce the resonance widths from the fit parameter Γ , several contributions to the measured width had to be subtracted. These contributions are the (assumed) Gaussian energy spread of the beam, the broadening of the resonance due to energy straggling in the target and the zero point motion of the H_2 target molecules. The quadratic sum (3.0 keV/u) of these functions was linearly subtracted from the fitting parameter to deduce the Lorentz-shaped natural width. This result was validated through simulation calculations which included beam energy uncertainty and straggling. From the resulting fit, the resonance strength was found to be $\omega\gamma = 556 \pm 41_{\text{stat}} \pm 65_{\text{syst}}$ meV, the resonance energy $E_{\text{cm}} = 821.3 \pm 0.9$ keV, and the natural width $\Gamma = 16.1 \pm 2.8$ keV, with a reduced chi-squared value of 2.3.

The data for the 1101 keV resonance in ^{22}Mg were taken in the energy range of $E_{\text{cm}} = 1090$ to 1135 keV and were analyzed in singles mode in a manner similar to that for the 821 keV resonance. Figure 56 shows the experimental yield curve for the 1101 keV resonance in ^{22}Mg , plotted as a function of incoming beam energy. As before, a least squares fit to the thick target yield function was performed, allowing the extraction

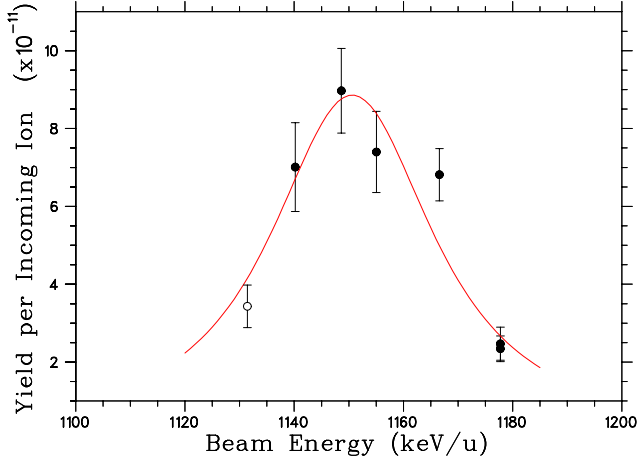


Fig. 56. The yield curve of the 1101 keV resonance as a function of incident beam energy. The lowest point is believed influenced by a neighbouring resonance and was not included in the fit.

of $\omega\gamma$, Γ , and E_{cm} . The displayed error bars arise from statistics and a similar 0.2% error in beam energy. In earlier studies of Ruiz et al. [Phys. Rev. **C65**, 042801 (2002)] there is another resonance about 20 keV lower that is believed to overlap with the low-energy tail of the 1101 resonance. Since the data were incomplete in this region, it was not possible to include this contribution. Ignoring the lowest energy yield point, the reduced chi-square for the final fit was 1.44 and the resonance strength was found to be $\omega\gamma = 368 \pm 47_{\text{stat}} \pm 41_{\text{syst}}$ meV at a resonance energy of 1101.1 ± 2.5 keV. A Γ of 30.1 ± 6.5 keV was deduced after subtracting experimental contributions.

Table VI summarizes the results of Expt. 824 with values of the energies and resonance strengths of seven resonances above the proton threshold in ^{22}Mg which are believed to play a role in novae and X-ray bursts. Errors on $\omega\gamma$ are the combined (in quadrature) statistical and systematic errors.

Figure 57 displays the respective resonant rates for each of the seven ^{22}Mg states populated in the $^{21}\text{Na}(p, \gamma)^{22}\text{Mg}$ reaction for temperatures consistent with ONe novae and X-ray bursts; an upper limit is shown for the possible resonance at 329 keV. Also

Table VI. Resonance strengths and level energies for $^{21}\text{Na}(p, \gamma)^{22}\text{Mg}$ reaction.

E_x (MeV)	E_{cm} (keV)	Γ (keV)	$\omega\gamma$ (meV)
5.714	205.7 ± 0.5		1.03 ± 0.21
5.837	329		≤ 0.29
5.962	454 ± 5		0.86 ± 0.29
6.046	538 ± 13		11.5 ± 1.36
6.246	738.4 ± 1.0		219 ± 25
6.329	821.3 ± 0.9	16.1 ± 2.8	556 ± 77
6.609	1101.1 ± 2.5	30.1 ± 6.5	368 ± 62

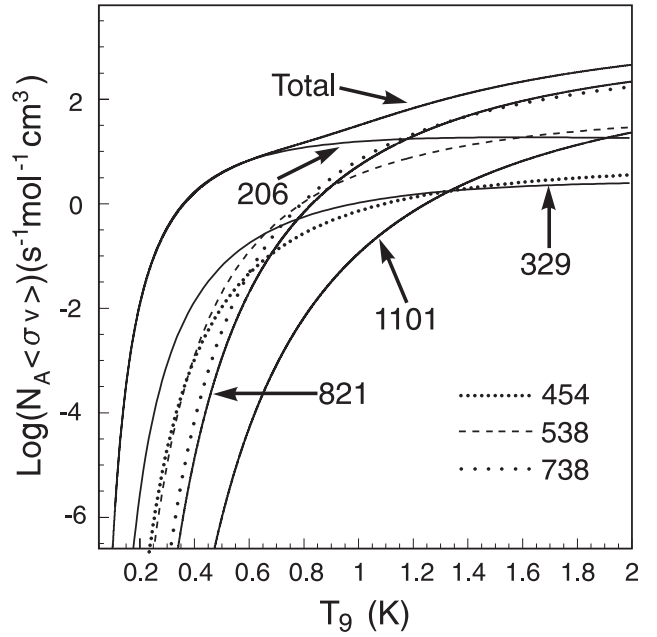


Fig. 57. Estimated reaction rate as a function of temperature based upon the resonances observed in this study. An upper limit for the possible resonance at $E_{\text{cm}} = 329$ keV was plotted.

included in the figure is the total $^{21}\text{Na}(p, \gamma)^{22}\text{Mg}$ reaction rate.

It is evident from our resonance strength measurements that the ^{22}Mg state at $E_x = 5.714$ MeV ($E_{\text{cm}} = 206$ keV) is the dominant contributor to the $^{21}\text{Na}(p, \gamma)^{22}\text{Mg}$ rate for the entire span of ONe novae temperatures ($\lesssim 0.4$ GK) and also up to temperatures of ~ 1.1 GK (X-ray burst range). The states at $E_x = 5.837$ (if it exists) and 5.962 MeV are wholly insignificant for ^{22}Na production in an ONe nova. Beyond 1.1 GK, other higher states start to play a role.

The strength of the 206 keV resonance, as determined in these studies, was used as an input into nuclear reaction network calculations of an ONe nova for purposes of the production of ^{22}Na . Abundance calculations were compared to those performed previously and it was found that the final mass fraction was reduced by 50%. This resulted from the fact that the measured $\omega\gamma_{206}$ is higher than used previously. A higher reaction rate indicates that the ^{22}Na is produced sufficiently quickly in the nova that it has time to react further, leading to its reduced presence at the end of the explosion. This could explain the lack of an observation of this radionuclide, ^{22}Na , using the discarded COMPTEL satellite. It also gives some criteria for searches with the new satellite, INTEGRAL.

In addition full hydrodynamic calculations were performed in which the role of the $^{21}\text{Na}(p, \gamma)^{22}\text{Mg}$ reaction was assessed in X-ray bursts. Basically two different models were used, one of which assumed that

the rate of the $^{21}\text{Na}(p, \gamma)^{22}\text{Mg}$ reaction was zero. The results of this calculation indicated that individual reactions do not play a critical role in X-ray burst models, except for specific rates related to potential waiting points. X-ray bursts occur at such high relative temperatures that different pathways to heavier masses are found.

Experiment 838

Double radiative capture on pionic hydrogen (RMC Collaboration)

Introduction

When negative pions are stopped in hydrogen they form pionic hydrogen atoms. These atoms can disintegrate via several modes that include the well-known processes of charge exchange $\pi^-p \rightarrow \pi^0n$, radiative capture $\pi^-p \rightarrow \gamma n$, and pair production $\pi^-p \rightarrow e^+e^-n$. However, an additional mode involving double radiative capture is expected also

$$\pi^-p \rightarrow \gamma\gamma n \quad .$$

The predicted branching ratio for double radiative capture is 5.1×10^{-5} [Beder, Nucl. Phys. **B156**, 482 (1979)], with a mechanism that is dominated by the annihilation of the stopped, real π^- on a soft, virtual π^+ , i.e. $\pi\pi \rightarrow \gamma\gamma$.

The underlying dynamics of $\pi\pi$ annihilation are rather intriguing. It led Ericson and Wilkin [Phys. Lett. **57B**, 345 (1975)] to suggest the reaction as a probe of the pion field in the nucleus, and Gil and Oset [Phys. Lett. **346B**, 1 (1995)] to suggest the reaction as a window on the $\pi\pi \rightarrow \gamma\gamma$ vertex. The possible sensitivity to the pion's polarizability of double radiative capture $\pi^-p \rightarrow \gamma\gamma n$ or radiative pion photo-production $\gamma p \rightarrow \gamma\pi n$ reaction is also of interest (see Wolfe *et al.* [Int. J. Mod. Phys. **E5**, 227 (1996)] and Drechsel and Filkov [Z. Phys. **A349**, 177 (1994)]).

Set-up

In Expt. 838 we have performed the first measurement of this rare mode of radiative capture. Our experiment was performed on the M9A beam line using the RMC spectrometer (see Fig. 58). The incoming pions were counted in a plastic scintillator beam telescope and stopped in a 2.7 l liquid hydrogen target. The outgoing photons were detected by $\gamma \rightarrow e^+e^-$ pair production in a cylindrical Pb converter and electron-positron tracking in cylindrical multiwire and drift chambers. An axial magnetic field was used for momentum analysis. The two-photon trigger was based on the hit multiplicities and the hit topologies in the trigger scintillator rings and the drift chamber cells.

A typical $\pi^-p \rightarrow \gamma\gamma n$ event is shown in Fig. 59. During our four week running period we collected

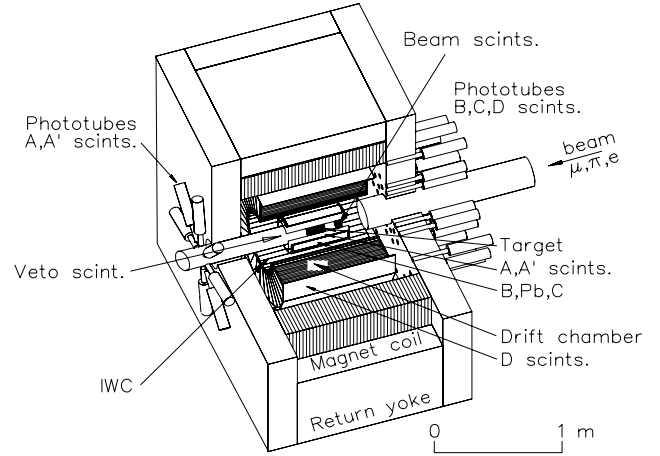


Fig. 58. The RMC spectrometer showing the hydrogen target, lead converter, cylindrical multiwire and drift chambers, trigger scintillators and spectrometer magnet.

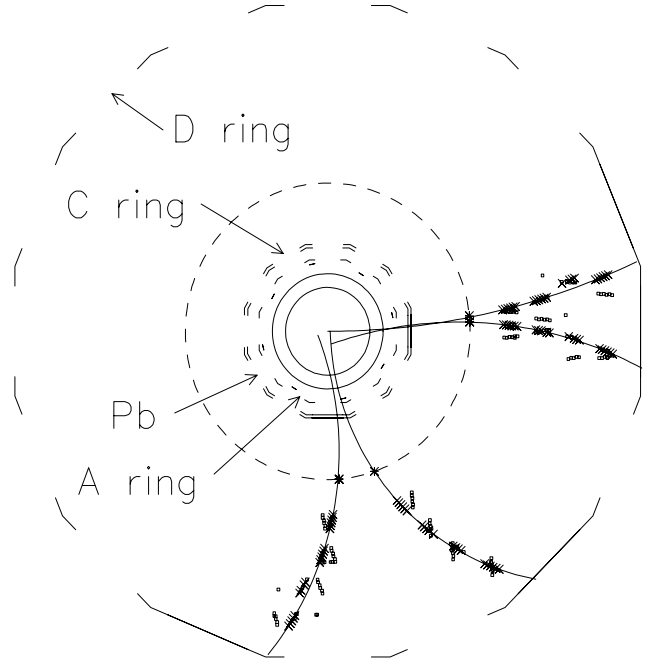


Fig. 59. A typical $\pi^-p \rightarrow \gamma\gamma n$ event. The plot shows the fit in the plane perpendicular to the beam axis. The electron-positron pairs converge at the lead converter and the reconstructed photon pairs originate from the hydrogen target located at the centre. The trigger pattern of zero hits in the A-counter ring, two hits in the C-counter ring, and four hits in the D-counter ring is also displayed.

$\pi^-p \rightarrow \gamma\gamma n$ data from 3.1×10^{11} pion stops in liquid hydrogen.

Analysis

One source of background was real $\gamma\gamma$ coincidences arising from $\pi^0 \rightarrow \gamma\gamma$ decay following $\pi^-p \rightarrow \pi^0n$ charge exchange. The π^0 s are produced by either at-rest or in-flight pion charge exchange. The at-rest source yields photon pairs with opening angles $\cos \theta < -0.91$, while the in-flight source yields photon pairs

with $\cos \theta < -0.76$. Thus a photon pair opening angle cut was necessary to separate the double radiative capture signal from the pion charge exchange background.

Another source of background was accidental $\gamma\gamma$ coincidences from simultaneous multiple π^- stops. Multiple pion stops in one beam bucket can yield a γ -ray pair by the accidental coincidence of one photon from the first pion and another photon from the second pion (via either single radiative capture or pion charge exchange). Thus a beam counter pulse height cut was necessary to separate the single pion stops from multi pion stops.

In addition, a tracking cut imposed minimum values for the number of points on the tracks and maximum values for the chi-squared of fits to the tracks, and a photon cut required that the electron-positron pairs intersect at the Pb converter and that the reconstructed photon pairs originate from the H_2 target. A total of 2.3×10^6 photon pairs passed both the tracking cuts and photon cuts, and a total of 635 events survived the opening angle cut and beam counter cut. After subtraction of residual backgrounds from $\pi^0 \rightarrow \gamma\gamma$ decay and multi- π stops, we obtained a total of 482 ± 42 $\pi^- p \rightarrow \gamma\gamma n$ events with summed energies $E_{\text{sum}} > 80$ MeV and opening angles $\cos \theta > -0.1$.

Results

To obtain the branching ratio for double radiative capture on pionic hydrogen we used the equation

$$B.R. = \frac{N_{\gamma\gamma}}{N_{\pi^-} \cdot \epsilon\Omega \cdot F \cdot c_{\text{bm}} \cdot c_{\text{stop}}}$$

where N_{π^-} is the number of lifetime-corrected pion stops, $N_{\gamma\gamma}$ is the number of background-subtracted $\pi^- p \rightarrow \gamma\gamma n$ events, and $\epsilon\Omega \cdot F$ is the detector acceptance. Note that the appropriate acceptance was obtained using Monte Carlo [Wright *et al.*, Phys. Rev. **C57**, 373 (1998); Wright *et al.*, Nucl. Instrum. Methods **A320**, 249 (1992)], with the $\pi^- p \rightarrow \gamma\gamma n$ kinematical distributions taken from Beder [*op. cit.*]. The factor $c_{\text{stop}} = 0.85 \pm 0.01$ accounts for the fraction of incident pions that stopped in hydrogen (see Wright *et al.* [*op. cit.*] for details) and the factor $c_{\text{bm}} = 0.99$ accounts for the efficiency of $\pi^- p \rightarrow \gamma\gamma n$ events passing the beam telescope cut. Using the equation above we obtained a branching ratio of $(3.05 \pm 0.27(\text{stat}) \pm 0.31(\text{syst})) \times 10^{-5}$. Note that the quoted uncertainty contains a statistical error of $\pm 8\%$ from $N_{\gamma\gamma}$ and a systematic error of $\pm 10\%$ in total. The systematic error is completely dominated by the $\pm 10\%$ uncertainty in the determination of the acceptance $\epsilon\Omega \cdot F$. The uncertainties in N_{π^-} , c_{stop} and c_{bm} were each $\leq 2\%$ and entirely negligible. We stress that the result we quote is the total $\pi^- p \rightarrow \gamma\gamma n$ branching ratio for all

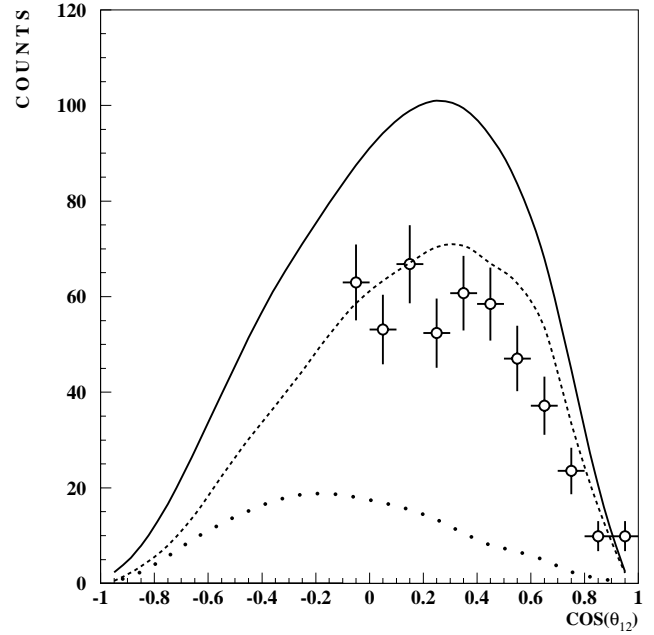


Fig. 60. Comparison of the opening angle distributions from the background subtracted experimental data (open circles) and the theoretical calculation (curves). The dashed curve is the $\pi\pi$ annihilation process, the dotted curve is the NN bremsstrahlung process, and the solid curve is the full calculation. These curves are convoluted with the response function of the RMC spectrometer.

photon energies ($0 < E_\gamma < m_\pi$) and all opening angles ($-1.0 < \cos \theta < +1.0$).

In Fig. 60 we compare our measured data with Beder's calculation [Beder, *op. cit.*]. The dashed curve assumes the $\pi\pi$ annihilation mechanism only, the dotted curve assumes the NN bremsstrahlung mechanism only, and the solid curve is the full calculation. Note that the curves have been convoluted with the response function of the RMC spectrometer. The figure shows that the $\pi^- p \rightarrow \gamma\gamma n$ branching ratio and opening angle distributions from experiment and theory are in reasonable agreement. The general consistency of experiment and theory supports the theoretical prediction of a dominant $\pi\pi$ annihilation mechanism.

However, our measured branching ratio is somewhat smaller than the theoretical branching ratio. We note that Beder's calculation was performed at tree-level and neglects contributions from pion loops, etc. We therefore speculate that higher order terms may explain the remaining difference between experiment and theory.

Significance

In summary, in Expt. 838 we have made the first measurement of double radiative capture on pionic hydrogen by recording γ -ray coincidences from π^- stops in liquid H_2 . We found the branching ratio to be $(3.05 \pm 0.27(\text{stat}) \pm 0.31(\text{syst})) \times 10^{-5}$ by assuming the

kinematical distributions from Beder [*op. cit.*]. Moreover, the measured branching ratio and opening angle distribution support the theoretical hypothesis of a $\pi\pi$ annihilation mechanism.

Experiment 862

Analyzing powers in the $\vec{p}(\pi, \pi\pi)$ reactions with CHAOS

(E.L. Mathie, Regina)

In this experiment, an attempt to use the Canadian High Acceptance Orbit Spectrometer, CHAOS, to observe at least two charged reaction products from 280 MeV negative pion interactions with polarized protons in the CHAOS polarized proton target was made. Cross section measurements for $\vec{p}(\pi, \pi\pi)$ reactions such as determined in the related CHAOS Expt. 624, have provided the best tests of the predictions of chiral perturbation theory (ChPT) in a fundamental interaction. Experiment 862 was the first (and only) attempt to measure a polarization observable in a kinematic regime which is a compromise between energies where the $\vec{p}(\pi, \pi\pi)$ cross sections are large enough and where the theory is best understood.

The polarization observable is sensitive to the spin orientation of the target proton and is defined in terms of the differential cross sections σ^+ (σ^-) for positive (negative) target polarization according to

$$A = \frac{1}{P_{\text{tgt}}} \frac{\sigma^+ - \sigma^-}{\sigma^+ + \sigma^-}$$

where P_{tgt} refers to the magnitude of target polarization and σ refers to any one of several differential cross sections which may be determined.

The polarized target was first developed for CHAOS Expt. 560. The control system was extensively changed to operate in a more modern control environment. The orientation of the proton spins is accomplished in an external, high homogeneity magnetic solenoid. The target material is first cooled to low temperatures using a helium 3-4 dilution refrigerator. Bombardment with suitably tuned microwaves induces polarization of the electron system, which is subsequently transferred to the proton system. Upon completion of this dynamic phase, the microwaves are turned off, leading to a rapid drop in temperature and the proton spin relaxation time to increase suddenly, effectively freezing the proton spin polarization. Once frozen, the target was physically moved from the polarizing solenoid above CHAOS into the spectrometer, where the normal magnetic field serves to preserve the polarization for days. During the actual movement of the target, a third small superconducting magnet, local to the target cryostat, was used to preserve the polarization. The target polarization was determined

by calibration of the NMR with the signal due to the small natural polarization arising from thermal equilibrium.

In previous pion production experiments, limitations to the maximum data acquisition rate meant the trigger had to discriminate against the prolific pion proton elastic scattering reaction. However, improvements to the CHAOS data acquisition before this experiment meant that this was no longer required, and new data for pion proton elastic scattering were simultaneously obtained. Experiment 862 received beam in the summer of 2002, however, a critical beam element degenerated and then failed completely before a significant data set of the relatively low rate $\vec{p}(\pi, \pi\pi)$ was accumulated.

During the brief period of running, data were collected for three cycles of the target polarization (both spin orientations form a cycle) and for one series of measurements with the background target configuration. This was sufficient time to produce a useful analyzing power distribution for the elastic scattering reaction, which was published in 2003; however, to date, all attempts to extract meaningful two pion distributions have failed.

Experiment 863

Ground state magnetic moments of $^{75,77,79}\text{Ga}$ (LTNO)

(P. Mantica, Michigan State)

Experiment 863 continued data-taking in 2003 with the goal of improving the statistical significance of the radiofrequency sweeps in the search for the nuclear magnetic resonance of ^{75}Ga . The experimental apparatus was improved by increasing the solid angle subtended by the β particle detectors, which consist of two plastic scintillator ΔE - E telescopes. In order to increase the count rate further, the low energy beam of ^{75}Ga was produced at the TRIUMF-ISAC facility using a 30 μA proton beam current on the Ta production target equipped with a surface ion source. The ^{75}Ga nuclei were implanted into an iron foil mounted on the cold finger inside the $^3\text{He}/^4\text{He}$ dilution refrigerator of the LTNO, which was held near 10 mK. The temperature of the cold finger was monitored by observing the γ -ray anisotropy from a ^{54}Mn thermometer sandwiched with the iron foil on the cold finger. Three HPGe detectors were placed at 0° , 180° , and 270° relative to the applied magnetic field to detect thermometer γ -rays as well as to detect γ -rays emitted from levels populated by the ^{75}Ga β -decay and subsequent decay of the daughter, ^{75}Ge . In this run as in previous runs there was no evidence of other $A = 75$ isobaric contaminants in the radioactive beam.

Polarization of ^{75}Ga was observed by detecting an

asymmetry in the emitted β particles at 0° and 180° . The polarization of ^{75}Ga was confirmed by observing an equal and opposite β asymmetry upon reversing the externally-applied magnetic field. The observed β particle asymmetry of 15% was of the same magnitude as that observed in previous runs.

Radiofrequency scans over the range 90 to 140 MHz were completed. Scans from a previous run indicated the possibility of an effect near the centre of this range and thus a major goal of the 2003 run was to look for resonant destruction of β asymmetry at a level better than 1%. The scans were performed to high precision due to the high implantation rate of ^{75}Ga and the high detection efficiency for β particles. The frequency range that was swept by the applied rf covered nuclear magnetic moment values from 1.6 to $2.5 \mu_N$. These data are currently under analysis.

Experiment 864

Measurement of the two-photon capture mode of the pionic deuterium atom

(P. Zolnierczuk, T. Gorringer, Kentucky)

To date, the only established system with a baryon number $B = 2$ is the deuteron. The experimental discovery of another dibaryon would certainly provide new insight into hadron dynamics at the GeV scale.

A recent claim for a dibaryon with mass 1956 ± 6 MeV and width ≤ 8 MeV has been published by the Di2 γ collaboration [Khrykin *et al.*, Phys. Rev. **C64**, 4002 (2001)], where they hypothesized that d^* dibaryons were first produced via the two-body process $pp \rightarrow d^*\gamma$ and then decayed via the three-body process $d^* \rightarrow pp\gamma$. Khrykin *et al.* have argued that $(J^\pi, T) = (1^+, 1)$ is the most natural choice for the d^* 's quantum numbers, being the lowest spin-isospin pp -decoupled state with zero orbital angular momentum.

Gerasimov [arXiv.org:nucl-th/9808070] suggested that double-radiative capture of pionic deuterium

$$\pi^- d \rightarrow nn\gamma\gamma$$

is an excellent candidate for further investigations of the dibaryon's existence. The $d^*(T_z = -1)$ dibaryon is first produced via radiative capture $\pi^- d \rightarrow d^*\gamma$ and then disintegrates via radiative decay $d^* \rightarrow nn\gamma$. Using a simple model, Gerasimov estimated that the branching ratio for the d^* mediated process might be as large as 0.5% exceeding by 2 orders of magnitude the expected two-photon branching ratio for non-resonant double-radiative capture in pionic deuterium.

We have found a total of 370 two-photon events (see Fig. 61) with a small opening angle between the two photons ($\cos\theta_{12} > -0.2$). This number of events should be compared to 580 ± 110 events from the non-resonant pion double-radiative capture on deuterium

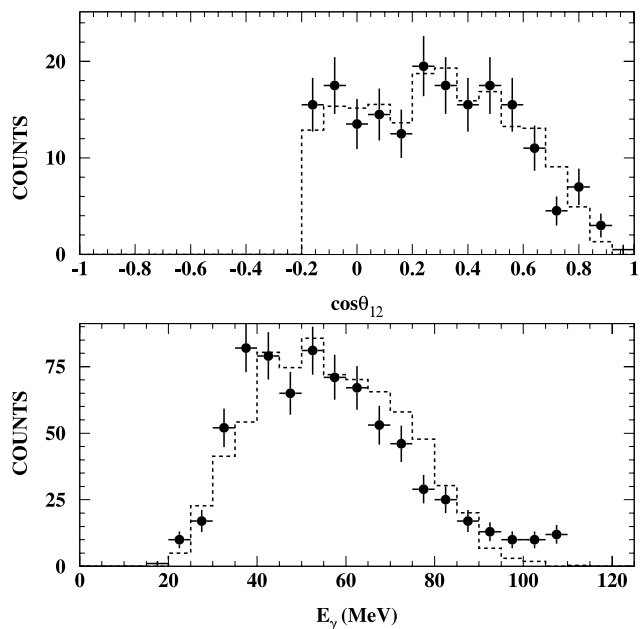


Fig. 61. The photon opening angle $\cos\theta_{12}$ (top) and summed photon energy spectra (bottom) for events passing the tracking cuts and photon cuts.

estimated using the measured branching ratio for non-resonant double radiative capture on hydrogen and assuming the ratio of single radiative capture to double radiative capture to be identical on a hydrogen target and a deuterium target. In addition, the opening angle distribution of the experimental data is consistent with the Monte Carlo simulations assuming non-resonant capture. The expected signature of dibaryon events, a monoenergetic peak from the production process $\pi^- d \rightarrow d^*\gamma$ and a three-body continuum from the decay process $d^* \rightarrow nn\gamma$, is not seen.

The resulting branching ratio upper limit on d^* production in $\pi^- d$ capture was obtained by determining the limits on the production γ -ray yield. It was found to be smaller than 6.7×10^{-6} (90% C.L.) for d^* 's in the mass range of 1920 to 1980 MeV and width of < 10 MeV (see Fig. 62).

We have found no evidence for narrow dibaryon production in $\pi^- d$ capture and in particular, we observed no evidence for a narrow dibaryon of mass $M = 1956$ MeV as claimed by Khrykin *et al.* Our upper limit on dibaryon production is several orders of magnitude below the yield estimate of Gerasimov and our null result is consistent with the null result of the WASA collaboration [Calen *et al.*, Phys. Lett. **B427**, 248 (1998)]. However, above and below the 1920–1980 MeV mass range, our experimental sensitivity rapidly deteriorates due to the energy cut-off in the spectrometer acceptance.

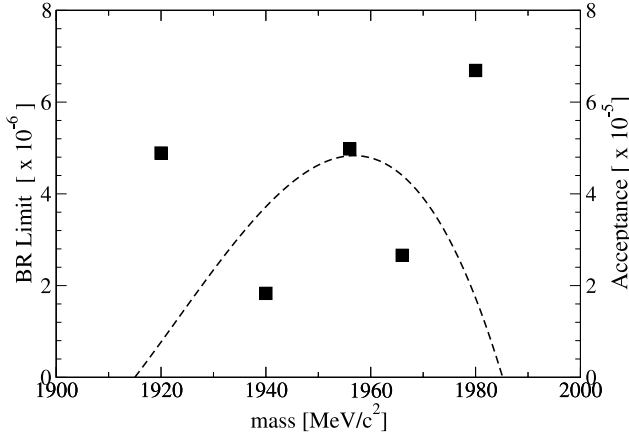


Fig. 62. The 90% C.L. dibaryon branching ratio upper limit versus the d^* mass (full squares and left-hand scale) and the Monte Carlo acceptance versus the d^* mass (dashed line and right-hand scale).

Experiment 871

Meson and quark effects in nuclear β decay of ^{20}Na

(K. Minamisono, JSPS/TRIUMF; K. Matsuta, T. Minamisono, Osaka)

In order to study the G -parity irregular term in the weak nucleon current, the alignment correlation term in the β -ray angular distribution from nuclear-spin aligned ^{20}Na ($I^\pi = 2^+$, $T_{1/2} = 449.7$ ms) has been measured for the first time. A large enhancement of the present result over the value calculated by the impulse approximation (IA) was preliminarily obtained and a discrepancy between the present result and β - γ angular correlation experiments was observed, which implies the importance of the contribution from higher order terms. In order to extract the very small G -parity violating induced tensor term, the alignment correlation term of the mirror partner, ^{20}F , has to be measured. In the process of measuring the alignment correlation term, we developed the technique of polarizing Na isotopes by the colinear laser pumping method and studied the hyperfine interaction of Na isotopes in several materials and measured the quadrupole moments of $^{20,21}\text{Na}$, which are also reported here.

Atomic polarization of Na isotopes

For the measurement of the alignment correlation term, we first developed the method of polarizing Na isotopes. The experiment was performed at the ISAC radioactive beam facility. For the production of $^{20,21}\text{Na}$ ($^{26,28}\text{Na}$) ions, the 500 MeV proton beam from the TRIUMF cyclotron was impinged on a thick SiC (Ta) production target, which was coupled to the surface ionization source. Na ions were extracted at an energy of 40.8 keV, mass separated, and transported to the polarizer beam line where they were polarized by the colinear laser pumping method. The atomic polarization

of neutralized Na atom passing through Na vapour cell was produced by pumping Na atoms on the D_1 transition ($3s\ 2S_{1/2} \leftrightarrow 3p\ 2P_{1/2}$) with circularly polarized laser light. Both ground state hyperfine levels ($3s\ 2S_{1/2}$ $F = I \pm 1/2$) were pumped to achieve high polarization using electro-optic modulators (EOM). Essentially the same technique was used as that developed for other experiments [Levy, Proc. 9th Int. Workshop on Polarized Source and Targets (World Scientific, 2002) p.334]. The optical pump laser was a Coherent 899-21 frequency stabilized dye ring laser pumped by a 7 W argon-ion laser. In order to compensate for the Doppler shift, the beam energy was scanned by changing the bias voltage of the Na vapour cell.

The atomic polarization was not measured, but we measured the nuclear polarization of Na isotopes by implanting Na ions into single-crystal NaF (cubic), which is known to keep the polarization well under a strong magnetic field. The nuclear polarization was checked by comparing the β -ray asymmetric angular distribution, $W(\theta) \sim 1 + A\mathcal{P}\cos\theta$, obtained with positive-helicity laser light compared to that with negative helicity. Here, θ is the angle between the direction of the β -rays and the orientation axis, A the asymmetry parameter, and \mathcal{P} the polarization. A typical result of laser pumping for ^{20}Na is shown in Fig. 63. In the

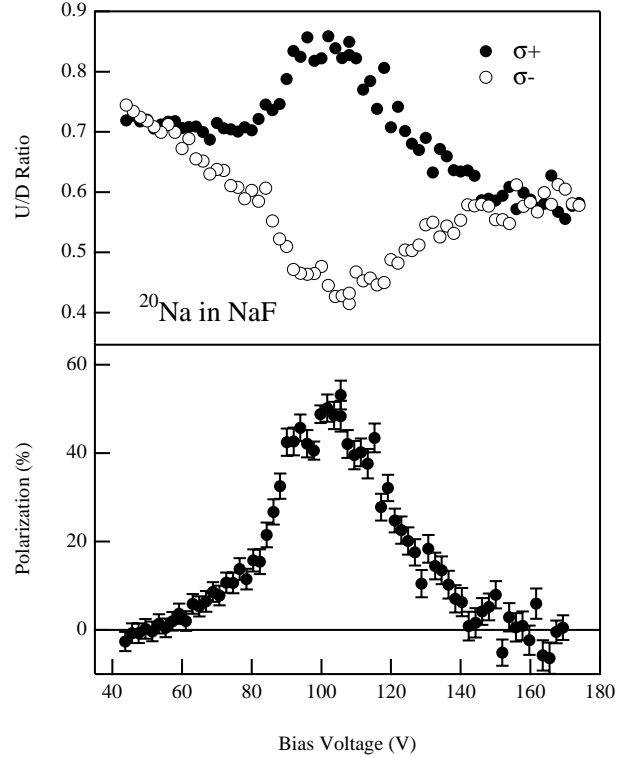


Fig. 63. Result of laser pumping method for ^{20}Na in NaF. In the upper part, the β -ray counting ratio between counters placed 0° (U) and 180° (D) relative to the polarization direction is shown. In the lower part, the deduced polarizations are shown, where $A = 1/3$ was assumed.

upper part, the β -ray counting ratio between counters placed 0° (U) and 180° (D) relative to the polarization direction is shown for the positive (σ^+) and negative (σ^-) laser helicities. In the lower part, the deduced polarizations are shown, where the asymmetry parameter $A = 1/3$ was assumed. A large polarization ($\sim 50\%$) has been achieved.

Hyperfine interaction

For the creation of a nuclear alignment to measure the alignment correlation term, the spin manipulation technique was applied; an artificial interchange and/or equalization of the population of the magnetic sub-levels, which is described below. For the spin manipulation, the Na atoms were implanted into a single crystal which has a proper electric field gradient q , under a strong magnetic field H_0 . The quadrupole interaction between q inside the crystal and the quadrupole moment Q of the nucleus, superposed on the magnetic interaction between the magnetic moment μ of the nucleus and H_0 , changes the energy of each magnetic sub-level as

$$E_m = -h\nu_L m + \frac{h\nu_Q}{12} (3\cos^2\beta - 1) \{3m^2 - I(I+1)\},$$

so that the single NMR frequency splits into $2I$ lines depending on the nuclear spin I , which correspond to the energy intervals of the magnetic sub-levels. Here, m is the magnetic sub-level, ν_L the Larmor frequency, $\nu_Q = 3eqQ/\{2I(2I-1)h\}$, and the asymmetry parameter of q is assumed to be symmetric. Under these conditions, a transition between two adjacent magnetic sub-levels can be selectively induced by applying an rf field (NMR).

An accurate knowledge of the quadrupole interaction is required for a reliable spin manipulation and thus the selection of the catcher, particularly for ^{20}Na , was one of the important keys for the measurement of the alignment correlation term. For this purpose, we tested several catchers and measured the polarization retained in the catcher and the relaxation time of the polarization. A typical result for the relaxation of ^{20}Na polarization is shown in Fig. 64. We found that ZnO and Mg, which have a proper electric field gradient for the spin manipulation of ^{20}Na , can retain the polarization with long relaxation times and that Pt can retain the polarization even better. The polarization of Na isotopes measured at ISAC is summarized in Table VII.

Quadrupole moments of $^{20,21}\text{Na}$

Introduction In the process of developing the spin manipulation technique for ^{20}Na , the electric quadrupole coupling constant was measured, from which the quadrupole moment can be extracted.

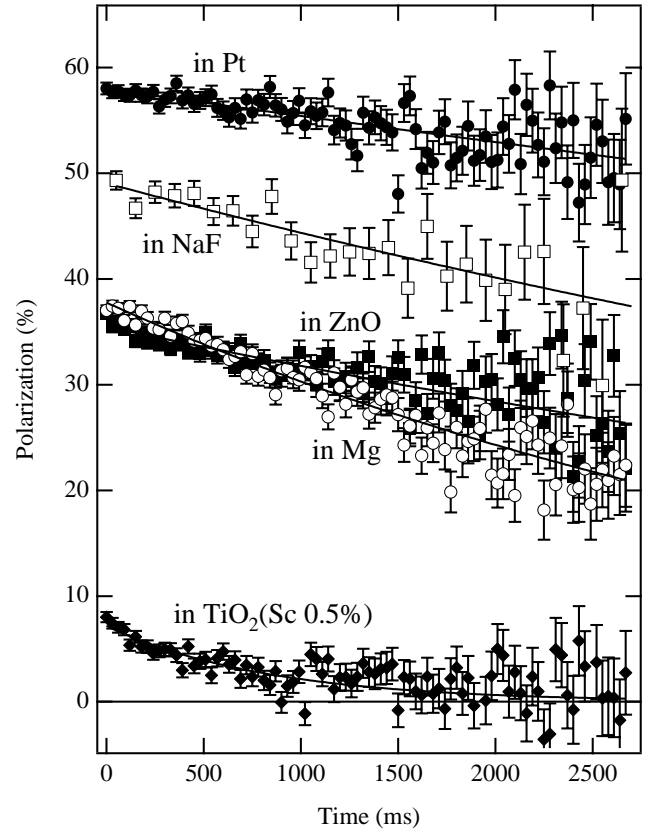


Fig. 64. Relaxation of ^{20}Na polarization in several catchers. The lines are the results of fits.

The quadrupole moments of long chains of Na isotopes have been measured in the experiment of on-line laser spectroscopy of hyperfine structure of the $3p\ ^2P_{3/2}$ state (D_2 line) [Touchard *et al.*, Phys. Rev. **C25**, 2756 (1982)] and in the β -NMR experiment [Keim *et al.*, Eur. Phys. J. **A8**, 31 (2000)]. However, some of the quadrupole moments have not been measured or have been measured with poor statistics. Since the quadrupole moment is very sensitive to a halo structure outside the spherical core, it is very important to have reliable values of the quadrupole moments. In the present study, the electric quadrupole coupling constants, eqQ/h , of $^{20,21}\text{Na}$ in single-crystal ZnO(hcp) were measured. Previously their quadrupole moments have been known only preliminarily or with poor statistics.

Results and discussion By applying the spin manipulation technique, nuclear quadrupole resonance (NQR) spectra of $^{20,21}\text{Na}$ in ZnO were measured as shown in Fig. 65. Here full circles are the data of ^{20}Na and open circles of ^{21}Na . The solid line is the result of a fit to the ^{20}Na data and the broken line for ^{21}Na . In the experiment, the crystalline c -axis was set perpendicular to the external magnetic field. Through the adiabatic fast passage method in NMR, the direction

Table VII. Measured polarization of Na isotopes at ISAC. The catchers indicated by stars were newly tested since last year's Annual Report. Here A is the asymmetry parameter, which is the integrated value of all measured decay branches, AP the typical measured asymmetry, T_1 the spin-lattice relaxation time, P_0 the initial polarization corrected for A and T_1 , eqQ/h the electric quadrupole coupling constant, and η the asymmetry parameter of the electric field gradient. For ZnO and Mg, $\eta = 0$ is assumed because of the symmetric crystal structure.

Catcher		^{20}Na	^{21}Na	^{26}Na	^{28}Na
	$T_{1/2}$	447.9 (ms)	22.49 (s)	1.072 (s)	30.5 (ms)
	I^π	2^+	$3/2^+$	3^+	1^+
	A	0.33	0.81	-0.94	-0.76
NaF	AP (%)	16.0 ± 0.4	20.8 ± 0.2	-46.6 ± 1.1	-35.9 ± 2.5
(cubic)	T_1 (s)	9.9 ± 3.1	9.0 ± 0.2	24.6 ± 4.2	—
	P_0 (%)	51.0 ± 1.3	33.5 ± 0.5	52.8 ± 1.3	47.3 ± 3.3
TiO ₂	AP (%)	5.3 ± 0.3	13.7 ± 0.3	-44.8 ± 0.5	-34.1 ± 2.5
(rutile)	T_1 (s)	3.4 ± 1.3	13.0 ± 0.5	32 ± 11	—
	P_0 (%)	18.3 ± 1.5	24.0 ± 0.5	46.8 ± 0.9	44.9 ± 3.3
	$ eqQ/h $ (MHz)	—	5.20 ± 0.03	—	—
	η	0.33 ± 0.03		—	—
LiNbO ₃	AP (%)	4.3 ± 0.3	5.3 ± 1.6	-40.4 ± 0.6	-26.3 ± 3.0
(ilmenite)	T_1 (s)	1.8 ± 0.5	1.3 ± 0.3	5.3 ± 0.5	—
	P_0 (%)	17.0 ± 1.7	56 ± 28	51.8 ± 1.5	34.7 ± 4
MgF ₂ *	AP (%)	—	—	-18.6 ± 0.6	—
(rutile)	T_1 (s)	6 ± 3	—	7.4 ± 2.0	—
	P_0 (%)	8.4 ± 0.6	—	22.3 ± 1.3	—
ZnO*	AP (%)	—	—	—	—
(hcp)	T_1 (s)	9.0 ± 0.5	9.63 ± 0.09	—	—
	P_0 (%)	35.5 ± 0.2	22.0 ± 0.1	—	—
	$ eqQ/h $ (kHz)	$683.7 \pm 2.7 \pm 5.3$	$939.3 \pm 1.9 \pm 8.2$	—	—
	η	0		—	—
Mg*	AP (%)	—	—	—	—
(hcp)	T_1 (s)	4.5 ± 0.1	—	—	—
	P_0 (%)	37.8 ± 0.2	—	—	—
	$ eqQ/h $ (kHz)	36.75 ± 0.06	—	—	—
	η	0		—	—
Pt*	AP (%)	—	—	-14.5 ± 0.4	—
(ccp)	T_1 (s)	22 ± 2	—	0.78 ± 0.08	—
	P_0 (%)	58.0 ± 0.1	—	55.0 ± 5.9	—

of polarization was reversed by applying a set of rf values, with both frequency (± 20 kHz and ± 50 kHz for ^{20}Na and ^{21}Na , respectively) and amplitude modulated. Since we measured the NQR spectra both with the positive-helicity laser light (σ^+) and with the negative helicity (σ^-) for the laser pumping method to produce the atomic polarization, we define the effective asymmetry change as the difference between the measured asymmetry change with σ^+ and that with σ^- as effective $AP \equiv AP(\sigma^+) - AP(\sigma^-)$, in order to maximize the NMR signal so that a reliable measurement was performed.

At first, a two component gaussian was fitted to the NQR spectrum of ^{21}Na in ZnO. We found two resonances, which may be caused by two final locations of Na isotopes in ZnO or other reasons. We call the larger resonance main and the smaller one sub. A

constant asymmetry change was observed because the transition between $m = -1/2 \leftrightarrow 1/2$ was always induced ($I = 3/2$) owing to the multi-rf technique. In the analysis of ^{20}Na in ZnO, the ratio of the main and sub resonances of ^{21}Na in ZnO was used because the measurement of the sub resonance of ^{20}Na in ZnO was not completed. The results are summarized in Table VIII together with a theoretical prediction and the quadrupole moments reported before. The second errors in the present results are the systematic errors owing to the unknown origin of the sub resonances. Here, one tenth of the width of the main resonance is considered as the systematic error and the error for the ratio $R \equiv Q(^{20}\text{Na})/Q(^{21}\text{Na})$ is a total error. The theoretical values are calculated by the shell model code OXBASH [Brown *et al.*, MSUCL Rep. N. 524] with *sd* model space, which reproduces the present experimental

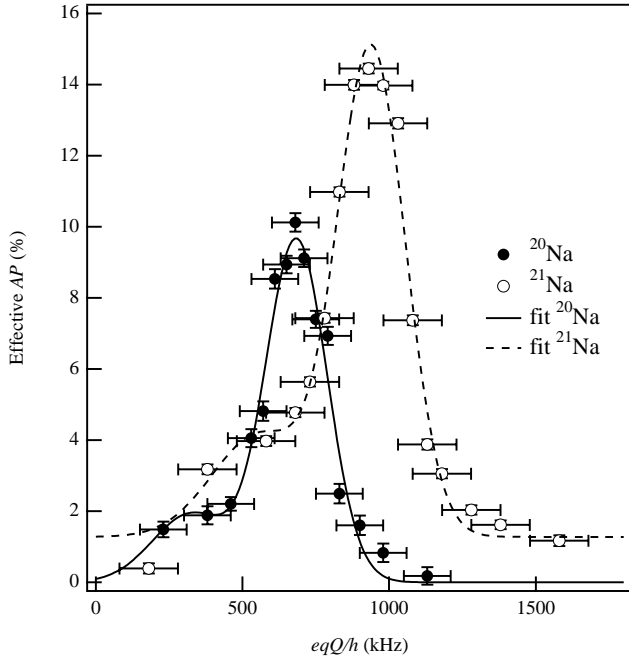


Fig. 65. Electric quadrupole resonance spectra of $^{20,21}\text{Na}$ in ZnO. The full circles are the data of ^{20}Na and open circles of ^{21}Na . The solid line and broken line are the results of fits.

Table VIII. Electric quadrupole coupling constants of $^{20,21}\text{Na}$ in ZnO. R is defined by the ratio between quadrupole moments of $^{20,21}\text{Na}$ as $R \equiv Q(^{20}\text{Na})/Q(^{21}\text{Na})$. The theoretical values were calculated by OXBASH. For experimental values see the text.

	^{20}Na	^{21}Na
$ eqQ/h $ (kHz)	683.7 ± 2.7 ± 5.3	939.3 ± 1.9 ± 8.2
R	0.728 ± 0.009	
$Q_{\text{theor.}}$ (mb)	+84	+110
R	0.76	
$Q_{\text{exp.}}$ (mb)	90 ± 10	61 ± 39
R	1.48 ± 0.96	

ratio of the quadrupole moments. Since the experimental quadrupole moment of ^{20}Na was taken from a figure in Keim *et al.* [ENAM98 (AIP **445**, 1998) p.50], it should be considered as preliminary data. The quadrupole moment of ^{21}Na was measured in Touchard *et al.* [Phys. Rev. **C25**, 2756 (1982)]. In Table VIII, a reanalyzed value of $Q(^{21}\text{Na})$ by the latest reference value of the hyperfine coupling constant $A(^2P_{3/2})$ and the quadrupole moment of ^{23}Na [Wo Yei *et al.*, Phys. Rev. **A48**, 1909 (1993); Jonsson *et al.*, Phys. Rev. **A53**, 4021 (1996)] is listed. For the first time, we determined the ratio of $Q(^{20}\text{Na})/Q(^{21}\text{Na})$ within $\sim 1\%$ relative error. In order to extract the quadrupole moment from the present electric quadrupole coupling constant, the reference value of the electric quadrupole coupling

constant, with well known quadrupole moment, will be measured.

Alignment correlation term of ^{20}Na

Introduction G parity is one of the important symmetries to be tested in the parity violating weak nucleon current. G operation is a product of the charge conjugation and the charge symmetry. It is a parity operation in the charge space. Many experimental and theoretical works have been performed and it was shown that there is no large G parity violation in the weak nucleon current. However, there still remains a possible small violation caused by the mass difference between the proton and neutron, or more fundamentally, between the up and down quarks inside the nucleon, or other reasons. A recent review can be found in the paper [Wilkinson, Eur. Phys. J. **A7**, 307 (2000)]. For this purpose, a high measurement experiment of the alignment correlation terms in the mass $A = 12$ system was performed by the Osaka group [Minamisono *et al.*, Phys. Rev. **C65**, 015501 (2002)]. In order to search for such a small G parity violating term, we need to extend the experiment to a variety of mass systems so that possible nuclear structure effects are eliminated. In the present study, the alignment correlation term of ^{20}Na in the $A = 20$ system was measured for the first time.

The β -ray angular distribution from an oriented nucleus is given by $W(E, \theta) \sim 1 + \mathcal{P}\hat{B}_1(E)P_1(\cos\theta) + \mathcal{A}\hat{B}_2(E)P_2(\cos\theta)$, where E is the β -ray energy, θ the angle between the direction of the β -ray and the orientation axis, \mathcal{P} the polarization, \mathcal{A} the alignment, $\hat{B}_1(E)$ the polarization correlation term and $\hat{B}_2(E)$ the alignment correlation term given by $\hat{B}_2(E) = -2\hat{H}_2(E, 0)/3$ [Holstein, Rev. Mod. Phys. **46**, 789 (1972)], where

$$\hat{H}_2(E, s) = \frac{E}{2M} \left(1 - \frac{d \pm d_{\text{II}}}{c} \pm \frac{b}{c} + (-1)^s \delta(E) \right).$$

Here \pm is for the electron and positron decays, respectively, M the nuclear mass, b the weak magnetism, c the Gamow-Teller matrix element, d the time component in the main axial vector current, d_{II} the G parity irregular induced tensor term and $\delta(E)$ the contribution from higher order matrix elements. Taking advantage of the symmetry between mirror β -decays, d_{II} can be extracted from the difference of the alignment terms as $\hat{B}_2(E)_{^{20}\text{F}} - \hat{B}_2(E)_{^{20}\text{Na}} = -2E(b - d_{\text{II}} - \Delta\delta(E))/(3Mc)$, where $\Delta\delta(E) = (\delta(E)_{^{20}\text{F}} - \delta(E)_{^{20}\text{Na}})/2$.

The angular correlation between the β -ray and subsequent γ -ray from the first excited state in ^{20}Ne to its ground state has also been used to test G symmetry. If we express the β - γ angular correlation as $W(\theta_{\beta\gamma}) = 1 + a(E)\cos\theta_{\beta\gamma} + p(E)\cos^2\theta_{\beta\gamma}$, the counterpart of the alignment correlation term is given by

$p(E) = \hat{H}_2(E, 1)/2$. Thus, these two experiments have different contributions from higher order terms, which provide us a chance to cancel the higher order term.

Spin manipulation In the present experiment, a single crystal ZnO (hcp) was used as a catcher. The polarized ^{20}Na were implanted into ZnO placed at the centre of an NMR magnet made of permanent magnet material (5250 Oe at the centre and parallel to the polarization). In ZnO, $(35.5 \pm 0.2)\%$ polarization and $T_1 = 9.0 \pm 0.5$ s were observed, as seen in Fig. 64. The spin manipulation and the measurement of the β -ray energy spectrum from the aligned nucleus were performed in accordance with a timing program. A typical result of the spin manipulation is shown in Fig. 66. A pulsed beam method was employed. After the beam was chopped, the polarization in counting section named I was converted into alignment in section III and back again to polarization in section V. Because we can't directly measure the degree of alignment, we calculated it from the polarization in sections I, II, IV, V and the efficiency of the spin manipulation, which was measured in a separate run. In section VIII, the alignment was created, which has an opposite sign to the alignment created in section III. The vertical lines in the figure are to guide the eye. The full circles

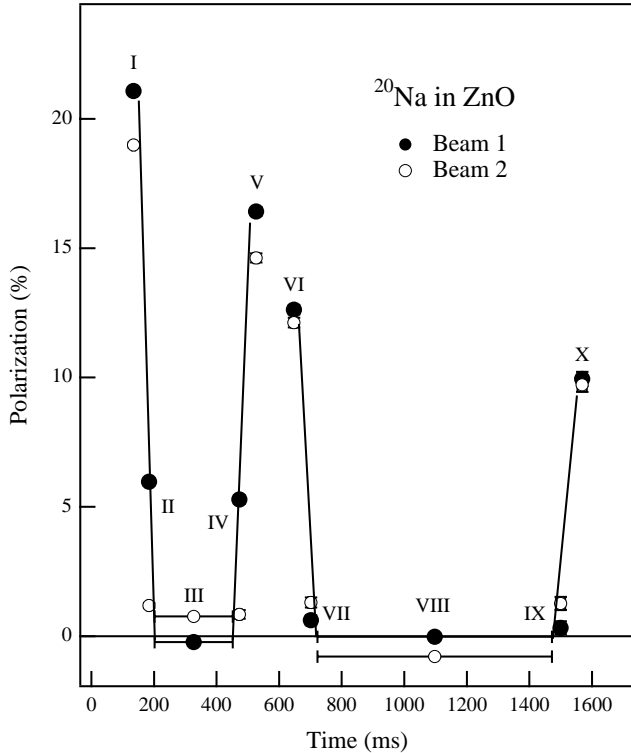


Fig. 66. Result of the spin manipulation of ^{20}Na in ZnO. The polarization change as a function of time is shown. At time zero, the beam was stopped. Roman numerals are the names of counting sections. The vertical lines are to guide the eye.

are the beam cycle named 1, in which the alignments were created in an order of minus to plus in sections III and VIII, respectively. In order to compensate for the relaxation of the polarization and alignment, the alignments were created in a different order in beam cycle 2, which is shown by the open circles. They constitute one cycle and the cycle was repeated until the required statistics were achieved.

Results and discussion From the ratio of β -ray counts between these positive and negative alignments, the alignment correlation terms were extracted as

$$\hat{B}_2(E) \sim \frac{1}{\hat{A}} \left(\frac{N(\mathcal{A}_1^+, E)}{N(\mathcal{A}_2^-, E)} \frac{N(\mathcal{A}_2^+, E)}{N(\mathcal{A}_1^-, E)} - 1 \right)$$

with

$$\hat{A} = \mathcal{A}_1^+ - \mathcal{A}_2^- + \mathcal{A}_2^+ - \mathcal{A}_1^-.$$

Here, \mathcal{A}_i^\pm is the degree of positive or negative alignment in beam cycle i and $N(\mathcal{A}_i^\pm, E)$ the β -ray counts from the aligned nucleus. By extracting the alignment correlation term from the ratio, we do not need to normalize the β -ray counts by the beam current so that the systematic error could be reduced. The obtained alignment correlation terms are shown in Fig. 67, where systematic corrections were applied for each data point.

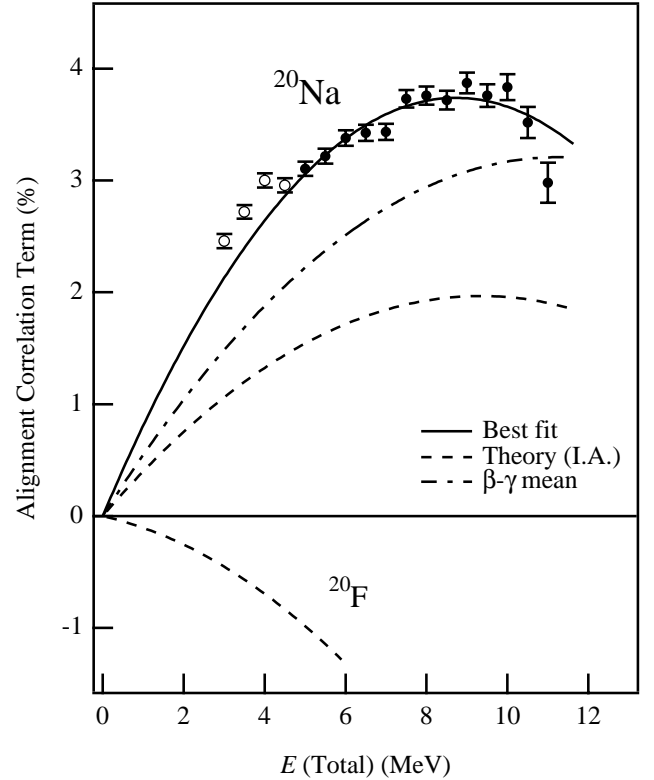


Fig. 67. Alignment correlation terms of ^{20}Na . The full circles were used for the fit and open circles were not. The solid line is the fit, the broken lines are theory(IA) and the dotted broken line is the result of β - γ angular correlation experiments.

In the figure, full circles were used for the fit and open circles were not because of a large scattering effect on the surface of the catcher. The solid line is the result of the fit and the broken lines are the theoretical predictions based on the IA [Calaprice *et al.*, Phys. Rev. **C15**, 2178 (1977)]. Together with the present result, the result of a fit of three existing β - γ angular correlation experiments [Dupuis-Rolin *et al.*, Phys. Lett. **79B**, 359 (1978); Tribble *et al.*, Phys. Rev. **C23**, 2245 (1981); Rosa *et al.* Phys. Rev. **C37**, 2722 (1988)] is shown by the dotted broken line, where the original β - γ angular correlation data were multiplied by $-4/3$ to plot the result of the fit in the figure. We found a huge enhancement in the present data compared with the theoretical calculation based on the IA, which might be explained by including meson exchange effects inside the nucleus as indicated in the result of the experiment on the alignment correlation term in the $A = 12$ system [Minamisono *et al.*, Phys. Rev. **C65** 015209 (2002)]. We also found a discrepancy between the present result and the result of β - γ angular correlation experiments. The contribution from higher order terms $\delta(E)$ should be considered in the analysis. Detailed analysis of systematic corrections and errors is now in progress. In order to reduce the scattering effect on the surface of the catcher, which has one of the largest contributions to the systematic errors, a new run with thin single crystal Mg is planned. For the extraction of very small f_T , the alignment correlation term of the mirror partner, ^{20}F , has to be measured.

Experiment 875

MuScat: muon scattering in low Z materials for muon cooling studies

(R. Edgecock, RAL)

Introduction

An important requirement of the Neutrino Factory accelerator complex is the ability to cool the muons in the transverse plane. Without this, it is likely the neutrino intensity will be considerably smaller than required for the physics program. Due to the muon lifetime, such cooling needs to be fast and the currently preferred technique is ionization cooling. In the case of the transverse cooling required for a Neutrino Factory, this involves passing the muons through an absorber in which they lose both longitudinal and transverse momentum. The lost longitudinal momentum is then restored using rf cavities following the absorber.

As well as a cooling effect coming from the ionization energy loss, there is heating coming from multiple scattering and the final cooling achieved is a balance between these. Theory suggests this balance is most favourable for elements with low atomic number, in particular, liquid hydrogen. However, an extensive

literature search has failed to find any measurements of the muon scattering distribution in light elements. The most relevant data found come from the scattering of 2.7 MeV/c electrons on Al, Be and Li. These data show a clear trend: as Z decreases, the agreement with Moliere theory gets worse. If this trend continues to hydrogen, there will be two effects:

- The level of cooling achieved would be less than expected.
- Due to the increased scattering in the tails, the fraction of muons scattered out of the cooling channel could be much bigger than expected.

Due to the importance of this to ionization cooling, the MuScat experiment has been created to measure the scattering of muons of various momenta in a number of low atomic number materials, in particular liquid hydrogen. As well as checking these observations, MuScat will compare a range of muon scattering models with the data.

A four week test period was allocated to the MuScat experiment in the M11 beam line at TRIUMF in June and July, 2000 and much was learnt about the experiment during this time. As a result, a number of changes were made and an improved version of the experiment was constructed. This was tested with cosmic rays and a proton beam at RAL at the end of 2002 and then sent to TRIUMF at the beginning of 2003. Time was allocated in the M20 beam line in April and May, 2003.

The following sections will describe the improved version of the experiment, the running in TRIUMF and the status of the analysis of the data. The aim is to have the analysis finished for NuFact'04 in Japan.

M20 beam line

The M20 beam line is a quadrupole muon decay channel, employing two bending magnets with quadrupole transport between them. This allows a dramatic reduction in the background to muons by selecting different momenta for the two bends and using a momentum slit in the quadrupole channel. By using forward decay pions, a muon beam up to almost 180 MeV/c is possible and this is how the beam line was used by MuScat. It should be noted that it is normally used for "surface" muons and was not used in the forward decay mode for 20 years before MuScat arrived!

The experiment

As the aim of the experiment is to make a precise measurement of the multiple scattering of muons, the amount of material that the muons must pass through has to be kept to a minimum. For this reason, it is not possible to do any tracking before the target and a collimation system is employed to reduce the beam

dimensions so that the incoming particle position is known accurately enough. In addition, the measurement of the position of the scattered muon relies on the first tracking detector as all subsequent detectors are affected by scattering in the first. Any additional detectors are only used to aid in noise rejection and for checking systematics. To minimize scattering in air, as much of the experiment as possible is mounted in vacuum. Finally, to eliminate particles other than muons, a good time-of-flight system is required.

The detector designed to satisfy these requirements and used in the M20 beam in 2003 is shown in Fig. 68. The most upstream parts are a veto shield and veto scintillator to eliminate beam halo. These are followed by the first trigger counter, which also acts as the TOF start. This is built from two fingers of scintillator, each 1 mm thick, 28 mm long and 3 mm high. These overlap by 20 mm in length and 3 mm in height. The timing resolution is about 250 ps. The TOF stop comes from the following rf-bucket of the cyclotron. This is almost a square-wave of length 1.9 ns, the smearing of the edges corresponding to a resolution of about 500 ps.

This trigger scintillator is followed by a 1 m long vacuum tube containing the collimation system. This consists of a 40 mm thick lead block at the front and a 160 mm lead block at the back, with two 10 mm disks behind the front collimator and another two in front of the back collimator. The first block has a slit 20 mm long by 2 mm high cut in it, while the slit in the second block is tapered to prevent large angle scatters off the internal face. With this arrangement, the scattering distribution is measured vertically, in the narrow direction of the slot. The second dimension is longer to increase the particle intensity. There are also two pairs of intermediate blocks each 10 mm thick with larger slits in them to prevent scattering off the internal faces and an active collimator in front of the back block. The latter consists of a strip of scintillator above and below the slit in the collimator. Finally, the whole collimator tube is wrapped in about 6 mm of lead.

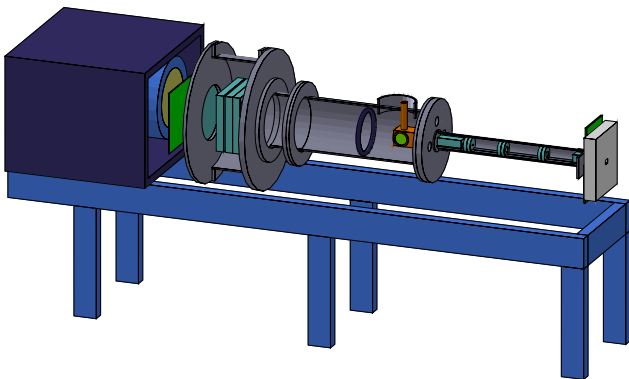


Fig. 68. The MuScat experiment in 2003.

The vacuum tube is connected to the main vacuum vessel, which contains the targets. These are:

- liquid hydrogen, 100 mm and 150 mm thick
- lithium, 12.7 mm and 6.3 mm thick
- beryllium, 3.7 mm and 1.0 mm thick
- carbon, 2.5 mm thick
- aluminum, 1.5 mm thick
- CH₂, 4.8 mm thick
- iron, 0.2 mm and 5.1 mm thick

The “thick” iron sample is used simply to blow the beam up to give a better coverage of the detectors and improve the measurement of the efficiency. The liquid hydrogen targets were built by the Targets group at TRIUMF. The two lengths were achieved in the same structure simply by rotating it through 90° in the horizontal plane.

The solid targets are mounted on a target wheel that can be controlled from outside the vacuum so it is unnecessary to break this each time a target is changed. The wheel has 12 slots, the last of which has no target mounted and is used to measure the intrinsic properties of the beam. These are monitored on a regular basis. In addition, two sets of lithium targets are used to allow systematic checks.

Three detectors built from scintillating fibres are used for tracking. These consist of two offset planes of 1 mm thick fibres in each dimension, to give a uniform efficiency and two dimensional readout. There are a total of 1024 fibres per chamber. The light from the scintillating fibres is transmitted to photomultipliers using clear fibres. The PMTs used are Hamamatsu R5900 L16s and contain 16 anodes, each 16 mm long and 0.8 mm wide. Bundles of 16 × 16 clear fibres are formed to match these anodes, thus giving a 16-fold multiplexing. To ensure that signals can be de-convoluted, the scintillating fibres are read out at both ends and the PMTs at each end are rotated by 90° with respect to each other. The detectors are mounted inside the vacuum vessel to minimize the amount of material between them and the target. The PMTs, on the other hand, must sit outside and this means the fibre arrays form the vacuum seal. The leak rate from these is sufficiently small, however, that a vacuum of less than 5×10^{-6} torr was achieved. The last of three detectors is shown mounted on the back plate of the vacuum vessel in Fig. 69.

A second scintillator for use in the trigger sits behind the tracking detectors, outside the vacuum. The final part of the detector is TINA, a NaI calorimeter of 460 mm diameter and 510 mm depth. It has a measured energy resolution (fwhm) of 3.6% at 90 MeV for electrons, with an energy dependence of $E^{-0.55}$. As it is not big enough to cover the full area of the tracking

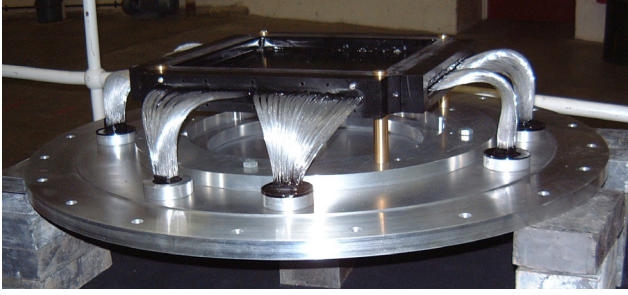


Fig. 69. The third Scifi detector mounted on the experiment end-flange.

detectors after extrapolation of the tracks, it is used offset from the centre of the experiment. Nevertheless, it is valuable for both a muon energy measurement and to check the beam composition.

Initial results from 2003

In 2003, MuScat had about 16 days of data-taking in the M20 beam line and recorded a total of 57 M triggers, as shown in Table IX. The analysis of these data so far has focused on three main areas: understanding the beam, understanding the detector and developing a full GEANT4 simulation of the detector. It should also be noted that theoretical work is being undertaken in Oxford University that will directly predict the scattering distributions that MuScat will measure. A strong collaboration has been created with the authors of this work. In this section, only a few aspects of the work done so far will be summarized.

Beam composition The time-of-flight distribution measured with the two bending magnets in M20 set to the same momentum and the momentum slit wide open is shown in Fig. 70(a) and under normal running conditions, with the bends set for forward decays and a narrow momentum slit in Fig. 70(b). In the former it is possible to identify peaks due to electrons, muons and

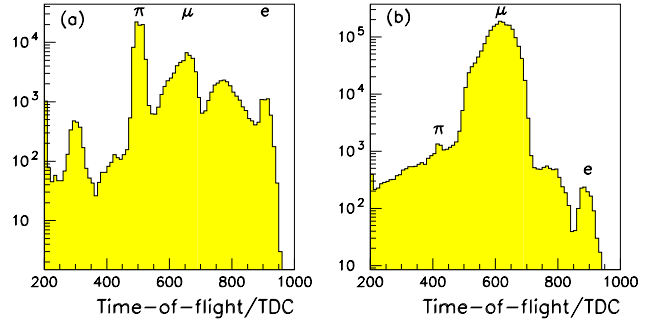


Fig. 70. Time-of-flight distributions.

taus. There are a number of other peaks which correspond to earlier rf pulses of the cyclotron and these are believed to be due to the protons. There are more than one of these because the protons do not penetrate all the way through the detector to the second trigger scintillator plane. Thus a “proton” trigger actually results from a proton signal in the first trigger counter and an accidental coincidence with another particle, pion, muon or electron, hitting the second trigger counter.

In normal running conditions, using forward muon decays and a narrow momentum slit, it can be seen that the backgrounds from particles other than muons are essentially eliminated. The shoulder on the muon peak is currently being understood, but is believed to be due to pion decays after the momentum slit.

Additional particle identification is possible with TINA. Although the details are still being understood, Fig. 71 shows the energy deposition of muons that strike the calorimeter well away from the edges. The tail to higher energies is believed to be due to electrons

Table IX. Number of triggers recorded in 2003.

Target type	Number of events
Liquid hydrogen 15 cm full	3.1 M
Liquid hydrogen 15 cm empty	3.9 M
Liquid hydrogen 10 cm full	7.9 M
Liquid hydrogen 10 cm empty	8.5 M
Lithium 1.3 cm	6 M
Lithium 0.6 cm	6 M
Beryllium 0.4 cm	3 M
Beryllium 0.1 cm	3 M
Carbon 0.3 cm	2 M
Aluminum 0.2 cm	3 M
Polythene 0.5 cm	2 M
Iron 0.02 cm	2 M
Iron 0.5 cm	2 M
Empty	5 M
Total	57 M

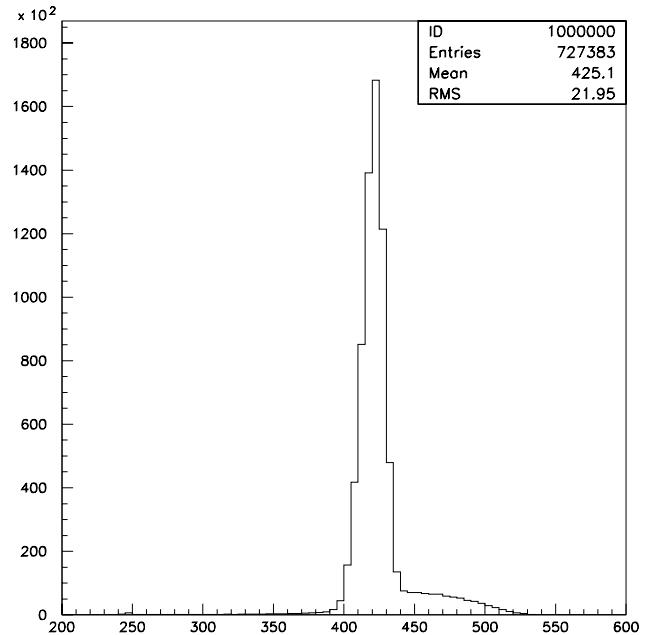


Fig. 71. Energy distribution of muons in TINA.

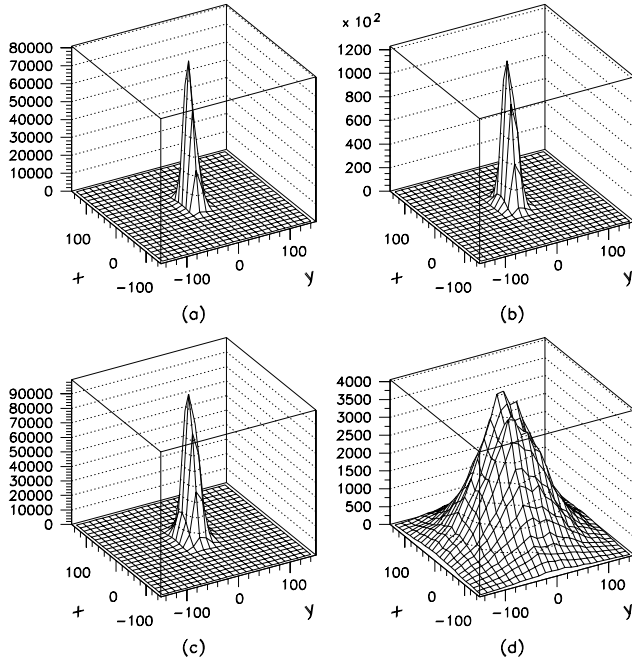


Fig. 72. Raw hit distributions in the first scintillating fibre detector with (a) no target, (b) thin lithium, (c) thick lithium and (d) thick iron. The distributions are broader in x as this is the long dimension in the collimator slits. The scattering will be measured in y .

which come from muon decays during the integration time of the electronics.

Beam momentum As M20 has not been used for forward muon decays for a long period, it is very important to have an independent measurement of the beam momentum. This is possible in two ways: (1) using the time of flight of a number of particle types and (2) using the kinetic energy depositions in TINA for these particle types. Both of these have been investigated and give a preliminary measurement consistent with expectations from the M20 magnet settings.

Tracking The tracking detectors are clearly the most important element of the experiment and a lot of work has been done to understand them. In particular, the pedestals and gains have been determined and the alignment, hit identification and error determination are almost final. Tests of the tracking algorithm are also almost complete. As an example, Fig. 72 shows very preliminary raw hit distributions, without tracking requirements, for running with solid targets. The algorithm for deconvoluting the real muon scattering distribution from these raw distributions has been developed and is also under test.

In addition, a detailed GEANT4 simulation of the whole experiment has been written. Much work has gone into comparing this with data, down to fine details, and this has brought many improvements to the simulation and a better understanding of the experi-

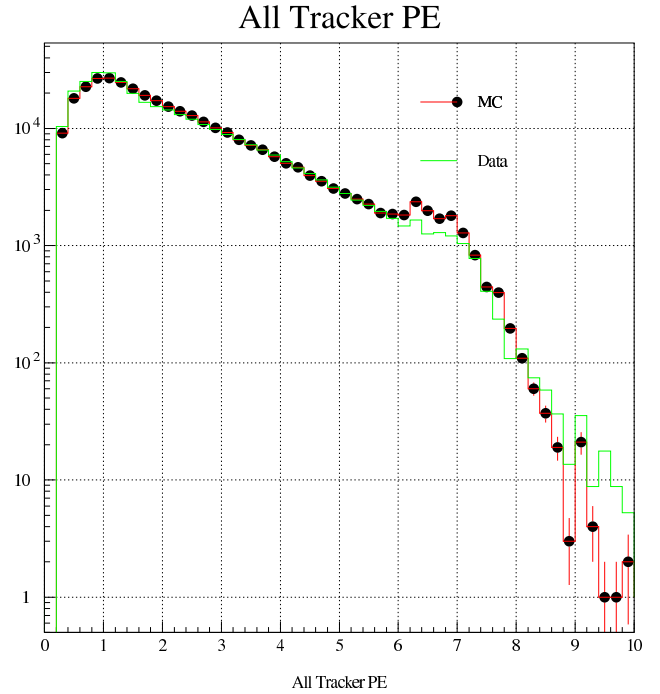


Fig. 73. Comparison of total signals from clusters found in the tracking detector, measured in photo-electrons, between data (solid line) and Monte Carlo (points). Note the differences above 6 pe are because a single saturation value for the electronics is used in the Monte Carlo, while there are variations for the real data.

ment. An example is shown in Fig. 73. A method of using a number of scattering algorithms as input to GEANT4 for comparison with the raw scattering distributions from the data is also under development.

Experiment 880

Ortho-para effect of muon catalyzed fusion in solid deuterium

(K. Ishida, K. Nagamine, RIKEN/KEK)

We measured the dependence of the rate of muon-catalyzed fusion in D_2 ($dd\text{-}\mu\text{CF}$) on the ortho-para state of deuterium molecules. In the $dd\text{-}\mu\text{CF}$ process, the resonant formation of $dd\mu$, $d\mu + D_2 \rightarrow [(dd\mu)dee]$, is one of the most important processes determining the overall efficiency of producing fusions. Since this process requires an energy matching between the initial state and the final state, the rate is very sensitive to the states of $d\mu$ (hyperfine states $F = 3/2$ or $1/2$, kinetic energy etc.) and D_2 (vibrational and rotational molecular states, kinetic energy etc.). Although the system had been experimentally investigated by changing various parameters such as the temperature and the density, full understanding was not achieved yet. In order to obtain further understanding of this process, we started to investigate the effect of another parameter, namely the ortho-para state of the D_2 molecule.

The measurement was performed at the M9B channel in June, 2000. We prepared two deuterium targets, one the “normal” D₂ (67% ortho and 33% para) and the other was an “ortho” D₂ (99.7% ortho and 0.3% para). A detailed explanation of the gas preparation procedure as well as the experimental set-up is given in references [Toyoda *et al.*, Phys. Lett. **B509**, 30 (2001); *ibid.*, Phys. Rev. Lett. **90**, 243401 (2003)]. The deuterium gas was solidified on a thin silver foil maintained at 3.5 K to make a solid D₂ target of 40 mm in diameter and 0.3 mm in thickness. To detect protons from fusion events, we used silicon surface barrier (SSB) detectors in pairs so that the “ ΔE vs. E ” particle identification method was applied. The fusion proton emission time spectrum after muon stopping as shown in Fig. 74 was analyzed to extract various parameters such as the effective $dd\mu$ formation rate from $d\mu(F=3/2)$ state, $\tilde{\lambda}_{\frac{3}{2}}$, and the hyperfine transition rate from $d\mu(F=3/2)$ to $d\mu(F=1/2)$ state, $\tilde{\lambda}_{\frac{3}{2}\frac{1}{2}}$. The obtained values are shown in Table X for normal D₂ and ortho D₂. It was found that the effective $dd\mu$ formation rate as well as hyperfine transition rate are decreased by increasing the ortho-deuterium concentration. This result is opposite to a calculation assuming the complete thermalization of $d\mu$ atoms, which predicts a slight increase of $dd\mu$ formation rate. We suspect that the solid-state effect plays an important role and a more detailed theory is necessary.

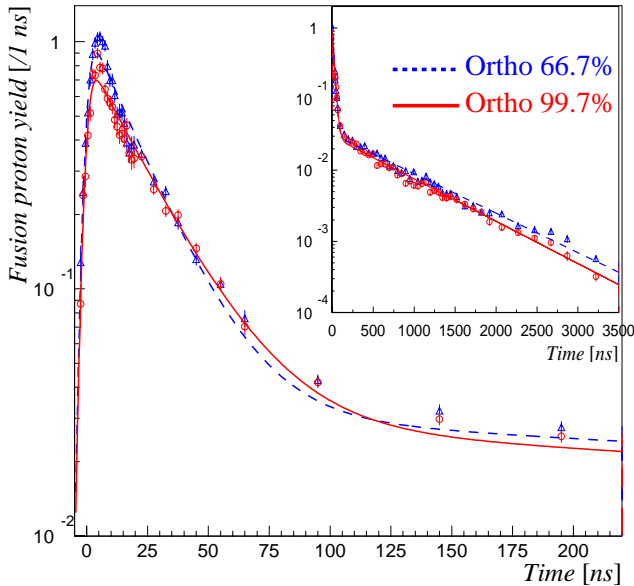


Fig. 74. Fusion proton time spectrum for normal deuterium (triangle data points and fitted dotted line) and that for ortho deuterium (circle points and solid line) are plotted. A significant difference was observed both in amplitude and decay rate of the fast component. The upper-right inset is for a different time range to show the slow component, which was used for the normalization.

Table X. Obtained value of the effective $dd\mu$ formation rate $\tilde{\lambda}_{\frac{3}{2}}$ and the hyperfine transition rate $\tilde{\lambda}_{\frac{3}{2}\frac{1}{2}}$ in normal D₂ and ortho D₂ and the relative effect due to ortho-para conversion.

	Normal D ₂	Ortho D ₂	Effect
$\tilde{\lambda}_{\frac{3}{2}}$	2.868(60)	2.131(43)	-26(3)%
$\tilde{\lambda}_{\frac{3}{2}\frac{1}{2}}$	36.14(84)	29.68(71)	-18(3)%

Table XI. Comparison of the $d\mu$ hyperfine-transition rate due to scattering [$\lambda_{d\mu}^{3/2\ 1/2\ \text{scat}}$ (μs^{-1})] and the $d\mu$ hyperfine-transition rate via back decay rate [$\lambda_{d\mu}^{3/2\ 1/2\ \text{back}}$ (μs^{-1})] between experiments (this work, Lauss *et al.* [Hyp. Int. **118**, 79 (1999); Voropaev *et al.*, Hyp. Int. **118**, 135 (1999)] and theories). Our experiment is for solid D₂ while others are for the liquid state.

	$\lambda_{d\mu}^{3/2\ 1/2\ \text{scat}}$ (μs^{-1})	$\lambda_{d\mu}^{3/2\ 1/2\ \text{back}}$ (μs^{-1})
This expt.	11.5 ± 4.2	24.7 ± 4.9
Lauss <i>et al.</i>	26.3 ± 3.0	11.0 ± 3.0
Voropaev <i>et al.</i>	23.6 ± 0.4	12.9 ± 0.4
Theories	~ 36	~ 14

Another interesting problem in $dd\mu CF$ is that there is a large discrepancy between theories and experiments concerning the $d\mu$ hyperfine-transition rate, to which two components are expected to contribute. Since one of the components (transition by back decay after $dd\mu$ molecule formation) is proportional to the measured effective $dd\mu$ formation rate with respect to the ortho-para conversion, while the other (transition due to scattering) is not dependent, we can use our data to separately determine the two components. Our result is shown in Table XI with previous experimental data obtained in the liquid state by completely different methods. It was confirmed that the scattering is much smaller than theoretical predictions.

Experiment 893

The hyperfine field of Rb in Fe, Ni and Co (LTNO at ISAC)

(P. Delheij, TRIUMF)

Principle

In the low temperature nuclear orientation (LTNO) set-up, a polarized nuclear ensemble is created by implanting the radioactive beam from the ISAC facility into a ferromagnetic target foil which is kept at a temperature near 10 mK. For these systems the polarization is determined by the factor $\mu H/kT$ through the Maxwell Boltzmann distribution. Here, μ is the magnetic moment, H the hyperfine field, T the temperature and k the Boltzmann constant. This polarization produces an anisotropy in the emission of the decay

products which depends on nuclear structure properties like spins, multipole mixing and parity mixing. By raising the temperature the normalization (isotropic distribution) is measured. The normalized anisotropies determine the parameter values.

If two of the three parameters in $\mu H/kT$ are known for the parent ground state, the third one can be determined. In this way (because μ and H are known) the temperature is determined by attaching a long lived source like $^{60}\text{CoFe}$ to the cold finger that cools the target foil.

The product μH can be determined directly with rf irradiation (NMRON technique). As the frequency of the rf field is stepped the anisotropy of any subsequent transition is measured to detect the change of this anisotropy when the Larmor frequency is passed. This technique avoids the systematic errors that are due to the temperature determination. This improves the accuracy typically by an order of magnitude. Either the magnetic moment or the hyperfine field can be determined if the other quantity is known.

Development

At present the goal of this experiment is to resolve the difference between the experimental and calculated value for the hyperfine field of diluted Rb in Fe. In 2000 a calculation of the hyperfine field of dilute impurities in Fe of the elements from Rb to Xe was published [Cottenier and Haas, Phys. Rev. **B62**, 461 (2000)]. Compared to earlier calculations the lattice constant around the impurities was treated as variable. This improved agreement between experimental and calculated values by an order of magnitude to the few per cent level. The exceptions were Rb and Sr. For Rb a discrepancy of a factor -5 exists. An NMRON measurement with ^{79}Rb in the LTNO set-up at ISAC can resolve this issue (Expt. 893). For Sr a discrepancy of a factor $+2$ was removed this year in Japan [Nishimura *et al.*, Phys. Rev. **B68**, 012403 (2003)].

During the preparations for the on-line measurements a problem with the top loading mechanism on the mixing chamber was encountered. The rebuilding required a substantial disassembly of the set-up. Then on-line measurements with ^{79}Rb and ^{75}Ga showed polarization effects on the 15 per cent level. However, no NMRON signal could be observed.

After that ^{91}Rb was implanted to populate the isomeric state at 555 keV in ^{91}Y . The hyperfine field for this system is known [Hinfurtner *et al.*, Phys. Rev. Lett. **66**, 96 (1991)] and the resonance frequency is 310 MHz without an external magnetic field. As shown in Fig. 75, an effect of 200% was observed for the intensity ratio of the detectors perpendicular (D90+D270) and parallel (D0+D180) to the external magnetic field due to the polarization.

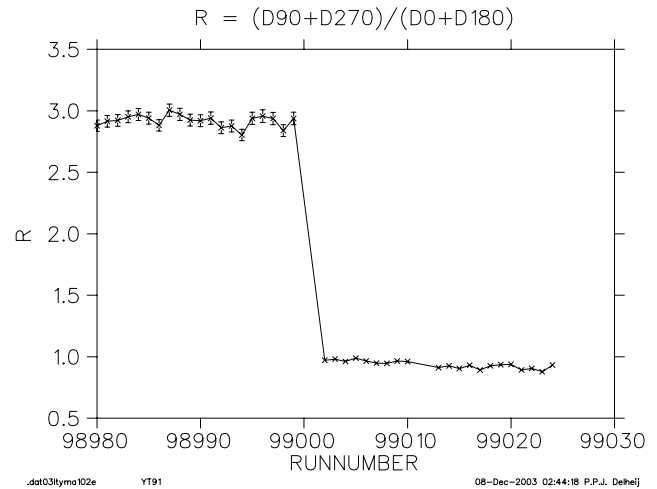


Fig. 75. Change of the intensity ratio R as the target foil is warmed up.

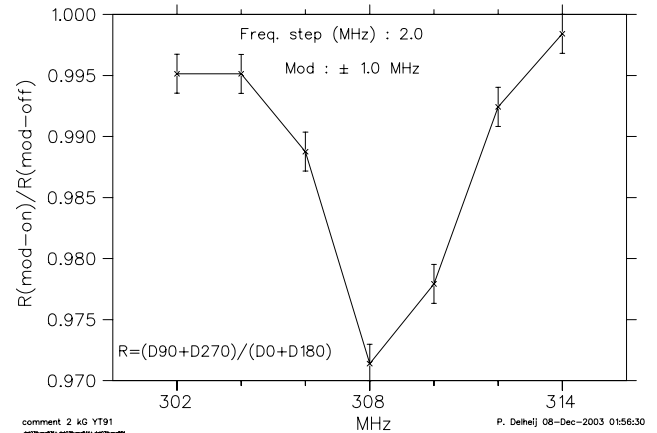


Fig. 76. NMRON resonance for $^{91}\text{RbFe}$ in an external magnetic field of 0.2 T. The ratio of R with the rf modulation on and the rf modulation off dips as the frequency is stepped through the resonance.

With this system a resonance was observed at 308 MHz as expected for the external field of 0.2 T (see Fig. 76). The rather small size of the resonance (a frequency integrated destruction of only 1/30 of the polarization signal) was a surprise, particularly in view of our earlier result for $^{60}\text{CoFe}$ (see last year's TRIUMF Annual Report) when a polarization destruction efficiency of 1/3 was observed at 165 MHz, approximately a factor 10 better. With the small polarization signal from ^{91}Y it was still possible to measure the spin-lattice relaxation for the first time. The result of 10 ± 5 s is in good agreement with the semi-empirical relation in Shaw and Stone [Atomic Data and Nucl. Data Tables **42**, 339 (1989)]. This might suggest that the small NMRON effect is less likely related to the sample preparation than to the operation of the rf system. To address this problem a mock-up of the rf transmission system was being built at the end of the year. Furthermore, computer simulations are in progress.

Experiment 909

Isospin symmetry breaking in superallowed Fermi β -decays

(C.E. Svensson, Guelph)

Precision measurements of the ft values for superallowed $0^+ \rightarrow 0^+$ Fermi β -decays between isobaric analogue states provide demanding tests of the standard model description of electroweak interactions. To date, superallowed ft values have been determined at the $\pm 0.1\%$ level for nine nuclei between ^{10}C and ^{54}Co and, once corrected for small radiative and isospin symmetry-breaking effects, their consistency has confirmed the conserved vector current (CVC) hypothesis at the level of 3×10^{-4} . However, the value of V_{ud} derived by comparing these β -decay data with the purely leptonic muon decay, combined with present knowledge of V_{us} and V_{ub} , indicates a violation of the unitarity of the Cabibbo-Kobayashi-Maskawa (CKM) quark-mixing matrix at the 98% confidence level [Towner and Hardy, Phys. Rev. **C66**, 035501 (2002)]. Should this discrepancy be firmly established, it would indicate the need for new physics, either in terms of explicit quark effects in nuclear structure or an extension of the minimal electroweak standard model. Before a definitive conclusion can be reached, all uncertainties contributing to the unitarity test must be carefully scrutinized and, if possible, reduced. For V_{ud} , the dominant uncertainties are those associated with theoretical corrections to the ft values, and the search for systematic effects has focused on the nuclear-structure dependent δ_C corrections that account for the breaking of isospin symmetry by charge-dependent forces in the nucleus.

Experiment 909 involves a series of measurements with the 8π spectrometer and SCEPTAR β array aimed at constraining the above-mentioned isospin symmetry-breaking corrections in superallowed Fermi β -decays. This program will take advantage of the unique beams of radioactive ions available at ISAC to study particular decays in which the predicted δ_C corrections show the greatest model sensitivity. An initial focus of Expt. 909 will be on lifetime and branching ratio measurements for ^{34}Ar , with the aim of establishing the superallowed ft value at the $\pm 0.1\%$ level. The first objective will be to improve the current half-life precision by approximately one order of magnitude. These measurements will be carried out by collecting samples of ^{34}Ar at the centre of the 8π and following their decay for ~ 30 half-lives by time-stamping γ -rays emitted from excited states in the daughter ^{34}Cl populated in Gamow-Teller decay branches of ^{34}Ar .

In anticipation of ^{34}Ar beams from the ISAC ECR ion source in 2004, tests of the experimental techniques to be employed in Expt. 909 were carried out with radioactive ^{26}Na beams. This isotope was chosen because

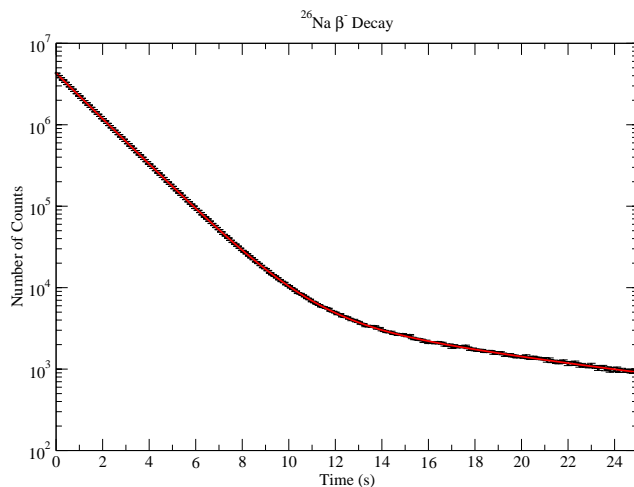


Fig. 77. Summed decay curve from β counting ^{26}Na samples with the 4π gas proportional counter at the ISAC GPS station. The second (longer lived) decay component results from a small ^{26m}Al contamination of the beam.

i) high yields were available from ISAC surface ion sources, ii) the half-life (~ 1.07 s) is similar to ^{34}Ar , iii) the daughter ^{26}Mg is stable, and iv) $\sim 99\%$ of ^{26}Na β -decays are followed by the 1809 keV γ -ray transition in ^{26}Mg , facilitating tests of the γ -ray lifetime technique to be employed for ^{34}Ar . The first requirement was to determine a precise value for the ^{26}Na lifetime. To this end, a ^{26}Na beam was delivered in 2002 to the fast tape system at the ISAC GPS station and its lifetime determined to high precision by the well-established β counting technique with a 4π gas proportional counter. The analysis of these data (a sample of which is shown in Fig. 77) is now complete, and the ^{26}Na lifetime has been established at the $\pm 0.03\%$ level.

In June, ^{26}Na beam was delivered to the 8π spectrometer to commission SCEPTAR (the scintillating electron positron tagging array) and to continue the

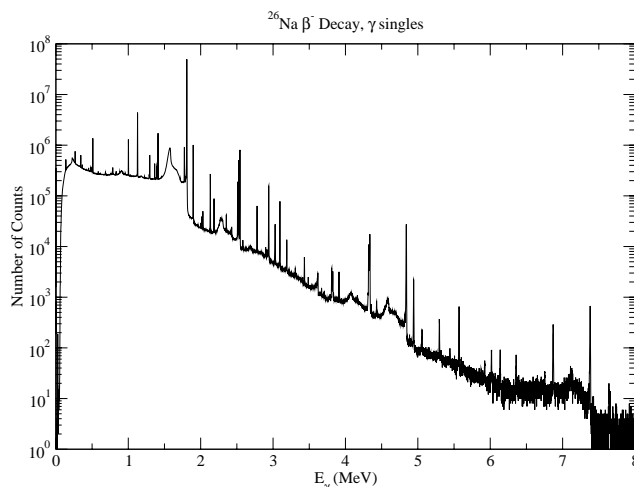


Fig. 78. γ -ray singles spectrum from ^{26}Na decay recorded with the 8π spectrometer at ISAC.

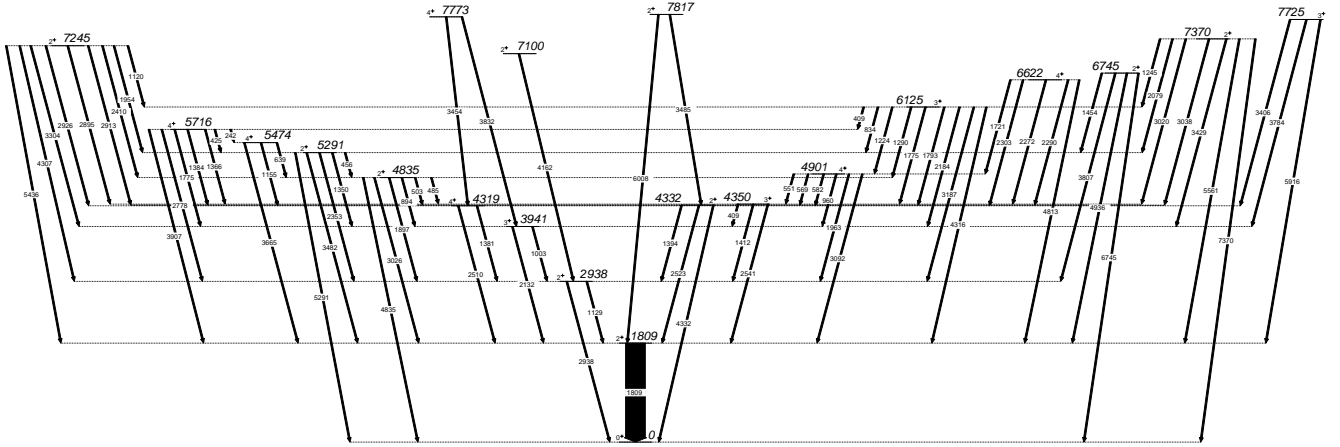


Fig. 79. γ -rays from the daughter nucleus ^{26}Mg identified with the 8π spectrometer following β -decay of ^{26}Na .

development of lifetime measurement techniques for Expt. 909. A γ -ray singles spectrum from ^{26}Na decay recorded in the 20 HPGe detectors of the 8π spectrometer is presented in Fig. 78. A total of 82 γ -ray transitions in the daughter ^{26}Mg were identified, with energies between 241 keV and 7.368 MeV and intensities ranging from 0.99 to below 10^{-5} per β -decay (see Fig. 79). Together with the above mentioned lifetime measurement and the previously known Q-value, these data have established precision ft values for 20 β -decay branches of ^{26}Na . The ^{26}Na beam also enabled further testing of the γ -ray lifetime technique to be employed for ^{34}Ar , and these data are currently being analyzed for comparison with the precise ^{26}Na half-life determined through β counting.

Following measurement of the ^{34}Ar lifetime, subsequent measurements with the 8π and SCEPTAR will focus on an improved determination of the ^{34}Ar superallowed branching ratio. Large, and model-dependent, isospin symmetry-breaking corrections are also predicted for the $A \geq 62$ odd-odd $N = Z$ nuclei. A program of precision lifetime measurements (Expt. 823) for these nuclei with the 4π gas proportional counter at the ISAC general purpose station is being led by G.C. Ball of TRIUMF. Future experiments with the 8π spectrometer and SCEPTAR will provide branching ratio measurements for these short-lived isotopes. Weak non-analogue Fermi decay branches that provide direct, and absolute, information on one component of the isospin symmetry breaking will also be measured. Initial measurements of ^{74}Rb decay by our collaboration with a single HPGe detector have identified a number of high-energy γ -rays from excited states in the daughter ^{74}Kr [Piechaczek *et al.*, Phys. Rev. **C67**, 051305(R) (2003)]. The high γ - γ efficiency of the 8π spectrometer will be used to clarify the coincidence relationships between these γ -rays and identify further γ -ray transitions following weak Gamow-Teller decay

branches, with the aim of establishing the superallowed branching ratio at the $\pm 0.05\%$ level. With the continued development of ion source technology at ISAC, these superallowed and non-analogue Fermi β -decay branching ratio studies will be extended to include ^{38}mK , ^{62}Ga and ^{70}Br .

Experiment 920

Nuclear charge radii and moments of short lived neutron deficient lanthanum and other rare earth isotopes

(H.A. Schuessler, Texas A&M)

We had our first on-line run scheduled September 5–9. The plan was to measure HFS and isotope shifts of short lived $^{129-134}\text{La}$ isotopes. In case of difficulties with lanthanum production, we were also ready to substitute short lived Pr isotopes for investigation. Initial field tests on a Ta foil target running at about 40 μA proton beam indicated that such experiments should be possible, even though more yield tests needed to be carried out to definitely confirm the required $\sim 5 \times 10^6$ ion/s for laser spectroscopy signals. Unfortunately shortly before our run started, the on-line ion source was destroyed, and nothing more could be done to pursue spectroscopy on either La or Pr. We hope that in a future ion source period our experiment will be scheduled closer to the beginning of the period to have a newer on-line ion source.

Since our experimental equipment was ready and needed to be tested, and since all the major collaborators were present, it was decided to try using the off-line plasma source (OLIS) with argon gas. We got excellent and fast support to arrange a stable beam run from the ISAC ion source management and the ion source operators.

Transitions accessible to laser dyes in the 550 nm region lie very high in Ar II and it was necessary to find transitions for which the lower level is metastable,

Ar II

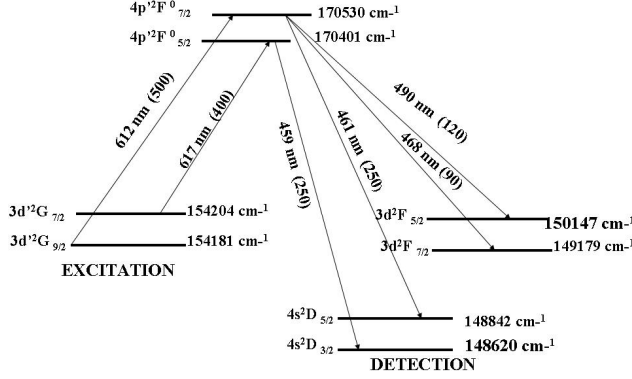


Fig. 80. Ar II level scheme of interest.

and populated by the plasma discharge of the source. The scheme used in our experiment is shown in Fig.80.

Laser radiation at $\lambda = 611$ nm and $\lambda = 617$ nm was employed for excitation and several lines between $\lambda = 459$ –490 nm for detection.

These excitation wavelengths lie on the border of the DCM dye range, so rather than change the dye in our laser (currently working with Rh110), we used Phil Levy's polarization beam line laser, which already operated with DCM.

We were successful in observing the laser spectroscopy signals even though the plasma ion source is not well suited for producing the required metastable states from which laser excitation starts. A signal from stable ^{40}Ar is shown in Fig. 81. It is hard to make a sensitivity estimate from this proof-of-principle experiment since it is unknown which minor fraction of the argon ion current is in the required metastable state (less than 10^{-4}). Also the signal line width is more than an order of magnitude broader than the lifetime limit due to the unfavourable conditions in the ion source plasma.

Nevertheless a milestone in our work was reached, since our experiment demonstrated that all our equipment is working and that we are ready for our first on-line experiment at ISAC.

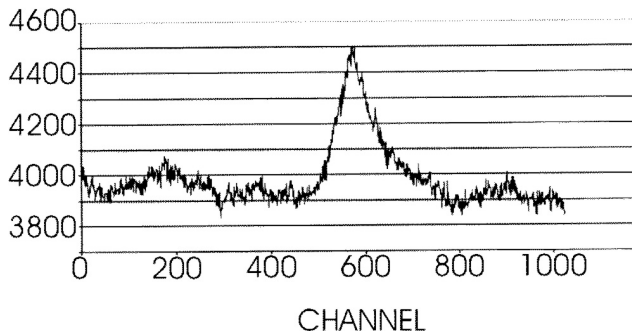


Fig. 81. Laser spectroscopy signal of ^{40}Ar .

Experiment 921

High- K isomers in the mass 180 region

(P.M. Walker, TRIUMF/Surrey, UK)

A program of high- K isomer studies has been initiated at TRIUMF-ISAC. In the first experiment, a radioactive source, prepared off-site, was measured with the 8π γ -ray spectrometer. Following this, measurements of $A \approx 180$ nuclides were made with the 8π spectrometer, in conjunction with the SCEPTAR electron detector array, on-line to the ISAC-I radioactive beam facility.

The motivation for these studies comes from the wish to understand the nuclear structure of high- K isomers, especially the transition rates of highly K -forbidden decays. The neutron-rich $A \approx 180$ nuclides provide a fertile testing ground for model predictions, which indicate the existence of an especially favoured region for the formation of high- K , multi-quasiparticle isomers. These may influence the r -process pathway of stellar nucleosynthesis. Furthermore, there is the prospect of exploiting isomers as novel energy-storage devices [Walker and Dracoulis, Nature **399**, 39 (1999)].

The spontaneous decay of 31-year $^{178\text{m}2}\text{Hf}$

A preliminary description of this experiment was given in the 2002 TRIUMF Annual Report. γ -rays from a 15 kBq source of the 31-year, $K^\pi = 16^+$ isomer were measured for 42 days with the 20-detector 8π spectrometer. The γ - γ -coincidence events were analyzed to produce level-scheme information. In this way, sensitivity to transitions with intensities as low as one in 10^5 parent decays was achieved. Detailed results have been published [Smith *et al.*, Phys. Rev. **C68**, 031302(R) (2003)].

The vast majority of the isomer decay proceeds by electron conversion, and the principal findings from the new measurements consist of the first unambiguous identification of direct γ -ray emissions from the 31-year isomer itself. These are 310 keV, M4, and 587 keV, E5 transitions with intensities of 15 and 6 parts in 10^5 , respectively. The high transition multiplicities set new boundaries for the operation of the K quantum number, broadly in line with expectations, i.e. their reduced hindrance factors are $f_\nu \sim 100$ (per degree of K forbiddenness).

In addition, the observation of a previously unknown E2 transition, between members of the two known $K^\pi = 8^-$ bands, has enabled the testing of a band-mixing model proposed by Emery *et al.* [KVI Annual Report, 1979] with consistent results.

It is notable that the M2 decay of the 4-s, $K^\pi = 8^-$ isomer was too weak to be identified (< 1 part in 10^5) with $f_\nu > 160$.

Search for new isomers in $A = 170 - 180$ nuclides

A K -isomer research program is now under way on-line to ISAC-I, to search for predicted isomers in neutron-rich nuclides. With a 30 μA beam of 500 MeV protons incident on a natural tantalum target connected to a surface ionizer, low-energy ions were extracted at 40 keV, mass separated, and transported to the 8π spectrometer. The latter has been supplemented with a large-solid-angle, 20-element array of plastic scintillators, SCEPTAR, for electron detection. The 40 keV ions were stopped at the centre of the 8π /SCEPTAR spectrometers in a remote-controlled tape, which periodically transported the accumulated activity to a lead-shielded location. In this way, short-lived isomers and β decays could be studied with minimum interference from long-lived isobars.

Preliminary results have been reported at the RNB-6 conference [Smith *et al.*, Nucl. Phys. A (in press)]. A significant aspect has been the observation of decays from a 3 ms, $1/2^+$ isomer in ^{179}Lu . While the isomer itself is well known, the short half-life had led to the expectation that it would not be observed with the present experimental arrangement. Therefore, its identification provides valuable evidence for the sensitivity to ms isomers.

Data analysis is in progress, with an emphasis in the present data on the search for new high- K isomers in ^{178}Lu and ^{179}Lu .

Experiment 927

$(^3\text{He}, p)$ as an alternative to resonant elastic scattering

(F. Sarazin, Colorado School of Mines/TRIUMF; P. Walden, TRIUMF)

The carbon-nitrogen-oxygen (CNO) cycles are thought to be the main source of energy generation in novae and X-ray bursts in their ignition phase. Under certain extreme conditions of temperature and pressure, these cycles may be broken by so-called breakout reactions such as $^{15}\text{O}(\alpha, \gamma)^{19}\text{Ne}(p, \gamma)^{20}\text{Na}$ or $^{18}\text{Ne}(\alpha, p)^{21}\text{Na}(p, \gamma)^{22}\text{Na}$, which link the CNO cycles to the rp-process, a long sequence of proton captures and β -decays. Precise knowledge of the structure of a few states above the relevant particle threshold in the compound nuclei is required to calculate the rate of the reactions involved in the breakout of the CNO cycles and in the subsequent rp-process.

In this context, resonant elastic scattering is a very valuable tool to identify astrophysically relevant states as demonstrated again recently at ISAC/TRIUMF [Ruiz *et al.*, Phys. Rev. **C65**, 042801R (2002)]. However, it is limited to low spin states and/or resonances of relatively large width. This technique also requires already having a fairly good knowledge of the com-

pound nucleus level scheme, so that the beam energy could be tuned to match the reaction excitation energy to that of known resonances. Experimentally, it requires time-consuming frequent beam energy changes to map out the excitation function for every state. We proposed to use the $(^3\text{He}, p)$ reaction in inverse kinematics at the TUDA scattering chamber at ISAC as an alternative to elastic scattering. For proton-rich nuclei this reaction has a high Q -value, which allows the population of a wide range of states with only one beam energy.

In early December, a first beam time period was allocated at ISAC/TRIUMF, mainly to test the method at ISAC energies (max 1.73 MeV per nucleon). At these energies, the deuteron transfer is expected to proceed mainly (but not exclusively) via a compound nucleus mechanism. Two stable beam tests ($^{20-21}\text{Ne}(^3\text{He}, p)^{22-23}\text{Na}$) and one radioactive beam test ($^{20}\text{Na}(^3\text{He}, p)^{22}\text{Mg}$) were performed.

Experimental set-up

The experimental set-up consisted of a 5 mm thick LN_2 -cooled ^3He gas cell at a pressure of 500 mbar. The entry and exit foils were 1.3 mg/cm^2 Ti foil. The target was designed, built and already used for experiments or secondary beam production [Harss *et al.*, Rev. Sci. Instr. **71**, 380 (2000)] at Argonne National Laboratory. It was shipped from Argonne to TRIUMF for the experiment.

The clear advantage of such a cold target is that for at the same operating pressure, it contains almost 4 times more ^3He atoms/ cm^2 than at room temperature. Therefore, it allows the target to be thinner, enabling better energy resolution.

A ΔE - E system, consisting of two stacked 300 μm LEDA detectors was placed, respectively, 8.1 cm (14 cm) for the $^{20}\text{Ne}(^3\text{He}, p)^{22}\text{Na}$ experiment (for the $^{20}\text{Na}(^3\text{He}, p)^{22}\text{Mg}$ and the $^{21}\text{Ne}(^3\text{He}, p)^{23}\text{Na}$ experiments) upstream from the target covering the $[123^\circ, 147^\circ]$ ($[138^\circ, 160^\circ]$) range in the laboratory frame. A 6 μm thick mylar foil was placed in front of the first LEDA to stop the beam ion particles which had backscattered off the Ti foils.

$^{20}\text{Ne}(^3\text{He}, p)^{22}\text{Na}^*$, $Q \sim 5.8$ MeV

The $^{20}\text{Ne}(^3\text{He}, p)^{22}\text{Na}^*$, using direct kinematics, has already been studied at various energies, including 2.8 and 3 MeV [Meynadier *et al.*, Nucl. Phys. **A161**, 305 (1971)]. The main goal of this first experiment was therefore to test the experimental set-up and evaluate the resolution obtained in inverse kinematics. The ^3He target was operated at room temperature. A 10^9 pps 1.73 MeV per nucleon ^{20}Ne beam was used for this first test. After about 8 hours, proton peaks were clearly seen in every strip of the silicon array. A prelim-

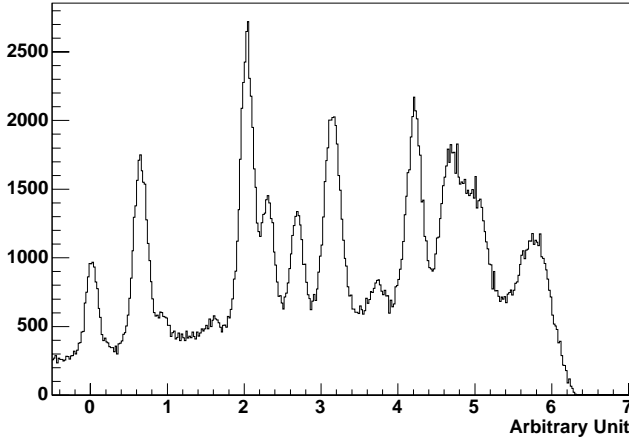


Fig. 82. Excitation function of ^{22}Na from the $^{20}\text{Ne}(^3\text{He},p)^{22}\text{Na}$ reaction.

inary excitation function, summed over all the strips, was extracted (see Fig. 82). As observed in the direct reaction, a large number of excited states are present, which confirms the potential of the reaction to find new excited states, as it seems to populate all excited states which are angular momentum accessible. The analysis of the ΔE - E spectrum showed that only protons were recorded in the detectors.

$^{20}\text{Na}(^3\text{He},p)^{22}\text{Mg}^*$, $Q \sim 14.9$ MeV

Following the initial success of the ^{20}Ne experiment, a 10^7 pps 1.73 MeV per nucleon ^{20}Na radioactive beam was used in the search of new states in ^{22}Mg . The precise knowledge of the level scheme of ^{22}Mg in the 5–7 MeV energy range is especially of importance for the $^{21}\text{Na}(p,\gamma)$ reaction, the rate of which is being investigated at the DRAGON facility. A very large background at low energy was observed in the detectors, due to the β -decay of the backscattered ^{20}Na implanted in the mylar foil. Another source of background was due to the β -delayed α -decay of ^{20}Na (20.5%). The energy of the alphas did not, however, overlap significantly with the energy region where the protons of interest were expected. After an initial 8 hour period, the ^3He target was cooled to LN_2 temperature. Although protons were clearly present from examining the ΔE - E scatter plot, no apparent structure could be seen in the accumulated energy spectrum. This suggested that the cross section for the $^{20}\text{Na}(^3\text{He},p)^{22}\text{Mg}$ reaction was much lower than for the $^{20}\text{Ne}(^3\text{He},p)^{22}\text{Na}$ reaction and it also suggested that the protons observed were coming from a separate distinct additional reaction. Currently, we speculate that the very significant loss of cross section is due to the larger Q -value of the reaction. A further investigation is in progress.

$^{21}\text{Ne}(^3\text{He},p)^{23}\text{Na}^*$, $Q \sim 11.4$ MeV

In order to gather some evidence for our speculation, we switched back to stable beam, namely ^{21}Ne .

The idea was to study a reaction with a somewhat lower Q -value with the advantage of the higher beam intensity offered by the use of stable beam (10^9 pps). As shown in Fig. 83, small peaks can be seen on the energy spectra. The peaks, however, sit on a much larger background than the one observed in the $^{20}\text{Ne}(^3\text{He},p)$ data. The evident loss of cross section compared to the nearby $^{20}\text{Ne}(^3\text{He},p)$ reaction seems to confirm the Q -value correlation with the cross section. The background was confirmed to be from a separate distinct reaction because a run without ^3He gas showed a similar background without the peaks (see Fig. 83).

The TUDA chamber was finally opened and the target foils examined. A large carbon build up was observed on both entry and exit foils. This carbon build up is likely to have occurred while the target was cooled and was therefore acting like a cold trap. The condensates were probably hydrocarbons which were carbonized by the ion beams. This built up as a function of time. The low background seen in our ^{20}Ne data was due to the fact that the build up had not yet occurred. As a last test, the target was replaced by a mylar foil to see if a reaction of the beam on the carbon build up was responsible for the background observed. A similar background was indeed observed.

Conclusions

Despite the apparent disappointing results of the radioactive beam experiment, much has been learned and improvements to the experimental set-up are being discussed. In particular, we are currently working towards the $^{18}\text{Ne}(^3\text{He},p)^{20}\text{Na}$ experiment, the subject of the original $(^3\text{He},p)$ proposal, which has a Q -value (Q 6.1 MeV) comparable to our successful $^{20}\text{Ne}(^3\text{He},p)$ test.

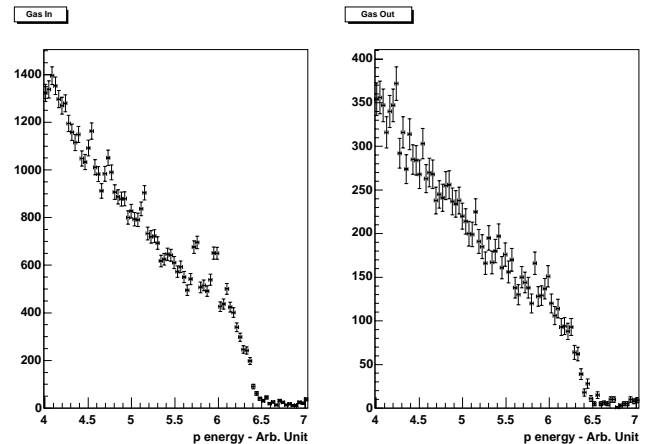


Fig. 83. Proton energy spectra obtained in the ^{21}Ne experiment. The figure on the left corresponds to runs with ^3He gas in the target. States in ^{23}Na can be seen although sitting on a large background. The figure on the right corresponds to runs without ^3He in the target, which shows that the background is due to protons unrelated to the $(^3\text{He},p)$ reaction.

Experiment 928

Level structure of ^{21}Mg : nuclear and astrophysical implications

(A. Murphy, Edinburgh)

Binary star systems are extremely interesting astrophysical phenomena due to their ability to undergo cataclysmic variability. The mechanism that drives these changes is thermonuclear runaway occurring in accreted layers of material transferred from a less evolved massive star on to the surface of its more evolved compact companion. Novae occur when the hydrogen rich outer layers of material from, for example, a red giant, are drawn off and deposited on the surface of a white dwarf companion. If the companion were instead a neutron star, the resulting detonation would occur in a much deeper gravitational potential, resulting in the hotter, faster event known as an X-ray burst. The criterion for the onset of the explosion is that the accretion rate is such that a degenerate layer builds up, which at some critical density then undergoes a thermonuclear runaway.

The rate of energy generation, and the amount of nucleosynthesis that develops, depends on the nuclear reactions that occur. A critical reaction path in novae and X-ray bursts may be breakout from the hot-CNO cycle to the rp-process and a key link in this chain is the $^{20}\text{Na}(p, \gamma)^{21}\text{Mg}$ reaction. A measurement of the $^{20}\text{Na}(p, p)^{20}\text{Na}$ reaction is able to determine many of the properties of the ^{21}Mg nucleus, and as the $^{20}\text{Na}(p, \gamma)^{21}\text{Mg}$ reaction rate is dominated by resonant contributions in these temperature regimes, such a measurement is highly important. This was the focus of Expt. 928 conducted at TRIUMF.

Accurate knowledge of the excited states of the ^{21}Mg nucleus are also of interest from a nuclear structure perspective. Properties may be compared to those of isobaric analogue states, allowing a study of the Thomas-Ehrman shifts to be made. Similarly, comparisons to predictions of recent shell model calculations will aid theoretical descriptions of proton-rich nuclei of similar masses. Finally, previous measurements of this and similar reactions have had to be made without the capabilities afforded by radioactive beam facilities such as TRIUMF. Consequently, indirect reaction techniques had to be applied, and conclusions drawn from complex model-dependent analyses of the reaction. Comparison of the data from this measurement with those of previous data sets will allow an assessment of these previous indirect techniques.

In order to determine the parameters of resonant states in ^{21}Mg , resonant elastic scattering of protons was employed. Experimentally, this consisted of impinging a radioactive ^{20}Na beam on to a hydrocarbon foil, and then detecting the recoil protons. The beam

was generated by ISAC, using a primary silicon-carbide target with a driver beam of typically 20 μA of 500 MeV protons. Typical beam currents on target in the TUDA chamber were a few pA, and during the experiment beam energies of 1.25 MeV/u and 1.60 MeV/u were requested. Accurate confirmation of the beam energies was assured by making measurements with the Prague magnet and then cross checking with the DRAGON spectrometer. This consisted of sending the beam in to each device and focusing the beam on to a set of exit slits (after the first magnetic dipole in the case of DRAGON), and then measuring each independently calibrated field. For the higher beam energy, where the field of the DRAGON MD1 magnet was unable to sufficiently bend the beam, this required first introducing gas in to the DRAGON target volume to slow the beam. Measurements of the required magnetic field were performed with various pressures of gas, and an extrapolation to zero gas pressure made. In all cases, an agreement between the beam energy measured with the Prague magnet and with DRAGON of ~ 1 keV/u was observed.

The target consisted of $\sim 795 \mu\text{g}/\text{cm}^2$ of CH_2 . Since the projectile loses a significant fraction of its energy in passing through such a thick target, the elastic reactions can occur over a wide range of energies, allowing an excitation function over a range of energies to be measured in a single experiment. For the lower beam energy, reactions can occur at ~ 0.51 – 1.20 MeV in the centre-of-mass, and for the higher beam energy between ~ 0.91 – 1.54 MeV, covering much of the astrophysically and structurally important resonances. Detection of the recoiling protons was achieved in two LEDA-design silicon detector arrays. These were placed downstream of the target at 19 and 62 cm.

Analysis of the data is ongoing. Various inconsistencies in calibration data have been resolved, and the data from the near detector are ready to be subjected to an R -matrix analysis. Progress on data from the farther detector is likewise expected. A multi-channel R -matrix code appropriate for the analysis of these data has been successfully developed at TRIUMF to support another experiment (Expt. 879) and is expected to be employed soon.

Experiment 929

Toward radon electric dipole moment measurements at ISAC

(T.E. Chupp, Michigan; C. Svensson, Guelph; J.A. Behr, M. Pearson, TRIUMF)

As a precursor to measurements of time-reversal violating electric dipole moments, Expt. 929 began tests of manipulating radioactive xenon beam in August. We demonstrated transfer of 40% of the ISAC beam into

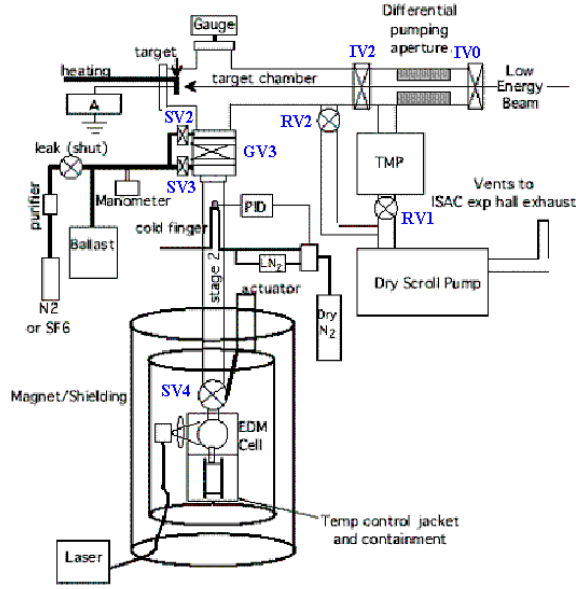


Fig. 84. Side view schematic of Expt. 929 test set-up at the GP2 station.

the form of xenon atoms in a mock-up of an eventual EDM cell.

The method is demonstrated in Fig. 84. We stop a ^{120}Cs beam from the ISAC surface source in a thin foil catcher. We irradiate for two half-lives of the ^{120}Xe daughter, isolate the system, and heat the catcher by direct current to release the Xe. We freeze it onto a cold finger at LN_2 temperature. Then we isolate this section, warm up the cold finger, and push the Xe efficiently into the cell with a burst of 1 atm of nitrogen buffer gas. The activity was monitored at all stages by Ge detectors. The cryogenic and gas push techniques are being written up for publication. Diffusion constants of xenon in platinum, tantalum, and zirconium foils were also measured and are shown in Fig. 85 and being prepared for publication. The control system, vacuum system, and diffusion measurements formed the senior thesis of Tim Warner of SFU.

These techniques should be applicable to radon atoms once they are available at ISAC.

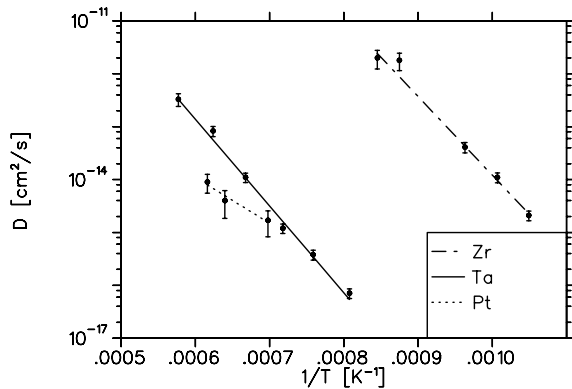


Fig. 85. Diffusion of Xe in Pt, Ta, and Zr foils.

Experiment 947

Evaluation of the competition between single-step and multi-step γ decay in the $^{12}\text{C}(^{12}\text{C},\gamma)$ reaction

(D. Jenkins, York)

Heavy ion radiative capture

Experiment 947 is intended to answer long-standing questions concerning the possibility of molecular-like configurations in nuclei. The $^{12}\text{C}+^{12}\text{C}$ system has long been regarded as the exemplar of the nuclear molecule hypothesis. Anomalous structures in the elastic and inelastic scattering of $^{12}\text{C}+^{12}\text{C}$ were explained in terms of the occurrence of short-lived molecular configurations. The heavy ion radiative capture reaction, $^{12}\text{C}(^{12}\text{C},\gamma)$ affords another perspective on the molecular hypothesis. Sandorfi and Nathan [Phys. Rev. **C24**, 932 (1981)] found that this reaction was strongly resonant with a total capture cross section of less than $1\text{ }\mu\text{b}$ (see Fig. 86). They employed a large single-crystal sodium iodide detector to observe capture to the first few low-lying states in ^{24}Mg . This decay mechanism was attributed to a coupling to the GQR strength in ^{24}Mg . Due to pile-up of low-energy γ -rays in the NaI detector, it was not possible to answer the important question of whether a substantial proportion of the capture decay might be mediated through high-lying doorway states in ^{24}Mg . This is especially topical as these doorway states are likely to be highly deformed since they are intermediate between the molecular-like entry

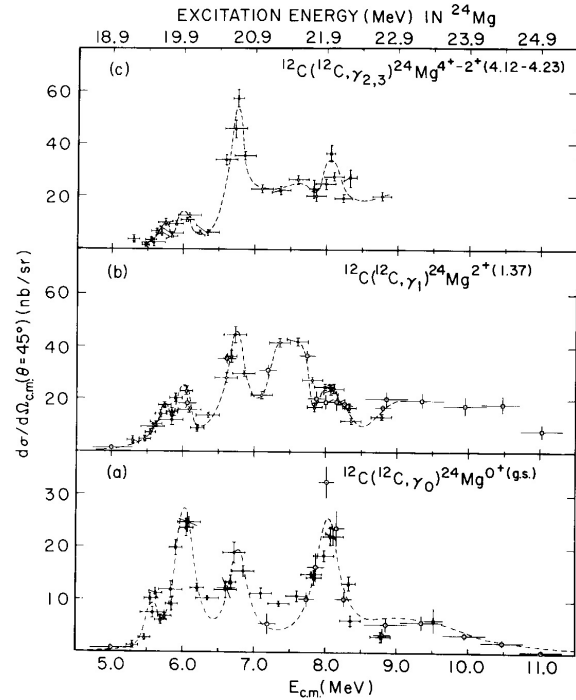


Fig. 86. Excitation functions for $^{12}\text{C}(^{12}\text{C},\gamma)$ measured by Sandorfi and Nathan.

state and the well-deformed ground state of ^{24}Mg .

Ongoing research

We have reopened the issue of heavy ion radiative capture with a series of measurements using the Gammasphere array of HPGe detectors at Argonne National Laboratory. These measurements strongly suggest that multi-step decay is, indeed, the predominant mechanism and that the total capture cross section is significantly larger than was previously believed. These studies, however, were complicated by the very poor efficiency of the Gammasphere array for the high energy (10–20 MeV) γ -rays involved in the capture mechanism.

Role of DRAGON

The unique combination of the DRAGON separator and its associated BGO detector array allows us to explore the full phase space for the decay mechanism by detecting the high energy capture γ -rays in coincidence with ^{24}Mg fusion residues. In order to perform these measurements, a solid target mechanism was designed and built for installation at the target position of DRAGON. An initial week of data was taken in November, at a beam energy corresponding to the resonance previously observed at a centre-of-mass energy of 8.0 MeV (see Fig. 86). It was possible to cleanly separate and identify ^{24}Mg residues at the focal plane. Moreover, high energy γ -rays were detected in coincidence with these residues. It should be noted that the recoil kick imparted by the high energy γ -rays means that depending on the angle of emission, only a fraction of the residues make it into the acceptance of the separator. This effect is qualitatively understood and is presently being modelled using the Monte Carlo modelling package, GEANT. This will allow absolute cross sections for the different decay pathways to be obtained from the observed γ -ray coincidences.

Future plans

The initial measurements have been very promising and it is planned to run for a further two weeks in early 2004, when we hope to cover lower energy resonances in the $^{12}\text{C}+^{12}\text{C}$ system.

Experiment 948

Proton and neutron radiation effects in silicon-on-insulator and bulk-silicon devices

(J.R. Schwank, Sandia National Laboratories)

Introduction

The primary goal of these experiments was to investigate proton radiation-induced effects on silicon-on-insulator and bulk-silicon devices for space applications. The proton energy range available at TRIUMF (~ 20 to 500 MeV) is well matched to the energy spectrum of protons in space. The experiments

were divided into four main tasks: 1) the investigation of proton-induced single-event effects in advanced SRAMs, 2) investigation of the effects of proton-induced displacement damage on the single-event latchup rate, 3) evaluation of TRIUMF's neutron source capability for simulating the terrestrial neutron environment, and 4) determination of the optimum laboratory radiation source for simulating the space environment.

Single-event effects

One of the most detrimental effects of the natural space environment on electronics is single-event effects (SEE). In memory circuits, information is stored at nodes in a circuit. If a high-energy heavy ion strikes a circuit node, it can create sufficient charge in a transistor to change the state of the node and cause false information to be stored. This type of failure is a non-destructive soft error and is known as a single-event upset (SEU). In addition to heavy ions, protons and neutrons can also cause single-event upset.

This year at TRIUMF, we performed several experiments investigating proton and neutron induced SEE in silicon-on-insulator and bulk-silicon ICs. Proton experiments were performed to investigate proton-induced SEE in advanced SRAMs. We also investigated the dependence of single-event upset cross section on angle of incidence by comparing front versus back-side exposure. Neutron experiments were performed to evaluate TRIUMF's newly developed neutron capability as a source for investigating the effects of terrestrial neutron exposure on commercial ICs. We also performed proton experiments to investigate the effects of proton-induced displacement damage and total-dose effects on the single-event latchup rate in SRAMs.

Space does not permit showing all of the test results. Two of the interesting studies are described here.

Evaluation of TRIUMF's neutron facility (TNF)

The TRIUMF neutron facility (TNF) comprises one of the neutron channels located at the high power beam dump. At this dump typically 100–150 μA of 450–500 MeV protons are stopped after passing through meson and isotope production targets. A track with a pulley system was installed in a vertical access channel to allow measurement instrumentation to be lowered to neutron beam level. Devices to be tested or activation foils are mounted on a trolley plate, which can be accurately placed in the beam.

To confirm the suitability of the TRIUMF neutron irradiation facility for terrestrial cosmic ray soft error rate (SER) characterization, 5 different SRAM types were irradiated that had previously been characterized at the Los Alamos National Laboratory Weapons Neutron Research (WNR) facility.

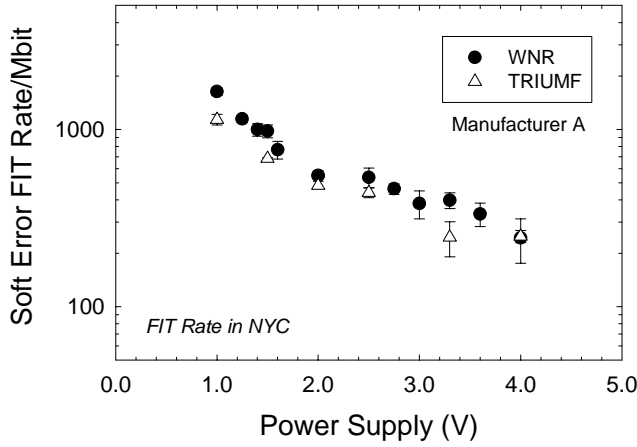


Fig. 87. Neutron-induced SER in 1.5/3.3 V 6T full CMOS 1 Mbit SRAMs from manufacturer A's 0.16 μm process as a function of power supply voltage. Ground-level FIT rates are shown for New York City.

Figure 87 shows the measured SER in 6T CMOS 1 Mbit SRAMs from manufacturer A's 0.16 μm process as a function of power supply voltage. The TRIUMF data are in reasonably good agreement with previous WNR tests, but appear to be systematically 10–30% lower than the SER calculated from the WNR data.

In contrast to the WNR neutron spectrum, the continuous neutron spectrum in the TNF includes a contribution from thermal neutrons. It has previously been shown that some ICs are sensitive to thermal neutrons, especially those whose construction incorporates boron-10. In Fig. 88, the neutron-induced SER in a 5 V 4 Mbit SRAM from a third manufacturer is plotted as a function of power supply voltage. Previous experiments have shown that this SRAM is sensitive to thermal neutrons. Data were taken at TRIUMF using both the unmoderated spectrum, and with a sheet

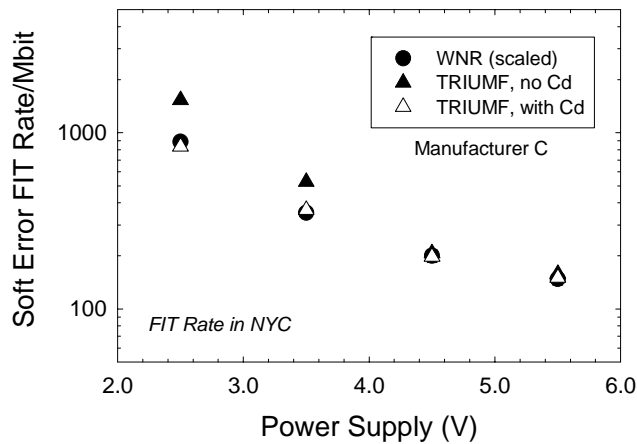


Fig. 88. Neutron-induced SER vs. power supply voltage in 5 V 6T TFT-load 4 Mbit SRAMs from manufacturer C. The WNR data were multiplied by 0.75 to match the TRIUMF data. Note increased SER at low power supply due to thermal neutron contribution in unmoderated TRIUMF spectrum.

of cadmium covering the SRAMs to remove all thermal neutrons. At low supply voltages, the unmoderated TRIUMF data lead to a calculated SER about a factor of two higher than with the cadmium sheet, indicating a significant enhancement in SER due to thermal neutrons at these voltages. In contrast, data taken with the cadmium sheet in place match the scaled WNR data at all voltages, indicating successful removal of the thermal neutron flux.

Total dose hardness assurance

The energetic electrons and protons of the space environment will generate radiation-induced charge in the gate and field oxides of bulk-silicon and silicon-on-insulator (SOI) devices. This charge buildup can cause parametric and/or functional failure of ICs. Recent works have demonstrated that proton degradation is more accurately simulated by X-ray irradiation, over a wide range of proton energies. Similarly, Co-60 gamma degradation was also shown recently to match electron degradation. This raises concerns about what laboratory source is best for qualifying bulk-silicon and SOI devices for space environments.

The work that we performed this year at TRIUMF culminates a three-year effort to determine the optimum laboratory radiation sources for qualifying bulk-silicon and SOI devices for space environments.

The samples were irradiated with 10 keV X-rays, Co-60 γ -rays, 41.4 MeV protons, and 1 MeV electrons, in the ON bias configuration ($V_G = 5$ V). During total dose irradiation, radiation-induced positive charge builds up in the field oxide. This charge buildup can turn on the lateral parasitic transistor structure, revealed by an increase in leakage current (drain current at $V_G = 0$ V). The results are displayed in Fig. 89,

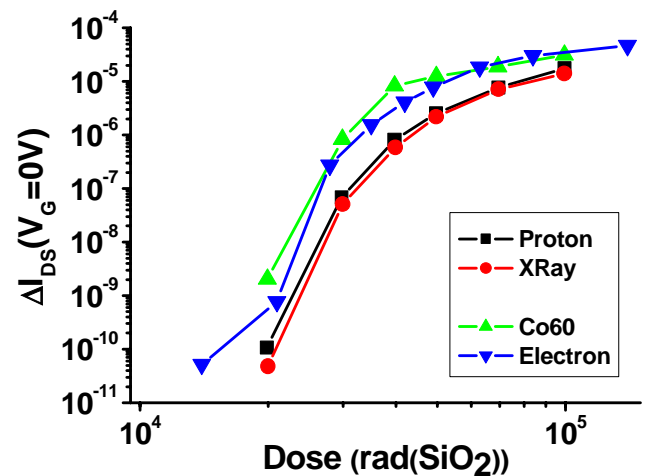


Fig. 89. Radiation-induced increase in leakage current (drain current at $V_G = 0$ V) versus total dose, for non-hardened bulk-Si transistors irradiated with 10 keV X-rays, 41.4 MeV protons, Co-60 γ -rays, and 1 MeV electrons. The transistors were irradiated with ON bias configuration.

where the increase in leakage current of the bulk-silicon transistors is plotted for the different radiation sources.

For the different technologies investigated here, the total dose degradation caused by protons with energies up to 200 MeV is well simulated by 10 keV X-ray irradiation, and the total dose degradation caused by 1 MeV electrons is well simulated by Co-60 γ -ray irradiation.

This work has been published in IEEE Trans. Nucl. Sci. **50**, 2310 (2003).

Experiment 952

A new measurement of $^{12}\text{C}(\alpha, \gamma)^{16}\text{O}$ reaction (*L. Buchmann, TRIUMF*)

The $^{12}\text{C}(\alpha, \gamma)^{16}\text{O}$ reaction determines the ratio of oxygen to carbon in the universe, among other things. Yet it is one of the remaining reactions in nuclear astrophysics of high relevance which is rather poorly determined. The reason is that there are no compound states of natural parity in ^{16}O at the energies corresponding to quiescent helium burning. In fact, there is a complex mixture of ground state and cascade transitions of different types.

The difficulty in determining this cross section so far has been the complexity of extrapolation combined with the overall low cross sections. In measurements of the emanating γ -rays considerable backgrounds are also encountered. In Exp. 952 it has therefore been proposed to measure both recoil particles and γ -rays in coincidence with the DRAGON facility at TRIUMF. Given acceptance restrictions of DRAGON, we decided to measure the high energy region first, roughly defined as energies above the first 4^+ state at $E = 10.36$ MeV. At these energies the cross section of the cascade transition into the $E = 6.9$ MeV state, which is a sub-threshold state important for determining the reaction rate, is directly proportional to the α strength of that 6.9 MeV state [Buchmann, Phys. Rev. **C64**, 022801(R) (2001)]. In addition, the transition to the ground state is most likely of pure $E2$ nature, contrary to lower energies, where the $E1$ transition is dominant.

We have made runs in April/May and November. We covered energies from 0.75 MeV/u to 1.5 MeV/u ($E = 2.25$ –4.5 MeV). In summary, we made the following observations:

- The recoil spectra are free of background. As an example, Fig. 90 shows the single recoil and the coincidence γ spectrum of the 1.07 MeV/u 4^+ resonance.
- The ^{12}C beam current which can be delivered by using a carbon stripper is marginal (about 50 pA), still big enough though to obtain events at the lowest measured energy. However, the data require information about angular distributions

and fits to cascade data, i.e. acceptable statistical accuracy.

- The acceptance of DRAGON is challenged for the present configuration given the recoil angle involved in the $^{12}\text{C}(\alpha, \gamma)^{16}\text{O}$ reaction. We found, however, sextupole polarities to be corrected and a more symmetric tune which, as tests have shown, delivers full transmission through DRAGON at higher energies.
- The angular recoil distribution for the ground state shows up very nicely in the energetic distribution of the recoil particles and thus delivers this crucial angular distribution with far better resolution than can be obtained from the BGO array of DRAGON.
- There is clear evidence for a cascade transition to the $E_x = 6.05$ MeV state in ^{16}O (see Fig. 91 for an example spectrum).
- Between the first and second 4^+ resonance cascade transitions are clearly dominant.

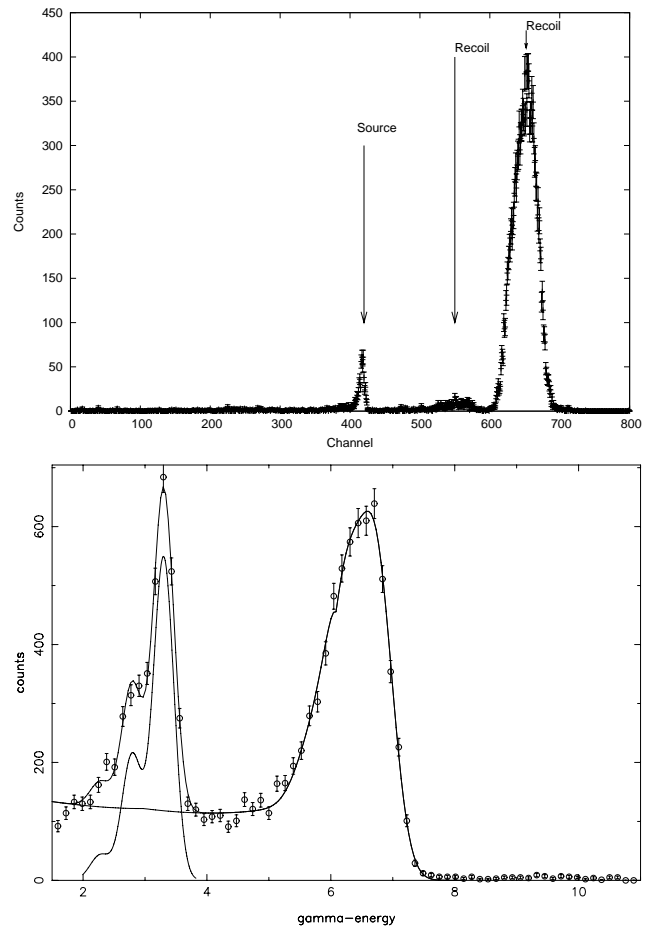


Fig. 90. Upper panel: Single recoil spectrum in $E = 3.2$ MeV resonance. Lower panel: γ spectrum gated by the recoil events of the upper panel. A fit to the cascade decay over the 6.9 MeV state is also shown.

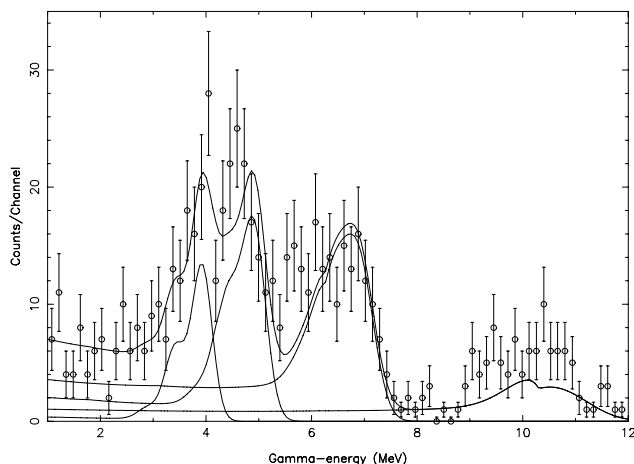


Fig. 91. Recoil gated γ -spectrum taken at 1.28 MeV/u and fit to its components. The primary transition to the 6.05 state is visible at 4.95 MeV.

Recently it has been demonstrated that the energy of the ISAC-DTL can be increased for a ^{12}C beam to 1.83 MeV/u. This will allow us to cover the $E_x=12.440$ MeV 1^- resonance which has a strong ground state $E1$ transition with its characteristic angular distribution centred around 90° . This will provide an acceptance test and a possible confirmation of our GEANT calculations of DRAGON which are in progress.

Experiment 955

Study of the β -decay of ^{32}Na

(F. Sarazin, Colorado School of Mines; G. Hackman, TRIUMF)

The structure of stable and long-lived nuclei is well understood in terms of the traditional magic numbers (2, 8, 20, 28, 50...) corresponding to large gaps in single-particle energy levels of nucleons in realistic mean-fields including a spin-orbit interaction. The evolution of shell closures far from stability is, however, a subject of much debate [Werner *et al.*, Phys. Lett. **B335**, 259 (1994); *ibid.*, Nucl. Phys. **A597**, 327 (1996)]. For example, a breaking of magicity has already been observed at the $N = 20$ shell closure, where an “island of inversion” in shell ordering has been shown to exist [Orr *et al.*, Phys. Lett. **B258**, 29 (1991); Warburton *et al.*, Phys. Rev. **C41**, 1147 (1990); Retamosa *et al.*, Phys. Rev. **C55**, 1266 (1997)]; more recently this has been seen at $N = 28$ for neutron-rich nuclei [Sarazin *et al.*, Phys. Rev. Lett. **84**, 5062 (2000)]. While understanding the apparent weakening or disappearance of the traditional shell closures far

from stability is a challenge for nuclear structure, it also has very important implications in nuclear astrophysics, as it will significantly affect the path of the r -process. In this context, a proposal for this experiment was submitted to the EEC in 2002 to probe the shell structure with β - and β -delayed γ -spectroscopy at ISAC/TRIUMF. The first nucleus studied was ^{32}Na , which β -decays to ^{32}Mg , a key $N = 20$ nucleus. The main goal of this experiment was to resolve some discrepancies observed in the ^{32}Mg level scheme. Two beam time periods (August 17–20 and October 8–17) in 2003 were allocated for the study of the β -decay of ^{32}Na .

The ^{32}Na beam was extracted from a tantalum production target and implanted onto a moving tape at the centre of the 8π /SCEPTAR facility described in the Experimental Facilities section of this Annual Report. In the course of the experiment, the intensity of the proton beam impinging the production target was increased from 40 μA to 50 μA . An estimated 2 ^{32}Na atoms per second was delivered to the 8π . At this very low rate, the combination of the 8π , SCEPTAR and tape system has shown its potential to produce very clean spectra. Several time cycles of the tape system were used in order to remove, efficiently, the build-up of the long-lived daughters of ^{32}Na .

γ -ray energy spectra from the first period are shown in Fig. 92. A significant part of the beam time during this test period was spent on optimizing ISAC optics settings. No new γ -ray lines were seen during this period. However, it clearly demonstrated the potential of the experimental set-up for seeing transitions in nuclei produced with very low yield.

The main data set (October 8–17) is currently being analyzed. Spectra obtained on-line show some previously unreported lines in the ^{32}Na spectrum. However, their placement in a decay scheme requires a more thorough analysis. A preliminary spectrum is shown in Fig. 93. The identified lines are transitions known or believed to originate from the γ -decay of ^{32}Mg following the β -decay of ^{32}Na .

This collaboration includes scientists from TRIUMF, Colorado School of Mines, McMaster University, University of Guelph, Queen’s University, Lawrence Livermore National Lab, Lawrence Berkeley National Lab, Georgia Institute of Technology, Louisiana State University, University of Surrey, and University of Vienna.

β -decay of ^{32}Na

- Test Run -

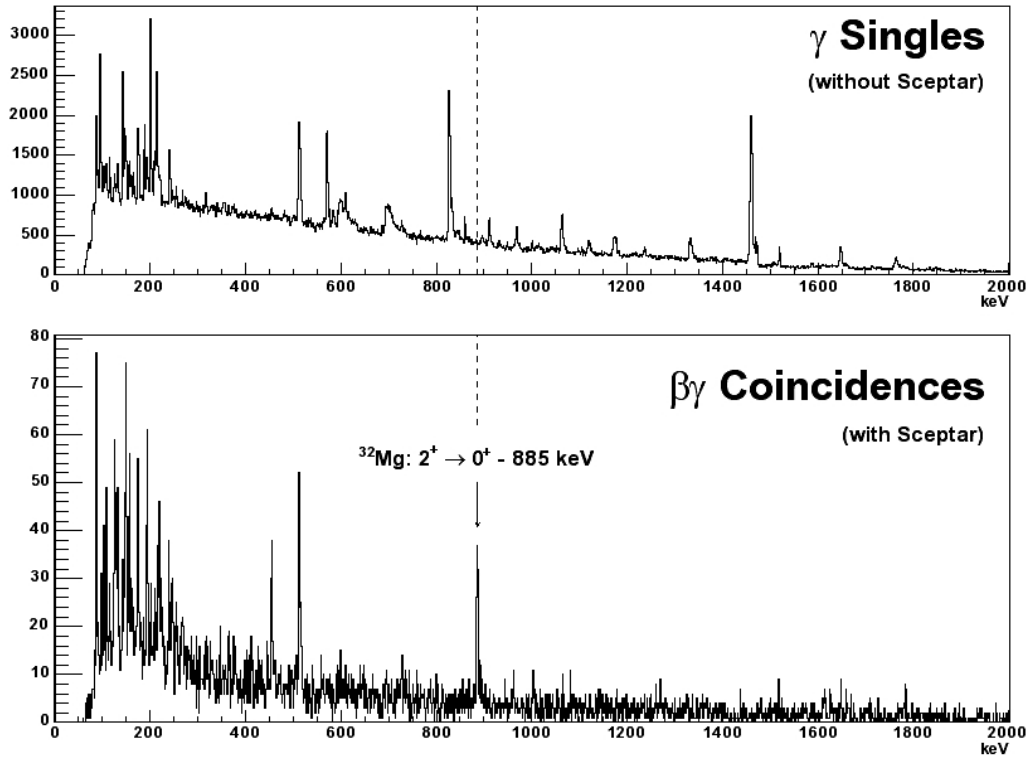


Fig. 92. Top: unconditional γ -ray spectrum; bottom: γ -ray spectrum in coincidence with β s detected in SCEPTAR, demonstrating the resolving power of the experimental set-up.

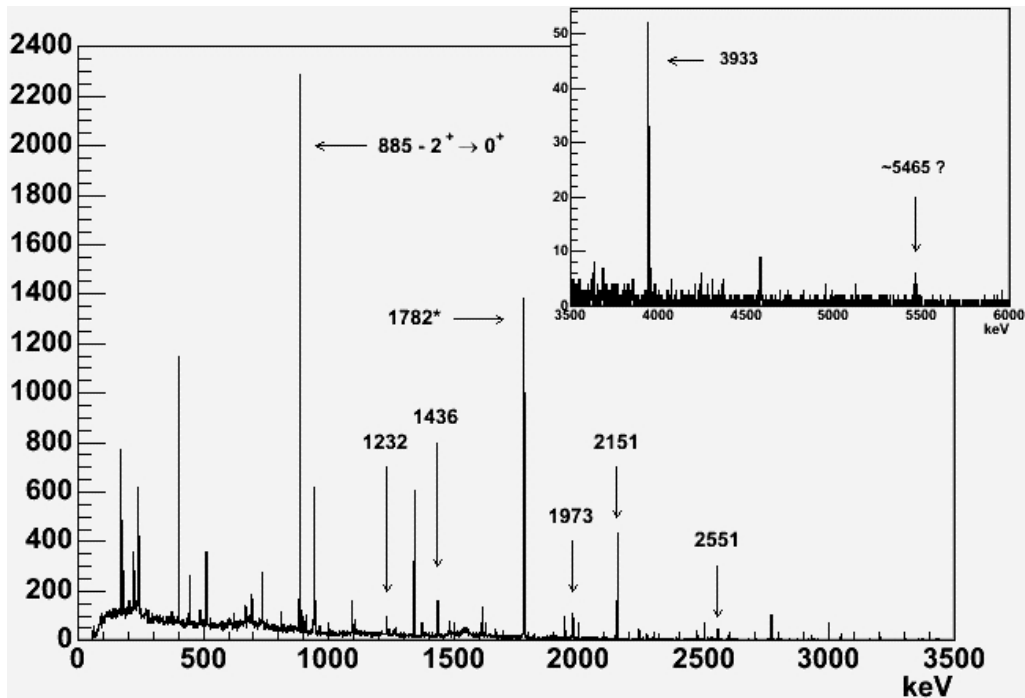


Fig. 93. (VERY PRELIMINARY) β -decay of ^{32}Na . The identified γ lines correspond to the decay of excited states of ^{32}Mg . The * sign indicates that the actual 1782 keV transition is part of a more pre-eminent transition coming from a contaminant. The ? sign indicates a possible new transition in ^{32}Mg .

Experiment 964

A study of the partial and total cross sections of the $^8\text{Li}(\alpha, n)^{11}\text{B}$ at astrophysically relevant energies

(A. Laird, York; P. Walden, TRIUMF)

The precise measurement of the $^8\text{Li}(\alpha, n)^{11}\text{B}$ cross section is an important measurement to know in the astrophysical sense. This reaction is deemed to play an important role in initiating r-process nucleosynthesis in core collapse supernovae, and in the production of light elements abundances in inhomogeneous big bang models (IBB). It is one of the few reactions that can play a key role in spanning the mass 8 gap and as such should be known and well determined. Cross section measurements to date have either large error bars or are conflicting.

The proposed experiment will measure the cross section directly in a large solid angle ion chamber which will be constructed. The future chamber has been designated with the name TACTIC (TRIUMF annular chamber for tracking and identification of charged particles). The experiment will be done with reversed kinematics using a ^8Li RIB beam from ISAC. Both the production of ^{11}B ions in the ground state and excited states would be identified. The excited states would be further selectively defined by a coincidence between the ion detection and the γ -ray picked off in an array of gamma detectors surrounding the chamber (the array will be initially borrowed from DRAGON).

The TACTIC concept is a specially designed cylindrical symmetrical ion chamber enclosing a full length cylindrical target with a larger diameter ion drift region. The dimensions of the chamber will be approximately 20 cm in length by 10 cm in radius. The size of the chamber and gas pressure used in TACTIC will be such that the ^{11}B ions will stop. The ion collectors will be mounted along the cylinder's outside radius to give "l" and " ϕ " coordinates. Drift time with respect to the ISAC accelerator rf will give the "r" coordinate. The path of the ion will thus be mapped out. The signal strength will be proportional to the dE/dx and will identify the ion type (e.g. ^{11}B or an elastically scattered α or ^8Li). The chamber as designed will not be just for one specific experiment. It can be used for other measurements. One experiment of significance that could use the TACTIC geometry is measurements of $^{12}\text{C}(^{12}\text{C}, \alpha)^{20}\text{Ne}$ and $^{12}\text{C}(^{12}\text{C}, p)^{23}\text{Na}$ fusion which are key reactions for understanding supernova type Ia events.

We have been experimenting with GEM signal amplification technology and have acquired several samples of GEM material to this end. A planar GEM chamber is to be constructed and tested. A cylindrical GEM chamber will be manufactured for the next stage. A

VME card has been acquired which has a 50 MHz sampling rate. The same card can be used for time and ADC extraction. Significant progress on the chamber is expected in 2004.

Experiment 967

Beta decay branching ratio of ^{21}Na

(S.J. Freedman, UC Berkeley-LBNL)

Our recent measurement of the β - ν correlation coefficient in the beta decay of laser trapped ^{21}Na , $a_{\beta\nu} = 0.5243 \pm 0.0092$, differs by 3.6σ from the standard model prediction of $a_{\beta\nu} = 0.558 \pm 0.003$ [Scielzo *et al.*, submitted to Phys. Rev. Lett.]. The uncertainty in the decay branching ratio to the excited state of ^{21}Ne ($5/2^+$) is the largest systematic uncertainty in the measurement.

The current accepted value of the branching ratio is 0.0502(13). This is in agreement with shell model estimates of 0.05(1), but there are large disagreements among previous measurements (see Fig. 94). The resulting systematic uncertainty in the ^{21}Na experiment is 0.7% in $a_{\beta\nu}$. Reducing the uncertainty in the branching ratio by a factor of 3 to a relative uncertainty of 1% will allow us to determine the β - ν correlation more accurately.

All previous measurements of the branching ratio used the ratio of 350 keV γ -rays which tag ^{21}Ne ($3/2^+ \rightarrow 5/2^+$) to 511 keV γ -rays which tag all $^{21}\text{Na} \rightarrow ^{21}\text{Ne}$ decays. They suffered from the presence of β^+ emitting contaminants. We are working on a different approach, taking advantage of recent developments in radioactive beams. The ISAC facility at TRIUMF is used to obtain a pure ^{21}Na beam with $<0.1\%$ contaminants. The technique counts individual accelerated ^{21}Na ions stopped in a thin scintillator and compares the particle number to the number of

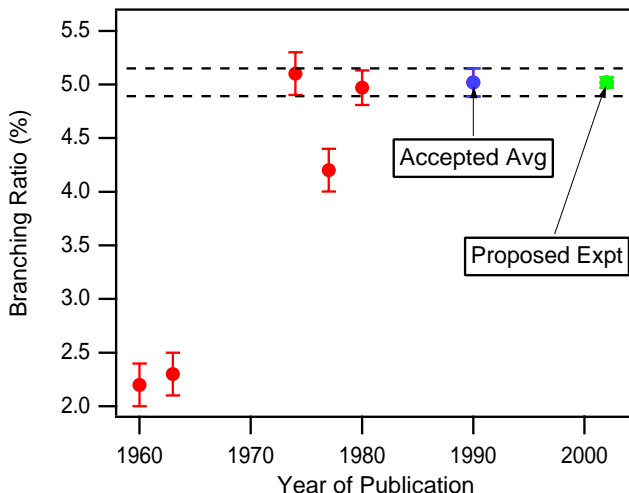


Fig. 94. Previous measurements of ^{21}Na decay branching ratio to the excited state of ^{21}Ne .

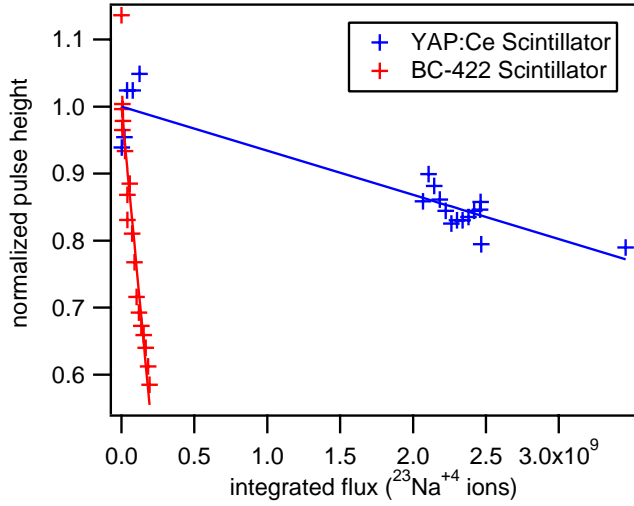


Fig. 95. Pulse height vs. number of incident ^{23}Na on YAP:Ce and BC-422.

350 keV γ -rays detected by a calibrated high purity Ge detector. The beam count rate of 10^5 – 10^6 ions/s is used to prevent pile-up. A total of 10^9 particles on target is required to reach the proposed sensitivity.

During the 2003 run, a plastic scintillator (BC-422) of 100 μm thickness was used. The rate of degradation of this scintillator due to radiation damage was unacceptably high. For the next run, we will use a YAP:Ce crystal scintillator which has been measured to have a higher radiation damage threshold by a factor of roughly 100 for γ -rays. A recent test at the LBNL 88 in. cyclotron using stable Na beam at similar energies of 1 MeV/u indicates that YAP:Ce is roughly 30 times more durable to heavy ion radiation damage than BC-422, and the damage will be limited for the dose required by this experiment (see Fig. 95).

Experiment 968

Ortho-para effect of muon catalyzed fusion in liquid deuterium; R&D of fusion neutron detection

(H. Imao, N. Kawamura, K. Nagamine, KEK)

The high resonant formation rate of $\text{dd}\mu$ in condensed deuterium has been one of the biggest problems in muon catalyzed fusion in pure deuterium ($\text{dd}\mu\text{CF}$). In order to solve this problem, a detailed understanding of the behaviour of muonic atoms and muonic molecules in condensed deuterium is necessary. Especially, the study of the ortho-para effect on μCF in condensed deuterium can provide much information to reveal the effects in condensed matter. However, the experimental study of the ortho-para effect on $\text{dd}\mu\text{CF}$ was carried out only in a solid [Toyoda *et al.*, Phys. Rev. Lett. **90**, 243401 (2003)]. The experimental ortho-para effect shows the opposite tendency against recent theoretical predictions. A further investigation

on the ortho-para effect in a wide temperature range can throw light on μCF phenomena. The aim of Expt. 968 is the observation of the dependence of the molecular formation rate and the hyperfine transition rate on the ortho-para states of deuterium in liquid and solid. To reach this goal, we have to obtain the time distribution of fusion neutrons for each state. The R&D of the fusion neutron detection system was performed with liquid normal deuterium at 19 K in November.

The experiment was performed on beam line M9B at TRIUMF. Our experimental set-up consists of the target cell in the vacuum chamber, the muon beam counters, neutron detectors, electron counters, a continuous-flow liquid cryostat and a gas handling system (GHS). The schematic view of our experimental set-up is shown in Fig. 96. The target cell was a cylindrical copper (2 mm thick) container, 30 mm in diameter, 30 mm in length and with a volume of 20 cc filled with liquid deuterium. Deuterium target status was monitored by measuring temperature and vapour pressure. In this run, we controlled the temperature of the liquid deuterium target at 19 K. The target gas was prepared by GHS, which is connected to the target cell. We used only normal deuterium gas, and the ortho-para conversion system was not used in this run. A μ^- beam was injected into the liquid target through the three collimators, of which the inner diameters were $\phi 50$ mm, $\phi 30$ mm and $\phi 25$ mm, respectively.

The muon incoming signal was created by the coincidence of the signals of two muon beam counters (B1, B2). A 60 MeV/c μ^- beam was used in the November run. One of the other detector signals coincident with the muon beam makes an event trigger and opens a 10 μs gate for data-taking. In order to eliminate the pile-up, the following condition is required: no muon incoming 10 μs before the event trigger, no subsequent muon incoming during 10 μs event gate. This condition reduces the background and suppresses distortion of the time spectra due to pile-up.

Muon decay electrons were detected by four pairs of plastic scintillation counters (E1–E8) placed around the target in order to determine the muon's stopping distribution. E1–E4 counters had a $\phi 5.5$ cm

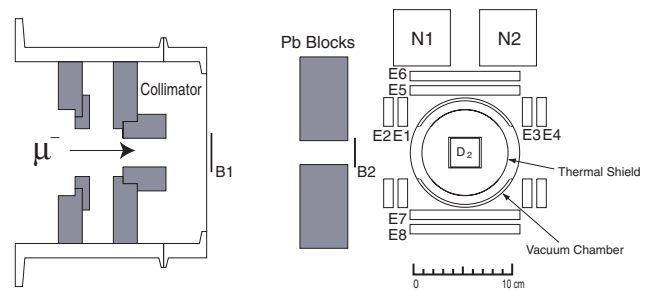


Fig. 96. Cross-sectional view of the experimental set-up in the November run.

hole at the centre for the muon entry. The timing and pulse height of coincidence signal from each pair of counters were recorded. As a neutron detector, $\phi 2$ in. \times L2 in. NE-213 viewed by a photo-multiplier (Hamamatsu H1161) was used. NE-213 was chosen for its pulse shape discrimination properties. We placed two neutron detectors (N1, N2) at 10 cm from the target perpendicular to the μ^- beam. Charge-veto for neutron detection was not necessary because of the perpendicular position. For discrimination between gammas and neutrons, a pulse shape analyzer (Ortec PSA552) and a delay line amplifier (Ortec DLA460) were adopted. The time difference of the output signals from the DLA module, which reflects the pulse shape, was recorded. The energy scale of the neutron detector was calibrated by the Compton edges of two gamma sources (^{60}Co and ^{137}Cs).

The method for analysis of neutron data is essentially the same as Knowles' method [Knowles *et al.*, Phys. Rev. **A56**, 1970 (1997)]. The neutron events consist of fusion neutrons, n_f , capture neutrons, n_c , and neutrons from ambient background, n_z . In order to obtain the fusion neutron spectra, the pulse-shape discrimination gate, the pulse-height cut, and the delayed electron coincidence condition (dele condition) with the efficiency ϵ_e were demanded. The pulse height window was chosen as 0.4–0.7 MeV electron energy scale (Fig. 97). The dele condition was satisfied if the muon decay electron was detected between 0.2 and 5.0 μs after the time of a candidate of fusion event. The time window efficiency includes the detector solid angle, Ω_e , as given by

$$\epsilon_e = \Omega_e \lambda_0 \int_{0.2 \mu\text{s}}^{5 \mu\text{s}} d\tau e^{-\lambda_0 \tau}.$$

The raw neutron spectra, n_r , and dele spectra, n_{dele} are given by

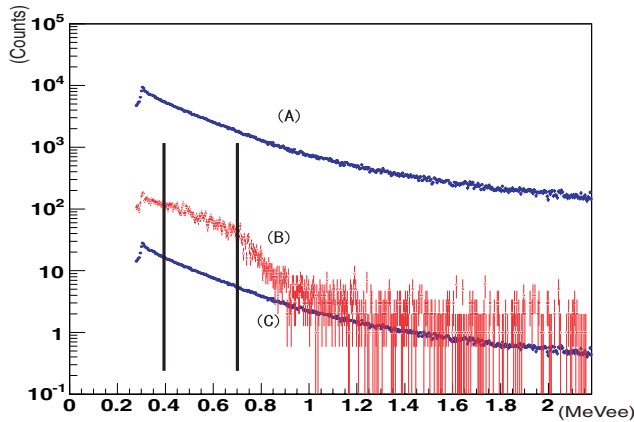


Fig. 97. Pulse height spectra without (A) and with dele condition (B) and accidental neutron spectra (C) in the deuterium target run. A pulse height cut was chosen, selecting events between the solid vertical lines.

$$n_r = n_f + n_c + n_z,$$

$$n_{\text{dele}} = \epsilon_e n_f + \epsilon_a n_r + \left(\Omega_e \lambda_0 \int_{t+0.2 \mu\text{s}}^{t+5.0 \mu\text{s}} d\tau \Theta(\tau - t_0) e^{-\lambda_0(\tau - t_0)} \right) n_z,$$

where ϵ_a is accidental efficiency. The dele condition strongly suppressed capture neutron background. As a result of these demands, the overall background was reduced to 10% for the fusion neutron measurement. Remaining background consists mainly of capture neutrons due to muon stops in the target cell.

Figure 98 is typical fitting results of neutron time spectra. The resonant $\text{dd}\mu$ formation rate and hyperfine transition rate are determined to be $\tilde{\lambda}_{3/2} = 2.6 \pm 0.1(\text{stat.}) \pm 0.2(\text{syst.})$ and $\tilde{\lambda}_{3/21/2} = 32.0 \pm 1.3(\text{stat.}) \pm 0.3(\text{syst.})$, which are consistent with other recent measurements [Demin *et al.*, Hyp. Int. **101/102**, 13 (1996)]. The muon loss rate by muon transfer process to impurities in the deuterium target was negligible in this run. This fact shows that some frozen impurities are deposited at the bottom in the liquid state target, and thus suppress the muon transfer process to the impurities. In the analysis, the empirically-based non-resonant molecular formation rate was used; $\lambda_{1/2} = 0.044 \pm 0.005$ [Scrinzi *et al.*, Phys. Rev. **A47**, 4691 (1993)]. In order to determine the absolute value of molecular formation rates, the calculations for the neutron detection efficiency and the muon stopping number in the deuterium target are performed.

Measurement of time distribution of fusion neutrons was carried out in liquid deuterium at 19 K. The results show that our neutron detection system can observe a few per cent difference of $\tilde{\lambda}_{3/2}$ and also $\tilde{\lambda}_{3/21/2}$ between ortho-rich and normal deuterium within our requested beam time. Toward the ortho-para experiment in August, 2004, many studies of ortho-para conversion are being promoted.

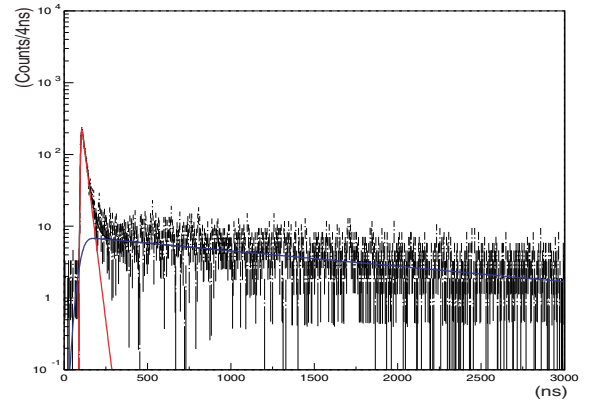


Fig. 98. Typical fitting results of time distribution of fusion neutrons with the accidental background subtracted.

Halo neutrons and the β -decay of ^{11}Li (F. Sarazin, Colorado School of Mines/TRIUMF)

The structure of ^{11}Li , a ^9Li core surrounded by two distant neutrons (the so-called halo), has been the subject of intense studies. In particular, the β -decay of ^{11}Li is expected to shed light on how the weak interaction affects (and is affected by) the two neutrons composing the halo.

In August, 2002, the β -decay of ^{11}Li was investigated at TRIUMF-ISAC with the 8π spectrometer, an array of 20 Compton-suppressed germanium detectors. ^{11}Li was produced by bombarding a 22 g/cm^2 Ta foil with a 500 MeV proton beam. A pure 30.4 keV ^{11}Li beam of about a thousand ions per second was extracted by surface ionization from the target and implanted into a 0.2 mm thick Al foil at the centre of the γ -detector array. A total of 8.1 M γ singles and γ - γ coincidence events were collected over a 2.5 day period (see TRIUMF 2002 Annual Report).

Most of the β -decay strength is observed to proceed through unbound states in ^{11}Be , which subsequently decay by one-neutron emission to ^{10}Be . This results in the observation of a γ -spectrum dominated by the decay of the excited states in ^{10}Be . As shown in Fig. 99, these transitions exhibit characteristic Doppler-broadened lineshapes.

A Monte Carlo simulation has been developed to analyze the complex shape of the γ -lines observed in this experiment. The lineshape of a given γ -peak mainly depends on the energies, widths and relative intensities of all the neutron branches feeding, directly or indirectly, the state from which the transition arises, and on the lifetimes of the excited states in ^{10}Be involved before the transition occurs due to the slowing down of the recoils. The lineshape of the peaks can also

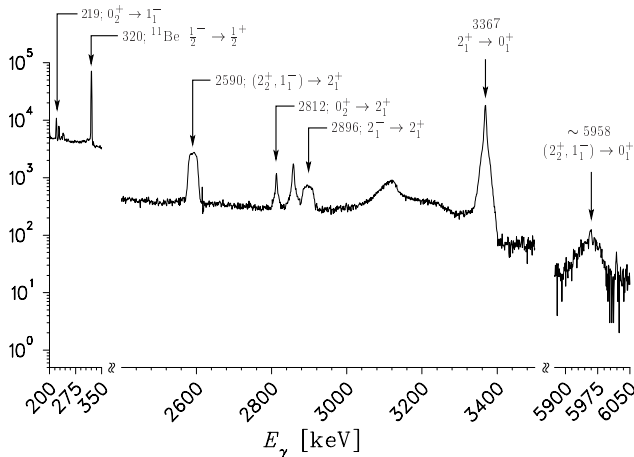


Fig. 99. Compton suppressed γ -spectrum following the β -decay of ^{11}Li . Only the relevant parts that contain the γ transitions observed in ^{10}Be and in ^{11}Be are shown (room background subtracted).

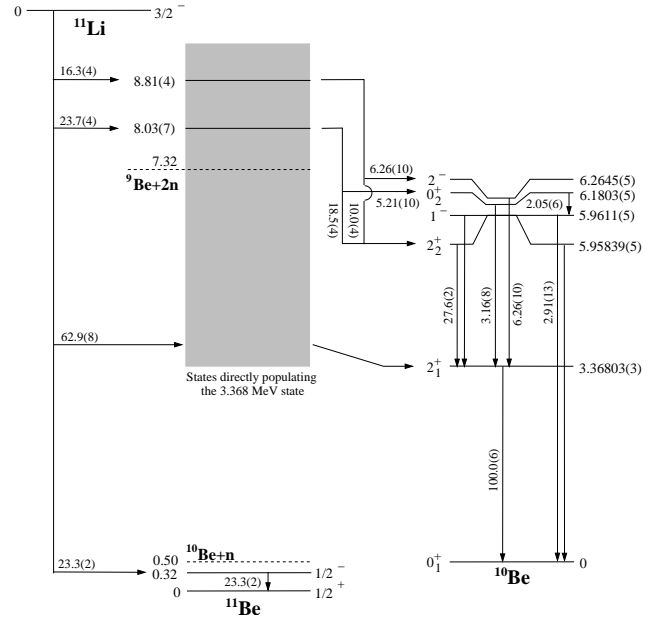


Fig. 100. Decay scheme of ^{11}Li deduced from this work. The energies of the two first excited states in ^{10}Be are the published values. All transitions are labelled with γ -ray intensities, normalized to the 3367 keV transition (100).

be affected by the angular correlation between the recoil and the γ -ray. The detailed β -decay scheme of ^{11}Li obtained from this experiment is shown in Fig. 100.

In this report, we present the conclusions of the lineshape analysis. A more detailed description of the procedure is presented in the upcoming publication [Sarazin *et al.* (submitted to Phys. Rev. C)]. The lineshape analysis of the 2896 keV transition originating from the 2^- state and of the 2812 keV transition originating from the second 0^+ state is fairly straightforward as no angular correlation between the recoil and the γ -ray is expected. This arises from the fact that the 2^- state is believed to be fed mainly by a $\ell=0$ neutron, whereas the γ -ray emission from a 0^+ state is naturally isotropic. The remaining free parameters are the energy of the given transition, the energy of the neutron that gives rise to the observed Doppler broadening and the half-life of the state of origin. We find that the lineshape of the 2896 keV transition is best described by a neutron originating from the 8.81(4) MeV state in ^{11}Be and a half-life for the 2^- state of $85(6)$ fs, whereas the lineshape of the 2812 keV transition is best described by a neutron originating from the 8.03(7) MeV state in ^{11}Be and a half-life for the 0^+ state of 871^{+75}_{-70} fs. No need was found to add any other neutron branch to fit the experimental lineshapes of both these transitions. The analysis unambiguously confirms the existence of the 8.03 MeV state suggested once [Aoi *et al.*, Nucl. Phys. **A616**, 181c (1997)], but not confirmed. It also shows that the uncertainties in the energy determination of the states in ^{11}Be in this experiment are,

remarkably, as small as those obtained from neutron spectroscopy experiments.

The analysis of the transitions originating from the $(1^-, 2_2^+)$ doublet states is more complex as it involves the indirect feeding from the 0^+ state and the feeding of the 2_2^+ state implies a $\ell=1$ neutron inducing possible angular correlation effect. We find that the lineshapes of the 2590 keV and of the 5958 keV transitions are a composite of, at least, 3 different contributions. Beside the indirect contribution of the 0^+ state to the line-shape, we show that two different neutron branches, from the 8.03 MeV and the 8.81 MeV states in ^{11}Be , feeding the 2_2^+ state are required to obtain the best fit of both transitions. Although it is not possible to rule out a (small) direct neutron feeding of the 1^- state, the best fits are obtained without the need to include one. A limit on the half-life of the 2_2^+ state was determined to be $30 < T_{1/2} < 160$ fs. It is not possible to get a better determination with the present data because of the strong correlation between the half-life and the angular correlation parameter A_2 .

The best fits for the four discussed transitions are shown in Fig. 101.

It has been suggested that if the β -decay of a halo nucleus takes place within its core, then it is possible for the halo wave function to retain its features after the β -decay, even though the core may now have a rather different structure. In this work, we show that two possible halo-like $(1n)$ configurations in ^{10}Be , namely the 2^- and 2_2^+ excited states, are fed by the β -

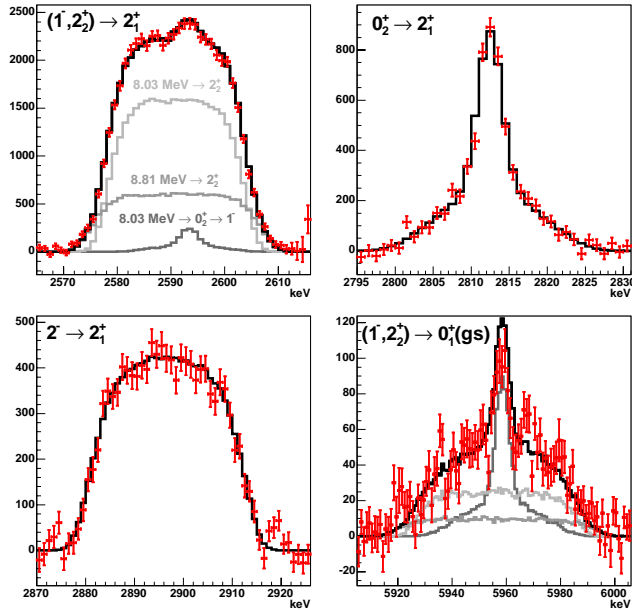


Fig. 101. Comparison between the experimental data and the best-fit obtained by the Monte Carlo simulation (black line). For the transitions involving the $(1^-, 2_2^+)$ doublet, a breakdown of the 3 contributions discussed in the text is also shown.

delayed neutron emission of ^{11}Li through the 8.81 MeV excited state in ^{11}Be . This excited state is strongly populated by 2n-transfer reaction and has been unambiguously shown recently to be the main excited state involved in the β -delayed two-neutron emission of ^{11}Li [Marques, private communication (2003)]. This strongly suggests that this state has a large overlap with a $^9\text{Be}+n+n$ configuration and that the β -decay of ^{11}Li to the 8.81 MeV state in ^{11}Be is likely to occur in the ^9Li core, leaving the two original halo neutrons of ^{11}Li undisturbed. The neutron emission path from this state is found to be consistent with the emission of one of the two halo neutrons, the surviving neutron giving the extended configuration suggested for the 2^- and 2_2^+ states in ^{10}Be .

LANSCÉ Experiment NPDGamma

Measurement of the parity-violating gamma asymmetry A_γ in the capture of polarized cold neutrons by para-hydrogen, $\bar{n} + p \rightarrow d + \gamma$

(S.A. Page, W.D. Ramsay, Manitoba)

Introduction

In this experiment at the Los Alamos Neutron Science Center (LANSCÉ), a beam of polarized cold neutrons is directed on a liquid hydrogen target where neutrons are captured via the $\bar{n}p \rightarrow d\gamma$ reaction. The γ -rays produced are expected to be emitted slightly more in the direction opposite to the neutron spin. Such an asymmetry is parity violating and is a signature of the weak nuclear force. The capture reaction is dominated by the long range part of the nuclear force, and the parity violating up-down asymmetry $A_\gamma \approx -0.11f_\pi$ provides a clean measure of the weak pion-nucleon coupling, f_π . (Some authors quote $H_\pi = f_\pi \frac{g_\pi}{\sqrt{32}}$, where g_π is the strong pion-nucleon coupling.) Despite several decades of intense experimental and theoretical effort, the strength of f_π is still a mystery. The most precise limit on f_π alone is believed to be from measurements of circularly polarized γ -rays from a parity mixed doublet in ^{18}F . These results, however, indicate a coupling constant consistent with zero, in contrast to a relatively large value implied by measurements of the anapole moment of ^{133}Cs via atomic parity violation. The np system is the only two nucleon system that is sensitive to the weak meson-nucleon coupling f_π^1 and, unlike the ^{18}F and ^{133}Cs results, can provide a clean measurement free of nuclear structure uncertainties. The best published $\bar{n}p \rightarrow d\gamma$ result, from a measurement at ILL Grenoble, is $A_\gamma = (6 \pm 21) \times 10^{-8}$, which is not accurate enough to impose a significant constraint. Advances in techniques for producing high intensity beams of polarized, cold neutrons now make possible for the first time a measurement of A_γ and hence f_π^1 to within 10% of model predictions.

The $\bar{n}p \rightarrow d\gamma$ collaboration involves 13 institutions, with Canadian collaborators from the University of Manitoba, and infrastructure support from TRIUMF. The authors of this report, S.A. Page and W.D. Ramsay, have taken responsibility for precision monitoring of the neutron beam flux, and have designed a new current mode beam monitor that was tested successfully in the fall of 2001 at LANSCE. Three additional beam monitors based on this new design have now been constructed for the experiment. In 2002, we expanded our role, with vital infrastructure support from TRIUMF, to include design and construction of an integrated stand for the gamma detector array and liquid hydrogen target with remote position control for calibration of the effective detector alignment *in situ*. This procedure requires that the entire one-tonne detector array be moved accurately in the vertical and horizontal directions by up to ± 5 mm. The required stand and motion control system was designed at TRIUMF, constructed at the Manitoba and TRIUMF shops, and is now undergoing final testing at Los Alamos. TRIUMF has also designed custom VME modules that permit the gain of each of 48 detector channels to be adjusted under computer control. One prototype is at Los Alamos for testing and 6 more will be fabricated at TRIUMF in 2004. We have engaged an M.Sc. student from the University of Manitoba who will do his thesis work on the commissioning run in 2003–4. A TRIUMF Co-op student has contributed to aspects of the detector package assembly, and a University of Manitoba NSERC USRA award holder worked on magnetic shielding and preparations for the new experimental cave during the summer of 2003. The Canadian group will also work on commissioning of the apparatus and diagnosis and minimization of systematic errors. The experimental cave is due to be completed in January,

2004, followed by a commissioning run early in 2004 and a first phase of data taking at LANSCE in late 2004.

Apparatus

The basic requirements of the experiment are an intense source of polarized cold neutrons, a liquid parahydrogen target, a high-efficiency, large solid angle γ -ray detector, and a means of reversing the spin of the neutron beam with minimal effect on other beam properties. At LANSCE, the neutron beam is produced by an 800 MeV proton beam pulsed at 20 Hz impinging on a tungsten spallation target; MeV neutrons emerging from the target are cooled in a liquid hydrogen moderator and transported via a supermirror guide to the experimental apparatus (Fig. 102), where they emerge with a time of flight distribution indicated in Fig. 103. The supermirror guide enhances the total neutron flux in the desired energy range (0–15 meV) by about a factor of 3 with respect to the Maxwellian distribution of neutrons emerging from the moderator. The pulsed beam enables the neutron energies to be determined from their times of flight.

Neutrons are polarized in the vertical direction by selective transmission through a polarized ^3He gas cell which acts as a spin filter, producing the energy dependent polarization spectrum indicated in Fig. 103 (top). The neutron beam intensity is measured with a current mode ^3He ionization chamber (Fig. 103, bottom) mounted on the end of the neutron guide. The transmission of the ^3He polarizer cell is measured with a similar device mounted immediately downstream, to provide an on-line measurement of its polarization and hence that of the neutron beam. A resonant rf spin flipper reverses the neutron spin every beam pulse according to a $+-+-+-$ reversal pattern, cancelling

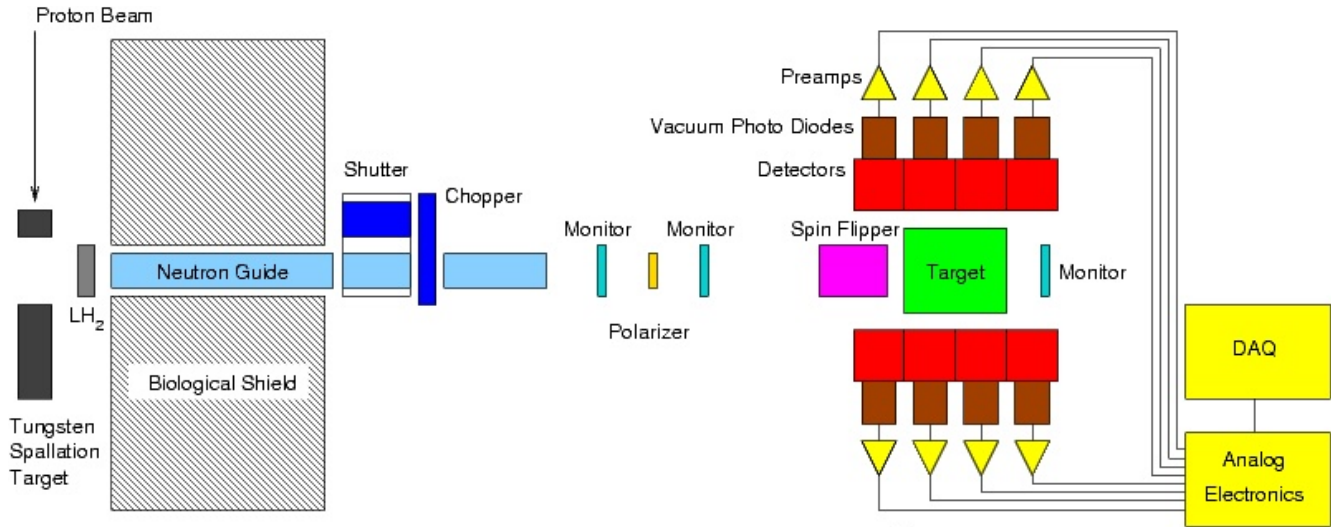


Fig. 102. $np \rightarrow d\gamma$ experimental apparatus at LANSCE.

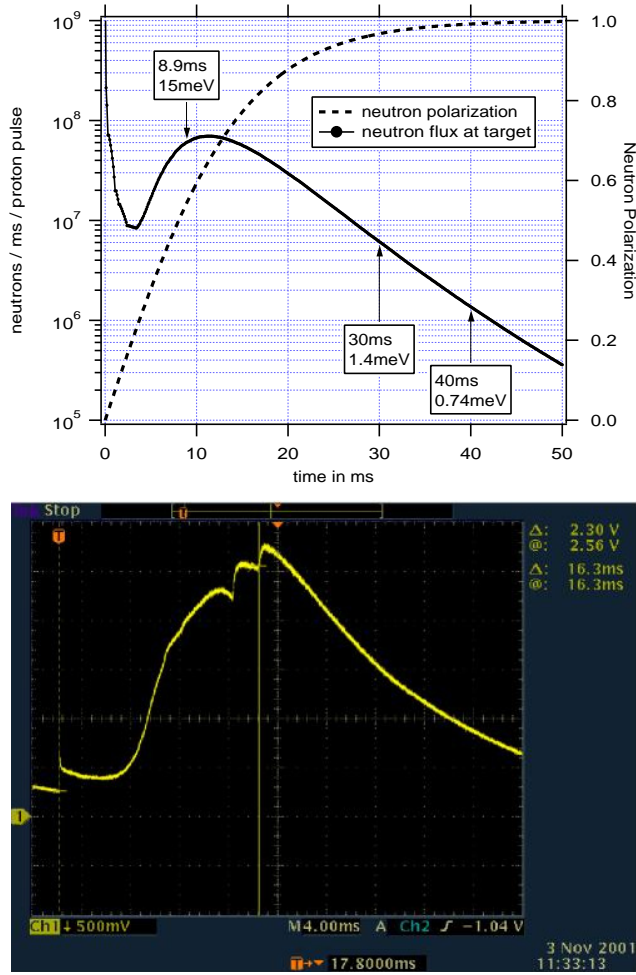


Fig. 103. Top: Predicted cold neutron beam flux and polarization. Bottom: neutron time-of-flight distribution measured by a dc coupled ^3He ionization monitor (frame overlap, the $1/v$ dependence of the capture cross section, and Bragg edges of Al beam windows account for the difference between top and bottom figures).

systematic drifts to second order. A uniform vertical guide field, $B_0 = 10$ G, preserves the neutron beam polarization as it is transported to the liquid hydrogen target; field uniformity at or below the 1 mG/cm level is essential for optimum performance of the ^3He polarizer cell, the rf spin flipper, and to avoid systematic errors due to the Stern-Gerlach effect.

It is important that the ortho-hydrogen fraction in the target be kept low ($\sim 0.05\%$). Low energy neutrons depolarize rapidly in ortho-hydrogen, while those below 15 meV retain their polarization in a para-hydrogen target. To monitor the ortho-hydrogen content, a third beam monitor positioned downstream of the target will provide on-line monitoring of the target transmission and hence a measure of the ortho:para ratio, since the neutron cross sections for the two species are markedly different.

The 2.2 MeV γ -rays from neutron capture in the

target are detected with an array of 48, $(15\text{ cm})^3$ CsI(Tl) crystals read out in current mode by vacuum photodiodes coupled via low noise I-V preamplifiers to transient digitizers. The time-of-flight information from the CsI detectors allows the γ -ray asymmetry A_γ to be deduced as a function of incident neutron energy; A_γ should be constant, but the experimental asymmetry $\varepsilon = P_n A_\gamma$ will reflect the energy dependence of the beam polarization from Fig. 103. A beam chopper eliminates frame overlap and provides for a beam-off background measurement at the end of each pulse, allowing us to measure the contribution of γ -ray asymmetries from beta decays of polarized nuclei produced by interactions of the beam with materials upstream of the hydrogen target. The expected NPDGamma asymmetry is $A_\gamma = -5 \times 10^{-8}$ based on the best available theoretical predictions, and we ultimately aim to measure A_γ to $\pm 1 \times 10^{-8}$ or better with systematic errors less than 5×10^{-10} .

Experimental errors

The statistical uncertainty in the measurement of A_γ is ultimately determined by counting statistics, set by the beam intensity, the detector solid angle, and the counting time. The γ -ray detectors and low noise preamplifiers have been designed to ensure that sources of instrumental noise are small compared to this limit. An exhaustive Monte Carlo study of systematic errors has been ongoing since the preparation of a major DOE proposal for the experiment in 1998. Care has been taken to identify all possible sources of error, to minimize the sensitivity of the apparatus, and to work out a program of ancillary measurements to quantify individual error sources. The conclusion of these studies is that it should be possible, with sufficient beam flux, to measure A_γ to $\pm 0.5 \times 10^{-8}$ with systematic errors no larger than 10% of the statistical error quoted above.

Systematic errors arising from interactions of the neutron spin are potentially the most serious for the experiment, including a number of reactions that take place in the hydrogen target in parallel with the $np \rightarrow d\gamma$ reaction. One particular class of systematic errors can arise from admixtures of small parity allowed left-right scattering asymmetries into the up-down angular distribution via a misalignment of the detector symmetry axis with respect to the neutron spin direction. To keep these false asymmetry contributions at or below the 5×10^{-10} level, we require a means of determining the detector alignment with respect to the neutron spin direction to 20 mr or better. This will be accomplished by scanning the detector array in x and y by a few mm with the target in place and measuring the effective γ yield in each detector as a function of the array position. As mentioned in the introduction, the motion control system to accomplish this was designed

at TRIUMF and built in the Manitoba and TRIUMF shops.

Current status and future outlook

Since the NPDGamma proposal was written and the apparatus funded by the DOE and NSF commencing in 1999, the upgraded spallation neutron facility at LANSCE has been brought on line, and a new neutron guide has been constructed for the experiment. Unfortunately, the present schedule is about a year and a half delayed, due in large part to a conflict that arose when the facility installed a large, unshielded, superconducting magnet on a neighbouring beam line that imposed enormous technical challenges in the design of magnetic shielding for our experiment. This issue is being addressed with the support of LANL management, but a technical solution has not yet been found that would allow both beam lines to run concurrently.

In the course of developing the experiment, the collaboration has dedicated several test runs to characterizing the apparatus and the neutron flux at LANSCE. In the 2000 test run [Mitchell *et al.*, Nucl. Instrum. Methods A (in press) nucl-ex/040109], we mounted a 10% model of the full apparatus, and measured parity violating (PV) asymmetries with Cl, La and Cd targets. We demonstrated that the model apparatus reached the error limit imposed by neutron counting statistics (Fig. 104). In the 2002 test run [Seo *et al.*, Nucl. Instrum. Methods (in press)], we measured the brightness of the new flight path 12 moderator and confirmed that the first 12 m of the new neutron guide performed according to design.

We have determined that the physics asymmetry A_γ can be measured at LANSCE with the full NPDGamma apparatus to $\pm 4 \times 10^{-4}$ per pulse with 120 μA proton beam on the spallation target. Our

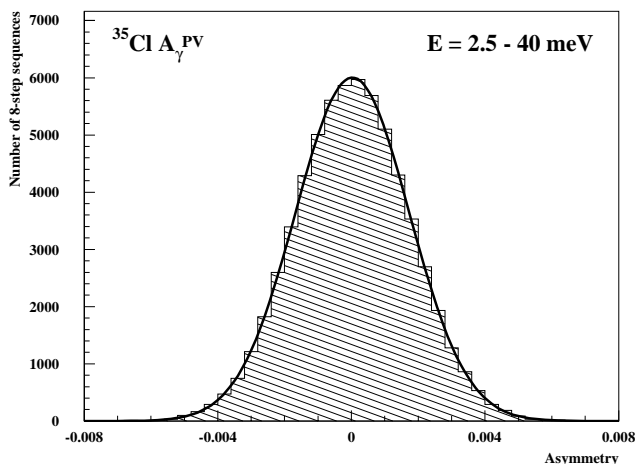


Fig. 104. Histogram of asymmetry values ($A_\gamma = (-29.1 \pm 6.7) \times 10^{-6}$) from test run on Cl [Mitchell *et al.*, *op. cit.*] used to validate our model of statistical errors for the full experiment.

test measurements have shown that expectations of the available neutron flux from the upgraded LANSCE facility (as advertised prior to the upgrade) were too optimistic by almost a factor of 4, with roughly equal contributions from reduced moderator brightness and reduced production beam current. An additional factor of 2 in running time for NPDGamma has effectively been lost due to the magnetic interference problem noted above.

In this context, the collaboration has carefully considered its options for commissioning and running the experiment at LANSCE in the near term. The experimental cave is scheduled to become available at the end of January, 2004. We will install and commission all elements of the apparatus (Fig. 105) with the exception of the target during the period January–March, 2004, when we anticipate approximately 8 weeks of beam to be available for the experiment. Once commissioned, the apparatus will be used to measure parity-violating asymmetries from cryostat materials and calibration targets, which are needed to understand backgrounds and possible systematic errors in the NPDGamma measurements. The liquid hydrogen target will be installed during the 2004 shutdown beginning in March.

We plan for a 1000 hour data run in calendar year 2004–05, which would result in a statistics-limited measurement of A_γ to $\pm 5 \times 10^{-8}$, or $\pm 100\%$ of the theoretical prediction based on the value of f_π as estimated by DDH. This measurement would be a factor of 4 better than the previous best published result $A_\gamma = (6 \pm 21) \times 10^{-8}$. While this would be a significant achievement, it falls short of our goals of either measuring or setting a meaningful upper limit on the weak-pion nucleon coupling that is currently known to be less than 30% of the best existing theoretical estimates. The compelling

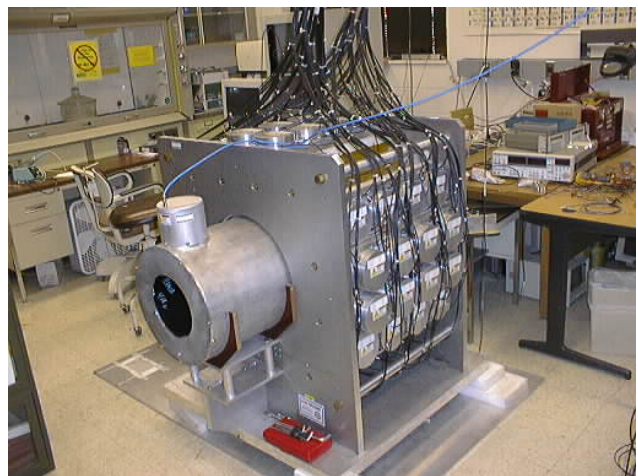


Fig. 105. Complete CsI detector array and spin flipper at Los Alamos mounted in the upper half of the detector position control stand designed by TRIUMF and built by the Canadian group.

physics case for a precise NPDGamma result merited recognition in the 2002 NSAC Long Range Plan for Nuclear Science (US), and the scientific priority of fundamental physics studies with cold neutrons has been confirmed with the approval of a new dedicated beam line for this work at the Spallation Neutron Source (SNS), currently under construction.

While the collaboration intends to pursue related measurements in the future at the SNS, we strongly prefer to complete the NPDGamma precision measurements on a much earlier timescale. We have informed the DOE of our desire to move the experiment to a new beam line at the Oak Ridge facility, HFIR, to pursue a much higher-statistics measurement than is currently possible at LANSCE. Conservative estimates indicate that HFIR could provide an order of magnitude higher neutron flux in the energy range of interest, and in addition the available running time per calendar year would be higher by a factor of 2–5. The new “CG”4 beam line suitable for NPDGamma could be ready as early as mid-2005, and only a modest capital investment would be required to adapt the experiment to

the new facility.

Collaborators (spokesman is underlined): C.S. Blessinger, M. Gericke, G. Hansen, M.B. Leuschner, G.L. Morgan, H. Nann, W.M. Snow (Indiana University); J.D. Bowman, G.E. Hogan, J.N. Knudson, S.K. Lamoreaux, G.S. Mitchell, C.L. Morris, S.I. Penttila, W.S. Wilburn, V.W. Yuan (Los Alamos National Laboratory); R.D. Carlini (Thomas Jefferson National Accelerator Facility); T.E. Chupp, K.P. Coulter, R.C. Welsh, J. Zerger (University of Michigan); M.S. Dewey, T.R. Gentile, D.R. Rich, F.E. Wietfeldt (National Institute of Standards and Technology); T. Case, S.J. Freedman, B. Lauss (University of California, Berkeley); S. Ishimoto, Y. Masuda, K. Morimoto (KEK National Laboratory, Japan); G.L. Jones (Hamilton College); F.W. Hersman, V.R. Pomeroy (University of New Hampshire); R.C. Gillis, S.A. Page, W.D. Ramsay (University of Manitoba); E.I. Sharapov (Joint Institute for Nuclear Research, Dubna); T.B. Smith (University of Dayton); D. Desai, G.L. Greene (University of Tennessee).

Experiment 768
Generalized FFLO state and anomaly of flux line lattice state in novel superconductors

(*R. Kadono, J. Akimitsu, KEK-IMSS, Aoyama-Gakuin*)

While the original goal of this proposal was to elucidate the anomalous magnetic response of quasiparticle excitation in CeRu_2 and related compounds, we have been looking for typical type II superconductors which could be compared with CeRu_2 as standard references. In 2003 we continued our search for such compounds including those which were newly discovered. Recently, a new ternary silicide, $\text{Sr}(\text{Ga},\text{Si})_2$, which has the AlB_2 -type structure similar to that of MgB_2 , was reported to be a superconductor with $T_c = 3.4$ K, stimulating active investigation of analogous compounds. In this class of materials, ternary silicide $\text{Ca}(\text{Al}_{0.5}\text{Si}_{0.5})_2$ has the highest critical temperature $T_c = 7.7$ K [Imai *et al.*, Appl. Phys. Lett. **80**, 1019 (2002)]. It is reported on this compound that the behaviour of electron-heat capacity deviates from that of the BCS-type, and that the effect of hydrostatic pressure on T_c is positive. Unfortunately, despite various experiments so far, there is very little known on the structure of superconducting order parameter in this compound. In order to obtain a clue in this matter, we measured magnetic penetration depth (λ) vs. temperature and field in a polycrystalline $\text{Ca}(\text{Al}_{0.5}\text{Si}_{0.5})_2$. The μSR experiments were performed on the M1 5 beam line using the HiTime spectrometer. The specimen, having a dimension of about $7 \times 7 \text{ mm}^2$, was mounted on the sample holder of a cryostat and then field-cooled at every magnetic field point to minimize the effect of flux pinning. The temperature (T) and field (H) dependence of transverse field (TF)- μSR spectrum was obtained at $H = 2.0$ T and $T = 2.0$ K, respectively. It is well established that the Gaussian relaxation rate σ measured by TF- μSR is predominantly determined by λ , and thus by the superconductive carrier density n_s in the following relation

$$\sigma^{-1} \propto \lambda^2 = \frac{m^* c^2}{4\pi n_s e^2}.$$

This equation indicates that λ is enhanced upon the reduction of n_s due to the quasiparticle excitation. For the ideal triangular flux line lattice (FLL) with isotropic effective carrier mass m^* , λ is given by the following relation

$$\sigma[\mu\text{s}^{-1}] = 4.83 \times 10^4 (1-h)[1+3.9(1-h)^2]^{1/2} \lambda^{-2}[\text{nm}],$$

where $h = H/H_{c2}$ with H_{c2} being the upper critical field. Therefore, provided that H_{c2} is known, one can deduce λ from σ at arbitrary field. The T dependence

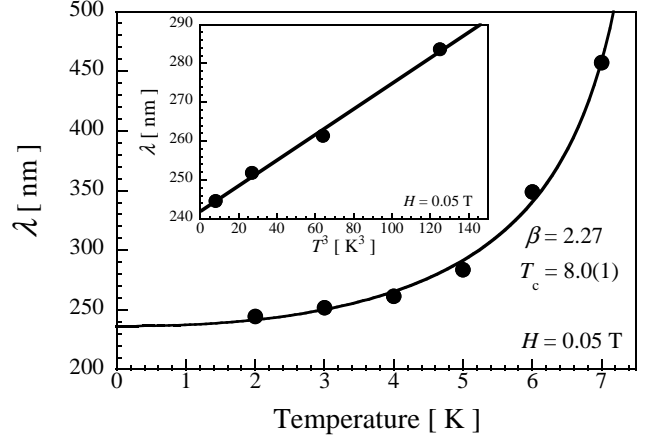


Fig. 106. Temperature dependence of the magnetic penetration depth λ at 0.05 T. The inset shows the λ plotted against T^3 . The solid line is a fitting result with $\lambda(t) = \lambda(0)/\sqrt{1-t^\beta}$.

of λ obtained from the analysis using a Gaussian model is shown in Fig. 106. Over the region below $T_c \sim 7.7$ K where the FLL is formed, λ increases with decreasing temperature. According to the empirical two-fluid model (which is a good approximation of the BCS theory), the following relation is expected to hold

$$\lambda(t) = \lambda(0) \frac{1}{\sqrt{1-t^4}},$$

where $t = T/T_c$. The solid line is the result of fitting analysis by a similar formula with an arbitrary power

$$\lambda(t) = \lambda(0) \frac{1}{\sqrt{1-t^\beta}}.$$

When both β and T_c are assumed to be free parameters, the above equation yields a good agreement with data for $\beta = 2.27$ and $T_c = 8.0(1)$ K. The result also means that the deviation of λ ,

$$\Delta\lambda = \lambda(t) - \lambda(0),$$

exhibits a tendency predicted for the case of line nodes (d -wave pairing) with some disorder (i.e. dirty limit, where $\Delta\lambda \propto T^2$). Compared with the case of isotropic gap ($\Delta_k = \Delta_0$), the quasiparticle excitations are enhanced along nodes ($|\Delta_k| = 0$) to reduce average n_s , leading to the enhancement of λ . As shown in the inset of Fig. 106, λ at low temperature behaves linearly against T^3 , suggesting that the order parameter in $\text{Ca}(\text{Al}_{0.5}\text{Si}_{0.5})_2$ has a large anisotropy. This is further supported by the magnetic field dependence of λ . As shown in Fig. 107, λ clearly exhibits a strong field dependence, where λ increases almost linearly with h . This is similar to the cases of NbSe_2 , $\text{YNi}_2\text{B}_2\text{C}$, and

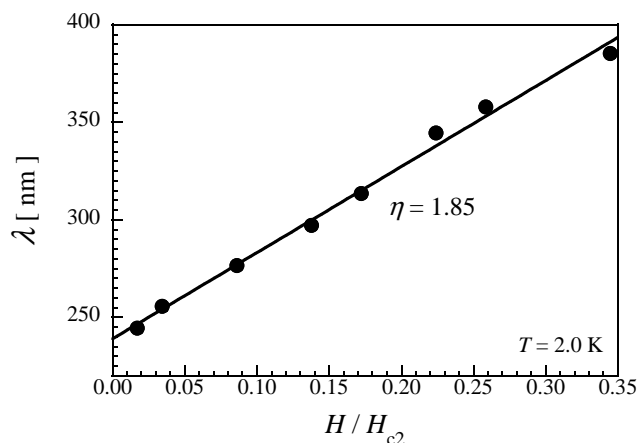


Fig. 107. Magnetic field dependence of the penetration depth λ at 2.0 K. The solid line is a fitting result with $\lambda(h)/\lambda(0) = 1 + \eta h$.

MgB₂, where such T/H -dependence of λ was observed; by now, there is ample evidence that they all have some anisotropy (including double gap) in the order parameter. The solid line is the result of fitting by the following linear relation

$$\frac{\lambda(h)}{\lambda(0)} = 1 + \eta h,$$

where η is a dimension-less parameter which represents the strength of the pair breaking effect. Fitting yields $\eta = 1.85$ (with $\lambda(0) = 239.05$ nm, $H_{c2} = 3.0$ T at 2 K) which is comparable with that in NbSe₂, YNi₂B₂C and MgB₂ (i.e. $\eta = 1.61, 0.97$, and 1.27 , respectively). Unfortunately, our results were obtained using a polycrystalline sample, which makes it difficult to deduce λ by analyzing data using the well-defined microscopic model.

Early experiments on high quality single crystal samples of Ca(Al_{0.5}Si_{0.5})₂ have reported that the upper critical field has an anomalous angular dependence which deviates from the Ginsburg-Landau anisotropic mass model. Moreover, very recent reports suggest that the crystal structure has clear five-fold and two-fold superlattice. Therefore, we are preparing high quality single crystals of Ca(Al_{0.5}Si_{0.5})₂ for further μ SR study of this compound in more detail.

Experiment 842

Mu-substituted free radicals in sub- and super-critical water

(P.W. Percival, SFU)

There is currently great interest in organic reactions in superheated water, and research in this area is motivated by a surprising diversity of applications: geochemical production of petroleum, biology in hydrothermal vents, corrosion in steam generators, destruction of hazardous waste, and the development

of environmentally benign chemical processes. However, progress on many of these fronts is hampered by lack of detailed knowledge of the kinetics and mechanisms of chemical reactions under hydrothermal conditions. Most studies to date have relied on end-product analysis and modelling to infer multi-step reaction sequences. Ideally, reaction intermediates should be studied in real time *in situ*. In practice most techniques are limited by the technical demands of the harsh environment – water is a corrosive solvent at high pressure and high temperature (hydrothermal chemistry is important up to and through the critical point of water, at 374°C, 220 bar). The study of free radicals is particularly difficult under such conditions.

Experiment 842 was designed to study free radicals in hydrothermal systems by using the positive muon as a spin probe. Since a positive muon can act as the nucleus of the hydrogen-like atom, muonium (Mu), it can be used to study H atom reactions and free radicals incorporating H. We were quickly able to demonstrate the feasibility of such studies by using transverse-field μ SR to detect muoniated free radicals over a wide range of conditions, all the way to supercritical [Percival *et al.*, Phys. Chem. Chem. Phys. **2**, 4717 (2000)]. However, unambiguous identification of free radicals requires knowledge of proton (or other nuclear) hyperfine constants, in addition to the muon hyperfine constant obtained by μ SR. In principle these hyperfine data can be obtained by muon avoided level-crossing resonance, and indeed we have done so in other projects, using the HELIOS spectrometer (see for example the report on Expt. 883). Unfortunately our high pressure cell was incompatible with HELIOS, which is based on a warm bore superconducting magnet with limited access, in contrast to the relatively open geometry of the SFUMU spectrometer used in previous high pressure experiments. Thus the project was stalled until the fall when a prototype high-pressure/high-temperature cell was built to fit HELIOS.

The new cell was a success, and immediately provided valuable new data. Since high momentum muons are required to penetrate the window of the pressure cell, Expt. 842 has to use beam line M9B, which does not have the spin rotation feature of M15 and M20. Thus it was expected that the longitudinal field installation of HELIOS would preclude standard transverse-field μ SR experiments. Surprisingly it was found that M9B has a significant transverse component of muon spin polarization, so that both μ SR and μ LCR experiments were possible in the same installation, with an appropriate adjustment of the positron counter positions.

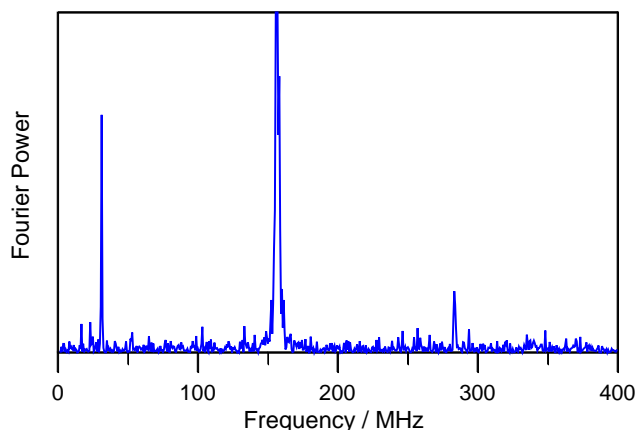


Fig. 108. μ SR spectrum of the *tert*-butyl radical in water at 300°C and 245 bar.

The transverse polarization on M9B has yet to be investigated systematically, but its utility is clearly demonstrated by the excellent spectrum evident in Fig. 108. The sample used for this spectrum was a solution of *tert*-butanol in water, which undergoes reaction in superheated water to form isobutene, $(\text{CH}_3)_2\text{C}=\text{CH}_2$. The reaction of muonium with isobutene results in the muoniated *tert*-butyl radical. The assignment of the *tert*-butyl radical structure, $(\text{CH}_3)_2\dot{\text{C}}\text{CH}_2\text{Mu}$, was originally based on the magnitude of the muon hyperfine coupling only. However, with the new cell it was possible to also collect μ LCR spectra. One example is shown in Fig. 109. There are two resonances apparent (two overlapping differential line shapes), as expected for the slightly different proton coupling constants for the CH_3 and CH_2Mu groups.

There was never much doubt about the identity of the *tert*-butyl radical formed in hot aqueous solutions of *tert*-butanol, hence its use as a test case. In contrast, the detection of more than one radical in superheated aqueous solutions of acetone presented a novel problem

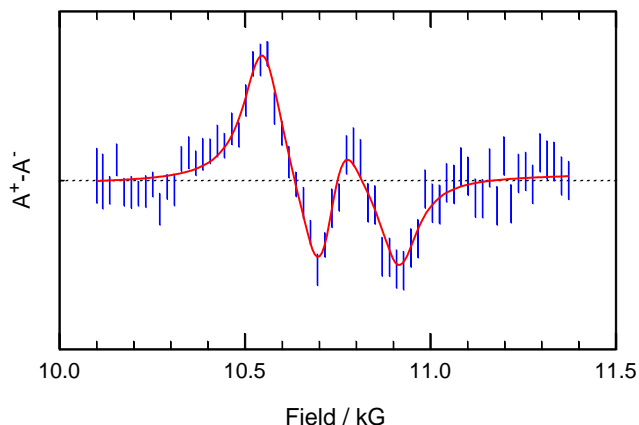


Fig. 109. μ LCR spectrum of the *tert*-butyl radical in water at 200°C and 250 bar.

of great interest to organic chemists. At low temperatures Mu adds to the ketone group of acetone, to form the radical $(\text{CH}_3)_2\dot{\text{C}}\text{OMu}$ (structure II in Fig. 110). On the strength of μ SR spectra alone, we suggested [Ghandi *et al.*, J. Am. Chem. Soc. **125**, 9594 (2003)] that at high temperature the keto form of acetone is in equilibrium with the isomeric enol form, which is more reactive by virtue of the $\text{C}=\text{C}$ double bond. Under these conditions reaction of muonium should result in the radical $\text{CH}_3\dot{\text{C}}(\text{OH})\text{CH}_2\text{Mu}$ (structure I), as indicated in the reaction scheme of Fig. 110. The μ LCR spectrum shown in Fig. 111 confirms this. Once again one sees the effect of two overlapping resonances, in this case even closer together than for the spectrum in Fig. 109.

Further studies should allow us to quantify the temperature dependence of the keto-enol equilibrium as well as the molecular dynamics of the radical products. It is important to realise that muonium is being used here as a passive probe of the keto-enol equilibrium, and that no other spectroscopic technique has ever been applied to probe this phenomenon under such extreme conditions. In fact literature data extends only up to 54°C!

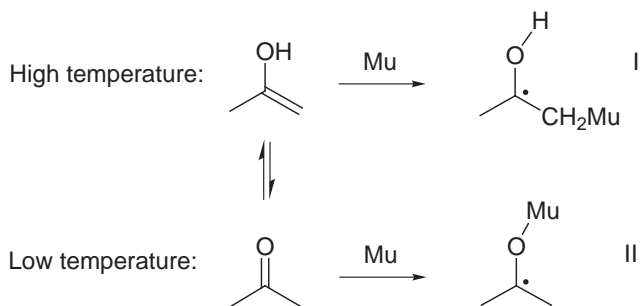


Fig. 110. Muonium addition to the enol and keto forms of acetone in water (upper and lower reactions, respectively).

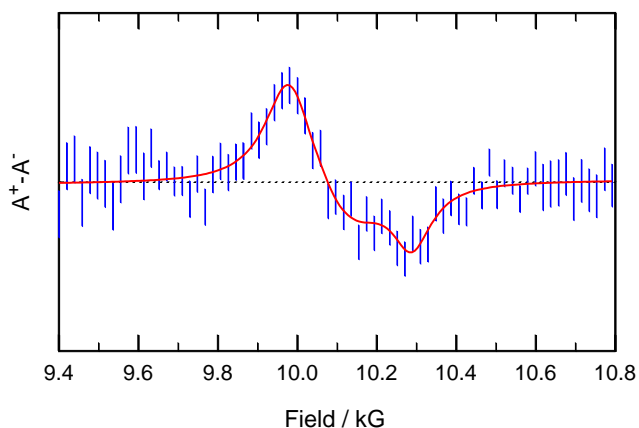


Fig. 111. μ LCR spectrum of the muoniated radical detected in an aqueous solution of acetone in water at 350°C and 250 bar.

Experiment 847

Electron-doped high- T_c superconductors

(J.E. Sonier, F.D. Callaghan, SFU)

Introduction

Our recent research on electron-doped high- T_c superconductors $R_{2-x}\text{Ce}_x\text{CuO}_4$ ($R = \text{La, Pr, Nd, Sm}$ or Eu) has been facilitated by progress in the growth of high quality single crystals of these materials. The issue of sample quality is one reason for the relatively slow advancement in our understanding of the electron-doped materials when compared with the more widely studied hole-doped superconductors. Another reason is the presence of both copper and rare earth magnetic moments. This makes it more difficult to isolate the contribution of the vortex lattice to the measured internal magnetic field distribution.

$\text{Pr}_{2-x}\text{Ce}_x\text{CuO}_4$ (PCCO)

In PCCO at a relatively low magnetic field strength (91 Oe), we observed an increase in local magnetic field at the muon stopping site below the superconducting transition temperature, T_c . Dipolar field calculations have allowed us to ascribe this to magnetic field-induced antiferromagnetic ordering of the Cu spins throughout the volume of the sample. The calculations show that the induced field at the muon site is due to a canting of the Cu spins out of the a-b plane by about 12° . The details of this work appear in a recent publication [Sonier *et al.*, Phys. Rev. Lett. **91**, 147002 (2003)].

$\text{Nd}_{2-x}\text{Ce}_x\text{CuO}_4$ (NCCO)

Most of our work in the last year has concentrated on NCCO. Whereas the ground state of the Pr^{3+} ions in PCCO is non-magnetic, the Nd^{3+} ions in NCCO have a relatively large magnetic moment – approximately $0.5 \mu_B/\text{ion}$ at 5 K in the parent compound Nd_2CuO_4 , which is reduced slightly in Ce-doped crystals due to a reduction in the magnitude of the Cu-Nd exchange field at the Nd site.

In order to induce superconductivity, it is necessary to lower the oxygen content by subjecting the Ce-doped samples to a severe annealing process. We studied a single crystal of NCCO in both the as-grown (pre-annealing) and superconducting (post-annealing) phases. The annealed crystal had a relatively sharp transition to the superconducting state at 23 K, which is indicative of a high quality, near optimally doped sample.

Zero-field μSR (ZF- μSR) measurements showed the magnetism of the as-grown and superconducting samples to be very similar down to temperatures of approximately 10 K, below which a marked difference emerged. Figure 112 shows the time-evolution of the muon spin polarization in each sample at $T = 2.75$ K.

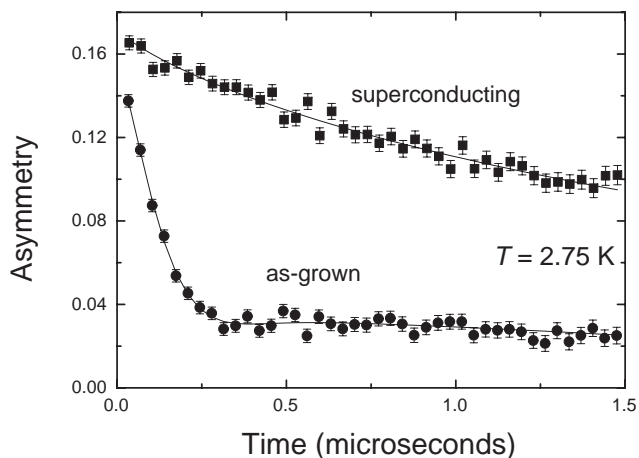


Fig. 112. Zero-field time-evolution of the muon spin polarization at $T = 2.75$ K in both the as-grown and superconducting phases of NCCO.

It can be seen that the muon spin polarization decays much more rapidly in the as-grown sample. In addition, the time-spectrum for the as-grown sample is best fit with a component oscillating at approximately 1 MHz, which is indicative of static magnetic order. The oscillating component first appears around $T = 6$ K and our analysis shows that by 2.6 K 80% of the sample is magnetically ordered. Based on a comparison with neutron and X-ray magnetic scattering experiments on the parent compound Nd_2CuO_4 , we postulate that the most likely source of such widespread order in the as-grown sample is antiferromagnetic ordering of the Nd^{3+} spins. It is known that both Ce-doping and annealing cause a reduction of the Néel temperature for Cu in these materials. This explains why we don't see Cu magnetic order in either the as-grown or superconducting samples. An interesting result is that Nd ordering is not observed in the annealed sample, which implies that Ce-doping has caused a reduction of the Nd ordering temperature. This is due to a suppression of the Cu moment in the annealed sample, which in turn lowers the induced moment on the Nd^{3+} ions due to the Cu-Nd exchange field. These results highlight the role of the Cu-Nd coupling in the ordering of the Nd^{3+} spins in current-generation single crystals.

Transverse-field μSR (TF- μSR) experiments were also performed. TF- μSR measurements at $H = 5$ kOe and parallel to the c axis of the crystal show a large negative μ^+ Knight shift, due primarily to the paramagnetic Nd^{3+} moments (see Fig. 113). The μ^+ Knight shift is a measure of the local magnetic susceptibility which is inaccessible to bulk probes as such measurements are dominated by the diamagnetic response of the superconductor below T_c .

The Nd^{3+} moments contribute a broad Gaussian component to the internal magnetic field distribution

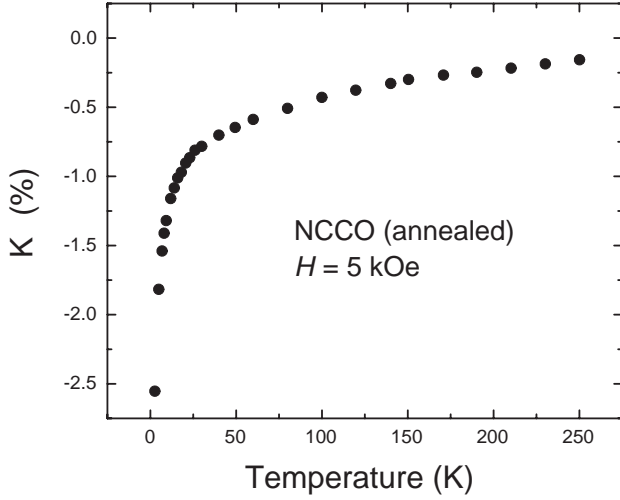


Fig. 113. μ^+ Knight shift in superconducting NCCO at $H = 5$ kOe.

in the vortex state. However, the high quality of the sample we studied allowed us to distinguish the asymmetric lineshape of the vortex lattice for the first time in this material. This means that the contributions from the vortex lattice and the electronic magnetic moments can now be separated, which is crucial for accurate measurements of the magnetic penetration depth and the vortex core size. An extensive analysis is currently under way to determine the temperature dependence of these quantities.

An example of such a lineshape can be seen in Fig. 114. The data were acquired at $T = 2.75$ K in a transverse magnetic field of 5 kOe directed perpendicular to the CuO_2 planes. The data are best fit assuming a square vortex lattice, in agreement with recent neutron scattering results. The pronounced shoulder in the lineshape at around 65.3 MHz is characteristic of a square vortex lattice.

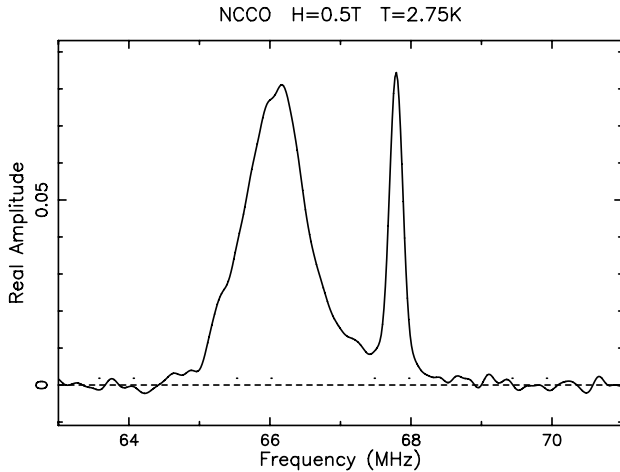


Fig. 114. Fast Fourier transform of the muon spin depolarization time-spectrum in the vortex state of NCCO. Note the characteristic asymmetric lineshape of the vortex lattice in a type-II superconductor.

Experiment 851

μ^+ SR in ruthenate and cuprate superconductors

(D.R. Harshman, Physikon Research Corp.)

The pairing state symmetry of $\text{YBa}_2\text{Cu}_3\text{O}_7$

Last year, we reported on our work [Harshman *et al.*, Int. J. Mod. Phys. **B17**, 3582 (2003); *ibid.*, Phys. Rev. B (in press); *ibid.*, SEMHTS Conf., Miami, FL] showing that the true character of the ground-state symmetry of $\text{YBa}_2\text{Cu}_3\text{O}_7$ is best described by the two-fluid model. We came to this conclusion by using a self-consistent model that incorporated temperature-activated de-pinning of the fluxons, which can mask the underlying order parameter. We showed that others had misinterpreted this pinning behaviour as evidence for d -wave pairing, and estimated that the probability that the non-local d -wave model [Amin *et al.*, Phys. Rev. Lett. **84**, 5864 (2000)] gives a better fit than the two-fluid model is less than 4×10^{-6} (best χ^2 per degree of freedom = 2.38 for two-fluid, compared to 13 for non-local d -wave).

We have continued our studies of single-crystal $\text{YBa}_2\text{Cu}_3\text{O}_7$, looking more closely at the character of the pinning. Recent transverse-field data acquired at 250 Oe show no evidence of a linear component, with the effective penetration depth exhibiting a flat temperature dependence as $T \rightarrow 0$ as is expected for s -wave superconductivity. The Fourier transform of data taken at 3 K is given in Fig. 115, and shows the familiar asymmetric lineshape associated with the formation of a vortex lattice. Little evidence of temperature-activated de-pinning is evident at this field, consistent with a strongly pinned vortex lattice. To show that the vortex lattice is, indeed, strongly pinned, we cooled the

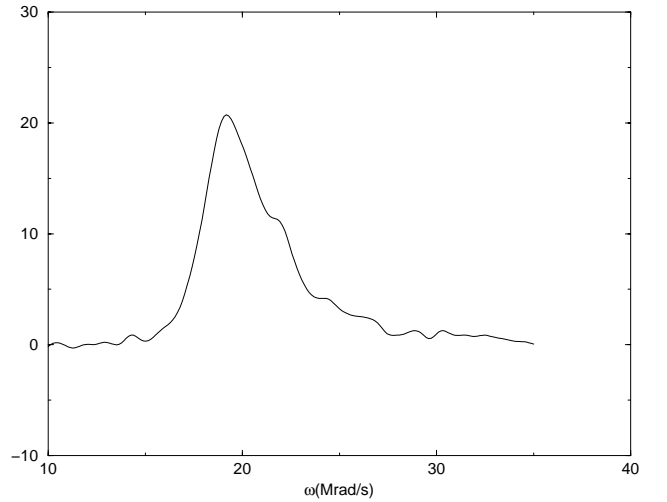


Fig. 115. Fourier transform of data taken at 3 K in 250 Oe.

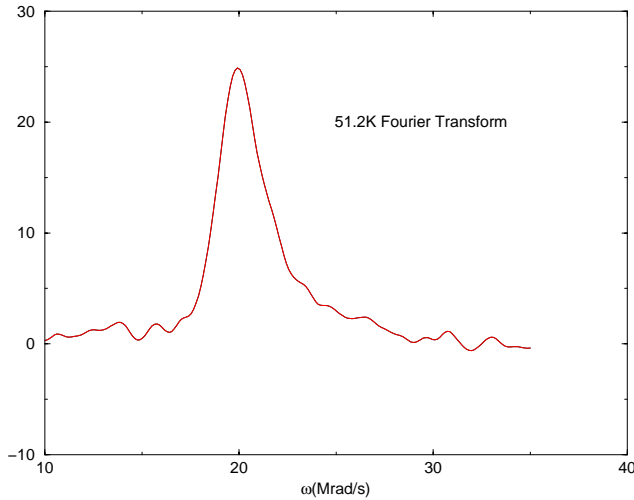


Fig. 116. Fourier transform of data taken at 51.2 K in 0 Oe.

sample in field to low temperatures, turned the field off, and acquired zero-field data at various elevated temperatures. The Fourier transform of data taken at 51.2 K is shown in Fig. 116. The characteristic shape reflecting the presence of a persisting vortex lattice is clearly evident, indicating that the fluxons are still pinned.

This result corroborates our assertion that strong pinning, which was earlier found to be present in powders [Harshman *et al.*, Phys. Rev. **B36**, 2386 (1987)] and early (heavily twinned) crystals [Harshman *et al.*, Phys. Rev. **B39**, 851 (1989)], suppresses the effects of temperature-activated de-pinning. It is only after the $\text{YBa}_2\text{Cu}_3\text{O}_7$ crystal quality improved that the effects of temperature-activated de-pinning, already observed in single-crystal $\text{Bi}_2\text{Sr}_2\text{CaCu}_2\text{O}_8$ [Harshman *et al.*, Phys. Rev. Lett. **67**, 3152 (1991)] became evident, masking the true *s*-wave character of the pairing state.

Experiment 852

Magnetic phases in geometrically frustrated rare earth pyrochlores

(S. Dunsiger, McMaster; R. Kiefl, UBC; J. Gardner, NIST)

Since Anderson considered the problem of antiferromagnetic ordering on the pyrochlore lattice in 1956 [Phys. Rev. **102**, 1008 (1956)], there has been a great deal of interest in systems where the magnetic ions occupy the vertices of edge or corner sharing triangular units [Ramirez, *Magnetic Materials: A Handbook on the Properties of Magnetic Substances and Related Phenomena* (2000)]. In these cases the natural magnetic coupling between ions is said to be geometrically frustrated. The pyrochlore transition metal oxides of general formula $\text{A}_2\text{B}_2\text{O}_7$ are composed of networks of corner-sharing tetrahedra such that it may not be pos-

sible to energetically satisfy all the magnetic interactions simultaneously. The curiosity about these systems stems from the possibility that if conventional magnetic order is highly frustrated then one may find novel low temperature behaviour. There is now considerable evidence that the low temperature state is fragile, i.e. it depends sensitively on a variety of factors such as anisotropy, the range of the spin-spin interactions, thermal and quantum fluctuations and residual disorder.

The purpose of Expt. 852 is to apply μSR to further our understanding of the effect of this frustration on the ground state and low lying magnetic excitations in the pyrochlores, in particular the rare earth titanates $\text{RE}_2\text{Ti}_2\text{O}_7$, where only the A site is magnetic. Recent theoretical efforts have focused on the effect of the dipolar interaction as the leading perturbation, particularly relevant in the study of rare earth systems, which have large dipole moments ($> 1 \mu_B$) and weak exchange interactions. Competing dipolar and superexchange interactions between Ising spins have been studied within the spin-ice type model by Siddharthan *et al.* [Phys. Rev. Lett. **83**, 1854 (1999)] and den Hertog and Gingras [Phys. Rev. Lett. **84**, 3430 (2000)].

$\text{Ho}_2\text{Ti}_2\text{O}_7$: a spin ice

Water ice is made up of oxygen atoms which form a hexagonal lattice (wurtzite structure). Of the 4 hydrogen atoms arranged tetrahedrally around each oxygen atom, two form strong covalent O–H bonds and are close to it to form a water molecule; the remaining two are hydrogen bonded and further removed. The hydrogen ion bonds between atoms form electric dipoles, so they can conveniently be represented by arrows placed on the bonds pointing towards the end occupied by the ion. The ice rule is then equivalent to saying that at each site there are two arrows pointing in and two out, as shown in Fig. 117.

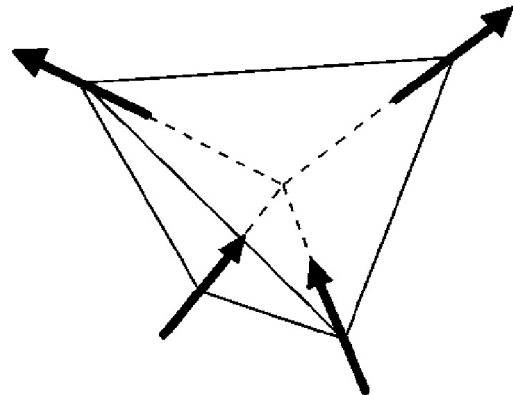


Fig. 117. Ground state configuration of spins on a single tetrahedron given ferromagnetic interactions and strong easy axis anisotropy along the dashed lines.

Spin orientation thus plays a similar role to that of hydrogen position in ice and magnetic analogues of water ice, so called “spin ice”, are currently of much interest [Ramirez *et al.*, Nature **399**, 333 (1999); Harris, Nature **399**, 311 (1999)]. Moessner [Phys. Rev. **B57**, R5587 (1998)] has shown that a strongly anisotropic classical Heisenberg model on the pyrochlore lattice can be mapped onto an Ising pseudospin model with an exchange constant opposite in sign. In the case of strong anisotropy ($|J/D| \ll 1$) the anisotropy term dominates, constraining the spins to lie along the $\langle 111 \rangle$ axes. The exchange term defines the direction in which they point, such that the enclosing angle between any pair may only take on values of 70.5° or 109.5° . Thus, counterintuitively, a system of spins situated on the vertices of corner sharing tetrahedra where the interactions are ferromagnetic may also be geometrically frustrated, provided the spins are constrained by anisotropy to point along the $\langle 111 \rangle$ axes.

Experimentally, the magnetic ions in a number of pyrochlores have recently been found to be subject to significant single ion anisotropies, whose local easy axis is along the $\langle 111 \rangle$ directions and which are thus candidates for spin ice behaviour. To date, the most extensively studied spin ice material is $\text{Ho}_2\text{Ti}_2\text{O}_7$ [Harris *op. cit.*; Harris *et al.*, J. Magn. Magn. Mater. **177-181**, 757 (1998)]. The Ho^{3+} ion is Ising like due to crystal field splittings which result in a ground state doublet with $J_z = \pm 8$ and the next excited state ~ 250 K higher [Siddharthan *et al.*, *op. cit.*]. This suggests that at low temperatures $\text{Ho}_2\text{Ti}_2\text{O}_7$ is well described as a quasi spin 1/2 Ising system. Neutron scattering measurements indicate that no long range order develops down to temperatures of at least 0.35 K in zero magnetic field, but instead, short range ferromagnetic correlations are observed [Harris *et al.*, J. Magn. Magn. Mater. *op. cit.*]. The idea which seems to be emerging is that there is no phase transition, but rather a continuous slowing down of spin fluctuations as the temperature is reduced, due to the development of energy barriers. A number of ordered phases have also been observed on application of a magnetic field, as well as history dependent behaviour. Monte Carlo simulations by Harris *et al.* [Phys. Rev. Lett. **81**, 4496 (1998)] show that the degree of degeneracy breaking depends on the direction of the applied field relative to the crystal axes and this has been confirmed by dc magnetization measurements [Cornelius *et al.*, Phys. Rev. **B64**, 060406 (2001)].

Monte Carlo simulations have been able to describe the magnetic susceptibility and diffuse magnetic neutron scattering results well, but the nature of the spin dynamics below 1 K has only been very briefly studied [Harris *et al.*, J. Magn. Magn. Mater. *op. cit.*] using

μSR . Our group has now completed a lengthy series of $1/T_1$ measurements on the $\langle 100 \rangle$, $\langle 110 \rangle$ and $\langle 111 \rangle$ orientations of $\text{Ho}_2\text{Ti}_2\text{O}_7$ in the dilution refrigerator on M15. In a low longitudinal field (LF) of 0.003 T the μ^+ spin depolarized too quickly to be observed. This is attributed to rapid Ho^{3+} spin fluctuations in the GHz range in the paramagnetic regime.

$\text{Ho}_2\text{Ti}_2\text{O}_7$ ($H \parallel \langle 100 \rangle$, $\langle 110 \rangle$ and $\langle 111 \rangle$)

Typical spectra at a higher field of 2 T applied along the $\langle 100 \rangle$ direction are shown in Fig. 118. At high temperatures of the order of 20 K, a full asymmetry non-exponential muon spin depolarization signal is observed. To account for the non-exponential behaviour, the data have been analyzed assuming a distribution of relaxation rates λ . In general, in low longitudinal field experiments in the “motionally narrowed” limit of rapid spin fluctuations, the muon spin depolarization associated with each magnetically inequivalent site i is well described by a single exponential $\exp(-\lambda t)$. The relaxation rate $\lambda = 2\Delta^2/\nu$, where $\Delta^2/\gamma_\mu^2 = \langle B_i^2 \rangle$ is the second moment of the internal magnetic field B_i ($i = x, y, z$), ν is the mean fluctuation rate for fluctuations in B_i , and γ_μ is the muon gyro-magnetic ratio. For simplicity, a flat distribution of relaxation rates has been assumed between $0 < \lambda < 2\Lambda$. The overall depolarization function then becomes

$$G_Z(t) = \frac{1}{2\Lambda t} [1 - \exp(-2\Lambda t)]. \quad (1)$$

The distribution of relaxation times observed in $\text{Ho}_2\text{Ti}_2\text{O}_7$ is remarkable. In dilute alloys this may be explained by the fact that the muon stops at different distances from the magnetic ion. However, one expects

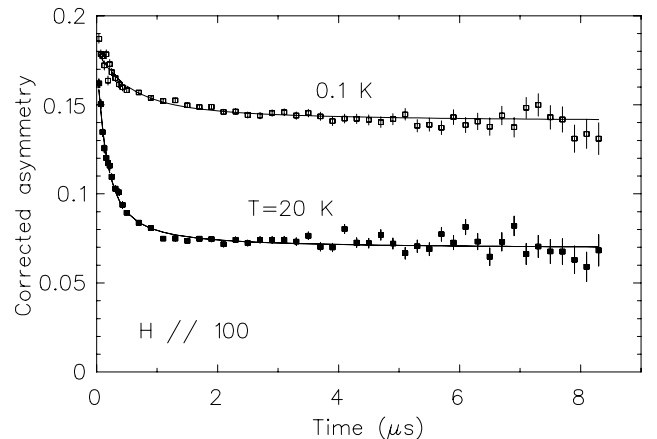


Fig. 118. Typical spectra in $\text{Ho}_2\text{Ti}_2\text{O}_7$ in a longitudinal field of 2 T applied along the $\langle 100 \rangle$ direction. A non-relaxing component due to muons which miss the sample, landing in the silver sample holder, is also present. As the temperature is reduced, an additional non-relaxing signal develops, which is attributed to static internal fields within the sample.

much less variance in a dense system of magnetic ions such as the oxide pyrochlores. This suggests that in this system there are a range of Ho^{3+} spin fluctuation rates.

The results of temperature scans in a longitudinal field of 2 T are summarized in Figs. 119 and 120. Above 5 K the data are well described by Eq. 1. The muon spin relaxation rate decreases with temperature as $\mu_B H/k_B T$ grows and the sample becomes increasingly magnetized. It seems likely that the spin dynamics are being altered as the electronic Zeeman splitting first becomes comparable with, and then exceeds, the exchange coupling \mathcal{J} . However, below 5 K the non-relaxing component develops (see Fig. 118) at the expense of the relaxing component. The amplitudes of

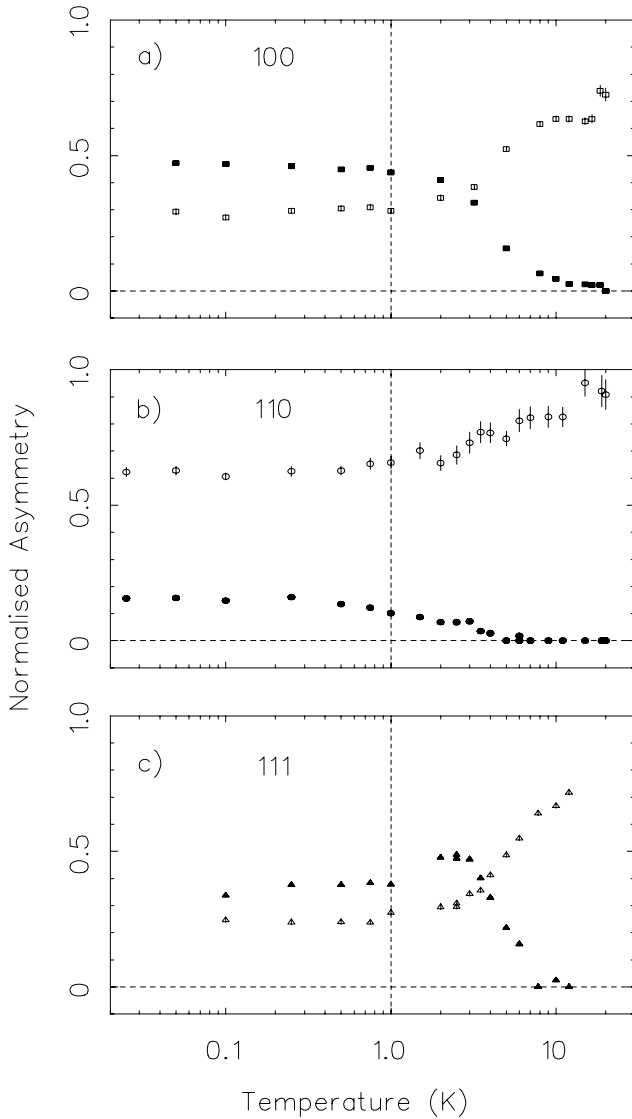


Fig. 119. Two component asymmetry in $\text{Ho}_2\text{Ti}_2\text{O}_7$ as a function of temperature. Magnetic field applied along the a) 100, b) 110 and c) 111 directions. The non-relaxing components are indicated by the filled symbols.

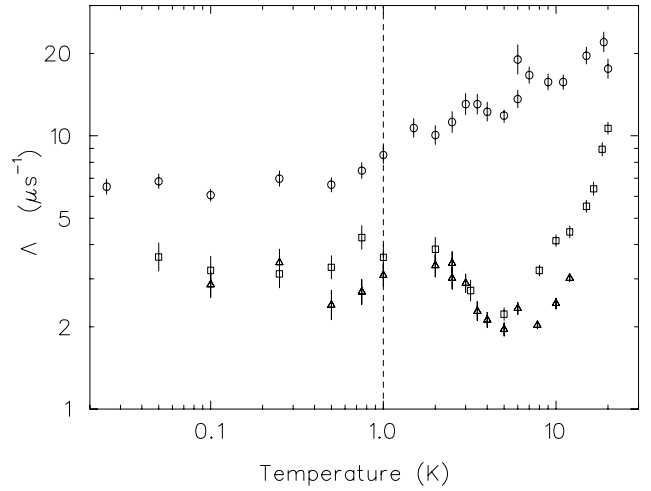


Fig. 120. Characteristic range Λ of relaxation rates of the muon spin polarization in $\text{Ho}_2\text{Ti}_2\text{O}_7$.

the signals have been normalized to the full amplitude found from a so called “indirect alpha” calibration. The non-relaxing component is attributed to the development of a static component of the order of 1 T. It should be pointed out that the muon has no sensitivity to a static internal field once it has been swamped by the high longitudinally applied field and the depolarization function is said to be “decoupled”. Thus in this regime the residual relaxing component observed in 20 kOe is thought to be dynamic by nature. If the muon spin depolarization were due to a static internal field Δ of the order of 1 T, it would take place on a time scale of $\Delta^{-1} \approx 1$ ns, too fast to be observed.

The most dramatic feature of the data taken in a longitudinal field of 20 kOe is the persistent, temperature independent spin relaxation observed below 1 K. Typically, in a conventional system some type of ordered phase would be favoured energetically at low temperature. In a 3 dimensional antiferromagnet below the transition temperature $T_1^{-1} \propto T^3$ for $T \gg T_{AE}$ and $T_1^{-1} \propto T^2 \exp(-T_{AE}/T)$ for $T \ll T_{AE}$, where T_{AE} is the gap in the spin wave spectrum due to anisotropy. In other words, below T_N , T_1^{-1} decreases rapidly as the magnetic excitations freeze out. Though difficult to understand theoretically, such partial ordering with persistent low temperature spin dynamics is a recurring phenomenon in the field of geometrically frustrated magnets.

Experiment 865

Electronic structure and diffusion kinetics of Mu in group III nitrides and related wide-gap semiconductors

(K. Shimomura, R. Kadono, KEK-IMSS)

Since the discovery of methods to produce sufficient *p*-type conductivity by Mg-doping, gallium nitride and related compound semiconductors are be-

ing aggressively developed for electronic and optoelectronic devices such as blue/green lasers and light-emitting diodes. Unique features such as a wide and direct band gap and high breakdown field make the nitrides ideal for such applications. However, as-grown undoped GaN epitaxial thin films, as well as bulk single crystals, commonly exhibit n -type conductivity with concentrations ranging from 10^{16} to 10^{19} cm^{-3} . Extensive experimental and theoretical studies have been undertaken to understand the origin of this n -type conductivity.

Here we report on the first observation of a paramagnetic muonium spectrum in GaN. The observed Mu^0 state has an extremely small and highly anisotropic hyperfine parameter. The location within the band gap for the $[0/+]$ energy level associated with this Mu state is estimated from the measured activation energy for thermal ionization. These results imply that an isolated hydrogen impurity would behave as a shallow donor if it were located at the same crystallographic site.

We performed μSR measurements on a GaN single crystal with the hexagonal (2H) wurtzite structure. The μSR experiment was conducted at the TRIUMF M15 beam line with the Belle spectrometer. Muons from a surface beam with their polarization transverse to the applied magnetic field were implanted into GaN ($[0001]$ orientation, n -type with a concentration of 10^{16} cm^{-3}).

Above 25 K, only a single (diamagnetic) precession signal is observed at the muon Larmor frequency. Relaxation of this signal is well described by Gaussian damping. This damping rate is satisfactorily explained by the dipole-dipole interaction of muons with $^{69,71}\text{Ga}$ and ^{14}N nuclei. The muon spin rotation signal changes drastically below 25 K. Figure 121 shows the angular and temperature dependence of the frequency spectra obtained by Fourier transform, in which one pair of satellite lines is clearly seen with their positions situated symmetrically around the central line, which corresponds to the precession of diamagnetic muons. The splitting of these satellites remained unchanged when the applied field was increased from 1.5 T up to 5 T, a result that is important in identifying the spectra as due to the hyperfine interaction of a Mu^0 centre. The splitting decreases when the $[0001]$ axis is tilted with respect to $\sim B$ as in Fig. 121d. Moreover, an equivalent frequency spectrum was observed when the $[1120]$ axis was rotated around $[0001]$, which was oriented at 35° to the applied magnetic field. These observations demonstrate the presence of a paramagnetic muonium state in GaN. The resulting hyperfine interaction is extremely small, about 10^{-4} times the vacuum value for a Mu atom, and is axially symmetric with respect to $[0001]$.

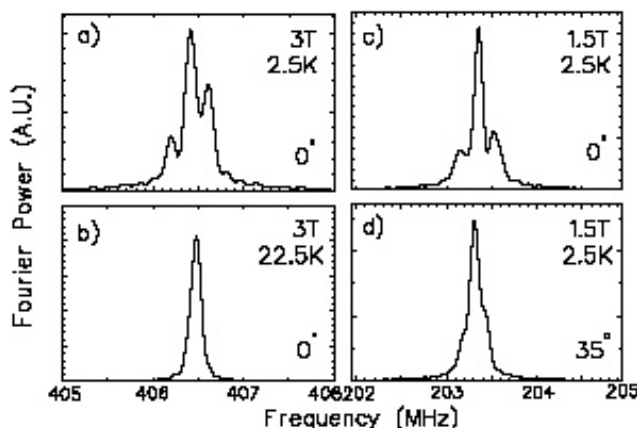


Fig. 121. Frequency spectra obtained for GaN at (a) 2.5 K and (b) 22.5 K with $B = 3.0$ T parallel to $[0001]$ axis, and with $B = 1.5$ T at 2.5 K, where $[0001]$ is parallel to B (c) or tilted by 35° from B (d).

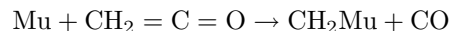
Because the population of the $Se = -1/2$ state is always larger in an applied field, the observations in Fig. 121 imply that the low-frequency line corresponds to $Se = +1/2$, thus to $A(\mu)$ is positive for the displayed orientations. From the detailed analysis, the parallel and perpendicular component of the hyperfine tensor is deduced to be $+337(10)$ kHz and $-243(30)$ kHz, respectively.

The temperature dependence measurement of the Mu^0 state shows their activation energy to be about 5 meV.

Experiment 883

Muoniated methyl and associated free radicals (P.W. Percival, SFU)

After an exciting excursion into a study of radicals formed from addition of muonium to stable carbenes [McKenzie *et al.*, J. Am. Chem. Soc. **125**, 11565 (2003)], Expt. 883 returned to its original focus in 2003, being a detailed study of the muoniated methyl radical, $\cdot\text{CH}_2\text{Mu}$, and its isotopomers. The first step in this project was to find a method of creating the radical. This was achieved by using ketene as the radical precursor:



as reported in the 2001 TRIUMF Annual Report and a subsequent paper [McKenzie *et al.*, J. Phys. Chem. **A106**, 7083 (2002)].

The new work involved the deuterated analogue, $\cdot\text{CD}_2\text{Mu}$, formed by addition of muonium to $\text{CD}_2=\text{C}=\text{O}$. Neither ketene nor deuteroketene are available commercially, since they are highly unstable molecules. Thus it was necessary to prepare fresh samples (by the pyrolysis of acetone or deuterioacetone) just prior to beam time, and store them in dry ice prior to

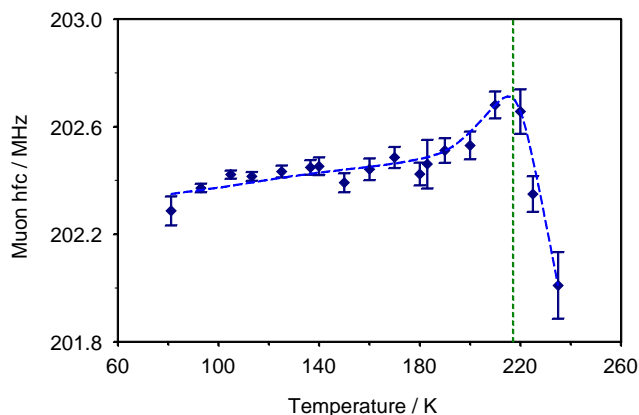


Fig. 122. Muon hyperfine constants determined for the $\cdot\text{CD}_2\text{Mu}$ radical. The dotted vertical line marks the boiling point of the ketene solvent.

mounting in a pre-cooled cryostat. As before, muon hyperfine constants were determined by transverse field μSR and proton or deuteron hyperfine constants were determined by muon level-crossing resonance, μLCR . Measurements were made over a wide range of temperature, from about 70 K to over 230 K, where the ketene dimerizes and it is no longer possible to form the muoniated methyl radical of interest.

The intent was to study the temperature dependence of the hyperfine constants and their isotopic dependence, to probe details of the vibrational motion of the radicals, specifically the out-of-plane (umbrella) bending motion, which is supposed to be the main cause of temperature dependence for the proton hyperfine coupling in the $\cdot\text{CH}_3$ radical. However, the effect of temperature was unexpectedly small for $\cdot\text{CH}_2\text{Mu}$ and $\cdot\text{CD}_2\text{Mu}$, a finding which can now be explained by the high frequency of the inversion mode for the muoniated radicals, as revealed by detailed quantum calculations.

The small temperature dependence of the hyperfine constants is probably due to solvent effects. In particular the significant feature observed near 220 K can be attributed to reduced intermolecular interactions close to the boiling point of ketene (217 K) and the subsequent formation of the dimer, which is itself solid at these temperatures (see Fig. 122).

The muon spin relaxation rate was also measured in the transverse field μSR experiments; the results for $\cdot\text{CD}_2\text{Mu}$ are shown in Fig. 123. The effective activation energy is too small for the relaxation to be due to chemical reaction. On the other hand the sign of the temperature dependence is opposite to that found for most organic free radicals, and which is usually attributed to the modulation of anisotropic g and hyperfine interactions by molecular tumbling. It is therefore concluded that the spin relaxation must be due to the spin-rotation mechanism, which only becomes dominant for small radicals undergoing very rapid

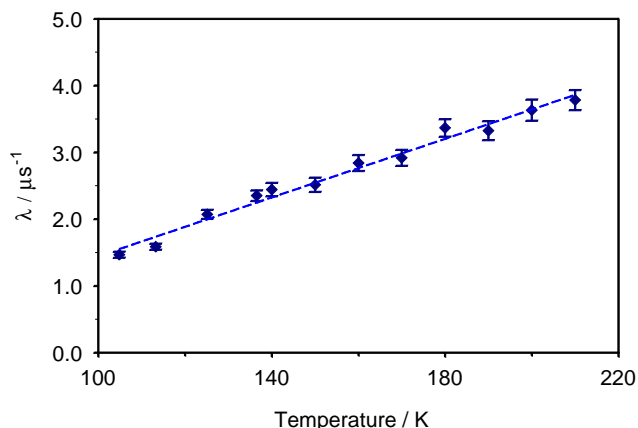


Fig. 123. Transverse muon spin relaxation rates measured for the $\cdot\text{CD}_2\text{Mu}$ radical in liquid ketene.

tumbling and would apply to the small, oblate shape of the methyl radical.

The research carried out in Expt. 883 forms a major part of the Ph.D. thesis of Iain McKenzie (Chemistry Department, Simon Fraser University, in press).

Experiment 895

Vortex structure and magnetism of electron-doped cuprate superconductors

(*R. Kadono, K.M. Kojima, KEK-IMSS, Tokyo*)

Recent observation of field-induced magnetism (FIM) in the mixed state of hole-doped (p -type) cuprates has attracted much interest, because it might provide a clue to resolve the true ground state in the normal phase of those compounds. Since the superconducting order parameter is locally suppressed in the vortex cores, there is a possibility that FIM may be a manifestation of the electronic ground state nucleated in the normal cores. However, while all of the observed effects are attributed to the antiferromagnetic (or quasistatic stripe) phase localized in the vortex cores, the evidence for the “antiferromagnetic (AF) core” remains elusive; for example, the results in $\text{La}_{2-x}\text{Sr}_x\text{CuO}_4$ [Katano *et al.*, Phys. Rev. **B62**, R14677 (2000); Lake *et al.*, Science **291**, 1759 (2001); Nature **415**, 299 (2002)] are all from neutron diffraction measurements which are not sensitive to the local structure over such a large length scale (vortices with a core size of $\sim 10^2$ Å, separated by 10^2 – 10^3 Å). The situation is less clear in electron-doped (n -type) cuprates because the information related with vortices is often masked by the influence of large magnetic moments of rare-earth ions in $R_{2-x}\text{Ce}_x\text{CuO}_4$ ($R = \text{Nd, Pr, Sm}$).

In 2003 we performed detailed high transverse field (TF) μSR measurements on the single crystalline n -type cuprate $\text{Pr}_{1-x}\text{LaCe}_x\text{CuO}_{4-y}$ (PLCCO) to study the mixed state. A specimen with $x = 0.11$, which is relatively close to the AF phase of PLCCO ($x \leq 0.1$), was chosen to examine the possibility of FIM. For

the study of FIM, PLCCO has an advantage over $\text{Pr}_{2-x}\text{Ce}_x\text{CuO}_{4-y}$ (PCCO) in that we can obtain single crystals in much larger dimensions, which allows systematic studies by various experimental techniques including neutron diffraction. The μSR measurements were carried out on the M15 beam line. A slab of $\text{Pr}_{0.89}\text{LaCe}_{0.11}\text{CuO}_{4-y}$ crystal ($T_c \simeq 26$ K, measuring about $5 \times 8 \times 0.5$ mm) with the c axis perpendicular to the plane was loaded onto a He gas-flow cryostat and a magnetic field ($\mathbf{H} = (0, 0, H_z)$) was applied parallel to the c axis (where $z \parallel c$). In the paramagnetic state, we have found that the muon Knight shift, K_μ^z , under an external magnetic field parallel to the c axis is significantly influenced by the in-plane susceptibility, χ_{ab} . This surprising result strongly suggests the presence of unconventional hyperfine interaction involving a non-diagonal Fermi contact-type term between muons and Pr ions. The muon hyperfine parameter A_μ^z is deduced from a comparison between the muon Knight shift and magnetic susceptibility χ . As shown in Fig. 124a, PLCCO exhibits a large anisotropy of χ between the in-plane (χ_{ab}) and perpendicular (χ_c) directions, where χ_{ab} exhibits a significant increase with decreasing temperature while χ_c remains almost unchanged. The corresponding muon Knight shift versus temperature is shown in Fig. 124b; it is clear that K_μ^z is mostly proportional to χ_{ab} . The K - χ plot in Fig. 124c for the data obtained in the normal state exhibits a linear relation with a small offset near the origin, from which we obtain $-969(2)$ Oe/ μ_B corresponding to the gradients of the K - χ line. Upon superconducting transition, the specimen exhibits a further peculiar magnetic response. As is evident in Fig. 125, showing the field dependence of the additional shift in the superconducting state, $\Delta B_z = B_0^S - B_0^N$, a large positive shift of the frequency is observed at $H = 200$ Oe. Note that the direction of the frequency shift is apparently opposite to that expected for diamagnetism in the mixed state. This result is quite similar to what has been observed in PCCO [Sonier *et al.*, Phys. Rev. Lett. **91**, 147002 (2003)]. Moreover, ΔB_z exhibits a steep decrease with increasing field to change its sign to negative above ~ 1 kOe. The strong field dependence at such low fields indicates that the effect of diamagnetism due to flux line lattice (FLL) is negligible over the entire field range. Meanwhile, ΔB_z is only weakly dependent on the field for 2–40 kOe, above which it exhibits a trend to increase further in the negative direction. These features above ~ 2 kOe are quite similar to those of field-induced moments detected by neutron diffraction. The field dependence of ΔB_z for $H \leq 40$ kOe can be understood by introducing an additional polarization of Pr and/or Cu moments that is controlled by the superconductivity. Assuming a simple Brillouin function for the

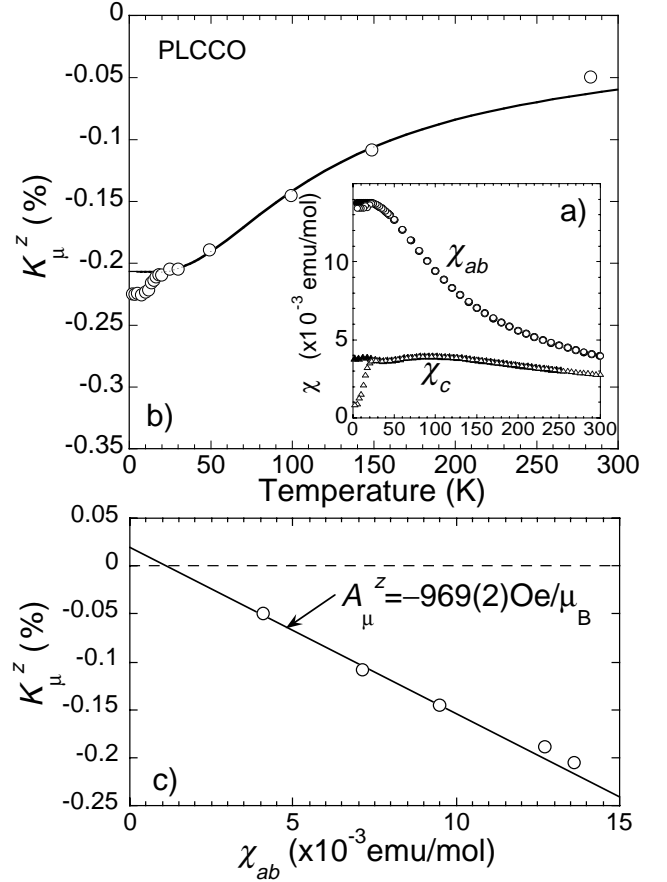


Fig. 124. (a) Temperature dependence of magnetic susceptibility at $H = 20$ kOe (open symbols) and 50 kOe (filled symbols) applied parallel (χ_c) and perpendicular (χ_{ab}) to the c axis. (b) The muon Knight shift with $H = 20$ kOe parallel to the c axis, where the solid curve in (b) is proportional to χ_{ab} . (c) The K - χ plot (with $\chi = \chi_{ab}$) for the Knight shift shown in (b).

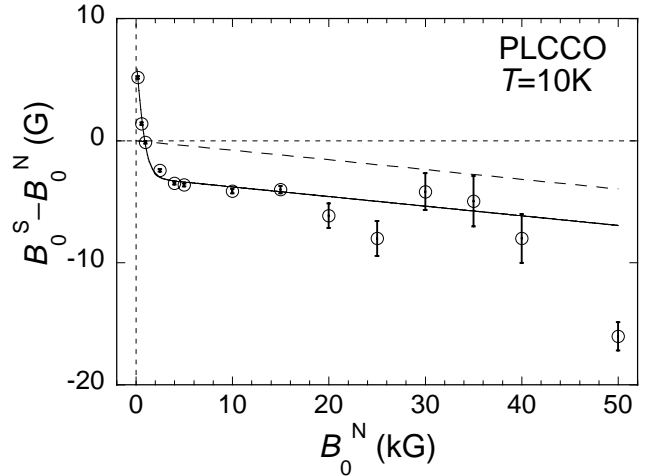


Fig. 125. Magnetic field dependence of the additional shift in the superconducting state, where B_0^S and B_0^N correspond to the internal field at 10 K and 30 – 40 K, respectively. The solid curve is a fitting result by the model described in the text (with the dashed line representing the contribution of residual demagnetization).

magnetic response, we analyze the data in Fig. 125 by an equation

$$\Delta B_z = B_z^* \tanh(H_z/H_p) + c_{\text{dm}} H_z + b_0,$$

where B_z^* is the field from the additional moment, H_p is a characteristic field where the direction of B_z^* is reversed, c_{dm} is the contribution of residual bulk demagnetization, and b_0 is an offset parameter. The solid curve in Fig. 125 is a result of fitting by the above equation, which reproduces data excellently with $B_z^* = 9.78(8)$ Oe, $H_p = 1.09(4)$ kOe, $c_{\text{dm}} = -7.9(1.4) \times 10^{-5}$, and $b_0 = 6.8(2)$ Oe. Since the emergence of B_z^* is perfectly correlated with the occurrence of superconductivity, the origin of B_z^* must be in close relation with the electronic state of CuO_2 planes. However, it has been demonstrated by very recent neutron diffraction measurements on the present specimen that the moment size of Cu ions induced by the external field is far smaller than that found in the AF phase of $\text{Pr}_{1-x}\text{LaCe}_x\text{CuO}_{4-y}$ ($x < 0.1$) with a quite non-linear dependence on the field; it remains almost constant over a range from 0 to ~ 40 kOe. Considering the hyperfine coupling between Cu ions and muons at the relevant site (which is usually dominated by magnetic dipolar interaction), it is unlikely that such small Cu moments directly contribute to B_z^* , in contrast to what has been suggested for the case of PCCO. Further analysis is still in progress.

Experiment 914/835

Zero-field μSR in Bi2212 and Bi2201 searching for effects related to pseudo-gap

(G.M. Luke, McMaster; P.L. Russo, Y.J. Uemura, Columbia)

In Expt. 914/835, we performed TF-MuSR measurements of Bi2201 in the underdoped, optimally doped, and overdoped regimes using mildly oriented ceramic specimens. Our initial motivation came from the work of Balakirev *et al.* [Nature **424**, 912 (2003)], who have performed Hall number measurements by suppressing superconductivity using high magnetic fields, and reported that the carrier concentration $n_{\text{Hall}} \sim 1$ hole per Cu at the optimum doping, as shown in Fig. 126. In most of the cuprates, it has been widely believed that the carrier concentration at optimum doping region is close to 0.15 holes per Cu. So, $n_{\text{Hall}} \sim 1$ in Bi2201 is anomalously large by a factor of 6 or so.

When we plot the μSR relaxation rate, which is proportional to n_s/m^* (superconducting carrier density / effective mass), versus T_c , Bi2201 systems follow the trend of various other cuprate systems, as shown in Fig. 127. Bi2201 has an average spacing $c_{\text{int}} \sim 12$ Å of CuO_2 planes, which is twice as large as $c_{\text{int}} \sim 6$ Å of 214, 123, and most other cuprate systems. Thus when

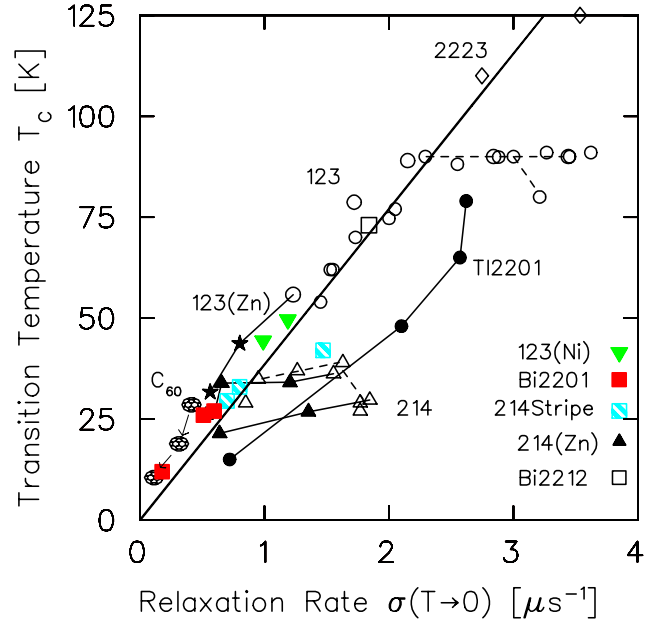


Fig. 126. Uemura plot updated with Bi2201 and Bi2212.

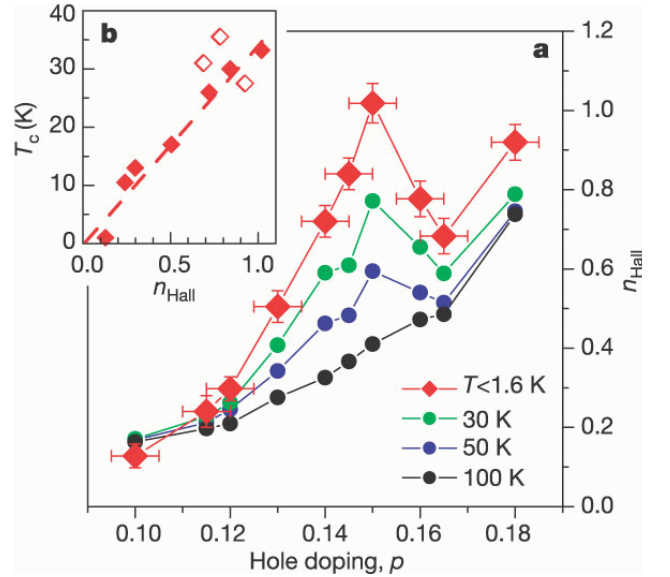


Fig. 127. Variation of Hall number with doping and T_c . **a**, Hall number (n_{Hall}) variation with doping (p). **b**, low temperature (n_{Hall}) and T_c for underdoped samples with $p \leq 0.15$ [Balakirev *et al.*, *op. cit.*].

we convert the results in Fig. 127 into a 2-dimensional superfluid spectral weight $n_{s2d}/m^* \propto \sigma \times c_{\text{int}}$, we expect about a factor 2 larger carrier density per Cu for Bi2201 compared to other cuprates, assuming that m^* values are nearly equal for all these systems. This is still not enough to account the factor ~ 6 anomaly.

Therefore, our results are not consistent with the anomaly of Hall number measurements unless, (1) the effective mass in Bi2201 is anomalously large, or (2) the

derived n_{Hall} somehow does not represent real carrier concentration.

Future plans

We are now checking the alignment of crystallites and developing a method to convert the relaxation rate to corresponding values for single crystal specimens. We would like to perform measurements using single crystal specimens of Bi2212 in several different applied fields in the future.

Experiment 915

Muonium in semiconductor alloys

(P.J.C. King, Rutherford Appleton Laboratory)

Experiment 915 has focused on investigation of muonium behaviour in $\text{Si}_{1-x}\text{Ge}_x$ alloys. Strained-layer $\text{Si}_{1-x}\text{Ge}_x$ alloys, grown epitaxially on to Si or SiGe substrates, have applications in transistor manufacture and provide the prospect of combining Si integrated circuit technology with optoelectronic components. The uses of epitaxial $\text{Si}_{1-x}\text{Ge}_x$ material have generated interest in the bulk, unstrained alloy, and this can be produced by the Czochralski technique in wafer form. Bulk alloy material offers the opportunity to study the intrinsic physical and electronic properties of the $\text{Si}_{1-x}\text{Ge}_x$ system. For example, regarding impurity behaviour within the system, the lattice site of dissolved oxygen has been investigated [Yonenaga *et al.*, Physica **B308-310**, 539 (2001)], with this species showing a preference for adopting a bond-centred location within Si-Si bonds. There have also been limited studies of hydrogen behaviour: DLTS investigations of very dilute (<1% Ge) material showed some modification of the properties of bond-centred hydrogen due to local variations in its environment; at the other end of the alloy spectrum, there is some evidence for the electrical activation of impurity Si atoms in Ge by hydrogen. The aim of this present experiment was to explore the behaviour of isolated hydrogen in bulk $\text{Si}_{1-x}\text{Ge}_x$ across the alloy composition, as modelled by its muonium analogue.

In November, 2001, three alloy compositions (Ge content 20%, 45%, 77%) were studied on M15 using the Belle magnet; these Czochralski samples were grown at Tohoku University. Qualitatively, the Mu_{BC} and Mu_{T} formation probabilities vary smoothly across the alloy range between the fractions expected in the unalloyed elements. Mu_{BC} was observed in all three samples and a linear variation of the average value of the isotropic component of its hyperfine parameter as a function of alloy composition was observed. The Mu_{BC} lines were broad, however, and further investigation of their nature was required. Mu_{T} signals were only seen in the alloy with 20% Ge content. The measured Mu_{T} hyperfine parameter was lower than that observed in pure Si

(whereas linear interpolation between the pure Si and Ge values suggests a higher value), and further investigation of the Mu_{T} hyperfine parameter in other low-Ge samples was of interest to confirm this behaviour.

In October, 2003 three $\text{Si}_{1-x}\text{Ge}_x$ samples were studied during low-intensity running at the start of a TRIUMF run cycle: Czochralski material with 11% Ge content from Virginia Semiconductor, material with 60% Ge content from Tohoku, and material with 20% Ge content which had been investigated previously.

In the 11% Ge material, both Mu_{BC} and Mu_{T} signals could be clearly seen. Figure 128 shows the asymmetries as a function of temperature for the two paramagnetic species together with the diamagnetic amplitude. This latter component is small and constant below around 150 K, above which it begins to increase due to Mu_{BC} ionization; the Mu_{T} amplitude remains constant above 20 K up to at least 230 K. However, both paramagnetic centres show a large dip in amplitude around 10 K, and the origin of this behaviour requires further exploration.

Material with 60% Ge content was studied very briefly in a single run; a Mu_{BC} line could be seen, and there is also some evidence for a Mu_{T} signal. Figure 129 shows a plot of the average value of Mu_{BC} hyperfine parameter versus alloy composition with the results from the 11% and 60% Ge samples added. Whilst the data point for 60% Ge has not benefited from the higher statistics that the other points had, the linear dependence on alloy composition is confirmed.

Figure 130 shows the Mu_{T} hyperfine parameter versus temperature as measured previously for the 20% Ge sample, together with new TRIUMF measurements for the 11% Ge sample. The parameter values are very similar between these two samples and below that expected for pure Si. For the 20% Ge case, there is the hint of a minimum in hyperfine parameter around 40 K; this is shown more clearly in the 11% Ge case.

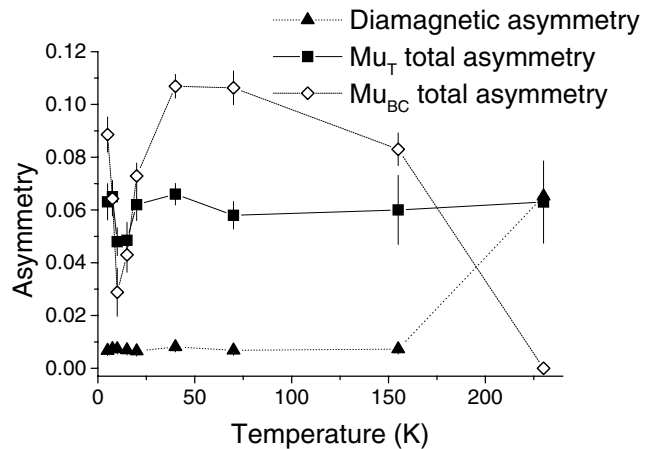


Fig. 128. Mu_{BC} , Mu_{T} and diamagnetic line asymmetries as a function of temperature from $\text{Si}_{0.89}\text{Ge}_{0.11}$.

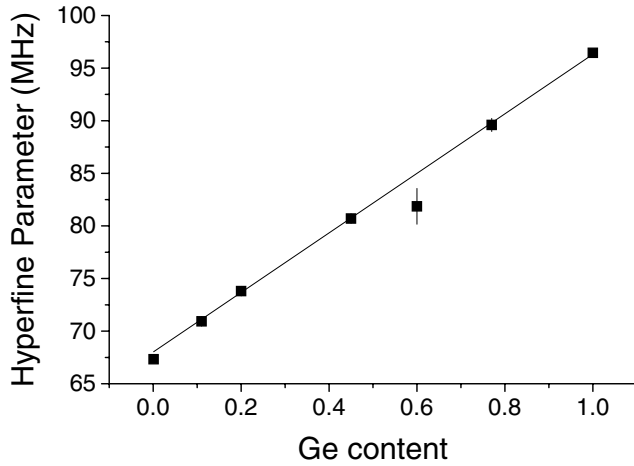


Fig. 129. Variation of the average value of the isotropic component of the Mu_{BC} hyperfine parameter with alloy composition. The line is a fit to the data.

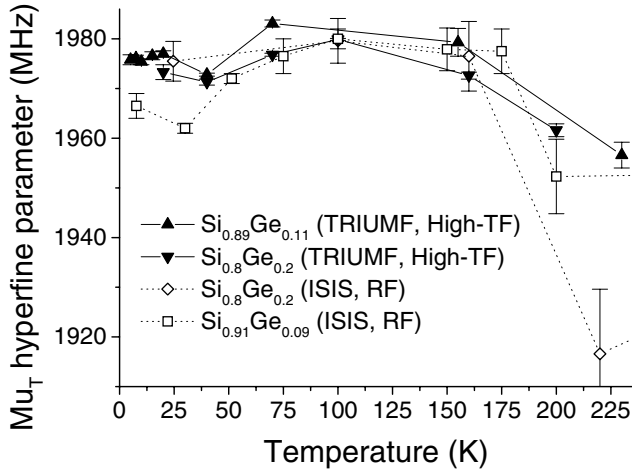


Fig. 130. Mu_{T} hyperfine parameter for different alloys measured either using high transverse fields at TRIUMF or RF- μ SR at ISIS.

Also shown in this figure are data from ISIS, where the Mu_{T} hyperfine parameter has been measured using radio-frequency resonance methods. Data from the 20% Ge sample agree closely with that taken at TRIUMF and measured using the high transverse field technique. In addition, ISIS data from a sample from Tohoku with 9% Ge are shown – these show a more pronounced fall in hyperfine parameter below 100 K, again with a minimum suggested at around 30 K.

The observed temperature dependence of the Mu_{T} parameter at low temperatures in these alloys is of interest. In pure Si, the Mu_{T} hyperfine constant decreases with falling temperature below around 75 K. Holzschuh [Phys. Rev. **B27**, 102 (1983)] attributed this decrease to Mu_{T} hopping between sites with slightly different isotropic hyperfine interactions. At low temperatures, these sites are populated according to the Boltzmann distribution which would preferentially give

more weight to those with lower hyperfine parameters. In low Ge alloy material, it might be expected that this effect would be greater, there being a wider possible variation in Mu_{T} sites owing to different numbers of Ge atoms surrounding cage centres. This may account not only for the fall in Mu_{T} hyperfine parameter with decreasing temperature below around 100 K, but also the low overall value compared with Si.

Further study of the data is ongoing. In particular, quantitative analysis of the variation with temperature of the Mu_{T} hyperfine parameter needs to be performed; in addition, high statistics data were also taken for the 20% Ge sample, and analysis to look for preferential occupation of specific bonding environments is proceeding.

Experiment 916

QLCR of diamagnetic muonium states in GaP (R.L. Lichti, Texas Tech)

Zero-field depolarization functions demonstrated that several different diamagnetic muonium states exist in doped GaP. The primary goal of TRIUMF Expt. 916 has been identification of these states using quadrupolar level-crossing resonances (QLCR). The two Ga isotopes produce a clear signature of a Ga near neighbour to the muon by nearly identical features at a field ratio of ~ 1.6 , while P has no quadrupolar nuclei, and thus is invisible to this technique. The standard Zn acceptor in GaP substitutes for Ga and has only a 4.1% fraction with a nuclear quadrupole moment, while the usual S donor has no quadrupolar isotope. The S donor will not be visible, but a small possibility exists that a Zn acceptor might be observed in QLCR experiments.

We have previously found the main Ga-related resonances associated with the Mu^+ defect centre at the bond-centre (BC) site in *p*-type GaP, and confirmed that the intensity of that spectrum decreases below roughly 100 K where the zero-field depolarization results indicate formation of a bound Mu-Zn pair. The Mu_{BC}^+ QLCR resonances lie between 200 and 400 mT and imply an electric field gradient (EFG) at the Ga that is roughly 10% larger for Mu^+ in GaP compared to that for the same state in GaAs. One of the remaining measurements for Expt. 916 beam time in late summer was to verify that a different resonance occurs below 100 K due to the Mu-Zn complex. We have observed a weak low-field Ga resonance at 670 K where a Mu-Zn complex is formed by Coulomb capture of the mobile Mu^+ by an ionized Zn^- acceptor. A major question is whether the structure of the Mu-Zn pair is identical at high and low temperatures, where the proposed process involves charge-exchange scattering between the mobile Mu_{T}^0 centre and a neutral Zn

acceptor as the first step toward pair formation.

Figure 131a shows the low-field QLCR spectrum obtained in heavily doped *p*-type GaP at 50 K. These resonances are too strong to be from Zn and very similar to the Ga spectrum seen at 670 K except that it is shifted to higher fields, implying that the EFG at nearby Ga nuclei is about 20% larger at 50 K than for the high-temperature complex. This result would seem to indicate that the Mu-Zn pair structure is very similar at these two temperatures. The fact that the same resonances are not seen in Fig. 131b at a temperature where Mu_{BC}^+ remains stationary, but the low-temperature pair formation process is not active because the Zn acceptors have ionized, shows that this spectrum is from a separate low-T state rather than due to the second-nearest Ga neighbours to Mu_{BC}^+ . Since the usual structure for an H-acceptor complex has the hydrogen in a BC location next to the acceptor, these results suggest that the structure of Mu-Zn is most likely not the standard one. We proposed a pair

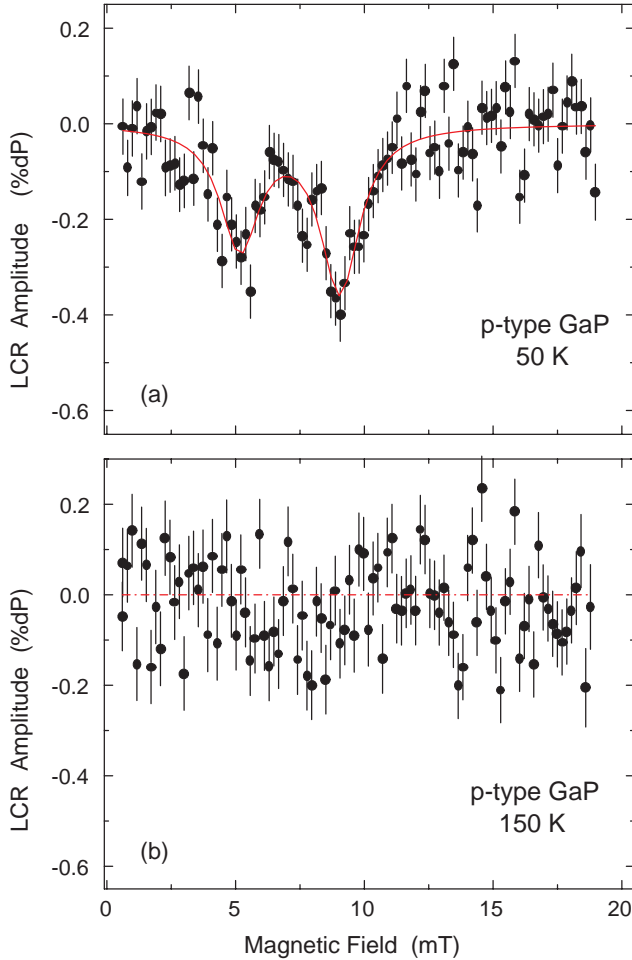


Fig. 131. QLCR spectra for Ga neighbours to the Mu location in a Mu-Zn complex formed at low temperatures (a). A similar scan (b) above the maximum temperature for low-T pair formation confirms a separate low-T state.

structure at high temperatures in both GaP and GaAs in which the Mu^+ resides behind the As or P neighbour to Zn_{Ga} , or is mobile among P-Ga (As-Ga) bonds one step removed from the Zn dopant as an explanation for these low-field resonances.

Figure 132 shows the spectrum obtained at 300 K in a heavily doped *n*-type GaP sample. We had previously identified Mu^- at 140 K where there is a peak in the diamagnetic fraction; however, the temperature dependence of that fraction was not as expected. Thus confirming Mu^- at the Ga tetrahedral location near room temperature became one of our goals for the most recent beam time as an identity check for a diamagnetic state that grows roughly linearly between 200 and 700 K. The resonance in Fig. 132 is essentially identical to that seen at 140 K, except for a small shift in the resonance fields. The odd dependences seen in *n*-type GaP above 100 K thus appear not to involve any state other than Mu^- .

We have now confirmed our preliminary identification of four of the five proposed diamagnetic states in doped GaP; Mu^- at T_{Ga} , Mu^+ at BC, a high-temperature Mu-Zn paired state formed by Coulomb capture of mobile Mu^+ by Zn^- , as well as the low-temperature Mu-Zn paired state formed by charge-transfer interactions between mobile Mu_T^0 centres and neutral Zn acceptors which is discussed above. The one remaining state is a low-temperature Mu-donor complex which should have the Mu located in a tetrahedral location surrounded by P atoms next to the S donor. An initial attempt did not find any low-field spectrum; however, this was not an exhaustive search. The expected structure is the least likely of all the proposed diamagnetic Mu centres to yield a QLCR signature in

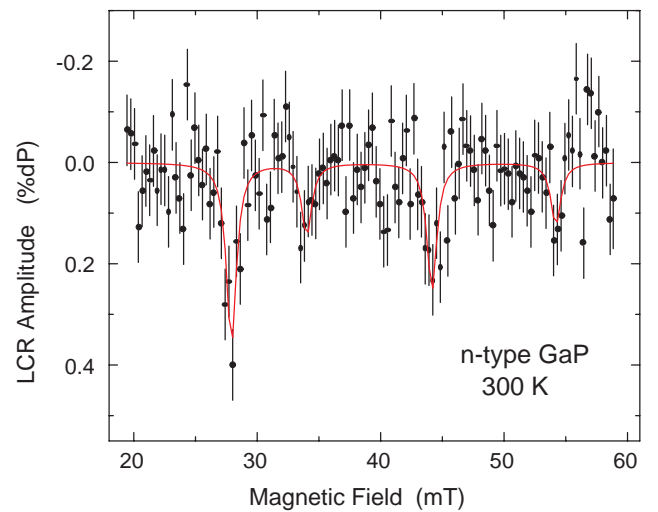


Fig. 132. QLCR spectra confirm Mu^- in the T_{Ga} site at 300 K for heavily doped *n*-type GaP. The electric field gradient at a Ga neighbour is slightly smaller at 300 K than at 140 K where the Mu^- fraction is larger.

GaP. Based on identification of a standard Mu^- centre as the main state at both 140 and 300 K, we conclude that the unusual dependences observed for diamagnetic fractions above 100 K may be the result of competing transitions out of the Mu_T^0 precursor to Mu^- . Answering that question requires a careful study of Mu_T^0 dynamics in n -type GaP which is being pursued as part of a separate experiment to define Mu defect energy levels in III-V compounds.

Experiment 917

Correlation between magnetism and transport properties of thermoelectric oxides

(J. Sugiyama, Toyota CRDL Inc.; J.H. Brewer, UBC-TRIUMF)

Although the widespread current interest in the layered cobaltites (i.e. 5 K superconductivity in $\text{Na}_{0.35}\text{CoO}_2 \cdot \text{H}_2\text{O}$ [Takada *et al.*, Nature **422**, 53 (2003)] was originally due mainly to their unique combination of high thermopower S with metallic transport properties, which makes them one of the most promising systems for power applications, we have shown that they also display interesting and complex magnetic orderings, directly correlated with the enhanced S . The richness of behaviour of the layered cobaltites is due to their intrinsic structure, namely: electrically active triangular planes of CoO_2 , which are separated by a variety of intermediate structures; their relatively strong electronic correlations; and the fact that the structures between the CoO_2 planes can be modified in a variety of ways to vary their dimensionality, ionic states, carrier doping in the CoO_2 planes and the relevant interaction strengths.

In order to elucidate the magnetism in the CoO_2 planes and the mechanism of the good thermoelectric properties, we have carried out positive muon spin rotation and relaxation ($\mu^+\text{SR}$) experiments on the layered cobaltites. As a result, we found the transition to a low- T commensurate or incommensurate spin density wave (C- or IC-SDW) state for $[\text{Ca}_2\text{CoO}_3]_{0.62}^{\text{RS}}[\text{CoO}_2]$ below ~ 100 K, [Sugiyama *et al.*, Phys. Rev. **B66**, 134413 (2002); *ibid.* **68**, 134423 (2003)], $\text{Na}_{0.75}\text{CoO}_2$ at 22 K [Sugiyama *et al.*, *ibid.* **67**, 214420 (2003)] and $[\text{Ca}_2\text{Co}_{4/3}\text{Cu}_{2/3}\text{O}_4]_{0.62}^{\text{RS}}[\text{CoO}_2]$ below ~ 200 K [Sugiyama *et al.*, J. Phys. Condens. Matter **15**, 8619 (2003)], where RS denotes the rocksalt-type subsystem. Here we summarize those results and report an almost dome-shaped relation between the transition temperature into the low- T magnetic state and the composition x for Na_xCoO_2 and/or the high-temperature asymptotic limit of thermopower in the more complex 3 and 4 layer cobaltites [Sugiyama *et al.*, Phys. Rev. Lett. **92**, 017602 (2004)]. This behaviour is explained using the Hubbard model on two-

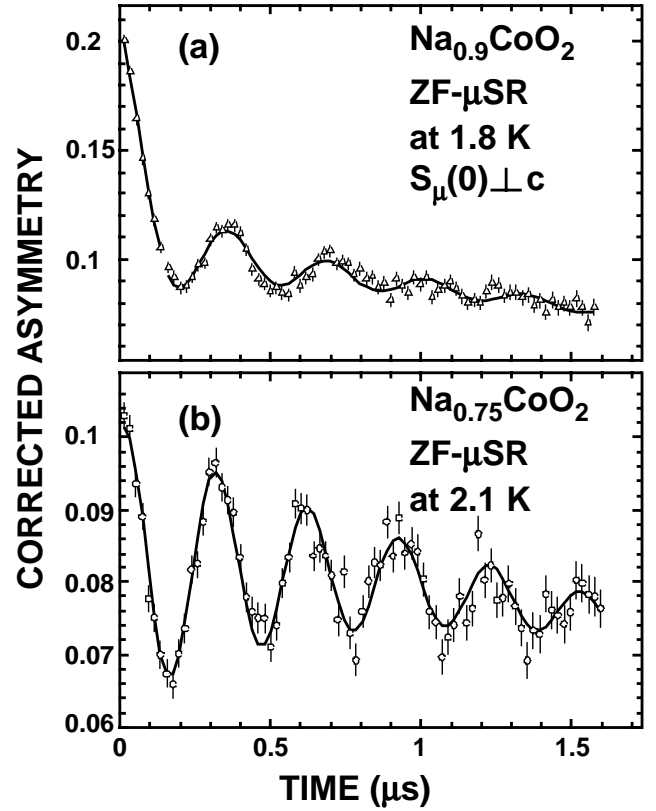


Fig. 133. ZF- $\mu^+\text{SR}$ time spectra of (a) single crystal platelets of $\text{Na}_{0.9}\text{CoO}_2$ at 1.8 K and (b) a polycrystalline plate of $\text{Na}_{0.75}\text{CoO}_2$ at 2.1 K.

dimensional triangular lattice in the CoO_2 plane.

Figure 133(a) shows a ZF- $\mu^+\text{SR}$ time spectrum at 1.8 K in the single crystal platelets of $\text{Na}_{0.9}\text{CoO}_2$; the spectrum was obtained with the initial μ^+ spin direction $\mathbf{S}_\mu(0)$ perpendicular to the c -axis. A clear oscillation due to quasi-static internal fields is observed only when $\mathbf{S}_\mu(0) \perp \mathbf{c}$. Also, the ZF- $\mu^+\text{SR}$ time spectrum for the polycrystalline $\text{Na}_{0.75}\text{CoO}_2$ sample, which entered a commensurate spin structure below 22 K, is shown in Fig. 133(b). Making comparison with the bottom spectrum, the oscillation amplitude in the top spectrum decays rapidly and the initial phase is delayed. The oscillation in the top spectrum is characteristic of a zeroth-order Bessel function of the first kind that describes the muon polarization evolution in an IC-SDW field distribution [Kalvius *et al.*, Handbook on the Physics and Chemistry of Rare Earths (North-Holland, Amsterdam, 2001) vol. 32, chap. 206]. The absence of a clear oscillation for the $\mathbf{S}_\mu(0) \parallel \mathbf{c}$ case indicates that the internal field is roughly parallel to the c -axis. Due to the strong anisotropy, the IC-SDW is thus considered to localize in the CoO_2 plane, with oscillating moments directed along the c -axis.

The magnetic phase diagram (Fig. 134) of Na_xCoO_2 can thus be sketched from the $\mu^+\text{SR}$ results

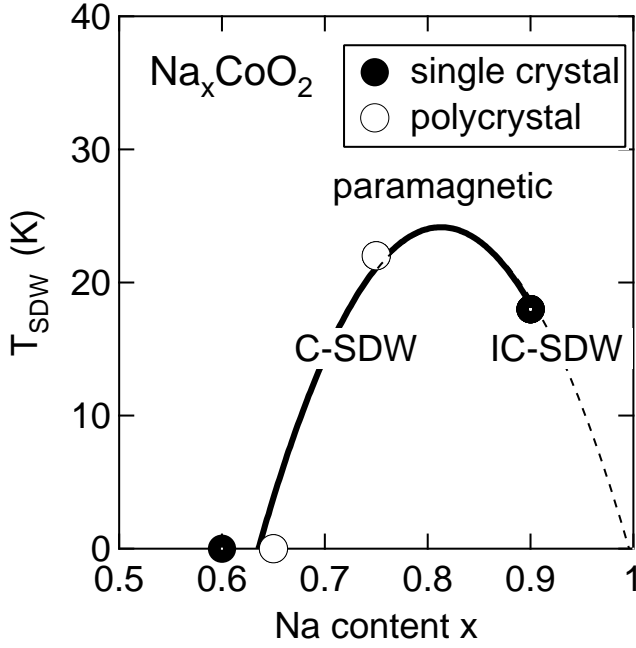


Fig. 134. Phase diagram of Na_xCoO_2 determined by the $\mu^+\text{SR}$ experiments. The point at $x = 1$ is extrapolated from the data on the related compound LiCoO_2 .

for polycrystalline samples with $x = 0.65$ and 0.75 and the $x = 0.6$ and 0.9 crystals. Since the oxygen deficiency δ in $\text{Na}_x\text{CoO}_{2-\delta}$ is negligibly small even for the $x = 0.9$ sample, the average Co valence is directly calculated from x . As x increases from 0.6 , the magnitude of T_{SDW} increases up to $x \sim 0.8$, then decreases with further increasing x . As a result, we obtain the dome-shaped relationship of Fig. 134 between T_{SDW} and x , viz. the Co valence for Na_xCoO_2 .

The Hubbard model within a mean field approximation can be used for explaining the magnetism of such a system as a function of electron filling n . At $T = 0$ and $n = 0.5$ (i.e. Na_0CoO_2), as the Hubbard on-site repulsion U increases from 0 , the system is a paramagnetic (PM) metal up to $U/t = 3.97$ due to geometrical frustration, then changes into a metal with a spiral IC-SDW, and then at $U/t = 5.27$ a first-order metal-insulator transition occurs, where t is the nearest-neighbour hopping amplitude [Krishnamurthy *et al.*, Phys. Rev. Lett. **64**, 950 (1990)]. The lack of magnetic transitions for Na_xCoO_2 with $x = 0.6$ and 0.65 suggests that $U/t \leq 3.97$. This means that Na_xCoO_2 is unlikely to be a typical strongly correlated electron system, because $U \gg t$ for such a system.

The calculations [Fujita *et al.*, J. Phys. Soc. Jpn. **60**, 2831 (1991)] also predict that, as n increases from 0 , the value of U/t at the boundary between the PM and SDW phases decreases, with increasing slope ($d(U/t)/dn$) up to $n = 0.75$. Even for $U/t = 0$, the SDW phase is stable at $n = 0.75$. The value of U/t then increases with further increasing n , with decreas-

ing slope. Therefore, the dome-shaped phase diagram is qualitatively explained by the calculations, although the measured maximum of the dome is located around $x = 0.8$ (i.e. $n = 0.9$). This is likely due to the simple band structure assumed in the above calculation, while calculations for Na_xCoO_2 suggest a more complicated one [Singh, Phys. Rev. **B61**, 13397 (2000)].

For the 3 and 4 layer cobaltites, $[\text{Ca}_2\text{CoO}_3]_{0.62}^{\text{RS}}[\text{CoO}_2]$ and $[\text{Ca}_2\text{Co}_{4/3}\text{Cu}_{2/3}\text{O}_4]_{0.62}^{\text{RS}}[\text{CoO}_2]$, the IC-SDW transition was also observed as a common behaviour in the CoO_2 planes. We have studied by $\mu^+\text{SR}$ the dependence of the IC-SDW transition on the Co valence for the variety of layered cobaltites. Figure 135 shows $T_{\text{SDW}}^{\text{on}}$ as a function of $S(300 \text{ K})$ for all the cobaltites measured. A clear dome-shaped relation is observed for all the available cobaltites with a variable number of layers (N) between the two adjacent CoO_2 planes. As N increases from 1 , the $T_{\text{SDW}}^{\text{on}} - S(300 \text{ K})$ curve shifts towards higher T , due to the increased two-dimensionality induced by the increase in the interlayer distance between CoO_2 planes.

Phenomenologically, the phase diagram is very similar to the well-known relationship between the superconducting T_c and the Cu valence in the high- T_c cuprates. Actually, both SDW and superconducting transitions are induced by an intrinsic instability of an electron system; that is, as T decreases, an energy gap appears at T_{SDW} and/or T_c to minimize the internal energy for both cases. Therefore, it is reasonable to expect a similar relationship between transition temperature and carrier concentration for both the magnetic cobaltites and the superconducting cuprates.

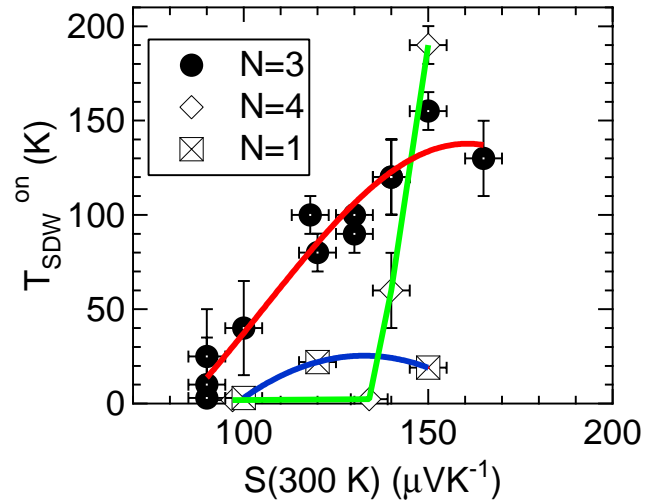


Fig. 135. The relationship between $T_{\text{SDW}}^{\text{on}}$ and thermopower S at 300 K . Solid circles represent the data for the cobaltites with a triple rocksalt-type subsystem, open diamonds a quadruple rocksalt-type subsystem and crossed squares Na_xCoO_2 . It should be noted that the magnetic susceptibility $\chi(T)$ curves for the 3- and 4-layer samples lacked a marked change at the $T_{\text{SDW}}^{\text{on}}$ detected by $\mu^+\text{SR}$.

Furthermore, the average Co valence for the maximum T_{SDW} indicates the optimal filling to induce an SDW transition at high T and enhance the effective mass of charge carriers through the AF interaction between spins. In other words, this dome relation provides important guidance in the search for improved thermoelectric properties of the layered cobaltites.

Experiment 918

High field study of La_2CuO_4 based superconductors

and Experiment 950

High field study of Zn doped/Eu doped/overdoped systems

(G.M. Luke, McMaster; Y.J. Uemura, A.T. Savici, Columbia)

In the previous report for Expt. 918 we showed an increased relaxation rate for the high transverse magnetic field μSR signal in the case of underdoped and optimally doped $\text{La}_{2-x}\text{Sr}_x\text{CuO}_4$ (LSCO). We observed no such effect in the overdoped sample or in the $\text{Bi}_2\text{Sr}_2\text{CaCu}_2\text{O}_{7-\delta}$ (Bi2212) one. We used a new way to look at the data, by studying the envelope of the signal. It is very easy to show if there is some field induced effect, the magnitude of magnetic fields that give enhanced relaxation and if the effect occurs in the whole of the sample or in just some fraction of the volume.

We extended our study in Expts. 918 and 950 to other samples, trying to determine a correlation between the parent compound, doping with Eu or Zn and the increased relaxation rate. In the case of $\text{YBCO}(\text{Zn}0.7\%)$ we found no field induced effect (Fig. 136). The relaxation rate is almost field independent, with a slow decrease as the external field increases. So far we found that increased relaxation occurs only in La_2CuO_4 based samples. In the case of the Europium doped LSCO, the effect is enhanced (Fig. 137). One interesting thing to note is the fact that we see an

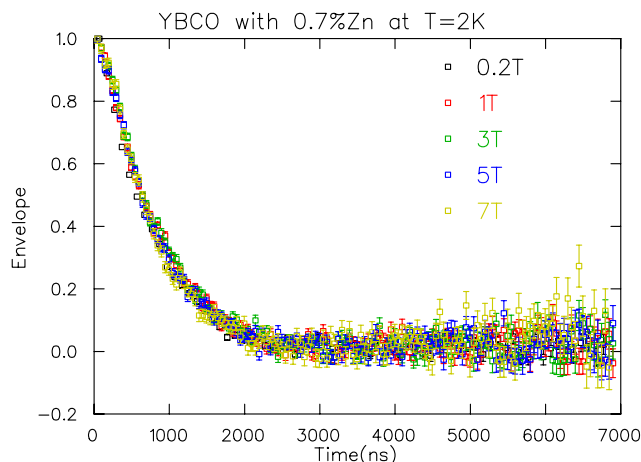


Fig. 136. Envelope functions at different magnetic fields for $\text{YBCO}(\text{Zn}0.7\%)$.

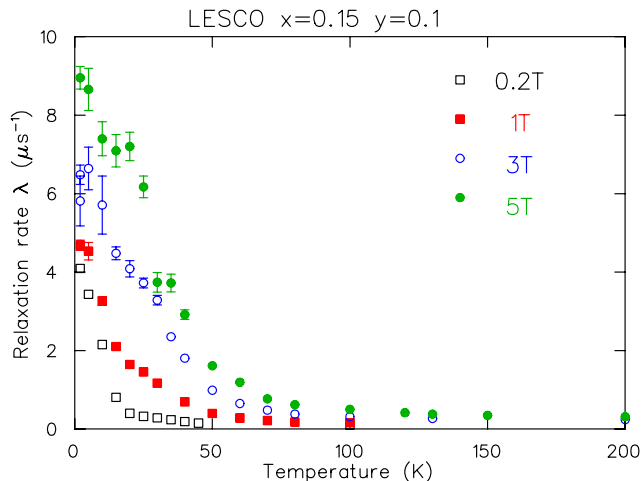


Fig. 137. Relaxation rates for exponential fits to TF- μSR signal in LESCO sample.

increased relaxation rate well above the superconductivity transition temperature.

Currently, we are working on determining the extent of the regions with induced magnetism.

Experiment 931

Magnetic properties of $\text{M}[\text{Au}(\text{CN})_2]_2 \cdot (\text{H}_2\text{O})_2$ ($\text{M} = \text{Cu}, \text{Ni}$) coordination polymers

(J.E. Sonier, D.B. Leznoff, SFU)

Introduction and background

Molecular magnetism deals with the magnetic properties of isolated molecules and groups of molecules, which contain one or more spin carriers. It is the combination of these spin carriers, the bridges connecting them, and their multidimensional assembly that generates materials with unique properties. At the heart of these investigations are two general goals: First, we seek to understand the magnetic interactions between spin carriers, both via direct bonding and mediated by ligand bridges. The key issue of interest is the strength and type of magnetic coupling (ferromagnetic or antiferromagnetic) for a given system. Second, methods to generate high-dimensional systems in a controlled fashion must be explored and applied to open-shell systems. Generally, high-dimensionality systems can show bulk properties (magnetic, thermal, optical) attributable to their polymeric nature. Metal-cyanide bridges have been extremely valuable in molecular magnetism research as they (a) readily form coordination polymers when reacted with transition-metal cations and (b) promote strong magnetic exchange. However, most studies have focused on octahedral $[\text{M}(\text{CN})_6]$ units. The Leznoff group has been exploring the use of linear cyanide units $[\text{M}(\text{CN})_2]$ ($\text{M} = \text{Ag}, \text{Au}$) as couplers in supramolecular open-shell systems. Dicyanoaurate and dicyanoargentate are unique

cyanometallates in that they are linear, form strong attractive M-M intermolecular interactions, and are luminescent.

Under Expt. 931 we have been examining the magnetic properties of some of Leznoff's multidimensional $[\text{Au}(\text{CN})_2]$ -containing coordination polymers that also incorporate paramagnetic transition-metal centres. In particular, the $\text{Cu}[\text{Au}(\text{CN})_2]_2 \cdot (\text{H}_2\text{O})_2$ system was shown in previous μSR studies to undergo a magnetic ordering transition at 250 mK. The questions we wished to probe included: (1) the nature of the magnetic exchange pathway in $\text{Cu}[\text{Au}(\text{CN})_2]_2 \cdot (\text{H}_2\text{O})_2$, i.e., whether the gold-cyanide unit or the copper-bound water molecules mediated the ordering phenomenon and (2) the effect of altering the paramagnetic metal spin carrier on the magnetic properties.

$\text{Ni}[\text{Au}(\text{CN})_2]_2 \cdot (\text{H}_2\text{O})_2$ was prepared and shown to have a very similar structure to the copper analogue. By using SQUID magnetometry between 2–300 K it was determined that this compound undergoes a magnetic phase transition at a much higher temperature than the copper analogue, but with complicated magnetic field-dependent behaviour. Field-dependent dc and ac measurements were conducted and a μSR investigation of this material was desired in order to aid the understanding of the magnetic phase diagram. The results are reported below. The results of these experiments are expected to be submitted for publication in the near future.

Both compounds examined by μSR have been characterized with a variety of other techniques (IR, elemental analysis, TGA etc.) but unfortunately, their structures have not been determined by single-crystal X-ray diffraction, although we are attempting to gain some structural information from powder diffraction data.

$\text{Cu}[\text{Au}(\text{CN})_2]_2 \cdot (\text{H}_2\text{O})_2$

To address the issue of the magnetic pathway in this material, the anhydrous copper/gold material, $\text{Cu}[\text{Au}(\text{CN})_2]_2$, was prepared. If the magnetic exchange interaction leading to ordering is via the metal-bonded water molecules via intermolecular hydrogen bonding, then the removal of these water molecules ought to greatly impact the ordering behaviour. If, however, the gold atoms are primarily responsible, then the ordering behaviour should persist.

We performed zero-field μSR on the anhydrous compound and found no evidence of magnetic order at temperatures down to 50 mK, as is evidenced by the lack of an oscillation in the time spectra presented in Fig. 138. In addition, the relaxation of the muon spin polarization at $T = 400$ mK was largely quenched in longitudinal fields as low as 200 G, indicating that the magnetic moments are primarily static in nature. The

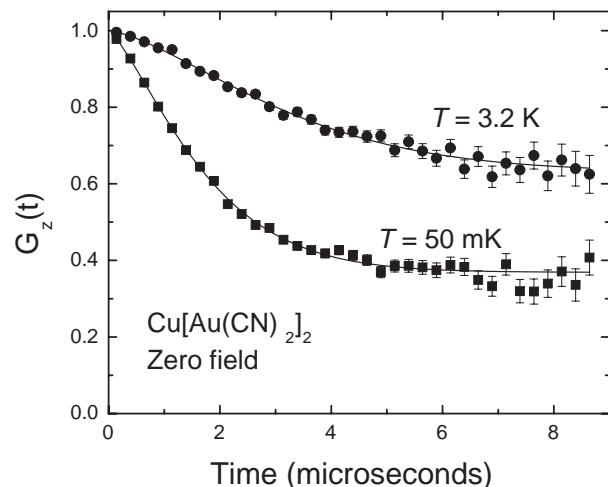


Fig. 138. Time-evolution of the muon spin polarization at various temperatures in $\text{Cu}[\text{Au}(\text{CN})_2]_2$.

lack of magnetic order is in stark contrast to the hydrated compound, and we can therefore conclude that the magnetic interaction in $\text{Cu}[\text{Au}(\text{CN})_2]_2 \cdot (\text{H}_2\text{O})_2$ is mediated by the metal-bonded water molecules.

$\text{Ni}[\text{Au}(\text{CN})_2]_2 \cdot (\text{H}_2\text{O})_2$

Zero-field μSR measurements as a function of temperature were performed on this material in an effort to determine the effect of altering the paramagnetic metal spin carrier on the magnetic properties. The zero-field time-evolution of the muon spin polarization at various temperatures is shown in Fig. 139. Figure 140 shows the corresponding relaxation rates extracted from fits of the time spectra to a stretched exponential function. It can be seen that the relaxation rate rises rapidly below $T \simeq 5$ K, indicating a slowing down of the fluctuations of the magnetic moments, but there is no indication of long-range magnetic order. This contrasts with $\text{Cu}[\text{Au}(\text{CN})_2]_2 \cdot (\text{H}_2\text{O})_2$ in which the spins freeze into an ordered state at the much lower temperature of 250 mK.

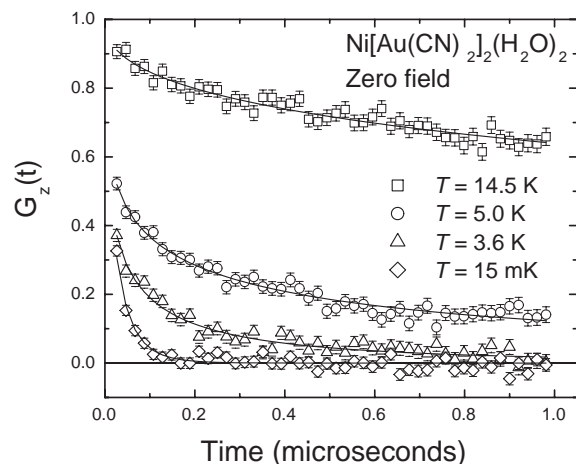


Fig. 139. Time-evolution of the muon spin polarization at various temperatures in $\text{Ni}[\text{Au}(\text{CN})_2]_2 \cdot (\text{H}_2\text{O})_2$.

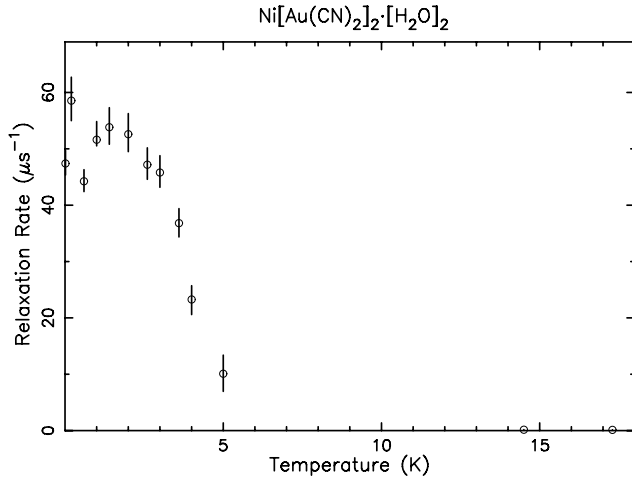


Fig. 140. Relaxation rate of the muon spin polarization as a function of temperature in $\text{Ni}[\text{Au}(\text{CN})_2]_2 \cdot (\text{H}_2\text{O})_2$.

Experiment 938

Muonium formation and ionization in semiconductors and insulators

(V.G. Storchak, Kurchatov; J.H. Brewer, UBC-TRIUMF)

Deep muonium in InSb

The exquisite time resolution and high magnetic field capabilities of TRIUMF's HiTime μSR spectrometer have facilitated the first direct observation of a muonium ($\text{Mu} = \mu^+ e^-$) bound state in indium antimonide. Figure 141 shows the characteristic field dependence of the three detectable frequencies (diamagnetic, ν_{12} and ν_{34}). Frequencies as high as 2.5 GHz have been observed in the HiTime spectrometer, whose true time resolution is estimated to be ~ 140 ps, but in this case the amplitude of the highest frequency signal was too small to follow above about 2 GHz.

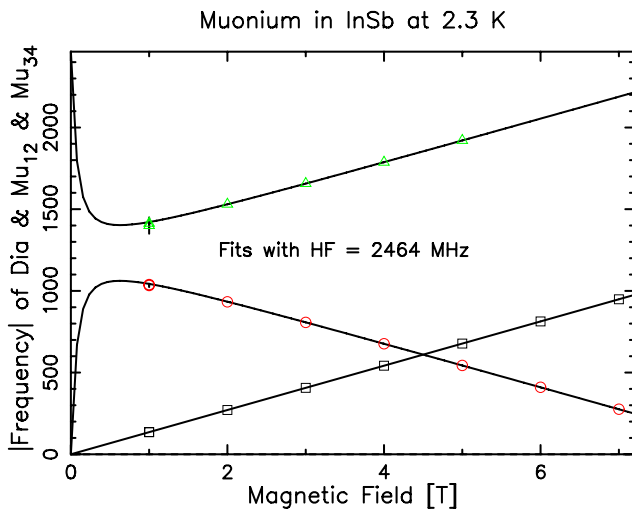


Fig. 141. Frequencies of diamagnetic (squares) and muonium (circles and triangles) precession signals in InSb at 2.3 K as functions of applied magnetic field.

The small-amplitude Mu signal was characteristic of “deep” tetrahedral muonium (Mu_T); there was no sign of the bond-centred Mu_BC state that has been so ubiquitous in other semiconductors [Patterson, Rev. Mod. Phys. **60**, 69 (1988)], nor was there any hint of the metastable “shallow” (weakly bound) Mu_WB state [Shimomura *et al.*, Phys. Rev. Lett. **89**, 255505.1 (2002); Eshchenko *et al.*, Physica **B326**, 120 (2003)] that was expected (given the high mobility and low effective mass of electrons in InSb).

However, there is a substantial “missing fraction” of muon polarization. Either Mu_BC or the shallow Mu_WB state may show up in subsequent experiments at dilution refrigerator temperatures.

The fractions of muon polarization shown in Figs. 142 and 143 have been corrected for the finite

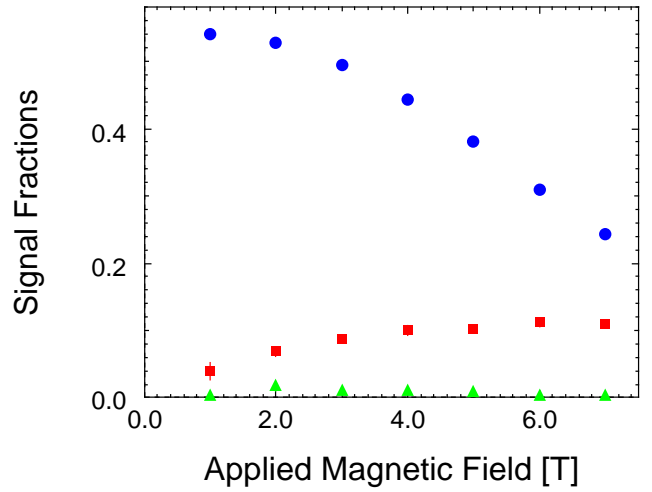


Fig. 142. Magnetic field dependence of diamagnetic (circles) and muonium (squares and triangles) signal amplitudes (expressed as fractions of the maximum muon decay asymmetry) in InSb at 2.3 K.

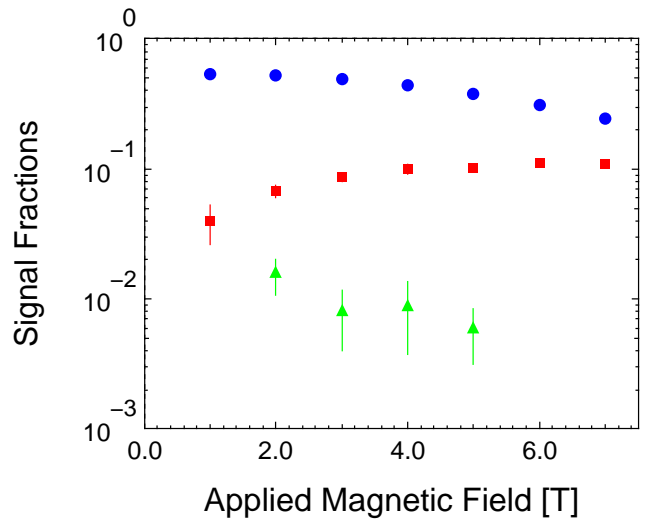


Fig. 143. Same as Fig. 142 except that the signal amplitudes are shown on a logarithmic scale.

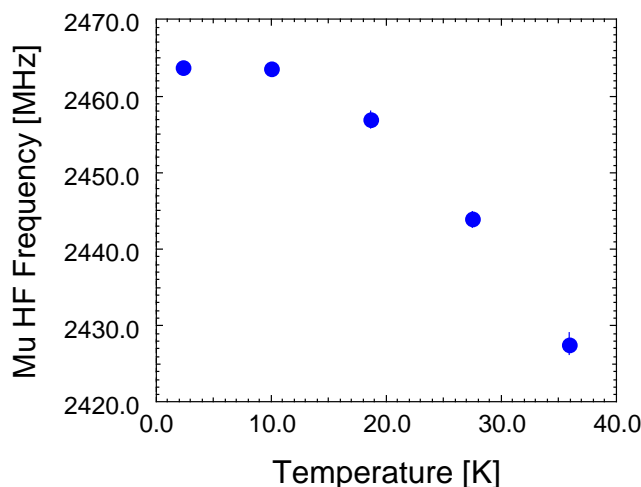


Fig. 144. Temperature dependence of the fitted hyperfine frequency of the deep muonium state in InSb.

time resolution of the HiTime spectrometer by dividing by the value at the same frequency of a smooth function fitted to the measured field dependence of the amplitude of a silver reference sample. The increase of the muonium fraction with field at the expense of the diamagnetic fraction is therefore a real phenomenon, and not a systematic effect. This is thought to reflect magnetic freezeout of radiolysis electrons into a weakly bound excited precursor state, as seen in GaAs [Storchak *et al.*, submitted to Phys. Rev. Lett.].

As can be seen from Fig. 144, the muonium hyperfine frequency was strongly temperature dependent, as seen in previous experiments in high magnetic field [Kiefl *et al.*, Phys. Rev. Lett. **53**, 90 (1984)].

Experiment 939

Guest-host interactions and Hfcs of Mu-alkyl radicals in zeolites

(D.G. Fleming, UBC)

In continuation of Expt. 939 as described in the 2002 Annual Report, the guest-host interactions and Hfcs of the Mu-ethyl radical were studied in the HY and USY zeolites, at 1 and 5 per supercage (SC) and 1 per SC, respectively. For details on experimental plans, loading techniques and terminologies please see that report. As seen in Fig. 145, differences in muon-hyperfine coupling constants (Hfcs) of Mu-ethyl in HY due to different loadings are quite small, differing by no more than 6%, suggesting that radical interactions with other guest molecules in the zeolite are negligible. Consistent with our previous data, however, cation-type effects on hyperfine coupling (due to zeolite type) are quite large, yielding an increase in Mu-Hfc of $\sim 15\%$ between HY and NaY. Unexpectedly, there was very little difference in the magnitude of Hfcs seen in HY and USY (a $\sim 100\%$ cation free zeolite), although the shapes of the temperature-dependence curves showed

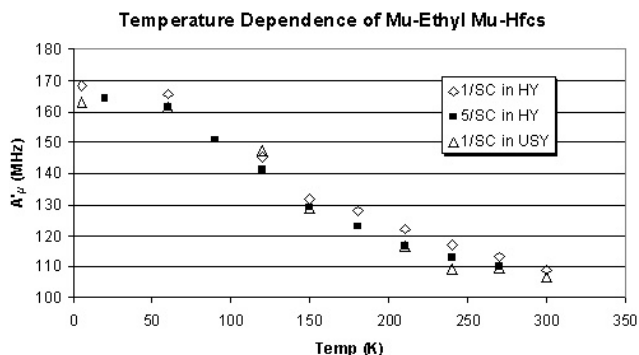


Fig. 145. Muon Hfcs for the Mu-ethyl radical in the HY (at 1 and 5 per supercage loadings) and USY (at 1 per supercage) zeolites. Note that it is the reduced muon Hfc, $A'_{\mu} = A_{\mu}/3.184$, that is plotted. It is also noteworthy that very little loading dependence exists in HY, and that radicals in the USY zeolite show a different T-dependence than those in the HY zeolite.

different curvatures at the inflection points and at low temperatures. USY shows a sharper inflection point than seen in HY suggesting two (or more) sterically-frozen orientations in the former case, a transition between which requiring overcoming a relatively large activation energy barrier. The McConnell plateau (at low temperatures, the y-intercept of which represents the Hfc of a molecule in the absence of internal rotation at 0 K) for the USY-bound radical is flatter, also supporting this idea. Alpha- and Beta-proton Hfcs (not shown in figure) were not well observed in USY, but in HY were shown to have a significant loading- and temperature-dependence, differing by 10–15% when compared at 1 and 5 per SC, and increasing by 10 MHz (15%) when the temperature was increased from 150 to 300 K.

In 2003, the only requirement for completion of the Mu-t-butyl study in Expt. 939 was to investigate the possible formation of the Mu-isobutyl radical in parallel with Mu-t-butyl. This radical is not easily observed, and it is thought rarely forms (by a pseudo-*anti*-Markovnikovian argument), but previous data from 2002 showed its potential presence in an LCR spectra at 240 K. High-statistics TF and ALCR tests were both performed on isobutene-loaded NaY at and around 240 K, showing the presence of no such radical. With the extra time available this summer, 2-cis-butene, 2-trans-butene, and 1-butene were surveyed in NaY and HY. Bulk 2-cis-butene was also investigated thoroughly, the results of which will be reported completely following Expt. 939's summer 2004 beam time. Figure 146 shows the preliminary results of the "butenes" study in zeolites. As is evident, there is little difference between the Mu-Hfcs from the addition of muonium to 2-cis-butene (studied from 7–320 K) and 2-trans-butene (only probed at 300 K). This is to be expected, as the radical yielded in both cases is

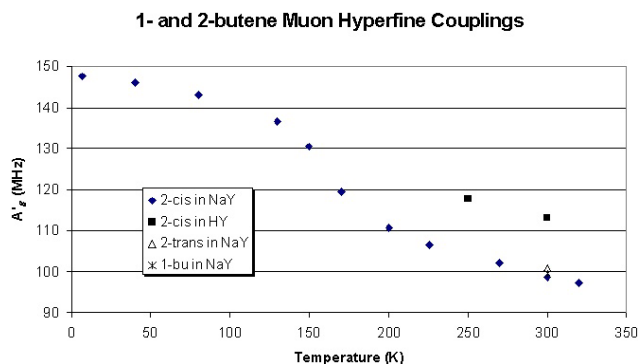


Fig. 146. Muon Hfcs for the Mu-butyl radical (from 2-cis-, 2-trans-, and 1-butene) in the NaY and HY zeolites at 2 per SC loadings. Again, it is A'_μ that is plotted. Note the significant dependence on cation type.

the Mu-butyl radical ($\text{CH}_3\text{CH}\cdot\text{CHMuCH}_3$). Addition of muonium to 1-butene also yields Mu-butyl, but of the form $\text{CH}_2\text{MuCH}\cdot\text{CH}_2\text{CH}_3$, which should yield different hyperfine coupling behaviour. At room temperature, all three butene-types in NaY yielded similar Hfcs; if this holds true at lower temperatures it has yet to be seen. The best potential for future investigation lies in the study of Hfc-dependence on cation type for 2-cis-butene (as is shown to be substantial at room temperature in the figure), and for 1-butene, which should yield some interesting differences from the former molecule. It is our intention to wrap-up the experimental project this summer.

Experiment 941

Investigation of spin statics and dynamics in the transition metal oxides $\text{Sr}_2\text{CaReO}_6$ and $\text{Li}_2\text{Mn}_2\text{O}_4$

(C.R. Wiebe, Columbia/McMaster; G.M. Luke, McMaster)

The topic of geometric frustration has been at the forefront of solid state physics for the last decade due to the remarkable number of interesting magnetic ground states observed. The plethora of lattice types which can accommodate the triangular motif of spins coupled with the arsenal of magnetic species to place on these sites has brought about a unique subfield of magnetism that will remain to be studied for a long time. In the last few years, the focus of study has shifted to the search for more exotic systems such as the spin liquid, which arises due to quantum effects from networks of frustrated low spin materials. For example, the pyrochlore $\text{Tb}_2\text{Ti}_2\text{O}_7$ has recently been shown to be a “cooperative paramagnet”, in which the system shows no magnetic long range order down to 0 K but instead forms a liquid like state. Neutron diffraction and μSR experiments were crucial in the elucidation of the important role of strong spin fluctuations that persist down to 0 K. Such discoveries provide the im-

petus to look for new materials that will continue to challenge and surprise the condensed matter community.

Despite this high level of interest, the number of examples of frustrated systems with isolated low-spin moments is relatively small. Spin liquids have proven to be difficult subjects of study with the exception of a few well known materials. The number of systems that display little disorder and have well-defined low spins on frustrated topologies is relatively low.

Spin freezing in the ordered FCC perovskite $\text{Sr}_2\text{CaReO}_6$

Two new materials have recently been synthesized at the Brockhouse Institute for Materials Research that are excellent candidates for displaying liquid-like ground states. $\text{Sr}_2\text{CaReO}_6$ is an FCC perovskite that has an ordered array of FCC $S = 1/2 \text{ Re}^{6+}$ moments. These form a network of edge-shared tetrahedra as displayed in Fig. 147. A FC/ZFC divergence in the DC susceptibility suggests a transition at 14 K. Neutron diffraction experiments failed to detect any long range ordering below this temperature. Recent heat capacity measurements hint at the presence of interesting spin dynamics at play through the appearance of an anomaly at T_G that is independent of the applied magnetic field. This is reminiscent of a spin singlet ground state, as suggested by Ramirez *et al.* from his work on the kagomé material $\text{SrCr}_9\text{Ga}_{12-9p}\text{O}_{19}$ (SCGO). Furthermore, the magnetic specific heat shows a T^3 dependence at low temperatures, which suggests that strong 3D spin fluctuations are present as $T \rightarrow 0 \text{ K}$. Similar behaviour is seen in SCGO, with a T^2 specific heat power law, indicative of 2D spin fluctuations that were later confirmed by μSR measurements.

μSR has long been used to study the dynamics of highly frustrated spin systems. For small S spin systems in particular, muons are perhaps the best probe of the low temperature magnetic ground state within a broad frequency range. Figure 148 shows several zero

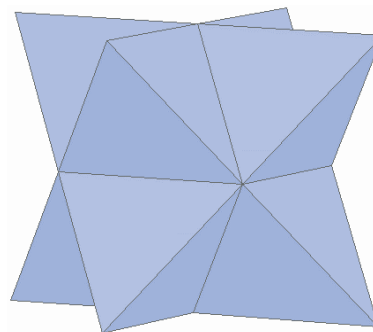


Fig. 147. The face-centred cubic lattice of Re^{6+} spins in $\text{Sr}_2\text{CaReO}_6$, which can be envisioned as a sublattice of edge-shared tetrahedra.

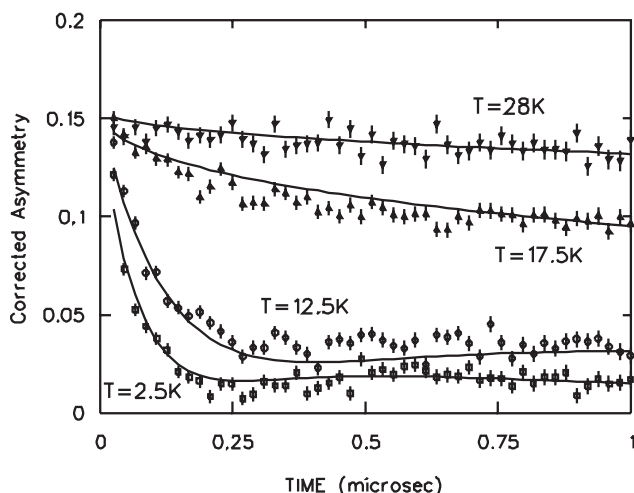


Fig. 148. ZF- μ SR measurements of $\text{Sr}_2\text{CaReO}_6$ at $T = 2.5$ K, 12.5 K, 17.5 K, and 28 K. The fits are based upon a generic spin glass relaxation function as described in the text.

field (ZF) scans taken between $T = 2.5$ K and $T = 28$ K. The two component nature of the spectra is immediately evident below $T_G \sim 14$ K, as opposed to the single component high temperature scans which is characteristic of a paramagnetic response. This response indicates a quasi-static distribution of internal magnetic fields developing below T_G , as noted in other spin glasses. The fit to the spectra indicated is modelled after Uemura's original treatment of these line-shapes in his pioneering μ SR work on AuFe and CuMn alloys. This is unusual with the absence of chemical disorder.

Although it seems like this system is a typical spin glass from the μ SR measurements, there are several departures from convention which merit further discussion. Firstly, the signal is somewhat weak, which is expected due to the small magnetic moment, but since it is feeble, it is truly difficult to tell if there is a weak ordering signal buried in the background. There could indeed be short ranged magnetically ordered clusters forming that are virtually undetectable by this technique. One would expect spin fluctuations at temperatures slightly higher than T_G to be visible in the spectra, but the nature of the transition itself is rather abrupt, with only the slightest hint of a second component appearing at $T = 17.5$ K. It is surprising that the second component develops quickly below T_G . The conventional way of understanding spin glasses is in the formation of islands of frozen spins which slowly develop as one passes through the transition. In our system, however, there is relatively little change in the muon signal from 12.5 K to 2.5 K, which suggests that the spins freeze out rather abruptly.

One can compare these results with the monoclinic $S = 1$ FCC ordered system $\text{Sr}_2\text{NiTeO}_6$ which shows a

lambda anomaly at $T_N \sim 28$ K indicative of magnetic ordering and a continuous phase transition. Nonetheless, magnetic susceptibility measurements show evidence for magnetic correlations at $T \sim 35$ K by a FC/ZFC divergence at temperatures higher than the cusp at T_N . In this case, approximately 70% of the entropy is recovered at the magnetic transition, but the ground state is ordered rather than glassy. As the Ni^{2+} ions in $\text{Sr}_2\text{NiTeO}_6$ have $S = 1$, this seems to suggest that it is the $S = 1/2$ moment on Re^{6+} that induces the spin glass ground state in $\text{Sr}_2\text{CaReO}_6$. This new ground state is believed to be caused by quantum effects of $S = 1/2$ spins on this highly frustrated lattice.

2D magnetic ordering in the 3D frustrated spinel $\text{Li}_2\text{Mn}_2\text{O}_4$

The other material of interest is the tetragonal spinel $\text{Li}_2\text{Mn}_2\text{O}_4$. This member is part of a series of materials, $\text{Li}_x\text{Mn}_2\text{O}_4$ ($x = 0-2$), which have been intensely studied as cathodes for secondary lithium ion batteries. All of these materials are in principle frustrated, since the Mn cations form a framework of corner-shared tetrahedra within the spinel structure (see Fig. 149). However, it is only the materials of low lithium content, such as $\lambda\text{-MnO}_2$ and LiMn_2O_4 that have been studied a great deal, due to interest by the electrochemical community. The fully lithiated species is difficult to synthesize without disrupting the structure unless one uses gentler methods, such as chimie douce. Insertion of Li by the addition of butyl-lithium to LiMn_2O_4 in an inert argon environment has been shown to be a successful method by our group to obtain the metastable $\text{Li}_2\text{Mn}_2\text{O}_4$ with only modest heating to 50°C .

$\text{Li}_2\text{Mn}_2\text{O}_4$ consists of a network of Mn^{3+} moments upon a lattice of slightly distorted corner-shared tetrahedra. Recently, Wills *et al.* have demonstrated that

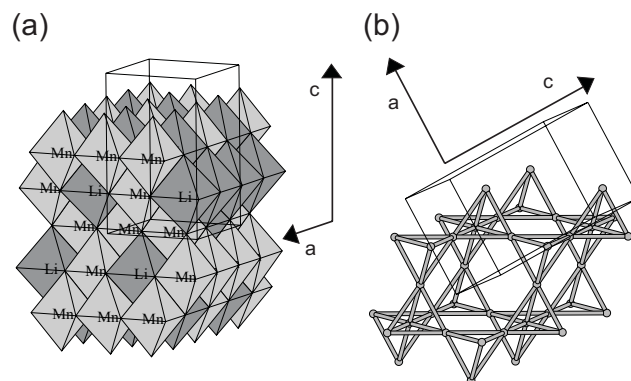


Fig. 149. (a) The spinel lattice, with Li and Mn octahedra. The a and c axis and the tetragonal unit cell are shown. (b) The Mn magnetic sublattice, shown as a network of corner-shared tetrahedra (which would be identical to the cubic pyrochlore sublattice if not for the tetragonal distortion). This can be thought of as a series of kagomé slabs normal to the $\langle 111 \rangle$ direction.

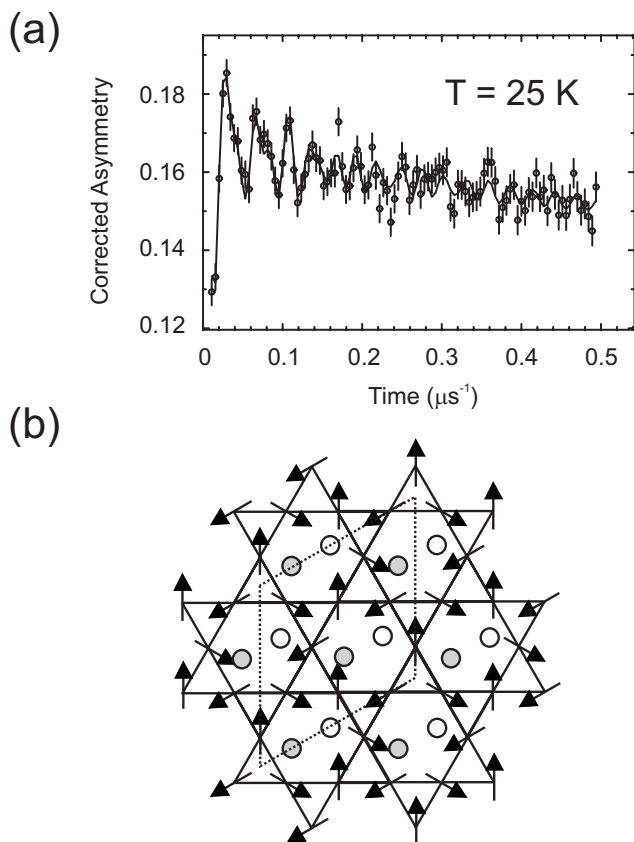


Fig. 150. (a) Early time ZF- μ SR spectra at $T = 25$ K. The fit is to a three frequency model. (b) The $q = \sqrt{3} \times \sqrt{3}$ magnetic structure. The muon sites in $\text{Li}_2\text{Mn}_2\text{O}_4$ are indicated on the figures as circles, slightly above (grey) and below (white) the kagomé planes. The magnetic sublattice in 2D is marked by dashed lines. There are six muon sites for the $q = \sqrt{3} \times \sqrt{3}$ structure, which give rise to the three frequency signal.

the frustrated lattice does not exhibit long-range order, but instead there is a transition to a short-range ordered state at 50 K. This is heralded by the appearance of several broad features in the elastic neutron scattering profile that can be fit to a Warren lineshape. As Warren indicated in his studies of graphite, these features are due to 2D correlations which arise in powder samples. In our case, the diffuse scattering is magnetic rather than structural, indicating strong 2D magnetic correlations. This is remarkable considering the fact that the connectivity of the frustrated lattice is fully three dimensional.

ZF- μ SR experiments on $\text{Li}_2\text{Mn}_2\text{O}_4$ have confirmed that a short-ranged ordered magnetic state sets in below ~ 150 K, which subsequently develops into a long-ranged ordered state below ~ 50 K. Longitudinal field measurements show that the fast relaxation seen in the regime $50 \text{ K} \leq T \leq 150 \text{ K}$ is static in nature, which is consistent with the broad features seen by neutron scattering. The ordering observed below 50 K

is compatible with the proposed two-dimensional $q = \sqrt{3} \times \sqrt{3}$ magnetic structure in kagomé planes that reside within the pyrochlore framework (see Fig. 150). The evolution of the order parameter at T_N resembles other 2D magnetic systems, but it is unclear why a three-dimensional network of tetrahedra would exhibit two-dimensional magnetism.

Experiment 943

Muonium formation and reactivity in sub- and supercritical carbon dioxide

(K. Ghandi, UBC)

Current data on muonium chemistry in supercritical water (Expt. 713/842) have established that the current models used in reaction kinetics of chemical reactions in supercritical water are wrong and they have led to a new model for chemical kinetics in supercritical water [Ghandi and Percival, J. Phys. Chem. **A107**, 3005 (2003); Ghandi *et al.*, Physica **B326** 76 (2003); Ghandi *et al.*, Phys. Chem. Chem. Phys. **4** 586 (2002); Ghandi *et al.*, Physica **B289**, 476 (1999)]. They have also led to novel mechanistic information relevant to green chemistry [Ghandi *et al.*, JACS **125**, 9594 (2003)]. In an attempt to extend those kinds of studies to supercritical CO_2 , we initiated Expt. 943.

The main focus of the first year of the experiment was to establish muonium formation over a broad range of thermodynamic states under sub-and supercritical conditions. In Figs. 151–153 we have compared our data with those in supercritical water [Percival *et al.*, Phys. Chem. Chem. Phys. **1**, 4999 (1999)] in a similar range of density and in high-pressure ethane [Kemp-ton *et al.*, J. Phys. Chem. **95**, 7338 (1991)] over a much smaller range of density. The comparison reveals significant difference in the radiolysis processes in supercritical CO_2 as compared to the other two fluids [Ghandi *et al.* (submitted to J. Phys. Chem. B)]. This may suggest that kinetics and interactions of thermal muonium

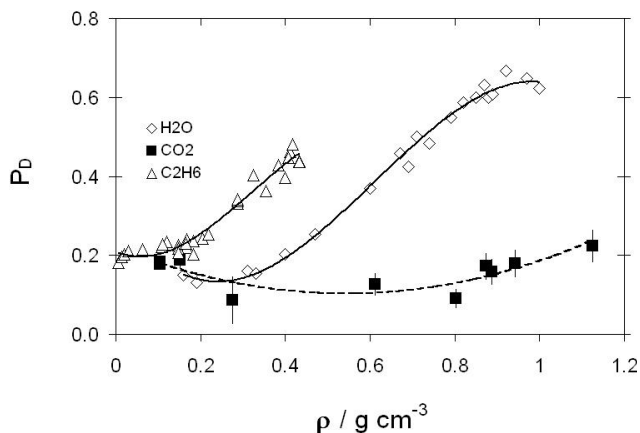


Fig. 151. Diamagnetic (P_D) fractions in pure CO_2 , H_2O and C_2H_6 as a function of density (error bars for C_2H_6 and H_2O data are not shown). The lines are to guide the eye.

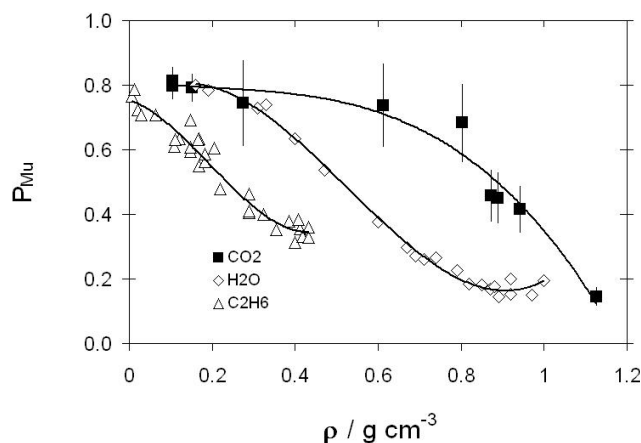


Fig. 152. Muonium (P_{Mu}) fractions in pure CO_2 , H_2O and C_2H_6 as a function of density (error bars for C_2H_6 and H_2O data are not shown). The lines are to guide the eye.

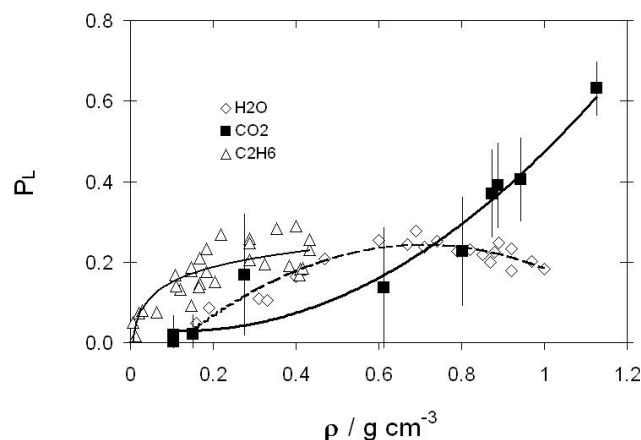


Fig. 153. Loss fractions (P_L) in pure CO_2 , H_2O and C_2H_6 as a function of density (error bars for C_2H_6 and H_2O data are not shown). The lines are to guide the eye.

are expected to be different compared to ones in supercritical water. To probe the change of interactions of Mu with solvent molecules (CO_2) with varying density, we have studied muonium hyperfine interactions at different densities. Our results, which are the subject of another publication, are shown in Fig. 154. This is the first demonstration, by any technique, of the effect of thermodynamic conditions in supercritical CO_2 on the atomic wave functions, and of a manifestation of change in intermolecular interactions between CO_2 and Mu. The data cover a much broader density range compared to the supercritical water data.

Also to extend the kinetic studies in supercritical water to supercritical CO_2 , we studied the reaction between NO and Mu. The rate of Mu decay is a result of two processes: spin exchange and addition of Mu to NO. Some early results are shown in Figs. 155 and 156 by using the $\frac{3}{4}$ law predicted by Senba [J. Phys. **B26**, 3213 (1993)] to separate the spin exchange from the additional component.

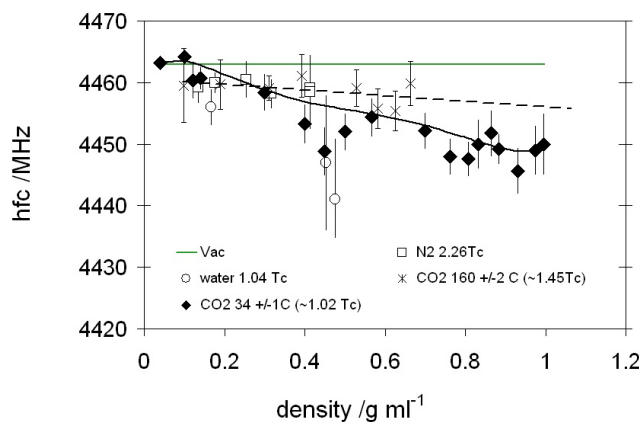


Fig. 154. Mu hyperfine coupling constant in supercritical CO_2 compared to in N_2 and in water.

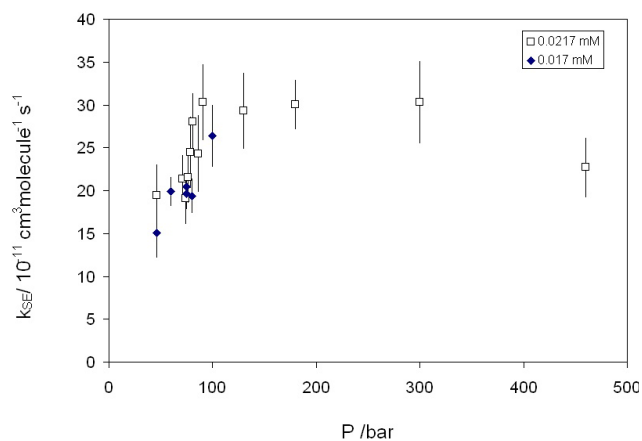


Fig. 155. The rate constant for spin exchange of Mu and NO at slightly above the critical temperature of CO_2 .

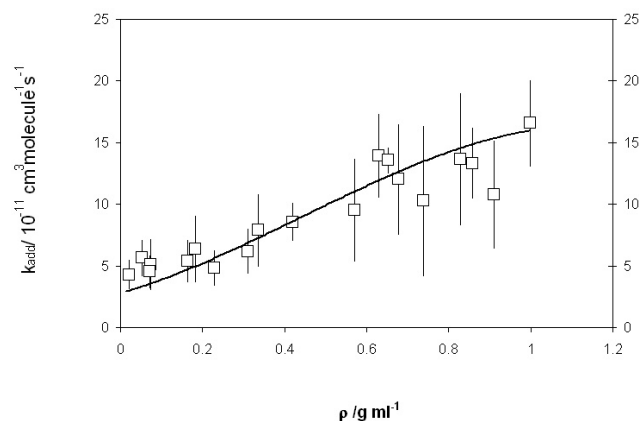


Fig. 156. The rate constant for the addition reaction of Mu and NO at slightly above the critical temperature of CO_2 .

The data on spin exchange may suggest a change in the diffusional and solvent cage properties in near critical CO_2 as observed for spin exchange between Mu and Ni^{2+} in supercritical water. The results for addition to NO show probably the first ever high-pressure limit for a reaction between Mu and a smaller than four atom molecule [Himmer *et al.*, J. Phys. Chem. **A103**,

2076 (1999); Pan *et al.*, Phys. Chem. Chem. Phys. **2**, 621 (2000)]. However, due to complications with addition to NO, more data, particularly in longitudinal field, are needed to confirm these results. It is intended to make such measurements over a wide density range at a few temperatures, with a view to separating the spin exchange from addition component by varying the magnetic field.

Experiment 944

Muonium in silicon carbide

(R.L. Lichti, Texas Tech; K.H. Chow, Alberta)

The main initial goal for TRIUMF Expt. 944 was to characterize the hyperfine interactions for neutral Mu centres seen in the three primary structures of SiC, namely 4H, 6H, and 3C. The cubic 3C structure was predicted to yield a shallow donor. We have not observed any Mu^0 hyperfine spectra in the *n*-type sample of 3C-SiC that was available, although features seen below 50 K suggest dynamics involving a possible shallow centre. Initial data for high-resistivity samples of the two hexagonal structures showed atomic-like neutral centres: two Mu^0 signals were observed in 4H as expected; and three strong Mu^0 signals were seen in 6H, but there were also hints of a possible fourth signal at some temperatures.

The three signals clearly observed in 6H-SiC do not correspond very well to the hyperfine values published some years ago [Patterson *et al.*, Hyp. Int. **32**, 625 (1986)]. The Mu^0 motion and related site averaging of A_{HF} that was expected to occur below 300 K based on the limited older data could not be confirmed. Instead we found that, although the precession signals of Mu^0 states disappeared between 100 and 200 K for the 6H sample, the same three signals reappeared at higher temperatures but below the onset of Mu^0 ionization near room temperature. Our main effort during this year's beam time was to examine *n*-type and *p*-type SiC to check for consistency in A_{HF} and to further characterize the unexpected Mu^0 dynamics.

In *n*-type 6H-SiC, two of the Mu^0 centres observed correspond to those seen in the high-resistivity material, but the third signal was significantly different, appearing in the region where hints of a possible fourth Mu^0 signal were seen previously. Table XII gives the zero temperature A_{\parallel} values in all 4H and 6H samples. We note that the values we find for *n*-type 6H are each about 20 MHz lower than the A_{\perp} values from the early results.

Figure 157 displays the temperature dependent hyperfine constants for one of the Mu^0 centres in 4H-SiC. The same two neutrals were seen in all 4H samples examined, and the data in Fig. 157 show typical

Table XII. The low-temperature hyperfine constants A_{\parallel} (in MHz) for Mu^0 centres observed with $\mathbf{B} = 6 \text{ T} \parallel \mathbf{c}$ in the 4H and 6H structures of silicon carbide.

Sample	High-resist	<i>p</i> -type	<i>n</i> -type
4H-SiC	3002.82 (0.01)	3002.77 (0.01)	3002.8 (0.1)
	2801.14 (0.06)	2801.07 (0.04)	2801.0 (0.2)
6H-SiC	2999.01 (0.01)		
	2984.34 (0.01)		2981.3 (0.1)
			2777.9 (0.2)
	2745.57 (0.01)		2745.5 (0.1)

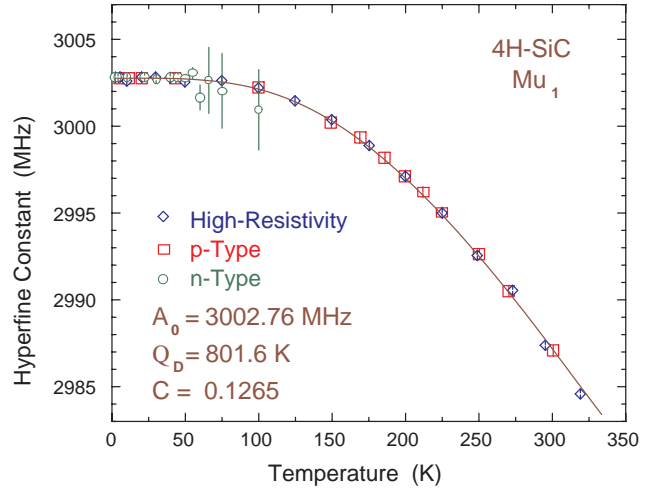


Fig. 157. Temperature dependent hyperfine constants for one of the two Mu^0 centres observed in 4H-SiC measured with $B = 6.0 \text{ T}$ applied along the *c*-axis.

sample to sample differences. For both *n*-type materials the Mu^0 spin precession signals broaden and disappear near 100 K where the nitrogen donors have ionized. The temperature dependence of A_{\parallel} fits well to a model in which the dominant cause of decreasing A_{HF} is interaction with long wavelength phonons. Each of the temperature-dependent A_{HF} curves in both 4H and 6H-SiC yields a Debye temperature of $\sim 800 \text{ K}$.

Longitudinal relaxation data were collected for the two *n*-type hexagonal samples as an initial attempt to identify specific transition or charge-exchange dynamics. Figure 158 shows the rate constants for the more rapidly relaxing fraction in *n*-type 6H-SiC. The amplitude associated with the feature between 100 and 180 K decreases with temperature, thus this feature probably represents a charge-state transition involving a single Mu^0 state, perhaps an electron capture to yield Mu^- at one of the occupied sites. Spin precession data for high-resistivity samples of both 4H and 6H suggest two diamagnetic states with a very small difference in frequencies of about 20 kHz out of 813 MHz, and the low-field precession data imply a transition between two diamagnetic states near 100 K.

The relaxing amplitude stays relatively constant across the higher temperature peak in Fig. 158, but

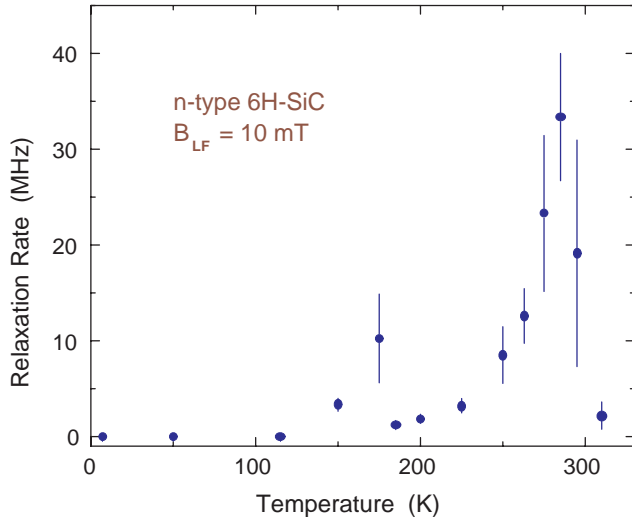


Fig. 158. Temperature dependence of longitudinal relaxation rates for the fast relaxing fraction seen in *n*-type 6H-SiC. Similar data for an *n*-type 4H-SiC sample show low rate constants and a sharp peak at 200 K.

then decreases above the peak. This is in the region where the spin precession data in *p*-type and high-resistivity samples imply an onset of Mu^0 ionization, thus we suggest a rapid $\text{Mu}^0 \leftrightarrow \text{Mu}^+$ charge-exchange cycle involving electron loss and recapture as the likely origin of this feature. These results show that a combination of spin precession and longitudinal relaxation data is beginning to provide hints of the origin of dynamics involving Mu^0 centres in hexagonal SiC.

Experiment 949

μSR study of magnetic order in high- T_c superconductors under high pressure

(J. Arai, Tokyo U. Science)

Anomalous suppression of superconducting transition temperature T_c observed in a narrow range of $x \sim 1/8$ for $\text{La}_{2-x}\text{M}_x\text{CuO}_4$ ($M = \text{Ba}, \text{Sr}$), which is called the “1/8 problem”, is one of the most important issues to understand the relation between superconductivity and magnetism in high- T_c cuprates. At the beginning, the 1/8 problem was considered to be particular to La-214 compounds. However, 1/8 anomaly is also observed in Bi-2212 and Y-123, suggesting that the 1/8 problem is a common property of high- T_c superconductors.

Structural instability is inherent in La-214 compounds, which are the most typical system in high- T_c superconductors. The crystal structure is closely related to the electronic state in this system. With decreasing temperature, La-214 compounds undergo a well-known phase transition from a high-temperature tetragonal (HTT) structure to a low-temperature orthorhombic (LTO) structure except for the overdoped region. In addition, $\text{La}_{2-x}\text{Ba}_x\text{CuO}_4$ (LBCO) displays

a second transition to a low-temperature tetragonal (LTT) structure around $x = 1/8$ at low temperatures. Because superconductivity is strongly suppressed in LBCO around $x = 0.125$ and slightly suppressed in $\text{La}_{2-x}\text{Sr}_x\text{CuO}_4$ (LSCO) around $x = 0.115$, it is widely believed that the LTT structure plays an important role in suppressing superconductivity around $x \sim 1/8$.

On the other hand, in La-214 compounds around $x \sim 1/8$, magnetic order has been observed by neutron scattering experiments [Tranquada *et al.*, Nature **375** (1995)] and μSR experiments [Watanabe *et al.*, J. Phys. Soc. Jpn. **61** (1992)]. These results indicate the close relation between the suppression of superconductivity and the appearance of magnetic order.

The μSR measurement is the most suitable experimental method to study the competition between superconductivity and magnetic order because we can investigate the Cu spin state in the absence of an external magnetic field. On the other hand, the LTT and LTO phases of LBCO with $x = 0.125$ are suppressed by applying pressure up to 0.6 GPa and 1.5 GPa, respectively [Katano *et al.*, Phys. Rev. **B48** (1993)]. Then we can control the two structural transition temperatures by applying pressure above 1.5 GPa.

To generate high pressure above 1.5 GPa, we have developed pressure cells made of non-magnetic alloy Ni-Co-Cr-Mo (MP35N) with a wall 8 mm thick. The size of the sample in the pressure cell is much smaller than that in conventional μSR measurements. To increase the SN ratio, we used the defining counter which is as small as the sample.

In order to clarify the relation among superconductivity, the magnetic order and the crystal structure, we have performed the zero-field μSR measurement in LBCO with $x = 1/8$ under high pressure up to ~ 1.3 GPa by using $\phi 7\text{T}8$ pressure cell at the M9B port at TRIUMF.

Figures 159 and 160 show the μSR spectra at ambient pressure and $P \sim 1.3$ GPa, respectively. Here we define the magnetic ordering temperature T_m as the temperature where an oscillation component starts to appear in μSR spectra. At ~ 1.3 GPa T_m exists between 35 and 40 K. The μSR spectra at 35 K under ambient pressure and ~ 1.3 GPa are quite similar. T_c at ambient pressure is the same as that at $P \sim 1.3$ GPa. Since the LTT structure vanishes above ~ 0.6 GPa, this result suggests that the magnetic order is not related to the LTT structure.

In order to investigate the relation between superconductivity and the LTT structure, we have carried out the resistivity measurement in LBCO with $x = 0.125$ at several pressures up to ~ 2.2 GPa. The superconducting temperature T_c which is determined by zero of the resistivity increases as the LTT structure

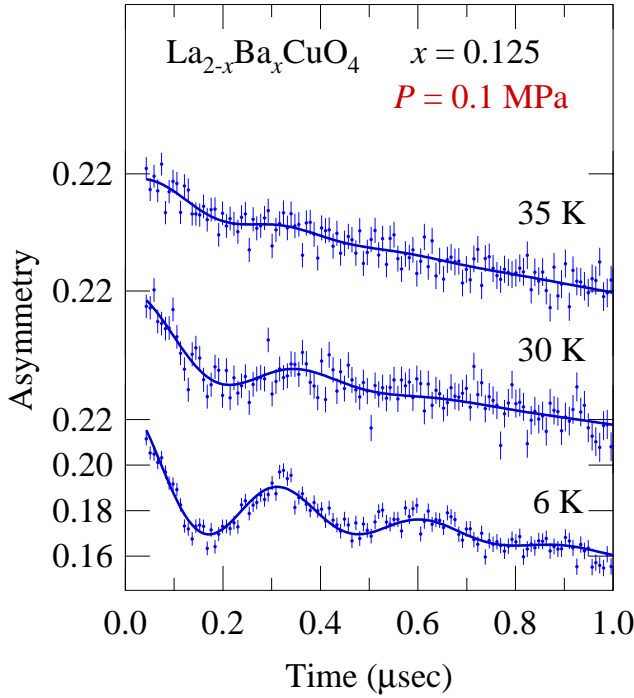


Fig. 159. ZF- μ SR spectra of LBCO with $x = 0.125$ at ambient pressure.

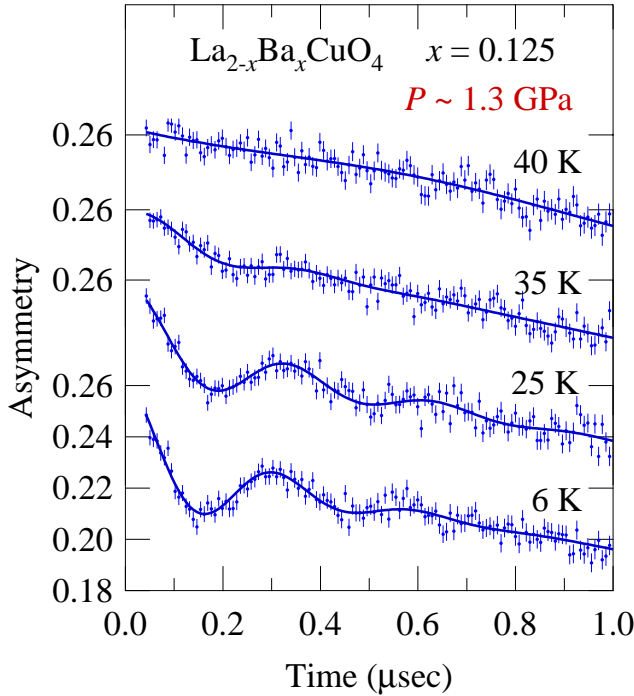


Fig. 160. ZF- μ SR spectra of LBCO with $x = 0.125$ at $P \sim 1.3$ GPa.

is suppressed. The suppression of superconductivity is closely related to the LTT structure.

T_m and T_c are plotted as a function of pressure in Fig. 161. With increasing pressure, T_c increases linearly with an initial rate of $dT_c/dP \sim +8.1$ K/GPa. At $P_d \sim 1.1$ GPa, dT_c/dP changes to $+1.9$ K/GPa.

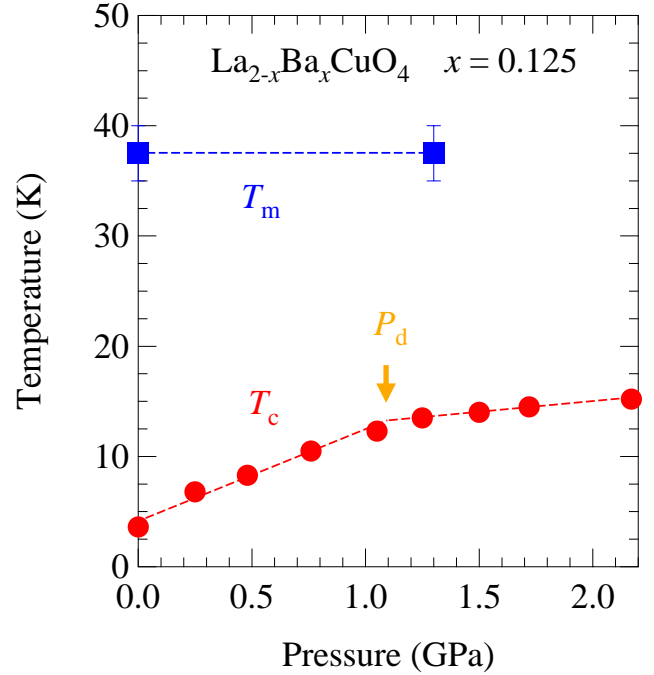


Fig. 161. Pressure dependence of magnetic ordering temperature T_m and superconducting temperature.

It seems that P_d indicates the LTT-LTO phase transition pressure. On the other hand, T_m is independent of pressure, suggesting that the magnetic order does not compete with superconductivity.

Experiment 951

Magnetism and flux line lattice structure of oxychloride superconductors

(K. Ohishi, R. Kadono, KEK-IMSS)

Alkaline-earth copper oxychlorides $A_2CuO_2Cl_2$ ($A = Ca, Sr$) are insulating antiferromagnetic compounds consisting of two-dimensional CuO_2 layers. They have a layered perovskite structure common to K_2NiF_4 with a body-centred-tetragonal symmetry ($I4/mmm$), which is free from any distortion. The Néel temperature (T_N) determined by neutron measurements is 255 K for $A = Sr$ [Vaknin *et al.*, Phys. Rev. **B41**, 1926 (1990)] and 247(5) K for $A = Ca$ [*ibid.*, Phys. Rev. **B56**, 8351 (1997)], respectively. While $Sr_2CuO_2Cl_2$ has yet to be carrier doped [Miller *et al.*, Phys. Rev. **B41**, 1921 (1990)], $Ca_2CuO_2Cl_2$ becomes a high- T_c superconductor (maximum $T_c = 28$ K at $x \sim 0.2$) by the doping of sodium [Hiroi *et al.*, Nature **371**, 139 (1994)]. While $Ca_{2-x}Na_xCuO_2Cl_2$ exhibits superconductivity upon doping holes by substituting Ca by Na, the magnetic property of those with $x < 0.10$ (which are non-superconducting) has not been investigated, except for $x = 0$. We have performed ZF- μ SR measurements to elucidate the magnetic phase diagram of $Ca_{2-x}Na_xCuO_2Cl_2$ over the underdoped region.

The ZF- μ SR measurements were conducted on the M15 beam line at TRIUMF. We prepared ten sets of $\text{Ca}_{2-x}\text{Na}_x\text{CuO}_2\text{Cl}_2$ specimens, $x = 0, 0.0025, 0.005, 0.01, 0.02, 0.05, 0.07, 0.10, 0.15, 0.20$, having a dimension of about $100 \sim 250 \text{ mm}^2$ with $\sim 1 \text{ mm}$ thickness. These samples were mounted on a sample holder and loaded to the ^4He gas flow cryostat. ZF- μ SR measurements were performed at temperatures between 2 K and room temperature, and transverse field (TF)- μ SR measurements were also performed at room temperature under applied field $H_{\text{TF}} \simeq 2 \text{ mT}$ in order to determine the geometrical factor. In this report, we show the result in $\text{Ca}_2\text{CuO}_2\text{Cl}_2$ ($x = 0$) for which the analysis is complete.

Figure 162 shows the time spectra of the muon spin polarization $P_z(t)$ observed in $\text{Ca}_2\text{CuO}_2\text{Cl}_2$ in zero field at several temperatures. The left and right figures show $P_z(t)$ over the respective time region of $7 \mu\text{s}$ and $1.0 \mu\text{s}$. For both time ranges, spin precessions with different frequencies are clearly observed below $T = 260 \text{ K}$. Therefore, μ SR data were analyzed with the following function;

$$P_z(t) = \sum_{i=1}^n A_i \exp[-(\sigma_i t)^2] \cos[2\pi(f_i t + \phi)] + A_{\text{non}} \exp[-(\sigma_{\text{non}} t)^\beta],$$

where A_i and A_{non} are the asymmetries of oscillating and non-oscillating components, f_i is the muon spin precession frequency, σ_i and σ_{non} are the relaxation rates, β is the power of the exponent.

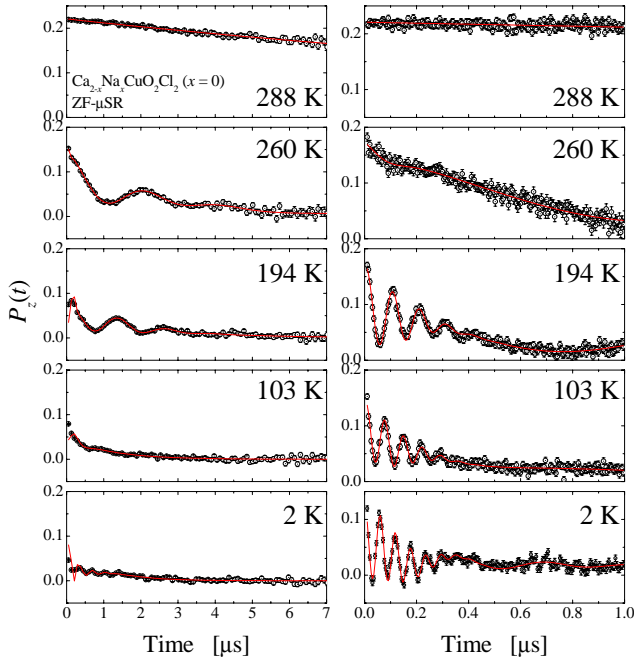


Fig. 162. ZF- μ SR time spectra of the muon spin polarization $P_z(t)$ in $\text{Ca}_2\text{CuO}_2\text{Cl}_2$ at various temperatures.

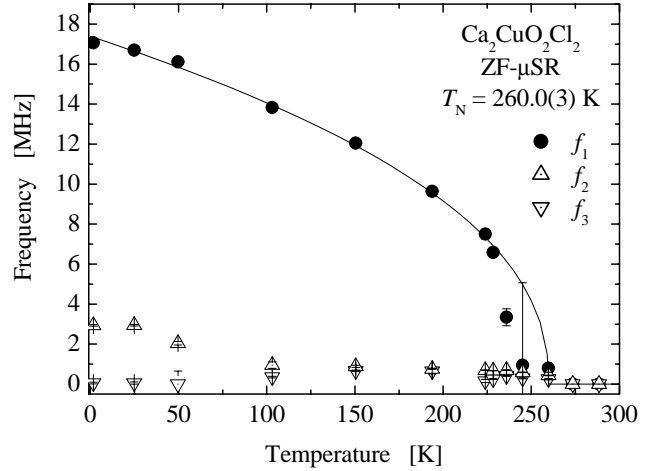


Fig. 163. Temperature dependence of the muon spin precession frequencies in $\text{Ca}_2\text{CuO}_2\text{Cl}_2$.

The temperature dependence of the muon spin precession frequencies is shown in Fig. 163. The frequencies are sharply reduced above 260 K, with their amplitudes disappearing around 275 K. This is consistent with the neutron results in which Bragg peak appears below $T_N = 247(5) \text{ K}$. It is also noticeable that one having lower frequencies further splits into two components below around 100 K. The high frequency component (f_1) is well fitted by a function $A(T_N - T)^B$, with $T_N = 260.0(3) \text{ K}$. This complex character of the internal field is in marked contrast with the case in $\text{La}_{2-x}\text{Sr}_x\text{CuO}_4$ where only a single frequency is observed. However, one of those (f_2) is almost the same as that in $\text{La}_{2-x}\text{Sr}_x\text{CuO}_4$ ($\sim 5 \text{ MHz}$) [Uemura *et al.*, Phys. Rev. Lett. **59**, 1045 (1987); *ibid.*, Physica **C153-155**, 769 (1988); *ibid.*, Hyp. Int. **49**, 205 (1989)] and f_3 is close to that in $\text{Sr}_2\text{CuO}_2\text{Cl}_2$ [Le *et al.*, Phys. Rev. **B42**, 2182 (1990)].

While the detailed analysis is still in progress, these findings suggest that the muon stopping site may not be unique. It is currently speculated that the muon sites are both at around apical chlorine, which is common to the $\text{La}_{2-x}\text{Sr}_x\text{CuO}_4$ case, and near oxygens in CuO_2 planes.

Experiment 953

Spin dynamics and quantum coherence in molecular magnets

(Z. Salman, TRIUMF; R.F. Kiefl, TRIUMF/UBC)

Molecular magnets are molecules consisting of ions coupled by strong ferromagnetic or anti-ferromagnetic interaction; these molecules crystallize in a lattice where neighbouring molecules are very well separated. At temperatures lower than the magnetic coupling J between ions inside the molecule, the spins of the ions are locked to each other, and the molecular magnets

behave like noninteracting spins, all with the same total spin quantum number S . The energy difference between the ground spin state of the molecule and the next excited spin state is of the order of J , therefore at low temperatures only the ground spin state S is populated. This state is $2S+1$ times degenerate in first order approximation. However, at even lower temperatures the degeneracy can be removed by additional magneto-crystalline anisotropic interactions such as the uniaxial term DS_z^2 , or rhombic term $E(S_x^2 - S_y^2)$ etc. When the temperature is high enough, transitions between different spin states of the molecules are thermally activated, but when the temperature is much lower than the energy difference between spin states, the transitions between them are only possible through a quantum mechanical process.

The $\text{K}_6[\text{V}_{15}^{\text{IV}}\text{As}_6\text{O}_{42}(\text{H}_2\text{O})]\cdot 8\text{H}_2\text{O}$ complex known as V_{15} [Müller and Döring, *Angew. Chem. Int. Ed. Engl.* **27**, 157 (1991)] is made of a lattice of molecules with fifteen V^{IV} ions of spin $1/2$, placed in a quasi-spherical layered structure formed of a triangle, sandwiched by two hexagons (see Fig. 164). When the temperature is lower than ~ 100 K the two hexagons of the V ions form an $S = 0$ state, leaving the three V ions on the triangle with an effective Hamiltonian [Chiorescu *et al.*, *Phys. Rev. Lett.* **85**, 4807 (2000); Barbara *et al.*, *Prog. Theor. Phys. Supp.* **145**, 357 (2002)]

$$\mathcal{H}_0 = -J_0 (\vec{S}_1 \cdot \vec{S}_2 + \vec{S}_2 \cdot \vec{S}_3 + \vec{S}_3 \cdot \vec{S}_1) - g\mu_B \vec{H} \cdot \sum_{i=1}^3 \vec{S}_i$$

where \vec{S}_i are the spins of the three V ions and $J_0 \simeq -2.445$ K is the effective coupling between the spins. At temperatures lower than 500 mK the V_{15} molecules reside in their spin $S = 1/2$ ground state, with negligible dipolar interactions (few mK) between neighbouring molecules. The V_{15} molecules have no anisotropy barrier and a large tunneling splitting at zero field, $\Delta_0 \simeq 80$ mK.

At very low temperature (below 2 K) the spin ground state of the V_{15} system is with spin $1/2$. At temperatures much lower than 2 K only transitions

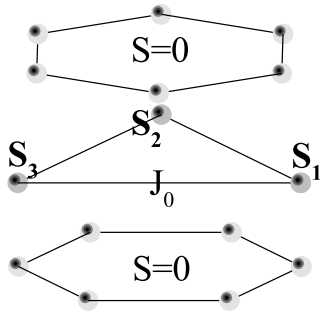


Fig. 164. The core of the V_{15} molecule. Only V ions are shown here.

between the $|+1/2\rangle$ and $|-1/2\rangle$ spin states are possible.

The muon spin lattice relaxation (SLR) rates, $1/T_1$, measured in V_{15} between 12 mK up to 300 K at various magnetic fields, are presented in Fig. 165. The high temperature SLR measurements show an increase in the SLR rates as the temperature is decreased due to the slowing down of the thermally activated transitions between the different spin states.

At $T \sim 100$ K a sudden increase in the SLR is observed at $H = 5$ G, a signature of the freezing of the V ions' spins on the hexagons (see Fig. 164), and the formation of $S = 0$ singlet state.

The relaxation rate at temperatures below ~ 10 K and at low fields (lower than 5 kG) becomes almost temperature independent, while at higher fields (5 and 10 kG) the relaxation rate decreases as the temperature is decreased down to 20 mK. At these temperatures mainly the $S = 1/2$ spin states are populated, and we attribute this decrease to the decrease in the thermally activated transitions between the $m = \pm 1/2$ states due to the Zeeman splitting. However, at even lower temperatures (less than ~ 200 mK) the SLR rate increases slightly, in agreement with ^1H NMR data [Yoneda *et al.*, *Physica* **B329-333**, 1176 (2003)].

The temperature dependence of the spin lattice relaxation at high temperatures indicates that the molecular spin dynamics at high temperatures is thermally activated. However, at low temperatures the spin dynamics is found to be temperature independent. This temperature independent behaviour is a strong indication that this spin dynamics is driven by the broadening and mixing of the spin states due to hyperfine interaction between the molecular and nuclear spins, and is the main contributor to the temperature independent spin lattice relaxation process observed.

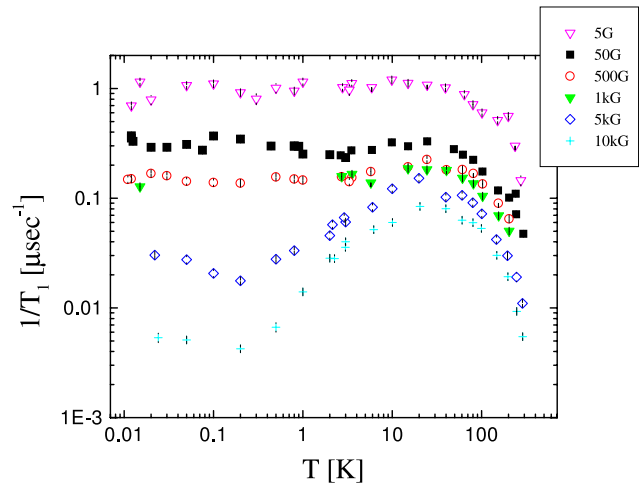


Fig. 165. The spin lattice relaxation rate as a function of temperature for different values of external magnetic field.

Experiment 960

Hydrogen (Mu) defects in II-VI chalcogenides (R.L. Lichti, Texas Tech; J.M. Gil, Coimbra)

Zn chalcogenides

The basic plan of this run was to follow the behaviour of the normal muonium line in ZnSe as a function of temperature (as done in 2002 with ZnS) with the high-frequency spectrometer HiTime in M15. We used commercially available ZnSe single crystals from Crystec and Alpha-Aesar.

The Crystec sample was measured with the (100) direction parallel to the incoming muon beam and to the applied magnetic field. At 3.4 K and a field of 7 T, two lines are clearly visible at about 679 MHz and 763 MHz, as shown in the Fourier transform of Fig. 166. No significant diamagnetic amplitude is seen. Both lines are identified by their field dependence as the ν_{12} precession frequency of Mu^0 . This is a surprising result, as only one muonium state was previously known, with $A_{\text{HF}} = 3456.7$ MHz corresponding to the observed 763 MHz line (Mu_{I}). The much broader second line at 679 MHz (Mu_{II}) may either correspond to a novel state or to anisotropy of the known Mu^0 centre. Further experiments with differently oriented samples should clarify this aspect.

The amplitudes of these lines are approximately two-to-one in proportion, with the larger spectral weight in the broader Mu_{II} line. The amplitude and relaxation dependence on temperature up to the disappearance of these lines at about 50 K are shown in Figs. 167 and 168. The Mu_{II} relaxation rate is two orders of magnitude larger than that of Mu_{I} at the lowest temperatures. Both rate constants increase to the resolution limit as the amplitudes decrease.

Data for a second crystalline ZnSe sample, obtained from Alpha-Aesar, confirms two paramagnetic lines

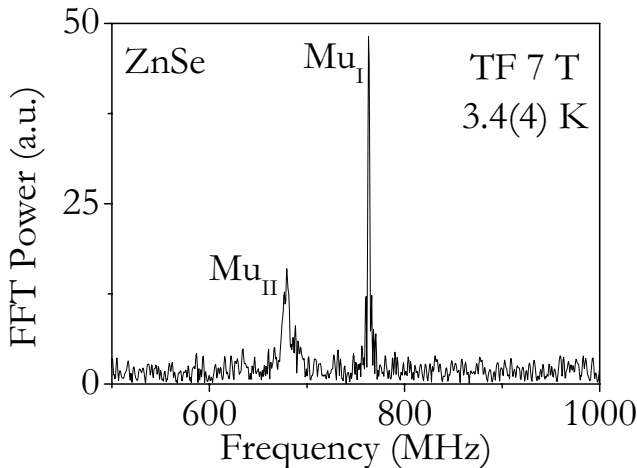


Fig. 166. Fourier transform of precession data for the ZnSe Crystec sample shows two paramagnetic lines, Mu_{I} and Mu_{II} , at low temperatures.

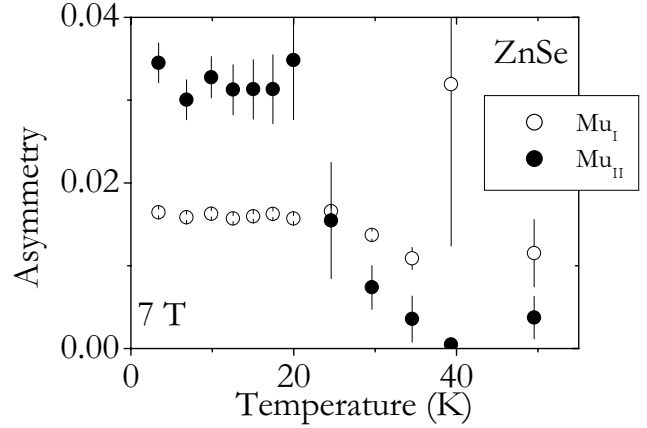


Fig. 167. Temperature dependent amplitudes of the paramagnetic lines observed for the ZnSe Crystec sample.

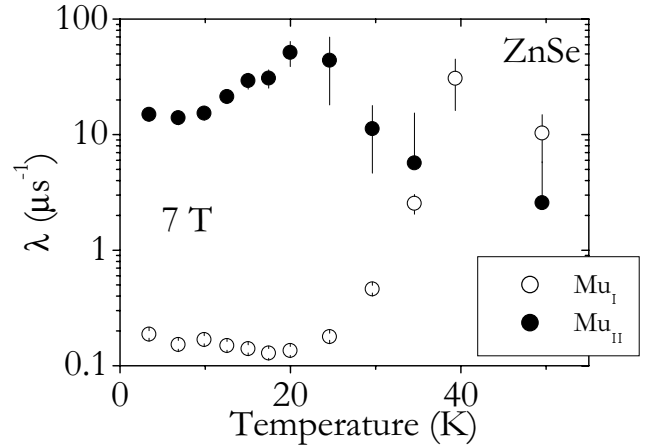


Fig. 168. Temperature dependent relaxation rates of the paramagnetic lines observed for the ZnSe Crystec sample.

with very similar amplitudes and relaxation rates at 3 K when compared to results from the Crystec sample. However, a crude temperature scan indicates persistence of the Mu_{I} line to much higher temperatures, whilst the Mu_{II} line seems to disappear at about the same temperature range in both samples. More detailed temperature dependences for the second sample deserve special attention in the near future. The sample related differences and different temperature dependences for the two lines seem to indicate two separate Mu^0 centres.

If we consider isotropic Mu^0 centres, a possible interpretation for the two states is that they would be located in the inequivalent tetrahedral cage sites of the zincblende structure. The hyperfine interactions obtained in this experiment match well with those calculated by Van de Walle and Blöchl [Phys. Rev. **B47**, 4244 (1993)], identifying Mu_{I} as located in the Zn cation cage and Mu_{II} in the Se anion cage.

CdTe

The case of CdTe is particularly interesting among the II-VIs in that both shallow and deep Mu^0 centres are apparently formed. The shallow Mu centre is visible at low temperatures in both n - and p -type materials with a low concentration of active native defects, and ionizes with an energy characteristic of a shallow-donor. The deep centre is inferred from a missing fraction and decoupling curves, but no precession signals are seen in transverse fields. In n -type samples, the diamagnetic fraction is involved in a dynamic process at temperatures above 150 K, revealed in low transverse fields by a decrease of its amplitude, large frequency and phase shifts, and an increase in the Lorentzian relaxation rate. This might indicate involvement of the deep centre in charge-exchange interactions with conduction electrons.

Measurements of T_1 relaxation as a function of longitudinal field and temperature are a way of extracting information on exchange rates and also of confirming the hyperfine interaction values of deep Mu^0 centres. One n -type undoped CdTe single crystal was measured in longitudinal fields with Helios in M20. Figure 169 shows the $1/T_1$ relaxation rates obtained as a function of temperature for a fixed low longitudinal field of 102 G.

Field scans were performed at the fixed temperatures of 220 K, 250 K and 265 K, as shown in Fig. 170. Although the decrease of the relaxation rate above 1 kG reveals the presence of a Mu^0 with a large hyperfine interaction, thus implying that a deep-level Mu^0 centre is the relaxing state, the slope of these curves does not have the B^{-2} dependence expected for a simple charge-exchange process involving an isotropic Mu^0 centre. We speculate that the processes responsible for the vanishing of the Mu^0 fraction in transverse fields, presumably a spin interaction during the final stages of thermalization of the implanted muon, might still play a role in this new situation.

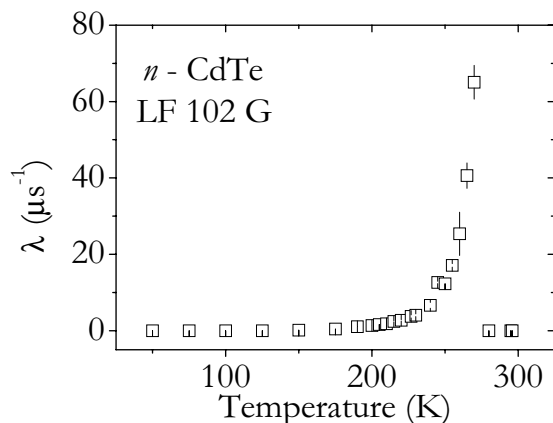


Fig. 169. Temperature variation of the relaxation rate at a fixed longitudinal field of 102 G, obtained for n -CdTe.

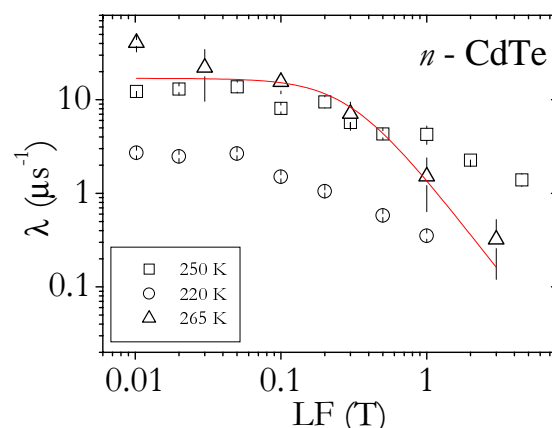


Fig. 170. Field variation of $1/T_1$ relaxation rates for n -CdTe, measured at a few constant temperatures.

Experiment 965

Investigation of spin dynamics in the new dipolar spin ice $\text{Ho}_2\text{Ru}_2\text{O}_7$

(C.R. Wiebe, Columbia/McMaster; G.M. Luke, McMaster; Y.J. Uemura, Columbia)

Frustration, a condition which describes the inability of a system to satisfy all of its individual interactions simultaneously, has become an important concept in the realm of condensed matter physics, being applicable to a wide range of phenomena such as high- T_c superconductors, liquid crystal phase transitions, and protein folding. A renewed interest in geometrically frustrated magnets has resulted from this general interest in frustration and the discovery of new magnetic ground states. One of these new states is the spin ice, which occurs on the pyrochlore lattice of corner sharing tetrahedra with weak ferromagnetic coupling between rare-earth ions subject to strong axial crystal fields. In particular, the $\langle 111 \rangle$ anisotropy of these sites promotes a “two-in, two-out” low temperature spin arrangement upon each tetrahedron, which is stabilized by dipolar interactions. The resulting ground state has a macroscopic entropy associated with the many ways that each tetrahedron can satisfy this condition independently of the other tetrahedra. The short-ranged order of this system maps onto the problem of proton ordering in the freezing of liquid water to ice. Pauling first realized the significance of the specific heat anomaly at the ice transition temperature as being due to the disorder at each oxygen site. An excellent agreement has been found between the spin ice model and physical properties including magnetization, specific heat, and neutron scattering experiments of the three spin ices, $\text{Dy}_2\text{Ti}_2\text{O}_7$, $\text{Ho}_2\text{Ti}_2\text{O}_7$ and $\text{Ho}_2\text{Sn}_2\text{O}_7$.

Recently, a new spin ice candidate has been discovered – $\text{Ho}_2\text{Ru}_2\text{O}_7$. Whereas other spin ices of the formula $\text{A}_2\text{B}_2\text{O}_7$ only have one magnetic species on

the A site, in $\text{Ho}_2\text{Ru}_2\text{O}_7$ both A and B sites are magnetic: Ho^{3+} $J = 8$ spins and Ru^{4+} $S = 1$ spins. Previous studies on the closely related pyrochlores in the series $\text{R}_2\text{Ru}_2\text{O}_7$ ($R = \text{Y}, \text{Nd}$) have revealed that the Ru^{4+} moments order at higher temperatures ($T \sim 100$ K). $\text{Ho}_2\text{Ru}_2\text{O}_7$ shows an anomaly in the magnetic susceptibility which agrees with these findings and suggests that the Ru^{4+} moments order at ~ 95 K. This claim was recently verified by neutron scattering measurements, which show very weak magnetic Bragg peaks forming.

The goal of our μSR experiments was to investigate how the Ru ordering influences the formation of the spin ice state at low temperatures. Zero-field (ZF) and longitudinal field (LF) measurements were completed on sintered powder samples of $\text{Ho}_2\text{Ru}_2\text{O}_7$. At ~ 95 K, there is no precession signal due to the paramagnetic Ho spins, which are much larger than the ordered Ru spins. However, we do observe a significant slowing down of spin fluctuations in the vicinity of T_N . The relaxation rate, obtained from fits to exponential relaxation, shows a dramatic rise at the transition (see Fig. 171). As well, the LF-spectra demonstrate a change in the spin dynamics below the transition at ~ 95 K (see Fig. 172). Recent neutron scattering measurements have shown that the Ho spins form spin clusters below ~ 95 K, which grow in size as the temperature is decreased. We see evidence for this with the change in spin dynamics in this temperature range.

Subsequent measurements were made at the Ho ordering temperature, where the ZF- μSR spectra show a highly damped response from the large ordered Ho moments. It is difficult to extract information as the relaxation rates move outside the window covered by conventional μSR .

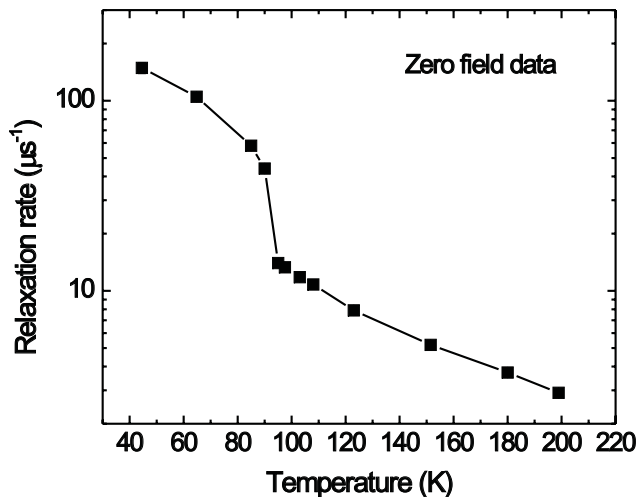


Fig. 171. Relaxation rates from ZF- μSR on $\text{Ho}_2\text{Ru}_2\text{O}_7$. Ru^{4+} spins are slowing down near the transition at ~ 95 K.

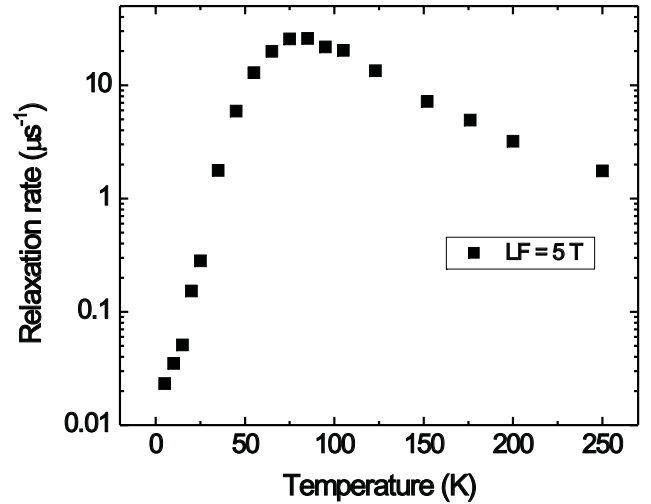


Fig. 172. LF- μSR on $\text{Ho}_2\text{Ru}_2\text{O}_7$ with $\text{LF} = 5$ T, indicating a change in spin dynamics in the region below the Ru ordering temperature (95 K), but above the Ho ordering at ~ 1 K. The Ho spins are believed to be forming spin clusters in this region.

Experiment 974

Unconventional superconductivity in $\text{Na}_x\text{CoO}_2 \cdot 1.3 \text{H}_2\text{O}$ and proximity to an ordered phase

(Y.J. Uemura, Columbia; C.R. Wiebe, Columbia/McMaster; G.M. Luke, McMaster)

Muon spin relaxation (μSR) measurements have been very effective in demonstrating unconventional superconductivity in high- T_c cuprate (HTSC) and organic superconductors. The absolute value of the measured penetration-depth λ established correlations between n_s/m^* (superconducting carrier density / effective mass) and T_c which, together with the pseudogap behaviour, suggest a formation of paired charge carriers occurring at a temperature significantly higher than the condensation temperature T_c . The temperature dependence of λ indicated d-wave pairing symmetry and line nodes in the energy gap. Zero-field μSR studies revealed and elucidated static magnetic order in parent compounds of HTSC.

To these superconductors based on strongly correlated electrons, the recent discovery of superconductivity in $\text{Na}_{0.35}\text{CoO}_2$ intercalated with $1.3 \text{H}_2\text{O}$ ($T_c = 4.2$ K) has added a unique compound which has highly 2-dimensional (2D) conducting planes of cobalt oxide in a triangular lattice structure with geometrical spin frustration. The original idea of resonating valence bonds was developed for this sublattice, but no superconducting system in this geometry has been known before the new cobalt oxide compound. Although extensive studies have been started, detailed characteristics of this system are yet to be demonstrated by conclusive experimental data sets.

Anhydrous Na_xCoO_2

We first describe zero-field (ZF) μSR studies of magnetic order in polycrystalline samples of non-superconducting anhydrous Na_xCoO_2 . Recent resistivity and susceptibility studies showed that the $x = 0.64$ system can be characterized as the “Curie-Weiss” metal, $x = 0.35$ as a “paramagnetic” metal, while $x = 0.5$ exhibits a transition from a high-temperature metal to low-temperature insulator at $T = 53$ K. In Fig. 173(a), we show the ZF- μSR time spectra of these systems. In the $x = 0.5$ system, the spectra above $T = 53$ K show slow relaxation without oscillation, i.e., a line shape expected for systems with nuclear dipolar fields without static magnetic order of Co moments. Below $T = 53$ K, a clear oscillation sets in, together with a rather fast damping. Below $T = 20$ – 25 K, we see two frequencies beating. Figure 173(b) shows the temperature dependence of these frequencies. The amplitude of the damping signal indicates that all the muons feel a strong static magnetic field below $T = 53$ K. The static magnetic order sets in at the onset of a metal-insulator transition, and the establishment of the second frequency takes place at $T = 20$ K, which roughly corresponds to the “kink” temperature in the resistivity shown in the inset. Although a conclusive picture requires neutron scattering studies, it seems that one of two interpenetrating Co spin networks acquires a long-range order below $T = 53$ K, followed by the other network establishing long-range order below 20 K. The spatial spin correlation should be antiferromagnetic (AF), since susceptibility shows no divergence at $T = 53$ K (evidence against ferromagnetism), and the damping of the $T = 25$ mK data is significantly slower than that of the Bessel function expected for the incommensurate spin-density-wave (ISDW) states (evidence against ISDW).

We also confirmed the absence of static magnetic order in anhydrous Na_xCoO_2 with $x = 0.35$ and 0.64 ,

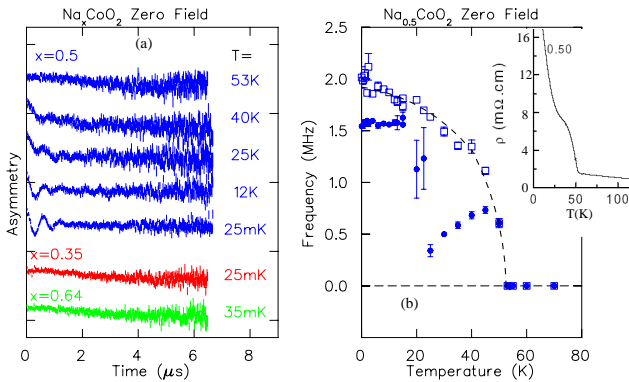


Fig. 173. (a) Muon spin relaxation time spectra observed in zero field in anhydrous Na_xCoO_2 with $x = 0.50$, 0.35 , and 0.64 . (b) The muon spin precession frequency observed in the $x = 0.5$ system, shown with resistivity in inset.

down to $T = 25$ – 35 mK, as shown in Fig. 173(a). Static antiferromagnetic order was reported for $x = 0.75$ – 0.9 by earlier μSR studies. Together, the present data establish a rather complicated evolution of the magnetic ground states from paramagnetic (PM) ($x = 0.35$) to AF (0.5) to PM (0.64) to AF (0.75) to ISDW (0.9), with increasing x . The ~ 2 MHz frequency in the $x = 0.5$ system is close to ~ 3 MHz in $x = 0.75$, suggesting that the ordered moment sizes in these systems are of comparable magnitudes. The existence of an insulating magnetic state in the vicinity of superconductivity resembles the case in the cuprates.

Superconducting $\text{Na}_x\text{CoO}_2 \cdot 1.3 \text{D}_2\text{O}$

We now focus on our results on powder samples of the superconducting phase, $\text{Na}_x\text{CoO}_2 \cdot 1.3 \text{D}_2\text{O}$. μSR data in transverse external fields (TF) reflect field broadening due to the flux vortex lattice in type-II superconductors, from which one can derive the magnetic field penetration depth λ . In Fig. 174, we compare the temperature dependence of $\sigma_{sc}(T) \propto \lambda^{-2}$ of $\text{Na}_{0.35}\text{CoO}_2 \cdot 1.3\text{D}_2\text{O}$ with various models, in a fit of 16 data points with $\sigma(T = 0)$ as a free parameter. The observed results clearly disagree with curves of the two-fluid model (normalized chi square NCS = 3.51) and s-wave BCS weak-coupling model (NCS = 1.75, Durbin-Watson value of a normalized residual error correlation DW = 1.11). Comparison with the scaled μSR results from YBCO yields NCS = 1.39 and DW = 1.59, showing a rather poor agreement yet in a statistically acceptable range. For a 5% confidence level, a model with NCS > 1.666 or DW < 1.1 or DW > 2.9 should be rejected, $1.1 < \text{DW} < 1.37$ or $2.63 < \text{DW} < 2.9$ is inconclusive, while $1.37 < \text{DW} < 2.63$ is comfortably acceptable.

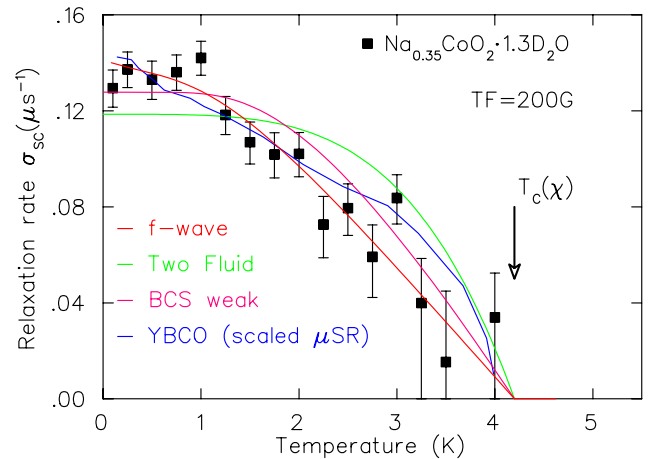


Fig. 174. Muon spin relaxation rate $\sigma_{sc}(T)$ due to superconductivity in $\text{Na}_{0.35}\text{CoO}_2 \cdot 1.3\text{D}_2\text{O}$, with $\text{TF} = 200$ G applied perpendicular to the aligned conducting planes, obtained by quadratic subtraction of $\sigma_{sc}^2 = \sigma_{exp}^2 - \sigma_n^2$. The results are compared with fits to several models and the scaled plot of μSR results on $\text{YBa}_2\text{Cu}_3\text{O}_{6.95}$ (YBCO).

For the cobalt oxide superconductors, several authors proposed f-wave models, which have a particular matching with the symmetry of triangular lattice. In Fig. 174, we also show a theoretical curve for an f-wave pairing, obtained by using a tight-binding fit of the LDA band calculation and by assuming a separable effective interaction supporting a simple f-wave order parameter. In the present system, there is a large Fermi surface around the Γ point as well as six small hole-pockets near the K points. The line in Fig. 174 represents a case where nodes of f-wave symmetry exist only on the large Fermi surface and not on the six hole-pockets, while the order parameter on each Fermi surface has the same maximum value. This f-wave model gives a good agreement with the observed data with $NCS = 1.19$ and $DW = 2.34$.

These results rule out a fully isotropic energy gap. Before concluding a particular pairing symmetry, however, one has to test various other models with and without the possible effect of impurities.

The penetration depth λ is related to the superconducting carrier density n_s divided by the effective mass m^* as $\sigma(T) \propto \lambda^{-2} \propto [4\pi n_s e^2 / m^* c^2] [1/(1+\xi/l)]$, where ξ is the coherence length and l denotes the mean free path. At this moment, it is difficult to prove the clean limit situation $\xi \ll l$ for the cobalt oxide superconductor, due to the lack of high-quality superconducting single crystals necessary to estimate the in-plane values of ξ and l . Derivation of the absolute values of λ and n_s/m^* is subject to modelling of flux vortex lattice line shapes, observed functional forms of field distribution, and angular averaging in the polycrystal samples. Based on the results of μ SR measurements on *c*-axis aligned YBCO and numerical works, we have adopted the conversion factor for polycrystal to aligned samples $\sigma_{\text{aligned}} \sim 1.4\sigma_{\text{poly}}$ to account for the effect of applying the TF perpendicular to the conducting planes of highly 2D superconductors. For σ to λ conversion $\lambda = A/\sqrt{\sigma}$, we have adopted a factor $A = 2,700 [\text{\AA}(\mu\text{s})^{1/2}]$ for the Gaussian width σ . With these conversion factors, the values of λ_{ab} of polycrystalline samples of underdoped YBCO with $T_c \sim 60$ K agree well with the value obtained using a single crystal specimen with comparable T_c in a more accurate lineshape analysis. The above factor A gives $\lambda = 7,200 \text{ \AA}$ for the in-plane penetration depth of the cobalt oxide system at $T \rightarrow 0$.

If we assume the charge carrier density to be equal to the Na concentration, we obtain the in-plane effective mass of the cobalt-oxide superconductor to be about 100 times the bare electron mass m_e . The heavy mass can be expected for strongly correlated carriers in a triangular lattice. The high effective mass is consistent with the electronic specific heat $C/T \sim 12$

[mJ/mole K²] of the superconducting cobalt oxide just above T_c . This value can be compared to ~ 2 [mJ/mole K²] of YBa₂Cu₃O₇. After normalizing the values to a unit sheet area of conducting planes, C/T for the cobalt oxide becomes about 25 times larger than that for YBCO. In the non-interacting 2D Fermi gas, C/T is proportional to m^* but independent of carrier density. Thus, within this approximation, we expect m^* of cobalt oxide to be 25 times that of the cuprates.

In conclusion, we have shown that the cobalt oxide superconductors have an anisotropic energy gap and a heavy effective mass $m^* \sim 100 m_e$. We have also established the existence of an antiferromagnetic insulating compound in the vicinity of the superconducting cobalt-oxide system without magnetic order, which suggests the possible involvement of magnetism in the superconducting mechanism.

Experiment 975 Magnetism and superconductivity in Na_xCoO₂·yH₂O and related cobalt oxides (W. Higemoto, R. Kadono, KEK-IMSS)

Recent discovery of superconductivity in a novel cobalt oxide, Na_xCoO₂·yH₂O ($x = 0.35, y = 1.3$) with the transition temperature $T_c \sim 4.5$ K, is attracting much interest [Takada *et al.*, Nature **422**, 53 (2003)]. The compound has a lamellar structure consisting of CoO₂, Na and H₂O bi-layers, where the two-dimensional (2D) CoO₂ layers are separated by thick insulating Na or H₂O layers. This structure is similar to high- T_c cuprate superconductors (HTSCs) in the sense that they also have a layered structure of 2D-CuO₂ sheets separated by insulating layers. It is well established that Cu²⁺ ($S = 1/2$) atoms on a square lattice exhibit antiferromagnetic (AF) ordering in the parent compounds of HTSCs, where the superconductivity occurs when the AF state is suppressed by carrier doping. On the other hand, Co atoms form a 2D triangular lattice on the CoO₂ layers, where a strong magnetic frustration is anticipated. Thus, while Na_{0.35}CoO₂·1.3H₂O may be viewed as an electron doped Mott insulator for a low-spin Co⁴⁺ ($S = 1/2$) with an electron doping $x = 35\%$, the electronic state may be considerably different from cuprates.

We conducted ZF- and HTF- μ SR measurements on the superconducting cobalt oxide and its deuterated specimen down to 2 K. We also made additional measurements on Na_{0.35}CoO₂·0.7H₂O with H₂O monolayers as a reference compound showing no superconductivity. The ground state property was examined by ZF- μ SR at KEK-MSL, while information on the superconducting pair correlation was investigated by the muon Knight shift deduced from HTF- μ SR at TRIUMF M15. Powder specimens of Na_{0.35}CoO₂·1.3H₂O

including a deuterated one ($D_2O \simeq 75\%$) were synthesized as described in Takada *et al.* [*ibid.*]. Each specimen was characterized by measuring magnetic susceptibility prior to μ SR measurement. For high field measurements, the powder specimen was secured with Apiezon-N grease to prevent an alignment of fine crystals in the specimen by strong field.

It turned out that the ZF- μ SR time spectra below 10 K can be well reproduced by the Kubo-Toyabe relaxation function. The lineshape exhibits the least dependence on temperature over the temperature range through T_c . A large difference in the nuclear dipolar width (Δ) between hydrate and deuterate specimens indicates that muons occupy a site close to the water molecule. By comparing Δ between those two specimens together with calculated mapping of Δ , the muon site is identified near (0.2, 0.25, 0.12). Since this site has a lower symmetry, it is unlikely that the internal fields from cobalt oxides happened to be cancelled. Thus, we conclude that there is no spontaneous internal magnetic field associated with the occurrence of superconductivity nor any symptom of magnetism down to 2 K.

The magnetic penetration depth (λ) in the hydrate specimen is deduced to be about 5000 Å from TF- μ SR data at lower fields. This long λ does not allow us to discuss the temperature/magnetic field dependence of λ in detail; the corresponding relaxation rate due to the flux line lattice (FLL) formation ($\sigma \simeq 0.1 \mu s^{-1}$) is too small to be determined experimentally with enough precision. On the other hand, the diamagnetism for such a long λ can be negligible at high fields, and thereby we can study the muon Knight shift without much ambiguity due to the FLL formation.

In general, the muon Knight shift $K(T)$ is expressed as $K(T) = K_s(T) + K_{orb}$. Here, K_s and K_{orb} are the spin and orbital component of the Knight shift, and only $K_s(T)$ is temperature dependent. Then, as shown in Fig. 175, $K_s(T)$ is determined by the slope of the muon Knight shift versus magnetic susceptibility (K - χ plot) irrespective of K_{orb} (which is set to zero in this analysis). Figure 176 shows the temperature dependence of $K_s(T)$ (at 60 kOe) and uniform susceptibility (at 10 kOe) in the randomly oriented sample of $Na_{0.35}CoO_2 \cdot 1.3H_2O$. The muon Knight shift decreases with decreasing temperature below 100 K and levels off below 10 K. Above 10 K, $K_s(T)$ is proportional to the uniform susceptibility, which clearly indicates that the upturn of the $\chi(T)$ below ~ 100 K is due to some intrinsic origin. The spin part of the muon Knight shift is expressed as $K_s = A_{hf}\chi$, where A_{hf} is the hyperfine coupling constant. From the above relation, A_{hf} is estimated to be ~ -134 Oe/ μ_B . It should be noted that

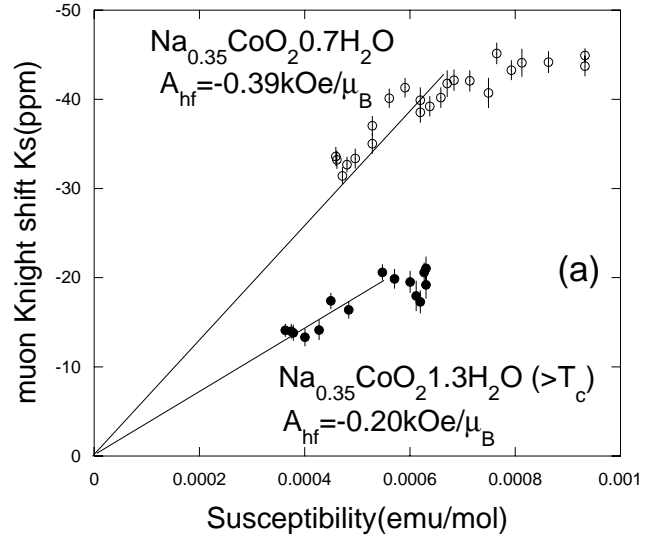


Fig. 175. The muon Knight shift (at 60 kOe) versus susceptibility plot in $Na_{0.35}CoO_2 \cdot yH_2O$; it exhibits superconductivity for $y = 1.3$ while it remains normal for $y = 0.7$.

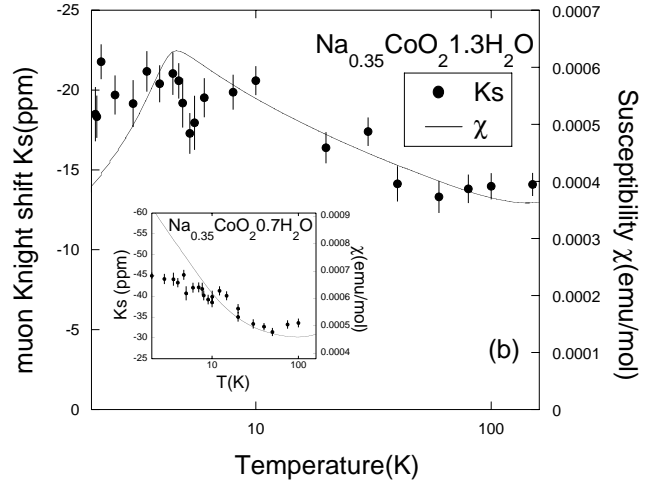


Fig. 176. Temperature dependence of the spin part of the muon Knight shift K_s (filled dot) and susceptibility (solid line). Susceptibility was measured at 10 kOe.

the anisotropic term of the Knight shift, or so called powder pattern, is not seen in the spectra. This implies that the anisotropy of the Knight shift is much smaller than the present resolution. In the case of s -wave pairing superconductivity, K_s decreases to zero with decreasing temperature following the Yoshida function. However, as shown in the inset of Fig. 176, the muon Knight shift does not show any appreciable reduction below T_c .

Since the observed muon Knight shift is negative, there remains a possibility that the reduction of K_s below T_c may be cancelled by the diamagnetic shift upon the formation of FLL. We estimated the magnitude of such a diamagnetic shift taking account of the effects of dense overlap of vortices and the Doppler

shift; the latter is present when the superconducting gap has nodes, leading to further enhancement of λ . This is reasonable considering the recent NMR measurements suggesting line nodes in this compound. Our simulation yielded that $\lambda \simeq 12 \mu\text{m}$ at 60 kOe where the

associated diamagnetic shift by the FLL formation is less than 2.8 ppm, which is too small to cancel out the predicted effect due to spin singlet superconductivity. Thus, we conclude that the result in Fig. 176 is mostly attributed to K_s .

LIFE SCIENCES

Introduction

This year saw the delivery of the two new scanners which were acquired through funds from the Canada Foundation for Innovation and the BC Knowledge Development Fund. High resolution research tomography (HRRT) is the state-of-the-art tomography designed to performed neurological research at a resolution of 2.5 mm and a sensitivity of greater than 6%. These metrics are made possible by the use of the new scintillator material, LSO. The other scanner is the microPET® which uses similar technology to achieve a resolution of sub-2 mm and is designed to perform functional imaging in rodents. Both of these scanners are the subjects of a number of research proposals for 2004.

In addition to the new equipment, a number of projects formerly supported through LS8, Radiotracers, have developed programs of their own and will be the subject of separate Life Sciences projects in 2004, thus the Life Sciences Program is poised to experience growth over the next few years through these new initiatives.

Experiment LS0

PET facilities

(K.R. Buckley, TRIUMF)

The PET facilities comprise the TR13 13 MeV H⁻ cyclotron, the ECAT 953B/31 tomograph, the new high resolution research tomograph (HRRT), and the new microPET R4 small animal tomograph, and ancillary equipment such as counting and data acquisition systems.

Personnel

A research associate joined the PET program early in the year as working on camera characterization and is actively involved in the maintenance and repair of all the cameras.

TR13 cyclotron

Usage of the TR13 cyclotron decreased significantly this year in delivered beam while the number of irradiations only dropped slightly. This was due in large part to the cessation of irradiations for the production of ⁷Be (LS8), ¹⁸F to the Cross Cancer Institute in Edmonton (LS32), and in mid-year, FDG to the local hospitals (LS13 and LS24). The total number of runs decreased to 970 vs. 1038 in total last year and delivered beam has dropped to 0.43 A min from 1.26 A min.

Downtime this year was caused by relatively simple failures such as water leaks and power supplies. Spare power supplies have been purchased for the control system since these supplies are now 10 years old and fail-

ures can be expected. The cryocompressor for the vacuum system exhibited some troubles for one day but then mysteriously started functioning correctly again before a fault was detected.

No extraction foil changes were required through the year and all targets were rebuilt at least once with the exception of the ¹⁶O-H₂O target for ¹³N production while the ¹⁸O-H₂O for ¹⁸F production was rebuilt 3 times. Four ion source filament changes have been done along with other miscellaneous service items.

Presently there are six target locations occupied of the available eight. These consist of

- one ¹⁸O-O₂ gas target
- one ¹⁸O water target
- one ¹⁶O water target
- one N₂/H₂ gas target
- one experimental gas target
- one experimental foil target.

A number of irradiations took place this year in support of LS8 but they were typically low current runs in support of the Botany Department or graduate student projects.

ECAT tomograph

Block detector failures and programmable array logic chips continue to be the dominant modes of failure for the camera. We are routinely repairing blocks in-house and have replaced 7 blocks again this year. We have still not assembled the necessary components to properly calibrate the blocks prior to returning them to the scanner. At present only a simple visual balance of PMT outputs is performed on the bench and the block set-up routine in the scanner performs the fine tuning. Programmable logic chips in the buckets continue to fail. Chips for 8 channels have been replaced this year. In addition to this, 2 analogue boards and 3 position/energy boards, and one bucket controller were replaced in the bucket assemblies. The ECAT 953B is now no longer officially supported by CTI and parts are only available if CTI has them in stock. No new parts will be manufactured. There were only six 953B scanners made and we have not yet been successful in obtaining a decommissioned one for parts. The ECAT 951 scanner uses the same detector block and bucket electronics so we remain optimistic that used parts will be available. We are aware of at least one used part vendor with a 951 from whom we have purchased a power supply in the past.

HRRT

The HRRT scanner arrived on June 2 and was installed in a few days. The scanner is undergoing char-

acterization and tests and has been used for some preliminary investigations with non-human primates. The patient couch has not yet been delivered. We have experienced a minimum of hardware troubles. We did some repairs when a high voltage capacitor failed and have replaced one analogue board and one phototube. The HRRT team at CTI are supplying parts and instruction as needed and team members have travelled to CTI a couple of times for service training before the machine arrived.

MicroPET

The microPET scanner was shipped with the HRRT. This scanner is shipped ready to run so it was simply a matter of plug and play to get the scanner up and running. Several members of the PET team were at Concorde MicroSystems for training on use and service of the scanner. We are a beta test site for Concorde and recently went through the installation of the latest beta software for the scanner. During that process we detected one analogue board that was faulty and it was replaced. With this exception the scanner hardware has been quite stable.

The room the microPET is housed in needs some additional modifications to accommodate the scanner and scanning procedures. The heat load of the scanner requires additional cooling to be added and oxygen and gas services still need to be plumbed into the room. We experienced delays in getting the mechanical drawings from the engineering consultant due to a change of staff there. At this time the drawings have been completed and are being reviewed by the hospital plant services. Work will proceed as promptly as possible.

Statistics

Tables XIII–XVI summarize the run and scanning statistics for the TR13, ECAT, HRRT, and microPET, respectively.

Table XIII. TR13 run statistics.

	2003	2002
Total runs conducted	970	1038
Total runs lost	18	16
Total beam delivered (μ A min)	430,630	1,258,376
Delivered to – LS 3	294090	301611
– LS 4	63279	40411
– LS 8	55636	605500
– LS 13*	14066	51410
– LS 24*	3559	17246

*Please note that LS13 and LS24 refers to the FDG production for use at local hospitals; it is not apportioned to particular LS projects since a single batch is made and subsequently divided among requesters.

Table XIV. ECAT scanning statistics.

	2003	2002
Total scans conducted	388	383
Total scans lost	75	37
Lost to – patient	23	8
– cyclotron	18	16
– chemistry	3	3
– scanner	20	7
– staff sick/away	9	0
– investigator	2	3

Table XV. HRRT scanning statistics.

	2003
Total scans conducted	23
Total scans lost	2
Lost to – chemistry	2

Table XVI. MicroPET scanning statistics.

	2003
Total scans conducted	66
Total scans lost	10
Lost to – cyclotron	1
– subject	6
– staff sick/away	3

Experiment LS3

Synthesis of radiopharmaceuticals for positron emission tomography

(*S. Jivan, TRIUMF*)

The PET group at TRIUMF continues to routinely produce up to 10 radiopharmaceuticals with 3 to 4 radiopharmaceuticals synthesized on any given day. FDG shipments to local hospitals (VGH, Lions Gate and St. Paul's Hospitals) were stopped as of April 1, 2003. Of the 10 radiopharmaceuticals, five (FDOPA, Raclopride, (+)DTBZ, Sch23390 and MP) are most heavily used. Two new tracers (^{11}C -Carfentanil and ^{18}F -SPA-RQ) have been successfully developed and are currently being used for non-human primate studies.

This year Health Canada requested that clinical trial applications (CTA) be submitted for all protocols using positron emitting radiopharmaceuticals for human research. We have been allowed to continue human studies with a timetable for 11 CTAs to be submitted by the end of May, 2005. Two CTAs (Raclopride and FDOPA) thus far have been submitted and approved.

Routine production

The total number of shipments to UBC Hospital for PET scanning was 400 and 74 deliveries to external users which include FDG for local hospitals and nitrogen-13 for the Botany Department at UBC. We had a total of 180 runs for research and development. These included testing new targets and checking radiochemical yields on new and existing compounds. The decrease in the number for external users is because we stopped delivering FDG to local hospitals as of April 1, 2003. There were also no shipments this year to the Cross Cancer Institute in Edmonton as they now have their cyclotron on-line and manufacture FDG on site.

We continue to use TBAF in most of the ^{11}C methyl iodide reactions to enhance and stabilize yields. Most precursors are made in-house by JML Biopharm Incorporated except Raclopride which is donated by ASTRA ZENECA AB.

New development

^{11}C -Carfentanil has been successfully synthesized and automated for routine production. The tracer is involved in looking at μ receptors in the opioid system in the brain. ^{18}F fluoromethylbromide has been successfully synthesized and is used to label SPA-RQ (substance P antagonist-receptor quantitation) which looks at neurokinin receptors.

Routine radiosyntheses for some PET radiotracers is performed *in-loop* [^{11}C]CH₃I-methylation of precursors. This year, a series of experiments was conducted to understand the mechanism of *in-loop* labelling with [^{11}C]CH₃I. These studies were applied to improve the yield and reliability of the radiosynthesis of [^{11}C]Carfentanil. This work was presented at the XVth International Symposium of Radiopharmaceutical Chemistry as well as being submitted for publication.

Experiment LS4

Targets for radioisotope production

(T.J. Ruth, TRIUMF)

The goal of this project is to develop targets for the TR13 cyclotron for production of positron emitting radionuclides. The past year has focused on the production of ^{18}F using gaseous oxygen-18 and $^{11}\text{CH}_4$ directly from the target.

Gas targets for the high yield production of ^{18}F -fluoride

With the growing pressure for increased yields for ^{18}F -fluoride around the world we designed and built a prototype target using gas target technology. This work has been published previously in the journal Applied Radiation and Isotopes **55**, 457 (2001).

The approach chosen made use of the ^{18}O -O₂ gas target concept in an analogous manner to the F₂ double shoot system. The first irradiation would generate the ^{18}F as fluoride that sticks to the walls. But instead of performing a second irradiation, the target is washed out with water in a similar fashion as used for ^{123}I production by MDS Nordion. Depending on the energy of bombardment, extremely high yields may be possible. For example the saturation yields at 13 MeV are approximately 200 mCi/ μA and 250 mCi/ μA at 18 MeV. At these rates one can imagine very long shipments. The advantages include straightforward recovery of the target material and efficient, higher beam currents possible than for water targets (liquids in general). Disadvantages include having to wash and dry the target between runs and finding the best material for this process. There are 2 patents pending for this system.

We have just been awarded a one year Proof-of-Principle (December 2003) grant from the Canadian Institutes of Health Research (CIHR) to build and test a working system on the CP-42 to operate at $>100\ \mu\text{A}$ with a design goal of producing $>15\ \text{Ci}$ in a 4-hour irradiation.

The outstanding issues to be addressed this coming year include:

1. What are the target parameters that have to be addressed in order to fabricate a fully functional target system?
2. Window strength and cooling for operating at $100\ \mu\text{A}$, or higher.
3. Target gas pressure/chamber-size ratio for cooling, density reduction, scatter and window strength.
4. ^{18}O -O₂ gas recovery to recycle enriched target material.
5. Target body material – compatible with washing to achieve high recovery factor.
6. Solution for recovering ^{18}F -fluoride to maintain chemical reactivity and target re-use compatibility.

^{11}C -CH₄ production

Our previous work on static irradiations of a H₂/N₂ target gas for the production of methane indicated that recoverable yields at 13 MeV plateaued at about 750 mCi at EOB. The relatively poor yields were attributed in part to Hot Atom interactions with the target chamber walls. In order to try and overcome this limitation, an aluminum bodied flow-through gas target was implemented and tested for the production of ^{11}C -CH₄ on the TR13 cyclotron at TRIUMF. Nitrogen gas with varying quantities of hydrogen has been used to investigate the optimum ratio for methane production. Comparison of the flow-through target with the static-target irradiations for production of methane indicates

that the yields are significantly better with the flow-through system but that the specific activity is lower. The source of the carrier carbon is under investigation.

In the mean time we built a niobium bodied target for methane production and preliminary results from this target are extremely encouraging. Yields ranged from 94 mCi/ μ A at saturation for a 10 minute run at 20 μ A to 77 mCi/ μ A for a 60 minute, 20 μ A run. We made more than 1.3 curies of methane in the one hour irradiation. With the Al target we could never go above 750 mCi, total. Specific activities of the final product tracers, such as DTBZ and raclopride, using the Nb body target have been comparable to the aluminum cone target (several Ci/ μ mole). A more detailed study of this target is under way.

Copper isotopes

Interest in foil irradiations has increased and we have in the past performed such irradiations using a special target jig, which uses He cooling on the foils to allow simple irradiations. For example, Pd foils for the ^{110m}Ag production for a researcher from the Physics Department at UBC have used this system.

A collaboration between the Australian Nuclear Science and Technology Organization (ANSTO) and TRIUMF has embarked on developing the use of copper isotopes for radiopharmaceutical development using Cu-61/64.

In addition, a researcher from Earth and Oceans Sciences at UBC (LS 60) has expressed an interest in using a copper isotope for her tracer studies in phytoplankton. Preliminary results indicate that we can make small amounts or relatively pure Cu-61/64, which is adequate for this program. However, we are in the process of exploring alternative means to allow for more remote handling approaches.

Experiment LS8

Radiotracers

(*T.J. Ruth, TRIUMF; A.D.M. Glass, UBC*)

Dr. Anthony Glass of the Botany Dept. at UBC continued to make use of tracers provided by the Life Sciences Group at TRIUMF. The Group continued to train scientists in the use of the tracer technique to address biological questions. Over the past year there was one Ph.D. student (Yu Wang), 3 PDFs (Wenbin Li, Wang Ye, Anshuman Kumar), and a visitor from Iran, Prof. Mansour Shariati.

Ongoing collaborations included researchers from the University of St. Andrews, Scotland (Profs. James Kinghorn, and Sheila Unkles), the University of San Diego (Prof. Nigel Crawford), and the University of Connecticut (Prof. Roberto Gaxiola).

Rice research

(*A. Kumar*)

Following his Ph.D. studies, Dr. Anshuman Kumar has been examining the manner in which cellular pools of carbohydrates and various nitrogen compounds regulate the expression of three ammonium transporter genes that he successfully cloned from roots of rice plants. This has involved measuring ammonium influx using $^{13}\text{NH}_4^+$, while measuring the cellular pools of these N and C compounds. It is evident that N and C interact at the cellular level so that the supply of N provided by the root ammonium transporters matches the availability of carbon compounds provided by leaf photosynthesis.

Nitrogen uptake in trees

(*Collaboration with CELLFOR: M.Y. Siddiqi, M. Shariati, W. Li*)

Our goal of increasing nitrate uptake in tobacco plants and poplar seedlings by over-expressing the high-affinity NO_3^- transporter gene (AtNrt2.1) was initially unsuccessful. We have confirmed our hypothesis that a second family of genes (the NAR2 family) must be co-expressed in order to achieve efficient NO_3^- uptake, and successfully demonstrated that mutants of Arabidopsis lacking a functional NAR2 gene fail to absorb nitrate. We have now developed strains of tobacco over-expressing both the AtNRT2.1 gene and the At-NAR 2 gene. Using $^{13}\text{NO}_3^-$ to measure nitrate uptake, we have obtained increased nitrate uptake and our preliminary growth measurements indicate increased growth in these lines. This working is actively being pursued.

$^{13}\text{NO}_3$ influx in the fungus *Aspergillus nidulans*

(*Collaboration with S. Unkles, J. Kinghorn, St. Andrews, Scotland; A.D.M. Glass, Y. Siddiqi*)

A structure function study of the NRTA gene sequence and NO_3^- uptake. With our Scottish collaborators, we have generated clones of *Aspergillus* modified at specific (putatively critical) arginine loci of the nitrate transporter protein. These arg sites are highly conserved in this gene family from fungi to higher plants. Replacement of arg 87 or 386 converts the protein from a high-affinity transporter with K_m s for $^{13}\text{NO}_3^-$ uptake around 10 μM to a low-affinity transporter with a K_m around 15 mM. We believe that this positively charged amino acid is critical in the transmembrane uptake of nitrate. Our data have been written up and submitted for publication.

The role of the NAR2 gene family

During his Ph.D. studies at UBC, Mamoru Okamoto isolated an Arabidopsis mutant disrupted in the NAR2 gene. We have demonstrated that mutant is unable to grow normally when nitrate is the sole

source of N and that $^{13}\text{NO}_3^-$ uptake is dramatically reduced. Thus high-affinity nitrate uptake requires the participation of genes encoding both the NRT2 and the NAR2 proteins. Using molecular methods we have evidence that the two proteins are associated in the plasma membrane for normal nitrate transport function.

Studies of fluxes and compartmentation of chloride ions in barley plants

(D.T. Britto, H.J. Kronzucker, Toronto)

With the increasing use of irrigation and fertilizers throughout the world, there have been associated increases in salt accumulation in agricultural soils, affecting ~50% of the irrigated agricultural land base globally. Soil solution concentrations of sodium, chloride, and other ions can sometimes reach excessively high levels, resulting in suppression of plant growth and, ultimately, loss of arable land. Because of the severity of this problem, much research has been focused on salt stress and its avoidance by tolerant species or cultivars. However, while the physiology of plant-sodium relations has been particularly well studied, the chloride ion, which often accompanies sodium, has been understudied in relation to salt stress in plants. The objective of our study was to establish a baseline of information regarding the transport and subcellular accumulation of chloride in barley (*Hordeum vulgare*) roots, particularly with regard to the influence of nitrogen strength and source.

The first analysis of chloride fluxes and compartmentation in a non-excised plant system is presented, examining ten ecologically pertinent conditions. The short-lived radiotracer couple $^{38}\text{Cl}/^{39}\text{Cl}$ was used as a Cl^- tracer in intact barley (*Hordeum vulgare* L. cv. Klondike) seedlings, which were cultured and investigated under four external $[\text{Cl}^-]$, from abundant (0.1 mM) to potentially toxic (100 mM). Chloride-nitrogen interactions were investigated by varying N source (NO_3^- or NH_4^+) and strength (0.1 or 10 mM), in order to examine, at the subcellular compartmentation level, the antagonism, previously documented at the influx level, between Cl^- and NO_3^- , and the potential role of Cl^- as a counterion for NH_4^+ under conditions in which cytosolic $[\text{NH}_4^+]$ is excessive. Cytosolic $[\text{Cl}^-]$ increased with external $[\text{Cl}^-]$ from 6 mM to 360 mM. Cl^- influx, fluxes to vacuole and shoot, and, in particular, efflux to the external medium, also increased along this gradient. Efflux reached 90% of influx at the highest external $[\text{Cl}^-]$. Half-times of cytosolic Cl^- exchange decreased between high-affinity and low-affinity influx conditions. The relationship between cytosolic $[\text{Cl}^-]$ and shoot flux indicated the presence of a saturable low-affinity transport system (SLATS) responsible for xylem loading of Cl^- . N source strongly

influenced Cl^- flux to the vacuole, and moderately influenced Cl^- influx and shoot flux, whereas efflux and half-time were insensitive to N source. Cytosolic pool sizes were not strongly or consistently influenced by N source, indicating the low potential for Cl^- to act as a counterion to hyperaccumulating NH_4^+ .

Isotope preparation The chlorine isotopes ^{38}Cl ($t_{1/2} = 37.2$ min) and ^{39}Cl ($t_{1/2} = 55.6$ min) were produced by irradiation of natural argon gas with 41 MeV protons accelerated by the CP42 cyclotron located at TRIUMF. A water-cooled aluminum target body of 75 cm³ volume was filled with approximately 250 psi (1.7 MPa) of Ar gas and irradiated with protons at currents between 5 and 7 μA . A typical run at a current of 5 μA for 30 min yielded approximately 555 MBq of Cl radioactivity, as measured 15 min following irradiation. The Cl isotopes adhered to the walls of the target and were rinsed off with a slightly alkaline aqueous solution after the target gas was released, then caught on a Sepak strong anion-exchange column. The only other radioisotope produced in appreciable quantities was ^{38}K ($t_{1/2} = 7.6$ min), which was removed by passage through the exchange column. The Cl isotopes were eluted from the Sepak with 20 ml of 10 mM CaSO_4 , and then used immediately for labelling experiments.

Results were published in *Planta*, an international journal of plant biology (available on line, December, 2003).

Experiment LS33

Evaluation and improvement of a dual head coincidence camera

(B. Pointon, UBC)

This study is now continuing exclusively as Barry Pointon's Ph.D. project. He is developing a model based random correction method in parallel to the scatter correction method. His methods will be tested on the ECAT 953B scanner located on the UBC campus. Results from this work have been presented at the 2003 SNM and the IEEE/MIC meeting.

Experiment LS35

Development of ^{18}F labelled nitroimidazole PET imaging agents for tissue hypoxia

(M.J. Adam, TRIUMF)

Hypoxia in cells and tissues is an important component of various pathological states (e.g. ischemia and stroke). Hypoxic tumour cells are extremely important within cancer treatment because they are more likely to survive radiation and chemotherapy, leading to an increase in tumour resistance to treatment. More recent evidence suggests that hypoxia is related to the aggressiveness of disease. Such studies employed a microelectrode, used in many centres, but were limited

because of invasiveness and requirement for an accessible tumour.

Derivatives of 2-nitroimidazole are used extensively as hypoxia markers. The 2-nitroimidazoles are not metabolized in oxygenated tissues, but bind to macromolecular proteins after reduction in hypoxic cells. This permits detection by a variety of techniques. For example, the products of such binding for the (pentafluoropropyl)acetamide (EF5) and (trifluoropropyl)acetamide (EF3) derivatives of 2-nitroimidazole can be detected by specific fluorescent antibodies.

The synthesis of ^{18}F -EF5 has now been developed and was achieved by preparing the allyl precursor and fluorinating it with ^{18}F elemental fluorine in trifluoroacetic acid. The radiochemical yield is 17% after HPLC purification.

Progress this year was stimulated by the arrival of Dr. Donald Yapp at the BC Cancer Research Centre and the installation of the MicroPET tomograph at the UBC Hospital. His main research interest is in the use of EF5 as a PET marker for hypoxic tissue. Since his arrival we have reactivated this project, improved the synthesis of hot EF5 at TRIUMF, and carried out our first MicroPET imaging in a mouse tumour model. This experiment took a significant amount of planning and coordination and established a strong link between the Cancer Agency and the TRIUMF/UBC PET program. From a chemistry perspective, the progress this year was to establish a QC HPLC system for the EF5 product and to reactivate the manual production system for the radiolabelling. If this project is to continue past the pilot study stage we will need to invest some resources into refining and automating the chemistry system.

The other significant development this year that had an effect on this project was the Health Canada regulations on the human use of positron emitting radiopharmaceuticals (PERs). Our original plan was to carry out human PET imaging first, however, that was not deemed feasible this year given the requirements of the regulations. We are planning to develop a Clinical Trial Application and submit it for Health Canada approval sometime in 2004. Upon approval we intend to bring back the human lung cancer and other studies that we planned to carry out this year. Due to the availability of Cu PET isotopes at TRIUMF we are also proposing to synthesize Cu-ATSM, developed by another group, as a hypoxia marker, and compare this agent to EF5 in animals.

Experiment LS39/LS44

Positron emission profiling (PEP) for pulp and paper fluid dynamic studies/ Development of a high-speed formation (areal density) measurement system for paper (*M. Martinez, UBC*)

Recently positron emission profiling has been shown to have utility in following certain physicochemical processes that have aided in the understanding of the mechanisms of these processes. The models used to describe the motion of fibres in the manufacturing of paper are limited by a lack of understanding about the micro-dynamics of the interaction of the various fibre sizes during motion. By labelling the fibres with a positron-emitting isotope it may be possible to monitor the sedimentation process to provide better parameters for the models.

Previously we have visualized the motion of different fibres sizes during sedimentation and we are in the midst of developing this method to visualize fibre motion in a new geometry, namely a hydrocyclone. A hydrocyclone is an industrial apparatus used to separate fibres into different length or weight fractions.

Flow visualization of a hydrocyclone using PET with applications for the pulp and paper industry

Papermaking fibres are hollow, flexible rod-like particles that have a wide distribution in both length and diameter depending upon species and growing conditions; when liberated from the tree they can curl or kink. North American fibres are typically 40–50% cellulose, 20–35% hemicellulose, 15–35% lignin, with the remaining fraction containing resins, tannins, ash and miscellaneous compounds. Solid-solid separation of papermaking fibre suspensions is of importance to the pulp and paper industry. Traditional unit operations such as screening, cleaning, and fractionation are traditionally described as solid-solid separation processes. For example, during fractionation, a dilute fibre suspension is separated into a number of different length-fractions. Despite the longstanding use of these unit operations, little is known about the mobility of the various fibre fractions that make up the suspension. One of the essential difficulties lies in the incomplete understanding of the long-range multi-body hydrodynamic interactions. Another difficulty is that these properties are strongly dependent upon the microstructure of the suspension which itself changes as these fibres tend to mechanically entangle or flocculate. Ascertaining these effects is not easy as these suspensions are opaque and difficult to visualize at reasonable penetration depths. These issues make the understanding of the behaviour of these suspensions particularly difficult. Clearly, there is a need to visualize the mo-

tion of the individual classes of components in a fibre suspension in order to better control the physical properties of paper.

Since 1999, the motion of ^{18}F radioactively-labelled papermaking fibres moving in the midst of a suspension of non-radioactive fibres has been studied using PET. These unique data were then used in conjunction with the equations of motion to characterize the rheological behaviour of these suspensions. This work has quickly been adopted by industry, namely Canfor (Prince George, BC), the Pulp and Paper Research Institute of Canada, and Cascade (Kingsey Falls, QC).

From these studies it is clear that this visualization technique has the potential to help clarify the behaviour of mixtures of fibres. We would like to extend this technique to measure the motion of fibres in a flowing device, in general, and to a hydrocyclone, in particular. We propose a hydrocyclone as this device (i) has relevance to industry; (ii) has a size and is operated in a manner which allows for PET profiling; (iii) has a geometry that is amiable to numerical analysis; and (iv) is supported by local experts in Vancouver who would help develop an industrially-relevant experimental protocol.

Recently, we have tested the feasibility of this idea by building a transportable hydrocyclone which we could profile using PET.

Experiment LS42

Configuration modelling and image reconstruction studies on a depth encoding research tomograph

(V. Sossi, UBC)

The HRRT tomograph was delivered in May. Hardware performance testing has been completed. The focus of the research on this tomograph will now be data quantification with more studies on reconstruction methods. However, since a large component of the present proposal was crystal simulation, we consider this proposal completed and we submitted a new proposal entitled “Quantification of high resolution brain imaging” which is intended to be a logical continuation of this proposal. The detector modelling part of this study was published [Astakhov *et al.*, IEEE Trans. Nucl. Sci. **50**(5), 1373 (2003)].

Experiment LS50

Antisense imaging nucleic acids for Parkinson’s disease

(H. Dougan, TRIUMF)

In recent years the UBC/PET neurologists have published *in vivo* antisense experiments focused on Parkinson’s disease. Antisense DNA directed to the D1 receptor mRNA and to dopamine transporter mRNA

was infused into rat brains. The rats developed behavioural disorders and biochemical changes consistent with depletion of the “sense” mRNA by the “antisense” DNA probe. The LS50 report for 2002 related how the UBC investigators wished to extend their observations with unlabelled DNA to make new imaging agents based on DNA radiotracers. During 2002, ^{125}I labelled antisense DNA was developed at TRIUMF for pilot *in vivo* trials. The labelling process involved incorporating a labelled radiochemical – (4-halogen-benzyl)-2-bromoacetamide (BBA) – into the DNA molecule. A separate project (LS56) was initiated to develop innovative new concepts for ^{18}F DNA. During 2003, extensive biological studies were carried out with antisense DNA labelled with ^{127}I BBA and preliminary imaging trials were carried out with ^{125}I BBA. The basic methodology is under investigation. A new DNA analogue – locked nucleic acid (LNA) – was labelled with ^{125}I BBA. LNA is quite stable *in vivo* and is significantly less toxic to brain tissue than phosphorothioate DNA, the original analogue used in this study.

A successful proposal (T. Ruth, PI) was submitted to CIHR, leading to funding related to LS50, LS56, and LS64.

Experiment LS51

Auger therapy for prostate cancer

(H. Dougan, TRIUMF)

Project LS51 examines the potential for treatment of prostate cancer through DNA damage and cell killing induced by the Auger electrons released following the decay of ^{123}I and ^{125}I . Radioiodine incorporated into an iodoandrogen steroid EMIVNT is brought into proximity of DNA by the androgen receptor protein (AR); the cancer cell DNA is consequently targeted by the Auger electrons of the radioiodine decay, followed by death of the cancer cell, in this proposed scheme for treatment. The basic idea is described in more detail in the 2002 TRIUMF Annual Report. TRIUMF is collaborating with The Prostate Centre. In previous years at TRIUMF we prepared a stannylated precursor for EMIVNT and developed radioiodination giving [^{125}I]EMIVNT at nearly 2,200 Ci/mmol and [^{123}I]EMIVNT at much higher specific activity. At The Prostate Centre, the graduate student has found that EMIVNT binds the rat androgen receptor with an affinity similar to testosterone. TRIUMF’s contribution to this project is complete, except to prepare EMIVNT as needed for The Prostate Centre. Now it is The Prostate Centre’s turn to perform the biological investigation for Auger killing.

Experiment LS53

Synthesis of ^{99m}Tc and $^{186,188}\text{Re}$ sugar derivatives

(M.J. Adam, TRIUMF)

An NSERC strategic grant was awarded (October, 2001, M.J. Adam, PI, \$78,200/year for 3 years) to carry out research on the synthesis of technetium and rhenium labelled carbohydrates for use in nuclear medicine imaging and therapy. Dr. Adam is collaborating with Dr. Orvig in the UBC Chemistry Dept. and AnorMED (M. Abrams, CEO). A post doctoral fellow (Dr. Simon Bayly) and two graduate students (Cara Fisher and Charles Ewart) have also been working on this project for approximately two years.

Radiolabelled carbohydrates have been of significant interest to nuclear medicine due to the success of 2- ^{18}F -fluoro-2-deoxy-glucose (FDG) as an imaging agent in positron emission tomography (PET). This success has naturally raised the question of whether a single-photon emitting glucose analogue with similar properties to FDG can be developed for use with single-photon emission computed tomography (SPECT). Because of the relatively short half life of ^{18}F (110 min) its use is limited to facilities that have an accelerator in close proximity to chemistry laboratories and medical facilities. This fact makes it impractical for the FDG method to be widely used in medicine. ^{99m}Tc is the most widely used isotope in SPECT due to the fact that it is a generator produced, commercial isotope which makes it convenient to use and relatively inexpensive. It also has ideal physical properties for imaging. The drawback to this isotope is that it must be attached to the molecule via a chelate or organometal conjugate, which may perturb the system being studied. A SPECT analogue based on a widely available isotope such as ^{99m}Tc would make these agents available to the broader medical community. Among elements of the same series as Tc, the isotopes ^{186}Re and ^{188}Re show promise in the development of therapeutic strategies. For a β^- emitting radioelement to be therapeutically useful, a half-life of between 12h and 5 days is preferred: moreover, for a 1 MeV β^- particle, the depth of penetration into tissue is approximately 5 mm. Furthermore, if some of the disintegrations are accompanied by 100–300 keV gamma photons, the behaviour of the radioelement can be conveniently followed by using a gamma camera. The nuclear properties of ^{186}Re and ^{188}Re are optimal for these purposes.

Progress this year centres around the synthesis of a number of bi- and tri-dentate sugar ligands. Several of these sugar derivatives have now been successfully labelled with ^{99m}Tc . HPLC conditions for the analysis of the products and the intermediate “Alberto” reagent have been worked out. Labelling kits (Isolink) have

been obtained from Mallinckrodt free of charge to prepare the Alberto reagent more consistently. A collaboration has been established with MDS Nordion to provide us with ^{186}Re in order to carry out test labelling. Several sugar complexes have been labelled with ^{186}Re but using different labelling conditions to that of the kit method used in Tc labelling. This year other radiometals are also being tested. For the PET imaging program we have an interest in Cu isotopes and other radiometals, such as ^{68}Ga . We have recently produced ^{61}Cu and ^{55}Co and both of these have been successfully incorporated into some of our sugar chelates. With regard to publications we have recently submitted a paper to Bioconjugate Chemistry and have presented this work at the International Radiopharmaceutical Chemistry Symposium held in Sydney, Australia (Fisher). This year (year two of the project), NSERC reviewed our progress report and deemed progress to be satisfactory and have released the funding for year 3.

Experiment LS56

Synthesis of radiolabelled nucleotides and oligonucleotides

(M.J. Adam, TRIUMF)

This is a progress report on the development of chemistry for the F-18 labelling of oligonucleotides. One of the strategies that we are pursuing is to develop a general method to label the phosphorous atom directly with nca F-18 fluoride so that there is little structural change to the molecule. Thus, the biological activity of the oligo will be preserved. Model compound systems were developed this year to determine if P(III) and P(V) containing derivatives could be labelled with nca fluoride. We were able to successfully incorporate F-18 into both P(III) and P(V) model compounds. Another approach makes use of the fact that fluoride anion reacts readily and quantitatively with ethers of silicon to give a very stable silicon fluoride bond. Grant applications to both NSERC and CIHR have been submitted to continue this work. An abstract to the 2004 Society of Nuclear Medicine meeting has been submitted and a manuscript is in preparation on the P-F work.

Experiment LS57

Quantitative imaging with the Concorde microPET

(V. Sossi, UBC)

The microPET R4 scanner was delivered in May. Preliminary camera evaluation studies have been performed and two areas that need further improvement have been identified: normalization and attenuation correction. Figures 177 and 178 show transaxial profiles of a cylinder uniformly filled with radioactivity for several scanning conditions (see legend). It is ap-

parent that both the absolute values and the shape of the profiles depend on the correction methods applied and none provides sufficient image uniformity. The optimum method thus needs to be developed and imple-

mented to achieve proper quantification. Preliminary results of these studies have been submitted to the Society of Nuclear Medicine meeting [Camborde *et al.* (in press)].

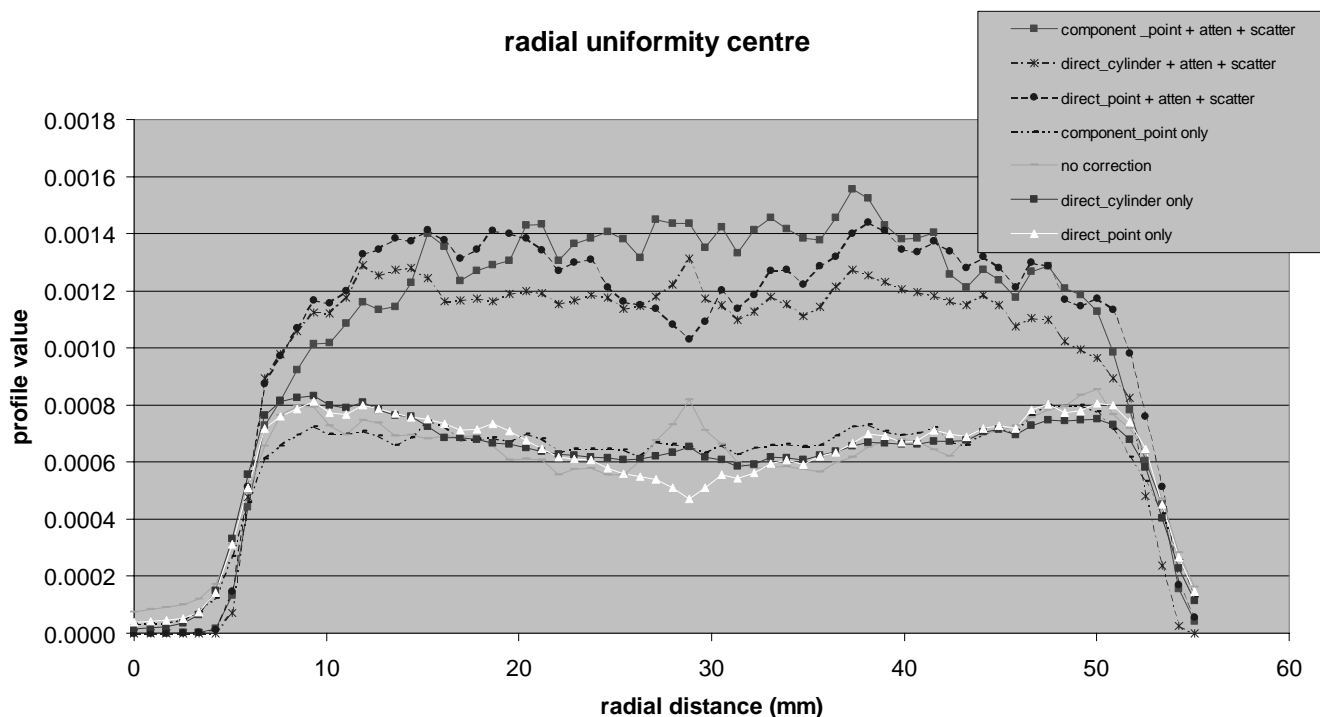


Fig. 177. Profiles obtained with and without attenuation correction using either a cylinder or a point source as normalization source and a direct or component based normalization procedure.

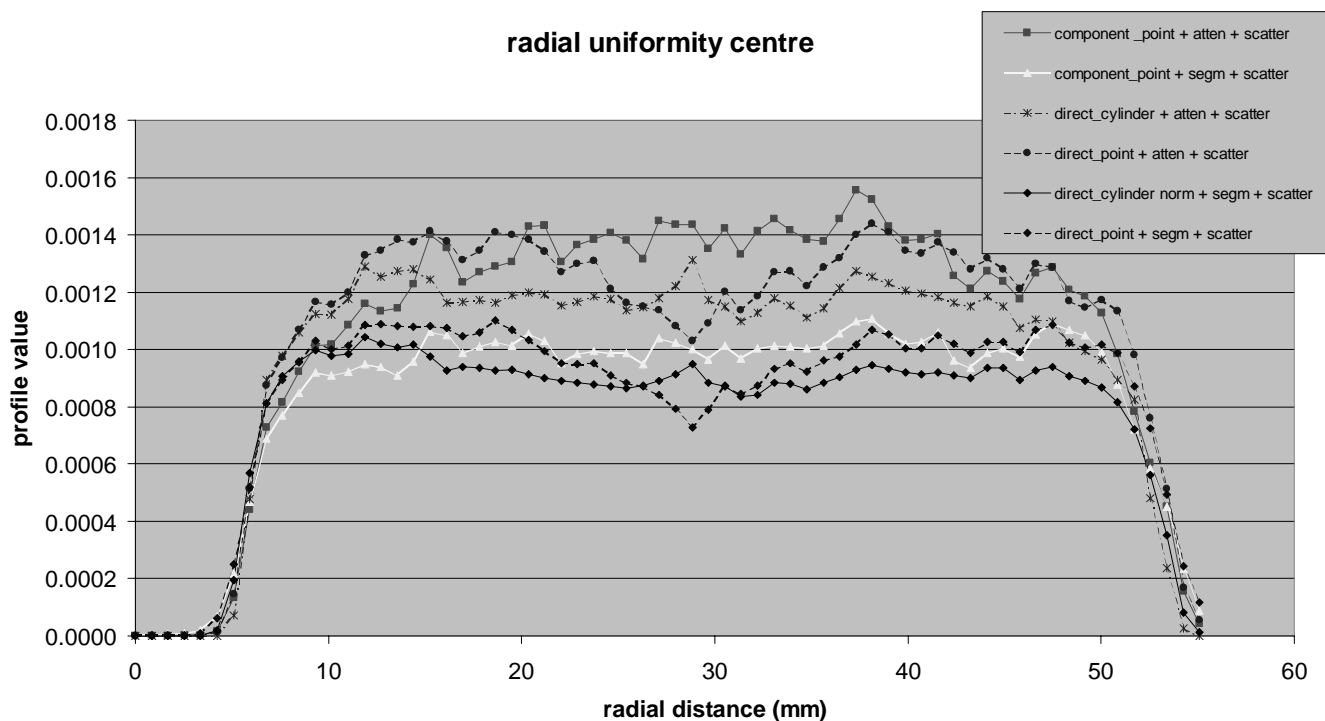


Fig. 178. Similar to Fig. 177, but now a measured (atten) and segmented attenuation correction methods are also compared.

Some preliminary animal measurements have also been performed: (+)¹¹C-dihydrotetrabenazine (DTBZ) and ¹¹C-methylphenidate (MP) scans on healthy, unilaterally mildly and more severely 6-hydroxydopamine (6-OHDA) lesioned rats, a triple RAC study with a 50 mg/kg IP of administration of levodopa (+ 10 mg/kg benserazide) approximately 45 min before the second RAC injection to investigate the feasibility of measuring levodopa induced raclopride displacement (an indirect measurement of DA turnover, see research proposal). This last study was also performed on a unilaterally lesioned rat. Two objectives were pursued with these studies: a) feasibility of the studies themselves, especially for the indirect measure of DA turnover and b) ability to measure differences between healthy state and lesions of different severity. In each study the binding potential was estimated using the tissue input Logan graphical approach. Results are presented in Tables XVII–XIX and Fig. 179.

These results clearly show the feasibility of measuring levodopa induced RAC displacement and to quantify pre-synaptic differences between healthy and lesioned striata. We have also tried imaging using the pre-synaptic tracer FD to investigate the possibility of a direct estimate of DA turnover. In agreement with verbal reports from other PET centres, not enough specific uptake was observed in the striata to allow the use of this tracer.

The next steps of this research will include the development of a correct attenuation and normalization method for this scanner to obtain quantitative images, further investigation of image reconstruction methods with particular emphasis on the development of methods that take into account the spatially variant nature of the point spread function, and development and validation of bloodless scanning procedures. In parallel we will also be evaluating the mass effect for several pre- and post-synaptic tracers.

Table XVII. Binding potential values obtained for DTBZ for 2 rats with unilateral severe and moderate 6-OHDA lesion.

	Un-lesioned	Mild lesion	Severe lesion
DTBZ	3.6	1.6	1.3

Table XVIII. Binding potential values obtained for MP in a rat with a severe unilateral 6-OHDA lesion.

	Un-lesioned	Moderate lesion
MP	1.05	0.43

Table XIX. Binding potential values obtained for the triple RAC scan in a rat with a moderate unilateral 6-OHDA lesion. 50 mg/kg IP of levodopa (+ 10 mg/kg benserazide) was administered approximately 45 min before the second RAC injections. The three injections were separated by 2 h.

	Lesioned side	Control side
RAC 1	2.31	2.72
RAC 2	1.67	2.56
RAC 3	2.56	2.22

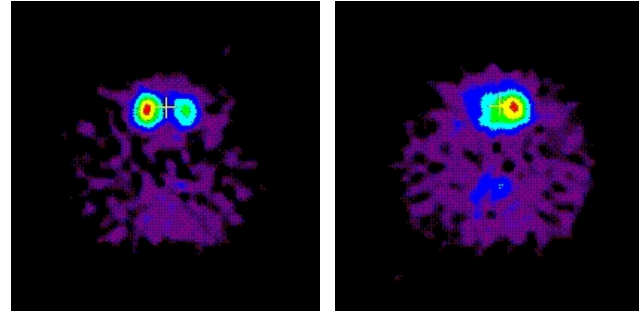


Fig. 179. RAC (left) and DTBZ (right) image of a severely unilaterally 6-OHDA lesioned rat. There is a lower DTBZ and a higher RAC uptake in the lesioned side as expected.

Experiment LS69

***In-vivo* studies on regulation of dopamine turnover using a Parkinson's disease rat model and a microPET**

(V. Sossi, UBC)

In this study we are planning to investigate disease and treatment induced regulatory changes of the dopamine transporter, their relation to dopamine turnover and to the onset of motor complications using a rat model of Parkinson's disease and a microPET. Preliminary data for this proposal can be found under LS57.

Experiment LS70

Quantification of high resolution brain imaging

(V. Sossi, UBC)

This proposal is a continuation of LS42. The proposal focuses on the implementation of the quantitative aspect and further development of reconstruction algorithms for the high resolution research scanner (HRRT) with the ultimate goal of assessing the HRRT ability to produce robust parametric images. Preliminary resolution measurements on this scanner show a reconstructed resolution better than 3 mm in each direction and a sensitivity of approximately 6%. This is the best performance to date for a human brain scanner and is expected to allow the investigation of new brain areas and the detection of more subtle and/or widespread disease induced changes of the neurotransmitter systems. In order to achieve this we are planning

to develop accurate data quantification with fast image reconstruction and image analysis methods that will allow for the investigation of the entire image volume.

This planned study builds on significant progress that we already made in the area of algorithm development – development of a list mode based reconstruction algorithm and development of a method that, given information on patient motion, incorporates such information into the reconstruction procedure. Figure 180 shows the effect of motion correction on the data on a simple phantom study. A radioactive line source placed into a cylinder was scanned in three separate scans: between each scan the cylinder with the source was rotated by a known amount. Data from the three scans were then summed into a single data file and reconstructed without and with motion correction. It can be easily seen that the motion correction algorithm correctly reconstructs the data as if the line source had not been moved. This correction is particularly important for the HRRT, since patient motion will not be negligible compared to the scanner resolution.

We also developed a new method to perform random subtraction in the iterative reconstruction algorithms. This new method substantially reduces the non-negativity constraint induced bias that is generally present in the high count rate – low number of acquired events data sets, thus improving quantification accuracy over a wide range of scanning conditions. Two papers related to this research are under revision [Rahmim *et al.* (submitted to IEEE Trans. Nucl. Sci.); Rahmim *et al.* (submitted to Phys. in Med. and Biology)].

Significant progress has also been made in the development of printed point sources. A successful technique has been designed that now allows us to obtain 0.5 mCi of activity in 9 point sources. An example of an image of such point sources is shown in Fig. 181. This method is now routinely used whenever we need to image very small point sources. This work has been submitted for publication [Sossi *et al.* (submitted to IEEE Trans. Nucl. Sci.)].

We are now planning to extend these techniques to the printing of extended sources. Detailed studies will be done to examine the feasibility of obtaining sources of sufficient uniformity to be used as scatterless normalization sources.

The results of the studies planned in this proposal

will impact all the studies performed in our centre. They will determine the optimum utilization of this brain scanner and will provide essential guidance in the estimate of the feasibility of new clinical studies. Their impact, however, will not be limited to our centre: they will directly benefit all the HRRT users and the PET imaging community. From a medical research point of view they will be instrumental in providing new tools to provide insights into presently unanswered questions.

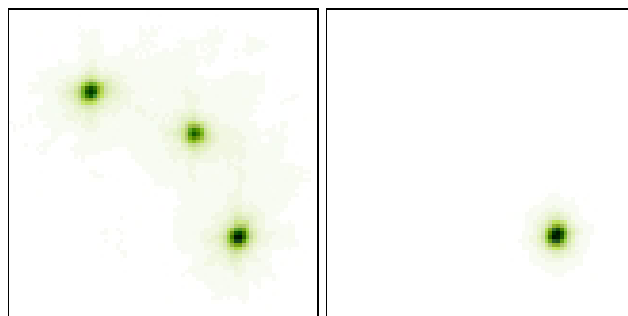


Fig. 180. Image reconstructed with (right) and without (left) correction for motion. A radioactive line source placed into a cylinder was scanned in three separate scans: between each scan the cylinder with the source was rotated by 45° .

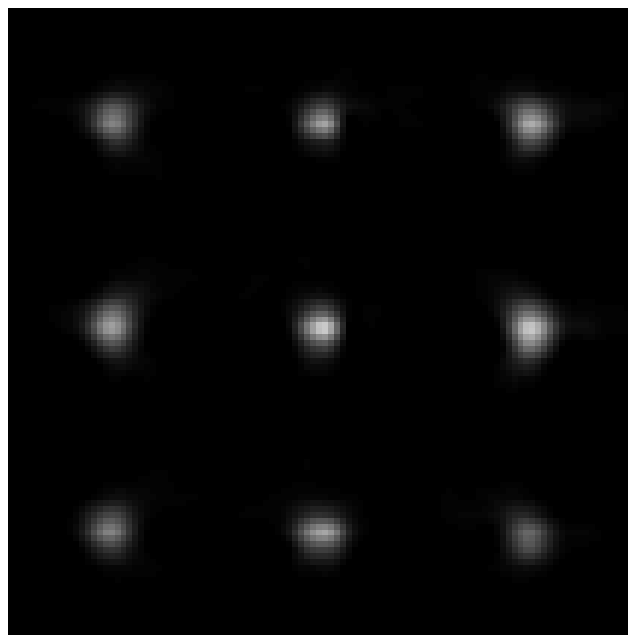


Fig. 181. Example of an image of 9 printed point sources obtained with the microPET. The sources are 0.5 mm in diameter and are separated by 1.5 cm.

THEORETICAL PROGRAM

Introduction

The TRIUMF Theory group provides a centre for theoretical research at TRIUMF and a group of active people involved in research in a wide variety of areas. Some of these areas are of direct relevance to the on-site experimental program. Others are more closely related to projects elsewhere involving TRIUMF and other Canadian scientists. Still others are more general, contributing to, and participating in, the efforts of the subatomic physics community both in Canada and elsewhere.

At present the group consists of four permanent staff members, six to seven research associates and a number of students and visitors. Currently the main research interests are nuclear structure and reactions, nuclear astrophysics, lattice QCD, effective field theories and chiral perturbation theory, few-body systems, and particle physics beyond the standard model.

The four permanent staff members of the group are: Harold W. Fearing, Byron K. Jennings (group leader), John N. Ng, and Richard M. Woloshyn. Erich W. Vogt (professor emeritus, UBC) is an associate member.

Research associates during 2003 were: R. Alahverdi, S. Ando, C. Barbieri, W. Chang, R. Cyburt (from September), A.K. Dutt-Mazumder (until December), C.P. Liu (until October), J.-M. Sparenberg, and L. Theussl (from September).

The graduate students associated with the group during 2003 were: F. Okiharu and K. Wong, both supervised by R. Woloshyn.

The visitors to the Theory group this year included: J. Al-Khalili, D. Atwood, B. Balantekin, T. Becher, S. Bilenky, C.W. Chiang, G. Carter, A. Datta, W. Detmold, W. Dickhoff, G. Drake, A. El-Khadra, V. Flambaum, C.Q. Geng, S. Godfrey, S. Groot Nibbelink, T. Hemmert, F. Herwig, K. Hornbostel, K. Langanke, M. Locher, K. Maltman, B. McElrath, R. Myers, A. Nogga, K. Nollett, M. Pospelov, A. Rinat, S. Scherer, I. Stetcu, T. Tait, M. Voloshin, N. Weiner, D. Wilkinson, M. Wingate and J. Yoo.

As usual, members of the group have been quite active, and below we briefly describe some of the many projects undertaken during the year by members of the group and longer term visitors.

Nuclear Structure and Reactions

Potential-model and R-matrix analyses of $^{12}\text{C} + \alpha$ elastic scattering phase shifts (J.-M. Sparenberg)

Using general results from the inverse problem in quantum scattering theory, it has been argued that, for a given partial wave, bound-state properties (num-

ber of bound states, energies, asymptotic normalization constants) are independent of one another and of the corresponding scattering phase shifts. This has been illustrated on the $\ell = 2$ partial wave of the $^{12}\text{C} + \alpha$ system in a simplified potential model: with the help of an inversion method based on supersymmetric quantum mechanics, potentials have been constructed, that reproduce the $\ell = 2$ phase shifts deduced from a recent re-measurement of the elastic-scattering cross sections. By construction, these *phase-equivalent* potentials (identical phase shifts) have a bound state at -245 keV describing the 2^+ subthreshold state of ^{16}O , which is known to have a strong influence on the $^{12}\text{C}(\alpha, \gamma)^{16}\text{O}$ capture reaction at astrophysical energies. However, the asymptotic normalization constant of this state, C_{12} , which is the key quantity for the capture reaction, is arbitrarily different from one potential to the other, despite their identical phase shifts and bound-state energy. This contradicts two recent R-matrix analyses of the $^{12}\text{C} + \alpha$ system, aiming at extracting C_{12} from the $\ell = 2$ phase shifts and the bound-state energy: both analyses have been shown to be unreliable, which explains the inconsistency between their results. In contrast, it has been shown that if the inversion potential is used to reproduce not only the $\ell = 2$ data but the whole $\ell = 0, 2, 4, 6$ rotational band, C_{12} is strongly constrained. Combining this result with other potentials from the literature has led to $C_{12} = 144.5 \pm 8.5 \times 10^3 \text{ fm}^{-1/2}$. This value is consistent with a theoretical estimate from the microscopic cluster model and with transfer-reaction data, provided small many-body effects are taken into account. On the other hand, it disagrees with cascade-transition data, a new measurement of which is foreseen at TRIUMF.

Construction of a Λ - Λ effective interaction for the calculation of hypernuclei

(J.-M. Sparenberg; Y. Fujiwara, Kyoto; K. Miyagawa, Okayama Science Univ.; M. Kohno, Kyushu Dental College; Y. Suzuki, Niigata; D. Baye, Brussels Free Univ.)

The 1S_0 Λ - Λ phase shifts generated by a QCD-inspired spin-flavour SU_6 quark model have been analyzed by a supersymmetric inversion method. This leads to a local potential which has been approximated by the sum of two Gaussian functions. This effective potential, together with Λ - N effective interactions obtained in the same way, has been used in microscopic calculations of the $^6_{\Lambda\Lambda}\text{He}$ and $^9_{\Lambda}\text{Be}$ hypernuclei with a new three-cluster Faddeev formalism based on the two-cluster resonating-group-method kernel.

Comparison of one-body functions deduced from microscopic models of the ^8B and ^{17}F nuclei

(J.-M. Sparenberg, C. Barbieri, B. Jennings; P. Descouvemont, Brussels Free Univ.)

Different ways of reducing a many-body problem to a two-body problem have been proposed in the literature, depending on the type of one-body function used. We have compared the approach based on the one-body overlap function to that based on an auxiliary function used in the microscopic cluster model. For the ^{17}F nucleus, as calculated by a microscopic Green's function-Faddeev equation method, both functions are very close to one another for states that have a strong $^{16}\text{O} + p$ structure, and appreciably different from one another for states that have a more complicated structure. For the ^8B ground state, as calculated by a microscopic generator-coordinate cluster model, an appreciable difference between both functions is also seen, despite the fact that this state seems to have a $^7\text{Be} + p$ structure with a good approximation. Only the one-body overlap function is close to the phenomenological $^7\text{Be} + p$ potential-model wave function, which tends to indicate that it has a stronger physical meaning than the auxiliary function.

Proton emission

(J. Al-Khalili, Surrey; C. Barbieri, B.K. Jennings, J.-M. Sparenberg, J. Escher, LLNL)

We have embedded the elegant Gurvitz-Kalbermann approach to proton emission [Gurvitz and Kalbermann, Phys. Rev. Lett. **59**, 262 (1987)] in a full many-body picture. We reduced the formalism to an effective one-body problem and demonstrated that the decay width can be expressed in terms of a one-body matrix element multiplied by a normalization factor. At first sight, this result agrees with the standard procedure for extracting spectroscopic factors from measurements via dividing an experimental width by a calculated single-particle width. The present work, however, clearly demonstrates that this procedure for determining spectroscopic factors is only valid if the phenomenological potential used to generate the single-particle width corresponds to the mass operator in the particle-hole Green's function. It is not *a priori* clear that this is actually the case. In fact, it has been strongly suggested [see Varga and Lovas, Phys. Rev. **C43**, 1201 (1991); Lovas *et al.*, Phys. Rep. **294**, 265 (1998) and references therein] this is not the case. While that study was carried out for alpha decay, the arguments given there can be carried over to a description of the proton emission process. Furthermore, the present work suggests that $\int_0^{T_t} dr \phi_r^*(r) \left[1 - \frac{\partial H_r(E)}{\partial E} \right] \phi_r(r)$ is the appropriate ob-

servable that can be extracted from proton emission experiments.

Low-energy nuclear structure and one-hole spectral function of ^{16}O

(C. Barbieri; W.H. Dickhoff, Washington Univ. St. Louis)

The best theoretical calculations presently available for the nucleus ^{16}O are still in disagreement with the experimental data obtained from $(e, e'p)$ reactions. In particular, the theory predicts too high values of the spectroscopic factors at small missing energies.

In order to approach this problem, we developed a formalism based on Green's function theory and the Faddeev equations technique. Results from such calculations tend to reduce the disagreement with the experimental data and suggest that further improvement should come from better treatment of long-range correlations. The latter need to be described in terms of low energy collective excitations, including the effects of fragmentation. For the particular case of ^{16}O it appears that the coupling of up to four-phonon states is required. Encouraging results have been obtained by considering the coupling of two phonons and the extension of our calculation to the full four-phonon case is under way.

The present calculations on ^{16}O are also meant to serve as a test ground for calculations with the above formalism, in view of possible application to other medium and heavy nuclei.

Study of short-range correlation by means of the $(e, e'pN)$ reactions

(C. Barbieri; W.H. Dickhoff, Washington Univ. St. Louis; C. Giusti, F.D. Pacati, Pavia)

Two-nucleon emission reactions have recently proved to be a powerful tool to study two-body (short-range and tensor) correlations in nuclei. In these studies, the effects of long-range motion are also important and need to be properly accounted for. The recent Faddeev studies of low-energy structure of ^{16}O (described above) have also produced improved results for the two-hole spectral function. These include the effects of self-consistency and of ground state correlation in the target nucleus. In collaboration with the Pavia group, we are now employing these two-hole spectral functions to study the two-proton and the proton-neutron emission from the nucleus of ^{16}O .

Nucleon-nucleus optical potential at low energy and proton capture

(C. Barbieri, B.K. Jennings)

The proton capture reactions $^7\text{Be}(p, \gamma)^8\text{B}$ and $^{16}\text{O}(p, \gamma)^{17}\text{F}$ play an important role in the understanding of stellar evolution. In this regime, the nuclear opti-

cal potential that describes the nucleon-nucleus interaction can present substantial energy dependence and is expected to be sensitive to the couplings between the nucleon and the surface vibrations of the target. Such low-energy modes have been considered for ^{16}O in earlier works. There, the nuclear self-energy was obtained using self-consistent Green's function theory.

In general, the nuclear self-energy at positive energies is a realization of the optical potential for the nucleon-nucleus scattering, while at negative energies it gives information on the binding of the final $A+1$ body system. Work is in progress to employ the above calculated self-energy as an optical potential to analyze the scattering and capture of nucleons at low energy.

Rescattering contribution to $(e, e'p)$ cross section at high missing energy and momenta

(C. Barbieri; L. Lapikás, NIKHEF; D. Rohe, Basel, for the E97-006 collaboration)

The contribution of rescattering to final state interactions in the $(e, e'p)$ cross section is studied using a semiclassical model. This approach considers a two-step process with the propagation of an intermediate nucleon and uses Glauber theory to account for the reduction of the experimental yield due to $N - N$ scattering. This calculation has relevance for the analysis of data at high missing energies and in particular at the kinematics of the E97-006 experiment done at JLab. It is found that rescattering is strongly reduced in parallel kinematics and that the excitation of nucleon resonances is likely to give important contributions to the final state interactions in the correlated region. For heavy nuclei, further enhancement to the rescattering is expected to be generated from the strength in the mean field region.

The analysis of data from the E97-006 collaboration is expected to yield, for the first time, experimental information on the spectral distribution of short-range correlated nucleons in finite nuclei.

Nuclear Astrophysics, Cosmology

Solar neutrino constraints on the BBN production of Li

(R.H. Cyburt; B.D. Fields, Illinois; K.A. Olive, Minnesota)

Using the recent WMAP determination of the baryon-to-photon ratio, $10^{10}\eta = 6.14$ to within a few per cent, big bang nucleosynthesis (BBN) calculations can make relatively accurate predictions of the abundances of the light element isotopes which can be tested against observational abundance determinations. At this value of η , the ^7Li abundance is predicted to be significantly higher than that observed in low metallicity halo dwarf stars. Among the possible resolutions to this

discrepancy are 1) ^7Li depletion in the atmosphere of stars; 2) systematic errors originating from the choice of stellar parameters – most notably the surface temperature; and 3) systematic errors in the nuclear cross sections used in the nucleosynthesis calculations. Here, we explore the last possibility, and focus on possible systematic errors in the $^3\text{He}(\alpha, \gamma)^7\text{Be}$ reaction, which is the only important ^7Li production channel in BBN. The absolute value of the cross section for this key reaction is known relatively poorly both experimentally and theoretically. The agreement between the standard solar model and solar neutrino data thus provides additional constraints on variations in the cross section (S_{34}). Using the standard solar model of Bahcall, and recent solar neutrino data, we can exclude systematic S_{34} variations of the magnitude needed to resolve the BBN ^7Li problem at $> 95\%$ CL. Additional laboratory data on $^3\text{He}(\alpha, \gamma)^7\text{Be}$ will sharpen our understanding of both BBN and solar neutrinos, particularly if care is taken in determining the absolute cross section and its uncertainties. Nevertheless, since it already seems that this “nuclear fix” to the ^7Li BBN problem is unlikely, other possible solutions are briefly discussed.

Primordial nucleosynthesis for the new cosmology: determining uncertainties and examining concordance

(R.H. Cyburt)

Big bang nucleosynthesis (BBN) and the cosmic microwave background (CMB) have a long history together in the standard cosmology. BBN accurately predicts the primordial light element abundances of deuterium, helium and lithium. The general concordance between the predicted and observed light element abundances provides a direct probe of the universal baryon density. Recent CMB anisotropy measurements, particularly the observations performed by the WMAP satellite, examine this concordance by independently measuring the cosmic baryon density. Key to this test of concordance is a quantitative understanding of the uncertainties in the BBN light element abundance predictions. These uncertainties are dominated by systematic errors in nuclear cross sections. We critically analyze the cross section data, producing representations that describe this data and its uncertainties, taking into account the correlations among data, and explicitly treating the systematic errors between data sets. The procedure transforming these representations into thermal rates and errors is discussed. Using these updated nuclear inputs, we compute the new BBN abundance predictions, and quantitatively examine their concordance with observations. Depending on what deuterium observations are adopted, one gets the following constraints on the baryon density:

$\Omega_B h^2 = 0.0229 \pm 0.0013$ or $\Omega_B h^2 = 0.0216_{-0.0021}^{+0.0020}$ at 68% confidence, fixing $N_{\nu, \text{eff}} = 3.0$. If we instead adopt the WMAP baryon density, we find the following deuterium-based constraints on the effective number of neutrinos during BBN: $N_{\nu, \text{eff}} = 2.70_{-0.90}^{+0.84}$ or $N_{\nu, \text{eff}} = 3.50_{-1.35}^{+1.39}$ at 68% confidence. Concerns over systematics in helium and lithium observations limit the confidence constraints based on this data. BBN theory uncertainties are dominated by the following nuclear reactions: $d(d, n)^3\text{He}$, $d(d, p)t$, $d(p, \gamma)^3\text{He}$, $^3\text{He}(\alpha, \gamma)^7\text{Be}$ and $^3\text{He}(d, p)^4\text{He}$. With new nuclear cross section data, light element abundance observations and the ever increasing resolution of the CMB anisotropy, tighter constraints can be placed on nuclear and particle astrophysics.

New nucleosynthesis constraints on hadronic decaying relic particles

(*R.H. Cyburt; J. Ellis, CERN; B.D. Fields, Illinois; K.A. Olive, Minnesota*)

We are exploring the constraints placed on the abundance of an unstable relic particle with lifetimes between 10^{-2} and 10^4 sec. We consider decays which produce hadronic showers, and constrain them through their effects on primordial nucleosynthesis. Hadronic showers change the light element predication in two ways, through hadronic induced pn-interconversion and nuclide disintegration. This project requires an intimate knowledge of hadronic thermalization processes and hadron-nuclide scattering and break-up cross sections.

Model independent $S_{17}(0)$ and error budget accounting

(*R.H. Cyburt, B. Davids*)

In an effort to combine all existing data, we use the data analysis formalism developed by Cyburt [astro-ph/0401091] and apply the methods to the specific case of $^7\text{Be}(p, \gamma)^8\text{B}$. Also, we detail all contributing sources of uncertainty, both statistical and systematic. We also show how inclusion of various theories can be used to reduce extrapolation errors, but we highlight that theory systematics must be taken into account in the error budget. In most cases, previous determinations of $S_{17}(0)$ have underestimated the true systematic uncertainty.

The cosmological concordance project

(*G. Huey, B.D. Wandelt, Illinois; R.H. Cyburt*)

This is an ongoing project that makes cosmological parameter extraction accessible to the general scientific community. The project Web page (<http://galadriel.astro.uiuc.edu/ccp/>) allows users to choose from a variety of observational data sets and theoretical constraints. The main motivation for the

work is to make it easy for experimentalists and theorists alike to explore and interpret the current state of cosmological knowledge.

Quick CMB parameter estimation

(*R.H. Cyburt; G. Huey, B.D. Wandelt, Illinois*)

With the growing precision and number of cosmological data sets, ever more complex and detailed cosmological models can be explored and constrained. With this added complexity, the field becomes computationally overtaxed and an exhaustive treatment becomes prohibitive. We outline a method for quick parameter estimation, detailing its advantages and range of applicability. Of particular usefulness are the theory sensitivities to these parameters, which will help limit the level of complexity a particular cosmological model can have. Another advantage of this method is that it allows a clear separation of individual data sets, allowing exploration of systematics. We use this method for parameter estimation including the second year WMAP data release.

Lattice QCD

Colour field distributions in the baryon

(*F. Okiharu, Nihon Univ.; R.M. Woloshyn*)

Chromo-electric and chromo-magnetic field distributions in mesons have been extensively studied but for baryons it is much more difficult to map the colour fields. Some special technique, such as using Abelian projected fields, to reduce statistical fluctuations needs to be applied. Once statistical fluctuations are under control the question of systematic errors has to be studied. We investigated the sensitivity of baryonic observables to the choice of the three-quark interpolating operator. It was found that consistent values for the static three-quark potential could be obtained in lattice QCD simulations for different (static) baryon interpolating operators. However, operator independence for the colour field distribution is more difficult and could not be achieved in present simulations. New techniques for reducing statistical fluctuations, which will allow for simulations with larger Wilson loops, are being investigated. Unitarized fat7 smearing, which was developed to suppress hard gluon interactions in hadrons made from staggered quarks, may be promising.

Lattice QCD simulations with dynamical improved staggered quarks

(*K.Y. Wong, SFU; R.M. Woloshyn*)

A major challenge for lattice QCD simulations is to include the effects of quark loops in the vacuum, so-called dynamical fermion effects. The most cost effective way of doing this is using staggered quarks. However, staggered quarks have species doubling and

“taste symmetry” among different species is broken by hard gluonic interactions. Recently a new class of improved staggered fermion actions has been proposed [Follana *et al.*, hep-lat/031104] in which the taste symmetry breaking effects are suppressed by unitarized fat7 smearing of the gauge field links. We have developed and tested computer programs, utilizing the hybrid molecular dynamics (HMD) algorithm, for these new actions. Parallelized versions of the programs (using MPI) have been developed for use at WestGrid and other large scale computing facilities.

Effective Field Theories and Chiral Perturbation Theory

Neutron beta decay in effective field theory

(*S. Ando, H.W. Fearing; V. Gudkov, K. Kubodera, F. Myhrer, USC; S. Nakamura, T. Sato, Osaka*)

Radiative corrections to the lifetime and angular correlation coefficients of neutron beta decay are evaluated in effective field theory. We also evaluate the lowest order nucleon recoil corrections, including weak-magnetism. Our results agree with those of the long-range and model-independent part of previous calculations. In an effective theory the model dependent radiative corrections are replaced by a well-defined low energy constant. The effective field theory allows a systematic evaluation of higher order corrections to our results to the extent that the relevant low-energy constants are known. We estimate the accuracy of our calculated observables to be of the order of 10^{-3} .

Effective field theory on the deuteron revisited

(*S. Ando; C. H. Hyun, Seoul/Sungkyunkwan*)

Pion-less dibaryon effective field theory for the deuteron is studied. The electromagnetic form factors of the deuteron and the cross section of radiative neutron capture on a proton, $np \rightarrow d\gamma$, are calculated within the theory. In accordance with the counting rule of the theory, we have the low-energy constants (LECs) in the higher order diagrams, which stem from integrating out high energy degrees of freedom from the effective Lagrangians, such as the meson exchange currents, and the values of the LECs should be fixed by experiments. We find that the contributions of the LECs of vector-two-dibaryon interactions turn out to be large, comparable to those of leading two-nucleon loop diagrams. We discuss the duality of two-nucleon and dibaryon field in the description of the deuteron, that is, those two kinds of diagrams are of leading order and the LECs can be fixed by the one-body interaction with an external probe. We find that this assumption reproduces well the results of effective range theory.

Second-class current on the nucleon in chiral perturbation theory

(*S. Ando*)

Experiments for investigation of the second-class current have been conducted at TRIUMF by a group from Osaka University for a long time. It was a challenge to detect this tiny quantity, since it is predicted theoretically that the magnitude of the second-class current (the axial tensor coupling constant g_T) is proportional to the mass difference between u - and d -quark, based on an estimate using QCD sum rules. Chiral perturbation theory (χ PT) provides the other systematic framework to incorporate the symmetry breaking patterns of QCD induced by the quark masses into the calculations. Though the isospin symmetry breaking terms have usually been neglected in the former calculations, the inclusion of the mass difference between the light quarks is straightforward except for the inclusion of the other isospin breaking effect, that is, the electromagnetic interactions. It would be interesting to estimate the coupling constant g_T by employing the χ PT.

Solar-neutrino reactions on the deuteron in dibaryon effective field theory

(*S. Ando*)

The recent experimental results at SNO show that the flavour of the solar-neutrino changes while it flies to the earth. This strongly indicates that the neutrino has a mass. The neutrino reactions on deuteron are the detecting reactions of solar-neutrinos at SNO and therefore it is essential to provide the theoretical cross sections for the reactions as accurately as possible to deduce the mass and the mixing angle of neutrinos from the data.

The cross sections have been estimated by using several different theoretical approaches so far: 1) standard nuclear physics calculations employing model Lagrangians to construct the exchange currents, 2) effective field theoretical (EFT) calculations employing the Weinberg’s counting scheme, and 3) EFT calculations employing the power divergence subtraction scheme. The results of those calculations turn out to agree well with each other. However, interrelations between these three approaches have not been well studied yet. We calculate the cross sections of the reactions employing dibaryon EFT without pions, which can correctly reproduce the results of the effective range theory, and compare the results with those of the former calculations.

Regularization procedures in relativistic chiral perturbation theory

(*S. Ando, H.W. Fearing*)

Relativistic chiral perturbation theory presents some problems not present in non-relativistic approaches because of the non-zero baryon masses in the chiral limit. In particular it is hard to obtain a systematic expansion scheme in the relativistic theory. A new renormalization scheme for relativistic ChPT with nucleons was proposed by Becher and Leutwyler and modifications of the approach have been intensively studied by Fuchs *et al.* These approaches seemingly correct the analytic structure of the amplitudes, and in the case of Fuchs *et al.* generate a systematic counting procedure which reproduces the results of heavy baryon chiral perturbation theory. We have been looking at these new approaches, examining the pros and cons, and trying to understand how they can best be applied to practical calculations.

Muon capture on a proton in relativistic chiral perturbation theory

(*S. Ando, H.W. Fearing; S. Scherer, Mainz*)

As an application of the new approaches to relativistic chiral perturbation theory which have been proposed, we have begun a calculation of ordinary, non-radiative, muon capture on the nucleon using the infrared regularization scheme of Becher and Leutwyler and the power counting proposals of Fuchs *et al.* The calculation will be compared to the non-relativistic heavy baryon ChPT approach used earlier [Nucl. Phys. **A631**, 735 (1998)]. This process primarily fixes the low energy constants needed for vector and axial vector interactions, and thus is a necessary first step for future applications to radiative muon capture, radiative pion capture and similar processes.

Reanalysis of nuclear PNC observables in the framework of effective field theory

(*C.-P. Liu; M.J. Ramsey-Musolf, Caltech/Connecticut; B.R. Holstein, Massachusetts*)

Traditional analysis of nuclear PNC observables is done by using the DDH potential. However, one big puzzle in this field is that the current constraints on PNC πNN coupling, obtained from various nuclear PNC observables, have not been very consistent, and they also do not agree well with the theoretical predictions, e.g., the DDH “best” value. One possible source of this inconsistency might be due to the fact that this widely-adopted potential is model-dependent. A new development by M.J.R.-M. *et al.* of formulating a model-independent PNC potential within the framework of effective field theory is in progress. Our goal here is using this new potential – parametrized by var-

ious low energy constants (LECs) – to reanalyze nuclear PNC observables and see if one can get a more consistent result in this framework. This work is still ongoing.

Few-Body and Medium Energy Processes

Induced pseudoscalar coupling of the proton weak interaction

(*T. Gorringer, Kentucky; H.W. Fearing*)

An extensive review of what is known, both theoretically and experimentally, about the induced pseudoscalar coupling g_P appearing in the weak nucleon current was revised and extended during the year. Most information comes from muon capture and radiative muon capture, and so these processes were extensively reviewed. The review has now been published in Reviews of Modern Physics. The most interesting new result to come from this work was the suggestion that, based on an updated analysis, the older measurements of muon capture on the proton may not be in as good agreement with the predictions of chiral symmetry as previously supposed. This enhances the importance of new experiments on this process which are now in progress.

Parity-nonconserving meson exchange currents

(*C.P. Liu; B. Desplanques, Grenoble; C.H. Hyun, Sungkyunkwan*)

The existence of meson exchange currents (MECs) has been acknowledged for quite a long time, and the inclusion of these currents is essential to guarantee the gauge invariance of any related calculation. A set of fully conserved parity-nonconserving (PNC) MECs is constructed within the framework of the DDH potential, the most widely-used model for the PNC nucleon-nucleon interaction, which consists of π -, ρ -, and ω -exchanges. This work has been done with the choice of the Feynman gauge for vector mesons. A further study will be using some other gauge, e.g., the unitary gauge, for vector mesons to insure the invariance property.

Deuteron anapole moment with heavy mesons

(*C.P. Liu; B. Desplanques, Grenoble; C.H. Hyun, Sungkyunkwan*)

Though the detection of nuclear anapole moment, a P-odd T-even electromagnetic moment, in light systems is still out of reach, there have been quite some theoretical works on the deuteron as it is one of the simplest systems to test nuclear parity nonconservation. We extended the earlier work by B.D. and C.H.H., which only included pion-exchange, to the full DDH model. It was found that the vector-meson exchange has little correction at the two-body level either through the polarization effect or MECs. However, its

contribution at the single-nucleon level (via loop diagrams) which produces the nucleonic anapole moment, is important, but still with a large theoretical uncertainty.

Deuteron photodisintegration

(*C.P. Liu; B. Desplanques, Grenoble; C.H. Hyun, Sungkyunkwan*)

While the asymmetry in polarized thermal neutron capture by hydrogen, which LANSCE plans to measure, provides information about the PNC πNN coupling constant, the asymmetry in its inverse process, i.e. deuteron photodisintegration by circularly-polarized light, is mostly sensitive to the isoscalar and isotensor parts of PNC heavy-meson-nucleon coupling constants. Therefore, these two experiments combined would provide valuable information about nuclear parity-nonconservation. Furthermore, some exciting calculations even suggested that at higher energies, the pion exchange dominates the deuteron photodisintegration asymmetry. Were this true, it could be an independent check on the LANSCE result.

With the advent of high-quality polarized photon beam, there is interest in doing this experiment at several places, which justifies an updated, more modern calculation. Within the framework of the DDH model and for photon energy up to 10 MeV above the threshold, we found that: i) near the threshold region, our results are consistent with the literature, and the asymmetry is of the order 10^{-8} , and ii) as the photon energy reaches 1 MeV above the threshold, the asymmetry drops to the order of 10^{-9} , and we did not see the great sensitivity to pion-exchange reported before. Therefore, our suggestions for such an experiment would be i) near the threshold, and ii) keeping away from the energy region about 4–6 MeV above the threshold, as a sign change in the asymmetry implies a great possibility of a null result.

Form factors in the point form of relativistic quantum mechanics

(*A. Amghar, Boumerdes, Algeria; B. Desplanques, LPSC, Grenoble; L. Theussl*)

Among the three forms of relativistic quantum mechanics proposed by Dirac (instant form, front form and point form), only the former two have been extensively used for describing few-body systems in the past. We consider the calculation of the electromagnetic form factor of the pion, but also electromagnetic and Lorentz-scalar form factors of scalar two-body bound states, in point form. In all cases, the comparison with results from an explicitly covariant Bethe-Salpeter approach evidences sizable discrepancies, pointing to large contributions from two-body currents in point form. The latter ones are constructed us-

ing two constraints: ensuring current conservation and reproducing the Born amplitude. The two-body currents so obtained are qualitatively very different from standard ones. Quantitatively, they turn out not to be sufficient to remedy all the shortcomings of the form factors in point form evidenced in impulse approximation. These results call for major improvements in the implementation of the point-form approach.

Generalized parton distributions of the pion in a Bethe-Salpeter approach

(*S. Noguera, Valencia; L. Theussl; V. Vento, Valencia*)

Generalized parton distribution functions are calculated in a field theoretic formalism using a covariant Bethe-Salpeter approach for the determination of the bound-state wave function. The procedure is described in an exact calculation in scalar electrodynamics, proving that the first higher order corrections vanish. The formalism is extended to the Nambu-Jona-Lasinio model, a realistic theory of the pion. It is found that in both cases all important features required by general physical considerations, like symmetry properties, sum rules and the polynomiality condition, are explicitly verified.

Z^* resonances: phenomenology and models

(*B. Jennings; K. Maltman, York*)

We explore the phenomenology of, and models for, the Z^* resonances, the lowest of which is now well established and called the Theta. We provide an overview of three models which have been proposed to explain its existence and/or its small width, and point out other relevant predictions, and potential problems, for each. The relation to what is known about KN scattering, including possible resonance signals in other channels, is also discussed.

Particle Physics

Rare tau decays in extra dimension models

(*W.-F. Chang, J.N. Ng*)

The recent neutrino experiment data show strong evidence that neutrinos have non-zero masses and mixings. This clearly indicates new physics beyond the SM in the neutrino sector and certainly implies the existence of lepton flavour violation (LFV) in the charged lepton sector. These LFV processes are either related or unrelated to the neutrino masses. They can also be used to discriminate different models. We discuss few examples of extra dimension models which give potentially testable LFV signatures. We compare the LFV processes in five dimension $SU(3)_W$ and $SU(5)$ GUT models where neutrino Majorana masses are generated radiatively without a right-handed neutrino. Also, we discuss the split fermion or multi-brane scenario where LFV coupling is generated geometrically.

Phenomenology of a 5D orbifold $SU(3)_W$ unification model

(*W.-F. Chang, J.N. Ng*)

We study the phenomenology of a 5D $SU(3)_W$ model on a $S_1/(Z_2 \times Z'_2)$ orbifold in which the minimal scalar sector plays an essential role of radiatively generating neutrino Majorana masses without the benefits of right-handed singlets. We carefully examine how the exotic scalars affect the renormalization group (RG) equations for the gauge couplings and the 5D $SU(3)_W$ unification. We found that the compactification scale of extra dimension is in the range of $1/R \sim 1.5 - 5$ TeV. The possibility of the existence of relatively low mass Kaluza-Klein excitations makes the phenomenology of near term interest. Some possible bilepton signatures can be searched for in future colliders and in neutrino scattering experiments with intense neutrino beams. The low energy constraints from muon physics and lepton number violating decay process induced by bilepton are also discussed. These constraints can provide new information on the structure of Yukawa couplings which might be useful for future model building.

Neutrino masses in 5D orbifold $SU(5)$ unification models without right-handed singlets

(*W.-F. Chang, J.N. Ng*)

We explore a mechanism for radiatively generating neutrino Majorana masses in a 5 dimensional orbifold $SU(5)$ unification model without introducing right-handed singlets. The model is non-supersymmetric and the extra dimension is compactified via a $s_1/(Z_2 \times Z'_2)$ orbifold geometry. The necessary lepton number violating interaction arises from the Yukawa interactions either between a 10-plet or a 15-plet bulk scalar field and the fermion quintuplets which are residents on the $SU(5)$ symmetrical brane located at one of the orbifold fixed points. The model is engineered to give realistic charged fermion masses and mixing and at the same time to avoid the rapid proton and neutron decays by geometric construction. The gauge unification can be maintained by adding extra fermion or scalar fields. The unification scale is found to be larger than 10^{15} GeV by adding a bulk vector decuplet pair whose zero mode has masses around the $10 \sim 100$ TeV range. We found that neutrino mass matrix of the normal hierarchy type is favoured by using 15-plet scalar. We give a solution of this type which has detectable $\mu \rightarrow 3e$ transition. On the other hand, by introducing 10-plet scalar, the leading neutrino mass matrix can only be inverted hierarchical and gives at most bi-maximal mixing.

Sleptogenesis

(*R. Allahverdi; B. Dutta, Regina; A. Mazumdar, McGill*)

We propose that the observed baryon asymmetry of the universe can naturally arise from a net asymmetry generated in the right-handed sneutrino sector at fairly low reheating temperatures. The initial asymmetry in the sneutrino sector is produced from the decay of the inflaton, and is subsequently transferred into the standard model (s)lepton doublet via three-body decay of the sneutrino. Our scenario relies on two main assumptions: a considerable branching ratio for the inflaton decay to the right-handed (s)neutrinos, and Majorana masses which are generated by the Higgs mechanism. The marked feature of this scenario is that the lepton asymmetry is decoupled from the neutrino Dirac Yukawa couplings. We exhibit that our scenario can be embedded within minimal models which seek the origin of a tiny mass for neutrinos.

Cosmological bounds on large extra dimension models

(*R. Allahverdi; C. Bird, S. Groot Nibbelink, M. Pospelov, Victoria*)

The existing cosmological constraints on theories with large extra dimensions rely on the thermal production of the Kaluza-Klein modes of gravitons and radions in the early universe. Successful inflation and reheating, as well as baryogenesis, typically requires the existence of a TeV-scale field in the bulk, most notably the inflaton. The non-thermal production of KK modes with masses of order 100 GeV accompanying the inflaton decay sets the lower bounds on the fundamental scale M_* . For a 1 TeV inflaton, the late decay of these modes distorts the successful predictions of Big Bang Nucleosynthesis unless $M_* > 35, 13, 7, 5$ and 3 TeV for 2, 3, 4, 5 and 6 extra dimensions, respectively. This improves the existing bounds from cosmology on M_* for 4, 5 and 6 extra dimensions. Even more stringent bounds are derived for a heavier inflaton.

Leptogenesis from a sneutrino condensate

(*R. Allahverdi; M. Drees, Munich*)

We re-examine leptogenesis from a right-handed sneutrino condensate, paying special attention to the B -term associated with the see-saw Majorana mass. This term generates a lepton asymmetry in the condensate whose time average vanishes. However, a net asymmetry will result if the sneutrino lifetime is not much longer than the period of oscillations. Supersymmetry breaking by thermal effects then yields a lepton asymmetry in the standard model sector after the condensate decays. We explore different possibilities by taking account of both the low-energy and Hubble B -

terms. It will be shown that the desired baryon asymmetry of the Universe can be obtained for a wide range of Majorana mass.

Modulated cosmological perturbations

(R. Allahverdi; L. Kofman, M. Peloso, CITA)

In an alternative mechanism recently proposed, adiabatic cosmological perturbations are generated at the decay of the inflaton field due to small fluctuations of its coupling to matter. This happens whenever the coupling is governed by the vacuum expectation value of another field, which acquires classical fluctuations during inflation. We discuss generalizations and various possible implementations of this mechanism. In many cases the second field can start oscillating before perturbations are imprinted, or survive long enough so as to dominate over the decay products of the inflaton. The primordial perturbations are then modified accordingly in such cases.

Leptogenesis in extra dimensions without a right-handed neutrino

(R. Allahverdi, W.-F. Chang)

As originally proposed by Zee, light neutrino masses can be generated by adding new Higgs fields (instead of a right-handed neutrino as in the see-saw mechanism) to the standard model. It is also possible to produce a lepton asymmetry in these models from

the decay of a heavy Higgs field with lepton number violating interactions. This, however, requires that at least two copies of that field be introduced. Recently, Zee-like models have been constructed in five dimensions which generate preferred neutrino masses and mixings. We show that leptogenesis with only one copy of Higgs is possible in these models, provided that it is a bulk field and fermions are localized in different positions along the fifth dimension.

Miscellaneous

JaxoDraw: a graphical user interface for drawing Feynman diagrams

(D. Binosi, Trento; L. Theussl)

JaxoDraw is a Feynman graph plotting tool written in Java. It has a complete graphical user interface that allows all actions to be carried out via mouse click-and-drag operations in a WYSIWYG fashion. Graphs may be exported to postscript/EPS format and can be saved in XML files to be used in later sessions. One of the main features of JaxoDraw is the possibility to produce \LaTeX code that may be used to generate graphics output, thus combining the powers of \TeX / \LaTeX with those of a modern day drawing program. With JaxoDraw it becomes possible to draw even complicated Feynman diagrams with just a few mouse clicks, without the knowledge of any programming language.

EXPERIMENTAL FACILITIES

Proton Irradiation Facility

(*E.W. Blackmore, TRIUMF*)

During the year there were six scheduled periods for proton testing on the low energy beam line BL2C, and during two of these periods the high energy beam line BL1B was also available. In addition the recently commissioned TNF neutron facility was used for single event testing by two outside groups.

The group from Sandia National Laboratories and CEA in France carried out Expt. 948, Proton Radiation Effects in Silicon-on-Insulator and Bulk-Silicon Devices, in two beam periods, one on BL2C at lower energies in May, and then on BL1B at energies up to 500 MeV in December. This experiment had a number of studies, including investigating the change in sensitivity of ICs to single-event latchup after extended proton irradiation. This group and the group from the Naval Research Laboratory used the higher fluence capability of both beam lines to irradiate at fluences up to 10^{14} protons/cm² at rates above 10^{10} protons/cm²/s. The NRL group irradiated GaAs solar cells at energies of 115 MeV and 50 MeV. The Sandia group also used commercial time for single event testing of various devices.

Table XX lists the proton flux and beam sizes for the high intensity set-up with a range of scatterers.

Groups from MD Robotics visited the facility four times during the year, testing components of a LIDAR system, and various other cards and devices. A special set-up with a 15 cm by 15 cm beam spot was developed for one test. Other Canadian space companies using beam this year included UTIAS, XIPHOS, Bristol Aerospace and ABB Bomem.

The high energy beam time in September was used by two groups, one from Bubble Technologies, Inc. (BTI), to test a new design of neutron spectrometer for space, and the other from Johns Hopkins University Applied Physics Laboratory to measure neutron energy spectra after 200–500 MeV protons strike different shielding materials. The BTI test required very low fluxes to below 10^3 protons/cm²/s. Another challenge was to reduce the effect of the 7–8 G cyclotron fringe field on the performance of the spectrometer, which used unshielded PMTs for readout.

The ATLAS group from the University of Alberta also used the beam session in September at lower energies for further testing of the readout electronics for the liquid argon calorimeters.

In May members of the Sandia group carried out a series of neutron single event effect tests using the TNF neutron beam line. Devices to be tested are lowered 5 m down a vertical slot in the TNF shielding to

Table XX. Proton flux and beam size measurements.

Beam line	Test	Range shifter or	Scatterer	Proton flux	Beam size	
Energy	I_{\max}	energy	material	per nA	80% uniform	
MeV	nA	MeV	thickness mm	cm ⁻² s ⁻¹ × 10 ⁸	X mm	Y mm
<u>BL2C</u>						
70	10	63	0	0.8 Pb	1.4	25
		52	15.5*	0	24	7.3
		50	15.5*	0.3 Cu	6.0	10
		50	780	0.8 Pb	1.1	28
116	6	115	0	0	41	5.4
		115	0	0.3 Cu	29	6.4
		111	0	0.8 Pb	6.2	16
		105	0	2.4 Pb	1.6	27
		85.5	2000	2.4 Pb	1.3	>27
		67	3800	2.4 Pb	1.1	>27
<u>BL1B</u>						
200	4	198	0	0.63 Pb	3.5	19
354	3	352	0	1.3 Pb	3.5	25
493	2	491	0	1.3 Pb	5.0	19

*Lucite absorber placed directly in front of test point

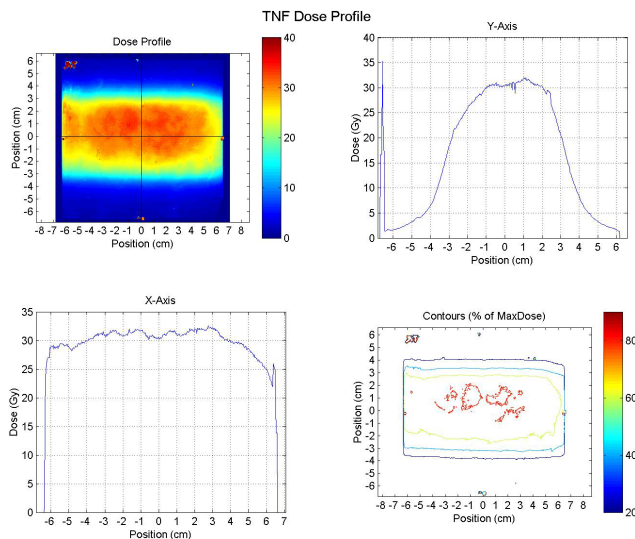


Fig. 182. The neutron beam profile at the TRIUMF neutron facility obtained by exposing GafChromic film at the test location.

intercept the neutron beam that is about 5 cm high and 12 cm wide (see Fig. 182). The flux of >10 MeV neutrons is 4×10^6 neutron/cm²/s at a BL1A current of 140 μ A. A unique feature of this beam is that it also contains thermal neutrons with a flux of 1.2×10^6 neutron/cm²/s. The sensitivity of devices to thermal neutrons can be tested by measuring the SEU rate with and without a cadmium absorber covering the device. The difference is due to thermal neutrons. Figure 183 shows such a measurement made by the Sandia group. This figure also shows the agreement between the SEU rate measured at the WNR facility in Los Alamos and TRIUMF. The data agree when the WNR fluxes are multiplied by a factor 0.75. In both cases the calibration is for neutrons above 10 MeV. The difference is

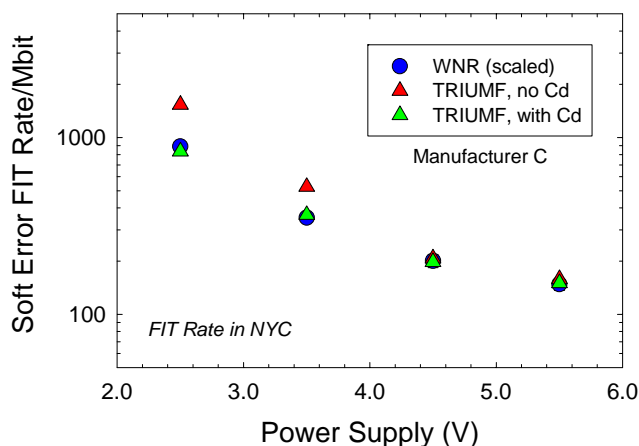


Fig. 183. Neutron-induced SER vs. power supply voltage in 4-Mbit SRAMs. The WNR data were multiplied by 0.75 to match the TRIUMF data. Note increased SER at low power supply due to thermal neutron contribution in TRIUMF spectrum.

partly due to the fact that the WNR neutrons extend to 800 MeV while the TRIUMF neutrons go to 450 MeV.

A similar set of measurements was carried out by the group from the Boeing Radiation Effects Laboratory in Seattle.

A paper titled “Improved capabilities for proton and neutron irradiations at TRIUMF” was presented at NSREC’03 and published in the IEEE Radiation Effects Data Workshop.

Proton Therapy Facility (E.W. Blackmore, TRIUMF)

In 2003, there were 12 patients treated with protons during the seven scheduled treatment sessions. This brings the total number of patients treated at TRIUMF to 89 as shown in Fig. 184. This year all of the patients were treated for a choroidal melanoma.

The PC version of EYEPLAN, obtained last year from the Clatterbridge group in the UK, was used for the planning of patients. This PC version is much more user friendly than the previous VAX version. The tumour contouring and editing tools are more flexible and simpler to use. The X-rays taken for simulation can be scanned and digitized directly on the computer screen. This is much quicker and more reliable than the previous use of the digitizing tablet. The PC version also incorporates special features to plan for iris and ciliary body melanoma, thereby increasing our patient base.

The only interruption to treatments during the year was failure of the X-ray equipment on the scheduled simulation day in October. This equipment was installed in 1994 and had experienced no prior problems. The fault was corrected by the next morning. It was due to a corruption of data in the permanent memory of the X-ray controls, and it is not clear if this was due to an upset error from earlier running for PIF or due to a battery charging problem.

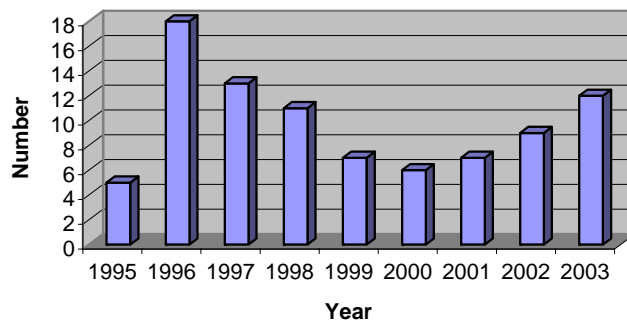


Fig. 184. Proton patients treated at TRIUMF.

μ SR User Facility

(S. Kreitzman, TRIUMF)

Overview

Operations The μ SR user facility operations in 2003 was a function of beam line availability and systems reliability. The former circumstance was characterized by the use of M20 during the first four weeks for tests on muon cooling. In the latter case the familiar situations concerning cyclotron operations were supplemented by the appearance of a leak in the final silver sintered heat exchanger in the DR (dilution refrigerator) just as it was being set down onto beam line for its summer run. This led to a hasty rescheduling of HiTime into the 6 weeks originally allocated to the DR. Successful repairs to the DR allowed those users who experienced the loss of that spectrometer in the summer to recoup it on a priority basis in the autumn. To that end, 62 beam weeks of μ SR experiments were carried out. The major spectrometer utilization was found to be (all in weeks) HiTime 20, LAMPF 17, Helios 14, DR 6, and SFUMU/OMNI' 5. In addition, 9 weeks of β NM/QR were carried out in the low energy ISAC facility.

Proposals, funding and future plans New and ongoing μ SR experimental programs continue on their course. As in the previous year, 19 new proposals were submitted during the two semi-annual Experiments Evaluation Committee reviews. With respect to funding, a new MFA (Major Facility Access) grant application was prepared and submitted to support the facility operations for the three fiscal years beginning April 1, 2004. Also, TRIUMF and the facility were part of a major condensed matter physics CFI (Canadian Foundation for Innovation) application sourced at McMaster University.

This year's MFA application (with its CFI counterpart) had a markedly different emphasis than recent predecessors insofar as it marked a quantum leap in the quantity and nature of the requested support. The prime factor motivating this approach is the significant role that μ SR assumes in TRIUMF's new 5 Year Plan (<http://tcmmms.ca/intro/ppt/TCMMS-Jeff/img0.html>). The interested reader will first notice a new name for the facility – now to be called the TRIUMF Centre for Molecular and Materials Science (<http://tcmmms.ca/>), a name inclusive to the science which is served by the current μ SR, β -NMR and β -NQR program. More to the point, however, is the substance of TRIUMF's plan which includes approximately \$6.3 million in capital spending to increase and enhance μ SR capability from T2 (see Fig. 185). Two additional surface muon beam lines are planned; one at the current location of M9A, the other a kicked Muons on Request (i.e. MORE) beam line. Fundamental flux, luminosity and transmission enhancements will come

from a redesigned T2 target and the use of dual compensated separator pairs for M20 and the new M9A.

The underlying scientific motivation for all this activity is simply the rapid growth of the number of (primarily Canadian) μ SR scientists who want to work in the field. This group now includes a rapidly expanding component of scientists who are not μ SR trained. To this end the design and operational mandate of the new M9A beam line will be to provide turnkey μ SR capability to an international community of the condensed matter researchers that are not μ SR cognoscenti. The modernization of M20, with high laminotomy and MORE, will further provide the community with the resources to carry out state of the art experiments on small samples and/or for longer times.

This scientific case, coupled with TRIUMF's adoption of an aggressive μ SR expansion in the upcoming 5 Year Plan, have together formed the underlying justification for the much broader MFA request. TRIUMF further provided the 60% matching funds commitment that is required for its portion of CFI request, an equipment grant which is meant to fund the new M9A spectrometer.

Facility developments

The major facility developments which highlighted the year were:

- Spectrometers: OMNI', Helios, DR, and HiTime update.
- Universal mounting system (UMS).
- Experimental control enhancements.
- Data acquisition hardware; the NIM I- μ SR module and the β -NQR frequency synthesizer.

The following report outlines these and related developments more fully.

Spectrometers

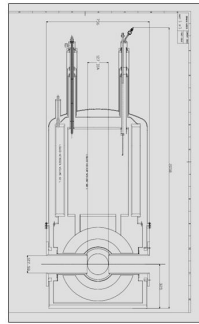
OMNI' The road to a new OMNI' spectrometer is progressing. The frame is built and the tables design is finished. Final detailing of the counter mounts should be completed by the first quarter in 2004.

Helios Helios has been adapted to run in M9A, and its initial run there was very successful. Maintenance to address the small helium leak, comprehensive temperature monitoring, and installation of vapour cooled superconducting leads is scheduled.

DR For the third time in its operational history, the DR developed a leak in the silver sintered heat exchanger which feeds into the dilution chamber. The occurrence of a leak just as the spectrometer was being set down into the M15 beam line for its spring scheduled run resulted in the last minute replacement of six weeks of DR experiments by ones which used HiTime.

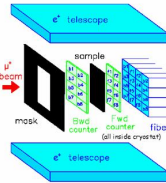


New μ SR Beam Lines and Facilities



M9A

- General condensed matter community user friendly spectrometer
- Dual access 2T magnet / axial & side entry / TF & LF optimized
- Fully automated and facility scientist supported infrastructure
- Multi use inserts supporting multiple pixel μ SR

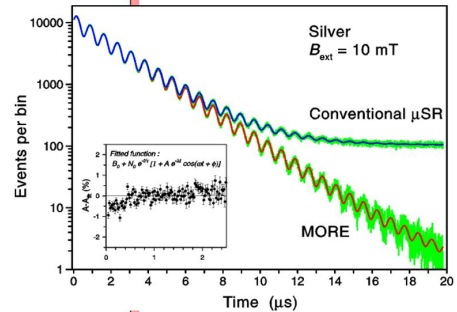
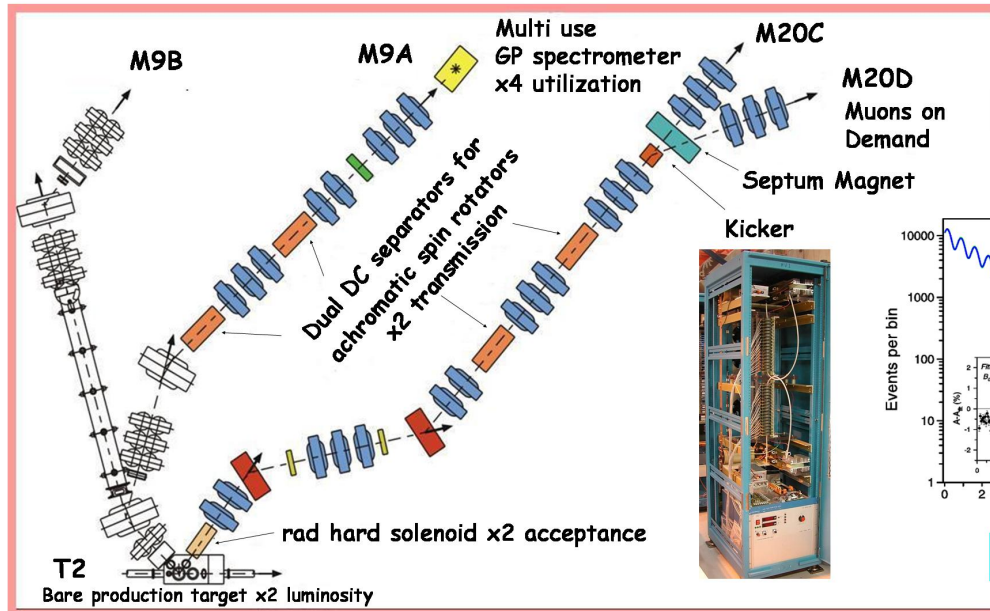


M20C

- High intensity general purpose beam line: Helios, Omni, SFUMU, Omni', Lampf, Virgin (VSU DR),
- 90° achromatic spin rotator / separator

M20D

- Muons on Request (MORE)
- Ultra low backgrounds — long time μ SR
- High efficiency muon utilization factor



More demonstrated at the PSI MuSR facility.

Fig. 185. A representation of the major μ SR related items which TRIUMF has included in its current 5 Year Plan.

The leaks in this unit are occurring more frequently, each incident coming in about 50% of the previous time interval. Thus the first leak took about 6 years to manifest, the second three years after that, and the most recent leak, less than two years after the second one. The leaks are all scattered about a small area close to the original leak. A new heat exchanger (from Walter Hardy's UBC laboratory, see Fig. 186) seems to have been found and may provide an avenue to permanently repair the problem. Otherwise, the VSU DR will be retrofitted to become the operational μ SR spectrometer for ultra low temperature physics.

HiTime Injecting the muon beam on axis into a high variable field spectrometer is a challenge if the geometry of the field distribution does not show perfect azimuthal symmetry. Due to the use of partially magnetic stainless steel in some aspects of the magnet construc-

tion, this is a problem which must be coped with in this spectrometer. The issue is further complicated by the fact that the wandering of the incoming muon beam is very field dependent. Our first approach was simply to mount the cryostat on an $X - Y$ table so that it could be moved to a position centred on the current beam location, but this approach results in the sacrifice of some homogeneity. A more successful strategy has now been found which has reduced the problem significantly. We have mapped both the fringe and central field regions to determine the locus of points which acts as the *significant* field axis. Adjusting the muon beam injection along this axis has substantially solved the injection problem, resulting in a radial beam wandering of less than ± 1 mm at all field values.

A program to enhance the timing resolution of this instrument is also proceeding.

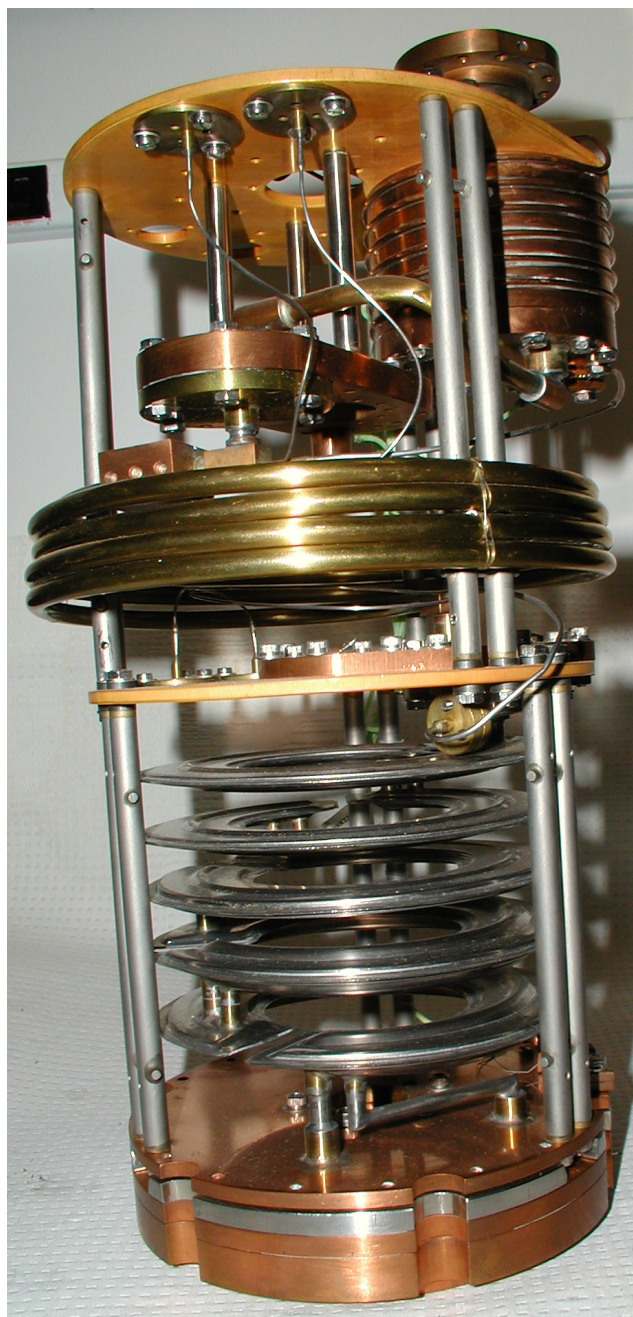


Fig. 186. A photograph of an unused, but with suitable vintage, dilution unit found in catacombs of the UBC Physics Department. It may prove to be transplantable into our current DR which is showing periodic arterial cryogenic failure.

μ SR universal mounting system (MuUMS)

The mounting of the plethora of cryostats, ovens, rf, and other specialized inserts into the various spectrometers has always been somewhat ad-hoc. We have now designed a universal system in which all inserts can be easily and quickly mounted independent of spectrometer. This holder provides for easy height and angular theta/phi adjustment. Every insert has a customized

adaptor that mounts on the universal holder and every spectrometer has its own holder. In those circumstances where two inserts must be mutually swapped during the run, each can be pre-aligned and reproducibly set down on the MuUMS holder at any time (see Fig. 187).

Experimental Controls

The facility has expanded its temperature control and monitoring equipment with the addition of a Thermo Haake Phoenix P1 circulator, and two multi-sensor Lakeshore 218 temperature monitors to be used with the Helios magnet and the Miss Piggy cryostat respectively (see Fig. 188).

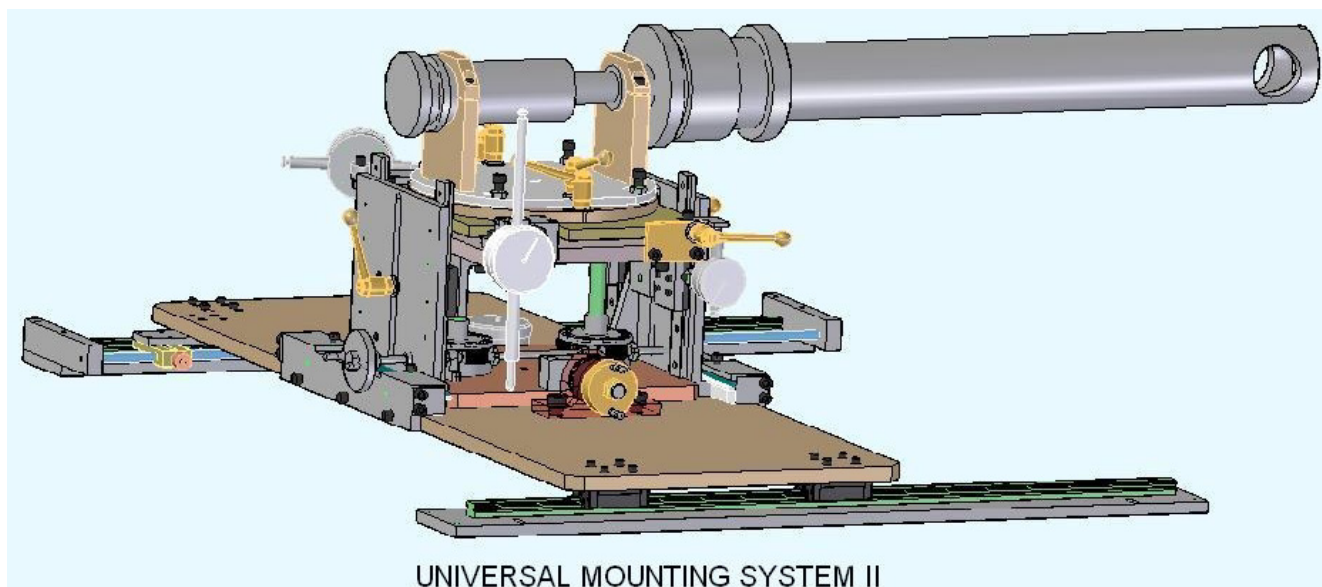
DAQ

Integral μ SR (I-muSR) now boasts a user interface that is integrated with the new Linux/Tkl GUI style that has proven to be so efficient and effective for the time differential μ SR experiments. Hardware enhancements have also been made. For I-muSR, the large number of NIM modules required to provide a general functionality has been replaced by one unit that was specifically designed for work with the VME GGL board (see last year's Annual Report). This provides a permanent I-muSR set-up for each area with enhanced functionality, specifically the capability of three levels of looping coupled to three different external experimental parameters, i.e. RF + EF + UV. For the β -NQR program an integrated frequency synthesizer/control device (Pol Synth) was designed and built. Complex modulation capabilities, coherent frequency sweep and external gating capabilities have all been built into the device (see Figs. 189 and 190).

Future perspectives

As mentioned above, this is the last year that the μ SR user facility name will grace the activities of the TRIUMF Centre for Molecular and Materials Science. Attendant with this name change is a purposeful change in orientation, one which will support a broader scientific community access to μ SR resources. The degree and speed at which this can be carried out depends in part on the success of the current MFA and CFI funding initiatives. The former will primarily provide for the manpower required to fully support users from outside the μ SR community while the latter will contribute to the construction of a state of the art μ SR spectrometer on the new M9A beam line proposed in TRIUMF's upcoming 5 Year Plan.

Regardless of the outcome of these important funding decisions, the facility will continue to provide innovative avenues to enhance the experiment capabilities which it can provide. In particular, plans for an axial ultra low background set-up, and a dedicated 4-pixel



UNIVERSAL MOUNTING SYSTEM II

Fig. 187. A 3-D rendering of the μ SR universal mounting system (MuUMS) with a typical axial cryostat attached.



Fig. 188. A modern temperature controlled circulation system (Thermo Haake Phoenix) widely used in the chemistry program to control sample temperature from -40 to 200°C .

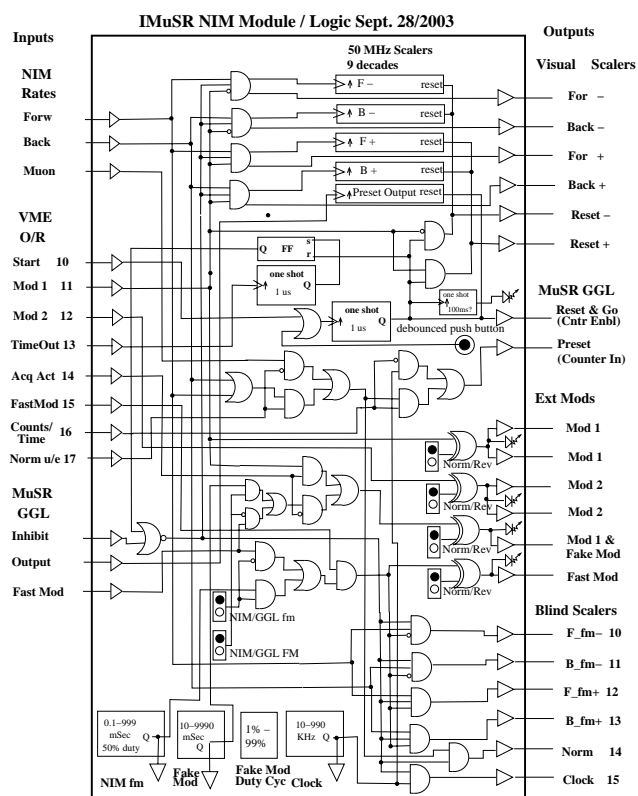


Fig. 189. The logic functionality contained in the I- μ SR NIM module that provides the new I- μ SR DAQ hardware.

version of the Multi insert will add additional capabilities to measure very small samples and efficiently carry out time differential experiments. The possibility of providing a He-3 cryogenic system for those experiments that would like to operate conveniently in the 0.3–100 K temperature range is also being considered. Further instrumental infrastructure support for the Physical Chemistry program will also be implemented.

The μ SR \rightarrow TCMMS facility therefore looks forward to a very dynamic juncture in its evolution and will, under any circumstance, continue to provide and facilitate access to the μ SR and β -NMR facilities at TRIUMF.

Facility information and documentation

Please refer to our Web site <http://musr.triumf.ca> for full access to a broad range of facility resources and information.

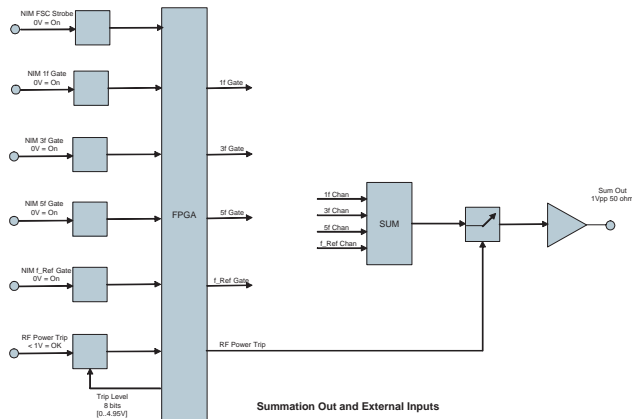
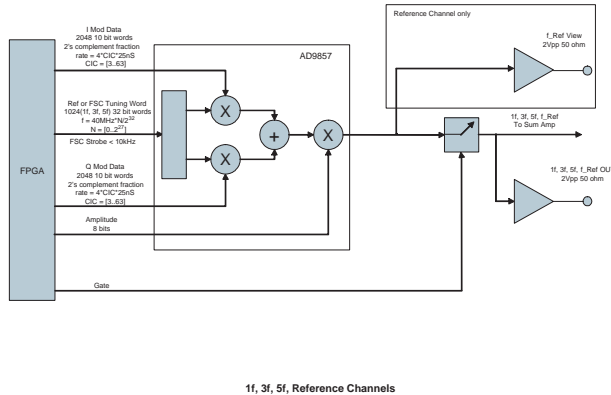


Fig. 190. The functionality of the β -NQR frequency synthesis and control VME board.

Cryogenic Targets

(C. Marshall)

Horizontal liquid hydrogen target

Installation and running was completed for a horizontal liquid hydrogen target used in Expt. 744 at M9. The 0.5 l target, designed and built at TRIUMF, incorporated a low mass vacuum structure manufactured from high strength foam (Divinycell) with a Kapton skin. The structure allowed a 360° scattering of particles with no intrusion from massive posts to support the vacuum load. The target cell had to be inserted 1.2 m horizontally within the M9 spectrometer, and allow a 5 cm clear path axially through the target's vacuum and refrigeration structures.

Liquid hydrogen target for Expt. 874

A rotatable liquid hydrogen target was designed and built for the muon-scattering experiment, Expt. 874. The target was rotatable to give full-length or half-length of a 0.5 l target.

Liquid xenon detector

A liquid xenon detector was designed for research into developing a better PET scanning machine. It is hoped with this detector to double the resolution as obtained with existing PET equipment.

Cryogenic engineering

Design work was carried out for the cryogenic components being built for the ISAC-II accelerator. The design involved cryogenic heat load, and flow calculations which were used to size the helium liquefier, and associated cryogenic distribution piping.

Computing Services

(C. Kost, TRIUMF)

Overview

The event of the year was moving Computing Services from the chemistry annex to the new ISAC-II building. That the final switchover was accomplished over the weekend preceding April 1 with little disruption to the site speaks volumes on the careful planning, expertise, and dedication of all those involved. This involved not only moving the people but also all the network equipment and computers (especially the Web, mail, Windows, print, and application servers). It was also necessary to complete the network infrastructure, not only for the new data centre but also for the many users, experiments and laboratories that would be occupying the new building. This meant the new building had to be cabled and patched for nearly 500 network connections. This was successfully completed by the April 1 deadline. The move was not without irony, however. After years of dealing with air conditioning problems in the old facility, the dual air con-

ditioners in the new facility both broke down within hours of our moving in. It was even more ironic that this was mostly due to a single line of bad code in the air conditioner's control system.

The emphasis for the duration of the year was in upgrading the network as well as dealing with two highly successful workshops, GEANT4 in September and HEPiX/HEPNT in October.

The UBC-TRIUMF component of WestGrid, the core of which is the 1008 3.06 GHz Xeon CPU cluster called Glacier, has continued to have a number of teething problems. Nonetheless, a small number of Beta users, one being TWIST, have successfully used the new facility, which is scheduled to be in full production in early 2004.

IBM compute cluster

2003 saw the de-commissioning of the lin01 and lin01a public Linux compute machines. These machines were running the outdated Red Hat Linux 6.2 and needed both a hardware and software upgrade. One of the problems faced in providing a generic public computing environment for the TRIUMF site is that it needs major upgrades both in software and hardware at regular intervals. In the past, TRIUMF computing services has typically purchased a new machine consisting of the best hardware available at the time and installing the most recent CERN supported release of Red Hat Linux. The lifetime of such an investment was typically 18 months. This year a new approach was taken. It was decided to build a small cluster of Linux machines. This approach has several advantages: firstly, only one machine need be known to the TRIUMF site, namely the head node, additional nodes can be added to, and removed from, the cluster with almost complete transparency to the users. This increases computational resources as they are needed, or removes nodes when they fail, resulting in much greater flexibility and robustness. Only the head node needs to be managed and kept running at all times. For this reason the head node should be highly reliable, consisting of hardware raid, redundant power and a responsive support contract.

One might think that the head node should be upgraded at the same 18 month interval as in previous years. However, by implementing the Openmosix kernel, as we have done, this is no longer a necessary requirement. An Openmosix kernel is a modified Linux kernel that allows automatic process migration to participating cluster nodes. That is, when a user logs on to the head node, the processes started by that user will migrate automatically to the other nodes in the cluster, maintaining an even load across the cluster. As the computing demands increase, more compute nodes can be added to the cluster. This is not your

traditional batch compute cluster, for if it were, then the head node would most likely need upgrading as in the past, since all interactive usage is constrained to the head node. By taking advantage of Openmosix, it is possible to spread the interactive usage across all nodes in the cluster.

In addition to the automatic migration properties of the cluster, it can also run as a traditional batch compute cluster, which most users are more familiar with. The cluster, which consists of six IBM x330's, having dual 1.4 GHz PIIs, with 512 MB memory, also runs the PBS queuing system. This same queuing system is used on the large WestGrid cluster. It can do this by turning off or suspending the process migration properties of various cluster member nodes when PBS jobs have been submitted to them. This gives some cluster nodes the ability to run exclusively single large computational intensive applications, without affecting the responsiveness of interactive processes, such as PAW, Netscape and ROOT.

This ability to perform as a traditional batch compute cluster as well as an automatic load sharing interactive cluster, is both unique and advantageous. It allows TRIUMF computing services to grow the cluster as required with minimal effort and transparency to the user community. It also improves the reliability of the computing environment and abandons the expensive and disruptive tear-down and rebuild approach we have taken in the past.

Servers

Figure 191 shows the main components of the computing services facility – notably the time, name, backup, mail, print, Web, file, application, and compute servers now located in ISAC-II. These servers are periodically upgraded to meet increasing demands of the user community.

To provide an alternative to sending large e-mail messages to multiple recipients a server, TRSHARE, which is both a file and Web server for use by everyone with an e-mail account, has been commissioned. It has a terabyte of raided disk space (with a hot spare). Web access can thus be used for global sharing of files. TRSHARE can serve clients under Windows, Mac, and Linux (via Samba). It is hoped that this will relieve some of the CPU and storage requirements on our mail server.

Network

In September, 2002 TRIUMF's Network and Computing Services took part in the world's first inter-continental high-speed, large-volume data transfer using an end-to-end (e2e) light path between TRIUMF and CERN. As part of these trials, TRIUMF had the opportunity to upgrade its WAN connection to the



Fig. 191. Computing services servers.

Internet. A coarse wave division multiplexer (CWDM) capable of carrying four 1 Gbps wavelengths over a single pair of fibres was purchased which currently provides separate services for (a) research and educational Internet traffic, (b) traffic to WestGrid, (c) end-to-end light path tests and high-speed large volume data trials, and (d) a wavelength reserved for commercial and commodity traffic which is currently carried by a separate 100 Mbps fibre link to UBC.

However, as of April, 2004 the commodity traffic will need to be moved to the fourth wavelength and at that time all of TRIUMF's Internet traffic will be on a single point of failure circuit which will be difficult to repair in a timely manner. To correct this vulnerability it is planned to purchase new equipment, as soon as possible, which will not only cost less than having a hot spare of one end of the existing hardware, but will

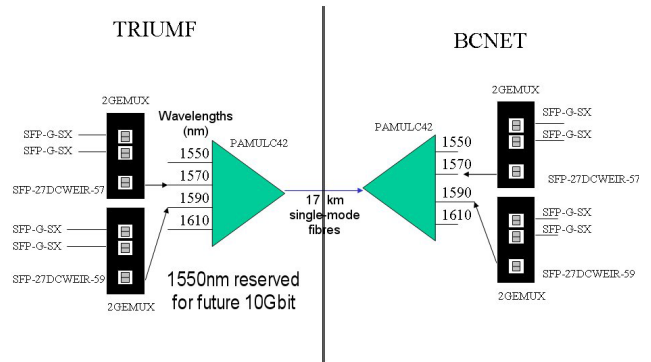


Fig. 192. Proposed CWDM solution.

provide growth to using 10 Gbps technology as well as allow capacity upgrades, while preserving the existing equipment as hot spares. The components are shown in Fig. 192.

Note that not only is the fibre multiplexed by using multiple wavelengths, but each wavelength is further time-division multiplexed by having two (SFP-G-SX) 1 Gbps circuits placed on each wavelength (each wavelength now handling 2.5 Gbps instead of just 1 Gbps on the current CWDM). It has been indicated that in the future it will be possible to do all this over a single fibre. Presently two fibres are used, one for sending and one for receiving the data. Essentially this would double the network capacity, yet again!

TRIUMF's Internet contract was also renegotiated through BCNET and not UBC. The 100 Mbps link to UBC, currently carrying TRIUMF's commercial and UBC traffic will be maintained but is currently unallocated. However, as of April 1, 2004, the commodity traffic will be moved onto one of the ports on the CWDM and the UBC traffic will be routed onto the research link. While this is a significant and desired improvement for all of TRIUMF's research and educational traffic, it has a potentially dangerous consequence for TRIUMF's commercial network traffic. As of April 1, 2004, TRIUMF will be volume charged for its commercial Internet traffic. Typical rates for commercial (or commodity traffic as it is sometimes called) is \$1 k per 1 Mbit of sustained traffic per month. With a gigabit connection to the Internet it is clear that TRIUMF needs to rate limit the traffic over this link. A 10 Mbps sustained network transfer over the commercial link for more than 36 hours would result in a monthly billing of \$10 k. Fortunately, all of TRIUMF research and educational network traffic is not volume charged; it is this research traffic which is generally the source of the large network transfers. However, applications such as Kazaa and E-donkey (which are contrary to TRIUMF's usage policy), typically associated with music and video file sharing as well as some Internet

radio stations that use the chain casting technology, can result in large network transfers over the commercial link. If left unchecked, as mentioned above, this could result in significant costs to TRIUMF. To address this concern, TRIUMF network services has installed a Linux machine at the network border that rate limits all commercial Internet traffic. Unwanted peer-to-peer file transfers can now be readily identified and tagged so as to limit their bandwidth to 100 Kbps. At present the rate limiting is relatively simple. However, if the situation becomes more complex requiring advanced packet shaping, protocol prioritizing and detailed analysis of Internet traffic, a commercial product may be necessary.

With the exception of the move from the chemistry annex to ISAC-II, the TRIUMF network infrastructure saw little fundamental change this year. Over the past four years TRIUMF network services has been migrating from an FDDI shared 10 Mbit topology to a switched Ethernet network with a gigabit backbone and 100 Mbit connectivity to the desktop. The migration has all but been completed with the exception of a few locations, namely the machine shop and a few locations in meson and proton annexes. It is estimated that 99% of the nodes at TRIUMF are now on the new network with 100 Mbit switched connections to the gigabit backbone. The remaining machines are still on the older 10Base2 shared 10 Mbit connections. A number of high demand areas such as ISAC-I and the second floor of the main office building were upgraded. The new high density, low profile, Nortel BayStack 470 switches replaced the older 450 switches. This enabled these locations to be completely re-cabled, leaving additional room for improved cable management. Previously, cable management was virtually non-existent in these wiring closets. In the case of the second floor of the main office building this resulted in a tangle of over 200 CAT5 network cables. This made it virtually impossible to trace and troubleshoot some network problems. A similar situation existed in ISAC-I, where the demand for network connections was initially underestimated, and additional connections were added in ad hoc fashion. The experience gained in improving the network core in these areas will be applied to other areas of the TRIUMF site in 2004, namely trailers Hh, Ff and the ground floor of the main office building. The decision was also made to activate every wired Ethernet port, thereby removing the confusion over which ports were enabled.

An important expansion to the TRIUMF core network this year was the addition of a dedicated 1 Gbps network connection to the 1008 3 GHz Xeon processor WestGrid computing cluster, with 10 Tbytes of disk and 108 Tbytes of tape storage at UBC, and 24 Tbytes

of disk and 135 Tbytes of tape storage at SFU. This was made possible because of the four-port CWDM described earlier. At the same time a second Nortel Passport router was purchased which allowed TRIUMF to separate the WAN (wide area network) connections from the LAN (local area network) connections. This was an important separation, as it allowed changes on the WAN router to be applied without affecting the local area traffic around TRIUMF. A third Nortel Passport router has been purchased for 2004. This will allow Network Services to add redundancy and reliability to the LAN network core. Details of our current configuration and further upgrades are shown in Fig. 193.

Computer security

As part of our “disaster recovery” plan, the most vital systems (Mailserver and Webserver) are now nightly backed up (RSYNCing) to other (slower) machines located in a different building and could be used for system recovery if disaster struck these servers. Slightly less critical machines (name and CUPS print servers) have their important files backed up every day. All this is in addition to our usual tape backup procedures.

Since air conditioners have by their nature been unreliable, networked sensors now monitor the main computing room temperature at two key locations and

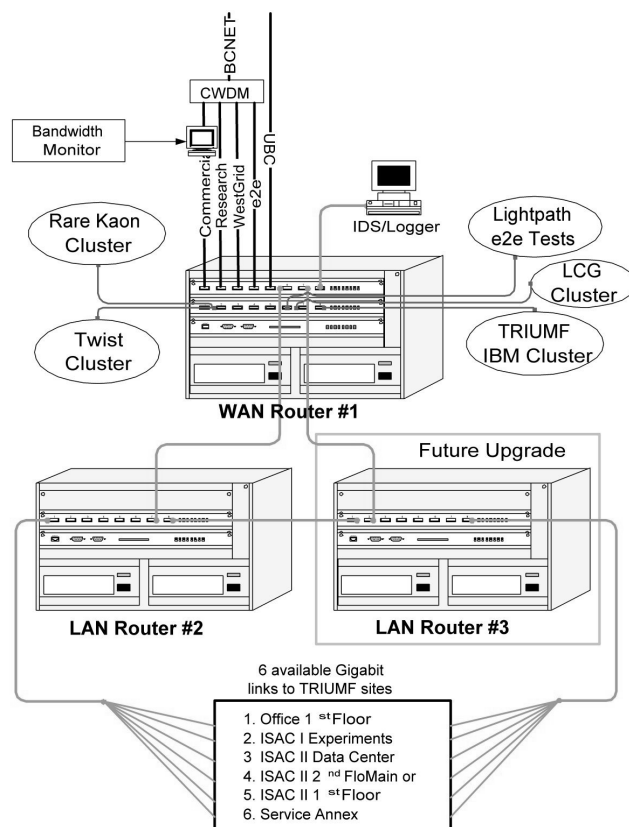


Fig. 193. Core network upgrades.

allow for e-mail and paging to alert staff should the temperature go outside the acceptable range.

On Friday, January 24 TRIUMF was hit by the Slammer worm. This was a rapidly spreading network worm affecting machines running Microsoft SQL server. Although only two machines on site were infected, the resulting large amount of traffic generated essentially halted the TRIUMF network overnight until the machines could be physically disconnected.

In the aftermath of this incident, we implemented procedures for notifying key personnel after hours independently of the network.

In August TRIUMF was affected by the Blaster worm, which affected machines running Microsoft Windows file sharing services. This occurred when some key personnel were on vacation but on-site staff were able to contain the problem. The network performance was unaffected but a large number of machines required updates. Though direct infection from the Internet was not possible, since we block these services from off site, it is believed that some infection occurred as a result of infected laptops being brought on site and connected to the TRIUMF network.

The PC Support group has installed a central server for Symantec AntiVirus. This allows efficient management of (about 250) systems running Microsoft Windows and for timely notification of infected systems. Together with the antivirus filter on the TRIUMF mail server this provides effective protection against the current generation of e-mail-borne viruses and worms – ones that require some human interaction (opening a message) to spread.

TRIUMF, and indeed all networked organizations, continues to be vulnerable to so-called Zero Day viruses and worms – a virus which is released as soon as a vulnerability is discovered, giving organizations no time to design and implement a patch.

In December an on-site machine was broken into and some critical passwords obtained. Over the Christmas vacation these were used to run an IRC chat room from a TRIUMF machine. No damage was done and security procedures have been re-evaluated.

The virus filter on the TRIUMF mail server reported some 19,000 infected machines to administrators during 2003, up from 900 in 2002.

Our computing security officer attended courses on computer security given by an internationally recognized organization, Global Information Assurance Certification (GIAC). The officer was awarded the GIAC Security Essentials Certification (GSEC) on September 30.

E-mail Again, TRIUMF continues to receive an ever-increasing amount of unsolicited commercial e-mail, or spam. The anti-spam tool SpamAssassin was upgraded

in 2003 to a later version with some enhanced features. Nevertheless, some inappropriate mail escapes the filter. In 2003, one of the on-line databases (Osirusoft) which was used to help filter mail came under attack and was closed down. For a short period the service was marking all mail as spam, causing some inconvenience to TRIUMF users.

A scheme was implemented which temporarily rejects certain incoming mail messages which are believed to be spam, based on their address of origin. Since many spammers do not respond to temporary rejects this can result in a reduction of the amount of spam finally delivered. This method is used more aggressively at the University of Calgary, where all incoming mail is delayed unless from a trusted source. This marks a watershed in anti-spam measures at TRIUMF – previously we had immediately accepted all mail and relied on users to filter it if they wished.

Videoconferencing

A Webcast server was used to record and transmit a number of events, including the HEPiX 2003 conference, TUG meetings, and the EMMA workshop.

TRIUMF received funding from WestGrid to establish a facility, based on the Access Grid Project (see <http://www.accessgrid.org>) for collaboration and visualization. Our security officer built up this facility (the videoconferencing room) in the ISAC-II building. A plan view is shown in Fig. 194.

As provided by the contractors, the room was acoustically insulated from adjoining rooms but hard-surfaced and not an optimal shape for conferencing (rectangular). Acoustic panels and wall covering were installed to reduce echo and reverberation. The room has been set up to allow a variety of different video, audio and local conferencing methods to be used. Two high-quality (1280*1024) digital projectors each

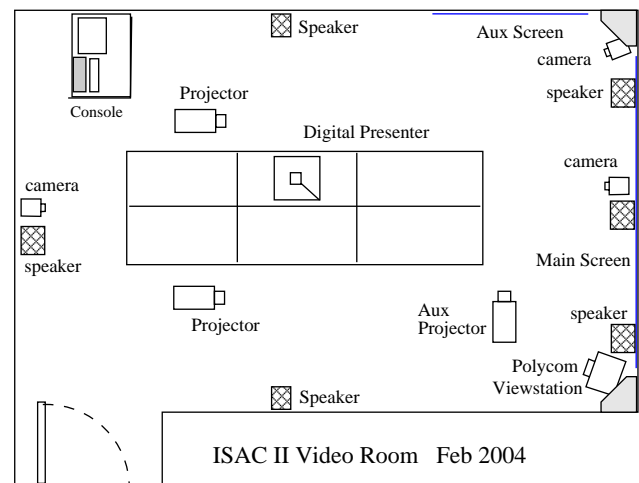


Fig. 194. Plan view of access grid facility for collaboration and visualization.

illuminate adjoining 2 m wide main screens while a third projector illuminates an auxiliary screen on the side wall. Each projector can be driven from a variety of sources including laptop computers. A multi-speaker surround sound system and multi-channel echo canceller with ceiling-mounted microphones allow sound from remote participants to be suitably positioned while ensuring adequate pickup from local participants around the room.

A “visual presenter” replaced the traditional overhead projector functionality for local meetings while allowing remote participants to see paper documents using a regular Web browser. ISDN and H.323 videoconferencing are provided by a Polycom Viewstation appliance; the ISDN telephone line has been rerouted to this room from its original location in the main office building.

VRVS and Access Grid conferencing are provided by a computer system which is capable of driving either one, two or all three projectors. All wiring is routed under the floor or above the ceiling to improve appearance and eliminate tripping hazards. The echo canceller, sound system and computers are located in an operator’s console in the corner of the room, together with a wireless hub which provides 802.11 network capability for laptops. A Bluetooth wireless keyboard and mouse allow the main computer system to be operated from the conference table. A “roomwizard” panel by the door shows bookings and integrates with the TRIUMF on-line room allocation service.

The room is being used regularly by several groups at TRIUMF.

Network measurements

We continue to participate in the SLAC Pinger and other network measurement efforts.

Software developments

Physica and other data analysis Physica is an internationally popular, general purpose data analysis/visualization program running on UNIX/Linux platforms. The port of Physica to the program Extrema on the Windows platform has progressed to the release stage. This Windows version has new improved features not found in the UNIX/Linux versions. Work has now begun on porting Extrema back to Linux and converting it into an Open Source project, making it even more accessible for world wide use.

Work was started on writing a GUI utilizing ROOT for display and analysis of MIDAS data. Rewriting of the analyzer code for the DRAGON experiment, originally written in C, is being rewritten in object oriented C++. Assistance, by writing several scripts, was provided to allow Physica to perform spectral analysis of experimental data. Assistance was also provided in the

conversion of neutrino simulation and analysis codes from the SUN-SPARC platform to Linux.

Beam dynamics

ACCSIM The multi-particle simulation code ACCSIM continues to be used in a wide variety of accelerator applications, principally for high-intensity proton synchrotrons and accumulator rings. The development of this type of simulation code, with self-consistent treatment of space charge, is now a very active field, as evidenced at the ICFA Mini-Workshop on Space Charge Simulation held at Oxford this year. A presentation on ACCSIM was given at this workshop and there was participation from many other institutions, with reports on new space-charge methods and advances in simulation software. One of the workshop goals was to produce a “master spreadsheet” of all known space-charge simulation codes, much of it done by direct interrogation of code authors or expert users who were present. The result can be found at [http://www.isis.rl.ac.uk/acceleratortheory/chris/Space Charge HALO03/Space Charge Spreadsheet.xls](http://www.isis.rl.ac.uk/acceleratortheory/chris/Space%20Charge%20HALO03/Space%20Charge%20Spreadsheet.xls).

Consultation and support activities with new and existing users continued. New ACCSIM applications emerging during the year included:

- High-intensity charge-exchange injection studies for the CERN PS booster;
- IHEP Beijing study of future Chinese Spallation Neutron Source rapid cycling synchrotron;
- Trapping in stable islands in the CERN PS;
- Intensity dependent emittance transfer in the CERN PS.

The latter two applications use a lattice description with nonlinear components based on measurements in the PS. Under an initiative from the ICFA workshop, this lattice, together with observation data from PS beam studies, will be used to benchmark and compare ACCSIM and other codes such as Orbit from ORNL. To accurately model the lattice requires adding a more general treatment of multipoles to ACCSIM, which is expected to be complete in early 2004.

Parallel Computing In conjunction with our contribution to the TRIUMF-CERN LHC collaboration beam dynamics tasks (reported elsewhere in this Annual Report), further experience in our group was gained with parallel computing on commodity clusters. The study of coherent beam-beam effects in the LHC involved large-scale multi-particle simulations with our parallel code BeamX, implemented on a small test-bed cluster at TRIUMF and on the THOR cluster at the University of Alberta Physics Department.

In the production phase of the study, jobs were run continuously in Vancouver and Edmonton over several weeks, with run control and analysis being done at CERN. With ~ 50 Mbytes of data being generated per run, it was important to come up with a simulation protocol which would ensure data integrity and streamline the run management and post-processing. The methodology that evolved, using ssh (with non-interactive authentication) and rsync (with ssh tunnelling) allowed data to be rapidly and securely replicated across platforms and gave immediate access to results via Matlab graphics. The existence of high-speed research networks connecting the three sites was of course a great boon to this project.

Late in the year, the first trials of this application were conducted on the new WestGrid facilities at the University of Calgary, utilizing an HP “CluMP” (cluster of multi-processors) alpha-based system. Initial timings (with the unmodified MPI-based code) showed up to a factor of 2 performance improvement. In 2004 we intend to test BeamX and other applications on the other WestGrid platforms (shared-memory and blade systems) as well, to find the best match to the computational problem.

RELAX3D Improvements were made to the GUI front-end for RELAX3D, the 3-dimensional electrostatic field solver still in frequent use at TRIUMF and many other sites. The GUI allows rapid and efficient control of most of the commonly-performed functions of RELAX3D and is particularly helpful for visualization of results. Automatic plot features, allowing one-click navigation and plotting of 2-d slices through the solution domain, were added to the internal graphics facility (contour plots) as well as to the external interface to Matlab (surface, contour, pseudo-colour and waterfall plots).

In the Matlab interface an intermittent problem with communication hang-ups between the GUI and Matlab was resolved, and erratic plot window updating in Matlab 6 was also corrected. An axis lock feature, for making series of commensurate plots, and support for multiple figure windows, were also added.

Printing A pilot study of two possible vendors of digital “all-in-one” printing, copying, sending (scanning) units, to both replace our aging analogue photocopy machines and high volume public printers resulted in a dead-heat tie and a lease of a Xerox 555 to replace one of the two main photocopy machines as well as the lease of a Canon Imagerunner 5000i to replace the ISAC-II central printing station. Response by the user community has been extremely positive and similar replacements are planned for 2004, possibly extending to colour capable units.

The capability to rapidly scan material and e-mail

the resulting pdf document, although currently limited to monochrome, has been particularly welcomed, as was the ability to scan a document only once to produce multiple copies, complete with optional hole punching and/or stapling.

To provide enhanced support for printing from Linux, the Common UNIX Printing System (CUPS) is now used for printing. It supports the new standard Internet Printing Protocol (IPP) which is now supported by nearly all printer manufacturers. With CUPS, users can now more readily manage and check their print status using their Web browser (eg. <http://cups:631>)

Miscellaneous Matlab 6.1 and Maple 8 were installed. These are site-licensed for unlimited use by both Linux and Windows environments. Due to high upgrade costs, Mathematica is now supported only as a legacy facility. Although not in the purview of our mandate, a novel way to address the need of multiple groups taking tours of the TRIUMF facility to be able to hear their guide, in what is often a very noisy environment, was to purchase 24 FRS (Family Radio Service, i.e. walkie-talkies) thereby enabling each tour member to clearly hear the presentations, no matter how distant they are from the speaker.

Data Acquisition Systems

(*R. Poutissou, TRIUMF*)

Overview

In 2003, the DAQ group introduced new systems for development of the TIGRESS detector and the T2K Neutrino group R&D while continuing to support a wide array of experimental groups and test stations. The DAQ group was involved in defining the next generation data acquisition system as a component of the Laboratory for Advanced Detector Development (LADD). The first phase of the development of MIROODAS, an on-line analysis package for replacement of NOVA, took place.

The TRIUMF data acquisition software package, MIDAS, is currently deployed over 34 stations managed by the DAQ group around the laboratory (see Table XXI). These machines also provide some off-line analysis resources and disk storage (see http://daq.triumf.ca/triumf_nodeinfo/).

MIDAS and MIROODAS

The core part of the MIDAS software has not changed much during this past year. There were minor changes, some bug fixes and support for new hardware. In particular, MIDAS was deployed and tested on a diskless VMIC/VME processor board. VMIC processors will be used in the future instead of PowerPC running the VxWorks operating system. Information about MIDAS can be found at <http://midas.triumf.ca>.

Table XXI. Computer systems managed by the DAQ group.

Name	Location	Type
isdaq01	ISAC-LE β NMR, TRINAT	2xPII/450
isdaq02	ISAC-LE, GP2, LTNO	PIII/500
isdaq03	ISAC-HE, TUDA	2xPIII/550
isdaq04	ISAC-HE, DRAGON	2xPIII/550
isdaq05	ISAC-LE, ISAC users	PIII/1000-256
isdaq06	ISAC-HE ISAC users	PIII/1000
isdaq08	ISAC-LE, 8π	2xPIII/1000
ltno01	LTNO CR DAQ	2xPIII/600
midtis01	TRINAT DAQ	2xPIII/550
midtis02	Detector Facility	Celeron 430
midtis03	LTNO platform DAQ	PII/350
midtis04	GP2 DAQ	2xPIII/550
midtis05	8π cryo	PII/300
midtis06	Neutrino Devel. DAQ	AMD/XP/350
midtig01	TIGRESS Devel. DAQ	2xAMD Ath/2000
midmes01	Detector Facility	PIII/500
midmes03	RMC DAQ	2xPIII/550
midmes04	M11 DAQ	PII/300
midmes05	Detector Facility	Celeron/335
midmes06	Neutrino Devel. DAQ	PII/400
e614slow	TWIST Slow Control	PII/400
midtwist	TWIST DAQ	2xPIII/1000
linm9b	M9B μ SR users	AMD Ath/1500
linm15	M15 μ SR users	AMD Ath/1500
linm20	M20 μ SR users	AMD Ath/1500
midm9b	M9B μ SR DAQ	2xPIII/1000
midm15	M15 μ SR DAQ	2xPIII/1000
midm20	M20 μ SR DAQ	2xPIII/1000
epicsm9b	M9B μ SR EPICS	PIII/550
epicsm15	M15 μ SR EPICS	PPro/200
epicsm20	M20 μ SR EPICS	PPro/200
daqlabpc	DAQ lab machine	PII/232
dasdevpc	DAQ development and Web server	PIV/1700
ladd00	LADD server	2xAMD Opt/1800

While MIDAS is mainly a data acquisition package, it includes a simple framework mechanism to interface to an on-line data analyzer tool. Currently two different analysis packages are routinely in use at TRIUMF: NOVA and PAW (physics analysis workstation). While NOVA is no longer officially supported by the TRIUMF DAQ group anymore, it will remain available as long as no major upgrade of the operating systems would brake it. For the CERN package PAW, the lack of future support and the limitations of the system in some specific areas, such as the live display, prompted our group to look at the new CERN data

analysis package ROOT. By using ROOT (fully OO compliant), TRIUMF will maintain its support capabilities for the next generation of experiments. ROOT is very flexible and already incorporates some of the current simulation tools like GEANT3. By providing a MIDAS/ROOT interface, the DAQ group feels that this package will keep MIDAS in the forefront of DAQ systems.

The status on that software interface at the end of 2003 includes: a mechanism in the MIDAS logger to save raw data in ROOT format (Tree), support for filling ROOT histograms in the standard MIDAS analyzer program and a simple on-line live ROOT histogram display GUI.

In parallel to this MIDAS/ROOT interface, the DAQ group has defined a new GUI ROOT application which will become a basic tool for on-line data display in the ROOT environment. This task was initiated with the help of Greg King (summer student) who developed an initial version. This work is also based on some major development done by the 8π group and their summer student (2002) Brian Eshpeter. Further development will continue in collaboration with TRIUMF Computing Services (Joe Chuma).

At the 2003 Real Time Conference, held in June in Montreal, Pierre Amaudruz, in collaboration with Stefan Ritt (PSI), gave a short course on MIDAS followed by a short course on ROOT given by its main author Rene Brun (CERN). Discussions on how to structure a MIDAS/ROOT connection took place between the experts. Rene Brun came to TRIUMF after the conference to give a seminar on ROOT and for further discussions with the DAQ group.

The LADD project

The Laboratory for Advanced Detector Development (LADD) is a CFI funded venture between TRIUMF and the University of Montreal. It provides infrastructure to support radiation imaging research in fields such as high energy and nuclear physics, materials and astrophysical sciences, and medical imaging applications. The LADD infrastructure at TRIUMF supports the development of new types of imaging detectors and systems for γ -rays and charged particles. One of the necessary components for detector development is a data acquisition system.

During 2003, the DAQ group, in collaboration with the first users of LADD, designed, specified and procured four new DAQ systems. Each consists of a VME crate with VMIC processor and readout modules and some NIM crates and NIM modules. The systems will be rolled out in 2004 for the KOPIO chamber tests, the T2K Neutrino photo detector tests, the liquid xenon prototype tests and a general use station. Since the VMIC processors are diskless, a disk and file server

system was also set up (ladd00).

DAQ systems

β NMR and β NQR at ISAC The second DAQ system used by the β NMR group to acquire data on the second leg of the ISAC-I low energy polarized beam line was renamed β NQR. Both systems are similar in nature.

Improvements made this year include the following. The DAQ software was simplified by combining the two experimental modes (integral type and time differential type). This makes the DAQ system simpler for the users, and very much easier to maintain. New features were added to the software, including two new experimental modes: a CAMP magnet scan and mode FAST (TD and I-type combined). Stopping the run automatically on error or after a requested number of cycles was also implemented. The EPICS and CAMP scans were made more reliable by adding code to allow them to reconnect and continue to scan if the connection to EPICS or CAMP is lost. Conversion from MIDAS format to the μ SR group's MUD format while a run is in progress (rather than from a saved file) was implemented.

μ SR systems

The TD- μ SR system continued to work well, and the new Linux-based Integral μ SR DAQ system was installed on all the μ SR beam lines (M15, M20, M9B). This system proved successful and as a result all the μ SR DAQ VAXes were promptly retired.

The search continued to find a suitable TDC front end module to support a MULTI type μ SR system. In this case, the detector is segmented in 8 sections and the DAQ has to handle the equivalent of 8 parallel experiments. We have chosen to use one of the new dead-timeless TDCs on the market. A first attempt at using a VME module developed in Japan around the ATLAS AMT chip proved unsuccessful due to bottlenecks in the readout part of the module. On the second attempt, we used a CAEN TDC built around the CERN HPTDC chip. This TDC used with a VMIC/VME processor appears to be fast enough to support the MULTI detector.

Other experimental stations

One major new system was requested last year by the TIGRESS group to study their first prototype detector. This required special software development for control of a scanning table. With the help of Dave Morris and his JACQ package, the system can be used to automatically scan the detector response over the full area of the detector. This DAQ is also used as a prototype to develop the full TIGRESS DAQ.

The newly formed Canadian T2K Neutrino group occupied the former ATLAS clean room to start detec-

tor development studies. Two standard CAMAC DAQ test stations were deployed. One of the stations will be replaced by a VME LADD system in the near future. This group is using the MIROODAS package for on-line analysis.

A special version of the polarimeter DAQ was set up for the McGill group (Expt. 920). On the TWIST system, new devices were added to the slow control front end programs as well as fine tuning of the beam line magnets for better stability. New slow control device servers were added to the LTNO system. KOPIO and DRAGON continued to use the test systems in the detector facility.

Support for external MIDAS users is still ongoing.

Detector Facility

(*R.S. Henderson, TRIUMF*)

This year has been an active one for the detector facility.

The TWIST project (Expt. 614) has been operating very well. This experiment at TRIUMF is a sophisticated attempt to measure the Michel parameters to ten times the precision they are now known. The various subsystems of this experiment continue to function extremely well. The detection system consists of scintillators, and 19 detector modules containing a total of 44 high-precision drift chambers (DC) and 12 MWPC planes (PC). In December, one of the MWPC planes failed – a broken wire is suspected. The spectrometer has been opened and the spare PC module will replace the damaged one, no beam time will be lost. A great deal of data has been collected already and the TWIST group is now involved in a massive blind analysis of the data sets. In addition, they spent several months of this year performing detailed measurements of the incoming muon beam characteristics. The TWIST experiment has been reviewed as extremely successful so far and its high priority has been reconfirmed.

A low pressure time expansion chamber (TEC) has also been designed by R. Henderson and G. Sheffer, for use just upstream of the TWIST spectrometer. It will be used to measure the muon beam properties. R. Openshaw designed the low pressure gas system. It was built and successfully tested in the facility. The TEC has also been built and is now being bench tested (Fig. 195). The beam line upstream of the TWIST magnet has been redesigned for the TEC. The new elements, including the TEC vacuum box and its stand, have all been installed, aligned and vacuum tested. The TEC is expected to be installed in Expt. 614 early in the next running period. If successful, a spare TEC will be fabricated and tested. This will probably mark the completion of the facility participation in the TWIST experiment, except for maintenance and repair.

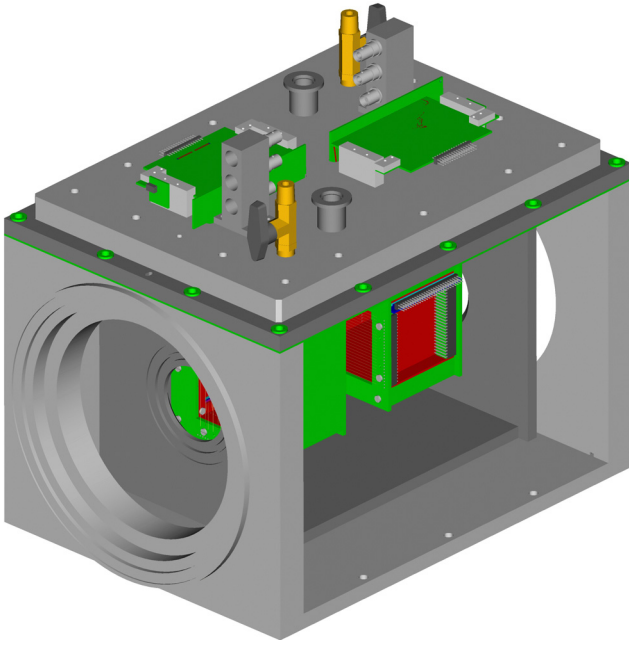


Fig. 195. A 3D rendering of the time expansion chamber (TEC) designed and built for the TWIST experiment (Expt. 614). The TEC is now undergoing bench tests and will soon be installed.

The scintillator shop continues to function as the heavily used machining centre for the facility. This year has seen a wide variety of scintillators fabricated for μ SR, the $G\theta$ experiment (at TJNAF) and the 8π experiment (ISAC). The larger mill in the scintillator shop was previously refitted as a 4-axis NC mill for the TWIST project, and allows us to machine the complex curved scintillator pieces for $G\theta$. The $G\theta$ scintillator designs were significantly delayed by the $G\theta$ group. The first scintillator sector has been finished and we are waiting for the testing before producing the other seven sectors. More KOPIO prototype detectors continue to be fabricated in this shop.

A highly significant project was completed in the scintillator shop this year. This is the 8π vacuum/scintillator unit, which is the central part of the scintillating electron positron tagging array (SCEPTAR). This vacuum/scintillator unit, with the array of Compton suppressed HPGe detectors and the fast tape transport system, form the 8π γ -ray spectrometer. Many experiments have already been approved for this new spectrometer (see Fig. 196).

This 8π vacuum/scintillator unit consists of 20 complex shaped, tightly fitting scintillators/light-guides in two hemispherical vacuum/scintillator assemblies. These were designed by H. Coombes and S. Chan, then fabricated and assembled in the scintillator shop. Both hemispheres have now been installed and successfully tested in the 8π spectrometer.

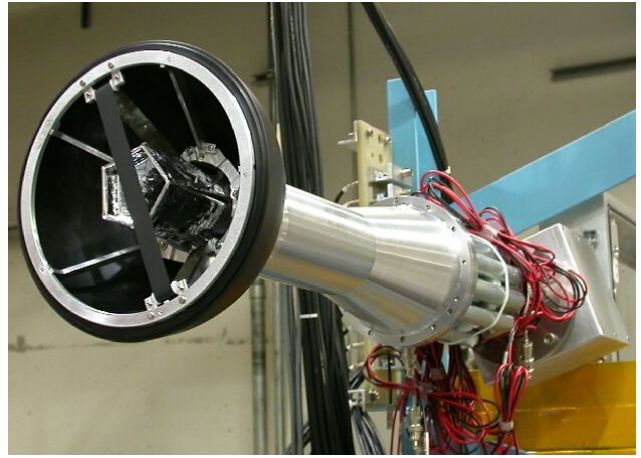


Fig. 196. Photograph of one half of the SCEPTAR vacuum/scintillator unit. The tape transport can be seen.

Design and prototyping have continued for the proposed KOPIO pre-radiator modules. KOPIO is awaiting approval by the US funding agencies. R. Henderson spent the majority of this year working in the KOPIO group. If approved, this project will be a very large detector project at TRIUMF, considerably larger and more complex than previous projects such as the ATLAS calorimeter fabrication, the BaBar drift chamber or the HERMES TRDs.

The present KOPIO design envisages having four quadrants of pre-radiator modules, each quadrant eight modules deep, for a total of thirty-two modules (plus two spares). Each of the modules would consist of two parts. The inner region (called the pre-radiator unit) is 2.15×2.15 m, and consists of eight drift chamber layers sandwiched between nine layers of extruded scintillator. The outer region (called the L-unit) would connect to, and support, the pre-radiator unit at the two orthogonal readout faces. Approximately fifty Shashlyk type calorimeter blocks would be mounted on these two edges of this L-unit, giving full calorimeter coverage in the experiment. Miniature coax cables will transport the 6,144 anode/cathode signals past the Shashlyk blocks to eight readout crates also mounted on the L-unit. In addition, both ends of approximately 1,800 WLS fibres will pass the Shashlyk blocks to over 300 PMTs (or APDs).

With each of the thirty-four pre-radiator modules $3.7 \times 3.7 \times 0.15$ m in size and weighing approximately 3 tons, the scale of the project becomes apparent. A great deal of development and testing is required. The detector facility is already contributing much of its manpower to this project in areas of design, mechanical mockup, thermal expansion testing, wire-chamber structural tests and scintillator painting tests. A full size module is scheduled for completion in mid-2005. If NSERC and TRIUMF management give final

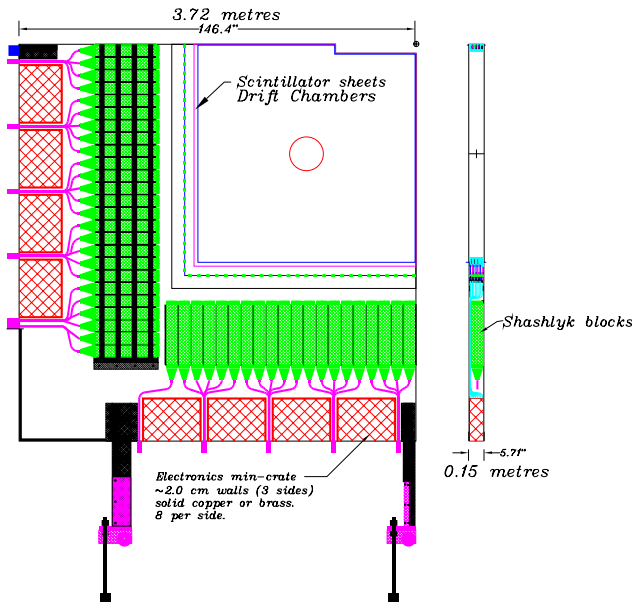


Fig. 197. Present design of KOPIO pre-radiator module.

approval, a full module production facility will also need to be implemented by mid-2005 (see Fig. 197).

CFI funding for LADD has been approved and spending has started. This money will be used to boost the detector development infrastructure at TRIUMF. LADD will take considerable time and effort to set up, and is planned to give TRIUMF a world class facility for continuing development of detector technologies, not just for physics experiments, but potentially for a wide range of R&D projects including a variety of medical detectors.

Experimental Support

(C. Ballard, TRIUMF)

The Experimental Support group provided technical assistance to experimenters and was responsible in part for the installation, alignment and maintenance of beam line elements and secondary channels. The Beam Lines group now has a permanent technical area complete with machine shop and welding room in the ISAC-II experimental hall. This allows better access for experimenters in search of technical assistance. For ISAC-I and ISAC-II, the Beam Lines group has provided technical support for the 8π detector as well as development for GPS, TITAN and TIGRESS. The group provided the layout of the “S” bend and helped plan the future installation of the transfer beam line scheduled for 2004. The Alignment group continued to provide precision alignment for TWIST, DRAGON, TUDA, Remote Handling and the RF group.

Routine preventative maintenance was performed in the vault, tunnel and other limited-access areas including the TNF and an improved Neutron Irradiation

Facility. Repairs were made to filters, magnets, valves, beam blockers and interlocks. Water and vacuum leaks were also investigated and fixed.

Beginning January, 2003, efforts were focused on the replacement of the final triplet for beam line 1A. The magnet frame assembly, insulators and cooling system upgrades were among the group’s contributions on this project.

Other projects in the meson hall included the continuation of the overhaul of the M9B solenoid and maintenance on the helium compressor and liquefier. New turbines were installed in the cold box as well as a new charcoal filter in the helium compressor room.

Improvements were made to the M15 and M20 separators. A new window assembly was installed in M20 that allows the thin window (isolating the separator vacuum) to be changed more efficiently with less experiment downtime.

The CERN Collaboration continued and involved three technicians on the assembly and testing of the PFN tanks destined for the CERN LHC. The same technicians also worked on the MULAN Kicker Magnet Project at PSI.

GEANT4

(P. Gumplinger, TRIUMF)

Modern particle and nuclear physics experiments require large-scale, accurate and comprehensive simulations of the particle detectors used in these experiments. The same is true for other disciplines, such as space science, nuclear medicine, accelerator design and radiation physics. In response to this demand, a new object-oriented toolkit, GEANT4, has been developed for the simulation of particles passing through matter. It provides a comprehensive, diverse, yet cohesive set of software components which can be employed in a variety of settings, from small standalone applications to large scale detector simulations for experiments at the LHC and other facilities. At the heart of this software system is an abundant set of physics models, including electromagnetic, hadronic and optical processes, over a wide energy range starting, in some cases, from 250 eV and extending in others to the TeV energy range.

GEANT4 was designed and is being developed by an international collaboration, formed by individuals from a number of cooperating institutes, HEP experiments, and universities. It builds on the accumulated experience in Monte Carlo simulations of many physicists and software engineers around the world. The origins of the collaboration go back to two independent studies done at CERN and KEK in 1993, which sought to investigate how modern computing techniques could be applied to improve what was offered by the existing GEANT3 program. These two activities merged in

1996 as CERN R&D project RD44, looking for additional collaborators with an interest in the LHC experimental program. TRIUMF was approached and joined this project almost immediately, in part because a number of its employees were experts in the field and were able to contribute immediately. This R&D phase was completed in late 1998 with the delivery of the first production release. The ambitious project, in terms of size and scope of code and the number of people involved, has demonstrated that rigorous software engineering practices and object-oriented methods can be profitably applied to the production of a coherent and maintainable software product, even with the fast-changing and open-ended requirements presented by physics research. Subsequently, the present collaboration was established to continue the development and refinement of the toolkit, and to provide ongoing maintenance and user support.

Although not a large contingent, the TRIUMF group has always been very active in some of the core activities of the collaboration and is represented in both the Technical Steering Board and in the Collaboration Board. The group had a strong voice in the discussion and design of the overall architecture of the program. One of our initial efforts was to port the hadron physics model GHEISHA from FORTRAN to C++, and its redesign to better match the object-oriented paradigm. Similar work was later done for part of the HETC (high energy transport code), originally developed at the Oak Ridge National Laboratory. We also implemented the hadronics portions of the test, validation and example suites that are part of the G4 distribution. TRIUMF collaborators have been active in many areas of user support, documentation, testing and quality assurance and in particular in the adaptation of associated tools from the Open-Source community: LXR, a www-based source code browser with cross-reference and full-text indexing; ViewCVS, a visual interface to a source-code and version management tool; and Tinderbox, an automated multi-platform system testing and reporting tool.

GEANT4 is an ideal framework for modelling the optics of scintillation and Čerenkov detectors and their associated light guides. This is founded in the toolkit's unique capability of commencing the simulation with the propagation of a charged particle and completing it with the detection of the ensuing optical photons on photo sensitive areas, all within the same event loop. This functionality of GEANT4 was developed exclusively by one developer at TRIUMF and is now employed world-wide in experimental simulations as diverse as ALICE, ANTARES, AMANDA, Borexino, Icarus, LHCb, HARP, KOPIO, the Pierre Auger Observatory, and the GATE (Imaging in Nu-

clear Medicine) Collaboration. This functionality is also exploited as part of the investigation to understand the optical properties of extruded plastic scintillator tiles for KOPIO and for the near detector of the long baseline neutrino experiment at J-PARC/SuperK. We are constantly responding to inquiries posted on the G4 Users Forum regarding the optical photon tracking. Questions and feedback arrive from people working in medical PET research, cosmic shower research, neutrino detectors, HEP experiments and also from cooperate research laboratories. We have prepared and presented invited tutorials at international user workshops held at SLAC, CERN, and most recently in early 2003, at the European Space Agency in the Netherlands.

The major players in the current collaboration are the international organizations: CERN and ESA/ESTEC; the national laboratories: INFN (Italy), IN2P3 (France), Helsinki Institut of Physics (Finland), Karolinska Institutet (Sweden), KEK (Japan), PPARC (UK), SLAC (USA) and TRIUMF (Canada); with strong support from these HEP experiments: BaBar (SLAC), ATLAS, CMS, HARP, LHCb (CERN). Additional expertise comes from 14 European, 4 Japanese, and 5 North American universities and 4 Russian institutes, for a total of about 150 collaborators. The TRIUMF participation in GEANT4 has fluctuated over the years, and is presently four researchers and software engineers. The toolkit is now in public release version 6.1 and is available for a variety of operating systems.

In summary, the GEANT4 project has brought a new level of computing expertise to our laboratory, one that has already filtered into the simulation efforts of TWIST, TIGRESS, T2K, LADD, KOPIO and plans for the BIG DRAGON.

GEANT4 collaborators: P. Gumplinger, F.W. Jones, C.J. Kost, M. Losty (TRIUMF).

Scientific Services

(*M. Comyn, TRIUMF*)

The Scientific Services group encompasses the Publications Office, Library, Information Office, and Conferences. Its activities during 2003 included: producing the 2002 Annual Report, the TRIUMF Review 1998–2003, conference proceedings, and the TRIUMF preprints; maintaining the Library; coordinating TRIUMF tours and assisting with the production of public relations materials; and supporting fifteen past, present and future conferences and workshops.

Publications Office

The TRIUMF Annual Report Scientific Activities has been truly electronic since 1998. Electronic files have been used throughout, from initial contributor submission, through editing, transmission to the

printer, and subsequent direct printing on a Xerox Docutech system. The same files are used for the WWW versions of the report which are available at <http://www.triumf.ca/annrep> in both Portable Document Format and PostScript file formats. Unlike the monochrome paper version, the electronic versions allow those figures which were submitted in colour to be both viewed and printed in colour. The WWW version of the 2002 report was available to readers three weeks before the printed version. It contained a record 322 pages and 259 figures. The Annual Report mailing list has been reduced and the trend is expected to continue as people become more accustomed to accessing the information over the WWW. This will result in less copies having to be printed, with subsequent cost savings.

In an attempt to aid and encourage authors to submit contributions in the correct format, the instructions available on the WWW were refined. The L^AT_EX 2_ε skeleton file was changed slightly and the instructions document which all authors should consult was reworded to include more explicit information on the correct production of Encapsulated PostScript files for the figures and the submission of original file formats.

Illegal code embedded in Encapsulated PostScript files continues to be a major problem in electronic publishing. Some software packages, such as the TRIUMF graphics routines, fully conform to the Encapsulated PostScript specifications, whereas many do not. In order to alert authors to problems encountered with files they submitted the previous year, and in an attempt to prevent similar problems recurring, a post-mortem of the 259 figures in the 2002 Annual Report was produced. This analysis and explanation of solutions is viewed as an ongoing project which will evolve as new procedures are devised and software packages become available for editing bad PostScript code. Superior TRIUMF scientific publications should result. See <http://www.triumf.ca/annrep/figures.html> for details.

TRIUMF preprints are now only produced electronically, and immediately posted on the WWW at <http://www.triumf.ca/publications/home.html> to allow rapid dissemination of the publications. This has replaced the traditional distribution of paper copies by mail, resulting in significant savings of both cost and labour.

The year began on three fronts with the kickoff for the TRIUMF Annual Report Scientific Activities 2002 submissions, the publication in March of a conclusions and abstracts booklet for the Italian-Canadian Interface for the Development and Exploitation of Stable and Exotic Ion Beams, which was held at TRIUMF October 16–20, 2002, and the final work associated with

the publication of the refereed proceedings of the 14th International Conference on Electromagnetic Isotope Separators and Techniques Related to Their Applications (EMIS-14), which was held in Victoria May 6–10, 2002. Extensive communications with Elsevier Science B.V. resulted in the publication of a special 846 page issue of Nuclear Instruments and Methods in Physics Research Section B, Beam Interactions with Materials and Atoms, Volume 204. It appeared in print in May and on the Web up to five months earlier.

In February work began on producing the TRIUMF Review 1998–2003, a companion document to the TRIUMF Five Year Plan 2005–2010. The scope of the document grew with time and its preparation became the main focus of the Publications Office for eight months. Initial work involved producing and approving templates in L^AT_EX 2_ε and MS Word for the submission of chapters and CVs. Chapters produced in MS Word were converted to L^AT_EX 2_ε to produce the final 232 page document which contained six chapters and two appendices. The task of producing Appendix A, Publications 1998–2003, was particularly onerous as it was derived from a compilation of the appendices in five annual reports, listings of life sciences and μ SR publications, additional material reported in CVs, and other sources. The 82 CVs formed a separate document. A secure Web site was maintained for use by the authors and the peer review committee.

Web site and other support was provided for the Summer Nuclear Institute at TRIUMF (SNIT 2003), held July 21–August 1.

Work began on preparations for the Eighth International Symposium on Nuclei in the Cosmos (NIC8), to be held in Vancouver, July 19–23, 2004. Quotations were obtained for the publication of the proceedings, and template files were prepared for producing the abstracts. Many procedures to be used for producing the abstracts booklet and the proceedings will be based on those developed for the EMIS-14 conference.

Due to the workload this year, activities on the Joint Accelerator Conference Website (JACoW) committee were limited to assisting with the electronic publication of the proceedings of the Particle Accelerator Conference (PAC 2003), held in Portland, Oregon, May 12–16.

Library

The Library budget was increased in 2003 to compensate for rising journal subscription costs and unfavourable exchange rates for 2004 renewals, thereby maintaining the list of journals which have been acquired since the last cutbacks in 1998. However, the journal subscription budget and electronic access alternatives are constantly under review. The Library continues to rely on donations for most of its book ac-

quisitions. The Library operates on a self-serve basis and manages with minimal support for day-to-day operations.

Information Office

The Information Office coordinated a record number of 261 tours for 2,019 people during 2003. The general public tours were conducted by a summer student during the June to August period when tours were offered twice a day. 255 people took a total of 65 tours during the three month period. Throughout the remainder of the year for the twice weekly general public tours, and for the many pre-arranged tours given to high school students and others, a small, dedicated group of TRIUMF staff acted as tour guides.

Table XXII shows the number of people taking tours, the number of tours, and the number of tour guides required to conduct them (groups of more than 15 require multiple tour guides) for each of the years 1999–2003 plus the totals. A steady increase can be observed. The numbers are broken down into four categories:

- General public: tours provided for members of the general public twice a week September–May, and twice a day June–August on a drop-in basis.
- Science: pre-arranged tours conducted for university/college physics, chemistry or science students with a specific interest in TRIUMF, scientists at TRIUMF for a conference or workshop, and scientific groups.
- Students: pre-arranged tours conducted for elementary and high school students and university/college non-science students.
- VIP: Specific tours, often conducted by senior management personnel, arranged for VIPs, review/advisory committee members, and the media.

The summer student also assisted with the production of presentation materials, with the Summer Nuclear Institute at TRIUMF, and as the coordinator of many student activities throughout the summer.

The TRIUMF Welcome Page, which is accessible directly at <http://www.triumf.ca/welcome> or via the TRIUMF WWW Home Page, continues to receive well over 5,000 visits each year. The series of WWW pages were developed by two co-op students and are intended to provide an overview of TRIUMF in a format understandable to the general public. The Information Office responds to any questions posed by visitors to the site. Some limited maintenance of the pages was performed during the year, but efforts began to totally overhaul those parts of the TRIUMF Web site directed at the general public.

Table XXII. Breakdown of TRIUMF tour numbers for the period 1999–2003.

Category	1999	2000	2001	2002	2003
<u>General Public</u>					
# people	350	368	421	499	482
# tours	96	107	110	131	126
# tour guides	96	107	111	134	126
<u>Science</u>					
# people	384	294	383	592	651
# tours	18	20	30	23	34
# tour guides	33	26	43	57	59
<u>Students</u>					
# people	794	612	839	894	626
# tours	46	40	30	40	38
# tour guides	70	53	60	70	50
<u>VIP</u>					
# people	145	171	258	193	260
# tours	37	37	59	53	63
# tour guides	38	40	65	55	71
<u>Total</u>					
# people	1,673	1,445	1,901	2,178	2,019
# tours	197	204	229	247	261
# tour guides	237	226	279	316	306

Various TRIUMF images found on the WWW pages continue to be in demand for use in text books and on other Web pages.

Support was provided to the TRIUMF Users' Group throughout the year by the TUEC Liaison Officer.

Conferences

Although TRIUMF did not host an international conference in 2003, it was still a busy year for workshops and meetings. Support was provided for seven workshops and meetings, along with preparations for six conferences and workshops in 2004 and beyond. Registration databases were created and managed for most of the workshops.

In addition, support was provided in the electronic proceedings office of the Particle Accelerator Conference (PAC 2003), held in Portland, Oregon, May 12–16.

TRIUMF hosted or supported the following conferences and workshops in 2003:

- Workshop on Functional Imaging in Basic Biomedical Research Through microPET Imaging, UBC, June 26–27 (57 delegates).
- Summer Nuclear Institute at TRIUMF (SNIT 2003), TRIUMF, July 21–August 1 (39 delegates plus 10 lecturers).
- GEANT4 2003 Workshop, TRIUMF, September 2–6 (53 delegates).

- International Union of Pure and Applied Physics (IUPAP) Meeting, TRIUMF, October 10–11 (24 delegates).
- HEPiX-HEPNT Autumn 2003 Meeting, TRIUMF, October 20–24 (76 delegates).
- TRIUMF Users' Group Annual General Meeting, TRIUMF, December 10 (55 delegates).
- EMMA Workshop, TRIUMF, December 11–12 (30 delegates).

In addition, preparations were made for the following future conferences and workshops.

- Fixed Field Alternating Gradient Workshop (FFAG 2004), TRIUMF, April 15–21, 2004.
- TRIUMF Summer Institute 2004, TRIUMF, July 5–16, 2004.
- Eighth International Symposium on Nuclei in the Cosmos (NIC8), Vancouver, July 19–23, 2004.
- Fifth International Symposium on Radiohalogens (5ISR), Whistler, September 11–15, 2004.
- 2005 CAP Congress, UBC, June 5–9, 2005.
- Particle Accelerator Conference (PAC 2009), Vancouver, 2009.

The DRAGON Facility

(D. Hutcheon, TRIUMF)

Introduction

DRAGON improvements included replacement of magnet power supplies, improved beam diagnostics and tuning methods, and development of a Web site containing information on how to use the facility. In addition there were developments specific to new experiments using stable beams: separator acceptance studies and a drive mechanism for solid targets.

General hardware improvements

Six of the separator magnets initially were given power supplies that were no longer needed on meson channels at TRIUMF. These power supplies proved to be unreliable, due to frequent water leaks developing in transistor pass-banks. During the winter shutdown they were replaced by new power supplies.

Addition of a dedicated CCD camera provided a valuable tool to aid in beam tuning. Light produced by passage of ion beams through hydrogen or helium gas targets could be detected in the camera which viewed the target from several metres downstream, through a magnet alignment port. This provided a non-destructive way to measure the beam position at the target, both for initial tuning and during production runs (Fig. 198).

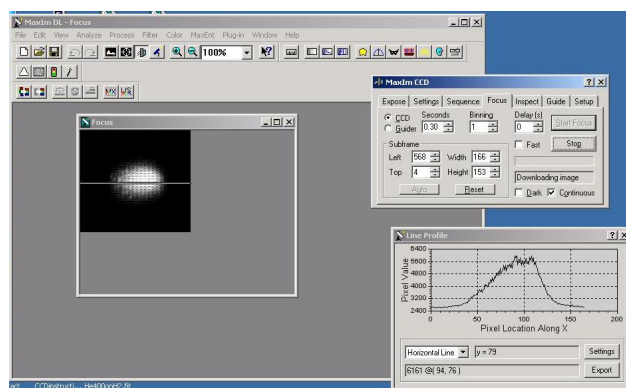


Fig. 198. CCD camera image of light produced by passage of a ^{12}C beam through a helium gas target. The beamspot is approximately 6 mm across at the base.

Under normal operation, the dry pump which backed the separator turbo pumps ran continuously, even though the amount of gas exhausted by the turbos was very small. To increase the time between expensive scheduled factory maintenance of the dry pump, a buffer tank was added to the turbo backing line. The vacuum control PLC was modified so that normally the backing dry pump was off, and was turned on only long enough to pump out the 200 l buffer tank when its pressure rose to 0.5 torr. Typically the backing pump would have to run for 2–3 min twice per day.

Information for users

Thanks to the efforts of several undergraduate students, a DRAGON Web site was made available to users. It has become the “instruction manual” of the facility, with detailed information about the use of hardware, data acquisition programs, beam tuning procedure, pre-run checklists, and links to useful ISAC Operations data. Its URL is <http://www.triumf.ca/dragon>.

Development for Expt. 952 ($^{12}\text{C}(\alpha, \gamma)^{16}\text{O}$)

This experiment had two features not seen in earlier proton capture experiments: the mass of beam ions was only 75% of the mass of the capture product ions; high γ -ray energies could result in product cone angles greater than 20 mrad.

The 3/4 ratio of beam mass to recoil product mass resulted in a separation by 12 cm at the mass selection slits, instead of the 2 cm more typical of proton capture reactions. This meant that it was possible to install an additional, fixed-position Faraday cup which could collect beam ions without interference from the slits. This cup, called FCM2, was the primary monitor of beam intensity for the experiment.

The alpha capture data revealed that the target/separator system acceptance was not large enough to transmit ions of ≈ 20 mrad cone angle. Because good

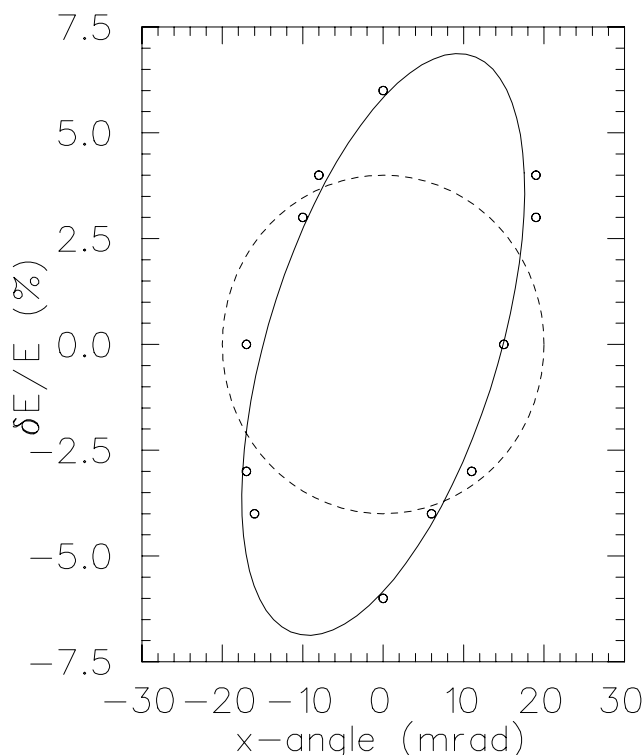


Fig. 199. Separator acceptance in horizontal angle and fractional change in ion energy, as measured using the wobbler magnet (open circles). The dashed circle indicates the angle-energy correlation of capture products having 20 mrad maximum emission angle. The solid line is an ellipse to guide the eye through the measured points.

transmission at 20 mrad and larger was important for Expt. 952, an extensive program was undertaken to understand where acceptance was being limited and how to improve it. One set of measurements consisted of replacing the gas target by a collimator and deflection magnet (the “wobbler”) and deflecting an ion beam to map out the limits of transmission of a nearly “pencil” beam. Figure 199 shows one result from this study, the acceptance correlation between angle and energy.

The pumping tubes between stages of the differentially-pumped windowless gas target had been designed for a recoil cone angle of 20 mrad. The downstream tubes were replaced by a new set, allowing transmission within a 25 mrad cone half-angle. With this change, plus a slight tune change suggested by the wobbler work, the alpha capture product ions showed a more symmetric transmission of higher-energy vs. lower-energy ions. However, there was still a clear loss of particles at the largest angles (at the middle of the energy distribution).

Extensive ion-optics studies were done, both with GIOS and a GEANT-based raytracing simulation, to try to understand where ions were being lost in the separator. The GIOS work suggested that a modification of the standard separator tune might give better

transmission, the trade-off being a possible reduction in the beam suppression factor. Measurements to validate the new tune were inconclusive due to unexpected fluctuations in resonant capture yields, possibly arising from beam energy instability during the course of measurements.

Several possible solutions have been considered, such as moving the gas target closer to the separator, adding quads between the target and separator, or replacing some existing quads with larger ones. Because of the cost and/or disruption to the radioactive beam program, there is no immediate plan to implement any of these solutions, until the cause of losses is better understood.

Solid target drive for Expt. 947 ($^{12}\text{C}(^{12}\text{C},\gamma)^{24}\text{Mg}$)

For this experiment it was desired to have thin foils of carbon, enriched in ^{12}C or ^{13}C instead of the extended gas target used in radiative capture experiments. Furthermore, γ -ray detection by the BGO array was not to be obscured by the target-mounting mechanism. The resulting design was a compact, chain-driven set of nine targets, with a stepping motor to permit remote changing of targets via EPICS (Fig. 200). The

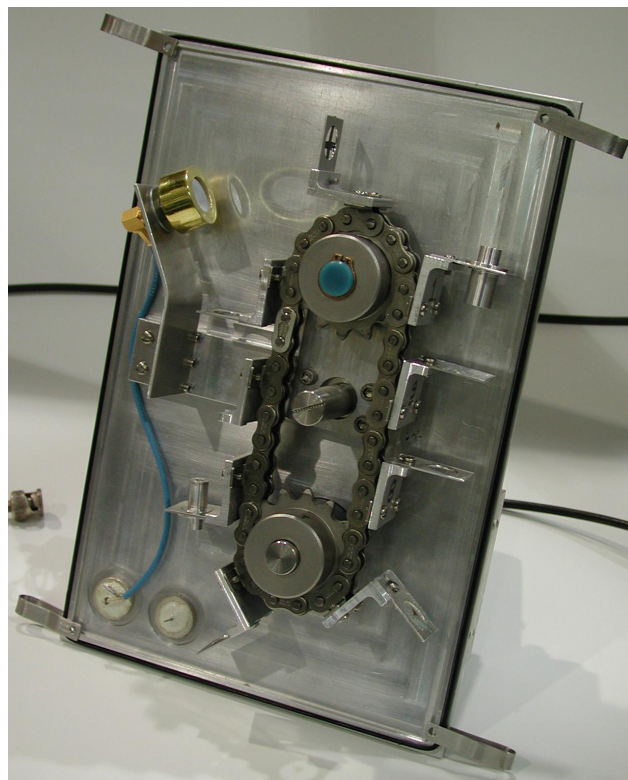


Fig. 200. Solid target changer mechanism. The mounting plate is a direct replacement for the gas target plate. The lower sprocket is driven by a stepping motor located outside the vacuum. A Si detector monitors beam intensity and target integrity by detection of products from elastic scattering.

system is mounted on a side-plate which mates to the standard target vacuum box in the same way as the gas target support plate does, making the change from gas target to solid targets relatively quick and easy.

Unlike gas targets of hydrogen or helium, the solid carbon foils did not emit enough light to be detected in the CCD camera when bombarded by heavy ion beams of a few nA intensity. It was discovered that microscope slide glass would give off sufficient light to be used for beam tuning at nA beam currents. At beam intensities of 50 nA or more the carbon foils did give off light at the beam position, probably incandescence due to heating by the beam.

8 π Spectrometer (G.C. Ball, TRIUMF)

During the past year the major accomplishment was the fabrication, installation and commissioning of the scintillating electron positron tagging array (SCEPTAR) that is required for β - γ coincidence studies with the 8 π spectrometer. SCEPTAR was designed to provide high β detection efficiency, a low energy threshold, minimum sensitivity to γ -rays, high count rate capability and a detector granularity comparable to the HPGe array. A schematic view of SCEPTAR is shown in Fig. 201. It consists of twenty 1.5 mm thick BC404 plastic scintillator detectors arranged in 4 pentagonal rings centred at approximately the same angles with respect to the beam as the four rings of HPGe detectors. The detectors centred near 80 and 110° are rectangular in shape while those centred near 37 and 143° are trapezoidal. Light produced in the scintillators is collected from one edge by segmented 1.5 mm thick UVT acrylic light guides which are contoured and subsequently glued to 1 cm diameter UVT acrylic rods which transport the light to 13 mm diameter phototubes located outside the vacuum chamber. The SCEPTAR detector array is mounted inside a spherical 8 cm

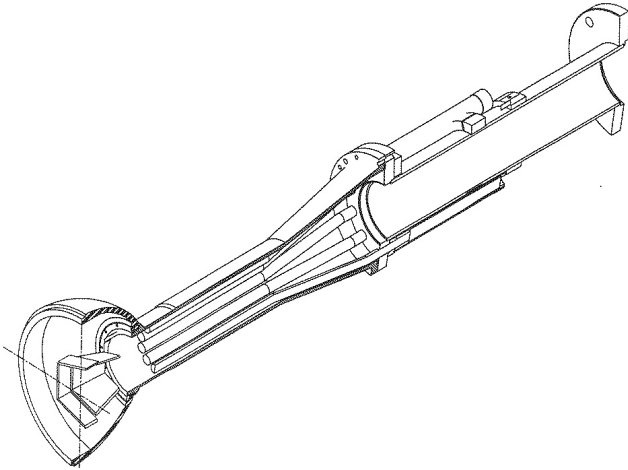


Fig. 201. Schematic view of one half of SCEPTAR.

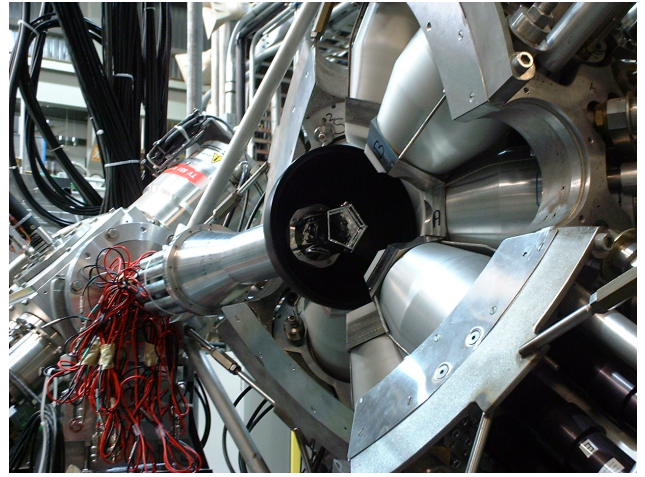


Fig. 202. Upstream view of SCEPTAR.

radius, 4 mm thick Delrin vacuum chamber divided into two hemispheres for easy access. The upstream half of SCEPTAR installed on the 8 π beam line is shown in Fig. 202. An integral part of SCEPTAR is a moving tape collector system designed and built by E. Zganjar (LSU) to remove long-lived daughter activities from the focus of the array. The low energy beams from ISAC are focused at the centre of the SCEPTAR chamber and deposited onto a 12.7 mm wide, $\sim 50 \mu\text{m}$ thick tape that is fed from a large aluminum storage chamber connected to the vacuum chamber containing the downstream half of SCEPTAR. A 5 cm thick lead shielding wall located immediately in front of the tape storage chamber shields the HPGe detectors from long lived activity remaining on the tape. The entire assembly is mounted on a stand that is moveable via linear bearings. The downstream view of SCEPTAR and the moving tape collector system is shown in Fig. 203.

The upgraded data acquisition system for the 8 π spectrometer described previously (TRIUMF 2002

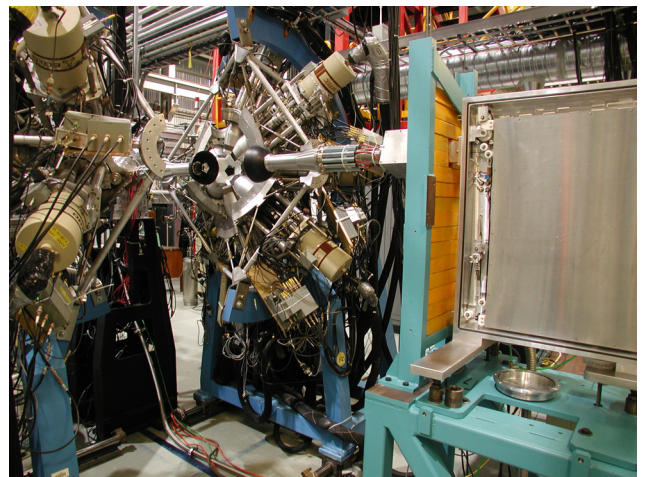


Fig. 203. Downstream view of SCEPTAR and the moving tape collector system.

Annual Report) was extended to include a separate FERA readout bus and VME triple port memory module for the SCEPTAR data stream. A second latching scaler was used to give an absolute time stamp required to correlate β - γ coincidence events. LeCroy 4300 FERA QDCs were used to encode the β energies and LeCroy multihit TDCs were used for the β times. The system also provided a number of possible hardware triggers to select the data that was readout. These included: γ , γ - γ , β , β - γ , and prescaled β s or γ s. A VME 32 input multichannel scaler module was also used to record the singles betas detected in each of the 20 SCEPTAR detectors.

Initial tests of the performance of SCEPTAR were carried out using a beam of $\sim 10^5$ ^{26}Na . The energy signals obtained from the individual SCEPTAR detectors for high energy betas that deposit about 400 keV are shown in Fig. 204. The low energy signals observed in the energy spectra for the rectangular scintillators result from high energy betas that pass through a trapezoidal scintillator and then produce Čerenkov light in the light guide of the adjacent rectangular detector, which passes behind the trapezoid. Data were also obtained from a ^{28}Mg source prepared by depositing a beam of ^{28}Na from ISAC onto the collector tape for about 12 hours. This source is ideal for measuring the efficiency of SCEPTAR as a function of beta end point energy. In particular, the decay scheme is well known and contains transitions with Q_β values that range from 0.2 to 2.9 MeV, all decaying to excited states in $^{28}\text{Al}/^{28}\text{Si}$ that subsequently gamma decay. The analysis of these data is in progress and will be compared to Monte Carlo predictions.

The first two 8π experiments to use SCEPTAR and the moving tape collector system were carried out in

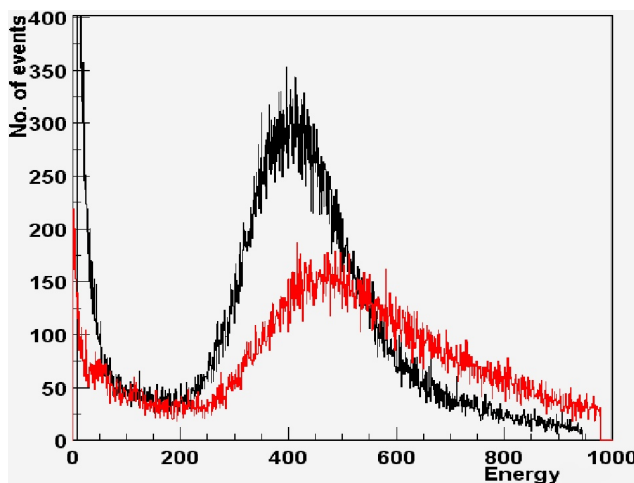


Fig. 204. Representative energy spectra obtained with SCEPTAR for high-energy betas from the decay of ^{26}Na . The rectangular detector is shown in black (upper curve), the trapezoidal detector in red (lower curve).

August–October. One of these (Expt. 921) was the search for new high-K isomers in the mass 170–180 region. A particular feature of this experiment was the detection of low energy ~ 90 keV conversion electrons with SCEPTAR in coincidence with γ -rays from the decay of the well-known $8^-, 4s$ isomeric state in ^{178}Hf populated in the beta decay of ^{178}Lu . In the second experiment (Expt. 955) designed to investigate the shell structure of light neutron rich nuclei, the beta decay of ^{32}Na was studied using a beam of only 1–2 ion/s. This experiment demonstrated that SCEPTAR, in combination with the 8π spectrometer, is a powerful tool for studying exotic short-lived (< 100 ms) nuclei produced at very low intensities. Both of these experiments are reported in more detail elsewhere in this Annual Report.

There are currently ten approved ISAC experiments that will use the 8π spectrometer (Expts. 823, 909, 921, 929, 954, 955, 957, 961, 984 and 988) including two which were approved by the TRIUMF EEC in December, 2003. The most recent proposals require the addition of a 10 element BaF_2 array and associated fast timing electronics that will allow the lifetime of γ -decaying states to be measured for states with lifetimes as low as 10 ps. For standard 8π spectroscopy experiments the time difference between the β particles detected in the plastic scintillators of SCEPTAR and the γ -ray detected in a BaF_2 detector will be used to measure lifetimes down to the sub-100 ps range. For shorter lifetimes down to 10 ps the time signal from the SCEPTAR array will be replaced with that from a single fast-plastic scintillator mounted immediately behind the beam spot of the moving tape collector. Tests using a ^{26}Na beam will be carried out in 2004 to measure the time response of SCEPTAR and optimize the design of the BaF_2 detectors. This development project is being led by Paul Garrett from LLNL.

Finally, during the past year a total of 40 collaborators from 14 institutions actively participated in the development and/or use of the 8π spectrometer, including: 7 undergraduate students, 6 graduate students and 5 post-doctoral fellows.

TIGRESS

(G. Hackman, TRIUMF)

To take full advantage of the physics opportunities presented by ISAC-II beams, a state-of-the-art γ -ray detector array with high efficiency and high resolution is needed. In 2003 the TIGRESS (TRIUMF-ISAC gamma-ray escape suppressed spectrometer) team continued towards its goal of building the detector in stages for early implementation in 2005 and full implementation in 2009. Highlights of the year's progress include: 1) successful competition and release of funds

for a Natural Sciences and Engineering Research Council (NSERC) RTI-3 Major Installation Grant; 2) testing of the HPGe prototype detector; 3) development of signal simulation codes; 4) receipt and initial testing of the BGO suppressors; 5) design of a single-unit detector stand; 6) fabrication and testing of a single-channel waveform capture board upon which the TIG-9 and TIG-10 DSP modules will be based.

1) NSERC funding: The TIGRESS RTI-3 proposal was reviewed first by a Technical Site Visit committee in January, the NSERC grant selection committee in February, and a prototype HPGe performance review (see Item 2) in July. Following the last review, funds were formally released for 12 units, amounting to \$8.03 M over six years. In 2003, an RTI-2 proposal was submitted by A.A. Chen for a silicon array for the first two EEC-approved TIGRESS-ISAC-II experiments on ^{58}Zn (Chen) and neutron-rich Ca isotopes (Austin).

2) HPGe prototype testing: Tests on the prototype HPGe [G. Hackman, 2002 TRIUMF Annual Report, p. 165] were performed in 2003. Energy resolutions of the readouts from all detectors and sub-units met specifications, and the total efficiency ($>36\%$ relative to standard on each crystal), peak-to-total, and total efficiency with add-back of the clover (215%) also met expectations.

Since sub-segment first-interaction location by pulse-shape analysis is a major component of TIGRESS's performance in ISAC-II experiments, a number of studies investigated the position sensitivity of the detector. These measurements used a "scanning table" (Figs. 205 and 206) to move a 0.5 mCi ^{137}Cs source held in a Densalloy 1.5 mm bore collimation vessel with a 1.5 mm bore in a plane perpendicular to the detector unit. In the "singles" scan, the source was moved on a grid with 3 mm $x-y$ spacing and all γ -ray events were recorded. The total yield of 662 keV photopeak (full-

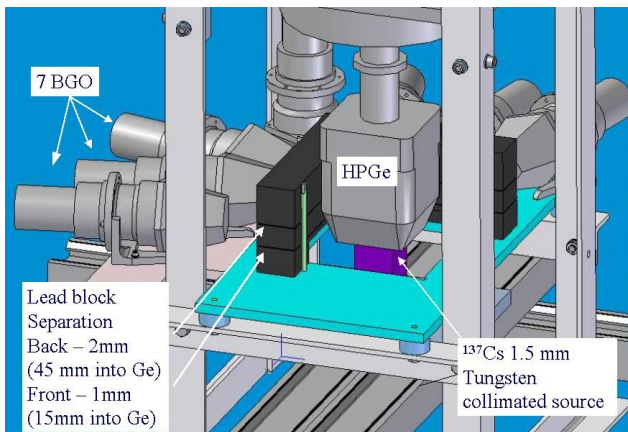


Fig. 205. Schematic rendering of the prototype HPGe scanning set-up.



Fig. 206. Photograph of the HPGe scanning set-up being assembled by TRIUMF undergraduate scholarship recipient Nick Cowan.

absorption in the clover unit) (Fig. 207) revealed the size of the inactive volume associated with the centre-contact bore and implantation. From these plots, the diameters of these dead volumes were deduced to be 11 to 13 mm, varying from crystal to crystal; this volume was largest on the crystals with the lowest

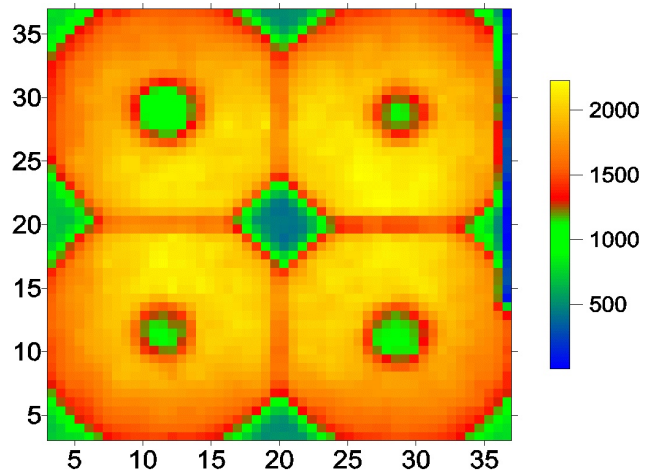


Fig. 207. Histogram of photopeak events as a function of (x, y) position of incident collimated 662 keV source. Horizontal and vertical axis labels identify discrete position number on a 3 mm square grid.

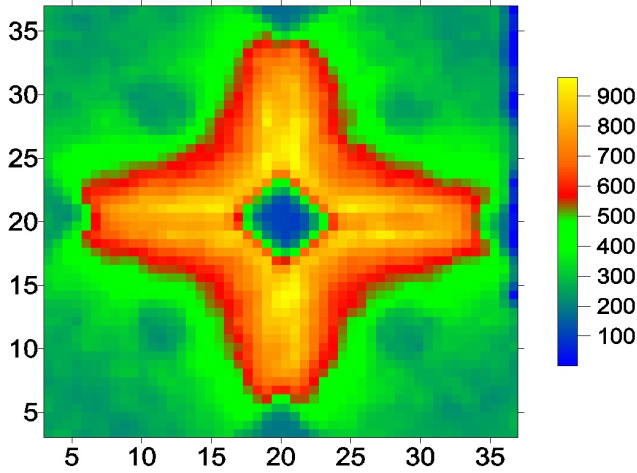


Fig. 208. As in Fig. 207, but selecting events with energy deposition in two or more crystals.

efficiency. By selecting those events where the full energy was absorbed in at least two or more crystals (Fig. 208), one observes that the “add-back” increase in total efficiency for a clover unit for 662 keV γ -rays comes dominantly from a narrow volume ~ 1.5 cm deep along adjacent crystal surfaces.

The “coincidence” scan was used to test the maximum achievable position sensitivity. Events were selected where the 662 keV incident γ -ray scattered out of the HPGe at a right angle, through planar Pb collimators, and into scintillation detectors, with energy depositions in the HPGe and BGO consistent with a 90° Compton scattering. These conditions localized the events to a volume approximately ~ 2 mm in each direction. Figure 209 shows a subset of the data from the

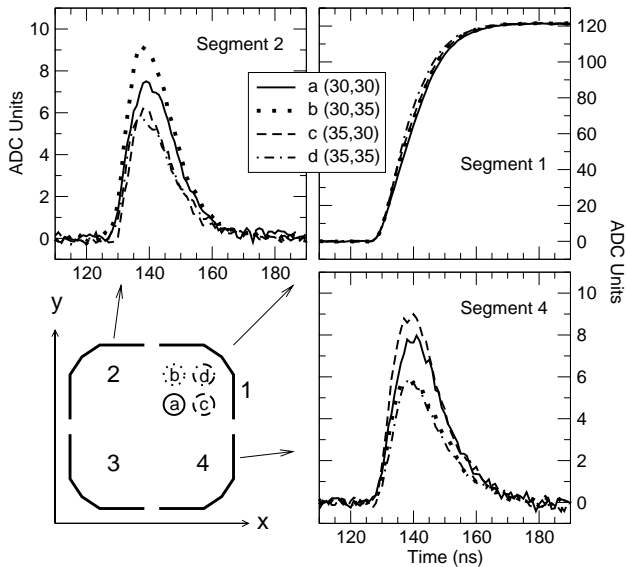


Fig. 209. Sample wave forms for select (x, y) positions collected in the coincidence scan measurement at a depth of $z = 15$ mm from the front of the crystal, with a sketch showing the relative positions of the sample positions and outer-contact segments for reference.

coincidence scan in the front segments of the detector. Following the definition of sensitivity proposed by Vetter *et al.* [Nucl. Instrum. Methods Phys. Res. **A452**, 223 (2000)], captured waveforms for a set of events at a given collimator position were averaged and the differences in waveforms from pairs of positions were compared with the baseline noise. In this analysis it was shown that the RMS position sensitivity is < 1 mm, or ~ 2 mm FWHM. This is well under the 5 mm FWHM that was used in modelling the performance of the array.

Manuscripts detailing the singles (H. Scraggs *et al.*) and coincidence (C.E. Svensson *et al.*) scans are being drafted.

3) Signal simulation codes: One strategy for analyzing the waveform data is to compare those waveforms captured in the experiment with a database of average waveforms from the scanning experiments, and perform a least-squares minimization to determine the interaction locations and energy depositions. However, such a strategy requires detailed knowledge of the waveforms throughout the entire detector. The coincidence scanning process itself is lengthy (1 point per day) and cannot access the innermost quarter of each crystal due to absorption of the scattered gamma. An alternative approach is to develop a reliable and verifiable means of calculating the waveforms generated over a fine and exhaustive grid. A first attempt at these calculations provided qualitatively correct overall waveform behaviour but did not achieve satisfactory agreement. Limitations were identified as including the precision of the RELAX3D electrostatics calculations, incomplete treatment of the drift velocities, and no considerations for crosstalk. These issues will all be addressed in 2004.

4) Receipt and testing of suppressor shields: One unit of BGO and CsI suppressor shields specified previously (Hackman, 2002) was received and tested for resolution and positional stability. A set of “first generation” charge-sensitive preamplifiers, based on a Swan Research design and fabricated at the University of Toronto, have been tested with these suppressors.

5) Design of a single-unit detector stand: Detailed design work on the full TIGRESS mechanical support structure continued this year. To facilitate installation of bottom detectors, the orientation of the inner structure is rotated 22.5° from the original conceptual design. To test the mechanical viability of the support structure design prepared in 2002 and to measure the performance of a full detector unit (HPGe plus suppressors), a single-unit stand mocking up $1/8$ of the 90° ring of the full array has been designed (Fig. 210). Fabrication was scheduled to begin in early 2004 with all

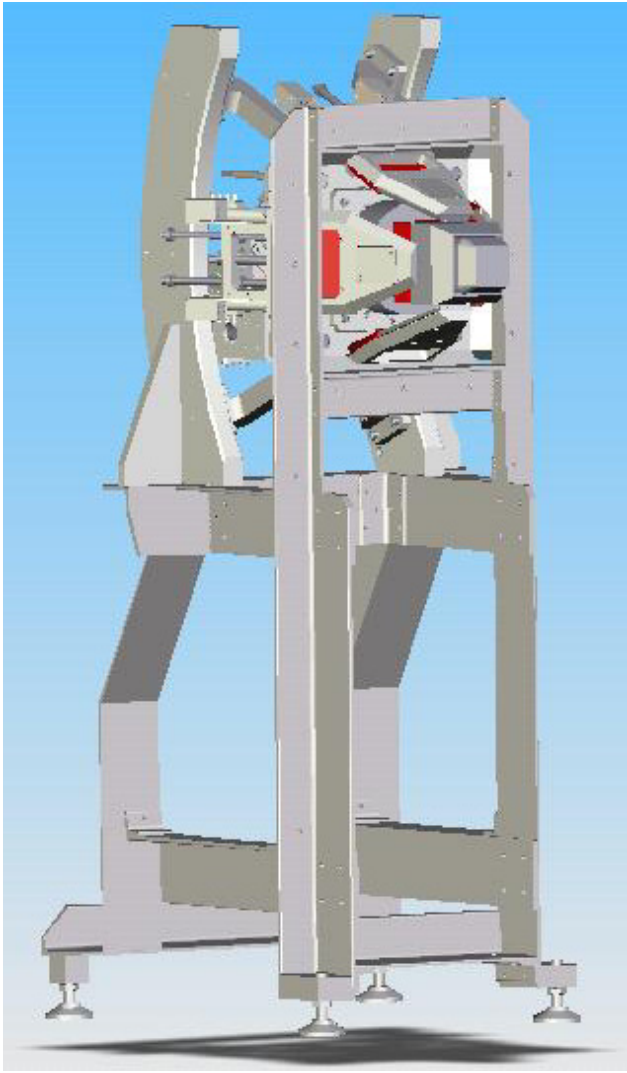


Fig. 210. Single-unit support and test stand.

mechanical, electrical, and detector performance tests scheduled to be completed in June, 2004. This single-unit test stand is conveniently designed so that the detector lies horizontally at the standard ISAC and ISAC-II beam line elevation.

6) Fabrication and testing of a single-channel waveform capture board: As part of parallel developments for KOPIO and TIGRESS, a single-channel waveform capture board was fabricated at Université de Montréal and tested with a large-volume HPGe detector at LTNO. These tests indicated a number of improvements needed in components to correct temperature-dependent gain drifts and susceptibility to power-supply noise and ground loops. These modifications will be incorporated into a full ten-channel card that should be ready for testing with the HPGe prototype in mid-2004.

Collaboration: The TIGRESS grant holders include

11 professors and staff from University of Guelph, McMaster University, Université de Montréal, University of Toronto, Université Laval, Simon Fraser University, and TRIUMF. The TRIUMF scientific team comprised G.C. Ball, G. Hackman, F. Sarazin, H. Scraggs, M.B. Smith, and undergraduate co-op students N. Cowan, G. Cronkhite, and L. Zimmerman. The collaboration has also benefitted from international collaboration with A. Boston of University of Liverpool, and C. Pearson and P.M. Walker of University of Surrey.

Status of the TITAN System

(J. Dilling, TRIUMF, for the TITAN Collaboration)

The TITAN (TRIUMF's ion trap for atomic and nuclear science) system at the ISAC low energy facility will allow high precision experiments in a variety of fields. Its main goal, however, is very precise mass measurements of short-lived isotopes, employing a Penning ion trap spectrometer. Different steps are needed in order to prepare the radioactive isotope beam from ISAC for those measurements, and therefore various ion traps are employed. The first step will be a linear gas-filled radio frequency quadrupole (RFQ) or Paul-trap system, which is used for cooling and converting the dc beam into a bunched beam. The next step is charge state breeding by use of an electron beam ion trap (EBIT). Presently these two systems are in the design and test phase, the RFQ system at TRIUMF and the EBIT system which is presently being built in Heidelberg, Germany in collaboration with the Max Planck Institute for Nuclear Physics. The Penning trap system is planned to be built and tested over the next two years (April, 2004 – April, 2006) and all components will move to their final location in the ISAC-I experimental hall in the spring, 2005. For this step a mezzanine will be erected above the existing low energy beam line area. In the following, the various components, which are presently under development or testing will be described in more detail.

The TITAN RFQ beam cooler and buncher

(J. Vaz, J. Dilling, TRIUMF; O. Hadari, UBC)

The TITAN RFQ beam cooler, designed for beam processing of the ISAC beam prior to injection into post apparatus, is currently being assembled in the TITAN test area. The radioactive ion beams (RIB) at RIB facilities are often of low quality due to the nature of the nuclear reaction mechanism of the production of the beams. A high beam quality, expressed in emittance or brilliance of the beam, is desired for optimal transfer of the precious ions to the various experiments. In order to achieve a better emittance, we employ a gas-filled RFQ cooler. It takes an energetic beam and through thermalizing collisions with a buffer gas, improves the beam quality. The use of this device

as a temporary store is also exploited such that a dc beam can be converted into a pulsed beam. A combination of rf and dc fields provides the required axial and radial manipulation of ion motion. RFQ beam cooler development by the TITAN collaboration at TRIUMF will incorporate several novel features in the device. The system can be oriented both horizontally and vertically in its present configuration and housing. The latter is used to couple the ISAC beam line to the TITAN components situated on a mezzanine level in the ISAC-I experimental hall. Reverse extraction from the beam cooler enables the processed beam to be delivered to other beam lines on the ISAC floor. Individual dc supply modules on each of the 24 electrodes of the RFQ rod structure allow for a user defined potential profile to be superimposed along the ion traversal region. The ion collection or trapping can therefore be executed at either ends of the device. The trapped ions are then ejected towards the nearest transfer aperture. This allows for more experimental stations to have access to cooled and bunched beams. The RFQ system is presently in the assembly and testing phase. A photo of the structure mounted on to the lid of the vacuum vessel is shown in Fig. 211.

The rf fields required for the beam cooler operation are generated using a unique RFQ driver system adapted from existing TRIUMF technology. A configuration of fast switching FET boards designed by the TRIUMF Kickers group is employed to deliver a 1 kV (peak-to-peak) rectangular waveform oscillating up to 3 MHz. These operation parameters allow for a mass range between 6–200 u to be transported efficiently through the beam cooler. The use of low-level TTL signals as FET switching triggers enables the rf field to be instantaneously turned off at the trapping ends of the device during ion extraction. This provides TITAN

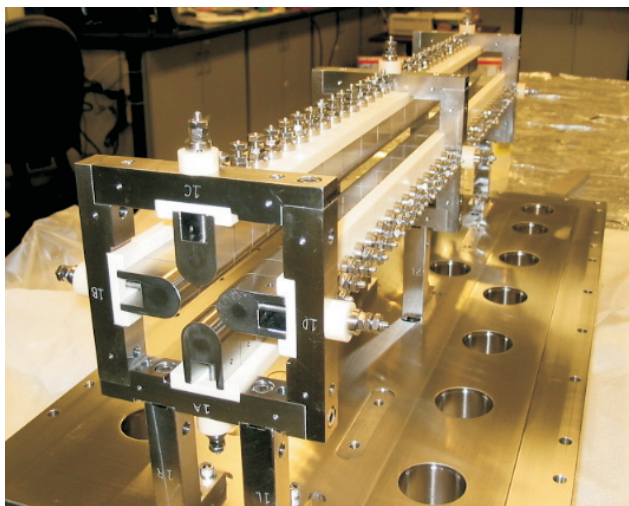


Fig. 211. Photo of the RFQ structure mounted on to the lid of the vacuum box.

with an opportunity to examine the beam quality during the extraction process without the influence of the rapidly changing rf field, often thought to be responsible for unwanted so-called rf heating. The careful investigation of this process would otherwise not be a trivial task, particularly when employing traditional transformer coupled sinusoidal rf drive systems.

Higher rf fields are required to effectively confine higher beam currents within the device. The higher fields counteract the space charge effects thus giving rise to a processed beam with a small emittance. This is crucial for experiments that require large samples of cooled bunched beam. A simple N (1 kV) stacking scheme of individual FET boards will yield higher rf voltages in the TITAN system. The current 1 kV drive can be scaled up as a test bed for an N (1 kV), $N = 2$ system at 3 MHz. This 1 kV base system will drive the RFQ cooler in the TITAN test area for an initial period to characterize injection/extraction optics in conjunction with the TITAN test ion source. Subsequently the entire RFQ assembly will form an injector system for the charge state booster (CSB) at the ISAC test stand location for tests on the effects of injection beam quality versus breeding efficiency, but ultimately, the RFQ will move to the ISAC-I hall in the spring, 2005.

Simulations of the RFQ buncher and cooler (*M. Smith UBC/TRIUMF; J. Dilling, TRIUMF*)

Detailed simulations are crucial when designing and optimizing complex devices and systems that rely on electromagnetic fields to transport and store charged particles. Consequently, extensive simulations of injection/extraction of an ion beam into/out of the RFQ device were carried out using, in this case, the commercial software SIMION 7.0 3d. This ion optics package determines the electric field for a user-defined electrode geometry using the over relaxation method. It furthermore allows the user to map out ion trajectories through the calculated electric field. Time dependent potentials on the electrodes can be defined, thus simulating rf fields. Originally, simulations of the plain ion optics geometry were carried out without considering how the optics would be held in place. However, with the finalization of the mechanical design for the optics, it became possible to investigate the ion paths including all details of the cylindrical symmetric and non-symmetric part of the optics support, vacuum vessel, etc. These simulations show that with the RFQ's current ion optics it will be possible to both inject and extract beam from both ends of the RFQ (see Fig. 212).

The SIMION 7.0 3d package incorporates features to simulate the presence of buffer gas, by means of an added force in a viscous drag model. Earlier studies have shown, however, that this oversimplifies the actual interaction. The results, particularly for smaller mass

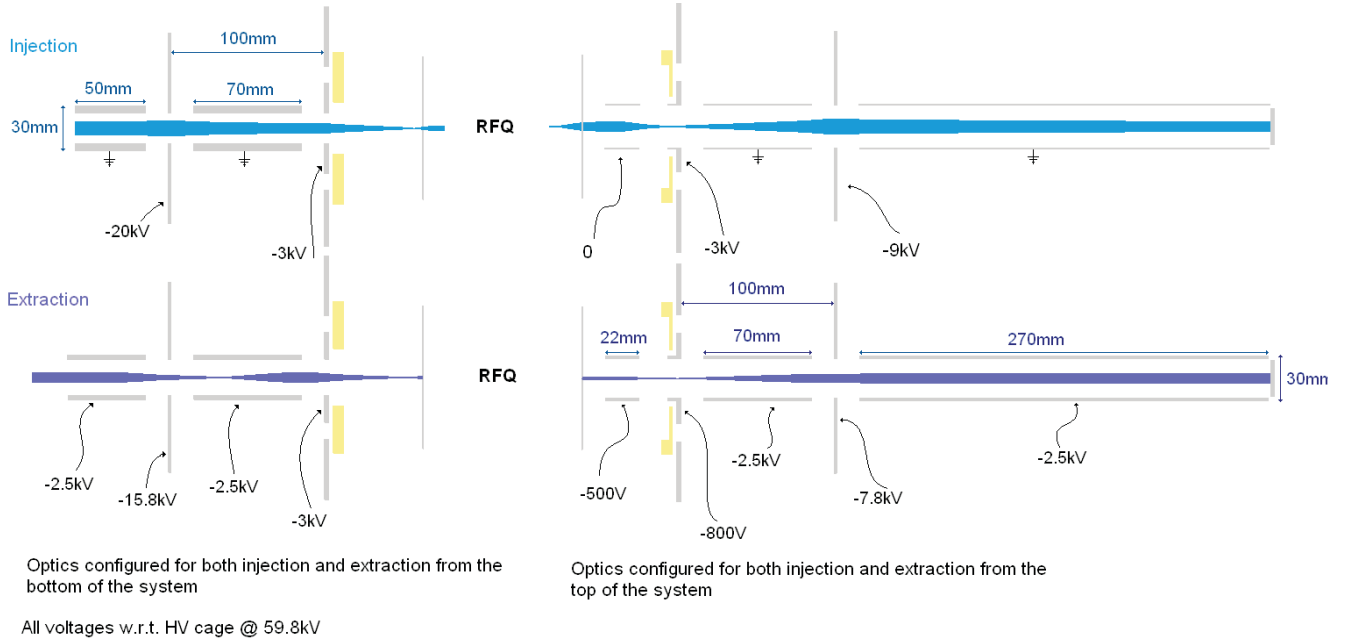


Fig. 212. Trajectories of ions injected (top) and extracted (bottom) at either end of the RFQ cooler and buncher, as simulated with the detailed geometry of the TITAN system.

differences between buffer gas and ions, differ dramatically from experimental observations. To overcome this problem, and to get more realistic results, in particular for the cooling of light ions like lithium, in helium buffer gas, a Monte Carlo code has been developed. It allows for the simulation of the collisional cooling process of the ions inside the gas-filled RFQ, employing documented ion-atom interaction potentials to calculate the scattering angle of an ion with respect to a gas atom in their centre of mass frame. Assuming a purely elastic collision, this scattering angle can be related to the energy lost by the ion during the collision. In order to test the precision of the code, simulations of the drift of ions in a gas-filled uniform electric field were carried out. It has long been known that a cloud of ions drifting in such a uniform electric field will move with an average velocity, the drift velocity, which is dependent on the ratio of the applied electric field to the gas number density. This velocity can also be related to a quantity known as the ion mobility which is the ratio of the drift velocity to the applied electric field. Such systems have been investigated and data exist for a large number of different ions drifting in various species of gas. The Monte Carlo simulation reproduced the experimental mobility data for both lithium and argon in helium to within experimental error. This code was then used to simulate the cooling of both lithium and argon ions inside the trap. It was found that for lithium ions cooled in helium at a pressure of 1.5×10^{-2} mbar with an applied rf field with a 400 V peak-to-peak voltage at a frequency of 2.7 MHz, a final cloud temperature of

around 1400 K was reached in approximately $700 \mu\text{s}$. This is expected to be significantly higher than room temperature due to the effect of rf heating. Although the average gain in energy for an ion oscillating in an rf field with no collisions is zero, when collisions are taken into account the particle's energy is scattered outside of the plane in which it is oscillating and hence the ion gains energy from the rf field. Figure 213 shows the velocity distribution or transversal energy of such a lithium ensemble after 2 ms. The temperature was taken from a 95% envelope of the distribution.

For argon ions in helium at 2×10^2 mbar with the rf field at 400 V peak-to-peak with a frequency of 1 MHz, a final temperature of under 900 K was reached in approximately $1000 \mu\text{s}$. This is expected to be lower than the final temperature of lithium as argon is much

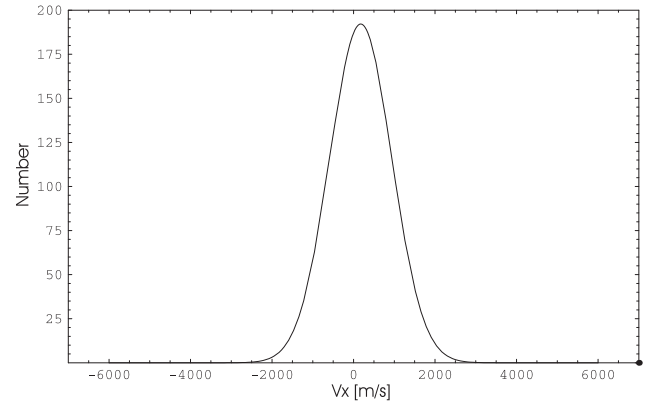


Fig. 213. Transversal emittance distribution of Li ions in a He buffer gas, as simulated with a collisional Monte Carlo code.

heavier than lithium and hence the average scattering angle is smaller, leading to a smaller probability of out-of-phase scattering.

Furthermore, simulations were carried out to investigate how driving the RFQ buncher with a square, as opposed to a sinusoidal, rf potential affects the final temperature of the trapped ion cloud. It was found that the final temperatures for argon were higher than those for the sinusoidally varying potential by around a factor of 2. This is due to the fact that the effective potential acting on the ions is steeper when trapping with a square wave as opposed to a sinusoid.

The code will now be used to look at the effect of cooling lithium in a trap driven with a square rf potential. The cooling of cesium will also be simulated such that results for heavy, medium and light mass ions are obtained. Furthermore the simulation of the extraction of the cooled ion clouds from the system will be carried out such that results can be compared to experimental data.

The TITAN high-current EBIT progress

(G. Sikler, TRIUMF; C. Osborne, Heidelberg/TRIUMF)

The main purpose of the TITAN electron beam ion trap (EBIT) is clearly the rapid charge-breeding of radioactive isotopes delivered by ISAC. In our planned system, a high-intensity electron beam is directed from an electron gun along the axis of a strong magnetic field, passing through the field and into a collector. Ions may then be injected into the field, and hence, into the path of the electron beam where they are radially trapped by the space-charge of the electron beam. Axial trapping is provided by potentials applied to drift tubes around the trap centre. The electron current will then ionize the atoms into higher charge-states, which may then be subsequently extracted and sent to the next trapping system of TITAN, the Penning trap, or examined *in situ*. The TITAN EBIT project is being built at the Max Planck Institute for Nuclear Physics in Heidelberg, Germany. This EBIT is expected to produce an electron beam of up to 5 A in order to rapidly and highly ionize short-lived isotopes. The EBIT design is based upon the existing Heidelberg EBIT, with a few notable design modifications – in particular, the superconducting magnet is a cryogen-free system, where the magnetic coils are coupled to an external cryo-cooler system. This superconducting magnet (see Fig. 214), following recent post-delivery tests, has been found to be very robust and user-friendly, and exceeding the initial specifications. The magnet is capable of producing fields of up to 6 T, with the superconducting coils held at 4.6 K. Electron gun designs have been completed for three different sizes of cathodes (necessary to achieve a full range of currents up to 5 A) and are currently under construction.

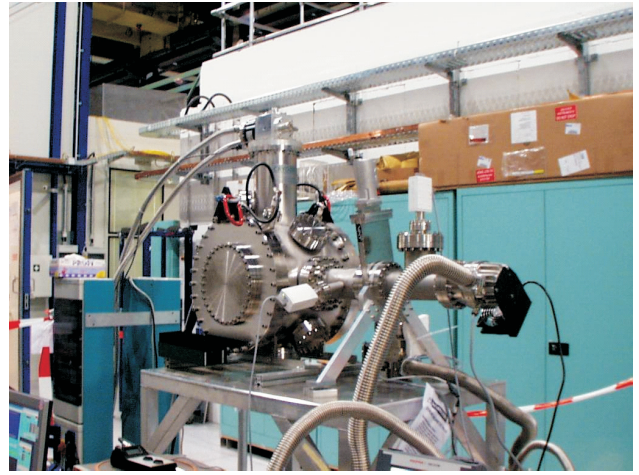


Fig. 214. Photo of the 6 T cryogen-free superconducting magnet, after delivery to the Max Planck Institute in Heidelberg, Germany.

The design of these guns has been driven largely by the results of simulations performed with the ion trajectory simulation software TRICOMP 5.0. With this software, the geometry of the EBIT (cylindrical symmetric) is defined using a triangular mesh in which electrodes are allocated potentials and magnet coils allocated currents. The software can, based on these parameters, calculate all of the electric and magnetic fields throughout the EBIT. Ion beam trajectories in the EBIT can then be evaluated, modelling space-charge-limited emission of electrons from a cathode surface. The passage of the electron beam through the EBIT is then determined, the electric fields being simultaneously recomputed to account for the local field modification due to the space-charge of the electron beam. The purpose of this is twofold: it facilitates design of electron gun components and other electrodes in order to deliver 100% of the electron beam cleanly through the EBIT, and produces space-charge-modified electric fields necessary for further modelling of injection and extraction of ions into and out of the trap. Figure 215 shows an example of electron beam trajectories for the medium-sized cathode, issuing from

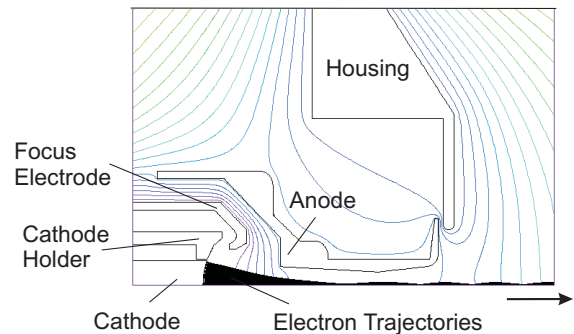


Fig. 215. Simulated electron trajectories calculated with the proposed TITAN-EBIT 5A e-gun geometry and including space charge effects. The X axis spans 5 cm.

the cathode surface and tracked beyond the electron gun aperture. The X axis spans 5 cm and electric field lines are traced on to the plot. So far these simulations have supported the design of all optical elements and determined optimal settings for all potentials and magnetic fields and their alignments relative to one-another. Component testing has shown that these optima all lie within the operating scopes of each element.

Beam monitoring system

(*H. Sharma, Manitoba/TRIUMF; R. Cussons, TRIUMF*)

The TITAN system is being set up for mass measurements of short-lived isotopes with high precision. The beam of radioactive nuclei from ISAC will be manipulated in various ways before transferring it to the Penning trap for the desired mass measurement. For this purpose the beam has to pass through devices such as a gas filled linear radio frequency quadrupole and an electron beam ion trap. For the optimal operation of these devices, and the subsequent beam transfer, it is important to monitor the beam characteristics at various stages. Hence, a general purpose beam monitoring detector has been developed which simultaneously allows an optical readout and digital recording of the beam profile and the beam intensity. It consists of micro-channel plates (MCP) in chevron arrangement, a phosphor screen and a fibre-optic image guide. The detector and a drift-tube have been mounted on an electrically isolated mechanically rotating feedthrough so that they can, alternatively, be brought in and out of the beam axis.

The beam impinging on the MCP produces a flux of secondary electrons which are further multiplied and subsequently accelerated towards the phosphor screen in order to produce a visual image of the beam. The beam image is transmitted to a view port via a fibre-optic image guide which is then recorded by a CCD camera and stored on a PC. Simultaneously, the current pulses from the aluminum-coded phosphor screen are processed by using a conventional electronic set-up, in order to estimate the beam intensity.

In order to observe the performance of the beam monitor, several test measurements have been carried out using a calibrated ^{241}Am alpha-source inside the vacuum chamber, at a pressure of about 3×10^{-8} mbar. The $57 \pm 4\%$ efficiency of the detector that was determined from these measurements was found to be in agreement with the 63% open area ratio quoted for the MCP. By using a mask with holes of 1, 2, and 3 mm the beam spots were resolved with a precision of 0.1 mm, as shown in Fig. 216.

The whole MCP surface was scanned using a mask with a grid of 1 mm holes, as shown in Fig. 217. The surface plot is in agreement with the intensity distribution of the incoming alpha particles.

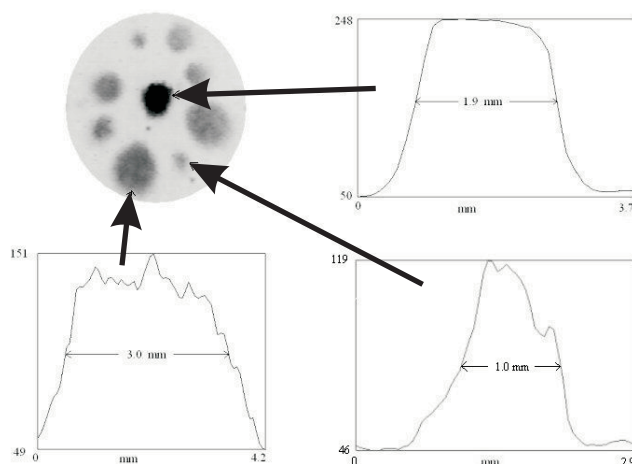


Fig. 216. Mask image with holes of different diameter and corresponding pixel intensity distribution for the beam spots.

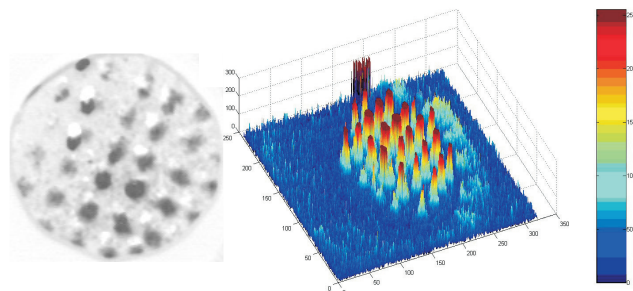


Fig. 217. The image of the mask (left) with equal-sized holes and corresponding surface plot. The lighter spots on the left image are artificial, due to the reduction of background.

R&D for the Time Projection Chamber for the International Linear Collider

(*M. Dixit, Carleton/TRIUMF*)

Introduction

The time projection chamber (TPC) is a prime candidate for the main charged particle tracker for the future international linear collider (LC). With more complicated event topologies and higher backgrounds than previous e^+e^- colliders, the LC TPC has to measure ~ 200 track points with a resolution of less than $100 \mu\text{m}$ for the full 2.6 m drift. The ambitious resolution goal is close to the limit from the ionization electron statistics and transverse diffusion in the gas. The target resolution is more than two times better than can be achieved by the existing TPC readout technology based on multiwire proportional chambers.

Using micropattern gas detectors (MPGD), such as the gas electron multiplier (GEM) and the Micromegas, for the readout will almost entirely eliminate the large $E \times B$ systematic effects which limit the performance of the proportional wire TPC systems. The MPGD-TPC has the potential to reach the LC resolution goal. With fast spatially confined charge signals, it

also has the potential for a much better double track resolution (in r - ϕ and in z) than the wire chamber TPC.

Due to reduced transverse diffusion at high magnetic fields, the maximum charge cluster size arriving at the LC-TPC anode readout will be on the order of 0.5 mm. The conventional TPC can measure the avalanche centroid position on the anode wire precisely with several mm wide cathode readout pads. To reach the same precision, the MPGD-TPC with standard charge readout will require a fully instrumented sub-millimetre width anode pad structure resulting in a significant increase in the cost and complexity of the detector.

MPGD-TPC R&D at Carleton

Depending on the pad size and the diffusion properties of the gas, the MPGD anodes do share some of the track ionization charge. Using cosmic rays, we have systematically studied the limits of achievable spatial resolution for a GEM-TPC with wide anode pads using conventional charge readout techniques. With the aim to achieve better resolution with wide pads, a new concept of position sensing from charge dispersion has been developed where the MPGD anode plane is made of a high surface resistivity material. The preliminary results are quite promising. These R&D activities are described below.

Cosmic ray resolution studies with a GEM-TPC

A small 15 cm drift TPC with a double-GEM readout endcap was designed and built to study the spatial resolution that could be achieved with wide pads using standard charge readout electronics. There was no magnetic field.

Resolution was measured for two gas mixtures: Ar:CO₂/90:10 and Ar:CH₄/90:10 (P10). The differences in the transverse diffusion for the two gas mixtures helps to disentangle various effects contributing to the observed spatial resolution. In addition, ArCO₂ has a relatively low transverse diffusion which leads to measurement conditions similar to those in a high magnetic field.

The anode readout board had a total of 192 pads in 10 rows. The pad sizes were different for different rows so we could study the dependence of the spatial resolution on the pad geometry. Wire preamplifiers, borrowed from Aleph TPC at LEP, were used for charge amplification. After 3-fold multiplexing, the signals were digitized at 200 MHz by 64 FADCs designed and built at the University of Montreal.

The data analysis used the technique of track reconstruction where all the pad data for the event is fitted assuming a Gaussian track profile from diffusion. The resolution as a function of drift distance for $2 \times 6 \text{ mm}^2$

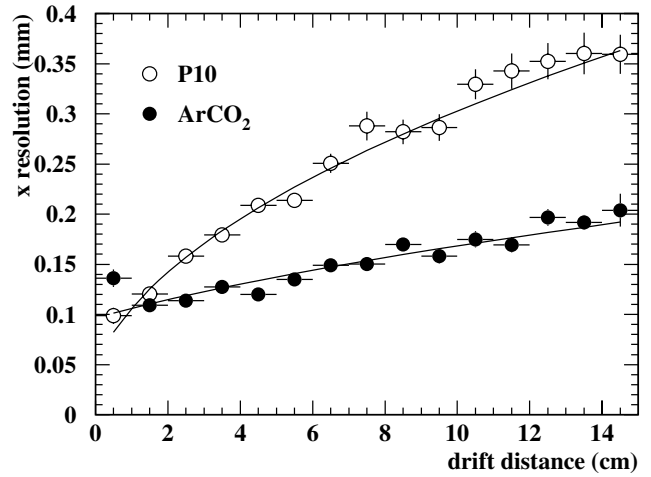


Fig. 218. Spatial resolution of the TPC as a function of drift distance for 2 mm wide pads for cosmic ray tracks with $|\phi| < 5^\circ$.

pads for small angle tracks is shown in Fig. 218. The measured spatial resolution for short drift distances for both gases was about 100 μm . From studies of 2.5 and 3 mm wide pads we find that, to achieve the best resolution, the pad widths should not be more than three times larger than the RMS charge cloud width. The resolution was also measured as a function of the track crossing angle in good agreement with the theoretical prediction.

The measured resolution values are about 50% larger than the limit from the ionization electron statistics and transverse diffusion.

Position sensing from charge dispersion in micro-pattern gas detectors with a resistive anode

We have developed a new concept to measure the position of a localized charge cluster in an MPGD using wide pads similar to those used in previous wire/pad readout TPCs. A high surface resistivity film, used for the anode, is bonded to the readout plane with an insulating layer of glue (Fig. 219). The resistive anode film forms a distributed 2-dimensional resistive-capacitive network with respect to the readout pad plane. Any localized charge arriving at the anode surface will be dispersed with the RC time constant determined by the anode surface resistivity and the

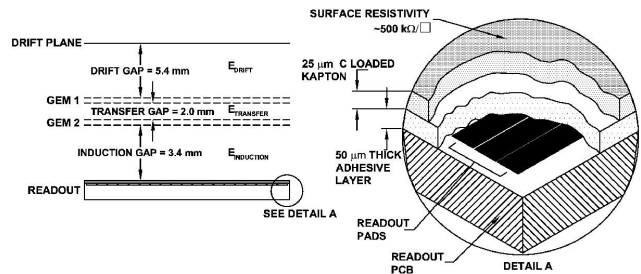


Fig. 219. Schematics of the resistive anode double-GEM detector for charge dispersion studies.

capacitance per unit area, the latter determined by the spacing between the anode and readout planes and the dielectric constant of the glue. With the initial charge dispersing and covering a larger area with time, wider pads can be used for position determination.

A simple model can explain the features of the new approach. Charge division, described by the well known Telegraph equation, is often used to measure the position of the avalanche on a proportional wire. We generalize the concept to 2-dimensions. At $t = 0$, a point charge is placed at the origin on a resistive anode surface of infinite radius (for simplicity). The space-time evolution of the charge density function ρ on the anode surface is given by the generalized 2-dimensional Telegraph equation:

$$\frac{\partial \rho}{\partial t} = h \left[\frac{\partial^2 \rho}{\partial r^2} + \frac{1}{r} \frac{\partial \rho}{\partial r} \right] \quad \text{where} \quad h = 1/RC$$

where R is the surface resistivity and C is capacitance per unit area.

The solution for the charge density function is given by:

$$\rho(r, t) = \frac{1}{2th} \exp(-r^2/4th).$$

The time dependent charge density function for the resistive anode is capacitively sampled by the readout pads. The charge pulse on a pad can be calculated from the pad geometry, the location of the pad with respect to the initial charge and the RC time constant of the system.

The charge dispersion GEM studies were done with a Ar:CO₂/90:10 gas mixture. A 25 μm thick film with a surface resistivity of $\sim 500 \text{ k}\Omega$ per square was glued to the pad readout board. The spacing between the anode and readout planes was about 50 μm defined by the glue thickness.

A $\sim 45 \text{ keV}$ bremsstrahlung X-ray source collimated to $\sim 50 \mu\text{m}$ was used for the measurements. A computerized translation stage moved the X-ray spot in small steps across a series of $2 \times 6 \text{ mm}^2$ pads read out with Aleph TPC charge amplifiers. The signals were digitized using Tektronix digitizing oscilloscopes.

Figure 220 shows the measured spatial resolutions for several pads as the collimated X-ray spot was scanned across the detector. The standard deviations of the position measurements, all in the range of 60 to 80 μm , are consistent with the size of the collimated X-ray spot at the detector.

The charge dispersion concept has been tested with the Micromegas with measured spatial resolution close to that for the GEM. The resistive anode additionally suppresses HV breakdown in Micromegas. We have demonstrated stable detector operation at unprecedented high gains near $5\text{--}6 \times 10^6$ in the limited

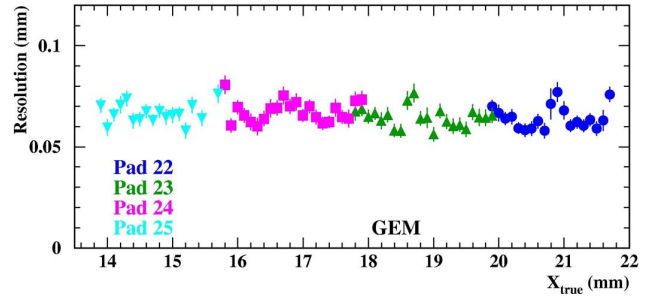


Fig. 220. Spatial resolution for $2 \times 6 \text{ mm}^2$ readout pads with charge dispersion readout measured with a collimated X-ray source. The anode resistivity was $0.5 \text{ M}\Omega/\text{square}$.

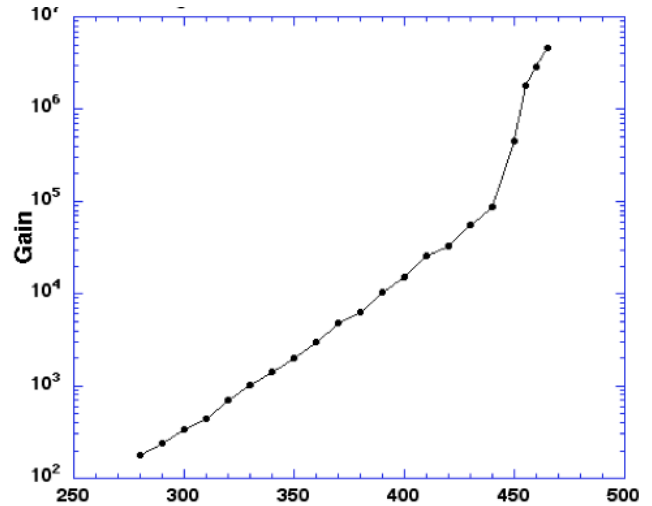


Fig. 221. Micromegas gain studies with a resistive anode. The resistive anode suppresses sparking and makes possible stable Micromegas operation at high gains in the limited streamer region.

streamer mode (Fig. 221). The Micromegas work is being done in collaboration with Saclay.

Future plans

The choice of technology decision for the LC accelerator will be made in 2004. A major LC TPC milestone goal is to test a realistic prototype by the year 2007. We expect to contribute significantly to this international effort. The following R&D steps are foreseen: i) completion of cosmic ray proof of principle spatial resolution tests of a small TPC with GEM and Micromegas with a resistive anode; ii) beam tests for two-track resolving power; and iii) magnetic field tests of a 50 cm diameter Saclay Micromegas TPC outfitted with a resistive anode.

Linear Collider TPC R&D group: R. Carnegie, H. Mes, K. Sachs (Carleton), M. Dixit (Carleton/TRIUMF), J.-P. Martin (Montreal), and D. Karlen (Victoria).

Linear Collider TPC Development

(D. Karlen, Victoria/TRIUMF)

In the summer, a time projection chamber with micropattern gas detectors was operated for the first time in a magnetic field, using the facilities at TRIUMF. This is an important step in demonstrating the capabilities of a new design for a large volume gaseous tracking system, suitable for large particle and nuclear physics experiments.

Introduction

A leading candidate for the central tracking system at a future linear collider experiment is a time projection chamber (TPC) readout by micropattern gas detectors (MPGDs), such as gas electron multipliers or micromegas detectors. This concept may offer two distinct benefits over traditional TPCs; improved tracking resolution and better two particle separation. When operated in a uniform magnetic field, the resolution of a traditional TPC, one with gas amplification provided by a wire grid, is limited by the so-called $E \times B$ effect. This refers to electric field components transverse to the magnetic field in the amplification region which cause segments of ionization to rotate. Since the ionization is not uniform along the track, the rotation results in degraded spatial resolution. The feature separation of an MPGD, the hole or mesh pitch, is much smaller than can be achieved with a wire grid. As a result, the transverse electric field components are much smaller and the $E \times B$ effect is significantly reduced. The electronic signals measured in a traditional TPC are primarily due to the motion of positive ions away from the anode wires. These signals tend to be relatively slow, are spread over a large region, and therefore limit the capability of separating two nearby tracks. The signals observed with a MPGD TPC are due to the motion of electrons across a small gap and by the collection of the electrons on pads, giving faster and narrower signals and therefore improved capability to separate two nearby particles.

The narrower signal distribution presents a new challenge for large scale TPCs, such as those being considered for a future linear collider. When operated in a strong axial magnetic field in a fast gas, the transverse width of the charge distribution as it reaches the TPC endplate may be only a few hundred microns across. Populating an endplate whose area is several square metres with pads with sub-millimetre dimensions would be cost prohibitive due to the associated electronic readout system. One solution to this challenge is to use gas diffusion in the region near gas electron multipliers (GEMs) to spread the charge over a wider area without sacrificing the track resolution.

Victoria TPC prototype

In order to demonstrate that the $E \times B$ effect is negligible and that gas diffusion after GEM multiplication can be used to spread the charge signals over multiple pads, a prototype TPC was designed for operation in a magnet at TRIUMF. The device, shown in Fig. 222, was constructed primarily of acrylic at the Science Technology Centre at Carleton University. A 30 cm long drift volume has a uniform electric field defined by 60 brass hoops connected to a voltage divider. Electrons produced in the ionization of gas by charged particles traversing this volume drift towards 2 GEMs separated by about 2 mm. The amplified electrons are then collected by pads 5 mm from the second GEM with dimension $2 \times 7 \text{ mm}^2$. The charge signals on the pads are amplified and digitized using readout electronics developed for the STAR TPC.

Results from tests

The TPC prototype was installed in the TRIUMF magnet and operated with a traditional fast gas, P10 (Ar CH₄ 90:10). A cosmic ray telescope was set up above and below the magnet in order to trigger the readout electronics when a cosmic ray particle passed through the TPC volume. The set-up is shown in Fig. 223.

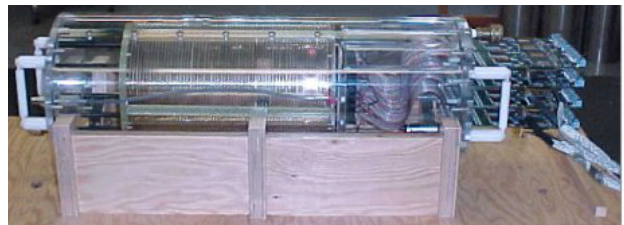


Fig. 222. Photograph of the prototype TPC constructed for magnetic field tests at TRIUMF. The outer diameter of 8.75 in. was chosen to fit inside the 9 in. bore, 0.9 T magnet. The drift volume is 30 cm long, followed by two GEM devices in front of an array of 256 pads, readout by front-end cards (on the right) produced for the STAR TPC.

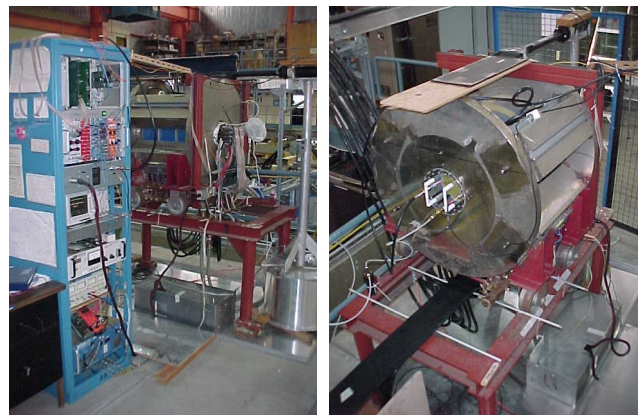


Fig. 223. Set-up of the TPC with the TRIUMF magnet. The cosmic ray telescope is visible in the photograph on the right.

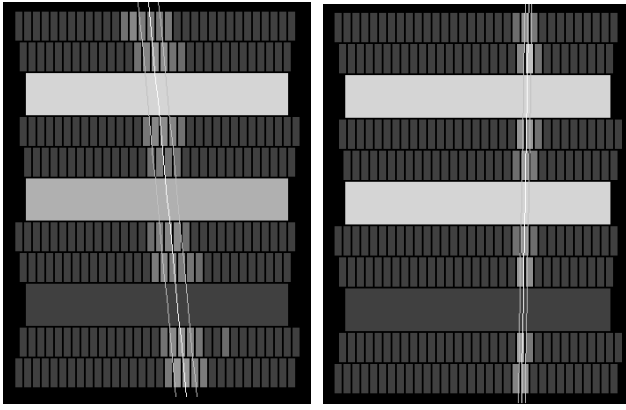


Fig. 224. Event displays from cosmic ray events recorded at zero field (left) and 0.9 T (right). The brightness of the pads represents the size of the signal recorded by the corresponding electronics channel. Each track drifted about 25 cm. The white lines show the results of track fits, with the outer lines showing the determined track widths. They are 2.3 mm and 0.8 mm for these events.

Event displays from cosmic ray events are shown in Fig. 224 for data recorded at zero and full magnetic field. For both events the drift distance was approximately 25 cm, and the reduction in transverse diffusion with magnetic field is easily seen. Eight rows of $2 \times 7 \text{ mm}^2$ pads are sampled at 20 MHz and digitized to 10 bits by electronics developed for the STAR TPC at RHIC.

A track fitting program has been implemented using a likelihood method. It determines the track orientation and transverse width from the observed pattern of charge sharing across each row. The program is used to estimate the resolution of a single row by comparing the track found by the other 7 rows, to the track location determined by one row. The resolution as a function of drift distance is shown in Fig. 225 for zero, half, and full magnetic field. For full field operation, the contribution to the resolution from transverse diffusion is significantly reduced, but is still observable.

A simple Monte Carlo simulation program has been developed to understand the performance of the GEM TPCs. Primary ionization clouds of electrons are produced and diffused through the gas volumes, amplified at the GEM foils and collected by the pads. Signals are generated on the pads according to the arrival time of the electrons and the response of the electronics. The simulated and real events are analyzed by the same program, and the derived resolutions are compared in Fig. 226. The agreement between the data and simulated resolution estimates is good.

Next steps

After the successful tests at TRIUMF, the TPC was brought to the DESY Laboratory in Hamburg, Germany, in the late summer for tests in magnetic fields

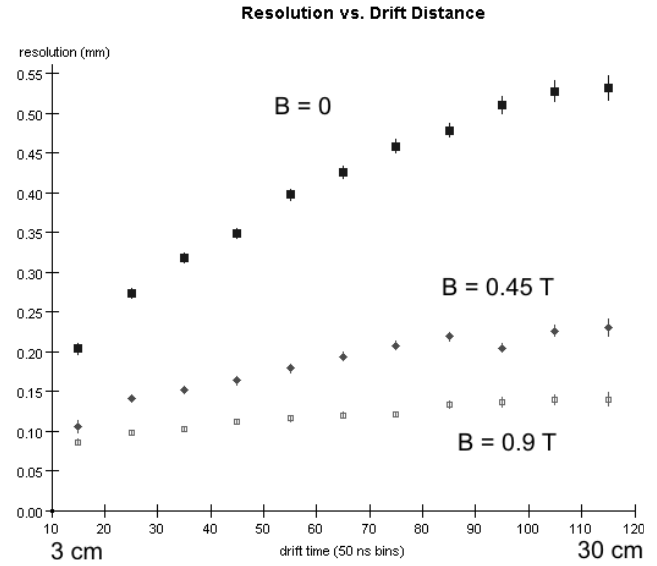


Fig. 225. Resolution (mm) is shown as a function of drift time (50 ns time bins). The horizontal axis corresponds to drift distances between 3 and 30 cm. The upper points are at zero field, the middle points are at 0.45 T, and the lower points are at 0.9 T. These data are from a preliminary analysis.

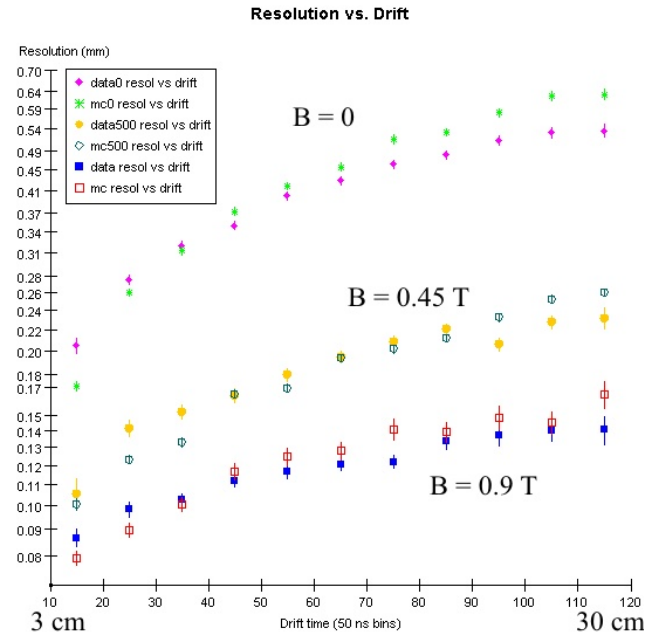


Fig. 226. Resolution (mm) is shown as a function of drift time (50 ns time bins). The horizontal axis corresponds to drift distances between 3 and 30 cm. The solid points correspond to real data, the open points are from simulated data. The results shown here are preliminary.

up to 5.3 T. A full analysis of these data is under way and a publication of this work is forthcoming.

In 2004, the group is preparing a second readout endplate to test with a micromegas device in place of the GEMs. Also, the TPC will be modified to allow tests with an ultraviolet laser. Data with consistent

ionization patterns from the laser will be useful for calibration studies with the GEMs and to develop a tracking algorithm for the micromegas device.

In the coming years, a technology decision for the TPC readout will be made and a large prototype constructed, in collaboration with an international group working on TPC R&D for the linear collider.

University of Victoria LC TPC group in 2003: Dean Karlen, Paul Poffenberger, Gabe Rosenbaum. This work has benefitted from the work of collaborators in Canada: R. Carnegie, H. Mes, K. Sachs (Carleton), M. Dixit (Carleton and TRIUMF), J.-P. Martin (Montreal).

CYCLOTRON OPERATIONS DIVISION

INTRODUCTION

During 2003 the cyclotron was available for $\sim 88\%$ of the hours scheduled, despite the unexpected problems encountered. However, the total number of available hours was 5176, exceeding the 4845 hours available in 2002. The total beam charge delivered at 500 MeV was 533 mAh of which 450 mAh were delivered to BL1A for meson production and 83 mAh were delivered to BL2A for RIB production. Beam was delivered for the first time down BL2A3 to the east target station (ITE) of ISAC. Approximately 117 mAh were delivered at 85 MeV to rubidium targets in beam line 2C4 for the production of ^{82}Sr that is used for medical diagnostics.

The 88% availability of the cyclotron was 2% lower than last year and the total downtime was 200 hours higher than average, due primarily to the problems with the inflector that forced an unscheduled lid-up in May. The low beam-charge delivery to BL1A was mainly caused by a water leak in one of the targets in the triplet assembly that forced us to run with a low average current for a while. A large water leak at an insulator on a quadrupole magnet (1AQ15) caused further reduction in the beam-charge delivery.

During the development shifts, two high current milestones were reached. A record-setting peak current of $420\text{ }\mu\text{A}$ was extracted at 25% duty cycle with 63% cyclotron transmission and a peak current of $370\text{ }\mu\text{A}$ at 50% duty cycle was extracted for ~ 3 hours with good stability and with a cyclotron transmission greater than 62%.

During the winter shutdown, the major beam line activities were the replacement of the chronically leaking BL1 triplet, replacement of crumbling blocks around the 1AT2 target, and replacement of shielding blocks to accommodate the new triplet. A number of water and vacuum leaks were repaired along with plenty of routine maintenance work. A chronological detailed description is presented in the Primary Beam Lines section. The major vault and tank activities include work on the extraction probes, slits, periscopes, correction plates, thermocouples, rf voltage probes, ground-arm-tip measurements, transmission line modifications, new tank ion gauges, and new inner and outer tank vacuum seals.

In the fall mini-shutdown, a decision was made to raise the lid to replace the water-cooled probe (WCP) that had failed earlier and to exchange the 2C extraction foils. In the meson hall, water leaks were repaired at the 1A triplet and M9Q5, and electrical connectors at M9Q1, which had melted and caused the M9 line to be shut down, were replaced. As well as tank and

beam line activities, the support groups were also very busy in their own respective areas.

RF downtime was similar to last year but it is worthwhile noting that only 20% of the downtime was due to sparking compared to 80% last year. Although most of this improvement in the sparking rate is due to the new ground-arm-tip control system that was installed in the September, 2002 shutdown, it was further improved this year by modifications to the software in the rf control system.

The major hardware failures were a 250 kW resistive load, damage to the transmission line, water leaks in the high-voltage power supply, and the failure of the 250 kW power tubes. Improvements in interlock protection circuitry, water cooling circuits, and reliability are being addressed to minimize hardware failure. During the winter shutdown the major activity was an extensive program to improve readings of the cyclotron voltage probes.

In the rf refurbishing program a second new combiner was installed. It operated reliably during the past year. A third new combiner was tested to 500 kW into a resistive load and will be installed in the winter shutdown next year. An upgrade to one of three capacitor stations in the matching section of the transmission line allows for faster replacement time, thus reducing the radiation dose for this job. The remaining two will be installed in the shutdown next year. A multiplexing and diagnostic system was built that provides first-event detection from as many as 24 monitoring points when rf sparking occurs.

In the Probes and Diagnostics group, progress was made on the refurbishment of the HE probe that included some prototyping of the probe-head mechanics. Several of the refurbished monitors were installed and a number of other monitor improvements were made.

The Vacuum group encountered a few problems with the B-20 cryogenerators related to lead loss in the 20 K regenerator, leaks in the helium gas plumbing, and the malfunction of the lubrication delay device. Despite these problems, downtime due to the vacuum and cryogenic systems was minimal. BL1A was upgraded to accept Varian turbo pumps, which involved a large amount of re-cabling and leak checking.

In ISIS, two new CUSP ion source bodies were built for use in the I1 terminal, the old wire-scanner PC-based data acquisition and display system was replaced, and four new sets of motor-driven variable-aperture slits were designed and built. The ISIS group is responsible for the inflector/deflector system and was very busy during the lid-up intervention in May for repairs.

The Controls group completed the new ISIS wire-scanner system controls, the rf spark first-event detector system controls, the phase out of the last VAX computer, the decommissioning of one of two DSSI disk systems, the implementation of a wireless infrastructure and its initial applications, and software upgrades.

Operational services, which include Remote Handling, Magnet Power Supplies, Electrical Services, and Mechanical Services, continue to play a vital role in the reliable operation of the cyclotron. Their services extend to the whole TRIUMF site and are appreciated site wide.

The work for “Safety-Critical Monitoring for Prompt Radiation Hazards” continued this year. Five pairs of safety-critical neutron and gamma monitors were installed around the proton hall. Eight safety-critical detector trips occurred during the year. A report, written for each event, included an estimate of the maximum radiation field outside of the shielding (at licensed beam current) had the beam not been tripped off and a record of whether the radiation field exceeded 50 mSv/h. A review meeting on the Conceptual Design of the Cyclotron Beam Trip and Prohibit System was held and the design concept was approved following some recommended changes in the documentation

BEAM PRODUCTION

Beam delivery for the year was reasonably successful although total charge production was down 10% from last year’s record. Cyclotron performance continued to be enhanced by the use of the rf booster which was on during much of the high current operation, partly to satisfy the occasional demand for 2 ns pulse-width beam but also to improve the cyclotron transmission (typically close to 65%) and reduce the measured tank beam spill (usually below $2.5 \mu\text{A}$). Thirteen weeks of shutdown left 5878 scheduled operational hours of which 5176 were achieved for an availability of 88%, 2% less than last year. These totals include 231 hours used for development and tuning and, as shown in Fig. 227, were split roughly 4:1 between high-current beam production and lower-intensity operation. The latter usually involved beam delivery to ISAC with the proton irradiation facility (PIF) using BL1B and BL2C1 running in parallel. BL2C1 was also used at 74 MeV for ocular melanoma treatments for nine patients during five proton therapy (PT) sessions. These PT sessions, with the high intensity source online, required the use of the ISIS pepperpot to limit the injected beam current during patient treatment times. Again this year there was no BL4 operation and no polarized source operation.

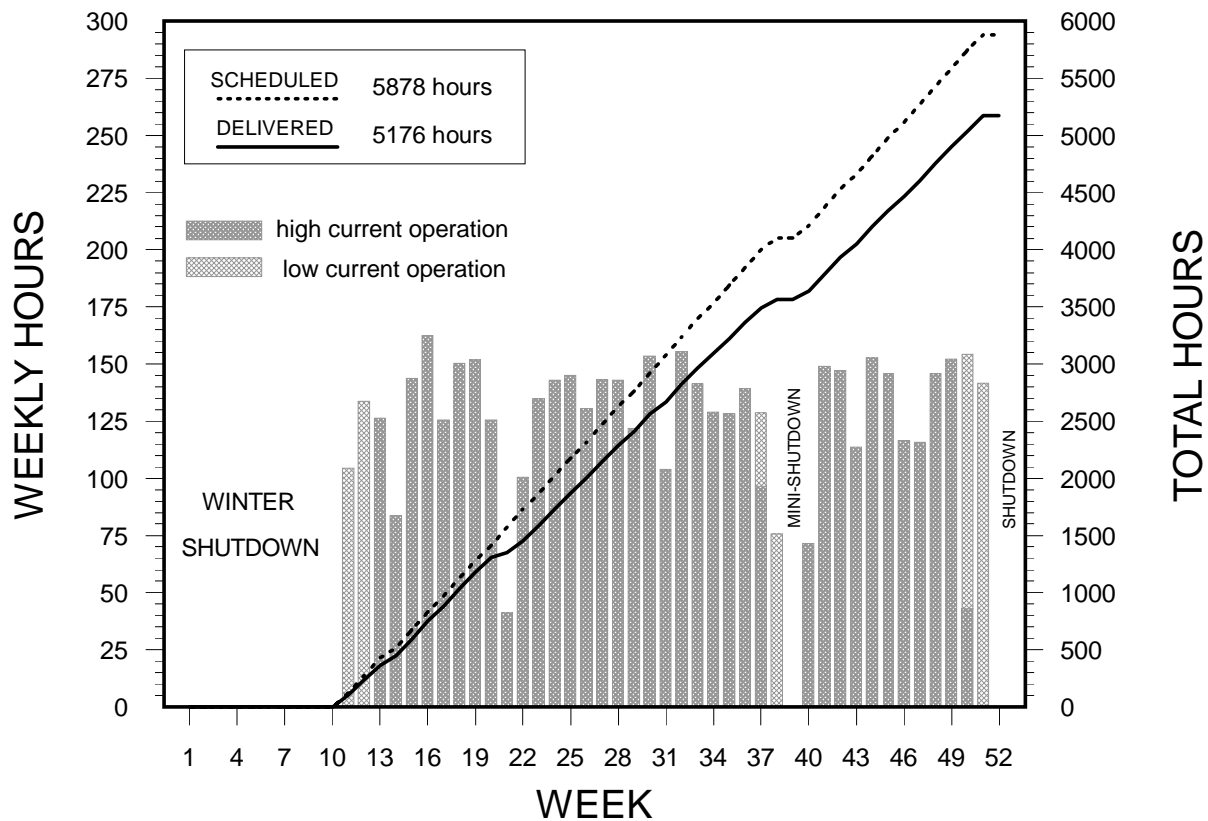


Fig. 227. Operational hours for 2003.

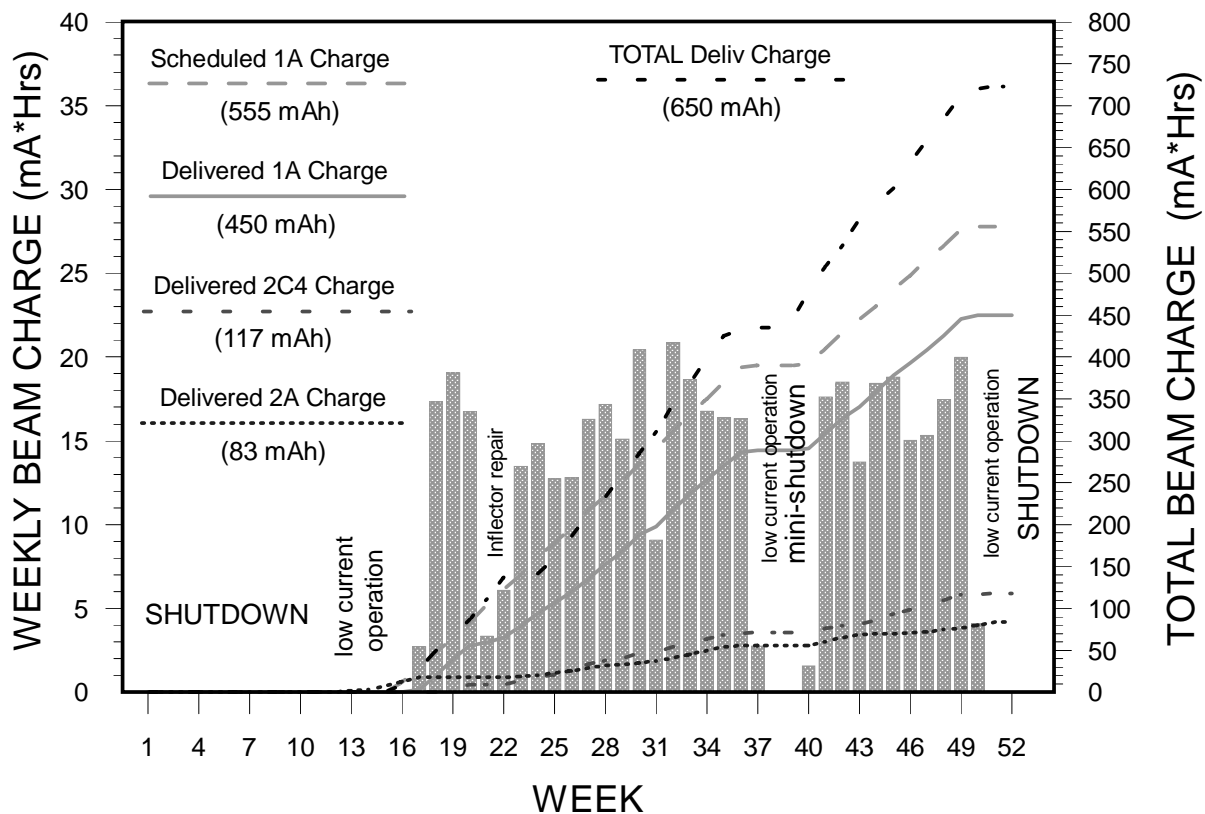


Fig. 228. Beam delivery for 2003.

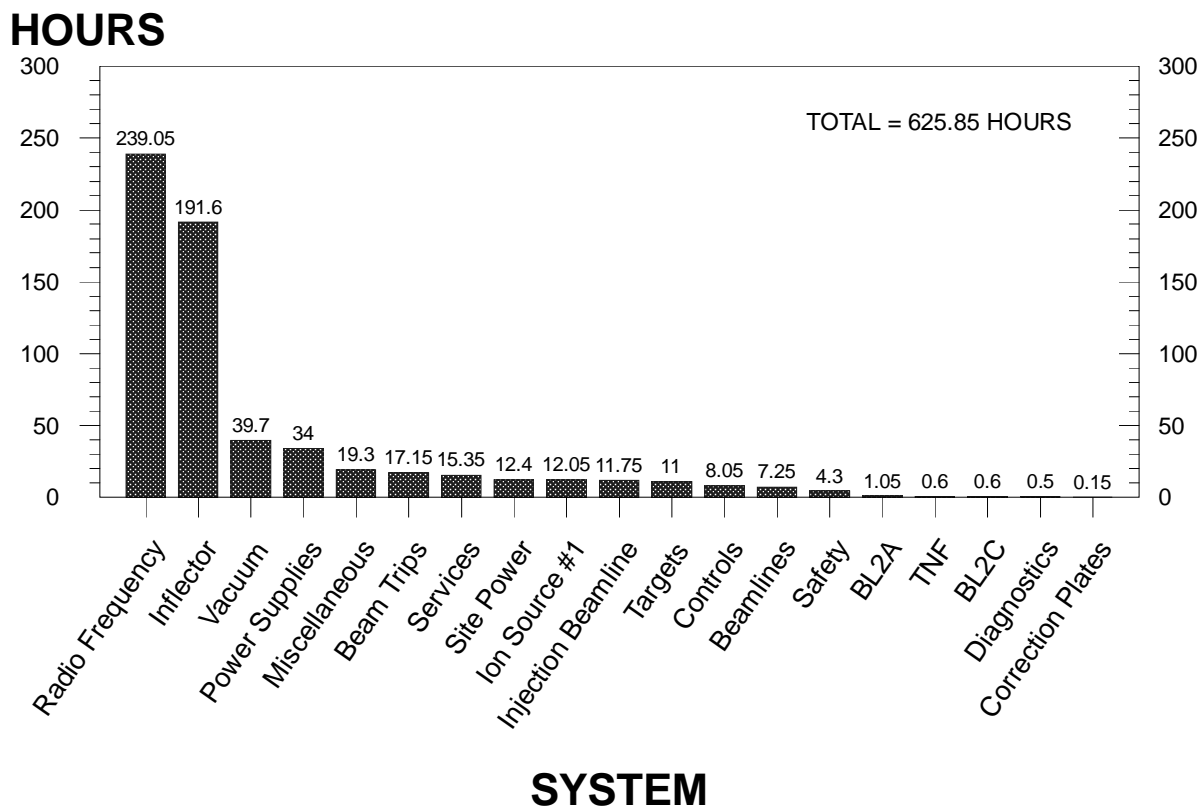


Fig. 229. Cyclotron downtime for 2003.

Table XXIII. Operational record for 2003.*

	Scheduled hours	Actual hours
<u>Cyclotron off:</u>		
Startup	163.0	131.10
Shutdown	2081.0	2104.90
Other	0.0	0.00
Cyclotron downtime	0.0	625.85
Overhead	31.0	84.60
Totals	2858.5	3562.65
<u>Cyclotron on:</u>		
Development	180.0	120.60
Cyclotron tuning	473.0	110.70
Beam to experiments	5224.5	4945.05
Totals	5877.5	5176.35
Actual/Scheduled = 5176.35/ 5877.5 = 88.1% availability		
<u>Beam to experiments:</u>		
1A Production	4167.5	3677.60
1A Development/tuning	127.0	40.20
1A Down/open/no user	549.0	836.80
1B Production	323.0	74.40
1B Development/tuning	0.0	8.25
1B Down/open/no user	58.0	307.80
Total 1A+1B production	4490.5	3752.00
2A Production	4627.5	2963.95
2A Development/tuning	0.0	25.95
2A Down/open/no user	597.0	1955.15
2C1 Production/tests	1247.0	201.50
2C1 Development/tuning	0.0	3.20
2C1 Down/open/no user	899.0	1499.40
2C4 Production/tests	3055.5	2731.50
2C4 Development/tuning	0.0	21.35
2C4 Down/open/no user	23.0	488.10
1A Beam charge (μAh)	555360.0	449495.00
2A Beam charge (μAh)	119300.0	83352.00
2C4 Beam charge (μAh)	143935.0	117379.00

* There was no BL4 production this year and the polarized source was not used.

Table XXIV. Beam to experiments for 2003.

Experiment*	Channel	Schedule #	Scheduled		Delivered	
			Hours	μAh	Hours	μAh
614	M13	103	2746.0	377785	2412.10	286410
614	M13	104	1317.5	165435	1265.50	157937
744	M9B	103	677.0	94780	659.75	81933
768	M15	103	150.0	21000	154.05	20862
782	M15	103	101.0	14140	95.00	13007
782	M15	104	148.5	19305	131.15	16741
791	M20B	103	127.0	17320	119.90	15966
842	M9B	104	254.0	33020	224.50	29269
843	M20B	103	150.0	21000	87.30	1918
843	M20B	104	81.0	10530	81.65	10538
844	M15	103	277.0	38780	273.00	24018
847	M15	103	150.0	21000	87.30	11918
847	M20B	103	150.0	21000	154.05	20862
851	M20B	104	127.0	16510	129.85	17412
875	M20B	103	423.0	56480	355.45	40958
877	M9B	103	150.0	19270	108.10	13563
877	M9B	104	150.0	19500	150.75	19198
883	M20B	103	150.0	21000	137.60	16933
883	M20B	104	117.0	15210	113.45	14808
895	M15	103	150.0	21000	141.60	18653
898	M20B	104	148.5	19305	131.15	16741
912	M20B	103	127.0	17780	116.05	15116
915	M15	104	94.0	6380	91.80	6411
916	M15	103	150.0	19270	108.10	13563
917	M20B	103	273.0	38220	269.65	36711
917	M20B	104	127.0	16510	98.75	13413
931	M15	104	127.0	16510	125.75	15856
932	M9B	103	127.0	17320	119.90	15966
938	M15	103	277.0	38780	274.05	30106
938	M15	104	127.0	16510	129.85	17412
939	M20B	103	265.0	33645	237.25	29837
939	M20B	104	244.0	25880	239.35	25142
941	M20B	103	127.0	17780	119.55	14850
942	M15	104	117.0	15210	113.45	14808
942	M20B	103	127.0	17780	135.75	10822
943	M9B	103	681.0	95340	550.45	60138
944	M15	103	150.0	21000	137.60	16933
944	M20B	104	150.0	21000	137.25	13196
949	M9B	103	127.0	16510	121.40	15540
945	M20B	103	150.0	21000	137.25	13196
949	M9B	103	115.0	14375	129.15	16274
949	M9B	104	127.0	16510	129.85	17412
950	M15	103	250.0	35000	246.20	25332
951	M15	103	127.0	17320	119.90	15966
953	M20B	103	254.0	35560	122.25	11976
953	M15	104	150.0	19500	155.05	19827
958	M15	103	273.0	36980	283.55	36970
959	M15	103	115.0	14375	129.15	16274

Table XXIV (cont'd.)

Experiment*	Channel	Schedule #	Scheduled		Delivered	
			Hours	μAh	Hours	μAh
960	M15	103	127.0	16510	75.90	4468
960	M15	104	150.0	19500	147.55	18731
962	M20B	103	150.0	21000	154.50	15256
963	M15	103	127.0	17780	131.90	17996
963	M20B	103	273.0	38220	265.55	32009
965	M15	103	127.0	17780	116.05	15116
965	M15	104	127.0	16510	98.75	13413
968	M9B	104	148.5	19305	131.15	16741
969	M15	103	172.0	24080	42.75	5708
969	M20B	104	150.0	19500	155.05	19827
974	M15	104	150.0	19500	150.75	19198
975	M15	104	69.0	8970	63.00	7922
977	M15	104	58.0	7540	58.40	7618
978	M20B	104	69.0	8970	69.10	8660
981	M20B	104	127.0	16510	125.75	15856
ISAC [†]	2A	both	4627.5	119300	2963.95	83352
ISOPROD	2C4	both	3055.5	143935	2731.50	117379
PIF	1B	both	323.0	0	74.40	0
PIF	2C1	both	815.0	0	184.70	0
P.THERAPY	2C1	both	432.0	0	16.80	0

* See Appendix D for experiment title and spokesman.

[†] Total proton beam on ITW and ITE for all ISAC RIB experiments and tests.

As Fig. 228 shows, the total beam charge delivered to meson hall experiments along BL1A was 450 mAh or 81% of the scheduled amount. This relatively poor outcome is a result of running with an average delivered current to beam line 1A of only 122 μA (for reasons described later) at the above reduced availability (88%). In addition to the BL1A charge, there were 117 mAh delivered at 85 MeV to rubidium targets in the solid target facility (STF) in beam line 2C4 for the production of radiopharmaceutical generators, about the same as last year. There were another 83 mAh, 8% more than last year's record, delivered to the two target stations in BL2A for the production of radioactive ion beams (RIB) for experiments in ISAC. A total extracted current exceeding 210 μA was sometimes shared by the three proton lines although 200 μA was more normal for extended production periods.

The annual downtime of 626 hours (Fig. 229) was about 200 hours higher than average mainly due to problems with the inflector (191.6 hours or 30.6% of the total). RF downtime was similar to last year at 239 hours (38%). Vacuum and power supply problems were distant runners-up, accounting for 6% and 5% respec-

tively. RF downtime arose from various faults but it is noteworthy that sparking, tamed considerably by software improvements late last year, played a relatively minor role at 20% of the total rf downtime or about 1 hour per week. The operational record and beam to experiments for the year are given in Tables XXIII and XXIV.

Winter Shutdown

For BL1A the winter shutdown was as long and involved as the previous year. Cyclotron work, however, was scheduled to finish a month earlier in order to deliver beam to PT, PIF and ISAC while activities in the meson hall continued. The main project there was the sorely needed replacement of the old and chronically leaking 1A triplet with a new one of a more serviceable design. This huge installation job began last year with the removal of interfering, defunct M8 front-end elements and involved rerouted services and custom shielding changes. Several crumbling shielding blocks in the area were also replaced and a number of water and vacuum leaks were repaired. These, as well as a plethora of more routine maintenance work, left no

time and dose remaining to remove the M11 septum, so that job that was postponed a year.

In the vault, the cyclotron lid was cycled briefly in early January in order to remove the highly radioactive copper beam blockers prior to some jack maintenance work. The lid was up most of February for diagnostics, rf and engineering physics systems maintenance. Diagnostics tasks included work on the extraction probes, slits, and periscopes while engineering physics systems maintenance involved correction plate and thermocouple repairs. The long list of rf jobs included voltage probe maintenance, resonator bellows chore pad replacement, ground-arm measurements, unplanned resonator repairs, centre region inspections, and transmission line modifications. The Vacuum group installed four new tank ion gauges (for rf) as well as replaced the tank inner and outer vacuum seals, one of the higher dose jobs, with the aid of a team of volunteers. Vault work finished as scheduled several weeks ahead of meson hall work so that beam to other proton lines started a few weeks prior to BL1A startup. The extent and complexity of the meson hall work, much of it involving very high radiation fields, resulted in some higher than usual doses that contributed to a total shutdown dose of 186 mSv distributed among 123 workers.

Beam Schedule 103

The cyclotron was started up in mid-March to deliver beam to PT and then PIF (both via BL2C1) before being joined by BL2A2 for delivery to ISAC toward the end of that month. A moderate amount of rf sparking as the high voltage settled, and some combiner and transmission line problems slowed things down a little at the start. Some undedicated time in the schedule offered the opportunity for a few days of maintenance in early April to improve rf stability, do a B20 defrost, fix a main magnet power supply leak, and fix monitor 2CVM1. When BL1A started in mid-April the downstream spills were unacceptably high. After some analysis it was realized that the rewiring done for the new, rotated quadrupole triplet had changed the direction of its associated asymmetric steering to a state incompatible with the sense of the quadrupoles. The triplet was uncovered and the problem corrected although some additional steering power was required to achieve the traditional beam tune. BL1A was running close to full intensity by the end of April, about ten days later than scheduled.

Although the startup period was beset with the above problems, the lower cyclotron availability (87%) for this beam schedule was due primarily to problems experienced with the inflector during the last half of May. The primary fault turned out to be a darkened insulator which, at the normal operating voltage, caused

excessive current draw on the positive power supply of the inflector. An initial attempt to run asymmetrically helped somewhat for a while, but it was soon decided that the lid needed to be raised to fix the problem. The actual repairs were completed quickly with a reasonably low dose (6.5 mSv) but the overhead resulted in a turnaround time of nearly a week. There was also another difficulty with the inflector that resulted in numerous exit skimmer trips and forced a temporary reduction in beam currents. The quality of the injected beam seems to have been a contributing factor but a bad cable or connection was the chief suspect. All told, the inflector was responsible for 190 hours or 40% of the total downtime for this schedule with the rf a reasonably close second at 148 hours or 31%. Currents were reduced somewhat during recovery from the inflector failure and subsequent 1AT2 target problems (described below).

Normal high current operation was under way by mid-July when a small tank vacuum leak developed at the water-cooled probe (WCP). The vertical flag was used instead to define the cyclotron off. The WCP was disabled in the OUT position and a vacuum pump attached to reduce the size of the leak. Because there was some suggestion that the rf booster was involved in initiating the leak (it turned out not to be), it was left off for the remainder of the schedule. The lack of the booster and the somewhat increased tank pressure resulted in slightly higher tank spills than normal although the cyclotron transmission remained well above 60%.

Apart from the high-current proton lines, which are discussed below, there was beam delivery to BL2C1 for both PT (four sessions, six patients) and PIF (four sessions totalling about twelve days). PIF also ran in BL1B for five days at the end of the beam production schedule (at 500, 350 and 200 MeV) as part of a two week, lower-current run scheduled to provide some cooldown prior to the fall shutdown. (BL2C1 currents were less than 5 nA, BL1B currents less than 1 nA.)

BL1A ran for 2412 hours or 85% of its scheduled time, receiving 289 mAh or 74% of its scheduled charge. The initial tuning problems associated with the triplet replacement job were finally sorted out and normal operation resumed ten days late. The current was as high as 140 μ A before the inflector problems but afterward was kept around 100 μ A largely because of problems at 1AT2. There, one of the targets developed a very small water leak in early June, apparently (on subsequent examination) because the beam was too low on the target. Other targets were deliberately positioned 3–4 mm low with reasonable beam-spot sizes and centring when yet another leak developed. This time the age of the target was suspected to be the cause. Once the target

problems were identified, including difficulties with the target motor control system, the current was raised toward 130 μA . Then there was a large water leak at an insulator on a quadrupole magnet (1AQ15) that was fixed during an emergency three-day repair in August. This held until the last few days of BL1A operation when the triplet leak again started a climb to 12 l/hr before beam was shut off.

The meson channels were fully subscribed with the following exceptions. M9 saw limited use because its first quadrupole developed an open circuit in July due to a bad power connection. Its repair would have to wait for the fall shutdown. M11 remained unusable as a meson channel because of the broken septum; it did, however, see limited use as a source of electrons for detector tests.

BL2A ran for 2050 hours or only 60% of its scheduled time, receiving 55 mAh of charge. A beam current of up to 50 μA was delivered to the first ITW target although one of 30 μA was more common on subsequent targets. Beam was delivered for the first time down BL2A3 to the east target station (ITE) of ISAC. Little charge was accumulated during the initial scheduled run because of uncertainties about the performance of the ECR source being tested there. After switching back to ITW, production was fairly steady until the last three weeks of the schedule when a required target change was held up because of a vacuum problem with the replacement target assembly. There was a reduction in the number of spurious BL2A beamspill monitor trips after a change to a more fully-intercepting extraction foil that was closely radially shadowed by the BL1 extraction foil.

BL2C4 ran for 1699 hours or 81% of its scheduled time, receiving 71 mAh or 70% of its scheduled charge. There was little BL2C4 downtime *per se*; rather the line remained idle during some of the lower injected current periods (BL1A startup problems, inflector troubles, BL2A-only times) until a reasonable running split could be obtained. The restored front-end wire monitor 2CVM1 was used to correct the tune before the first production run – the previous beam tune was found to be steered far to the right, accounting for the melted indium seal last year. Beam delivery was generally good but during the last month of operation there was difficulty in maintaining a tune that kept the collimator temperature from climbing toward warning levels. It was thought that the extraction foils were to blame, but when they were examined during shutdown only one of the three foils appeared obviously worn out. The other two had fine separations visible between the whiskers but otherwise appeared normal. If this was caused by a combination of a slightly broadened foil together with a decreased beam aperture due to the

kink in the beam line, it was suggested that the problem might be alleviated by using a somewhat narrower (0.200 in.) foil.

Fall Mini-Shutdown

Because of extended maintenance work, the fall mini-shutdown had a very ambitious schedule. It was decided to raise the lid to replace the WCP and exchange the BL2C extraction foils after an initial assessment of turnover time and dose cost deemed it reasonable. The shutdown was advanced several days by chopping the last bit of the ISAC schedule, which was somewhat moot because of target problems anyway. This left PIF as sole user for the last nine days after high current ended and allowed for some significant cooldown time, enough to reduce the residual cyclotron fields (with the south-side shadow shields in place) to tolerable levels, about 50% higher than last spring. This allowed the WCP replacement and the BL2C4 foil exchange to proceed. Meanwhile, meson hall shutdown work was able to get under way a few days earlier than vault work because BL1A became accessible as soon as PIF was finished with BL1B. The main jobs in the meson hall were to repair water leaks at the BL1A triplet and M9Q5, replace the electrical connections at M9Q1, and repair a small air leak at the M20 beam blocker. The final total shutdown dose for the fall mini-shutdown was 28 mSv distributed among 47 workers.

Beam Schedule 104

Cyclotron availability for this quarter improved to 91%, slightly better than the long term average of 90%. The leaking water-cooled probe was replaced in the fall shutdown with the result that tank spills were a little lower with the return to normal tank vacuum conditions. The rf booster was also able to be turned back on to help keep the cyclotron transmission around 65%. Total downtime was 147 hours of which 86 hours were caused by rf system failures (mostly HVPS and PA problems) while another 14 hours were caused by power supply failures. In addition to the high-current proton lines discussed below, there was beam delivery to BL2C1 for both proton therapy (one session, three patients) and proton irradiation facility experiments (two sessions, about a week each). PIF also ran in BL1B for a week at the end of the beam production schedule and there was some use of the neutron irradiation facility at TNF while BL1A was operating.

BL1A ran for 1266 hours or 96% of its scheduled time, receiving 160 mAh or 97% of its scheduled charge for an average current of 130 μA . The current was capable of going higher (and indeed did during a high current development shift) but was not pushed as there was no overwhelming demand. Triplet water-leak re-

pairs in the fall shutdown held tight with no new ones arising there. The M9 channel saw some use after repairs were made to the power connections of its first quadrupole, but did suffer a couple of large water leaks in some downstream elements. The M20Q1-1AT2 vacuum leak was a constant concern as it wandered up and down depending, apparently, on the flange temperature (beam heating versus CuALCW cooling). There were suggestions of another leak in the 1AT2 volume that needs to be investigated during the M20Q1 seal repair in the 2004 winter shutdown. There were no more target problems at 1AT2 as the target was kept 3–4 mm “low” all of the time. However, there was a two-week period of elevated BL1A tunnel air activity that seemed to be caused by a small CuALCW system water leak at the 1AT2 water-package plumbing that seeped through the shielding blocks into the BL1A tunnel. The readings often hovered around the warning level but eventually settled back to normal values (about half of warning) after the leak was repaired.

BL2A ran for 914 hours or only 74% of its scheduled time and received 28 mAh for an average current of around $30\ \mu\text{A}$. Things went fairly well when BL2A was on the air but the beam was turned off for two five-day stretches to repair target vacuum leaks caused by HV sparking. That accounted for virtually all of the downtime on this beam line. The schedule finished as the year began with BL2A the sole high-current user while PIF ran nanoamperes in parallel.

BL2C4 ran for 1032 hours or 106% of its scheduled time, receiving 46 mAh or 111% of its scheduled charge. The main reason for the high percentages was the turnover of unused BL2C1 (PT) time to BL2C4. New foils from the mini-shutdown helped achieve an average extracted current of $45\ \mu\text{A}$ without collimator heating problems. A 0.200 in. foil tested at the end of the year looked promising for future operation as it helped maintain even cooler (10° less) collimator temperatures than obtained with the new 0.250 in. foils. There is a plan to straighten out the STF in the 2004 winter shutdown so as, hopefully, to dispense with the corrective steering magnet introduced two years ago. A dose study estimates the whole job to cost around 15 mSv.

Most cyclotron systems were turned off following a two day development shift over the weekend before Christmas. Before the end of the year about six dozen large BL1A shielding blocks were removed to temporary storage near the machine shop in preparation for the next round of BL1A and meson channel refurbishments and repair. These include repair of the 1AT2 area vacuum leaks (particularly M20Q1), replacement of the 1AM10 crumbling block, and the possible removal of the M11 septum magnet. In the vault there

is the STF realignment work. The cyclotron lid is being raised for the usual tank MRO work on correction plates, probes, thermocouples, resonators, and inflector.

Apart from the many tasks associated with beam delivery, various operators were again very involved with fire alarm system improvements, card access system installation and implementation, AUTOCAD drawings, training, equipment repair, computer and console upgrades and maintenance, beam transport modelling, coordination of software improvements, etc., as well as actively helping out with many shutdown jobs.

BEAM DEVELOPMENT

Cyclotron Beam Development

High current beam development work, aimed at increasing TRIUMF’s extracted current from the present level of $\approx 200\ \mu\text{A}$ to $\approx 300\ \mu\text{A}$ continued in 2003. The higher currents will be required in 2007 when ISAC is scheduled to start operating with $100\ \mu\text{A}$ and $\approx 400\ \mu\text{A}$ which will be required in 2009 if TRIUMF goes ahead with its plan to build an additional independent $100\ \mu\text{A}$ target facility for ISAC.

Two high current milestones were reached. In July a record setting peak current of $420\ \mu\text{A}$ was extracted at 25% duty cycle with 63% cyclotron transmission. In October, as shown in Fig. 230, a peak current of $370\ \mu\text{A}$ at 50% duty cycle was extracted for ≈ 3 hours with good stability and with a cyclotron transmission greater than 62%.

Each of TRIUMF’s centre region quadrants contains electrostatic correction plates for vertical steering. Figure 231 shows how each upper and lower set of plates is mounted on a tray fastened to the dees. Vertical beam scrapers have been attached to the leading edges of the trays. As shown in Fig. 232, the thermocouples, mounted on the upstream side of the

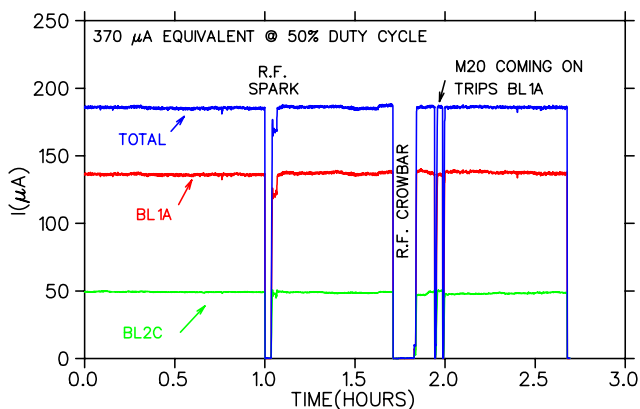


Fig. 230. $380\ \mu\text{A}$ peak current at 50% duty cycle.

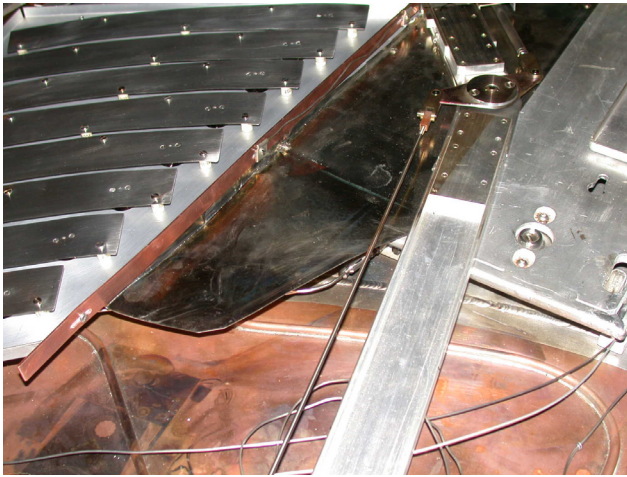


Fig. 231. Quadrant 4 lower correction plates showing the beam scraper and thermocouples.

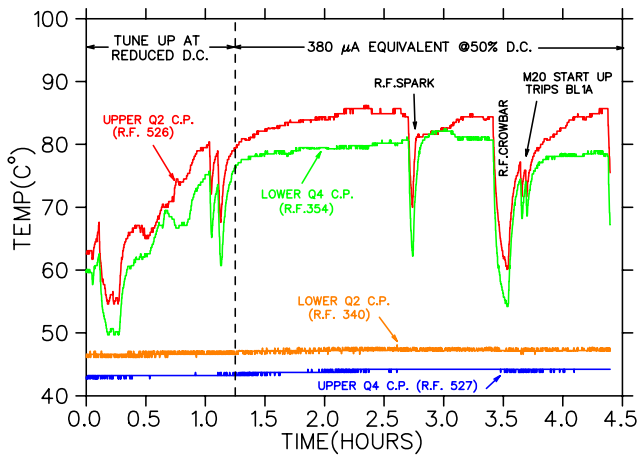


Fig. 232. Quadrant 2 and 4 correction plate thermocouple readings versus time with $380 \mu\text{A}$ peak current at 50% duty cycle.

scrapers, show that the beam heats up the upper scraper in quadrant 4 and the lower scraper in quadrant 2. The other scrapers remain cool. Some beam development time was devoted to trying to understand this phenomenon, and it is now thought to be caused by misalignments of the trays. These will be corrected in 2004. In addition, the thermocouples will be moved from the upstream to the downstream side of the scrapers to make sure that they are measuring the scrapers' temperature and not just responding to direct hits by the stray beam. Hopefully these measures will solve the problem.

Two new devices were installed during 2003 to assist with high current development. A pair of movable energy-limiting slits were installed in the dispersive plane at the centre of the ISIS vertical bend. Within the cyclotron a high resolution head with five vertical fingers was installed on low energy probe LE1. Both were tested successfully.

ISIS Beam Dynamics Development

The high-intensity CUSP ion source and injection line continued to operate well for the past year. The major development activity undertaken was to further model its optics better. An experiment with beam was made to clarify the polarities of some quadrupoles in the downstream portion of the vertical section where the wiring is not conveniently accessible. It was found that there are three consecutive quadrupoles with the same polarity. This is an error; fixing it should result in a better match to the cyclotron.

An experiment was performed to determine the initial beam parameters (radius, divergence and emittance) at the exit of the 300 kV acceleration tube. The initial beam should be axially symmetric. Although this was not the case, the reasons are unknown.

The horizontal and vertical profiles were measured with a wire scanner for a number of different settings of the upstream quadrupole strength at beam currents of 400 and $660 \mu\text{A}$. The rms sizes were used in the beam optics calculations with TRANSOPTR to fit the initial beam parameters.

Using these initial beam parameters and the actual operational voltage settings of all the quadrupoles, we calculated the ISIS beam envelopes for a current of $520 \mu\text{A}$. The result is shown in Fig. 233, where the measured beam sizes are plotted as well for comparison. One can see that in the horizontal section the calculated beam envelopes are in good agreement with the measured beam sizes and it is well matched, whereas the vertical section is obviously mismatched. This unmatched beam may be responsible for the observed

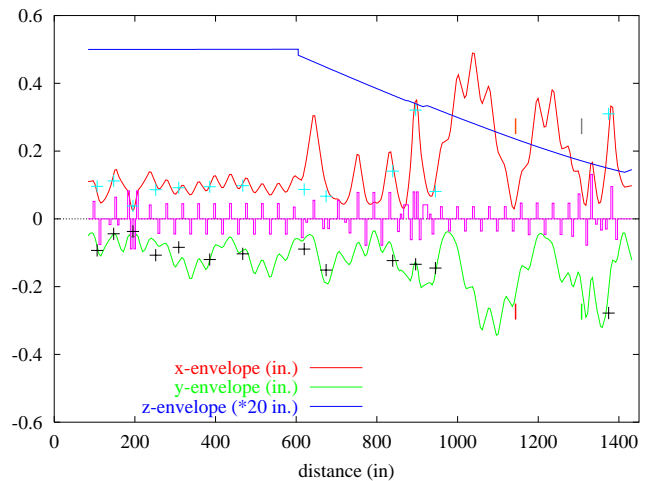


Fig. 233. Calculated beam envelopes in ISIS using the initial beam parameters inferred from a fit of rms sizes versus quadrupole setting, and the actual operational voltage settings of all the quads. The plus marks represent the measured beam sizes. The beam current is $520 \mu\text{A}$. The vertical bars occurring at 1144 in. and 1308 in. represent two collimators.

spills often occurring in the vertical section, although the beam size still stays within the aperture of the two collimators in this section.

BL1 Beam Dynamics Development

The operational tune of beam line 1A is known to differ from the theoretical tune by $\sim 10\%$. Experiments were therefore performed to determine the effective length of the quadrupoles. The main result is that the effective length is 10–15% less than the length calculated from the field map. The discrepancy is under investigation.

RADIO FREQUENCY SYSTEMS

RF Operation

The total rf downtime for the year was 234 hours. Although at the level of the previous year, the contribution of different factors has dramatically changed; for example, the downtime due to sparking was reduced to 48 hours from about 170. This was achieved with two major activities: an extensive program of resonator tuning using a new ground-arm-tip control system that was installed at the end of 2002, and an upgrade of

the rf control system in which the timing sequence for spark recovery was changed to allow a fast recovery of the system following a spark.

A detailed weekly downtime chart is shown in Fig. 234. Bars on the histogram represent the accumulated number of hours over a one week period that were lost while the system recovered from a specific failure. The failures are grouped into four categories: sparks, high voltage power supply (HVPS) crowbars, rf self-excited (out of driven (OOD)) mode, and other, which represents unique hardware failures. It is obvious that the largest part of the downtime ($\sim 62\%$) was attributed to unpredictable failures of major hardware (the Other category). Among these was the failure of a resistor in the 250 kW waster. This caused heavy sparking in the transmission line and substantial damage to it (see Fig. 235). On another occasion, damage to the transmission line was triggered by parasitic-mode excitations in the rf combiner. Both failures demonstrated a deficiency in protection of the system against a high standing wave ratio (VSWR) in the transmission line. Interlock circuitry is being developed that triggers rf drive cutoff in the case of high VSWR.

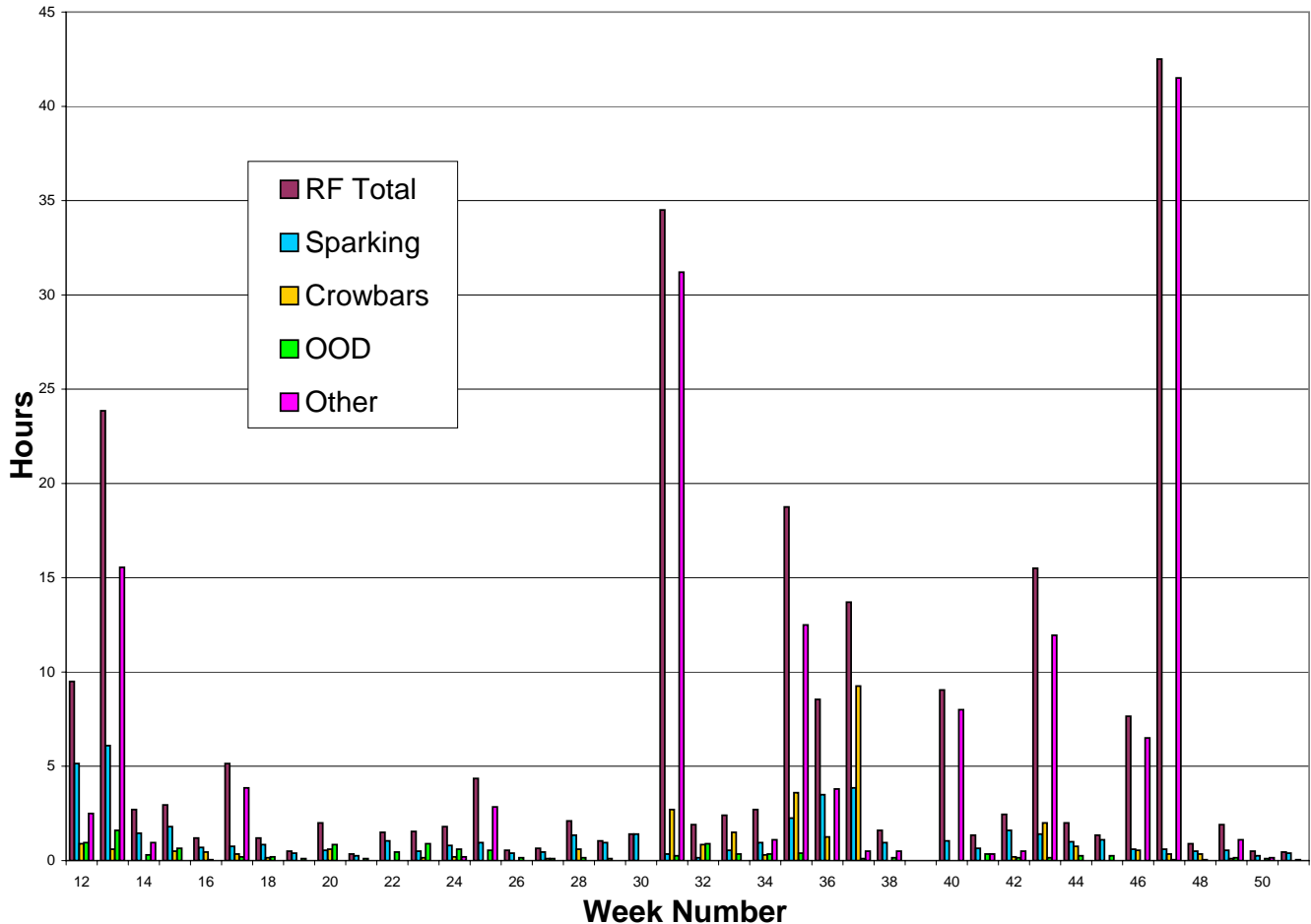


Fig. 234. 2003 rf system downtime.

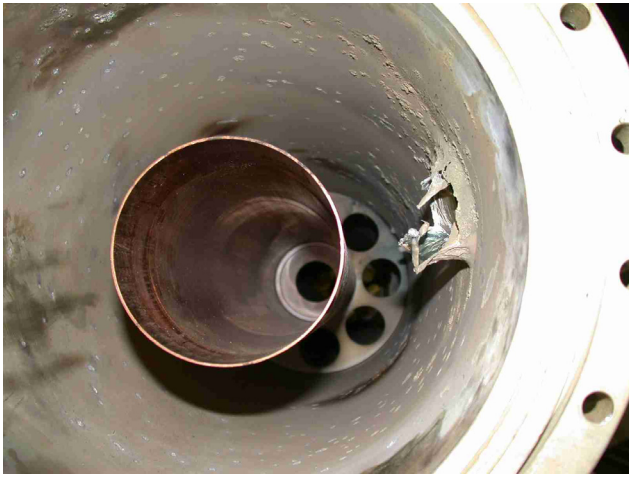


Fig. 235. Spark-damaged 9 in. transmission line.

Another series of failures was associated with HVPS water leaks. HVPS crowbars caused pressure bursts in the cooling line of the high power resistors which, in turn, caused subsequent damage to the plastic hosing. One of the floods caused damage to electronic circuitry in the HVPS. An improved cooling circuit was designed and is to be implemented next shutdown.

Over the year, two of the 4CW250000 power tubes failed. Their replacement and conditioning caused about 25 hours of downtime. While troubleshooting these failures, it was found that the tube protection circuit associated with the crowbar firing schematics had a few deficiencies in its design. Thus when running power amplifier (PA) number 3 without tube protection a screen power supply, a tube cathode shunt, and some crowbar firing-circuit components were burnt. A new approach to the crowbar firing circuitry is being developed to improve the reliability of the system.

During the winter shutdown an extensive program was carried out to improve reading of the cyclotron voltage probes. There are 64 probes installed at every resonator ground-arm panel (excluding resonators number 1 and 10). Six broken voltage probes were repaired and the readings of all 64 probes were recalibrated. This involved measurements of the capacitance of the pickups and the positions of the resonators ground-arm-tips (GAT) and hot-arm tips (HAT), fixing the 20 Db attenuators, and calibration of the adjustable rectifiers (64 channels). GAT positions were measured directly in the rf gap using a special tool (see Fig. 236). This operation was very delicate and associated with a personnel radiation exposure of 3.62 mSv for the ~150 measurements. Apart from the distance calibration, we were able to identify a few spots of damage to the resonator panels caused by rf breakdowns (see Fig. 237) and parasitic rf currents across adjacent

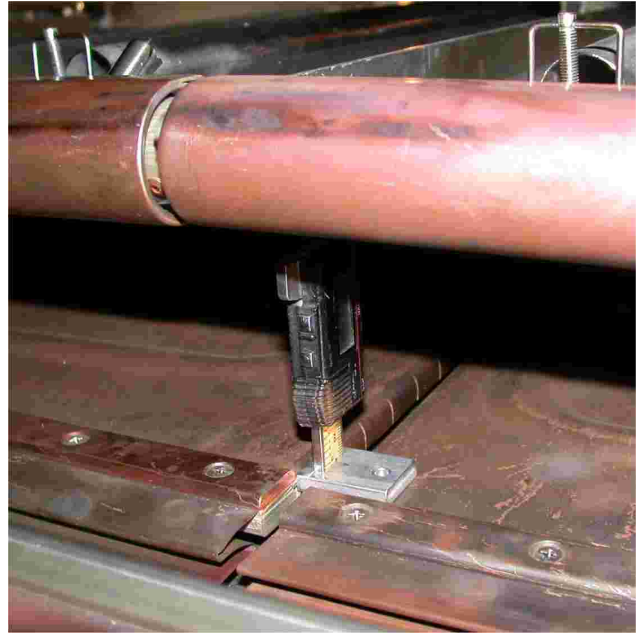


Fig. 236. Ground-arm-tip position measurement.

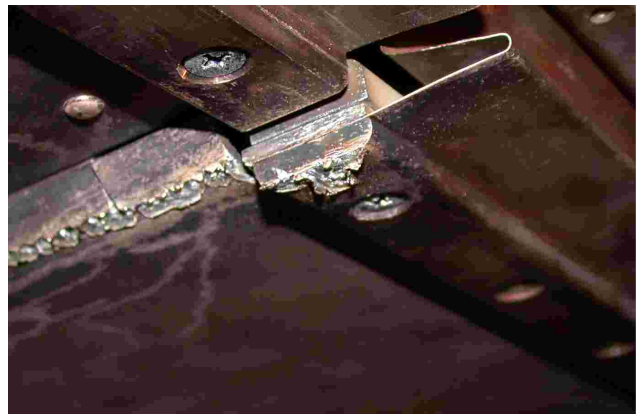


Fig. 237. UQ2 resonator number 3 spark damaged panel.

panel junctions. Problems were observed between resonators number 3 and 4 in quadrants 2 and 3. Eroded surfaces were polished and bent finger contacts were straightened to fix this problem.

Other shutdown activities in the cyclotron tank included:

- maintenance cleaning and insulator replacement of the centre region correction plates in quadrants 2 and 4;
- relocation of the two centre region thermocouples RF516 and RF107;
- relocation of two thermocouples from LQ2 resonator 2 to LQ2 resonator 1 for monitoring the resonator strong-back temperature;
- installation of four new thermocouples on LQ1 resonator 1, LQ3 resonator 1, and LQ3 resonator 2 strong backs;

- assessment and repair (where possible) of failed thermocouples RF543, RF406, RF507, RF303, RF323, and RF345;
- 1U2, 2L2, 3U2 GAT manual adjustment;
- continuation of the program of the replacement of copper chore pads with the fibreglass ones for another 20 resonators in the upper octant numbers 1 and 2.

In addition, all four rf power amplifiers (PA) were carefully retuned. This resulted in an increase of the overall PA efficiency to $\sim 60\%$ from $\sim 50\%$. A remote, PC control interface for a LECROY digital scope was developed that allows instant data logging. This helped us in the spark diagnostics and in the debugging of the new control system during its upgrade.

RF Refurbishing

A substantial effort was dedicated to the rf refurbishing program. In the winter shutdown, rf combiner number 2 was installed. It has operated reliably during the past year. RF combiner number 3 was tested to a power of ~ 500 kW and is being prepared for installation in the forthcoming shutdown. A new layout of the rf room for the power combining was developed that incorporates a new 900 kW rf switch. This set-up will allow a fast switch to the $50\ \Omega$ dummy load for PA fine tune-up and troubleshooting.

An upgrade to a fast replaceable capacitor station number 2 was implemented in the matching section of the transmission line (see Fig. 238). A major modification of the cooling circuit for all the capacitor stations that will provide higher reliability and serviceability was included. New capacitor stations numbers 1 and 3 were prepared for installation during the next shutdown.



Fig. 238. New capacitor station number 2.

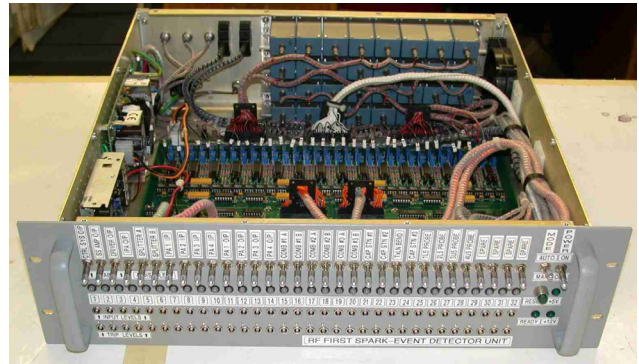


Fig. 239. First-event rf spark detector unit.

A multiplexing and diagnostic system was built that provides a first-event detection from as many as 24 voltage pickups when rf sparking occurs. It has proved to be an essential tool for troubleshooting the rf system. A view of the electronic module is shown in Fig. 239.

With the help of a student, one more automatic system was developed that switches rf signals from all of the transmission-line directional couplers (32 channels) to a Hewlett Packard vector voltmeter that is linked to the main control system via a GPIB interface. This device opens the possibility of monitoring the performance of the rf system; it also provides data logging. Another student was involved in simulations of the cyclotron electrodynamics using the HFSS program. A detailed three-dimensional model of the resonator structure was created. This work is ongoing and is aimed at obtaining a better understanding of how the rf modes are excited and, eventually, to suppress cyclotron sparking. A set of four additional ion gauges was installed in the cyclotron tank. These will allow local vacuum monitoring and are expected to be useful instruments in the troubleshooting of rf breakdown.

RF Support

The RF group was also dedicated to the following major ISAC projects (details are reported in the ISAC section):

- operation and maintenance of the ISAC Linacs;
- development of the RFQ HVPS soft-start circuit;
- upgrade of the DTL tuners and couplers;
- development of ISAC-I rf amplifier remote controls;
- set-up of the SCRF laboratory;
- design, test, and characterization of the SCRF cavities and accessories;
- development of a cryomodule alignment (WPM) system;
- development of an ISAC-II transfer-line re-buncher system.

RADIO FREQUENCY CONTROLS

In conjunction with the RF group the RF Controls group has performed tests with the goal of reducing rf downtime in the main cyclotron. By ignoring some of the smaller sparks and using a more aggressive recovery of rf voltage on the larger ones, the rf downtime has been reduced significantly.

The rf control system of the booster has been upgraded using the VXI standard. This provides better performance in voltage and phase regulation as well as a configuration that is easy to upgrade. Better communications and data logging are also incorporated into the new system. The new system has been tested and is ready for commissioning.

The rf control system for the superconducting rf cavity has been tested with the fast tuner-feedback control. Amplitude and phase regulations have also been tested. A procedure for conditioning the superconducting cavity has been developed that allows a new cavity to be powered within minutes rather than the hours required previously.

PROBES AND DIAGNOSTICS MECHANICAL MRO

In addition to normal MRO activities and ISAC work, more progress was made on the HE probe refurbishment, including some prototyping of the probe-head mechanics. Several of the refurbished monitors were installed, and a number of other monitor improvements were made. This year, non-routine repairs were made on the following devices: water-cooled probe, SE periscope, and the ISAC IMS:DB0 slit and Faraday cup.

For more details, the Diagnostics group meeting notes are available electronically via the Operations CYCINFO information service on the site computer cluster (accessible also through the TRIUMF home page on the WWW). The winter cyclotron shutdown activities are summarized in detail in the Diagnostics group meeting notes of April 11, 2003. The fall shutdown report is included in the meeting notes of October 10, 2003.

Probes MRO

The extraction probes for beam lines 2A and 2C were removed for routine service in the winter shutdown. The low- and high-energy probes were inspected *in situ* and a new five-finger head was installed on LE1. The vertical drive screws were replaced on the SE periscope; square threaded screws were replaced with standard ACME threads. The SE periscope prism was replaced during the September shutdown when the lid was raised to replace the water-cooled probe, which had developed a vacuum leak in the retraction bellows

during the summer operation. Dose limitations did not permit replacement of the NW periscope prism, which will be serviced in the 2004 winter shutdown. The PIP3 vertical drive screw was cleaned and relubricated during the September shutdown.

The ferrofluidic feedthroughs (f/t) for slits H3 and H4 and the vertical flag were inspected during the winter shutdown and found to be in good condition.

Monitor MRO

All vault and standard beam line monitors were serviced during the shutdowns. Refurbished monitors were installed at 1BM5 and 1BM5.5. Monitors 1VM1, 1VM2, and 2CVM1 were modified to work without gas; they now use the new VME signal processing system. New signal and HT wiring was installed for 2CVM1. Monitor 2AM10 was re-aligned. A spare 1AM9 monitor was manufactured and lifting hardware was mounted on the box lid to facilitate handling during service.

ISAC Diagnostics

The IMS:DB0 slits were changed during the winter shutdown and a slit drive misalignment was fixed. The Faraday cup was replaced during the September shutdown. New absolute encoders were commissioned. They should solve deficiencies in the reliability of software control of the slit and Faraday cup positions.

A number of foils were prepared and loaded on the MEBT stripper.

CYCLOTRON VACUUM AND CRYOGENICS

The cyclotron vacuum/cryogenics system worked well during the year. There were a few problems with the B-20 cryogenerators. These were related to lead loss in the 20 K regenerator, leaks in the helium gas plumbing that had developed over the years due to vibration, the failure of a seal ring, and the malfunction of the lubrication delay device. There was little impact on beam production because of the timely and efficient work of the Vacuum group on cryogenerator repairs.

Cyclotron cryopumps were maintained and serviced regularly throughout the year. Leak checks of the turbo-pumps backing system were conducted during the winter shutdown. One leak was detected on an oil lubricant canister of the north turbo pump. The canister was replaced.

The inflector box was leak checked in May.

The main seals of the cyclotron were replaced during the winter shutdown. A decision to install new seals was based on noticeable vacuum changes in the tank that were correlated with the main cyclotron magnet tuning on or off.

Four new ion gauges were installed on the cyclotron. They were located in the four quadrants of

the cyclotron tank so as to provide better vacuum mapping. These gauges are used by the rf group for diagnostic purposes.

A TRIUMF vacuum workshop took place on September 29. The main questions discussed were the status of the cyclotron vacuum controls and their possible refurbishment, the cyclotron vacuum status and possible improvements, the status of the ISAC vacuum, and the beam line vacuum.

The Vacuum group looks after maintenance and repair of the leak detectors. Because the older detectors require more and more attention with time, we are proceeding with a program to replace them. Four new leak detectors arrived on site this year.

Beam Line Vacuum

In preparation for the upgrade of BL1A to accept Varian turbo pumps and gauges, eleven cables were installed to connect the vacuum rack on the meson hall mezzanine to the 1A tunnel. Adapter pieces were designed and manufactured for the Varian turbo pumps, which will be installed in the BL1A tunnel. Turbo pump 11 was replaced after a failure. No spares are available for the old pumps. A leaking indium seal was replaced in the BL1A vault section, the controller for the Leybold turbo was repaired, and two controllers for interlocks summary and gate valves were refurbished and made ready as spares. A few leaks in the area of M20Q1 and triplet were diagnosed and scheduled for repair during the spring, 2004 shutdown.

A few leaks located on BL1B were fixed during the spring, 2003 shutdown. Since then the beam line vacuum has been good and is performing well.

Beam line 2A performed well during the year with an average vacuum level of 4.0×10^{-7} torr. A few leaks developed in the vault section because of radiation damage and these were repaired by replacing O-rings. A roughing pump in the ISAC-I tunnel is showing signs of wear; it is scheduled to be replaced during the spring shutdown of 2004. One of the turbo pump controllers was refurbished and is back in operation.

The vacuum system of BL2C worked well throughout the year. The BL2C radiation-hard valve and its nitrogen supply have been repaired.

The vault section of BL4 is kept under high vacuum to protect the cyclotron vacuum. It performed well during the year. The backing pump for the turbo in this section was refurbished.

A few repairs in the 1AT2 area were made. An automatic venting for the 1AT2 blower has been installed. Additional remote helium lines with manifolds for remote helium leak checking were traced in 1AT2.

The turbo pump backing valve of the M9 channel has been repaired. Leak checks were done on the M13

beam line following repairs. A convectron gauge was installed on beam line M13; this gauge replaced an old thermocouple gauge.

Vacuum and Cryogenics Support

The Vacuum group has been involved in ISAC-I and ISAC-II in major projects related to SC Linac development, leak checking, the installation of vacuum equipment and mechanical assemblies, the design of cryogenic systems, the production of vacuum and cryogenic diagrams, testing the SC solenoid, etc.

ISIS

The CUSP ion source and injection line continued to operate well for the past year with only minor downtime that was caused by a failed control module. Although many ISIS personnel were involved in other TRIUMF projects, a few significant projects were undertaken during the past year.

Two new CUSP ion source bodies were built for use in the ISAC-I terminal, one of which was installed and commissioned in March. This source ran successfully through December of this year. The second source will replace the first source for commissioning in March, 2004.

In conjunction with the Controls group, the old wire scanner PC-based data acquisition and display system has been replaced with a new system that allows distributed remote control using X Windows. The save and restore scan functions allow on-line profile and statistical parameter comparisons. The system has been commissioned and has been particularly useful for beam development work.

Four new sets of motor driven variable aperture slits have been designed and built. Three of these sets are variable aperture in both the x - and y -directions; the fourth assembly is in the y -direction only. Two sets of slits will be installed into the first common periodic section of the ISIS beam line to define the emittance of the beam injected into the cyclotron. The third assembly will replace the existing 5:1 slits and will provide enhanced beam current control. These devices will be installed in the winter, 2004 shutdown. The fourth set of slits (y -direction only) was installed in the September shutdown and has been successfully commissioned. They reside between the two 45° vertical bend elements to limit the dispersive energy tails of the beam from reaching the cyclotron.

The inflector/deflector system experienced a series of failures during the last week of May and the first week of June and accounted for 175 hours of downtime. The inflector/deflector was serviced during the winter shutdown and ran well for 10 weeks at which time a high voltage insulator failed, requiring a lid-up intervention for repair. A high voltage cable breakdown as

well as poor connections slowed the repair effort. After the insulator replacement and attachment of the spare high voltage cable the system ran well for the balance of the year.

Last year we reported the successful effort to produce a broad ISIS tune at the 300 μA equivalent extracted current level at better than 60% cyclotron transmission. This year we made significant progress toward demonstrating the feasibility of 400 μA operation. In July we achieved 412 μA equivalent extracted current at 25% duty cycle. Although both the ISIS and cyclotron transmissions were good, the tank spills inside the cyclotron were a factor of 4–5 higher compared with nominal operating parameters. Later in the year we achieved a 370 μA equivalent tune (185 μA extracted at 50% duty cycle) with nominal transmissions and tank spills that were only 25% higher than the extrapolated nominal operating value. This work is described in greater detail in the Beam Development section of this report.

PRIMARY BEAM LINES

The year began with a three-month shutdown in which it was planned to replace the quadrupole triplet downstream of the 1AT2 target, repair water and vacuum leaks in the front-end of the M20 channel, and replace some of the crumbling concrete shielding blocks. In addition to these, normal MRO activities were undertaken.

The shutdown began with vacuum repairs upstream of the 1AT2 target. O-rings were replaced on the window valve upstream of the target, on monitor 1AM9, and in another valve downstream.

The highly active, iron bridge-blocks that required removal in order to gain access to the triplet and M20 areas were craned to a temporary bunker to expose the M20Q1/Q2 quadrupoles. The leak in M20Q1, previously measured to be ~ 10 l/hr, was located in an insulator. After loose contamination had been vacuumed from the magnet, the insulator was replaced. The Hansen O-rings were found to be leaking and they were replaced. During this work a ground fault showed up on this quadrupole, remaining when the magnet was electrically isolated from its power supply. It is suspected that water damage to the insulation of the pyrotenax has occurred, leading to a chemical reaction that is causing a battery effect. Although this ground fault could not be repaired, the magnet can be run from an isolated supply as long as another fault does not occur.

After 20 years in a radiation environment the cooling hoses of M20Q2 had become rigid and brittle and had begun to leak. These too were replaced.

A vacuum leak was found on the top plate of a box between quadrupole M20Q2 and dipole M20B1. A

new O-ring was installed. Leak checking showed that a small leak remained. It was so small that it was felt that the radiation dose required to diagnose it was not justified. All three magnets were powered and no trips occurred in an overnight run. The shielding blocks were reinstalled and MRO work concluded in the 1AT2 area.

The 1AS1 scraper downstream of the 1AQ14/15/16 triplet was removed, bagged, and placed in the bunker. The location and arrangement of the power supply terminations to the triplet were verified. With some difficulty (and with a bit of persuasion) the triplet was removed, bagged, and taken to the remote handling warm cell where alignment measurements could be taken.

Contamination of the beam line vacuum system was prevented by blanking it off at collimator B, which lies immediately upstream of the triplet, and keeping the beam line under vacuum. All services for the triplet that were attached to the trench blocks were removed. Work began to replace the crumbling blocks under the 1AT2 water package.

Earlier, the water lines and cabling had been disconnected from the water package and the package itself had been moved from its operational location. A number of shielding blocks were removed from the trench and the trench cleared of debris and all obsolete services. The two crumbling shielding blocks supporting the water package were removed. As more blocks were being removed the hand-stacked wall that separated the M8 treatment room and the beam line 1A blocks began to shift. Although this wall was in no immediate danger of collapsing, a plywood retaining wall was built to prevent any blocks from falling into the 1A tunnel. Removal of a crumbling tunnel block provided a view of other crumbling blocks. Some were in worse condition than that of the block removed; it was necessary to jackhammer one in order to remove it.

Following replacement of the crumbling blocks, preparation for the installation of the new triplet began. The 1AT2 water package was returned to its normal location and water, diagnostic, and electrical connections were restored. New cabling was added for the new flow meters and other diagnostic equipment that had been added to the assembly. The plywood retaining wall was removed and the beam line trench was cleared of debris and vacuumed. Two special wall blocks supporting the cooling lines to the triplet were installed and the water lines craned in. Flexible copper lines running the length of the water lines were installed. These lines will become part of a new remote leak-checking package. Assembly of the electrical buss bars was begun.

The new triplet was moved to the warm cell where its vacuum box was aligned to that of the old triplet.

Some modification of the triplet stand was required to meet the alignment requirements. Asymmetric steering was connected to the outer quadrupoles of the triplet. The triplet was lowered into the beam line trench, a temporary rubber seal was inserted at the joint between collimator B and the triplet, and the beam line was pumped down. The joint was found leak tight. Measurements were made to ensure the alignment of the electrical leads, the vacuum joint was broken, and the triplet was removed.

The scraper was moved to the warm cell where a substantial amount of indium was scraped from the flange that connects it to the triplet. Buss bars were installed in the trench, supports for the water lines were added, and the triplet was returned to the trench. New interlock cables and water connections were connected. In the new configuration the quadrupoles have individual copper and stainless cooling lines, flow meters, control valves, and upgraded fittings for back-flushing. A water test showed a small leak and attempts to resolder the connection failed. The leak finally was sealed successfully by applying epoxy.

The scraper was craned into position and indium rings were installed in all vacuum joints. A leak check of the system found it vacuum tight, although a small leak was observed in the connection between the 1AT2 target and the M20 channel. Bridge blocks were installed and all magnets were examined for water leaks; none were found. A test at full power for 1.5 hours showed no ground faults or temperature warnings. The next layer of shielding was added and a power test over the weekend showed no problems. The remaining shielding was added so that beam delivery could begin.

Shortly after beam delivery began it was found that an error had been made in the wiring of the asymmetric steering of the triplet. The triplet area was opened again and the steering problem corrected with little loss of beam time.

In addition to the above, the Beam Lines group was involved in servicing the active water filter systems, repairing the M9B solenoid, upgrading the beam blocker and diagnostics for the TWIST experiment, and repairing vacuum leaks in their area.

In early July the first quadrupole of the M9 channel, M9Q1, had developed an open circuit that rendered the channel inoperable. Inspection at that time found that the power connections from the magnet power supply had melted. It was planned to replace the six connections to M9Q1 and, if necessary, the four connections to M9Q2 in the September shutdown.

In early August a water leak was detected in the centre quadrupole of the new triplet. The area was again opened and the insulator replaced. It was noted that two other insulators had small leaks. Be-

cause no insulators were available they were not replaced. By early September the leak rate had increased to ~ 12 l/hr. The area was opened again during the September shutdown. The two damaged insulators were found to be leaking badly. All eight insulators on the supply side of 1AQ15 were replaced with insulators that had been made in the machine shop. A similar repair was made to an insulator on 1AQ14. No leaks were observed when the water supply was turned on.

Inspection of the M9 channel in September prompted the decision to replace all power connections to these quadrupoles. Cabling was replaced and an electrical continuity check ensured that each connection was isolated from the others and from the service stand. O-rings in the Hansen connectors were replaced. Ten new power cables were prepared and positioned remotely. Shielding was replaced and the vacuum system restarted. A substantial leak was found and isolated to a feed-through for a convection gauge. This was repaired *in situ*; no other vacuum leaks were found. All work was completed as scheduled before the shutdown.

The Beam Lines group was also involved in assessing the upgrade of the M13 beam-blocker. A new window valve assembly was installed at the downstream end of the M20 separator and a new booster pump was installed in the triplet cooling system.

In non-shutdown activities throughout the year the Beam Lines group replaced the hosing of the 1VQ4/5/6 quadrupoles and repaired water leaks in 4VQ1 and vacuum leaks at 2CQ4. A flow switch was installed on a steering magnet on beam line 2C4, leaking fittings repaired on 1AQ8, and problems were sorted out with interlock wiring on M9B1 and M13Q4. A gate valve was installed in M13, hosing was replaced on quadrupoles M9BQ9/10/11, and water leaks repaired on M20BQ11.

In addition to ongoing support of experimenters for TWIST, DRAGON, TUDA, HEBT, and β NMR, the Beam Lines group was involved in alignment measurements of the triplet in the hot cell, cyclotron probe *in situ* measurements, and ISAC-II beam line/floor measurements. They also took part in the measurements of the sag of the roof beams in the cyclotron vault, total station reliability and limitations investigations, and MRO of existing survey devices and equipment.

The majority of the work during these shutdowns was done by members of the Beam Lines and Remote Handling groups. Because of their dedication the work was completed on schedule despite the many unforeseen problems that were encountered.

Beam Line 2C

The production of the radioisotope ^{82}Sr in the solid target facility (STF) on 2C4 continued to be the major user of 2C beam time. Operating time was increased

from 149 days in 2002 to 170 days in 2003. The beam line ran very well on limited support with no interruptions due to beam line or target failures. The dose was decreased slightly from 123.35 mAh with a yield of 45.80 Ci in 2002, to 116.1 mAh with a yield of 41.66 Ci in 2003. Eight natural rubidium targets were irradiated in 2003, the same number as in 2002. However, to meet isotope demands, all of the 2003 targets were processed with better optimization of the dose and target processing.

The beam extraction foil that is used for isotope production is a 0.250 in. wide curtain of 0.001 in. diameter pyrolytic graphite fibres. Because the foils were splitting after extended operation, different assembly techniques were tested during isotope production. Unfortunately, positive results were not achieved. An emergency cyclotron lid-up in September allowed the Diagnostics group to load another set of foils. A 0.2 in. wide foil was tested for 7820 μ Ah of isotope production at a beam current of 50 μ A. The beam spot was approximately 10% smaller than that of the wider foil, making beam tuning much less sensitive to the beam halo. No damage was observed on the rubidium target window. Operation in 2000 with a 0.1 in. wide foil had burnt a small hole in the target window because of a higher beam density. The test of 0.2 in. wide foils will continue to higher currents in 2004.

The Diagnostics group rebuilt the profile monitor, 2CMWIR01, and repaired the actuator of the blade scanner monitor, 2CSWM04, in the 2003 shutdown. The operating diagnostics facilitated the correction of a chronic misalignment problem at the front end of the beam line. The beam was routinely too close to the vacuum pipe wall and it destroyed the O-ring upstream of 2CQ1 in December.

Considerable time was spent preparing for correction of the solid target facility (STF) misalignment in 2C4 and repair of the STF limit switches in the 2004 shutdown. Two alignment jigs that can be used remotely were designed and built. Consideration of an upgrade of the STF to increase isotope production will go ahead in the 2004 shutdown.

There were 35 days scheduled for proton therapy on 2C1 and 40 days scheduled in the proton irradiation facility (PIF) on 2C1.

PROMPT RADIATION HAZARD

Safety-Critical Devices

In response to questions from the Canadian Nuclear Safety Commission, a review of prompt radiation at TRIUMF was initiated several years ago. A number of recommendations came out of that review. Work on those recommendations, and subsequent developments, has progressed well during the year.

Five pairs of safety-critical neutron and gamma monitors were installed around the proton hall. This completes the installation of monitors for the existing beam lines. In addition to these hardware changes, a series of operational procedures were drafted to describe the appropriate response to safety-critical monitor trips. The procedures require each trip event to be documented.

Eight safety-critical detector trips occurred during the year. A report, written for each event, included an estimate of the maximum radiation field outside of the shielding (at licensed beam current) had the beam not been tripped off and a record of whether or not that radiation field exceeded 50 mSv/h.

In response to another recommendation, the Safety Systems group convened a Conceptual Design Review for a redesigned beam trip/beam inhibit system. Proposals for both an interim and a final configuration were approved. An interim proposal will be implemented during the 2004 shutdown. This interim configuration will have three existing ISIS safety beam control devices terminating beam for all categories of safety trips (gamma, neutron, emergency, and access). The final proposal cannot be implemented until several ISIS electrostatic elements are re-engineered for use as safety beam control devices. This re-engineering is scheduled to be completed during the 2005 shutdown. When this work is completed the safety-critical gamma and neutron monitoring beam trip systems will be totally independent of each other. One set of three beam control devices will terminate beam for safety-critical gamma monitor trips and another set of three devices will terminate beam for safety-critical neutron monitor trips. The trip functionality of each set of safety beam control devices is tested weekly to demonstrate their reliability.

CONTROLS

The Central Control System (CCS) ran well during 2003. Operation of the CCS remains reliable and requirements for cyclotron operation, developments, experimental use, and other users were fulfilled as needed. To meet this year's new requirements, functionality was added in numerous areas.

Despite being a good year, there were some problems. The loss of scheduled beam time because of CCS faults was recorded by the Operations group as 8.7 hours. This is up somewhat from previous years but it is still a minor contributor to overall cyclotron downtime. The faults that result in downtime continue to be largely caused by unpredictable hardware failures such as power supply problems. A new hardware diagnostic module has been developed and its deployment may help to detect some issues before downtime occurs.

The goals set for this year were mostly attained. These included such items as the completion of the new ISIS wire-scanner system controls, the rf spark (first event) detector system controls, the phaseout of the last VAX computer, the decommissioning of one of two DSSI disk systems, the implementation of a wireless infrastructure and its initial applications, and software upgrades. In addition, there were numerous changes made in areas where unforeseen requirements arose. The Controls group remains extremely busy meeting new requirements and maintaining a reliable system.

CCS Facilities

The ISIS wire scanner system was completed and commissioned during 2003. This set-up provides a much more flexible interface to ISIS wire scanners and the data they provide than did the previous system.

The wireless Ethernet infrastructure used by Controls has been expanded and reorganized to meet new needs. These changes have been made to support developments in the use of monitoring and control of cyclotron devices using wireless, handheld devices. Initially, wireless notebook computers were used but this has evolved to the use of Personal Digital Assistants (PDAs). PDAs are usually employed as a repository for phone numbers and to-do lists but new models now support Web browsers and X Window displays. The first application was a Web-based program that allows the Operations group to do their weekly testing of the safety-critical monitors. This new set-up shortens the time required for testing while it also reduces the staff needed for the testing. More developments in the next year should see PDAs being used as important diagnostic tools.

Support was added in the CCS for the new ISIS slits. Slits are important beam control devices but the old unit did not operate as desired. The new system is expected to be commissioned at the end of the 2004 shutdown.

A system for detecting low voltage in the rf system (often caused by sparks) has been developed and deployed. It has multiple voltage detectors and the capability to identify the first location to detect a voltage drop. This "first event" or spark detector is still being debugged, but the software and hardware to monitor the detector system and to display the data have been developed and commissioned for the CCS. Further work will be done in 2004 as the spark detector system is fine tuned.

Another project was started to support rf developments. This system is for multiplexing rf signals and comparing their amplitudes and phases using a vector voltmeter. Software and hardware developments commenced during the year and should be completed in

2004. This system will automate the recording of these values, which now is done manually. In addition, this system will provide the trending information that is currently unavailable.

A replacement for the aging X Window terminals is being pursued. The old system of VXT 2000 X Window terminals has run very well, providing good functionality while requiring very little software management. Approximately 50 of these terminals are in use. Unfortunately, because this equipment is more than 10 years old, it is slow compared to more modern hardware and it lacks certain functionalities. The hardware components are failing frequently due to age. A candidate set-up has been configured in hardware and the software is under development. It should support simple management, secure connections, and multi-headed displays. One or more new X Window display stations should be deployed in 2004.

Within the CCS infrastructure there were a number of hardware developments. The DSSI disk-storage system in the development cluster of computers has been phased out. During this process all of the disk files were moved to a new storage system. As part of the move, a reorganization and cleanup were done. The new set-up has a much better directory/file organization and its performance is significantly better. Although clearly worth the effort, phasing out the old system was a larger task than anticipated and took longer to complete. The same procedure has been started for the DSSI system of the Production Cluster, but there are fewer files and the organization is now fully determined. This task should be completed during 2004.

Another network switch was added, providing 24 more ports and reflecting the ever expanding need for network connections. Changes to the computers included memory enhancements and a swap of CPUs to provide a faster CPU for one of the production computers. Within the main console, the old 17 in. CRTs are being phased out and replaced by 18 in. LCD monitors. The LCD monitors provide a particular bonus because, unlike the CRTs, the fringe field of the main magnet does not adversely affect them.

Of the many other developments only two more will be cited here. The last of the VAX computers in the CCS was decommissioned. OpenVMS continues to be used successfully and is now running exclusively on Alpha computers. OpenVMS was upgraded to version 7.3-1 during the year and will likely be upgraded early in the new year to the recently released 7.3-2. With the port of the VMS to the IA64 architecture, VMS may be seen running on PCs in the CCS in the future. The last example of infrastructural developments is the removal of old terminal servers and their replacement by a new generation of hardware. More terminal servers

may be replaced during the next year.

In addition to the development of new applications, many of the existing applications received enhancements. Examples of programs that received changes are XTpages, Xsoftwatch, Xstrip, and the Safety Panels. In another area, a significant start has been made on allowing the device numbering system to move from octal to decimal. Within the CCS, cyclotron devices are identified by a system ID and a device number (often called the thumb-wheel number). This change will permit much larger device tables, but it does mean work on some applications and modifications to device selection lever-wheels. The change to decimal device numbering should be completed during 2004.

Secondary Beam Lines

Progress on the new secondary beam line controls continues to go well. The controls for M15, M20, M9A, and M9B have been implemented and there is ongoing effort for testing and commissioning these beam lines. M11 and M9 solenoid crates have been added to the CAMAC serial highway. A multiplet tuning application has been developed for M15 and M20 and the EPICS version has been upgraded to R3.13.8.

Other Systems

Support for the proton therapy facility is continuing. During 2003 the computer handling the operator interface was upgraded as expected to a DS10 and the previous computer was freed up to act as a spare for the beam line 2C CPU. To improve the quality of the operator displays, one of the CRTs in the proton therapy control room was changed to an LCD monitor.

There has been increased activity in the neutron irradiation facility (NIF) and to support this work a special display page was developed. Functionalities such as charge timers have been added.

OPERATIONAL SERVICES

Remote Handling

ISAC

Remote Handling technicians began assembly work of the shield plug, service cap, and containment box for target module #4 (TM4). Hot cell activities for the year included four scheduled target changes for TM1, the installation of new targets on TM2 and TM3 modules, and the replacement of steering plate assembly in TM1. Specialized handling equipment was designed, built, installed, and used to exchange a damaged manipulator at the south hot cell.

Cyclotron servicing

The winter shutdown was dedicated to the usual routine of Cu-blocker and shadow shield handling,

along with video and radiation surveys. The 2C extraction probe was removed remotely and replaced for the Diagnostics group during its annual service. A pair of screw jacks at station #4 of the cyclotron elevating system were routinely exchanged for servicing.

Beam lines servicing

During the winter shutdown (January through March, 2003) the new replacement beam line 1A triplet magnet (Q14/15/16) assembly was installed downstream of the T2 target. The previous triplet assembly was removed from the beam line, bagged, and transferred to the active equipment storage pit. Shielding blocks to the south of the beam line trench at the triplet location were removed to replace water damaged crumbling blocks in the area beneath the former M8 beam line and to create a chase for the triplet cooling services to the beam line 1A tunnel. Electrical power conductors were extended in the beam line trench from the previous location beneath the triplet to buss connections along the north wall. The new triplet was installed, guide fixtures aligned for future remote positioning, and the vacuum beam tube was connected, pumped and leak checked. Water cooling connections, utilizing a radiation-hard metal seal coupling recently designed by the Remote Handling group, were made up and the power buss links remotely connected. The magnets were fully power tested prior to, and after, installation of the first cover layer of steel shielding.

A fairly large job at the M20 beam line front end required repair of cooling-water leaks at the M20Q1 quick-connect fittings and replacement of a cracked ceramic insulator. The M20Q1 magnet was disconnected and investigated to determine the cause of ground fault in one of the coils. During the M20Q1 work a water leak was created at M20Q2 by disturbing and cracking a rubber cooling supply hose. This required replacement of the hose.

Other shutdown jobs included: repair of separate vacuum/air leaks at the M20 jaws box, the 1AWVA2 window valve, and at the 1AVA8 valve. The tentatively scheduled rejuvenation work for the M20 beam line front end continued throughout the year, taking a more intensive approach of a major refurbishment of the M20B1 magnet as well as replacement of the M20Q1/Q2 magnets, stand and vacuum box. The removal of the failed M11 septum magnet for failure mode examination, scheduled for the winter shutdown, 2004, prompted the issue that M11 experimenters are still able to gather some limited data from operation of the beam line without powering the septum magnet. This ability would be totally lost with installation of the straight-through beam line 1A septum bypass vacuum beam tube. Design began in November for modifications to the bypass to provide an M11 take-off leg.

This beam tube would replace the septum magnet with a comparable septum-Y vacuum box.

Hot cells and targets

Annual target station cooling package maintenance was performed during the winter shutdown. The 1AT2 cooling head was rewired for an electrical upgrade and both 1AT1 and 1AT2 cooling package flow meters were measured and recalibrated. A leak in the T2-Mk1 target required the metal C-seals to be replaced. The beam profile monitor on T2-Mk1 was also replaced. In June the T2-Mk1 target was inspected in the hot cell. The beam spot profile was documented and target travel positions were measured and recorded. This was all in an attempt to explain the low beam spot believed to be responsible for the recent target failure. The damaged TNF beam dump cooling vessel was removed from storage, prepared, and cut in sections to reduce storage volume.

Assistance was given to beam line 2C operations with hot cell target installations during the year, and preparation for the 2C4 solid target realignment to be performed in the winter, 2004 shutdown

Magnet Power Supplies

The vast majority of 2003 activity was related to MRO activities for the power supply system that is part of the original TRIUMF installation.

The copper water-distribution headers in the main magnet rectifier cabinet developed two water leaks, one of which was repaired by soldering and the other was repaired by peening the metal at the joint. This may indicate problems in the future that may require the replacement of the header system.

New supplies were installed and commissioned for DRAGON. These replaced the supplies for MD1, MD2, Q9, Q10, SX3, and SX4. Their original power supplies had been recovered from M8 but they proved to be unreliable.

Leaking pass-bank chill plates were replaced with a new copper version, which was procured from VR Electronics. This activity continues as new leaks develop in other heat sinks.

Silicon hoses, which developed leaks after 18 years in service, were replaced in the main magnet power supply. Silicon hoses were a vast improvement over the originally installed braided hoses that were replaced in 1985. The braided hoses seemed to have leaks every few weeks and caused excessive downtime.

A necessary retrofit of trim and harmonic power supplies was developed to address code compliance of the bays. Bay 4 will be addressed during the winter, 2004 shutdown.

Because of the installation of the new triplet in

BL1A the asymmetric steering supply system was upgraded to provide additional steering for the triplet.

Quadrupole power supplies were purchased for the ISAC S-bend beam line. These are to be installed in 2004. Power supplies were purchased and commissioned for the charge state booster.

A KAON factory era high-voltage supply was cleaned up and commissioned for the target conditioning station at ISAC.

Electrical Services

The ISAC-II project continued to be the major focus of the engineering and coordination efforts. About 35 engineering and installation work orders were carried to completion (the larger portion for ISAC). Among them worth noting in this section are the variable speed drives for the first 8 motors of the main cyclotron cooling tower, the office renovation in the chemistry annex for Nordion use, UPS power to the proton therapy facility and the fire alarm system operator graphic interface, conduit runs for the safety-critical radiation protection system, new services and improved grounding in the micro-electronics lab, deficiency corrections in the M20 counting room, UPS power for the new Nordion access system and power to various air conditioning services.

Continuing engineering support was provided to Nordion for the new TR30-2 radioisotope production facility project and to the ATG group for maintenance of the electrical services and the lighting of the operating facilities. A planned upgrade of the fluorescent lighting system was postponed because of the significant financial and manpower effort required to complete it in one year. We are currently in discussions with representatives from the BC Hydro Power Smart program to explore different ways to proceed with this important project to lessen its impact on a given fiscal year.

Typical maintenance activities included servicing lighting systems, motors and associated controls, air conditioning controls, panel boards and transformers, HV switchgear, breakers and capacitor banks, and the fire alarm system. Approximately 230 calls were answered (about 40 from ISAC-I and 50 from Nordion facilities) in addition to lighting maintenance. After stopping water infiltration in the conduit housing the 15 kV cable feeding the main office building, and after further consideration, it was concluded that cable replacement could be postponed.

In the summer, an incident with trim harmonic bay 4 revealed a deficiency in the wiring method of the bay control-wiring distribution. Temporary wiring was provided and the procedures for removal of a power supply from service were changed. Further study indi-

cated that a better solution would be to change design and tap the control power directly from within each power supply. Each power supply will be retro-fitted with plug-ins as well. With this approach, turning a power supply breaker off will de-energize the unit and allow its safe removal.

A failure of the outside lighting in front of the main office building was traced to an electrical short in the underground wiring. A failure of one of the main breakers in the ac distribution of the rf system prompted a review of the whole system. The installed technology is obsolete and spare parts are in short supply. This situation demands an upgrade in the near future of the whole ac distribution in this room.

Power delivery

Power delivery continued to be very reliable without major events or outages. Scheduling coordination continued regularly for large power HV with Power Tech High Voltage Laboratory short-circuit tests. These tests produce small transient disturbances to which, unlike other facilities, TRIUMF is particularly sensitive. However, thanks to our good working relationship with the management of Power Tech, scheduling of these events is carried out in close coordination with TRIUMF Operations, therefore causing minimal impact on our operations.

The monthly averaged peak power demand has increased 7.7% from 6834 to 7358 kVA. This was expected because of the addition of the ISAC-II building. However, the maximum peak demand decreased 2.7% from 8944 to 8702 kVA. This year, the peak was reached in November (Fig. 240) in keeping with ISAC-II increased activities over the months. The electricity

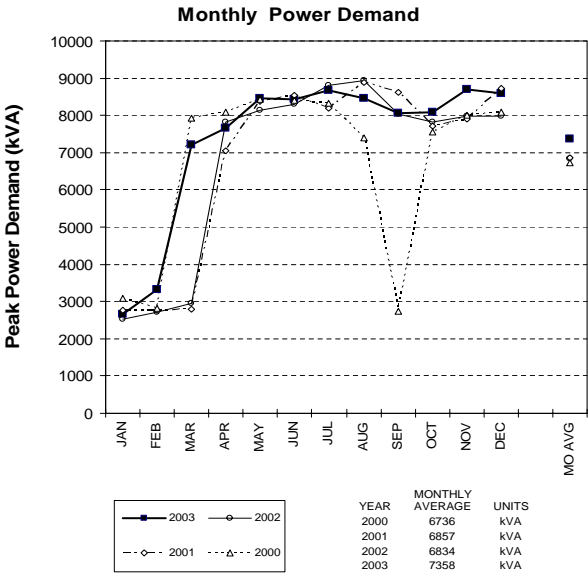


Fig. 240. Electrical power demand – four year comparison.

consumption followed suit, increasing about 5.9% from 53.3 to 56.4 GWh (Fig. 241). The largest consumption also occurred in November (5.83 GWh).

The power factor (PF), averaged over the calendar year, inched up marginally to 96.3% from 96.1% (Fig. 242). However, the PF for a typical production month improved thanks to the addition of three automatic power factor correction capacitor banks that were brought into service in April. The benefits of this addition will be even more important when the new BC Hydro rates (7.3% higher) take effect next April.

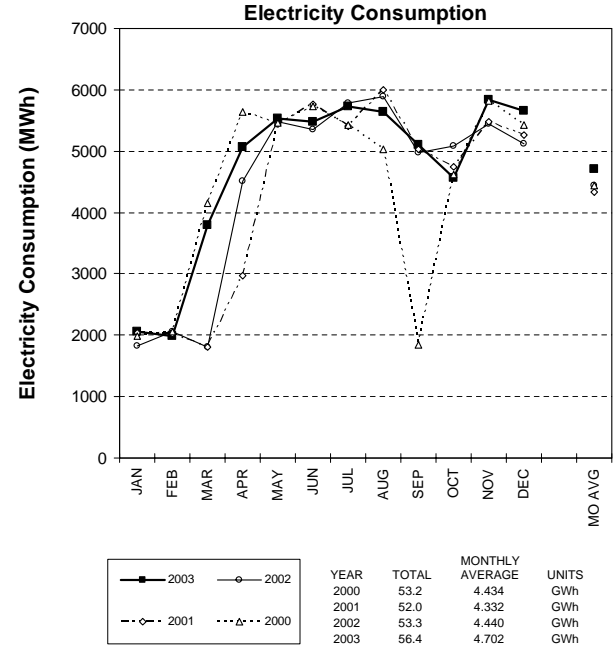


Fig. 241. Electricity consumption – four year comparison.

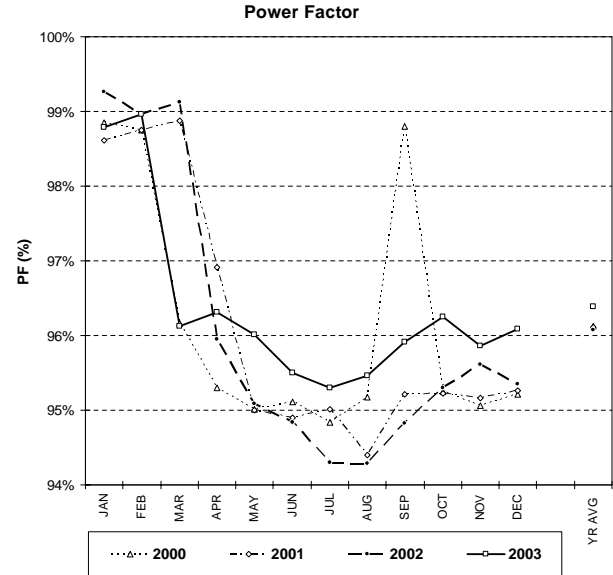


Fig. 242. Electrical system power factor – four year comparison.

Mechanical Services

One of the more interesting jobs was the completion of the installation of the variable-speed drives for the cooling fans in the cooling tower. These fans now regulate the temperature of the raw water much better than the old “flaps”, and the stability has led to better machine stability. The city-water lines to the cooling-tower were replaced.

There was a lot of work for rf cooling-water services, including the vault transmission line capacitors, the rf room inlet filter, the high voltage power supplies, and the transmission line. A start was made in re-commissioning the former MRS air compressor as a backup site air compressor. New pumps were installed

in the building perimeter drainage sump and for the beam line 1A triplet. Other piping jobs included replacement of the original city water lines that had become corroded in the ISIS area, some hot water lines in the chemistry annexes, and the discharge lines of the M13 vacuum pump. Trailer X services were disconnected.

A new air extraction system was provided for the removal of toxic powder from the machining of G10 material in the machine shop of the probes laboratory. Air conditioning service was provided for the RMC room, trailers Gg and P, M8, the main office building air handling units 1 and 5, the ATLAS clean room, and the service annex Buffalos at elevation 264.

ISAC DIVISION

INTRODUCTION

The following ISAC sections outline the various activities in ISAC-I operation, ISAC-I developments and the progress towards finishing ISAC-II. Although, there have been many highlights during the year, only a few are outlined here. Operational experience had pointed out the need to reduce the impact of the time needed to safely exchange targets. Considerable proton beam time was not being used due to this significant scheduling overhead. Consequently a second target station was brought into operation this year to increase the exotic beam availability. There were numerous target and ion source highlights. Six targets, including a new ZrC, were used to provide a wide variety of thermally ionized beams. The charge state booster was used on the test bench to produce multi charged ions of various species (i.e. performed as charge state booster). A resonant laser ion source test stand has been set up. An initial ECRIS test failed to demonstrate the anticipated performance, although subsequent measurements are leading to a much better understanding of the ECRIS operating specifications. A high power target has been developed and tested in the conditioning chamber. This target design has the potential of permitting full power operation at ISAC in the coming year. The accelerators achieved a remarkable 94% availability for the second year in a row. The ISAC-II civil construction was completed and technical staff moved in to convert the new building into a functioning laboratory. In ISAC-II, a major effort was to prepare the superconducting rf clean assembly area for assembly of the cryomodules since nearly half of the medium beta superconducting rf cavities have been fabricated and are already at TRIUMF. Good progress is being made on achieving adequate cavity tuning and rf coupling. Resource (personnel and financial) limitations prevented ISAC from realizing its full potential. Nevertheless, as the result of detailed planning and careful resource allocation, the major objectives for the year were successfully achieved.

ISAC OPERATIONS

This year, routine RIB operation provided beams to DRAGON and TUDA in the high energy area and to low energy experiments at LTNO, 8π , GPS β -NMR and Osaka. As in previous years, the first quarter was devoted to shutdown activities. Beam schedule 103 began in the second quarter and carried on through the summer. Beam schedule 104 followed a short shutdown in September. An overview of RIB operation is shown in Fig. 243 in terms of proton beam on the production targets. The hours of RIB and stable beam operation

for schedules 103 and 104 are shown in Figs. 244–247.

Operational performance statistics are provided for the ISAC beam production of RIB from ITW and ITE and stable beam from OLIS. These are summarized separately for each beam schedule in Tables XXV to XLIV (p. 208–216).

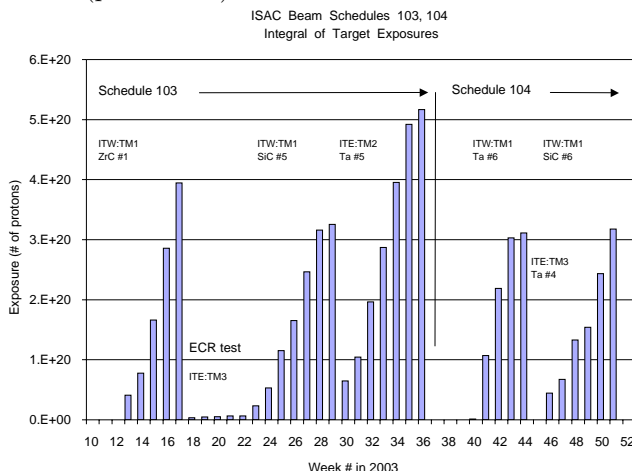


Fig. 243. Integral target exposures by week for RIB delivery in 2003.

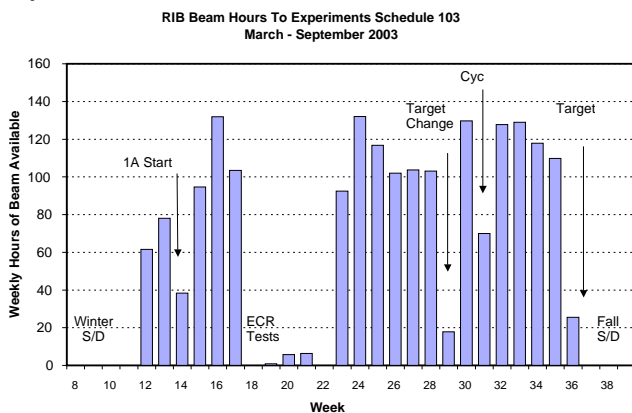


Fig. 244. Weekly hours of RIB beam available to experiments during schedule 103.

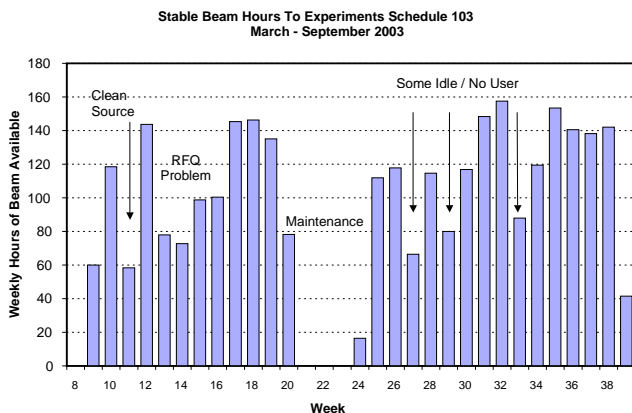


Fig. 245. Weekly hours of stable beam available to experiments during schedule 103.

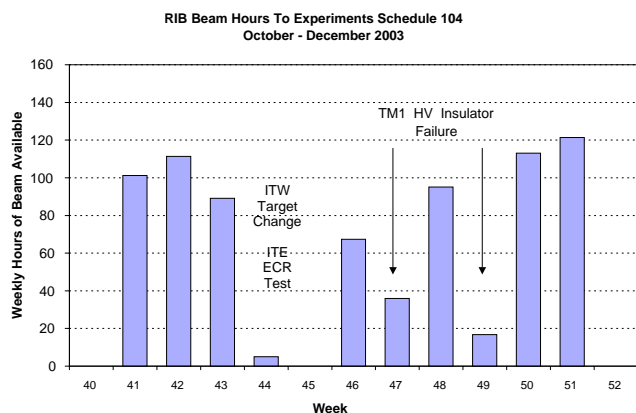


Fig. 246. Weekly hours of RIB beam available to experiments during schedule 104.

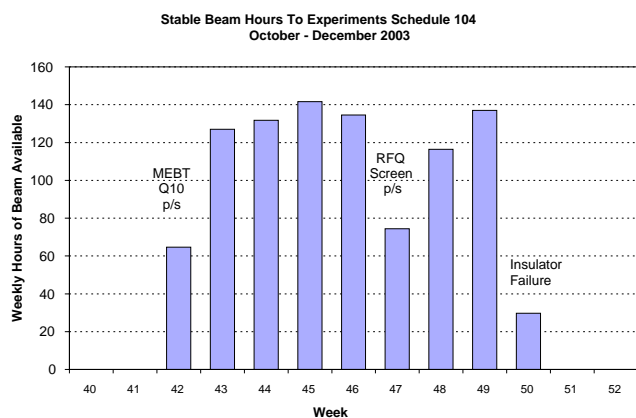


Fig. 247. Weekly hours of stable beam available to experiments during schedule 104.

In some instances OLIS was used by an on-line experiment as part of procedures to change mass or energy. Other times it was used for commissioning or when the RIB was unavailable such as during a maintenance period. The RIB availability as an indicator of operational efficiency is complicated by the incentive to minimize activation when the beam is not required, and by the coincident use of OLIS. Furthermore, while a surface source was available and operated on TM 2 in ITE, the uncertainty in the schedule for the commissioning of the ECR source on TM 3 affected the beam scheduling of the ITW modules and as a result, a number of experiments were affected. In the performance statistics presented here, the “combined facility efficiency” is quoted giving the actual beam delivered to experiments in comparison to the scheduled hours. This summary information includes the effects of experiment operational performance, ISAC system performance and proton beam availability with overhead as well as downtime components. The ISAC system performance is quantified by comparing the unscheduled downtime to the availability. Some interpretation is required to extract the relevance of overhead due to

operational procedures such as the extensive time required to set up the beam transport and accelerator systems for different beams. The OLIS performance is affected by its part-time use during parasitic operation simultaneous with RIB production to another user who has higher priority for technical support. Finally, there are some impacts on the schedule caused by logistical constraints of target hall operation. For beam schedules 103 and 104, the total unscheduled downtime for RIB and OLIS was 1637 hours compared to total scheduled user time of 7839 hours giving an availability of 79.1% for combined cyclotron, ISAC system performance.

A major milestone was achieved in beam schedule 103 when the first proton beam was delivered on a target module in the east target station on April 30 (week 18). This was also the first attempt at commissioning the ECR target/ion source on TM 3. The proton beam exposure on TM 3 was limited for the duration of the four week test to facilitate subsequent inspections and maintenance/development of the ECR TIS. The ECR progress is reported on p. 220. The east target station was used later in the summer with a tantalum target (Ta #5) and a surface ion source mounted on TM 2. Due to scheduling constraints related to the ECR development program, this target was operated beyond its normal life expectancy and it failed in week 36 due to an ionizer tube open circuit. Because beam from the SiC #5 target had exhibited an instability in the source optics, the optics tray was replaced during the target change, which added several weeks to the time that TM 1 was in the hot cell. As a result, TM 1 was not ready for operation when Ta #5 failed, and beam time was lost in the turn around. This was further compounded when a vacuum leak occurred in the TM 1 shutter bellows. The downtime carried into the scheduled fall shutdown which occurred in week 38. Beam delivery in schedule 104 was very good until a vacuum leak occurred in a HV feedthrough on TM 1 in week 47. This was caused by HV sparking from an unused thermocouple lead, which had held for extended operation with a bias at 30 kV, but became problematic when the bias was increased above 40 kV for normal operation. (The system had been conditioned to over 50 kV but only for brief periods.) A similar leak had occurred previously and, as then, the insulator was replaced. In this instance due to the higher bias requirements, the sparking recurred shortly after startup and the new insulator developed a leak in week 49. The problem was finally identified as arising from field emission from a small tube that carried the thermocouple lead into the vicinity of the nylon feedthrough. It was addressed by making minor modifications to the geometry, including the use of a corona cap.

A new position was created within ISAC Operations to provide console hardware and software applications support specifically for Operations and beam development activities. Chris Payne assumed this responsibility in September at the end of beam schedule 103, vacating his shift position. Working closely with the target chemist and beam line physicists, yield and collection station tunes were investigated, with the goal of developing standard tuning procedures for the front end of the low energy beam lines. A tool to easily compare harp and RPM data to accepted standard scans has been created, which aids tracking and correction of drift in the beam tune. A new network firewall was installed, doubling bandwidth to the rest of TRIUMF to nearly the theoretical limit. Operations consoles were updated to the latest version of RedHat Linux, and new and upgraded consoles were installed in the ion source and ISAC-II control rooms respectively. As part of an effort to consolidate electronic record keeping systems (electronic logbook, fault reports, work permits), a number of electronic systems of other labs were investigated for applicability, with the conclusion that an in-house solution will work best. An SCRF electronic log based on the current ISAC e-log was set up for tracking SCRF commissioning. The ISAC-II control room is now available for insulated off-line training, including simulating all EPICS functions as well as e-log, e-fault and work permit tasks. Further console and control system improvements and development of beam tuning applications are on-going.

The staffing complement remains critical, with five on-shift operators required for skeletal operation (one operator per shift) of a multiple source, complex RIB facility. The operators are assisted by two day-shift coordinators, who are responsible for beam quality assurance and the coordination of maintenance activities. The coordinators are also required to fill in for operators who are off shift due to illness or vacation – which is approximately 30% of the time. Including the coordinator absences, beam quality and maintenance tasks are supported at a level less than 60%. With the loss of one operator, shift coverage was down by one throughout beam schedule 104. Two new operators were hired in October. When they are trained, the shift complement will include a contingency of one operator, but any single-coverage shift will remain stressed at times of simultaneous activities. A recruitment plan has been proposed to increase the resources within ISAC Operations to provide adequate coverage on all shifts.

Documentation and training responsibilities continue to command the full-time attention of Mike Hauser, who has been assigned those duties within ISAC Operations. In compliance with the Quality Assurance program being implemented at TRIUMF, a 31-

page document, entitled “Document Planning for an ISAC Operations Manual” was produced. It describes the methodology for preparing and revising the ISAC Operations Manual. Development of the SAT training program for ISAC Operations continued although progress was slower than planned due to the time required for the training of new personnel. The development phase was completed June 30 and approved in the fall. Some progress was made on the design phase (third of five phases), but efforts were diverted to the orientation and training of four operators: the two hired in October and two from the 500 MeV Facility Operations Group. The four trainees completed the ISAC orientation in December and will undergo the latest version of the training program in the new year. They should be ready for unaided shift responsibilities by May, 2004. The two Facility operators will return to the main control room, but will be available to assist in ISAC if required.

The MEBT and HEBT beam operation has become more routine. This year, while new beams and large energy changes required support from the beam dynamic experts, a large fraction of the experts’ time was devoted to establishing effective tuning procedures. Again, as always with complex accelerator systems, there are still occasions that challenge even the experts. The members of the ISAC operations group take great pride in their contributions to the success of the experiments and major ISAC milestones that have been highlighted elsewhere in this Annual Report. In the coming year, in addition to providing beam for the scheduled experiments and performing systems maintenance, the major effort will be to complete the SAT training program for ISAC operators, migrate many of the control functions to the ISAC-II Control Room, and to continue to improve the ability of ISAC Operations to provide the beams of interest to the ISAC science program.

A concerted effort was undertaken to schedule and perform regular systematic yield measurements in order to track the target performance (RIB yield) as a function of operating hours to better understand how to schedule and operate high power targets. The target histories are given in Table XLV (p. 217); yield results are given in the target ion source report.

The target hall and hot cell operations have become quite well organized. The engineering that has been done for the east target station module access area (MAA) services will be applied to upgrade the west target systems, which were installed as prototypes. There were four target changes done this year, each one completed as planned and without incident. The history of operation of ISAC production targets for 2003 is given

in Table XLV. Schedule 103 started with ZrC #1 – a target of zirconium carbide pellets. The Ta #4 target installed on TM 3 (the ECR ion source module) was installed twice for development tests. For scheduling purposes, Ta #5 on TM 2 was run for more than its expected lifetime. It failed due to an open circuit in the ionizer heater. Initial experience with two working target stations indicates that careful planning is required to be able to manipulate the service requirements during brief maintenance periods in the beam schedule. Also, operation with the ECR gas loads has an impact on the capacity of the containment of the vacuum exhaust system. These activities will be better optimized with more operational experience.

Figure 248 shows the beam operation on the first target (ZrC #1) that ran on TM 1 in ITW from March 24 to May 8. The graph has two components: the proton beam delivered on target (up to 50 μ A at 500 MeV), interspersed with the residual radiation

fields recorded during maintenance periods. The radiation monitor is located near a target primary vacuum turbo pump where volatile products impinge on the vanes and many decay to adhering daughter products. The ZrC target has interesting characteristics in that the residual radiation includes the build up of progeny from the primary products that come to dominate the fields after the end of beam. Initially the field decays with a short half-life, characteristic of the primary production. Later the field shows a growth and much slower decay – from the progeny that has collected at the pumps. Until now, all other targets have had decay curves of short enough duration that a two-day cool down is sufficient for access to the module for target service (e.g. target SiC #6 shown in Fig. 249). The experience shows that beam scheduling must include consideration of the cool down requirements for the subsequent service of the various production targets.

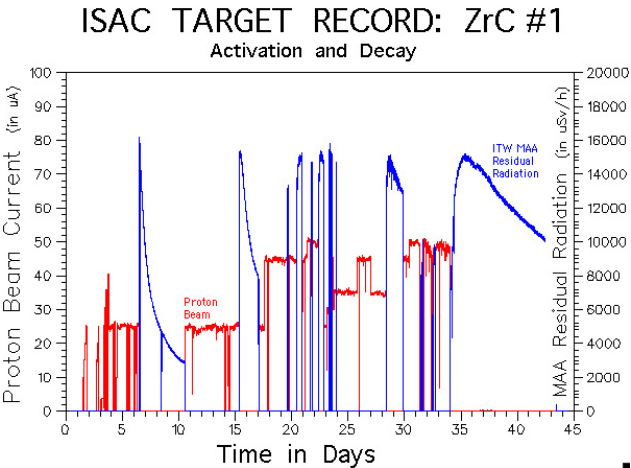


Fig. 248. Beam operation showing the proton beam current delivered and the residual radiation fields for the ZrC#1 target which was operated on TM 1 in ITW from March 24 to May 8 during schedule 103.

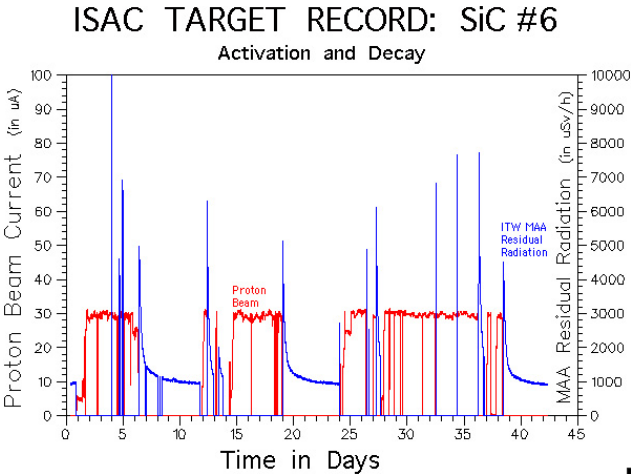


Fig. 249. Beam operation showing the proton beam current delivered and the residual radiation fields for the SiC#6 target operated during schedule 104.

Table XXV. ITW beam schedule 103 (surface ion source targets ZrC #1 and SiC #5): February 19 – September 30 (weeks 8–39) (reporting period is from Monday, February 17 to Monday, September 29). ITW beam to ISAC experiments (hours).

Experiment	Scheduled	Actual	Tune	Off	Total
Etest ILY	216.0	52.9	2.5	0.0	55.4
E815 BNMR	275.0	200.0	18.6	8.5	227.1
E816 BNMR	360.0	261.1	38.0	4.3	303.4
E823 GPS	192.0	144.9	11.6	0.3	156.8
E824 DRA	0.0	56.7	1.5	0.0	58.2
E871 OSA	239.0	170.4	0.2	11.5	182.1
E909 8PI	132.0	12.0	9.5	13.0	34.5
E967 HEBT	156.0	22.1	12.2	3.8	38.1
<hr/>					
Available		120.1			120.1
Totals	1570	920.1	94.1	41.4	1175.7

Total RIB experiment time = 920.1 hours

Combined facility efficiency = 58.6% (reflecting combined efficiency of cyclotron, ISAC and experiment systems; efficiency = (actual beam to the experiment / scheduled)).

Table XXVI. ITW beam schedule 103: detail of ITW beams to experiments (hours).

Experiment	Line	Isotope	Beam hours
815	BNMR	^8Li	200.0
816	BNMR	^8Li	261.1
823	GPS	^{62}Ga	144.9
824	DRA	$^{20}\text{Na}^{5+}$	21.4
824	DRA	$^{21}\text{Na}^{5+}$	35.3
871	OSA	^{20}Na	134.5
871	OSA	^{21}Na	35.9
909	8PI	^{26}Na	12.0
967	BRK	$^{21}\text{Na}^{5+}$	22.1
Test	ILY	Various	52.9
Total			920.1

Table XXVII. ITW beam schedule 103: detail of ITW RIB to HEBT experiments (hours).

Energy	Species	Experiment	Hours
488 keV/u	$^{21}\text{Na}^{5+}$	E824 DRA	56.7
Total			56.7

Table XXVIII. ITW beam schedule 103: ITW systems downtime and overhead.

ISAC systems	Hours
<u>Downtime – unscheduled</u>	
Controls	10.8
Magnet power supplies	7.9
Ion source	12.6
Polarizer	2.1
Stripper	0.1
DTL rf	0.5
Safety	0.6
Services	34.5
Site power	23.2
Vacuum	168.9
Subtotal	261.2
<u>Downtime – scheduled</u>	
Cyclotron maintenance	279
Cyclotron development	50.3
Beam line 2A off	165.3
ISAC shutdown	688.0
ISAC maintenance	48.0
ISAC development	77.7
ISAC idle	60.5
Procedures	146.6
Target conditioning	279.9
Target change	2125.5
ISAC startup	15.3
ITW cooldown	2.0
Subtotal	3938.1
Total	4199.3

RIB available from ITW = 1175.7 hours
ITW operational performance = 81.8% (reflecting the performance of ISAC systems; performance = available / (available + unscheduled downtime)).

Table XXIX. ITE beam schedule 103 (initial commissioning and development of new facility. ECR source and gases for target Ta #4 and surface ion source Ta #5): ITE beam to ISAC experiments (hours).

Experiment	Scheduled	Actual	Tune	Off	Total
Yield	372	45.0	1.8	2.8	49.6
E816 BNMR	110	88.0	6.0	4.8	98.8
E863 LTNO	144	97.6	2.3	1.3	101.2
E893 LTNO	144	7.5	2.1	58.8	68.4
E909 8PI	72	76.4	1.4	1.2	79.0
E920 POL	84	0.0	0.0	0.0	0.0
E921 8PI	240	155.1	6.7	18.7	180.5
E929 GP2	108	47.1	0.0	43.5	90.6
E955 8PI	60	38.4	2.2	0.0	40.6
<hr/>					
Available		14.0			14.0
Total	1334	555.1	22.5	131.1	722.7

Total RIB experiment time = 555.1 hours
Combined facility efficiency = 41.6%

Table XXX. ITE beam schedule 103: detail of ITE beams to experiments (hours).

Experiment	Line	Isotope	Beam hours
816	BNMR	⁸ Li	88.0
863	LTNO	⁷⁵ Ga	68.5
863	LTNO	⁹¹ Rb	29.1
893	LTNO	⁷⁹ Rb	7.5
909	8PI	²⁶ Na	76.4
921	8PI	¹⁷² Lu	4.4
921	8PI	¹⁷⁸ Lu	100.5
921	8PI	¹⁷⁹ Lu	27.2
921	8PI	²⁵ Na	7.0
921	8PI	³⁰ Na	4.9
921	8PI	³¹ Na	11.1
929	GPS	¹²⁰ Cs	47.1
955	8PI	³¹ Na	2.0
955	8PI	³² Na	36.4
Test	ILY	Various	45
Total			555.1

Table XXXI. ITE beam schedule 103: ITE systems downtime and overhead.

ISAC systems	Hours
<u>Downtime – unscheduled</u>	
Controls	14.7
Diagnostics	11.5
Services	0.8
Ion source	316.1
Site power	13.0
Vacuum	59.8
Subtotal	415.9
<u>Downtime – scheduled (overhead)</u>	
ISAC maintenance	16.0
ISAC development	373.3
ISAC idle	800.7
p+ off	128.3
Procedures	132.7
Target conditioning	59.5
Cyclotron maintenance	111.8
Cyclotron development	38.5
Shutdown	527.0
Startup	827.1
Cooldown	4.0
Target change	1217.5
Subtotal	4236.4
Total	4652.3

RIB available from ITE = 722.7 hours

ITE operational performance = 63.5%

Table XXXII. OLIS beam schedule 103 (microwave source and gases): OLIS beam to ISAC experiments (hours).

Experiment	Scheduled	Actual	Tune	Off	Total
E824 DRA	120	104.3	6.3	4.2	114.8
E863 LTO	24				
E870 TUDA	312	33.9	6.2	0.3	40.4
E879 TUDA	120				
E893 LTNO	32	8.0	2.6	0.0	10.6
E909 8PI	12				
E920 McGill	76	75.3	1.0	0.0	76.3
E921 8PI	60	0.0	9.0	0.0	9.0
E952 DRA	1291	860.8	44.1	4.5	908.4
E967 POL	48				
<hr/>					
Available		1827.9			1827.9
Total	2095	1082.3	69.2	1836.9	2988.4

Total RIB experiment time = 1082.3 hours

Combined facility efficiency = 51.7%

Table XXXIII. OLIS beam schedule 103: detail of OLIS beams to experiments (hours).

Experiment	Line	Isotope	Beam hours
824	DRA	$^{12}\text{C}^{3+}$	26.9
824	DRA	$^{20}\text{Ne}^{4+}$	7.6
824	DRA	$^{20}\text{Ne}^{5+}$	60.5
824	DRA	$^4\text{He}^{1+}$	9.3
870	TUDA	$^{12}\text{C}^{3+}$	33.9
893	LTNO	^{14}N	8.0
920	POL	$^{132/136}\text{Xe}$	60.0
920	POL	^{40}Ar	15.3
952	DRA	$^{12}\text{C}^{3+}$	662.4
952	DRA	$^{13}\text{C}^{3+}$	46.0
952	DRA	$^{16}\text{O}^{4+}$	152.4
Total			1082.3

Table XXXIV. OLIS beam schedule 103: detail of OLIS stable beams to HEBT experiments (hours).

Energy	Species	Experiment	Hours
0.200 MeV/u	$^{20}\text{Ne}^{5+}$	DRA test	16.2
0.200 MeV/u	$^4\text{He}^{1+}$	824 DRA	5.8
0.200 MeV/u	$^{20}\text{Ne}^{5+}$	824 DRA	25.8
0.200 MeV/u	$^{12}\text{C}^{3+}$	952 DRA	13.0
0.400 MeV/u	$^4\text{He}^{1+}$	824 DRA	1.5
0.400 MeV/u	$^{20}\text{Ne}^{5+}$	824 DRA	14.1
0.450 MeV/u	$^{13}\text{C}^{3+}$	952 DRA	8.6
0.540 MeV/u	$^{13}\text{C}^{3+}$	952 DRA	5.5
0.556 MeV/u	$^{13}\text{C}^{3+}$	952 DRA	11.1
0.571 MeV/u	$^{13}\text{C}^{3+}$	952 DRA	2.0
0.572 MeV/u	$^{13}\text{C}^{3+}$	952 DRA	5.7
0.650 MeV/u	$^{13}\text{C}^{3+}$	952 DRA	16.2
0.750 MeV/u	$^{12}\text{C}^{3+}$	952 DRA	58.9
0.775 MeV/u	$^{16}\text{O}^{4+}$	952 DRA	31.7
0.776 MeV/u	$^{16}\text{O}^{4+}$	952 DRA	72.9
0.778 MeV/u	$^{16}\text{O}^{4+}$	952 DRA	7.9
0.782 MeV/u	$^{16}\text{O}^{4+}$	952 DRA	1.1
0.810 MeV/u	$^{12}\text{C}^{3+}$	952 DRA	35.6
0.860 MeV/u	$^{12}\text{C}^{3+}$	952 DRA	36.4
0.900 MeV/u	$^{12}\text{C}^{3+}$	952 DRA	15.2
0.940 MeV/u	$^{12}\text{C}^{3+}$	952 DRA	40.1
0.965 MeV/u	$^{16}\text{O}^{4+}$	952 DRA	7.7
0.972 MeV/u	$^{16}\text{O}^{4+}$	952 DRA	20.5
0.975 MeV/u	$^{16}\text{O}^{4+}$	952 DRA	16.1
1.00 MeV/u	$^{12}\text{C}^{3+}$	952 DRA	20.6
1.02 MeV/u	$^{12}\text{C}^{3+}$	952 DRA	22.8
1.04 MeV/u	$^{12}\text{C}^{3+}$	952 DRA	15.2
1.05 MeV/u	$^{12}\text{C}^{3+}$	952 DRA	9.8
1.06 MeV/u	$^{12}\text{C}^{3+}$	952 DRA	2.5
1.07 MeV/u	$^{12}\text{C}^{3+}$	952 DRA	46.5
1.08 MeV/u	$^{12}\text{C}^{3+}$	952 DRA	17.1
1.09 MeV/u	$^{12}\text{C}^{3+}$	952 DRA	11.9
1.100 MeV	$^{12}\text{C}^{3+}$	952 DRA	19.7
1.110 MeV	$^{12}\text{C}^{3+}$	952 DRA	20.7
1.130 MeV/u	$^{12}\text{C}^{3+}$	952 DRA	13.1
1.160 MeV/u	$^{12}\text{C}^{3+}$	952 DRA	24.1
1.190 MeV/u	$^{12}\text{C}^{3+}$	952 DRA	15.6
1.220 MeV/u	$^{12}\text{C}^{3+}$	952 DRA	13.0
1.250 MeV	$^{12}\text{C}^{3+}$	952 DRA	22.1
1.280 MeV/u	$^{12}\text{C}^{3+}$	952 DRA	21.4
1.300 MeV/u	$^{12}\text{C}^{3+}$	952 DRA	19.1
1.310 MeV/u	$^{12}\text{C}^{3+}$	952 DRA	151.4
1.460 MeV/u	$^{12}\text{C}^{3+}$	824 DRA	13.9
1.460 MeV/u	$^{12}\text{C}^{3+}$	870 DRA	33.9
1.460 MeV/u	$^{20}\text{Ne}^{5+}$	824 DRA	12.8
1.500 MeV/u	$^{12}\text{C}^{3+}$	952 DRA	0.5
Total			997.3

Table XXXV. OLIS beam schedule 103: OLIS systems downtime and overhead.

ISAC systems	Hours
<u>Downtime – unscheduled</u>	
Controls	19.2
Diagnostics	1.0
Magnet PS	8.3
RF controls	14.6
Pre-buncher	2.0
RFQ	156.9
DTL rf	43.8
Charge-exchange stripper	11.3
MEBT rf	1.0
Services	86.7
Site power	23.0
Vacuum	34.8
Ion source	45.5
Subtotal	448.1
<u>Downtime – scheduled (overhead)</u>	
ISAC maintenance	223.5
ISAC idle	502.0
ISAC shutdown	579.7
ISAC startup	59.3
Procedures	319.5
Etest Development	254.5
Subtotal	1938.5
<u>Total</u>	<u>2386.6</u>

OLIS beam available = 2988.4 hours
OLIS operational performance = 87.0%

Table XXXVI. ITW beam schedule 104 (surface ion source target Ta #6 and SiC #6): September 29 – December 29 (weeks 40–52) (reporting period is from Monday, February 17 to Monday, September 29). ITW beam to ISAC experiments (hours).

Experiment	Scheduled	Actual	Tune	Off	Total
E817 BNMR	168	206.7	17.1	7.5	231.3
E824 DRA	168	25.2	1.8		27.0
E826 LTNO	120	29.7	12.4	38.4	80.5
E871 OSAKA	60	79.0	2.2	4.5	85.7
E927 TUDA	108	64.5	0.5	4.0	69.0
E955 8PI	144	125.0	7.5	2.9	135.4
Etest ICS	72	52.7			52.7
Etest ILY	204	52.1	1.9	6.9	60.9
<hr/>					
Available		13.6			13.6
<u>Totals</u>	<u>1044</u>	<u>634.9</u>	<u>43.4</u>	<u>77.8</u>	<u>756.1</u>

Total RIB experiment time = 634.9 hours
Combined facility efficiency = 60.8%

Table XXXVII. ITW beam schedule 104: detail of ITW beams to experiments (hours).

Experiment	Line	Isotope	Beam hours
817	BNMR	^8Li	206.7
824	DRA	$^{21}\text{Na}^{5+}$	25.2
826	LTNO	^{79}Rb	5.7
826	LTNO	^{91}Rb	24
871	OSAKA	^{20}Na	76.9
871	OSAKA	^{21}Na	1.1
871	OSAKA	^{26}Na	1
927	TUDA	$^{20}\text{Na}^{5+}$	64.5
955	8PI	^{28}Na	1
955	8PI	^{31}Na	0.8
955	8PI	^{32}Na	123.2
Test	ILY	xLi/Al/Na/La	52.1
Test	ICS	^{26g}Al	52.7
Total			634.9

Table XXXVIII. ITW beam schedule 104: breakdown of ITW RIB to ISAC experiments (hours).

Species/ Experiment	8PI E955	LTNO E826	BNMR E817	OSAKA E871	ICS Etest	TUDA E927	DRA E824	Energy
^{79}Rb		5.7						45 keV
^{91}Rb		25.2						45 keV
^8Li			206.7					30.6 keV
^{26g}Al					52.7			30.6 keV
^{20}Na				76.9				30.6 keV
^{21}Na				1.1				30.6 keV
^{26}Na				1				30.6 keV
^{28}Na	1							30.6 keV
^{31}Na	0.8							30.6 keV
^{32}Na	123.2							30.6 keV
$^{20}\text{Na}^{5+}$						64.5		1.730 MeV/u
$^{21}\text{Na}^{5+}$							0.2	1.115 MeV/u
$^{21}\text{Na}^{5+}$							9	1.130 MeV/u
$^{21}\text{Na}^{5+}$							2	1.135 MeV/u
$^{21}\text{Na}^{5+}$							0.4	1.14 MeV/u
$^{21}\text{Na}^{5+}$							2.8	1.145 MeV/u
$^{21}\text{Na}^{5+}$							1.5	1.15 MeV/u
$^{21}\text{Na}^{5+}$							5.3	1.160 MeV/u
$^{21}\text{Na}^{5+}$							4	1.175 MeV/u
Total	125	30.9	206.7	79	52.7	64.5	25.2	584
Available				13.6				597.6

Yield Etest xLi/Al/Na/La 52.1 hours.

Table XXXIX. ITW beam schedule 104: ITW systems downtime and overhead.

ISAC systems	Hours
<u>Downtime – unscheduled</u>	
Controls	2.5
Ion source	237.2
Polarizer	0.8
RFQ	2.2
Site power	0.5
Subtotal	243.2
<u>Downtime – scheduled (overhead)</u>	
Cyclotron maintenance	122.7
Cyclotron development	46.0
Beam line 2A off	134.5
ISAC shutdown	369.5
ISAC idle	8.5
Procedures	141.3
Target conditioning	137.7
Target change	127.5
ITW startup	90.5
ITW cooldown	7.5
Subtotal	1185.7
Total	1428.9

Total RIB available from ITW = 756.1 hours
ITW operational performance = 75.7%

Table XL. ITE TM 3 beam schedule 104 (Ta #4 target with ECR source and gases; commissioning and development of new facility): ITE beam to ISAC experiments (hours).

Experiment	Scheduled	Actual	Tune	Off
Etest	312	0	0	0
Subtotal	312	0	0	0
Total	312	0	0	0

Total RIB experiment time = 0 hours
Combined facility efficiency = 0%

Table XLI. ITE TM 3 beam schedule 104: ITE systems downtime and overhead.

ISAC systems	Hours
<u>Downtime – unscheduled</u>	
Services	29.5
Subtotal	29.5
<u>Downtime – scheduled (overhead)</u>	
ISAC development	32.0
ISAC idle	971.0
Procedures	4.3
Target conditioning	67.6
Shutdown	865.0
Target change	215.6
Subtotal	2155.5
Total	2185.0

Total RIB available from ITE = 0.0 hours
ITE operational performance = 0.0%

Table XLII. OLIS beam schedule 104 (microwave source with gas feed): OLIS beam to ISAC experiments (hours).

Experiment	Scheduled	Actual	Tune	Off	Total
E824 DRA	24.0	34.1	2.0	0.0	36.1
E870 TUDA	36	0.0	0.0	0.0	0.0
E871 OSAKA	24	0.0	0.0	0.0	0.0
E927 TUDA	96.0	19.4	7.6	2.1	29.1
E947 DRA	108.0	134.2	4.3	0.0	138.5
E952 DRA	565.0	268.5	17.5	16.3	302.3
DEV	180	0.0	0.0	0.0	0.0
<hr/>					
Available		451.2			451.2
Total	1484.2	456.2	31.4	18.4	957.2

Total OLIS experiment time = 456.2 hours
Combined facility efficiency = 30.7%

Table XLIII. OLIS beam schedule 104: breakdown of OLIS beams to ISAC experiments (hours).

Species	E952 DRA	E947 DRA	E927 TUDA	E824 DRA	Total	Energy
$^{12}\text{C}^{3+}$	0.2				0.2	0.879
$^{12}\text{C}^{3+}$	2.7				2.7	0.881
$^{12}\text{C}^{3+}$	42.2				42.2	0.894
$^{12}\text{C}^{3+}$	29.7				29.7	0.895
$^{12}\text{C}^{3+}$	40.4				40.4	1.314
$^{12}\text{C}^{3+}$		99.7			99.7	1.340
$^{12}\text{C}^{3+}$		12.4			12.4	1.400
$^{12}\text{C}^{3+}$		22.1			22.1	1.420
$^{12}\text{C}^{3+}$	73.1				73.1	1.460
$^{12}\text{C}^{3+}$	80.2				80.2	1.462
$^{20}\text{Ne}^{5+}$			9.8		9.8	1.5/1.8
$^{20}\text{Ne}^{5+}$			9.6		9.6	1.73
$^{21}\text{Ne}^{5+}$				34.1	34.1	1.130
Total	153.3	134.2	19.4	34.1	456.2	

Table XLIV. OLIS beam schedule 104: OLIS systems downtime and overhead.

ISAC systems	Hours
<u>Downtime – unscheduled</u>	
Controls	4.3
Beam lines	19.2
Magnet PS	16.2
RF controls	6.3
Pre-buncher	3.5
RFQ	28.2
DTL rf	17.8
Charge-exchange stripper	15.9
MEBT rf	4.1
Site power	0.5
Vacuum	119.5
Ion source	3.6
Subtotal	239.1
<u>Downtime – scheduled (overhead)</u>	
ISAC maintenance	95.7
ISAC idle	97.7
ISAC shutdown	624.0
ISAC startup	33.0
Procedures	120.3
ISAC development	18.0
Subtotal	988.7
Total	1227.8

Total OLIS beam available = 957.2 hours
 OLIS operational performance = 80.0%

Table XLV. ISAC target history for 2003.

Target ID	In date	Out date	Exposure # of protons	Power $\mu\text{Ah} \cdot \text{g}/\text{cm}^2$	Comments
ZrC #1	28-Feb	11-Apr	5.11E+20	1.00E+06	33.21 gZr/cm ² + 10.88 gC/cm ² (435 foils 0.13 mm C + 0.24 mm ZrC).
Ta Foils #4 ITE:TM 3 R1	4-Apr	18-Jun	6.49E+18	6.30E+03	21.79 g/cm ² Ta in the form of 525 \times 0.025 mm foils.
SiC #5 ITW:TM 1	26-May	30-Jul	3.25E+20	3.84E+05	26.5 g/cm ² SiC in the form of 425 \times 0.23 mm foils. Steering optics replaced during scheduled service.
Ta Foils #5 ITE:TM 2	24-Jun	28-Oct	5.17E+20	5.01E+05	21.79 g/cm ² Ta in the form of 525 \times 0.025 mm foils. Failed due to ionizer open circuit.
Ta Foils #6 ITW:TM 1	25-Sep	31-Oct	3.11E+20	3.02E+05	21.79 g/cm ² Ta in the form of 525 \times 0.025 mm foils.
Ta Foils #4 ITE:TM 3 R2	28-Oct	5-Nov	* 5.08E+19	* 7.16E+04	21.79 g/cm ² Ta in the form of 525 \times 0.025 mm foils.
SiC #6 ITW:TM 1	6-Nov		2.74E+20	3.23E+05	26.5 g/cm ² SiC in the form of 425 \times 0.44 mm foils

* includes amount from R1: 4-Apr to 18-Jun.

ISAC TARGETS

ZrC Target Material

In 2003, ISAC target development involved production of new ion beams from previously commissioned target materials as well as initial operation of a new composite ZrC target material. The ZrC/graphite composite target foils were fabricated in an analogous manner to the SiC and TiC composite targets commissioned the previous year. In addition to ZrC, three Ta foil targets and two SiC composite targets were operated on-line during 2003.

The ZrC target was operated to explore the production of Rb, Sr, Y and especially Ga isotopes. Previous attempts to observe ^{62}Ga ($t_{1/2} = 116$ ms) from Nb metal foil targets were not successful, although ^{63}Ga ($t_{1/2} = 32$ s) was observed in $10^4/\text{s}$ quantity. The suppression of the shorter lived ^{62}Ga was attributed to a long effusion time resulting from strong physical and chemical Ga absorption on Nb surfaces. Thermochemical calculations suggest that the formation of metal-gallide phases of gallium with metals such as Nb, Zr or Ta is energetically favoured. However, for the same metals, the metal oxide and carbide phases are thermochemically more stable. With this in mind, ZrC was chosen as a potential target material based on calculations that suggested the Zr-Ga interaction could be blocked by the presence of a stronger Zr-C interaction. Additionally, the interior of the tantalum target container was coated with TaC to block tantalum gallide formation as well as to suppress reactions between ZrC

and Ta. The ZrC was operated at a maximum proton current of 50 μA and proved to be a very good target material for Ga production with ^{62}Ga observed for the first time, as well as ^{62}Ga ($t_{1/2} = 168$ ms). Additionally, Rb, Sr and Y (as the YF_2^+ ion) production was observed. Table XLVI lists the surface ionized Ga yields from the ZrC target.

Increased ^{11}Li Production from Ta

Of the previously commissioned target materials, the highest observed ^{11}Li ($t_{1/2} = 8.4$ ms) yield was from Ta metal foils. Target Ta #1 consisted of 512 Ta foils (each 0.025 mm thick) with a total thickness of 21.3 g Ta/cm². At 20 μA proton current on target, the measured ^{11}Li yield was $1.4 \times 10^4/\text{s}$. For the Ta #2 target, the number of foils was approximately doubled to 1050 for a total thickness of 43.6 g Ta/cm². Doubling of the target thickness did not produce a doubling of the ^{11}Li yield; at 20 μA proton current on target, the ^{11}Li yield was only $5.2 \times 10^3/\text{s}$. At 40 μA proton current, the ^{11}Li yield from target Ta #2 was $2.2 \times 10^4/\text{s}$, less than twice the Ta #1 20 μA yield.

The decrease in ^{11}Li yield can be attributed to longer effusion delays for the very short-lived ^{11}Li . Doubling the number of target foils also doubles the surface area of the target as well as doubling the volume of the target container. The associated delays resulting from increased ^{11}Li interactions with target surfaces are sufficient to decrease the observed yield below the increase expected from the doubled target thickness. To verify the effusion effects on overall

Table XLVI. Comparison of Ga yields from ZrC and other targets.

Beam	Composite target	Yield (/s)	p^+ (μA)	Other target	Yield (/s)	p^+ (μA)
^{61}Ga	ZrC	10	50.0	not observed	—	—
^{62}Ga	ZrC	8.5×10^2	36.2	not observed	—	—
^{63}Ga	ZrC	7.9×10^5	35.7	Nb	1.6×10^4	29.2
^{64}Ga	ZrC	3.1×10^7	40.0	Nb	4.3×10^5	9.5
^{65}Ga	ZrC	5.1×10^8	40.0		—	—
^{66}Ga	ZrC	2.7×10^8	44.4		—	—
^{67}Ga	ZrC	8.0×10^8	44.9		—	—
^{68}Ga	ZrC	4.1×10^8	45.5		—	—
^{70}Ga	ZrC	2.2×10^8	45.5		—	—
^{72}Ga	ZrC	6.7×10^6	45.3		—	—
^{73}Ga	ZrC	9.0×10^6	45.1		—	—
^{74}Ga	ZrC	2.2×10^6	45.1	Nb	3.4×10^5	9.5

^{11}Li production, targets Ta #5 and Ta #6 were fabricated with 525 Ta foils with a total thickness of 21.8 g Ta/cm². For Ta #6, the 20 μA ^{11}Li yield was $1.0 \times 10^4/\text{s}$, similar to the Ta #1 target. Furthermore, at 40 μA , the ^{11}Li yield was $4.4 \times 10^4/\text{s}$, double the yield observed with the thicker Ta #2 target. Clearly, effusion delay effects can dominate in comparison to target thickness when very short-lived products are considered. The ^{11}Li yields as a function of proton current for targets Ta #1, Ta #2 and Ta #6 are displayed in Fig. 250. In the case of Ta #6, the proton beam current limit was raised to 50 μA , producing a ^{11}Li yield of $5.1 \times 10^4/\text{s}$.

^{26}gAl Beam Development

A total of six SiC targets have now been operated at ISAC. Since the SiC/graphite foils composite targets came into operation, $^{26\text{m}}\text{Al}$ activity has been observed in β -spectra of ^{26}Na used to cross-calibrate the ISAC yield station scintillator detector against the measured

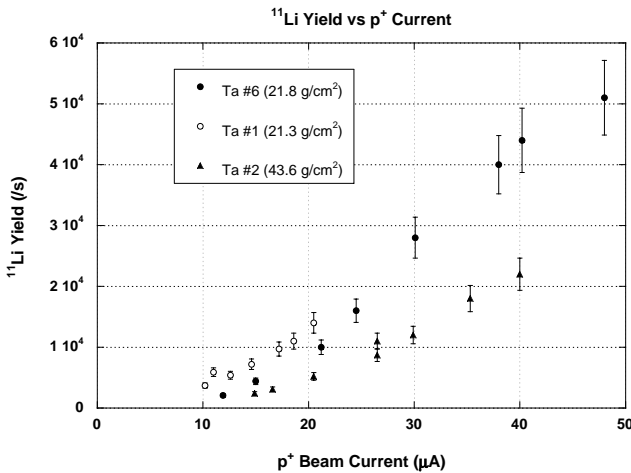


Fig. 250. Yield of ^{11}Li as a function of proton beam current on tantalum targets of varying thickness.

γ -activity observed using the yield station HPGe detector. As well, the Na beams extracted from SiC targets operating under high proton currents are sufficient to be measured as ion beam currents on Faraday cups throughout the ISAC low energy beam transport system. Generally, the yields of ^{20}Na , ^{21}Na , ^{24}Na and ^{25}Na deduced from measured currents agree well with yields determined by γ -counting of deposited activity at the ISAC yield station. Differences of up to a factor of 2 can be attributed to distortions of the current measurements by intense β^+ or β^- activity of the ion beams. However, for ^{26}Na the Faraday cup current yields are consistently 2 orders of magnitude above the ^{26}Na and $^{26\text{m}}\text{Al}$ yields obtained by γ and β counting. Since long-lived $^{26\text{g}}\text{Al}$ is an isotope of significant interest to nuclear astrophysics, investigations were undertaken to determine if the excess current at $A = 26$ was due to an $^{26\text{g}}\text{Al}$ beam. After excluding the possibility of ^{26}Mg or ^{26}Si contamination, the $A = 26$ beam was deposited in the ISAC collection station used for collecting samples of long-lived activity for off-line use. Two sample collections were made. The first collection was conducted with proton beam on target ($\sim 30 \mu\text{A}$ average) over a period of 21 hours. The average $A = 26$ beam current was $\sim 160 \text{ pA}$ corresponding to a yield of $\sim 10^9/\text{s}$. A second additional collection was conducted over a period of approximately 60 hours with either proton beam on target or resistive target heating during p^+ beam off periods. A running total was kept of integrated $A = 26$ beam current at the collection position.

The collected sample was counted in β - γ coincidence in the ISAC 8π detector after decay of the short-lived ^{26}Na and $^{26\text{m}}\text{Al}$ activities. A 12.75 hour count of the sample yielded a total of 150 counts for the 1809 keV γ -branch (99.8%) of $^{26\text{g}}\text{Al}$, corresponding to an estimated 1.6 Bq activity of $^{26\text{g}}\text{Al}$. A second count of 18 hour duration yielded 200 counts for an estimated

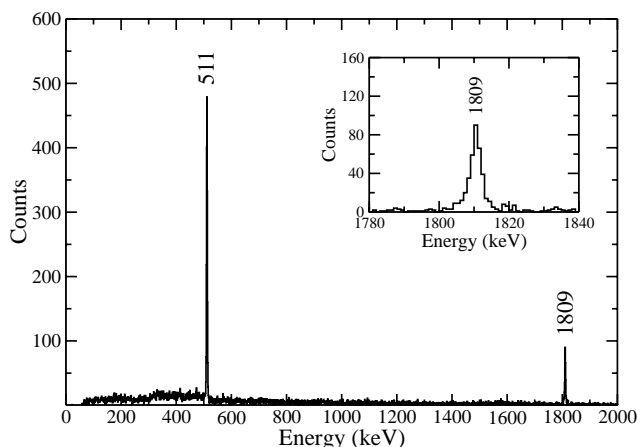


Fig. 251. A coincidence spectrum of the collected $A = 26$ beam obtained using the 8π spectrometer.

1.3 Bq activity. The integrated current on the collection station (if attributed entirely to ^{26}gAl) would provide an activity of 1.2 Bq. The β - γ coincidence spectrum of the ^{26}gAl sample is shown in Fig. 251.

High Power Target Development

Existing foil targets can accommodate up to $40\ \mu\text{A}$ beam intensities and the available intensities of many radionuclides can be expected to scale with the proton beam currents. However, production targets capable of withstanding proton beam intensities up to $100\ \mu\text{A}$, without compromising the radionuclide yield and the lifetime of the target, are a challenge. Several approaches to the dissipation of the power in such targets have been investigated and a realistic solution for the removal of the heat from the target container is proposed.

The electron beam heating system

It is crucial to test off-line the high power target before going on-line to make sure that the thermal calculations are correct and to test the reliability of the target under such power.

The direct heating system uses a $10\ \text{V} - 1000\ \text{A}$ power supply that directly heats the target container by resistive heating. The maximum power we can achieve with such a system is around $4.5\ \text{kW}$. To go above that limit we developed an electron beam bombardment system. The electron beam heating system was built around an existing power supply capable of delivering $16\ \text{A}$ at $1.2\ \text{kV}$. Figure 252 shows a schematic diagram of the heating system.

A filament located on the axis of the target tube is resistively heated to $2300\ ^\circ\text{C}$ and biased negatively with respect to the target tube. The electrons leaving the hot filament impinge onto the target inside wall.

Schematic drawing of the Electron Heating System

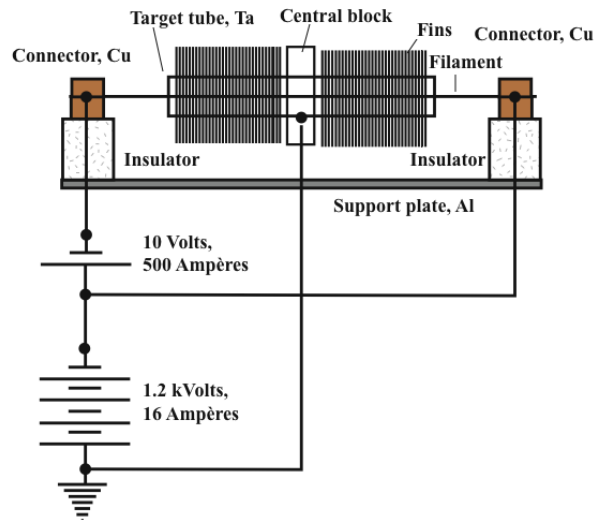


Fig. 252. Schematic drawing of electron heating system.

Instrumentation and measurement method

The target was equipped with a type C (W-Re) thermocouple attached to the corner of the fins. A second thermocouple measured the temperature of the heat shield. Two holes, $6\ \text{mm}$ in diameter, in the copper heat shield allow us to measure the tube and central block temperature using a 2 frequency pyrometer. The output cooling water was recorded using a type K thermocouple. The filament temperature was also monitored during the test using the same pyrometer.

Figure 253 shows a photograph of the fin target installed in the conditioning box. First we bring the filament to its operating temperature ($\sim 2300\ ^\circ\text{C}$) using a $10\ \text{V} - 500\ \text{A}$ power supply. We found that the best way to stabilize the arc was to regulate the voltage on the filament power supply.

We discovered that the central part of the target (we call it the central block) which connects the two

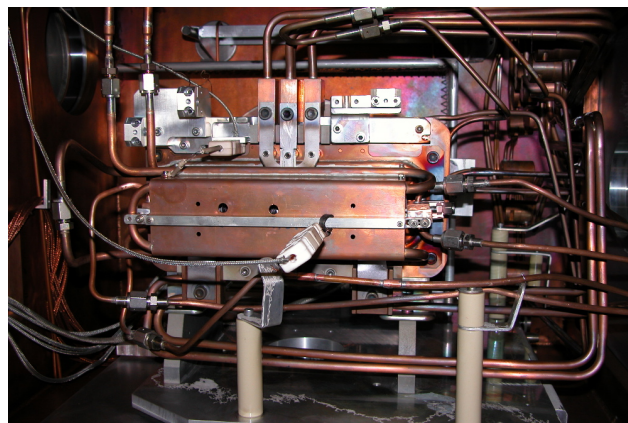


Fig. 253. Photograph of the high power target installed in the conditioning box.

Ta tubes was getting very hot. We had an excess of 450 °C at 13 kW. We decided to retrofit fins on the central block. The fins were machined from the same material thickness as the block, 9.5 mm in height and 1.5 mm apart. We operated the high power target up to 17.7 kW and observed that the central block temperature dropped to slightly lower than the tube.

Results and discussion

We measured the temperature of the fin, tube and central block as a function of the bias voltage. The input power originates from the electrons' power and the power radiated from the filament.

$$P_{in} = V_{EB} * I_{EB} + \sigma A \epsilon_{Ta} (T_{Fil}^4 - T_{Tgt}^4) ,$$

where V_{EB} is the bias, I_{EB} is the electron current, σ is the Stefan-Boltzman constant, A is the filament emitting area and ϵ_{Ta} is the tantalum emissivity. T_{Fil} and T_{Tgt} are the filament and tantalum tube temperature, respectively.

In Fig. 254, the green triangles show the temperature of the actual ISAC target that does not have fins. The maximum power we can dissipate is only 4.5 kW. These results were obtained by resistive heating. The

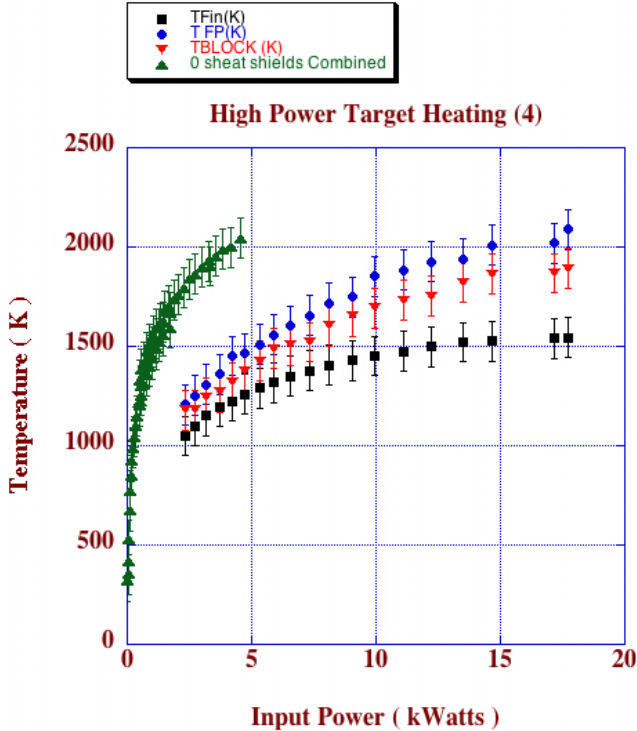


Fig. 254. Plot of the temperature as a function of the input power. The green points are the result of the resistive heating test for a Ta target without fins which goes only to 4.5 kW. The other three sets of points represent the temperature obtained with the electron beam heating system. The temperature of the tube, the central block and the fins is represented by the blue dots, red inverse triangles and the black squares, respectively.

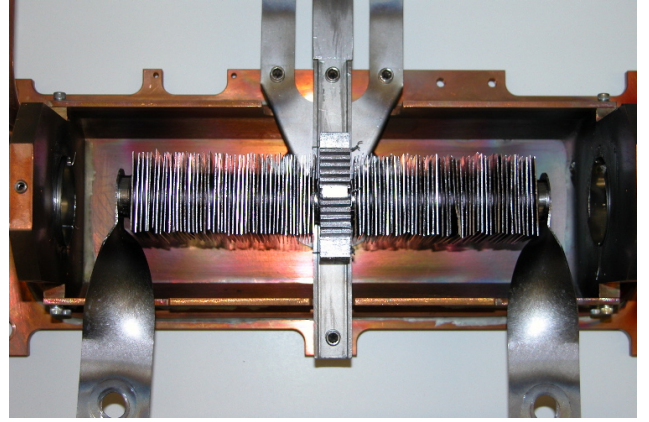


Fig. 255. Photograph of the high power target after the tests, with the heat shield removed. We can see the fins we added on the central block.

other three sets of points represent the temperatures obtained using the electron beam heating system. The temperature of the tube, the central block and the fins is represented by the blue dots, the red inverse triangles and the black squares, respectively.

Figure 255 shows a photograph of the target itself after the tests. Even though the target was operated up to 17.7 kW there is no sign of degradation of the target and the fins.

ISAC ION SOURCES

ECRIS-1 Tests

The ECRIS-1 was installed for the first time in the east target station at ISAC in the summer of 2002. The ECRIS-1 at that time was equipped with an extraction hole of 5 mm in diameter. Extensive stable beam studies were carried out to establish a good tune. Unfortunately, the beam intensity was such that we experienced large copper sputtering from the interaction of the ion beam with the copper collimators located in front of each quadrupole lens. The copper coated all the insulators inside the exit module 1 and 2. The optics elements in the two exit modules had to be rebuilt and we added the following improvements to our design:

1. Two water-cooled collimators were installed after the extraction system and before the first quadrupole.
2. Current limits on these collimators provide a warning and if no action is taken after 30 seconds then the high voltage bias is turned off to avoid sputtering.
3. Current limits on all of the collimators in front of each quadrupole have also been implemented.
4. Shielding cups were added on each insulator to prevent deposition of metallic vapour coming from sputtering onto the insulator.

5. A smaller extraction hole of 3 mm replaced the 5 mm one in order to reduce the extracted beam intensity and consequently limit the sputtering.

The ECRIS-1 went back to the east target station in May, 2003 and we resumed operation with stable beam. We measured the neon ionization efficiency using a calibrated leak. A Ta target was installed onto the ECRIS-1 and we measured noble gases yield, Xe, Kr, Ar, Ne and He. These yields can be compared to the well known alkali yield of Cs, Rb, K, Na and Li measured already at ISAC and at ISOLDE, CERN for example. We found that the yield of the noble gases was low by a factor of 10 to 100.

We noticed that the efficiency dropped significantly with the proton beam current on target and discovered that the efficiency is greatly affected by the pressure increase when the proton beam hits the target.

Tests were performed during the shutdown period in order to determine the effect of the pressure on the neon ionization efficiency. At first we spent time to ensure we would obtain the best operating conditions to optimize the neon ionization efficiency by varying the magnetic field using the two coils, the rf, and the support gas flow. We were able to reproduce the neon ionization efficiency of 2 to 2.6% which was observed on the off-line test stand. In the best operating conditions, we measured an ionization efficiency of 25.9% for Kr^{1+} and 62.1% for Xe^{1+} . Once we had the operating condition optimized we began injecting krypton and xenon into the ECR.

The intent of this study was to determine the operating range under pressure of the ECR-1 installed in the east target station. Kr and Xe gases were injected into the ECR and we have measured the neon ionization efficiency with respect to the injected flux of gas. We also recorded the pressure increase inside the containment box, the extracted current, and the beam emittances as a function of the flux of gas.

We observed that the ionization efficiencies dropped by two orders of magnitude for a pressure increase of 1.5×10^{-6} torr while injecting Kr or Xe (see Figs. 256 and 257, respectively).

The measurements show also that the emittance increases with the gas flux injected into the ECR. Furthermore, we observed a low energy tail formation that increases with the injected gas flux. This is a sign that part of the beam experienced collision inside the accelerating gap.

We can conclude that the source is stable over a pressure range between 1×10^{-6} to 1.5×10^{-6} torr. Above that pressure the ionization efficiency starts dropping. That corresponds to an estimated flux of 10^{14} atoms/s. If we want to run the ECR on-line we have to make sure that we stay within those limits if

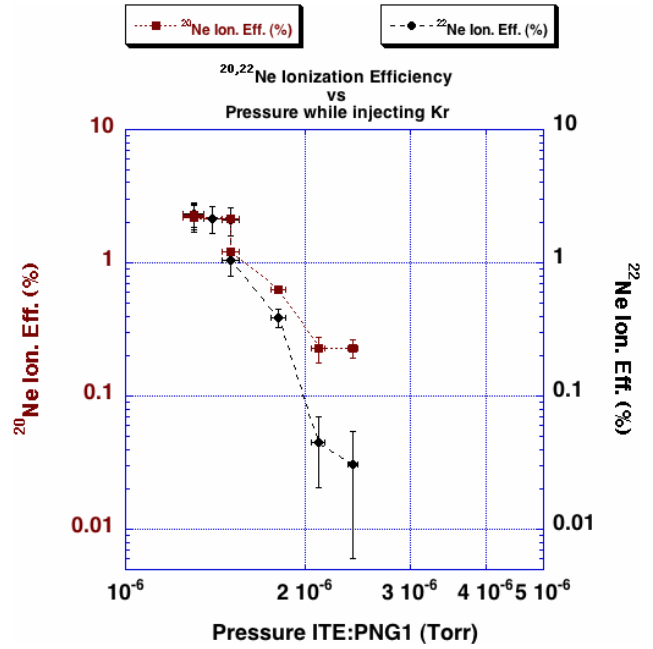


Fig. 256. Neon ionization efficiency as a function of the pressure while injecting krypton into the ECRIS-1.

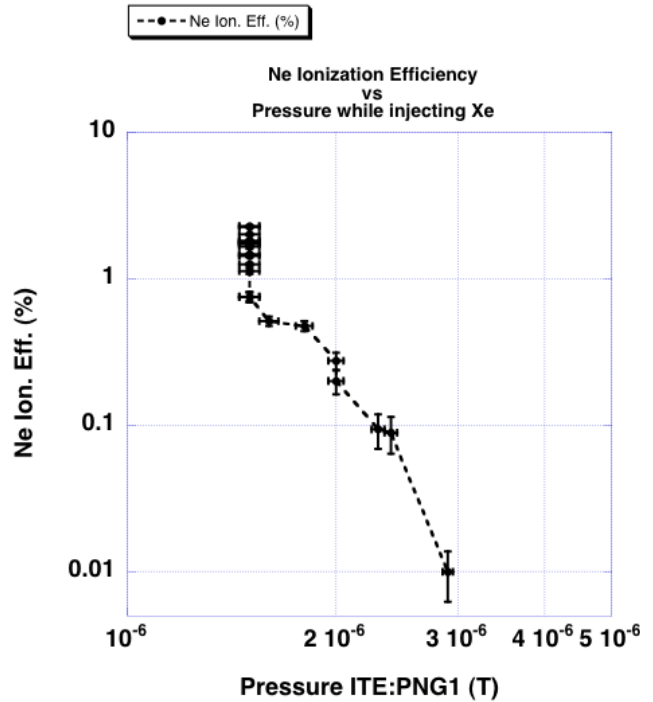


Fig. 257. Neon ionization efficiency as a function of the pressure while injecting xenon into the ECRIS-1.

we want to maintain the 2% ionization efficiency. On-line tests are scheduled in May, 2004 with a SiC target. The aim will be to produce ^{18}Ne for a high precision half-life determination.

Charge State Booster (CSB)

The 1+ ion source test stand (ISTS) facility has been extended to incorporate the CSB for tests and further development. The installation of the CSB, the beam transport and diagnostic elements, the high current and high voltage power supplies, the 14.5 GHz – 2 kW microwave generator and the vacuum and high-pressure water cooling systems has been completed.

Figure 258 shows the 1+ beam transport system upstream of the CSB during installation. Figure 259 shows the N+ beam transport system downstream of the CSB including the M/Q magnetic and electrostatic analyzing systems. Space has been provided in the 1+ beam line for the future installation of the rf beam cooler for tests with the charge state booster.

The computer control system (hardware and software) of the ISTS has been extended to include the control of the CSB test facility.

With some delay, due to lack of technical support

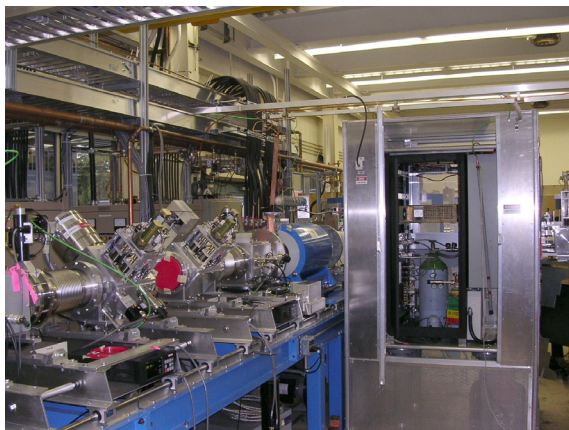


Fig. 258. Photograph taken during the assembly of the 1+ portion of the beam transport system. The CSB is the blue cylindrical object located at the left of the H.V. rack, which houses the gas supply system and auxiliary equipment.

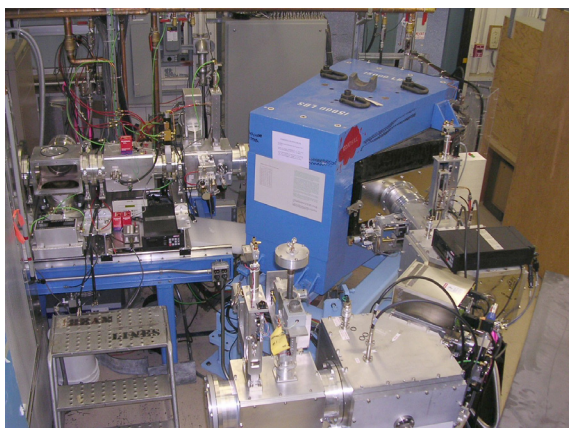


Fig. 259. This photograph shows the beam transport components downstream of the CSB. Seen are the 90° magnetic and the 2 × 45° electrostatic analyzers.

at the assembly stage, the CSB was operated for the first time in November. This first run was principally to commission most of the devices including tests of the personal safety and machine interlock systems.

The CSB was operated as an ECR ion source (26 kV extraction – 150 W rf power) for a short time using oxygen as a buffer gas. The extracted beam consisting mainly of oxygen atoms was analyzed. Figure 260 shows the M/Q spectrum taken with the Faraday cup located at the exit of the analyzing magnet.

The preliminary layout to implement the CSB in the ISAC-I building has been finished and is waiting for approval.

The first three months of 2004 will be devoted to fully commission the CSB facility including the electrostatic analyzing system and diagnostic elements. Beam optic tuning and 1+/N+ operation is expected to begin in April.

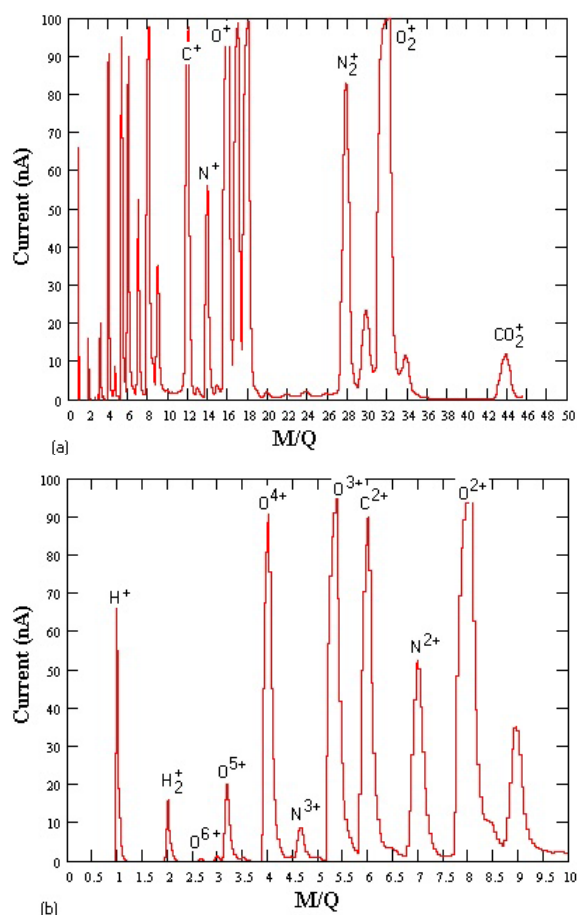


Fig. 260. (a) M/Q spectrum. This scan was made soon after the CSB was put into operation for the first time. The current amplifier for the O_2^{1+} peak is in saturation. Logarithmic current amplifiers have been designed and tested but not yet implemented. (b) Same spectrum but to $M/Q = 10$. The different charge states of oxygen are clearly seen here. The other peaks arise most likely from the out gassing process in the plasma chamber and from the rest gas.

Resonant Ionization Laser Ion Source (TRILIS)

Within the radioactive ion beam (RIB) development at ISAC a resonant ionization laser ion source (TRILIS) is to be implemented to provide radioactive ion beams complementing the existing ion sources. TRILIS uses multi-step resonant laser excitation and ionization and capitalizes on the potential for element-selective, efficient photo-excitation and ionization, with the major components of the LIS located far away from the highly radioactive target ion source.

The basic set-up of TRILIS is shown in Fig. 261 and is identical for off-line development and on-line beam production. In general TRILIS can supply beams of metals and transition elements that are otherwise difficult to obtain. Tunable, high-power, high repetition-rate, narrow bandwidth, and synchronizable pulsed lasers are required. Typical excitation schemes employ two and more commonly, three laser excitation steps for ionization, with the laser wavelength for the first excitation step usually being in the blue to ultraviolet region of the spectrum. In a typical laser excitation ladder each additional step requires higher spectral energy density. Therefore autoionizing states in the continuum are best suited for efficient ionization. These states have to be determined experimentally for each element individually. The initial beam development in 2003/04 is focused on Al and Ga. Figure 262 details the laser excitation schemes used in the initial investigations.

The TRILIS laser system employs state of the art, frequency-doubled YAG lasers pumping Q-switched solid-state titanium sapphire (TiSa) lasers (collaboration with Mainz University). This reduces the over-

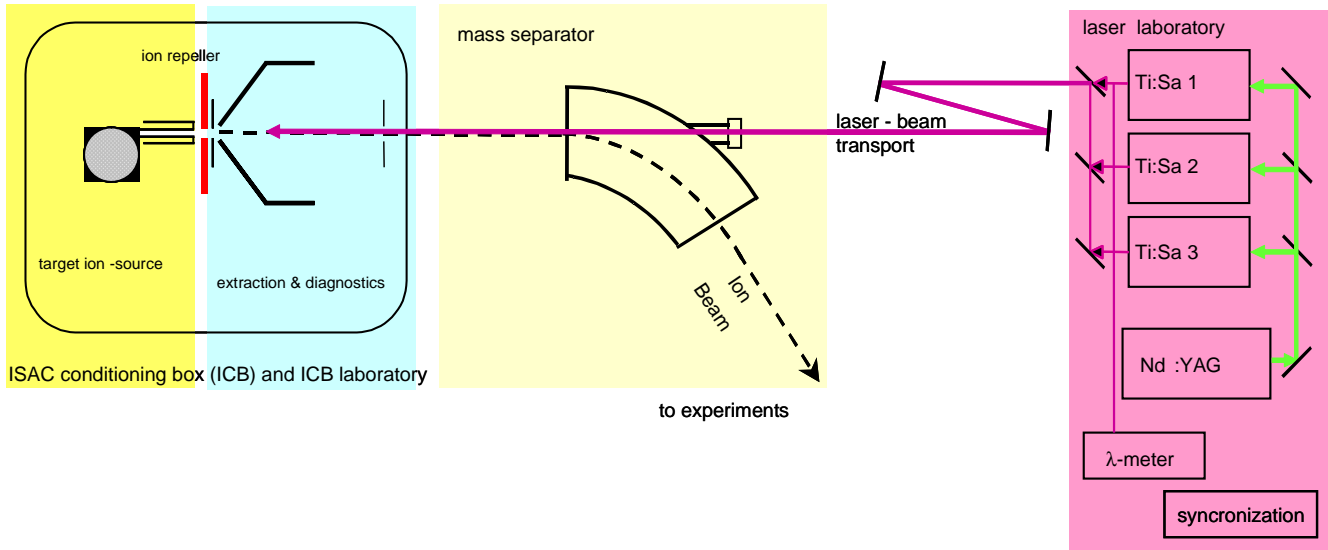


Fig. 261. Schematic of the TRILIS off-line development station with the principal functional groups: target ion source, mass separator and laser system. For TRILIS on-line the laser beam transport distance increases approximately five fold, thus requiring beam expansion and 2 in. diameter optics.

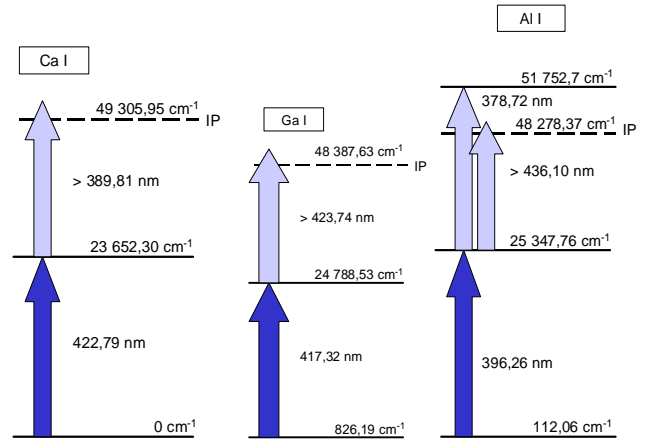


Fig. 262. Simple one-step resonant one-step non-resonant (1+1') laser excitation schemes used for off-line excitation scheme development and search for auto-ionizing state for the initial target elements Ga and Al.

all installation and operation cost over the competing copper-vapour laser-dye-laser combination. It does, however, involve the development or adaptation of some technologies:

- new laser ionization schemes, as the wavelength range covered by the TiSa lasers differs from that of the dye-laser systems,
- frequency-tripling for efficient laser excitation of elements such as Be (under development at Mainz University), and
- pulse amplification of ionizing TiSa laser (future work).

After the completion of the proof of principle tests with the Mainz TiSa lasers in 2002, we fabricated,

installed and tested a set of 3 TiSa using the Mainz design. At the same time the pump laser pulses and beam quality were fully characterized.

On the electronics side, a new Q-switch driver electronics built around a commercial fast push-pull transistor switch and a remotely programmable 3 channel trigger/digital delay generator with 0.5 ns resolution for TiSa laser synchronization were developed, prototyped and built by the TRIUMF Electronics Development group. The construction and commissioning of the laser laboratory and the laser systems was supported substantially (3 months) by Dr. Roland Horn, who graduated from the Mainz group, and Thorben Windeler a MSc. student in applied laser technology from FH Ostfriesland in Emden (Germany). Safety approval for the off-line laser lab and the lasers therein was obtained. Basic laser parameters of the TiSa lasers were determined, the lasers were operated in Q-switched mode and two manually controlled frequency doubling units were set up and operated in order to gear up for off-line ionization scheme development. The complete TRIUMF Mainz TiSa laser system is shown in Fig. 263.

First on-line work is planned with the fundamental and the frequency doubled laser wavelengths as this allows for substantially simplified laser beam transport into the west target station (ITW) which was designated for first laser ion source tests in the fall of 2004. Off-line testing will be done with quantitative

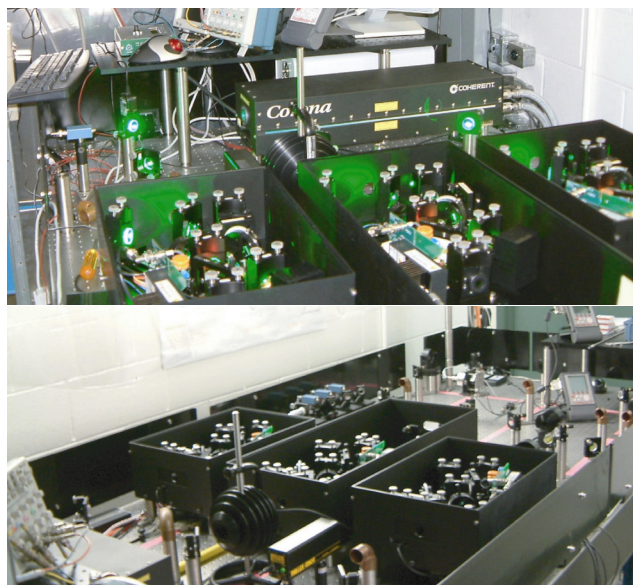


Fig. 263. TRILIS off-line laser laboratory adjacent to the ISAC conditioning station (ICB). Shown are the wavelength meter and wavemeter input multiplexing, the compact 75 W, 5 kHz–25 kHz Coherent Corona75 pump laser and the three TRIUMF built Mainz University narrow bandwidth, tunable titanium sapphire (TiSa) lasers. Not shown are the two frequency-doubling units.

evaporation of elements from crucibles attached to the standard ISAC target ion source surface ionizer/transfer tube. The heater-crucible combination is being tested with the surface ionizer and negative ion source in the ISAC conditioning box (ICB). This highlights the synergies in the RIB development group, however, it also shows the high level of facility sharing resulting in limited access for development work.

The laser beam transport from TRINAT to ITW was calculated and opto-mechanics installed for laser beam transport. This included modifications to the laser port on the pre-separator magnet during the 2002/2003 shutdown.

Further improvements to the TiSa lasers were tested and will be implemented as time permits. Preparation of the TRILIS laser laboratory location in the TRINAT clean-room for on-line work continues.

ISAC POLARIZER

Production of polarized lithium and sodium isotopes became routine and very reliable. The dye laser was used for polarizing all lithium isotopes, as well as sodium. DCM is the dye used for the red region of the spectrum including the Li transitions, and the solvent recommended by the laser manufacturer was ethylene glycol. However, ethylene glycol is very hygroscopic, and water forces DCM out of solution. Very stable operation was achieved by changing the solvent to EPH (ethyleneglycol phenyl ether).

An ATOS LM007 wavemeter was purchased and installed, after tests with one borrowed from the TRILIS group demonstrated its usefulness. It is an order of magnitude more accurate than the wavemeter it replaced. Formerly, one tuned the laser to an undetermined order of the spectrum analyzer (free spectral range 300 MHz), locked the laser frequency to a specific fringe spacing between it and a reference He-Ne laser, and finally scanned the Na cell bias to Doppler-tune the isotope beam energy onto resonance. If the laser frequency lock were lost, one would have to scan the Na cell bias again, since the wavemeter was not accurate enough to tune the laser to the same fringe order in the spectrum analyzer. The new wavemeter is accurate enough to tune back to the same order, eliminating the need for a Na cell scan. This upgrade is especially useful when running low intensity beams, when a Na cell scan takes too much time.

Concepts for producing polarized paramagnetic ion beams such as $^{11}\text{Be}^+$, $^{15}\text{O}^+$ and $^{20}\text{F}^+$ were explored. The polarization of such a beam would normally be lost during transport to the experiment, due to precession of the electron magnetic moment coupled to the nuclear spin. The simplest solution, applicable to all isotopes, is simply to extend the guide field to the ex-

periment. Magnetic coil field calculations showed that this is feasible for both the existing BNMR platform and the polarimeter beam line. An optical pumping scheme for atomic metastable fluorine was identified.

The polarizer beam line is well suited for doing collinear laser spectroscopy. The Texas/McGill group modified a fluorescence monitor, originally used for tuning the laser to ^8Li , for detecting laser induced fluorescence from metastable La ions. Their experimental set-up was tested during the summer with an Ar^+ beam, and Ar^+ resonance lines were observed.

REMOTE HANDLING / TARGET HALL FACILITIES

Modules

Work began this year on the fourth target module (TM #4) with assembly of the shield plug, containment box, service cap and completion of the services tray.

Remote Handling

Regularly scheduled target exchanges for target module #1 (TM #1) operating in the ISAC west target station (ITW) are becoming a full time operation for both the remote crane system and the target handling hot cell.

In January the SiC #4 target was exchanged for the ZrC #1 target on TM #1, in May this was replaced with the SiC #5 target, with the Ta #6 target in July, and finally with the SiC #6 target at the beginning of November. The spent targets from all TM #1 operations were inspected and documented, packaged and remotely transported to the spent target storage vault in the target hall.

The spent target storage vault is now at one half of its storage capacity with 12 spent target pails, and the failed TIS service tray removed from TM #1 in 2001. At the rate of presently scheduled target exchanges for TM #1 alone, we will reach maximum target storage capacity by 2006. With TM #2 and TM #3 now beginning operation in the ITE station, this date will no doubt be reached even sooner.

A mechanical system for replacement handling of the hot cell tele-manipulators was designed and installed at the south hot cell. This was employed in June to replace a problematic manipulator for repair.

The TM #3 module, with the installed ECR source was serviced after initial trial operation in a contamination control enclosure within the target hall. The original ECRIS quartz tube was replaced with an alumina version, and the Ta #4 target subsequently reinstalled on the module in the hot cell.

ISAC CONTROLS

This year saw some slowing down of the frantic installation of new systems, which had to be dealt with during the past years. This “breathing space” was used to enhance the consistency, maintainability and reliability of the ISAC control system.

As in the years before, the Electronics Development Group supplied the hardware support for the ISAC control system, both for design and maintenance. Chris Payne from the ISAC Operations Group became an honorary member of the Controls Group and took over the responsibility of managing the console Linux workstations in the control room.

New Systems

Charge state booster

At the ion source test stand, the control system was expanded to support the new charge state booster system. This amounted to more than doubling the existing system. A small EPICS IOC, based on the PC104 form factor, was installed to supervise the vacuum controls PLC. A Linux packet-switching firewall was installed to shield the PC104 CPU from rogue network traffic. Beam optics and beam diagnostics controls were integrated with the existing VME based EPICS IOC. Two new PLC breakout cabinets were installed, one at ground and one at HV potential. Hardware and software support for 83 vacuum devices, 22 power supplies, and 22 beam optics devices, including 2 emittance measurement stations was provided.

TITAN rf cooler

The conceptual design for the TITAN rf cooler set-up in the proton hall extension was finished. A VME based EPICS IOC will be located in the high voltage rack. This IOC will drive the trap power supplies and the voltage switches, and control the beam optics via ISAC style CANbus controllers.

The majority of the detailed design was finished. For the control of the trap supplies and pulse sequencing, special VME modules were developed (for details see the Electronics Development section of this Annual Report). EPICS device and driver support for these new modules is complete.

For the vacuum system, the PLC program was developed and simulation tests were performed. The PLC breakout panel was pre-wired and is ready for installation.

ISAC-II cryomodule

The control system for the ISAC-II superconducting cavity was disassembled at the BC Research location, moved to the new ISAC-II building and re-commissioned. In addition, the system was upgraded

to fully support the new ISAC-II cryomodule in the test location at the SCRF facility.

OLIS surface source

EPICS and PLC support for the new OLIS surface source was implemented. This also required modifications to the existing vacuum and beam optics systems.

Other small systems

For the GP2 experiment, a concept design for the experiment control system was developed. The experiment's summer student was guided during the implementation of the front-end Modicon Momentum PLC system. An EPICS system was implemented, which includes an operator interface and extensive sequencing control. For this, minor enhancement to the TRIUMF/EPICS cppe sequencing tool were implemented.

RF amplifier monitoring

The conceptual design of a monitoring system for all relevant parameters of the 14 ISAC rf amplifiers was finished. It consists of a Modicon Momentum PLC system, which uses the new Advantys I/O system and implements one I/O drop per amplifier. PLC code and EPICS support was developed. The PLC was installed and one amplifier was instrumented. This subsystem awaits final signal hook-up and is ready for testing. In addition, remote control of the RFQ amplifier was implemented.

Functionality Enhancements

The Probes Group installed absolute encoders for position read-back of all the motor systems in diagnostic box DB0 after the pre-separator magnet. EPICS support was implemented and the previously used tedious calibration procedures could be retired.

Work on the rf phase measurement system continued. A first version of the GPIB based readout of a vector voltmeter was implemented. It uses a dedicated PC104 EPICS IOC, which interfaces to GPIB via the GPIB-Enet10 module from National Instruments. Support code was written to support this interface using the EPICS stream device driver. This system has known performance and reliability problems, but it was the only available solution given time and manpower constraints. An upgrade, which will replace the GPIB-Enet10 controller with a PC104 board is being worked on at the moment. This upgrade will also move the signal selection from VME to PC104 and provide a dedicated phase measurement solution.

At the ITE target station, an interlock system was implemented in order to cope with the higher currents from the ECR source. This system balances the requirements of machine protection and operational convenience in a staged approach, increasing the machine protection the longer an overcurrent situation prevails.

Sequencing code for automatic startup and shutdown of the ECR source was developed.

Optically isolated, CANbus based charge integrators were installed at the TUDA experiment for low current readout.

At the target conditioning box, many small modifications were made to support changing requirements for testing of the laser ion source and high current targets. A new 8-channel water flow controller with flow readout via CANbus was installed. The newly developed EPICS support for this device was tested.

Additions to the 8π vacuum system, both PLC and EPICS, were implemented to support extra devices for the new tape collector system.

An EPICS device and driver support were developed for a new TRIUMF-designed 8-channel VME ADC.

System Support

The homecoming of the superconducting cavity test set-up from BC Research freed up one SUN workstation. This allowed the reconfiguring of the production environments for the EPICS control systems outside the ISAC firewall (ion source test stand, target conditioning box, evaporator, TIGRESS). The responsiveness of the conditioning box system was considerably improved and the system topology was altered for future firewall protection of these systems.

Again this year, a considerable amount of time went into system maintenance on the development and production machines, especially operating system upgrades both for Solaris and Linux. Some time was spent evaluating a low-maintenance, commercial firewall system, which was finally abandoned because of insufficient throughput. In its place a PC/Linux-based firewall was installed to protect the development nodes in Trailer GgExt.

The introduction of PC104 based IOCs was delayed by several months due to problems with unexplained communication lock-ups. These did happen frequently, when the IOC was located on the site network, but not when located behind a firewall. Although the source of the problem was never clearly identified, it was resolved by upgrading the vxWorks Kernel from version 5.4 to 5.5.

In preparation for ISAC-II, a new VME CPU was evaluated. It is based on the Intel Pentium (Celeron) chip and provides a good balance of price and performance. Support for vxWorks 5.5 was implemented and all ISAC drivers and device support were built and tested with this CPU. Field tests at the ion source test stand are scheduled for the new year.

Development Support

In order to better control software deployment, the IOC boot system was reorganized. A Perl tool was developed which configures the IOC boot directories and allows roll-back to a previous IOC configuration.

As a major project during the fall, the ISAC database tools underwent a major upgrade with the goals of:

- converting from Paradox to PostgreSQL as the underlying relational data base system;
- implementing the existing functionality with a Web interface;
- integrating many of the group's development tools with this Web application.

After a short evaluation comparing Java, PHP, and Perl CGI, the latter was chosen for implementation of the tool applications.

The design of the database tables was reviewed and improved. Then the table data were exported from Paradox and imported with few difficulties into PostgreSQL.

The functionality of the Paradox application was recreated in Perl using the DBI module for accessing PostgreSQL. Other development tools, such as generation of Capfast schematics for building IOC software, PLC interlock checking, the IOC boot configuration system, and device control panel building, were integrated into the Web application. An automatic event registration system was implemented in order to keep track of control system changes.

Commissioning and Operation

The ISAC controls Web site was reorganized for better optics, navigation and information retrieval. More documentation, tutorial material and troubleshooting information was added.

The ISAC control system operation matured during this year, with the system settling down. Most IOCs were smoothly upgraded to vxWorks 5.5. A problem area remains the communication with the rf control PCs, where erratic behaviour occurred with unacceptable frequency late during the year and is not yet understood. A different approach is being tested for ISAC-II and may be retrofitted to the ISAC-I system as well.

VACUUM

ISAC-I

The Vacuum group supported all vacuum equipment for beam production and distribution, as well as some vacuum systems for the experiments. Most of the turbo pump repairs, including replacement of bearings and rebalancing of rotors, were done on site. More than

15 pumps have now been restored and returned to operation.

CAD-generated vacuum diagrams for CSB, S-bend transfer line, HEBT roughing system upgrade, RFQ cooler, cryomodule, GPS-2 and TUDA have been produced, most of the components purchased, and some of the systems have already been implemented.

Targets

Several vacuum leaks, located on the isolators of the service cap of the ISAC target west, have been repaired. The Vacuum group has been involved in turbo pump installation on target modules and leak checks of the target module cooling system.

The ion gauge has been replaced on TM #2.

The east target station is performing very well and holding an average vacuum of 8.0×10^{-7} torr. The new gas-insensitive membrane gauges are scheduled for installation during the spring shutdown of 2004.

A turbo pump failed on the IMS beam line and was replaced. A test was done by the addition of a cryo pump to improve the vacuum in that area for future requirements.

LEBT

ILY The Penning gauge controller failed and was repaired and replaced twice during the year. It is planned to replace the gauge and controller with an inverted magnetron from Varian.

8 π An extra turbo pump was installed for lowering the vacuum in the detector area. The gate valve was rebuilt with new seals.

Polarimeter Two turbo pumps failed during the year. One was replaced with a rebuilt pump, the other one has been removed and the port planked off. The gate valve was rebuilt with new seals.

MEBT

RFQ All brass valves were refurbished or replaced with new ones. A turbo on the RFQ failed and was removed and will be rebuilt or replaced.

DTL Two turbo pumps failed and were replaced with new ones. The DTL tanks are performing very well and are holding an average vacuum of 4.5×10^{-7} torr. A few vacuum leaks were diagnosed and repaired by the Vacuum group.

HEBT

Two turbo pump controllers were repaired and are back in operation. Air cooling units have been added to all turbo pumps.

TCB The Vacuum group provided support for the installation of an extra turbo pump and the diagnosis of various vacuum leaks.

TUDA A new high vacuum gauge was installed and the Vacuum group diagnosed and repaired a few vacuum leaks.

Berkeley experiment The vacuum system has been set up for the experiment on the straight HEBT section.

Vacuum/Cryogenics, ISAC-II

Vacuum property measurements for different materials have been conducted on the vacuum test stand. These materials are intended for use in the ISAC-II cryomodule.

The CSB vacuum system has been assembled and is functioning well. The copper wool filters have been selected, purchased and installed to prevent migration of Teflon dust from the dry mechanical Scroll 300 pump to the vacuum chamber.

The Vacuum group participated in some of the cryogenic activities related to ISAC-II SC linac development, including participation in the design and development of the main components on the new SC linac, and the manufacturing and assembly of the nitrogen heat shield for cryomodule #1. CAD-generated cryogenic diagrams have been produced for the cryomodule, including the temperature sensors, level probes, heaters, and pressure gauge positions. Pressure relief valves have been tested.

The Vacuum group designed and assembled the SC solenoid helium test cryostat and tested the SC solenoid built by Everson.

Liquid Helium and Liquid Nitrogen

The Vacuum group is responsible for liquid helium and liquid nitrogen deliveries and distribution on site.

The liquid nitrogen service to BCRI was cancelled in September when the SCRF laboratory moved to its new home in the ISAC-II building.

The ISAC-II nitrogen distribution system has been inspected, and is scheduled for commissioning in the spring, 2004.

ISAC-I RF SYSTEMS

ISAC rf systems performed well over 2003 with a total availability of about 94%, the same as in the previous year.

RFQ

The RFQ operated reasonably well, though it contributed the most rf system down time (188 hours). Major problems were associated with a power amplifier (PA):

- two PA tubes (4CW150000) failed and were replaced with spares;

- screen bypass capacitor burnt. To fix it, the fabrication burrs on the screen plate were removed and a kapton insulator was replaced;
- driver power supply regulation circuit failed. A smaller dc supply was promptly built to provide temperate operation while troubleshooting the original unit;
- air conditioning deficiencies caused a few PA interruptions during the hot summer. Both ISAC hall and HV power supply air conditioning configurations were improved;
- ac distribution for the RFQ controls tripped due to overload from the experimental set-up energized from the same panel. The distribution was reconfigured to supply rf controls from UPS.

During the winter shutdown a soft start circuit was installed in the RFQ high voltage power supply and has shown reliable operation since. It is based on SCR elements and allows a slow voltage rise to prevent high inrush currents. It also provides very fast power cut off (8 ms compared to 24 ms in the mechanical switch) to reduce ignitron tube overloads. Soft start circuit implementation also allowed a PA remote controls update, permitting amplifier remote turn on/off. Previously this was not possible due to ac mechanical switch gear manual reset requirements. An RFQ PA filament power supply transformer was replaced during the September shutdown, providing proper tapping for reduced filament voltage in order to increase tube lifetime.

Bunch Rotator

The MEBT 105 MHz bunch rotator was routinely used in operation to allow a desired beam quality. Its amplifier failed once due to a burnt motor in an air blower. At that time a temperate 400 W amplifier was set up to ensure uninterrupted operation while ordering and replacing the broken unit.

During the course of the year, we realized that rotator startup is somewhat troublesome. After a day of idling it normally requires up to 30 minutes of conditioning to overcome a multipactor discharge, which does not happen to any other rf system. To investigate the problem the cavity was taken off-line and dismantled. The problem was traced to an extensive secondary electron discharge ignited between split-ring stem and cavity endplates (see Fig. 264). This area is exposed to low rf voltage and prone to multipactoring. A special surface treatment is foreseen to tackle this problem and will be accomplished during the next shutdown.

MEBT Rebuncher

The MEBT rebuncher solid state amplifier was replaced with a home made unit in 2002 and we have not

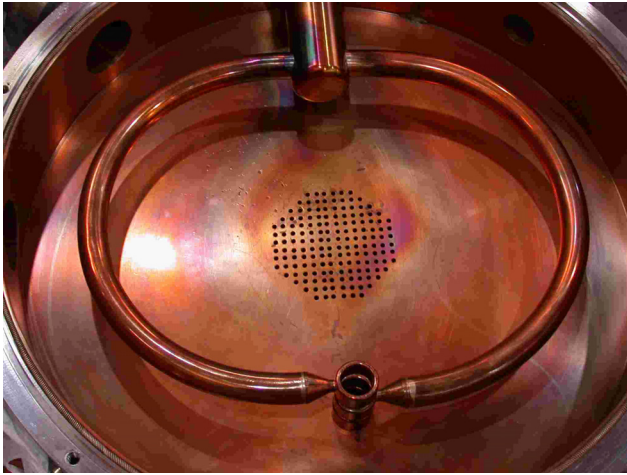


Fig. 264. MEBT bunch rotator structure with multipactor discharge traces around the stem.

experienced any trouble in its operation since. A cavity state has attracted our attention while servicing its cooling circuit. The endplates made of mild steel were originally nickel plated inside the cooling channels to prevent corrosion. Over time this coating has degraded and iron was exposed to water. As a result, heavily ionized water has contaminated the return circuit, painting the plastic flow meter cover in red. Buncher cooling requirements were reconsidered and a high power test was performed without water cooling of the endplates. The results have proven our estimate of insignificant power dissipation in the endplates. Running a system at 1.5 kW (50% over the nominal) we observed a temperature rise from 22 to 36° C. So a decision has been taken to operate this unit with non-cooled endplates.

DTL

DTL systems routinely operated mostly at about 4/9 full power ($A/q \approx 4$) according to the scheduled experiments. During the winter shutdown we continued the program of fine tuner modification. This time we have removed fingerstocks, which were scratching the tuner shafts, from DTL #3 and #4 tuners. None of the 9 modified tuners has shown any trouble in operation.

All rf pickups were removed from the cavities for detailed inspection. Two of them were replaced due to poor conditions traced back to original installation. Buncher #1 pickup loop was replaced with a capacitive probe giving more stable read back signal. The original loop showed a coupling dependence on the rf power level.

DTL #1 tank has shown the same problem with iron endplates as the MEBT rebuncher did. It has also been put under high power test with hope that we might be able to run without endplate cooling. The test has confirmed that cooling is vital. Under nominal 4 kW power, non-cooled tank structure has rapidly

warmed up to about 60° C, and the frequency regulating tuner has reached its limit. To minimize the intervention with structure modifications it was decided to apply external detachable heat sink for endplates cooling. All required parts have been designed and will be installed next spring.

About 15 regulation valves were replaced in the DTL cavities cooling circuits in order to provide smooth water flow adjustment. The original valves were too coarse to satisfy the regulation requirements.

DTL amplifiers

After extensive maintenance in 2002 the DTL amplifiers did not require any specific service over the last year and worked very reliably. The only unit we worked on was a transmission line from PA to DTL tank #3. It showed an elevated standing wave ratio (VSWR) and excessive heat dissipation. The problem was traced to a distorted line section at a sharp bend where the internal insulator was melted (see Fig. 265) in 2000 during the commissioning period. To fix the problem, the entire Tx-line was replaced with a new piece.

An amplifier remote control system was developed and prototyped with DTL #5 PA. It provides all amplifier subsystem status signals, operational ac and dc voltages and currents, and forward and reverse rf signals to the ISAC main controls system via EPICS interface. All signals will be archived for postmortem analysis. This system will give us, as well as ISAC operators, a powerful tool for rf system troubleshooting and preventive maintenance. According to budget availability we plan to build such a controls for all rf amplifiers.

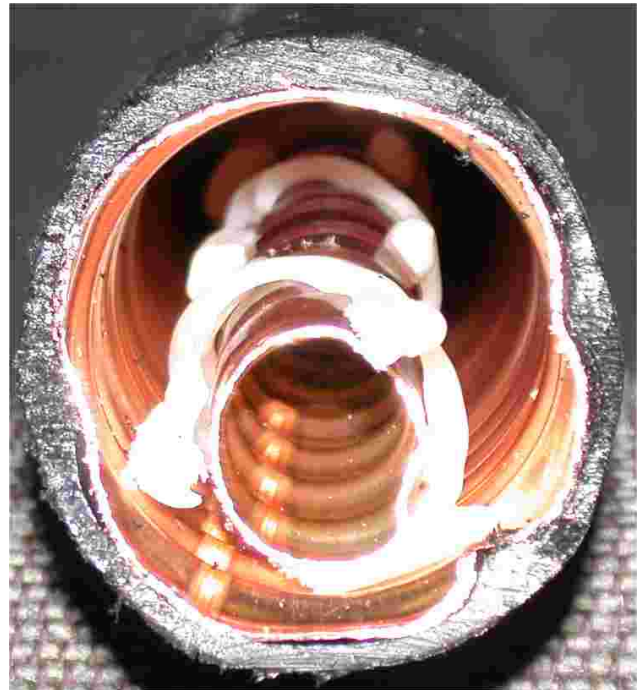


Fig. 265. Damaged semi-flexible Tx-line.

DTL couplers

During last year the previously troublesome coupler windows worked fine after some preventive and monitoring measures were taken (see last year's Annual Report). Nevertheless during the winter shutdown all the couplers were again taken out for inspection, which confirmed their good state. Then all coupling loops were copper plated to avoid possible spattering from the brazed joint, which we experienced in the past. Buncher #1 coupler was tested with the aim of better operation stability. Its coupling loop was found to be oversized, which caused excessive coupling, both inductive and capacitive acting in opposite polarity. A new smaller loop was installed that dramatically reduced the capacitive component and improved system stability.

HEBT High Beta Buncher

The 35 MHz buncher was tested to operate with a modified DTL#4 tuner (without fingerstocks), showing a temperature rise on a bellows of about 20° C. This is still acceptable for operation, though it is much more elevated compared to the DTLs. The difference is explained by another type of structure (spiral), which generates rf currents through the tuner shaft, heating it up, while in the DTL all tuner currents are localized on the tuner plate, which faces opposite voltages on the drift tubes, and thus shaft currents are compensated. Then the original buncher tuner was modified to improve operational reliability. Subsequent tests showed much more pronounced heat impact on the bellows than in the beginning. The difference appeared to be in the tuner design. It has a longer shaft providing higher coupling to the structure, and thus absorbing more rf power. The tuner was set close to the outer limit of the regulating range to keep the temperature reasonable (below 70° C) for the current operation. Next shutdown we plan to standardize the tuner design to be compatible between different rf cavities and to satisfy the operational temperature requirements.

Phase Measuring System

An auxiliary phase measuring system (PMS) has been commissioned for the ISAC rf system. It provides precise ($\sim 0.2^\circ$) phase difference measurement between the reference rf source and each individual rf device. All hardware was tested and calibrated in 2002. Last year an EPICS based control system was commissioned. It provides remote control over the measurements both in manual and automatic modes. In manual mode a single cavity phase can be acquired with a variable repetition rate between 0.2 and 2 s. In automatic mode the system scans all 18 rf devices with 2 s intervals providing relative phase read back update every 36 s. At every

point a number of samples is measured, and an average value together with a standard deviation is being archived for rf system troubleshooting and beam instabilities investigation.

Two additional rf pickups were installed in the MEBT and HEBT bunchers providing independent inputs for PMS. For other rf systems the amplitude monitoring signal is split to give an input for PMS.

Eventually PMS is expected to provide the rf reference settings for accelerator tune up.

RF Controls

Over the year the RF Controls group regularly provided routine tune up of the rf control system. Upgrade work had been done for the VSWR protection circuitry: new rf filters have improved system stability.

Upgrade of rf controls hardware has extended this year over 3 more personal computers (PC): 1 was replaced and 2 others were superseded with a modern PC. The latter operation required a substantial software upgrade. New equipment has demonstrated very stable and reliable operation giving no more computer crashes since they were upgraded.

ISAC-II Transfer Line 35 MHz Buncher

The RF group continued development activities for building a 35 MHz buncher for the transfer line to ISAC-II linac. The buncher tank was copper plated. Cooling pipes were attached to the spiral resonator, leak checked, and copper plated (see Fig. 266). The

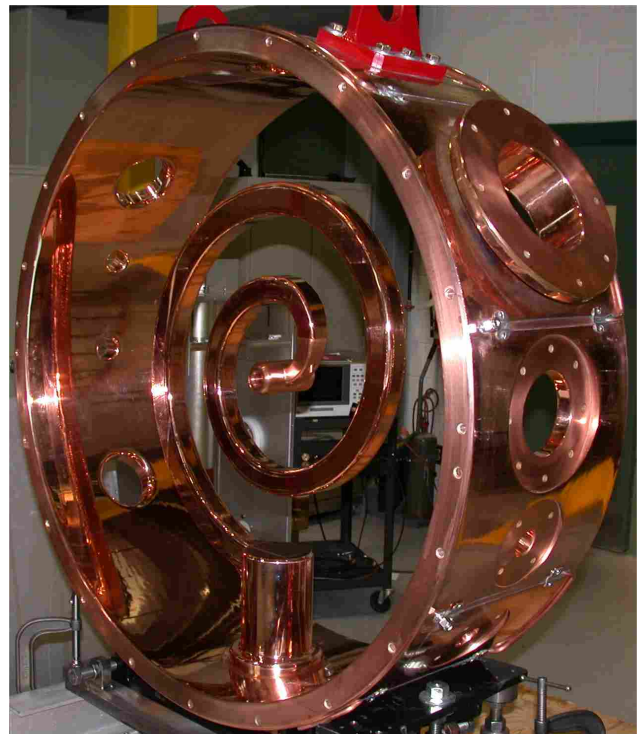


Fig. 266. New transfer line 35 MHz buncher.

structure assembly is ongoing. Fine and coarse frequency tuner drawings were updated for fabrication. Drawings for rf amplifier parts and sub-assembly have been made and submitted for production in the machine shop. The bias and screen power supplies and driver rf amplifier have been made in-house and tested. RF cold testing of the anode circuit, coupling loop and neutralization circuit was done. As a result of the test, the length of the outer tube for the anode circuit was reduced and sent for silver plating. The coupling loop size was re-designed and the external anode capacitor was modified.

BEAM DYNAMICS

LTNO Optics

Almost all of the focusing element settings in the low energy beam transport (LEBT) section are at or very near their theoretical values. The only exception has been the low temperature nuclear orientation (LTNO) optics. This consists of an ungridded electrostatic mirror, followed by a symmetric quadrupole triplet. These optics were obtained from ORNL and are not a TRIUMF in-house design.

From measurements of the beam centroid at a profile monitor downstream of the triplet, as a function of triplet setting, it was concluded that the mirror acts as an ideal mirror plus defocusing lenses at entrance and exit. The fitted focal lengths were on the order of 50 cm.

The electric potential inside the mirror was calculated numerically with RELAX3D, and particles were tracked through. These calculations confirmed the experimental findings.

GUIs

A graphical user interface (GUI) has been developed for beam envelope calculation. It has the capability of calculating beam envelopes for any section of beam line, and also to fit settings to a given set of constraints and free parameters. The purpose of this is to allow operators to calculate beam envelopes on the fly as they are changing beam line tunes. It is foreseen as a tool to aid in tuning all the ISAC beam lines, as well as ISIS and the cyclotron extracted beam lines.

ISAC DIAGNOSTICS

The accelerating components of the ISAC-II cryomodels must remain aligned at liquid helium temperatures: cavities to $\pm 400 \mu\text{m}$ and solenoids to $\pm 200 \mu\text{m}$ after a vertical contraction of $\sim 4 \text{ mm}$. A wire position monitor (WPM) system based on a TESLA design is being built and will be used to test a prototype cryomodule. The system is based on the measurement of signals induced in pickups by a 215 MHz

signal carried by a wire through the WPMs. The wire is stretched between the warm tank walls parallel to the beam axis providing a position reference. The sensors, one per cavity and two per solenoid, are attached to the cold elements to monitor their motion during pre-alignment, pumping and cool down. A WPM consists of four 50Ω striplines spaced 90° apart. A GaAs rf multiplexer scans the WPM signals and a Bergoz Instrumentation card converts them to dc X and Y voltages. National Instruments ADC and I/O cards read the dc signals and control the multiplexer. The data acquisition is based on a PC running LabVIEW. The system was developed in collaboration with LASA INFN Laboratory and the software was written at the SIDEA Corporation, both of Milan. The system will be used for initial alignment only and will be moved from one cryomodule to the next as they are built.

The amplitudes of the stripline signals vary nonlinearly with their position w.r.t. the wire. A test stand was constructed to calibrate the WPMs (see Fig. 267). A 0.5 mm diameter copper-bronze wire tensioned by a 10 lb weight passes through the WPM under test. A pair of Oriel translator stages, each with 1 in. of travel, forms an XY table to move the WPM about the wire. Optical encoders inside the dc servo motors provide $0.1 \mu\text{m}$ resolution. Figure 268 shows a plot of the electrical X and Y signals from the Bergoz unit as a WPM is moved in a raster scan under computer control. A scan of 3600 points using 0.2 mm steps covers a range of $\pm 6 \text{ mm}$ and requires about 2 hours to perform. A 2D third order polynomial curve fit is used to reduce the data to a set of calibration coefficients. Though the range beyond $\pm 4.5 \text{ mm}$ is still useable, signal compression occurs and these points were not included in the curve fits. A fitting error of less than $20 \mu\text{m}$ was achieved over most of the $\pm 4.5 \text{ mm}$ range (see Fig. 269).

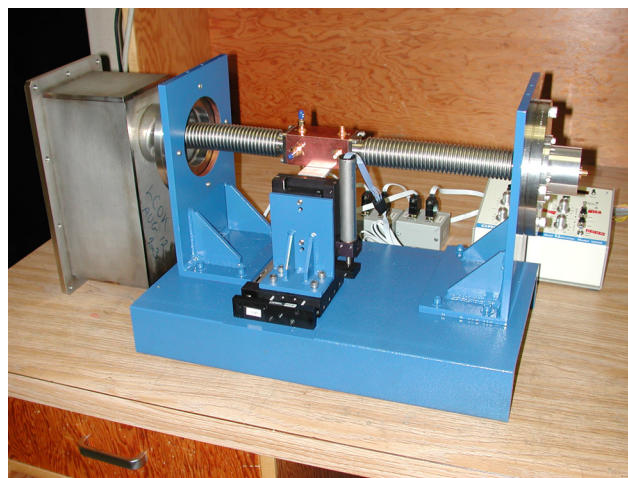


Fig. 267. The WPM calibration stand with the weight box on the left and the Oriel electronic interface behind. The stretched wire passes through bellows which form the outer conductor of the rf coaxial structure.

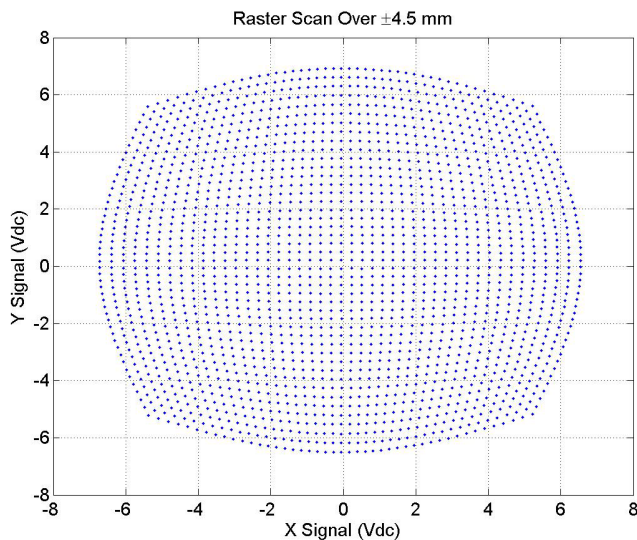


Fig. 268. Non-linearity away from centre is apparent in this plot of the electrical signal amplitudes collected during a raster scan of a WPM over ± 4.5 mm.

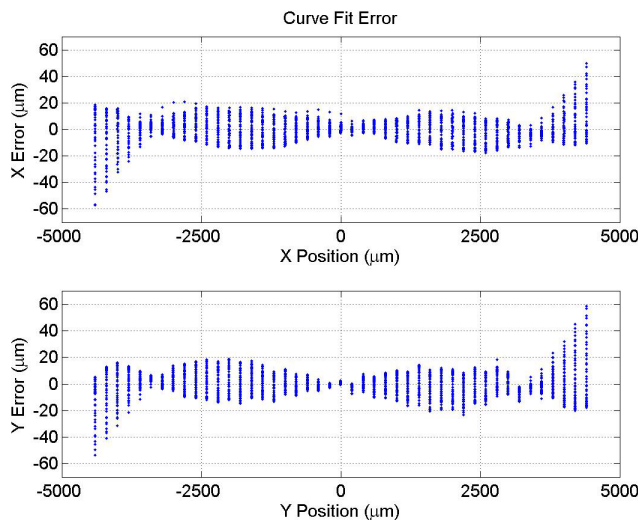


Fig. 269. The curve fit error is less than $20 \mu\text{m}$ over most of the ± 4.5 mm range.

EXPERIMENTAL SUPPORT

The Experimental Support group provided technical assistance to experimenters and was responsible in part for the installation, alignment and maintenance of beam line elements. The Beam Lines group now has a permanent technical area complete with machine shop and welding room in the ISAC-II experimental hall. This allows better access for experimenters in search of technical assistance. For ISAC-I and ISAC-II, the Beam Lines group has provided technical support for the 8π detector as well as development for GPS, TITAN and TIGRESS. The group provided the layout of the S-bend and helped plan the future installation of the transfer beam line scheduled for 2004. The Alignment group continued to provide precision alignment

for DRAGON, TUDA, Remote Handling and the RF group.

ISAC-I CONVENTIONAL FACILITIES AND INFRASTRUCTURE

This was an uneventful year on the operation and maintenance front without major breakdowns to report. Continuing engineering support was lent to the laboratory users. This included attendance at regular and engineering meetings, participation in engineering design review, cost estimating, services design, specification, procurement and installation coordination, as well attending to operational problems and maintenance.

Mechanical Services

Program debugging and re-commissioning of the radiation exhaust pressure zoning required additional effort during the implementation of the distributed digital controls.

A new heating coil and a new water pressure relief valve were added to the TRINAT air conditioning system heating coil. ISAC-I experimental hall services work included replacement of polyflo tubing for the RFQ, new valving for DTL, GP2 vacuum pump and glass tube venting to the radiation exhaust system, and cooling for DRAGON power supplies and the new laser room. Roof top air exhaust units were fitted with insect screens. Design Office HVAC work included a new pressure relief system and a balance damper for one of the diffusers. Target hall work included relocation of the target zone depression sensor to the middle leg of the extraction system to obtain a more equal depression between east and west targets, and consultation regarding the crane hook rotation system. Sprinkler heads were relocated in the south hot cell service area to accommodate the new manipulator removal system.

Electrical Services

Power distribution centre MCC-X was finally replaced during the winter shutdown.

A new power factor correction capacitor bank was added to MCC-T. The power factor in the unit jumped from 82% to about 98% under the present load. Engineering efforts focused on experimental facilities services (TITAN and GP2). The HV electrical interlocks for the CSB and TITAN were reviewed and are ready to be installed.

Upon review of the load requirements in light of the planned beam line and experimental additions to ISAC-I and the loading of the power distribution centre MCC-T, it was concluded that the most economical approach would be to relocate the RFQ amplifier feeder to MCC-U. After the capacitor bank was

brought into service, MCC-T was running at 65% demand capacity (650 kVA), leaving only 350 kVA for future load growth. The planned installation of TITAN (about 150 kVA demand) and CSB (about 350 kVA demand) exceeds the remaining capacity.

About 20 installation orders were processed for ISAC-I. Among them were services to GP2 and the TITAN test stand. Services and lighting were re-arranged in the south target hall support area to make room for the new hot cell manipulators.

Conduit runs were completed for the electrical room radiation safety lock-up system and the future link of the ISAC-I safety system to the control room which will be relocated in ISAC-II.

ISAC PLANNING

This year the Planning group was involved in planning, scheduling, coordinating and expediting several sub-projects for ISAC-I (ECR source and upgrades to 8π and β -NMR); ISAC-II (medium-beta cavities, wire position monitor, cryogenics system, high-beta cavities, charge state booster (CSB), HEBT transfer, H-HEBT); ISAC experimental facilities (TIGRESS, TITAN); two step target, and actinide target test.

The Planning group was also extensively involved in preparing manpower and cash flow estimates for various ISAC projects included in the Five-Year Plan (2005–2010).

Technical details and progress on PERTed activities are described elsewhere in this report under the respective principal group. However, following is a summary of the main projects along with the major milestones achieved.

Various plans and PERTs were prepared and updated regularly with manpower estimates and analysis to identify critical areas and resolve any problems. ISAC priorities were evaluated and higher priority was assigned where necessary to optimize the scientific output.

ISAC-I

ECR source

ECR design improvements were made after tests with stable beam from the ECR-1 installed on TM 3 in late 2002. Two exit modules were damaged due to high current and absence of proper skimmers. Then skimmers with current limits and cooled collimators were installed, insulators were changed, and the aperture was reduced from 5 mm to 3 mm. Tests were done first on the test stand, followed by tests with stable beam and then with RIB in April, but still the efficiency and amount of RIB delivered was less than expected. After analyzing the test results, the design was modified and ECR-2 was fabricated and tested extensively on the

test stand. The plan is to install and test the ECR-1 with modifications (mainly central piece with boron nitrate), first without the target and then with a target, in February and April, 2004 respectively, for further investigations and to optimize ECR performance.

Experimental facilities

Several modifications and upgrades were made to 8π and β -NMR during 2003.

ISAC-II

Medium-beta cavities

The major milestones achieved included: cavities #1–9 were fabricated, inspected, chemically treated and received at TRIUMF. Cavities #10–20 were fabricated and received at TRIUMF and are expected to be chemically treated by May, 2004. Tuners, coupling loops and amplifiers for the first two cryomodules have been received, with the remaining components expected to arrive early in 2004. The first cryomodule tank was received in July; all the internal components were fabricated and assembled in the tank by early December. A cold alignment was achieved with the wire position monitor before year-end. Cold tests and rf tests on cryomodule 1 were delayed due to manpower problems and technical challenges and are now planned for completion by April, 2004. The tanks for cryomodules 2–5 could not be ordered due to lack of funds and will therefore be ordered and received in 2004, with the last one to be at TRIUMF by October, 2004. Cold tests and rf tests on cryomodules 2 and 3 will require extensive expediting of components and appropriate manpower allocations to meet the scheduled completion dates of July and October, 2004 respectively. The plan is to install the last cryomodule, #5, and be ready for tests by fall, 2005.

Cryogenics system

It took much longer to prepare the specifications for the cryogenic system including the distribution system. After receiving the bids in October, it was decided that the distribution system would be designed, procured and installed by TRIUMF with help from outside contractors, to meet budget constraints. A detailed Work Breakdown Structure (WBS) and PERT was developed for this project. The contract for the cold box, compressor/ORS and He ambient vapourizer was awarded in November to Linde. These components will be arriving at TRIUMF in July and September, 2004. The buffer tank will be ready to be ordered by March, 2004 and ready to install on its pad by September, 2004. The plan is to complete the process and instrumentation drawings (PID) in January, 2004, with an aim to do a design review in February and specify all components, explore potential vendors and award

contracts by May, 2004. Installation of the refrigeration and distribution systems should be done in early 2005 and the overall system commissioning by May, 2005.

High-beta cavities

Preliminary physics specifications for the high-beta systems were done with an aim to complete the conceptual design by July, 2004 and order Nb for all high beta cavities in April, 2004.

Charge state booster (CSB)

The CSB system, matching sections and analyzing magnet were installed. ECR mode and breeding mode were commissioned by the end of November. Tests with the rf cooler will take place in summer, 2004, and optimization will continue until the end of the year, when the CSB will be ready to move to its final location.

HEBT transfer

The 4 dipoles were designed and ordered in November and are expected to be received in July, 2004. All 20 quads were received and field mapped by July. Eight steering magnets were assembled and field mapped by December, and will be ready to install by March, 2004. The rebuncher was received at TRIUMF in March, and assembly of the components on to the rebuncher continued with an aim to be ready to install in the DSC line by July, 2004. The rebuncher was fabricated and assembled with an aim to do signal and power level tests in May, 2004.

H-HEBT

Due to manpower constraints, physics specifications and design of the H-HEBT were delayed and are planned to start in March, 2004.

Experimental Facilities

Detailed plans were developed for two major experimental facilities – TITAN and TIGRESS. Work breakdown structures (WBS) and detailed plans and schedules were developed for both projects along with some manpower analysis and planning. Following are some major highlights of these projects.

TITAN

The overall planning and scheduling of TITAN included the following major components:

RFQ cooler High voltage platform, RFQ, beam line support, RFQ cooler tests and related controls, and power supplies. High voltage platform design was reviewed in May, and fabricated in November with a plan to install by March, 2004. Fabrication of RFQ components was delayed to December due to the heavy workload in the Machine Shop. The plan is to assemble the components and test in proton hall extension in May,

2004, with an aim to test on the test stand by August, 2004.

EBIT EBIT modifications and ion optics that were designed at Heidelberg with a plan to finish fabrication and assembly by April, 2004. The TRAP was designed at TRIUMF in December to finish fabrication and assembly by April, 2004. A prototype electron gun was tested. EBIT superconducting magnet was ordered in June, with an expected delivery at MPI in May, 2004. The plan is to assemble the EBIT system by July, 2004 and test by the end of 2004 in Germany. A prototype Wien filter was received at McGill and the plan is to test by June, 2004.

Penning trap No progress as the postdoc who will do the simulations required to specify trap parameters will be joining the TITAN group in March, 2004.

Platform and services Initial concept for platform started towards the end of 2003 with an aim to design by May, 2004, fabrication by August, 2004, and installation in January, 2005 shutdown.

TIGRESS

The overall planning and scheduling of the TIGRESS project included the following major components with their main milestones:

Prototype substructure The plan is to make it initially for one detector and later for 4 or more detectors after tests. The stand and substructure was designed and reviewed by the end of the year with a plan to fabricate and assemble by April, 2004. The Ge detector was sent to the manufacturer for repairs. The electronic and readout system was designed with some help from collaborators, with a plan to test the prototype substructure by June, 2004.

4 detectors system The specifications were reviewed and negotiations for procuring 4 Ge detectors and BGeO's started to meet cashflow constraints.

Other components The conceptual specifications for target chamber, beam dump, beam line components with diagnostics, controls and services started with an aim to finish the overall assembly and prepare for beam by October, 2005.

CONTRACT ADMINISTRATION

In the past year three contracts were awarded: Linde Kryotechnik A.G. of Switzerland will supply one refrigeration system for the first phase of the ISAC-II linac. Sunrise Engineering Ltd. of Delta, B.C. manufactured 4 steel sub-assemblies and assembled all four HEBT S-bend dipole magnets for ISAC-II, with Alpha Magnetics Inc. of California supplying the eight excitation coils. Amplifier Systems Inc. of California will

supply twenty rf amplifiers for the ISAC-II medium beta superconducting cavities.

Personnel Resources

ISAC-I

In 2003 the average monthly personnel effort for ISAC-I decreased by approximately 7.5 people per month to an average of 43.28 FTE people per month (see Fig. 270). In 2002 the FTE effort per month was 50.76 people.

The total work effort expended on ISAC-I from the start of the project on January 1, 1996 to December 31, 2003 has been 516.81 years, based on a FTE work-month of 150 hours per person.

Figure 271 shows the FTE persons per month for the various sections of ISAC-I in 2003.

ISAC-II

The recording of work effort for ISAC-II started October 1, 2000 (see Fig. 272). The work effort was recorded as “Project Management and Administration” up until March 31, 2002. Commencing April 1, 2002 the work effort was monitored by section. In 2003 the average monthly personnel effort for ISAC-II increased by approximately 6.5 people per month to an average of 19.5 FTE people per month (see Fig. 272). In 2002 the FTE effort per month was 13 people.

Figure 273 shows the FTE persons per month for the various sections of ISAC-II in 2003.

The total work effort expended on ISAC-II from the start of the project on October 1, 2000 to December 31, 2003 has been 35.79 years, based on a FTE work-month of 150 hours per person.

Figure 274 shows the FTE years of work effort for each section of ISAC-II since the project began.

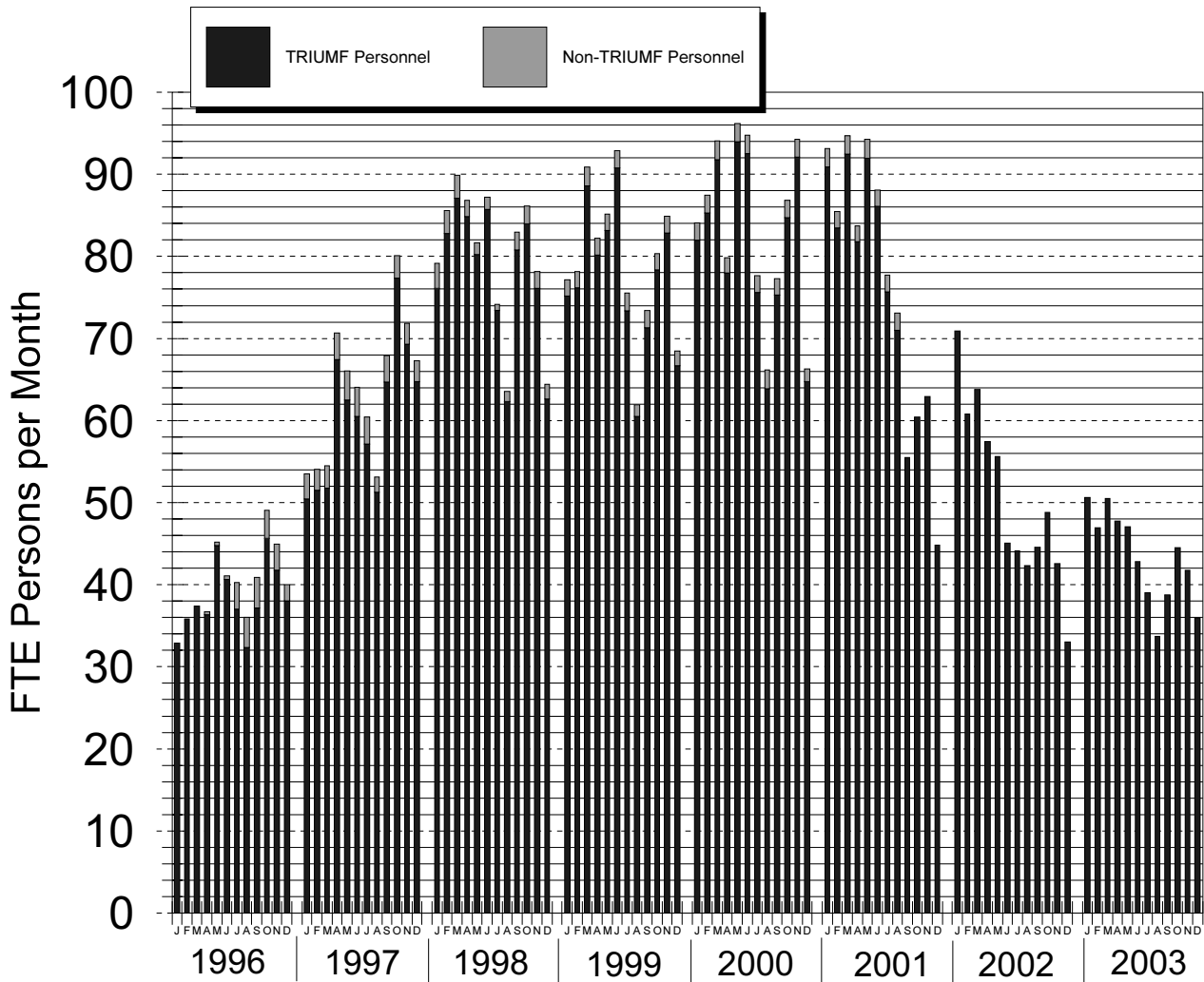


Fig. 270. ISAC-I monthly personnel effort, January 1, 1996 to December 31, 2003.

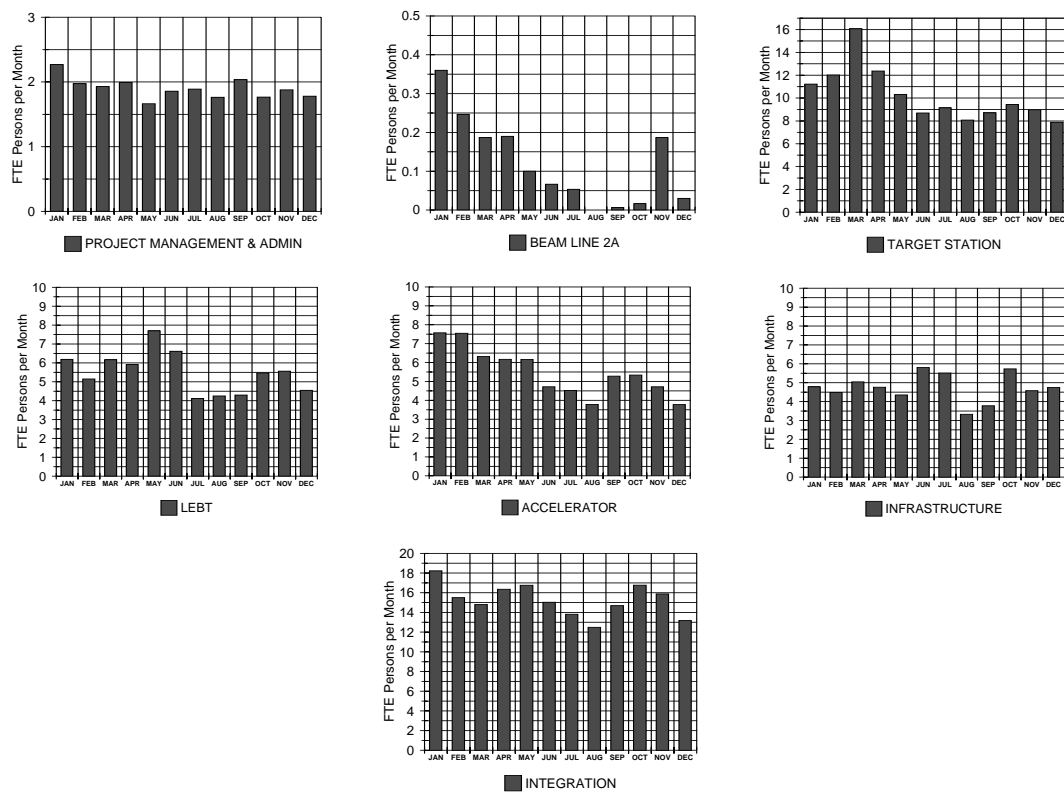


Fig. 271. ISAC-I monthly personnel effort, shown by section for 2003.

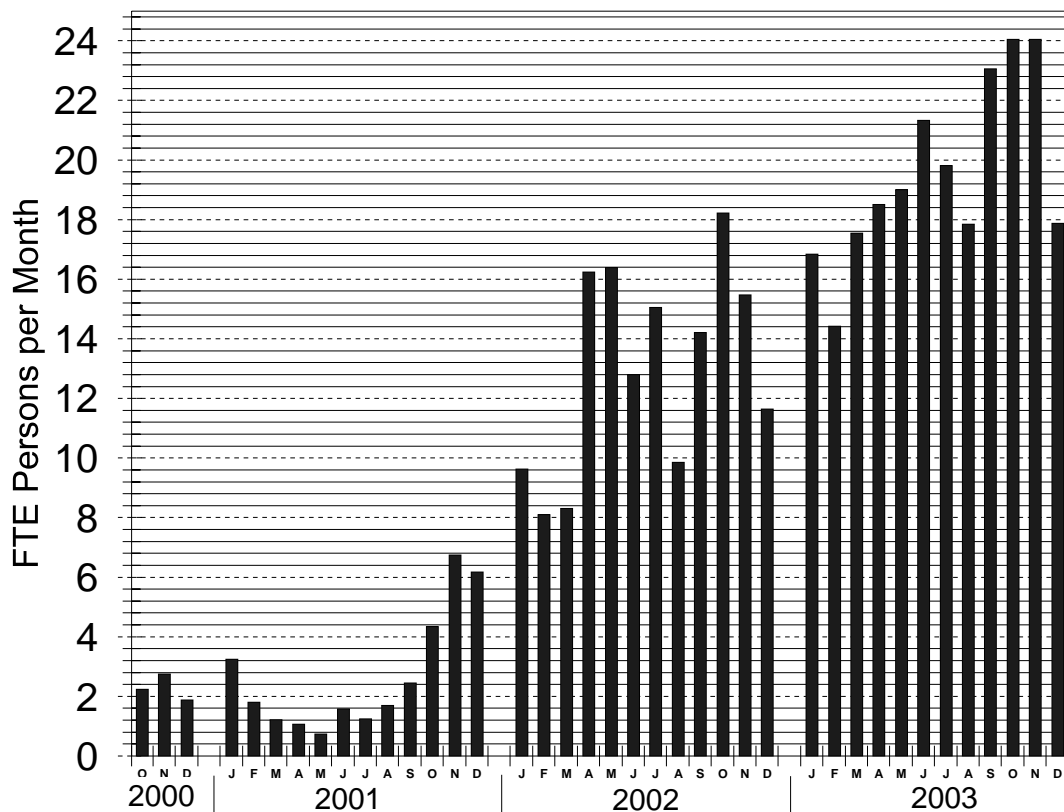


Fig. 272. ISAC-II monthly personnel effort, October 1, 2000 to December 31, 2003.

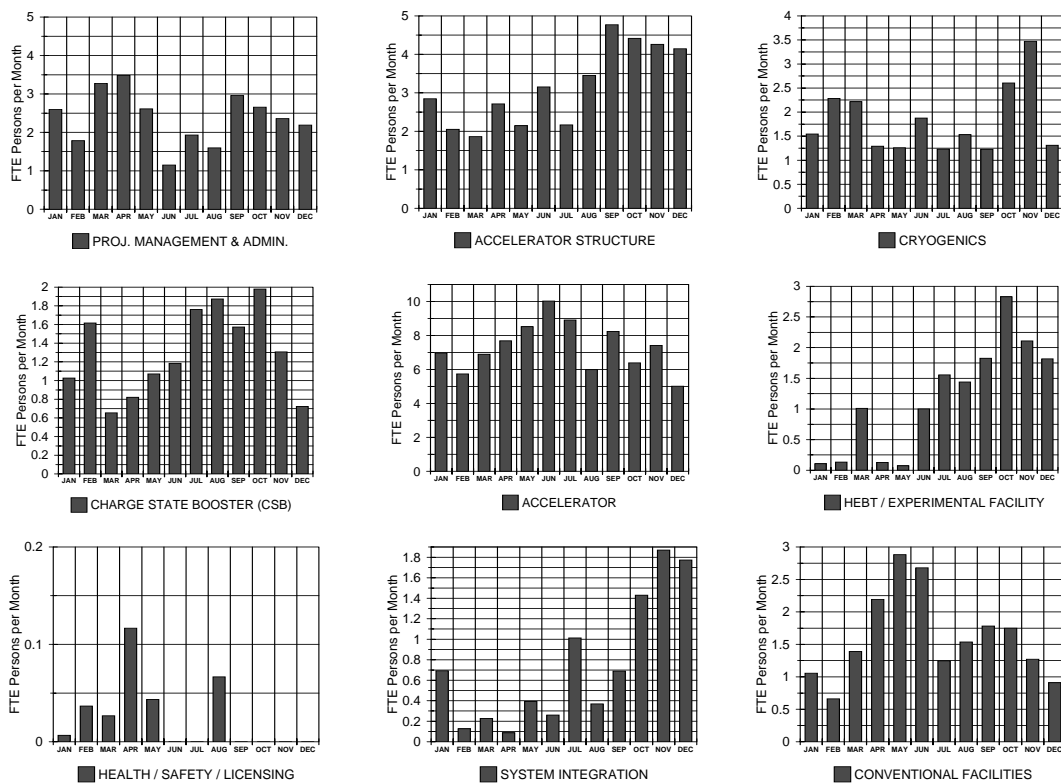


Fig. 273. ISAC-II monthly personnel effort, shown by section for 2003.

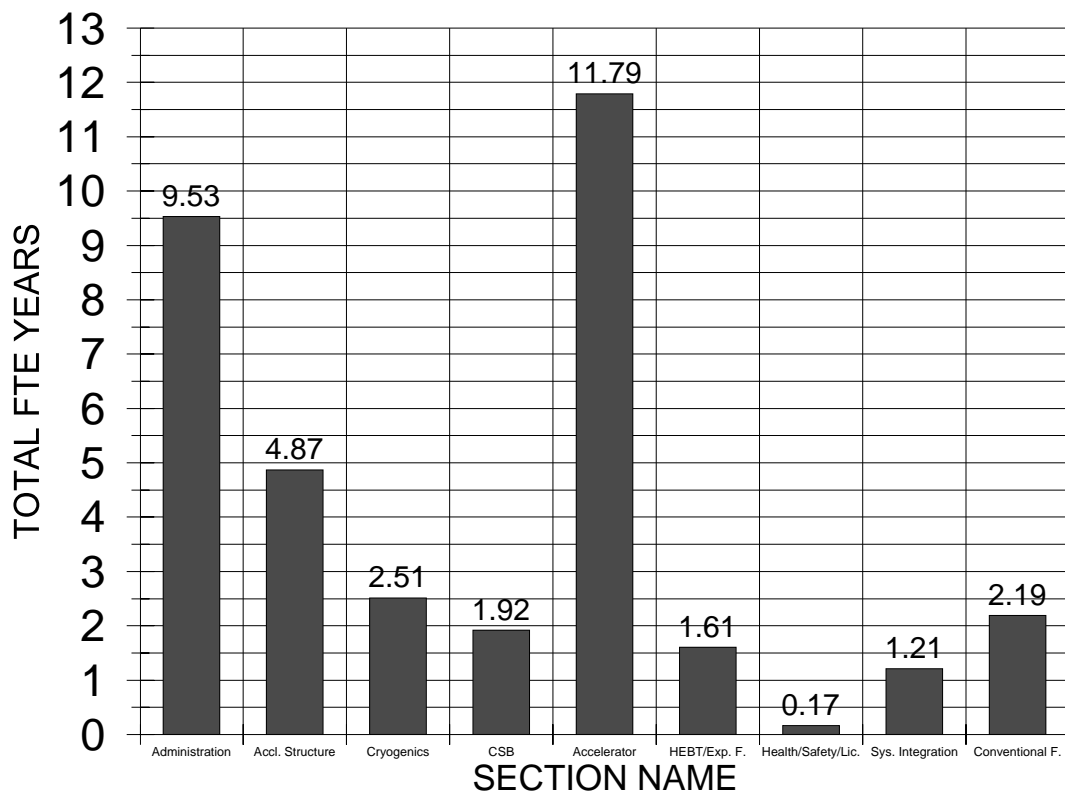


Fig. 274. ISAC-II total personnel effort, October 1, 2000 to December 31, 2003 shown by section.

ISAC-II CONVENTIONAL FACILITIES AND INFRASTRUCTURE

The highlight of the year was the delivery, under the direction of UMA Management Services Ltd., of the ISAC-II buildings (March, 2003) that culminated with the official opening on June 11, 2003 by the Hon. Gordon Campbell, Premier of British Columbia.

Upon completion of data and voice services by TRIUMF staff in April, a large number of technical and experimental staff relocated and took residence in ISAC-II. Formal building occupancy was granted on June 4, 2003 upon satisfactory submission of the Fire Safety plan also prepared by staff.

Architecturally, ISAC-II marks a departure from the traditional box structure of older TRIUMF buildings. The new facility's landscaping and pleasant modern features make it a vibrant place to work in (see Fig. 275). The buildings were completed on a tight budget and even tighter schedule. ISAC-II features a long Z-shaped, thick-walled vault, interconnected to ISAC-I, to house the future accelerator structures and connecting beam lines, an experimental hall surrounded by support shops and assembly areas, and locales for auxiliary systems and services. It also provides offices for approximately 95 technical support and experimental staff, a working clean room for the SCRF cavity research program first and for their maintenance later, and other laboratory spaces in support of the rf development program and experimental activities.

With the continuing support of UMA and PBK/Cochrane Engineering, the greatest single effort was the commissioning of the building systems and to address and rectify a number of construction deficiencies. The implementation of the DDC building controls required more effort than initially anticipated due to early device failures and program debugging. Work continues to optimize ambient temperature in various locales.

Parallel activities included:

- The installation of services (power, racks gas and vacuum vent lines, rinse water installation, and clean room air balancing) and commissioning of infrastructures to meet the stringent requirements of the SCRF clean room. The rented lab at BC Research was dismantled.
- Services for laboratory space in support of the accelerator and experimental program.
- The completion of infrastructures for the data network, video conferencing and on-line meeting room booking ("the wizard").
- A start to the rf test stand area in the experimental hall.
- Design and delivery of electrical and mechanical services from the CSB test area.



Fig. 275. A view of the ISAC-II building taken from the west side of the parking lot.

Other engineering work included participation in the preparation of the helium refrigeration work package, rf coupling loop thermal calculations, and revision of the oxygen detection system. The original design intent (nitrogen hazard detection) of the O₂ detection system was expanded to also cover the helium hazard. We plan to install the revised design in 2004. The S-bend services and logistics support went through design review and, once approved, working drawings were prepared.

Three new power factor correction capacitor banks (for a total of 1,125 kvar) were brought into service in April. Their function is to limit the kVA power demand increase by reducing the reactive power supplied by B.C. Hydro. As the kVA demand is paid in hard currency, the benefit of this installation will be even more noticeable when the B.C. Hydro rate increase (+7.23%) goes into effect in April, 2004.

ISAC-II S-BEND HEBT

The ISAC-II superconducting accelerator complex comprises a low beta, a medium beta and a high beta section. The energy range is between 400 A keV to 6.5 A MeV for mass $A = 150$. Due to budget and manpower constraints the construction will be done in three phases. The first phase will take the beam from the ISAC-I accelerator complex which has an output energy of 1.5 A MeV for $A = 30$. The beam will then be injected into the medium beta section. The beam will be accelerated to 4.3 A MeV and delivered to the ISAC-II experimental hall for experiments starting in December, 2005.

The second phase consists of the addition of the high beta section with an output energy of 6.5 A MeV. A third phase is necessary which will take $A/q < 30$ beam from the RFQ at 150 A keV. A room temperature or superconducting linac will accelerate the beam to 400 A keV and then a stripper foil will boost the charge state to $A/q < 7$. The beam will then be injected into the medium beta section to be accelerated to the final energy.

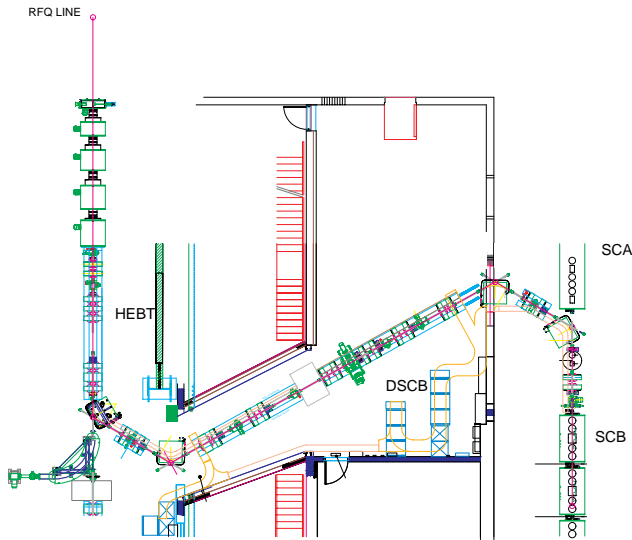


Fig. 276. Layout of the transfer beam line from the ISAC-I IH-structure linac to the ISAC-II superconducting linac.

Figure 276 shows the layout of the new transfer beam line.

We received all the necessary quadrupoles and the four dipole specifications were submitted for bid and the contract was awarded to Sunrise Engineering for the steel manufacturing and to Alpha-Magnetic for the coil fabrication. The coils will be completed in April, 2004 and the first magnet will arrive at TRIUMF in June, 2004.

ISAC-II ACCELERATOR DEVELOPMENT

Due to experimental pressure and budget limitations the installation of the linac has been grouped into three stages highlighted in Fig. 277. The initial Stage 0 to be completed in 2005 includes the installation of a transfer line from the ISAC DTL ($E = 1.5 \text{ MeV/u}$) and the medium beta section to produce 18 MV of accelerating voltage for initial experiments. Stage 1, to be completed two years later, includes the installation of the three high beta modules for a further 18 MV. The ISAC-II accelerator final Stage 2 is foreseen for 2010. A new building complete with linac vault, experimental areas, office and laboratory is now complete. Present

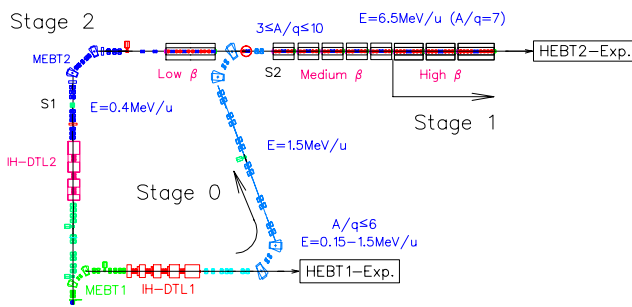


Fig. 277. Stages 0, 1 and 2 for the ISAC-II upgrade.

studies are concentrating on design and development for the first stage installation.

Hardware and Development

Work is ongoing on several fronts with the goal of realizing beam delivery in 2005. The first major milestone is the cold test of a completed medium beta cryomodule in spring, 2004. An SCRF lab, set up in a neighbouring facility, was used for development where cold tests were completed at the rate of one per month. The lab was closed in September and moved to the new ISAC-II SCRF lab. The new lab is an expanded space with clean assembly and rinse areas, a large high bay rf test pit area, a measurement console area and a preparation area. The lab was ready for cold tests to resume by year end. A summary of the year's developments is given below.

RF Systems Ancillaries

In previous linac installations the tuning of quarter wave cavities has been accomplished with mechanical or pneumatic tuners characterized by slow response, poor resolution and/or large backlash. Detuning by microphonic noise or rapid fluctuations in helium delivery pressure is accommodated by either overcoupling to reduce the loaded Q or with a variable reactive load using a PIN diode network at the cavity. A slow tuner response affects the required Q -loading and may limit the accelerating gradient due to constraints on the stored energy.

The ISAC-II medium beta cavities have a design gradient of 6 MV/m . This corresponds to a peak surface field of $\sim 30 \text{ MV/m}$ and a stored energy of $U = 3.2 \text{ J}$ and is a significant increase over other operating heavy ion facilities. To achieve stable phase and amplitude control, the natural bandwidth of $\pm 0.1 \text{ Hz}$ is broadened by overcoupling to accommodate detuning by microphonic noise and helium pressure fluctuation (1 Hz/torr). A rough rule is to use a loaded bandwidth of six times the microphonic noise plus twice the resolution of the mechanical tuner. The ISAC-II medium beta cavities are outfitted with a passive mechanical damper and the microphonics are not expected to be more than a few Hz RMS. The chosen tuning bandwidth of $\pm 20 \text{ Hz}$ demands a cw forward power of 200 W and peak power capability of 400 W to be delivered to the coupling loop at the cavity.

Two complementary developments are ongoing at TRIUMF to achieve the design goal. In the first a new rf coupling loop is being developed with the goal to operate at 200 W forward power with less than 1 W of power being added to the helium load. Secondly TRIUMF is developing a mechanical tuner capable of both coarse (kHz) and fine (Hz) frequency adjustments of

the cavity. The goal for the ISAC-II cavity tuner is to achieve fine (1 Hz) tuning capability with a response time to control fast helium pressure fluctuations allowing stable operation within a bandwidth of $\Delta f = \pm 20$ Hz.

Cavities

A prototype of the $\beta_o = 7.1\%$ cavity, designed in a collaboration with INFN-LNL, was routinely used for early SCRF development tests. The niobium sub-assemblies of the twenty cavities of the medium beta section, composed of eight $\beta_o = 5.7\%$ and twelve $\beta_o = 7.1\%$ cavities, are now delivered from industry. An initial delivery of four cavities was chemically polished at CERN and cold tested at TRIUMF. Three of these cavities meet specification but the fourth suffers from a poor Q . This fourth resonator does have a small dark spot on the rf surface at the root end that developed after chemical polishing. The plan is to recover this cavity with a combination of local hand polishing and further chemical treatment. To keep the schedule, the fourth cavity in the first cryomodule will be taken by the prototype cavity. A summary of cold tests for the cavities of the first cryomodule, consisting of three production cavities and the prototype is shown in Fig. 278. All cavities meet the ISAC-II gradient specifications (6 MV/m in 7 W) but the field emission at higher gradients evident in several of the cavities should be reduced through high pressure rinsing and rf conditioning. The remainder of the medium beta cavities will be chemically polished at Jefferson Lab prior to testing at TRIUMF.

RF Controls

The rf control system for the superconducting cavities is a hybrid analogue/digital system. Each system consists of a self-excited feedback loop with phase-locked loops for phase and frequency stabilization. Amplitude and phase regulations, as well as tuning control,

are performed using digital signal processors. Special pulsing circuitry is incorporated into the system to facilitate “punching” through multipactoring. We have demonstrated fixed amplitude and phase regulation at the design gradient with the phase error used to drive the mechanical tuner to maintain cavity frequency.

Mechanical Tuner

Tuning plate The tuning plate (see Fig. 279) consists of 1 mm thick RRR niobium sheet of 240 mm diameter fixed to the bottom niobium flange by bolts and retaining flange. A flat plate can be used but the deflection force required is parabolic with distance and tends to assume a concave shape upon cooling leading to highly non-linear behaviour. To overcome these problems the ISAC-II tuning plate is spun with a single “oil-can” convolution and milled with eight radial 1 mm slots. The plate is capable of allowing ± 20 kHz (± 3 mm) of tuning range before yielding. Further, if required, the plate can be plastically deformed while cold by the mechanical tuner, removing the necessity of complicated tuning procedures on the finished cavity. Cold tests with the plate give Q and gradient values consistent with the flat plate performance (see Fig. 280).

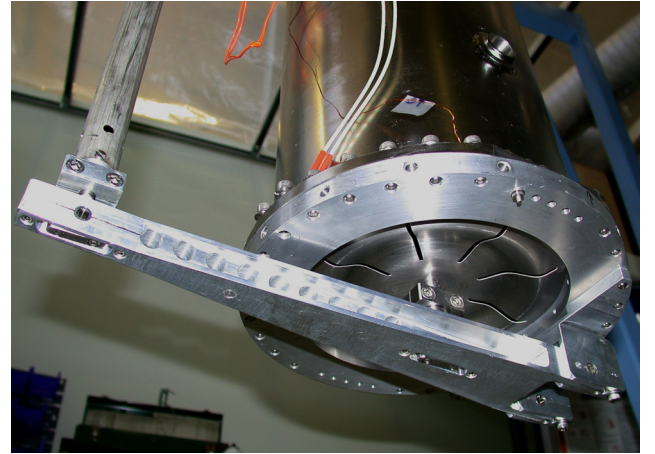


Fig. 279. The tuner plate, lever arm, bottom of push-rod and cavity viewed from below.

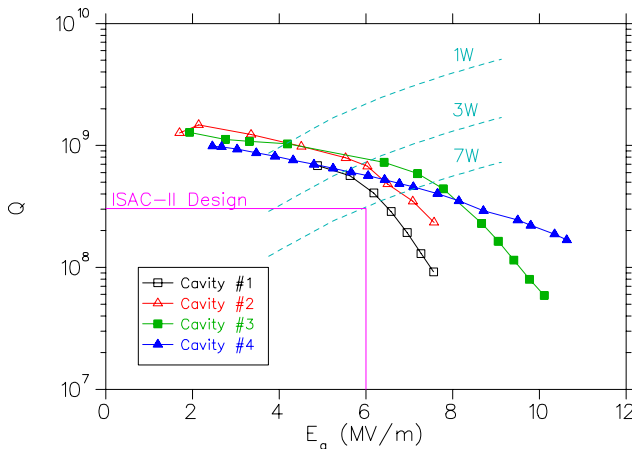


Fig. 278. Cold test results for the cavities of the first medium beta cryomodule.

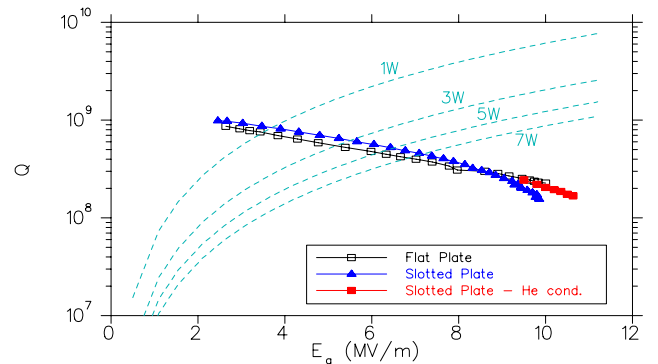


Fig. 280. RF cold test results comparing cavity performance with a flat tuner plate and the new slotted plate.

Mechanical tuner The tuning plate is actuated by a vertically mounted permanent magnet linear servo motor, at the top of the cryostat, using a “zero backlash” lever and push rod configuration through a bellows feed-through. The system resolution at the tuner plate centre is $\sim 0.055 \mu\text{m}$ (0.3 Hz). The demonstrated dynamic and coarse range of the tuner are ± 4 kHz and 33 kHz respectively. The tuner on-line performance is measured by altering the cavity frequency by forced variations of the helium pressure. Figure 281 gives the pressure change, the associated position drive signal for the tuner and the voltage and phase error at the design gradient. The tuner responds accurately to the pressure variation with a resolution better than $0.1 \mu\text{m}$ (0.6 Hz). The demonstrated response bandwidth is presently limited to 20 Hz by a mechanical resonance.

Coupling Loop

Original cold tests with a prototype quarter wave cavity were done with an adjustable coupling loop copied from an INFN-Legnaro design that we identify as Mark I. The loop consists of a brass outer housing, a copper plated stainless steel outer conductor and copper inner conductor. The outer conductor is driven in/out through a rotating mechanical shaft attached to a stepper motor on the cryostat lid via a rack and pinion mechanism on the loop housing. The original in-vacuum rf drive line consisted of a 1 m length of flexible coaxial cable with a 30 cm rigid section of

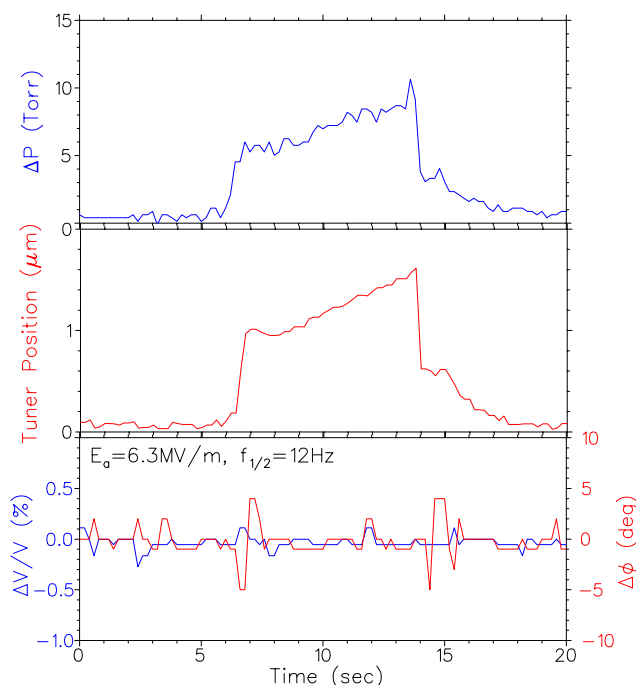


Fig. 281. Tuner response to forced helium pressure fluctuation ($\frac{\Delta f}{\Delta P} = 1$ Hz/torr) and corresponding voltage (blue) and phase (red) errors for high field ($E_a = 6.3$ MV/m) and a bandwidth of ± 12 Hz.

copper coated stainless steel for thermal isolation. The loop was designed to operate at gradients of 3–4 MV/m with a forward power of about 50 W. Early cold tests at higher power showed significant heating of both the drive system and the loop assembly with several W of power being deposited in the helium. Cold tests are done by first measuring the static heat loss based on the helium boil-off rate after full thermalization. The cavity is then powered until thermal equilibrium is reached and the new static heat load is measured. The temperature of the loop is monitored by several sensors during power on and power off cycles.

The loop prototypes maintain the Legnaro dimensions and loop adjustment system but the loop materials are altered and LN_2 cooling is added. In Mark II the housing is changed to thin walled stainless steel for better thermal isolation and the outer conductor is copper. A copper heat exchange block is fastened to the outer conductor. Copper braid thermally links both the block and current maximum points on the cable to an LN_2 cooled copper pipe (Fig. 282). The stainless steel rigid line section is removed and replaced by one continuous flexible cable.

With an initial forward power at the loop of 140 W in fixed gradient mode the temperature of the inner conductor becomes sufficiently high to change the coupling and the forward power grows to 200 W during thermalization. The loop heating causes 4.5 W extra static boil-off. A reduction in heating to 2.5 W is obtained by adding heat shields tied to the LN_2 pipe around the rf cable.

The Mark III loop is identical to Mark II but two 1 cm long pieces of aluminum nitride (AlN) dielectric are added to thermally connect the inner and outer conductor of the loop near the heat exchange block to reduce inner conductor heating. In this case the loop heating adds only 1.5 W to the static heat load and



Fig. 282. The Mark II loop prior to cold test.

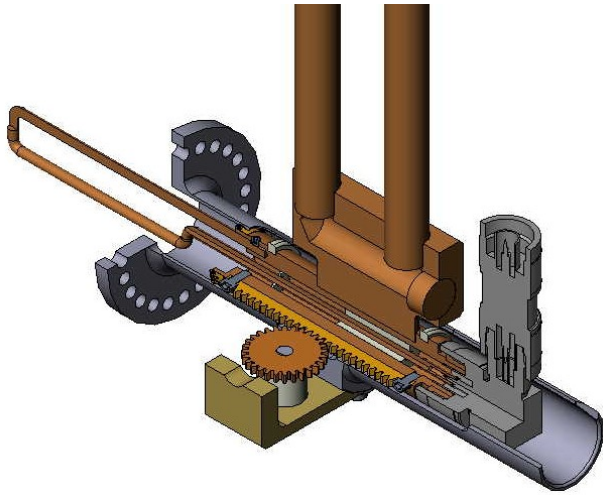


Fig. 283. A cut-away rendering of the Mark IV coupling loop.

the coupling and forward power remain constant at 200 W throughout the test. In addition the improvement in the thermal path reduces the thermalization time from 6 hours to 2 hours.

In the Mark IV prototype (Fig. 283) the outer conductor and heat exchange block form a solid piece. A cooling channel running through the block allows direct cooling with LN_2 .

Solenoids

Focusing in the SC linac is provided by 9 T 26 mm diameter bore SC solenoids of lengths 16, 34 and 45 cm corresponding to the low, medium and high beta cryomodules respectively. The solenoids are equipped with bucking coils to actively limit the fringe field in adjacent cavities to less than 0.1 T to prevent reduction in cavity performance. The magnets are mounted in a liquid helium vessel fed from the common helium header. An order for five medium beta and two high beta solenoids placed in industry has been delayed as the company has gone into receivership. The prototype magnet was obtained from the company and was completed and tested at TRIUMF. The magnet reached the design field of 9 T without a quench (Fig. 284). A contract for the remaining seven magnets has been let to Accel in Germany.

Alignment

The cavities must be aligned to within 0.4 mm and the solenoid to 0.2 mm. TRIUMF is developing a stretched wire alignment system based on the TESLA design. Wire position monitors (WPM), each consisting of four striplines, are attached to the cavities and solenoid by off-centre alignment jigs. A wire running parallel to the beam axis and through the monitors carries an rf signal at 215 MHz. A Bergoz BPM card converts the rf signals from one monitor into dc X

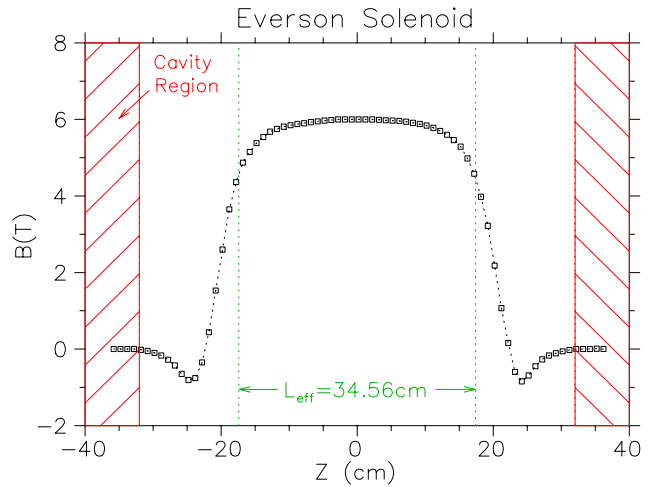


Fig. 284. Mapped axial field for the first superconducting solenoid.

and Y signals while a multiplexer with GaAs switches scans through the monitors. A National Instruments ADC and I/O card controls the multiplexer and reads the dc signals. The striplines are fabricated and have been calibrated on a test bench.

Progress in ISAC-II Cryogenics

Refrigerator

The refrigerator system will be installed in two equal stages. The first stage includes a 500 W helium refrigerator with associated compressors, oil removal system (ORS), helium buffer tank, helium dewar, room temperature piping, helium distribution transfer lines, and nitrogen distribution network. The phase I cryogenic system supplies 4.5 K helium to five medium beta cryomodules and to two high beta cryomodules. Progress on definition of the cryogenic system continued in 2003. The main goal was to secure a contract for the phase I system. Initially TRIUMF was seeking a turnkey facility with a single source. Two vendors bid on the job but the cost of both were beyond the project budget. In meetings with each vendor the scope of the contract was reduced to the supply of the refrigerator main components with TRIUMF taking responsibility for the installation, the helium buffer tank, the helium dewar, the warm piping and the cold distribution. In November Linde was chosen as the supplier of this reduced contract. Delivery and installation is expected in the latter part of 2004.

The refrigerator-liquefier on order is the Linde TCF50 with liquefaction rate of about 5.2 g/s and refrigeration rate of 530 W at 4.5 K with simultaneous liquefaction rate of 0.71 g/s. The vendor supplied system consists of a cold box/liquefier, a main and recovery compressor, as well as oil removal and gas management system. The main compressor is a Kaeser ESD441SFC direct drive screw compressor of 268 KW

producing a compressed helium flow of 79 g/s at 14 bara pressure to be delivered to the cold box/liquefier in the cryogenic room via the warm piping. The main compressor has a variable frequency drive option allowing part load performance during normal operating modes depending on the active load from the accelerator. The second compressor is a recovery compressor allowing the helium gas inventory to be recovered and compressed into the storage tanks. It is a Kaeser BSD62 screw compressor of 37.5 KW producing a compressed helium flow of 12 g/s at 14 bara pressure. The Linde refrigerator local control is designed to self adjust to flow returning from the distribution system. The variable frequency compressor allows the refrigeration power to vary. The refrigeration output will not be continuously variable since each level requires a control initialization. Linde promises to set up three such operating levels with refrigeration power suitable for a) rf off, b) rf on/maximum, peak liquefaction, and c) rf on/intermediate.

Distribution system

The design of the TRIUMF cryogenic system was solidified in 2003. Briefly, the refrigerator cold box delivers LHe to a main supply dewar located in the cryogenics (refrigerator room). The main supply dewar supplies LHe to the main distribution trunk line with a moderate push pressure. The ISAC-II cryomodules (CMs) are fed in parallel from the main distribution line with U-tube transfer lines. Each cryomodule has two associated female bayonet cans, one for the delivery bayonet and one for the cold return bayonet. There is also a main warm return line that takes warmer gas (>20 K) from the CM back to the suction side of the main compressor during cooldown. There is also gas from the solenoid power leads and for cooling of the stack that is valved into the warm return line through throttle valves. Internal to the cryomodules is a manifold system and valve that can force cold helium vapour to the bottom of each cold element during initial cooldown. Control of the helium levels in each cryomodule is monitored by a level probe in each helium reservoir and adjusted by the proportional liquid delivery valve into each cryomodule. The level in the helium main dewar is controlled during normal operation with the heater in the dewar. Each cryomodule reservoir has an immersion heater that can also be used for level control. It may be useful perhaps to use the cryomodule heaters to compensate for variations in rf power in that cryomodule.

The cryomodules contain a LN₂ cooled thermal shield consisting of a 1/2 in. copper tube soldered to a copper box. Liquid nitrogen is supplied to the cryomodules via a parallel distribution scheme from a local nitrogen dewar/phase separator. The dewar is fed

LN₂ from an external 9000 USG nitrogen tank via existing nitrogen vacuum isolated piping. A separate LN₂ circuit is used to cool the vacuum jacketed cold distribution system.

During normal operation the linac will be cold and the rf will be on to accelerate the beam. The total expected cryogenic load for phase I is 390 W. This can be broken down into 192 W of static losses and 198 W of active rf loss. The static loss budget is split half and half with 96 W for the cold distribution system and 96 W for the cryomodules. This assumes static losses of 13 W and 14 W for the medium and high beta CMs respectively. The liquefaction loss from the cryomodule power leads is expected to be 0.7 gm/s. There will be times where a cryomodule or cryomodules will have to be cooled down from room temperature. A flow of 6 liquid l/hr of 100% liquid nitrogen will cool down the medium-beta cryomodule LN₂ shield in ~ 24 hours. The bulk of the cold mass will cool by radiation to ~ 250 K. Cold tests indicate that a flow of 20 liquid l/hr of helium is a sufficient flow to pre-cool the cavity from 250 K to 4 K in about four hours. The medium beta cryomodules require 100 l/hr and the high beta modules 150 l/hr for efficient cooling. The CMs are cooled one at a time and each filled cryomodule is topped up periodically as the cold mass thermalizes.

ISAC BEAM DYNAMICS

Operating the DTL Above 1.5 MeV/u

The ISAC DTL is designed for a maximum energy of 1.53 MeV/u and for a maximum $A/q = 6$. The DTL essentially operates as a fixed velocity accelerator with voltage and phase detuning in the last operating tank to accelerate to a reduced energy. The full energy range from 0.153–1.53 MeV/u can be spanned by this method. Conversely it is possible to reach a higher final energy than specified by increasing the voltage in the last operating tank and optimizing the phase for maximum acceleration. Assuming that the maximum voltage in a tank occurs for $A/q = 6$ then these higher energies are only possible for $A/q < 6$ values. Since the higher voltage increases the particle velocity above the design value, phase slippage during the tank crossing occurs. Therefore as the relative voltage increases, the incident particles must be pushed to more and more positive phases to achieve maximum acceleration. Some additional energy can be achieved by increasing the relative voltage on the second to last tank to maximize the energy entering the last tank.

Simulation results from LANA are summarized in Fig. 285. The results show that the tanks are short enough that a significant increase in final energy can be achieved by maintaining a fixed voltage near the maximum for the tank and optimizing the phase. The

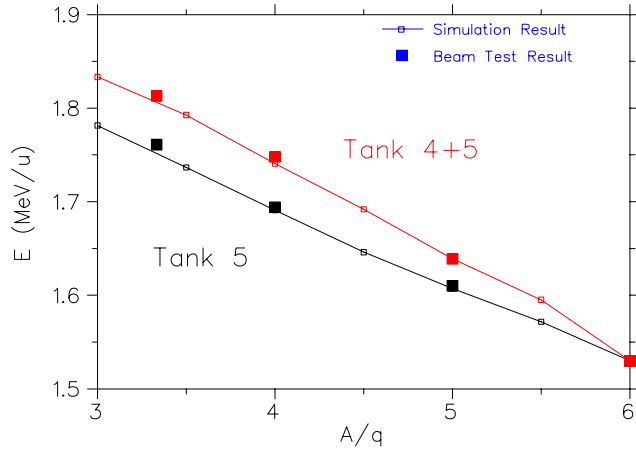


Fig. 285. Maximum energies of ISAC-DTL from simulations and experimental tunings.

gain cannot be duplicated by increasing the voltage in all tanks since the large phase slip caused by accelerating particles with a velocity higher than designed does degrade longitudinal beam quality. Beam test results from August are also reported that confirm the accuracy of the simulations.

ISAC-II HEBT

The beam line for the new ISAC-II experimental hall has been revisited during this year. We took advantage of several workshops with the ISAC-II users community to clarify some of the design goals and to obtain from the users the crucial specifications for the beam on target. This allowed us to propose a simpler and cost effective approach. We propose to use two Y dipoles and 22 quadrupoles that we acquired from Chalk River Laboratory. Figure 286 shows the

proposed layout of the new ISAC-II experimental hall.

From discussions with future users it became clear that the multi detector array will be the common type of detection system foreseen at ISAC-II. Some good examples of that are the TIGRESS (16 HPGe detector array), HERACLES, and LEDA. It was clear also that sensitive diagnostics are necessary to tune in a time effective manner the low RIB intensity onto the user's target. We have designed the beam line in order to have a unit transformation from, and intermediate focus to, the final focal point. This allows the installation of a diagnostics box that can be equipped with all the state of the art diagnostics.

The superconducting linac was designed to take advantage of the possibility of accelerating several charge states. The beam line that can accommodate this has to be not only achromatic but also isochronous. The direct beam line and the one going to the recoil spectrometer are designed to accommodate multi-charge state ion beams.

ISAC-II CRYOGENIC SYSTEM

Refrigeration System

A specification was written for the phase 1 refrigeration system as a complete turn-key system. This included everything up to the delivery and transfer of 'U' tubes at the cryomodules. TRIUMF was responsible for all services necessary to support the refrigeration system. The two major suppliers of cryogenic refrigeration systems, Linde and Air-Liquide, responded to the tender package with a quotation. Unfortunately both quotations were beyond what TRIUMF had budgeted. At that time TRIUMF decided to negotiate with

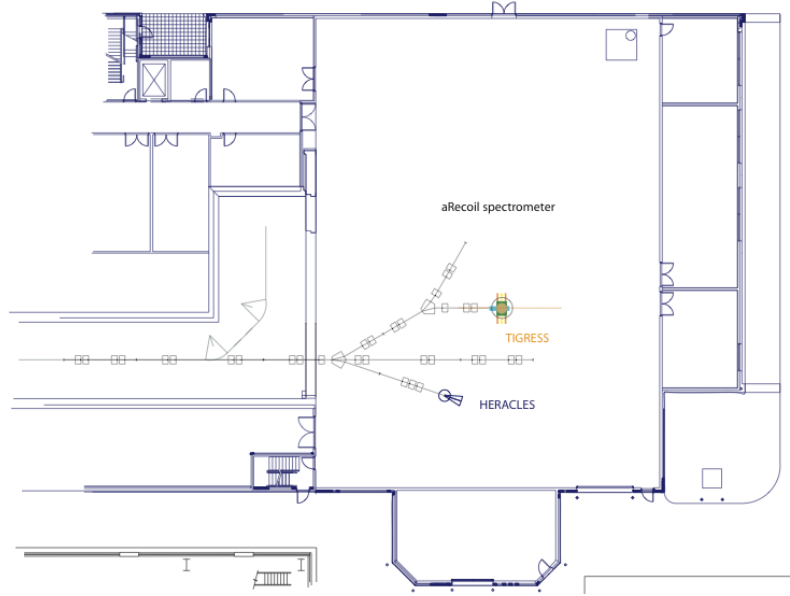


Fig. 286. Proposed layout of the new ISAC-II experimental hall beam lines.

both tenderers, asking for quotations for the supply of the refrigeration system components only, including process and instrumentation diagrams, installation instructions, etc. Quotations were received and a contract was awarded to Linde in November. TRIUMF will be the project manager for the refrigeration system which can be broken down into 3 categories:

1. Refrigeration system component installation including all services, warm piping and buffer storage tank.
2. Accelerator vault access platform and distribution system support structure.
3. Cryogenic distribution system (all vacuum jacketed, liquid nitrogen shielded piling from the liquifier cold box to the cryomodels, including the liquid helium dewar).

The third item is the most complex and specialized (other than the refrigerator itself), and a task force was formed to discuss how TRIUMF would approach the design, purchase and installation of such a system based on the simplest and most cost effective system but also one that has as high a transmission efficiency (low heat load on helium) as possible. To this end a conceptual design was produced, flow schematics were created and a package of information was put together along with a letter requesting interested parties to respond early in 2004. The intent is to have a complete phase 1 refrigeration system operational and commissioned by April, 2005.

Cryomodels

A complete description of the medium-beta cryomodel was presented in the 2002 Annual Report and will not be repeated here. The design was well under way by the beginning of this report period and drawing release began in March. The vacuum tank arrived in May, followed by the lid and the internal components

such as the helium reservoir, support beam, struts and solenoid mounting frame.

The μ -metal was ordered for all 5 medium-beta cryomodels, however, it was not flat and was outside of our required tolerance. This required return of the shipment which was reworked to specification. A μ -metal liner was then produced that was installed adjacent to the inside vacuum tank wall. At the same time work commenced on the liquid nitrogen thermal shield box. The box is constructed of 0.125 in. copper sheet with copper tubes soldered in an array on the inside surface of all sides by a special fluxless solder procedure prior to the box being riveted together. There is a separate lid mounted thermal shield piece that overlaps the edges of the box when finally installed.

An assembly frame was constructed to support the lid and allow the installation of all the internal components. The helium reservoir mounts to the stack flange of the lid and all other components are suspended from 3 adjustable mounting lugs on the lid. This allows for cryo element alignment adjustment relative to the vacuum tank. The assembly frame also mimics the vacuum tank beam ports and wire position monitor ports allowing cryo elements to be aligned with respect to each other as well as the theoretical beam line, and this alignment is also transferred to 3 target posts on the lid since the beam ports will not be visible once the cryomodels are installed in the accelerator vault.

Assembly has progressed to the point where the assembly frame and internal components had been through the cleaning cycle, moved into the class 3 clean room and reassembled on the frame allowing the commencement of alignment. The vacuum tank and thermal shield box had been moved to the class 2 clean room awaiting completion of the lid assembly. The goal is to complete a cryomodel cold alignment investigation in March, 2004.

ACCELERATOR TECHNOLOGY DIVISION

INTRODUCTION

The Accelerator Technology Division is responsible for most of the engineering and design at TRIUMF as well as support of the beam dynamics effort for international collaborations. Other responsibilities include planning for projects and shutdowns, electronics development and services, the Building department, the Design Office and Machine Shop. This year, as for the past number of years, much of the available effort went into supporting the ISAC program, in particular the ISAC-II cryomodule design and specification of the helium refrigeration system. In the Requests for Engineering Assistance (REA) that were submitted during the year, there were 37 ISAC related jobs and 30 non-ISAC in mechanical engineering and design.

The Canadian Nuclear Safety Commission requires TRIUMF to develop and adopt a quality assurance program for all activities at the laboratory. A task force, which included two members of the division, was set up to develop this program and for the most part the new plan is adopting many of the policies and procedures that already exist at TRIUMF. In some cases the documentation and formalization of the procedures will have to be improved and this will have some impact on the work of the division. Hopefully there will be an overall benefit emerging from adopting this quality management system.

In addition to the CERN work described elsewhere, the Beam Dynamics group provided support in calculating the 50 GeV ring impedance for J-PARC, played a key role in some new FFAG developments, and carried out studies on a lattice for a radioactive storage ring. A number of magnets were designed and two contracts for the fabrication of superconducting solenoids for the ISAC-II linac were supervised. The Kicker group, in addition to the LHC injection kickers, designed and built a muon kicker for an experiment at PSI and started a program of research on the use of IGBTs for pulsed power applications.

The engineering and design groups worked on many parts of the ISAC-II superconducting linac; the first medium-beta cryomodule was fabricated and assembled, cavity tuners were developed, the refrigeration system was specified, the contract for the 500 W at 4.5 K system was awarded, and a decision was made to take responsibility for the liquid helium distribution system in-house. Designs for the TITAN rf cooler prototype and the TIGRESS detector were other parts of the ISAC work that were supported this year. In the support of external experiments the KOPIO detector work continued, the support stand for the NPDGamma experiment at LANL was commissioned, an engineer

was assigned to supervise the contract for the Qweak coils for an experiment at Jefferson Lab., the ATLAS calorimeter fabrication at Victoria and TRIUMF was completed, and at Carleton the forward calorimeter is nearing completion.

The Planning group looked after the scheduling and coordinating of a number of ISAC projects, the planning of the cyclotron shutdowns and provided project information for the development of the TRIUMF Five-Year Plan (2005–2010). The Machine Shop is under new management with the retirement of Roland Roper, who served in this position since 1980. Ivor Yhap is now the new Machine Shop supervisor. Two new machinists were hired into the shop. The Building department was involved with a number of maintenance and repair jobs, some structural designs, and review of designs for the new TRIUMF House.

In the Electronic Services area a major task was installation of the network communications infrastructure in the new ISAC-II building. Hardware support was given to a number of experimental groups, the CERN kicker work and controls group, and software support to TIGRESS, μ SR, and ISAC motor systems.

The Electronics Development group continued to provide all of the hardware installation, maintenance and upgrades for the ISAC control system. EPICS/PLC systems were provided for several applications, and some application-specific VME-based modules were designed and built. The development of the prototype data acquisition boards for CERN continued with the fourth version DAB-IV under design.

BEAM DYNAMICS

J-PARC Collaboration

The Japan Proton Accelerator Research Complex (J-PARC) is an amalgamation of the formerly proposed Japan Hadron Facility (JHF) at KEK and the Neutron Science Project (NSP) at JAERI. Under construction at the Tokai campus, the J-PARC will pursue frontier science in particle and nuclear physics, materials and life sciences, etc., using a new proton accelerator complex at the highest beam power in the world. TRIUMF scientists have a particular stake in this endeavour: J-PARC-Nu, the Next Generation Long Baseline Neutrino Oscillation Experiment. J-PARC consists of a 400 MeV linac followed by 3 GeV and 50 GeV rapid cycling synchrotrons, and the neutrino beam line will use fast extracted beams from the latter machine.

In preparation for later involvement with the construction of particle-beam damping systems, TRIUMF was asked to consult on ring impedance estimates and advise on potential beam instability in the 50 GeV

main ring. A wide range of impedance sources was considered, and in particular kicker magnets with reactive terminations – for which there were no previously existing formulae. Both bunched and coasting beam, longitudinal and transverse, instability thresholds and growth rates were estimated. This is complicated by the fact that there are vastly different parameter sets during injection, ramping and the fast and slow extractions. For the bunched beams, a key issue was to understand the stability of high-order head-tail modes at very large chromatic tune shift, which is an unusual condition. Recommendations and cautions made to the “Accelerator Technical Advisory Committee” included: (i) not to operate the ring with near or zero chromaticity during slow extraction; (ii) to be wary of introducing resonant transverse impedances into pumping-port enclosures and rf cavities by careless design; and (iii) to add small resistive loads to the TW-type kicker magnets to reduce troublesome reflections.

Radioactive ion storage ring

Last year’s report described some preliminary studies of the feasibility of storing radioactive ions from ISAC for more efficient experimental use. This work continued in 2003, focusing on issues affecting injection into the ring, and on the design of a suitable magnet lattice.

The TSR at MPI Heidelberg has demonstrated successful storage of stable ions over a wide mass range, those that are highly stripped exhibiting lifetimes of many minutes. But the conventional injection process takes 10 minutes and captures only one charge state. The radioactive ion beams from ISAC-II, which contain a wide charge state distribution (CSD), clearly require a faster and more inclusive process. Injection by foil stripping offers this possibility.

Figure 287 shows the dependence on atomic number Z expected for various properties of the beam leaving ISAC-II, including A/\bar{q} (where \bar{q} is the average charge), and $n_e = Z - \bar{q}$, the average number of electrons remaining, before (S2) and after (S3) stripping at final energy E/A . The parameter $\Delta = (q_+ - q_-)/2\bar{q}$, where q_+ and q_- are the charge states enclosing $\geq 99\%$ of the CSD. Apparently $\pm 9\%$ charge acceptance in the ring would be sufficient to contain 99% of the ISAC beam.

Injection by stripping would be simple and instantaneous, so that the ISAC beam could be fed into the ring continuously during the accumulation period. Moreover, stripping would:

- increase the average ionic charge \bar{q} , reducing the bending power and diameter required for the ring;

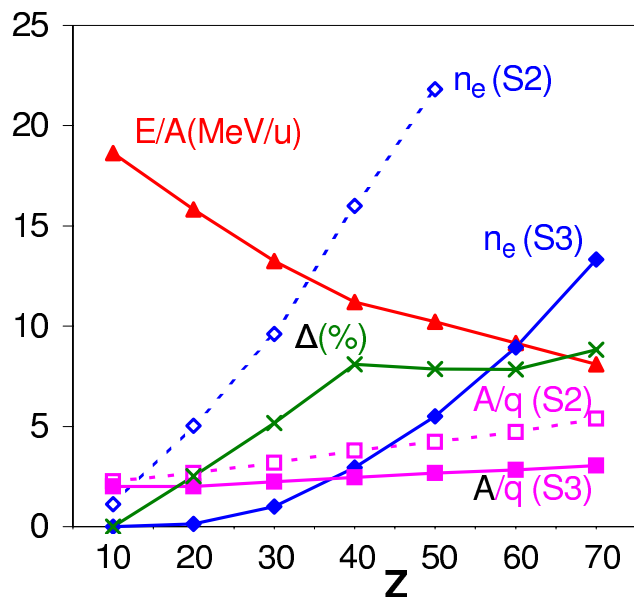


Fig. 287. ISAC-II beam properties vs. atomic number Z .

- reduce the fractional width of the CSD, enabling a greater fraction of the beam to be contained;
- make possible capture of the multiple charge states present in the ISAC-II beam.

The basic drawback to injection by stripping is that the stored beam may make further passes through the foil, leading to loss of beam quality and possibly of the ions themselves. Assuming a $260 \mu\text{g}/\text{cm}^2$ carbon foil, sufficiently thick to give an equilibrium CSD, neither multiple scattering nor energy straggling should cause significant damage. The energy loss is also tolerable for light ions, but it could rule out storage of those with the highest $Z(>50)$. Electron transfer is the most serious threat: on each passage the CSD will re-equilibrate and the empty charge states outside the ring’s acceptance will be repopulated; that fraction of beam will be lost on each pass through the foil. It is clearly vital to maximize the charge acceptance and minimize the number of foil interceptions. Fortunately, the interception rate can be significantly reduced by painting the incoming beam over the acceptance. If this is done in both transverse planes, the average rate can be reduced to 1 in 400 turns.

These considerations have two major implications for the ring design: firstly, a high charge/momentum acceptance requires a low dispersion lattice, large aperture magnets, and careful control of higher-order effects; and secondly, storage of multiple charge states requires zero dispersion at the stripping foil, ruling out momentum painting.

Initial lattice studies have focused on the 2.6 T-m “Midi” ring, capable of storing 80 MeV/u fully stripped C ions. This is conceived as being four-sided, with the

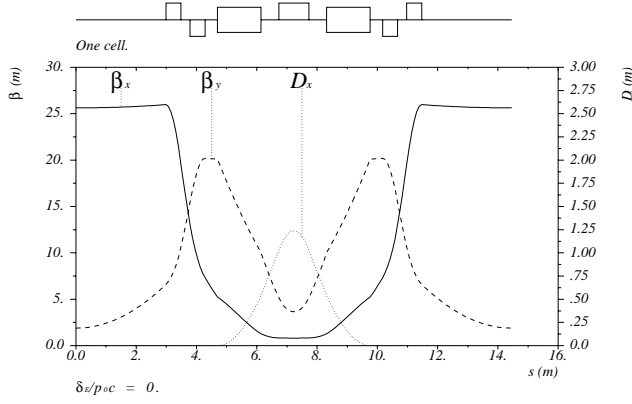


Fig. 288. Twiss functions for the lattice under study.

long straights assigned to injection, cooling, acceleration and experiment. As all these functions require zero dispersion, a natural choice for the arcs has been a double-bend achromat (DBA). The lattice chosen, of the form 0FD0B0F0B0DF0, restricts the dispersion to a narrow region with a low peak value of 1.24 m and also low β_x – crucial features for realizing a high charge acceptance (see Fig. 288). The circumference is 57.8 m, the tunes 2.57(x) and 1.84(y), and the transition energy 7.08. Initial tracking studies have shown good behaviour for charge or momentum excursions up to $\pm 4\%$ – sufficient to contain 99% CSD for ions with $Z \leq 25$.

With ion losses kept to the $\lambda = 1\%$ level for each foil traversal, and transverse painting reducing the average traversal rate to $1/400$, then if charge Q is injected on each turn, the stored charge will exponentially approach $Q/\lambda F_x F_y = 40,000 Q$. A more practical aim would be to stop after 40,000 turns (≈ 40 ms) with $\approx 25,000 Q$ – a sizeable improvement over present beam intensities.

Muon Acceleration in an FFAG

The collaboration with BNL and FNAL on the design of FFAG accelerators for a future neutrino factory and/or muon collider continues. “Non-scaling” (i.e. variable-tune) FFAGs spanning the energy range 5–20 GeV hold the promise of reduced acceleration costs and reduced cooling requirements compared with the alternative, recirculating linacs. The FFAG designs are rapidly approaching maturity and TRIUMF has played a key role in this achievement. The discovery of a new mode of acceleration coupled with a new understanding of the lattice optimization based on thin-element models for the optics, has led to a three-fold reduction in machine circumference and cost.

To achieve rapid acceleration ($\approx 10 \mu\text{s}$) the FFAG ring is filled with rf cavities operating at fixed frequency. This sets limits on the phase variation allowable during acceleration. Although not isochronous,

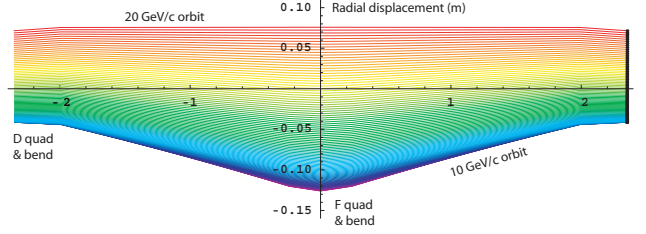


Fig. 289. Single cell, length 5 m, of FFAG showing closed orbits of momenta from 10–20 GeV/c (cold to hot) as a function of radius (m).

the quadratic variation of path length on momentum in the non-scaling FFAG is the origin of a novel mode of acceleration in which the beam slips back and forth across the crest of the rf waveform. This is understood in terms of a libration manifold, shown in Fig. 289, which opens up once the acceleration per cell exceeds a critical value depending on the range of pathlengths, and is the result of strongly non-linear longitudinal dynamics. The manifold links injection to extraction energy yielding a near linear dependence of machine energy range on accelerating voltage, which is a considerable benefit.

A hallmark of the non-scaling FFAG lattices is their ability to compact a very wide range of momenta into a narrow radial band, a property which is helpful not only in terms of lowering magnet aperture and cost, but also in restricting path length variations with momentum. As shown in Fig. 290, $\Delta R/R$ is of order 10^{-3} for $\Delta p/p$ of order unity. This property is associated with the use of F0D0 or FDF triplet lattices in which the F magnet provides a reverse bend.

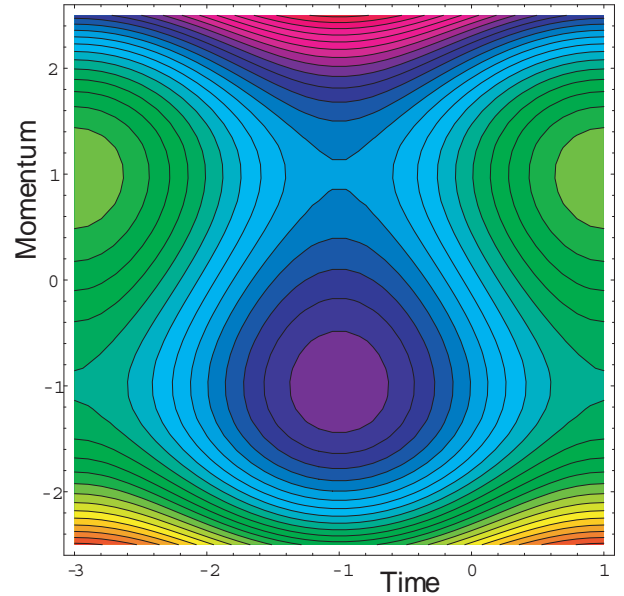


Fig. 290. Phase space generated by quadratic pendulum oscillator.

Thin-element models of the non-scaling FFAG lattices have been used to derive simple analytic formulae for key properties, such as orbit displacement and path length. These confirm the parabolic dependence of path-length on momentum observed with standard orbit codes, reveal the factors which should be adjusted to minimize path-length variation, and form a useful starting point for thick-element design (for which analytic formulae have also been developed). In the case of a 10–20 GeV/c muon ring, the thin-element formulae are in reasonable agreement with the predictions of standard orbit codes – somewhat better for F0D0 than for triplet lattices. The thick-element formulae are in excellent agreement for both.

MAGNETS

In addition to supervising the contract for the fabrication of the CERN twin aperture quadrupoles, described in the CERN collaboration section, work was carried out on a number of other magnets during the year.

In 2002, a small $X - Y$ steering magnet was designed to fit between the ISAC-II cryomodules. In 2003, 8 of these magnets were constructed.

In 2002, Everson Electric Company (Bethlehem, PA) was contracted to design and build 5 superconducting solenoids for the ISAC-II medium-beta cryomodules. In 2003, Everson went bankrupt before completing the first magnet. As the coils for the prototype had been wound and potted in wax, we obtained the coils from the receiver and completed the magnet at TRIUMF. On December 11, the magnet reached 9.02 T without quenching.

Since ISAC needed 5 solenoid magnets, and Everson was only able to produce part of one, Accel Instruments (Germany) was contracted to supply a prototype magnet and 4 production magnets. At year-end, Accel was ready to test their prototype magnet.

A high field C-frame dipole was designed for the ISAC HEBT (S-bend) transfer line [TRI-DN-03-4]. The transfer line needs 4 of these magnets. A contract was awarded to Alpha Magnetics (California) for the coils. The contract to machine the steel and assemble the magnets was awarded to Sunrise Engineering (Delta, BC). These magnets are expected to be on site in May, 2004.

Work began on fulfilling TRIUMF's commitment to assist the Canadian collaboration on the Qweak experiment at Jefferson Lab. TRIUMF is assisting in the purchase of the large coil assemblies for the QTOR spectrometer. The spectrometer is being designed at MIT-Bates Laboratory. MIT-Bates expects to issue final coil drawings in February-March, 2004. Once these drawings are available, TRIUMF will request tenders

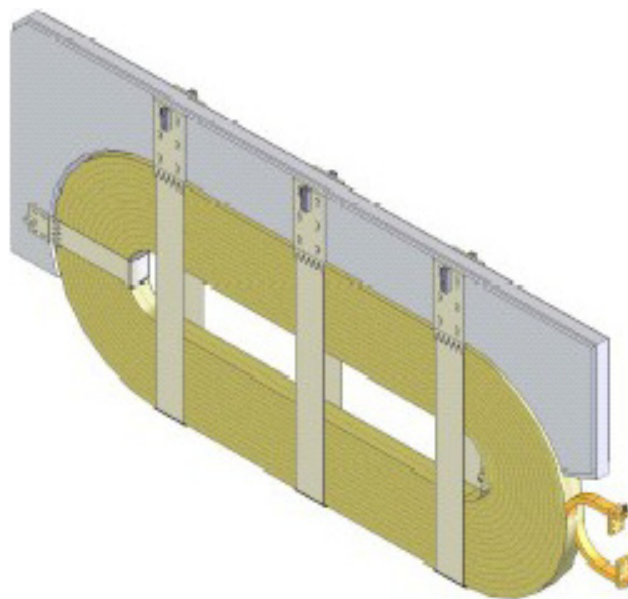


Fig. 291. Single coil arrangement for the Qweak spectrometer.

for the manufacture of the 8 coils plus a spare. Figure 291 shows the single coil arrangement.

Magnet Measurements

Experiment 614 – TWIST

The first part of the year was occupied surveying the TWIST solenoid in M13. Measurements were carried out from the upstream end of the solenoid to the quadrupole (Q7) in front of the solenoid.

TOSCA 3D simulations have previously been carried out for the TWIST magnet. These simulations provide important information because the measurements provide only one component (B_z) of the field at a limited number of space points. By contrast a good TOSCA computer model can provide the three field components at any point in space. A detailed comparison was made between field maps taken for the TWIST solenoid, at a field of approximately 2 T and the TOSCA predictions. Within the TWIST iron box (i.e. ± 147.2 cm from the centre of the solenoid) the maximum discrepancy between the predicted and measured B_z field is 20 G. Upstream of the TWIST magnet the discrepancy between predictions and measurements increases: 220 cm from the centre of the solenoid the predicted B_z field is approximately 70 G less than the measured field. 106 cm from the upstream end of the TWIST iron box there is a quadrupole (Q7) that contains a significant quantity of iron; a further 54 cm upstream there is a second iron core quadrupole (Q6). A further 74 cm upstream is a dipole that has an estimated weight of approximately 18 tonnes. The iron associated with the two quadrupoles and dipole would act to increase the field at the upstream end

of the magnet and could therefore explain the discrepancy between measurements and predictions. A revised TOSCA 3D model, which includes the iron of the 2 quadrupoles and dipole, is currently being set up.

Other magnets

Other magnets surveyed this year included a HiTime superconducting solenoid from M15, the Strovink solenoid, twenty ISAC-II transfer line quads, an ECR source magnet assembly, the M20Q1 and Q2 replacement quads, an ISAC S-bend quad, eight ISAC-II double steering magnets, and an ISAC-II 9 T superconducting solenoid.

KICKERS

NLC collaboration

The Kicker group is collaborating with kicker experts at SLAC carrying out research into the application of high power insulated gate bipolar transistors (IGBTs) for high efficiency, high reliability, and low cost pulsed power modulators for the Next Linear Collider (NLC). The IGBTs are stacked in series, with a voltage of approximately 140 kV dc per stack. Under normal conditions the IGBTs conduct 3 kA current pulses for 3 μ s, but under fault conditions the IGBTs may have to conduct currents of 6 kA or more. IGBT modules from EUPEC, a German manufacturer of power electronic devices, were frequently failing at SLAC under fault conditions (see Fig. 292). These EUPEC modules contain sixteen IGBT dies, two of these dies are referred to as “A” and “B” as shown in Fig. 292. When the damaged IGBT modules were opened, it was found all of the observed failures occurred in the B dies; these dies are closest to the emitter. Observations on the failed units suggest that the failures might be the result of unbalanced lead inductances within the IGBT package.

The approach adopted at TRIUMF to understand the failure mechanism is to derive an equivalent circuit of the layout of the IGBT, primarily the parasitic inductance (Fig. 293), and simulate the equivalent

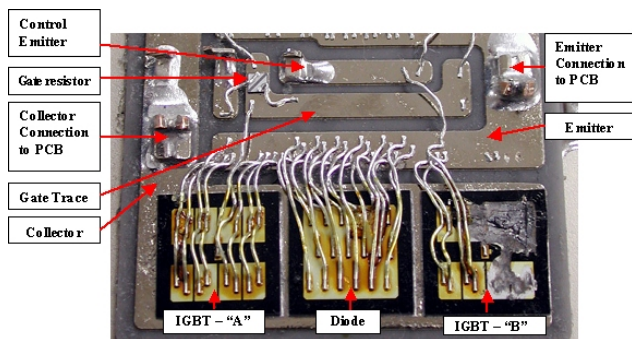


Fig. 292. Lower half of one EUPEC IGBT “raft”.

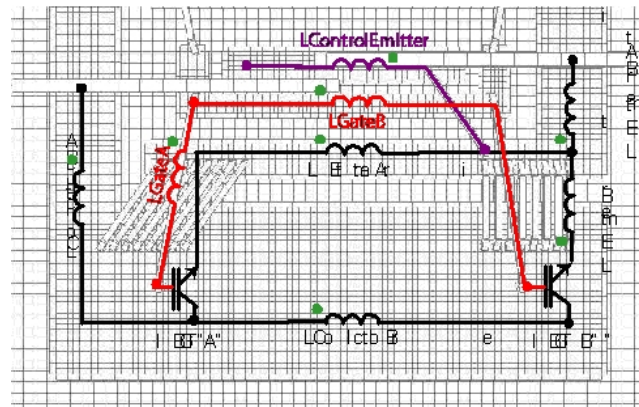


Fig. 293. Extracted inductors and node locations for EUPEC IGBT module.

circuit using PSpice. A 3D electromagnetic code has been used to extract both the self and mutual partial inductances for the layout of both a EUPEC FZ800R33KF2 module and a SLAC designed rectilinear layout. An NSERC research grant was received to carry out research into the high power IGBT switches. Two co-op students have worked on this research project at TRIUMF during 2003.

The EUPEC and a SLAC IGBT have each been simulated under normal working conditions as well as hard and soft short circuit conditions. The PSpice simulations show that the current is well balanced between the IGBT die under normal operating conditions. However, under fault conditions there can be a significant imbalance between die A and B in the EUPEC module. Figure 294 shows a prediction for die A and B in the EUPEC module under soft short circuit conditions: IGBT die B, which is the die that generally failed at SLAC, conducts significantly higher current than die A. Simulation results also show that the proposed SLAC rectilinear IGBT module exhibits well balanced current between the die.

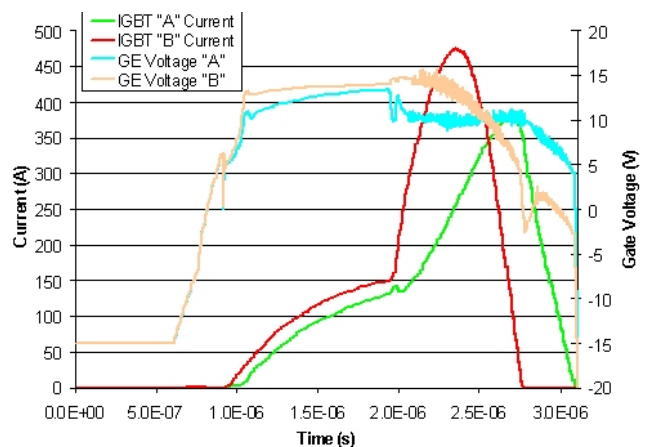


Fig. 294. EUPEC current imbalances and corresponding gate voltages: soft short circuit.

J-PARC collaboration

The Japanese Hadron Facility (J-PARC) includes a ring in which the beam is accelerated from an energy of 3 GeV to 50 GeV. One of the proposed experiments, which require the beam to be extracted from this ring, is the long baseline neutrino oscillation experiment. Space constraints in the lattice of the ring result in a requirement for a novel bipolar combined function kicker that can be used for fast extraction or abort. Magnetic field pulses with a rise time of approximately 1.1 ms and 4.3 ms flat top duration are required. One of the stringent design requirements of the extraction system is a flat top ripple of less than ± 1 . The proposed kicker system is composed of 6 kicker magnets of 1.5 m length each, powered by pulse forming lines (PFLs). To achieve the required kick angle of ± 5.32 mrad, low characteristic impedance has been chosen. Several different concepts for the kicker system have been considered including system impedance, and kicker magnet type (transmission line, lumped inductance and hybrid-transmission line). The conclusion of the research was that a $5\ \Omega$ lumped inductance magnet with capacitors, or either a $4\ \Omega$ or $5\ \Omega$ four-cell hybrid magnet meets the specifications while avoiding the complexity and expense of a transmission line magnet. For the HV cable to be reliable for both thyatron and IGBT switches, the cable should be rated for at least 68 kV and 56 kV pulsed for $5\ \Omega$ and $4\ \Omega$ systems, respectively, with a voltage gradient of not more than 9 kV/mm.

Thyratrons will initially be used for the switches of the kickers. It is planned to carry out research and development work at TRIUMF to build an IGBT switch that can be used to replace the thyatron switches. The IGBT switch will improve the reliability and reduce the maintenance required.

PSI MuLan collaboration

An international collaboration plans to measure the lifetime of the muon to a precision of 1 ppm. The MuLan experiment will take place at PSI in Switzerland. The central idea employed in MuLan invokes an artificial time structure on an otherwise dc beam. The MuLan method requires a fast beam line kicker, which can turn the beam on and off at a repetition rate of up to 75 kHz. The TRIUMF Kicker group was contracted to design and build the kicker. The kicker runs with a standard “on-off time cycle”, or in a “muon on request” mode. The MuLan kicker consists of 2 pairs of deflector plates mechanically in series, driven by 4 FET modulators. Each pair of plates is 0.75 m long. One plate of each pair is driven by a +12.5 kV FET based modulator and the other plate is driven by a -12.5 kV modulator. The potential difference



Fig. 295. MuLan kicker racks installed in beam line at PSI.

between a pair of deflector plates is variable up to 25 kV. Each modulator consists of two stacks of FETs operating in push pull mode. The specifications for the kicker demand that the rise and fall times of the deflector plate voltage are not more than 45 ns; rise and fall times of 40 ns or less were achieved. There is a requirement for an adjustable output voltage from 0 V to ± 12.5 kV per deflector plate, a minimum pulse duration of 200 ns (160 ns achieved), and adjustable repetition rate up to a maximum of 75 kHz (77 kHz achieved), continuous. In addition, short turn-on and turn-off delays of 200 ns were achieved. A novel concept was developed for the design of the MuLan kicker; a PCB containing a 1 kV MOSFET, high-speed driver, power supply and fibre optic receiver has been developed. The printed circuit board layout for this design is very critical due to the fast switching times (< 2 ns on the board) and the presence of kV transients that could otherwise be superimposed on low voltage fibre optic control voltages (5 V). The kicker was successfully commissioned at PSI in July (Fig. 295). However, as a result of the very fast switching times of the MOSFETs (< 2 ns compared with approximately 30 ns in the previous generation of our kicker cards), and the interconnection required for the 4 kicker racks, significant rf noise is generated. It is planned to ship the kickers and deflector plates to TRIUMF in early 2004, to investigate and implement measures to reduce the rf generated noise.

One co-op student worked on this project at TRIUMF during 2003. A very similar kicker is required at TRIUMF as part of the Five-Year Plan for M20 upgrade.

Electromagnetic software

The extraction of parasitic inductance and capacitance for both the IGBT project and the MuLan kicker

required the use of 3D electromagnetic software. However, the TOSCA software used is not presently suitable for extracting partial inductances or capacitances. In addition the TOSCA 3D simulations for the TWIST magnet require a considerable amount of computer memory (>1 GB) to simulate only one-eighth of the geometry; at least one-quarter of the geometry is finally required to be modelled. Hence other electromagnetic software codes have been evaluated. The codes from a Canadian company, Integrated Engineering Software (IES), have been extensively tested for their ability to calculate partial inductance, and the code has proven to be both versatile and accurate. The IES codes may be much more efficient for simulating problems such as the TWIST solenoid: it is planned to simulate the TWIST solenoid in early 2004.

MECHANICAL ENGINEERING

Mechanical engineering work at TRIUMF is initiated by the submission of a Request for Engineering (REA) form which is assessed and assigned according to the size, complexity and schedule of the task. Large, complex tasks usually require a team approach guided by a project engineer. The ISAC-II superconducting accelerator refrigeration system and cryomodels fall into this category.

During the year there were 37 ISAC REAs and 30 non-ISAC REAs submitted, along with a number carried over from the previous year.

As in the past there was continuous participation of engineering personnel in performing engineering analyses, consideration of safety related issues, design reviews, and other ad hoc engineering related small jobs.

ISAC-I

Modules

Work recommenced on target module 4 (TM 4) which had been previously built to house a special high power target for tests conducted in December, 1999 (100 μ A tests). For those tests the module was incomplete and did not have the normal internal components. TM 4 will be completed as a fully serviced module able to accept a surface source or an ECRIS. However, it will initially be used as a special target development test module later in 2004. Completion is scheduled for the summer of 2004.

ISAC-II

TRIUMF is building a superconducting linear accelerator to be installed in the ISAC-II accelerator vault. The first phase of the project involves manufacture, assembly and construction of the 5 medium-beta cryomodels (and eventually 2 of the 3 high-beta cryomodels) and the refrigeration system necessary to support their operation. Phase 1 of the refrigeration

system will be a 500 W at 4.5 K system based on the heat load of the phase 1 components plus distribution losses with a suitable margin. Phase 2 is not at the present time completely defined but will include an addition to the refrigeration system as well as completion of the high-beta cryomodels.

Refrigeration system

A specification was written for the phase 1 refrigeration system as a complete turn-key system. This included everything up to the delivery and transfer of "U" tubes at the cryomodels. TRIUMF was responsible for all services necessary to support the refrigeration system. The two major suppliers of cryogenic refrigeration systems, Linde and Air-Liquide, responded to the tender package with a quotation. Unfortunately both quotations were beyond what TRIUMF had budgeted. At that time TRIUMF decided to negotiate with both tenderers asking for quotations for the supply of the refrigeration system components only, including process and instrumentation diagrams, installation instructions, etc. Quotations were received and a contract was awarded to Linde in November. TRIUMF will be the project manager for the refrigeration system which can be broken down into 3 categories:

1. Refrigeration system component installation including all services, warm piping and buffer storage tank.
2. Accelerator vault access platform and distribution system support structure.
3. Cryogenic distribution system (all vacuum jacketed, liquid nitrogen shielded piping from the liquifier cold box to the cryomodels, including the liquid helium dewar).

The third item is the most complex and specialized (other than the refrigerator itself), and a task force was formed to discuss how TRIUMF would approach the design, purchase and installation of such a system based on the simplest and most cost effective system but also one that has as high a transmission efficiency (low heat load on helium) as possible. To this end a conceptual design was produced, flow schematics were created and a package of information was put together along with a letter requesting interested parties to respond early in 2004. The intent is to have a complete phase 1 refrigeration system operational and commissioned by April, 2005.

Cryomodels

A complete description of the medium-beta cryomodel was presented in the 2002 Annual Report and will not be repeated here. The design was well under way by the beginning of this report period and drawing

release began in March. The vacuum tank arrived in May, followed by the lid and the internal components such as the helium reservoir, support beam, struts and solenoid mounting frame.

The μ -metal was ordered for all 5 medium-beta cryomodules, however, it was not flat and was outside of our required tolerance. This required return of the shipment which was reworked to specification. A μ -metal liner was then produced that was installed adjacent to the inside vacuum tank wall. At the same time work commenced on the liquid nitrogen thermal shield box. The box is constructed of 0.125 in. copper sheet with copper tubes soldered in an array on the inside surface of all sides by a special fluxless solder procedure prior to the box being riveted together. There is a separate lid mounted thermal shield piece that overlaps the edges of the box when finally installed.

An assembly frame was constructed to support the lid and allow the installation of all the internal components. The helium reservoir mounts to the stack flange of the lid (see Fig. 296) and all other components are suspended from 3 adjustable mounting lugs on the lid. This allows for cryo element alignment adjustment relative to the vacuum tank. The assembly frame also mimics the vacuum tank beam ports and wire position monitor ports allowing cryo elements to be aligned with respect to each other as well as the theoretical

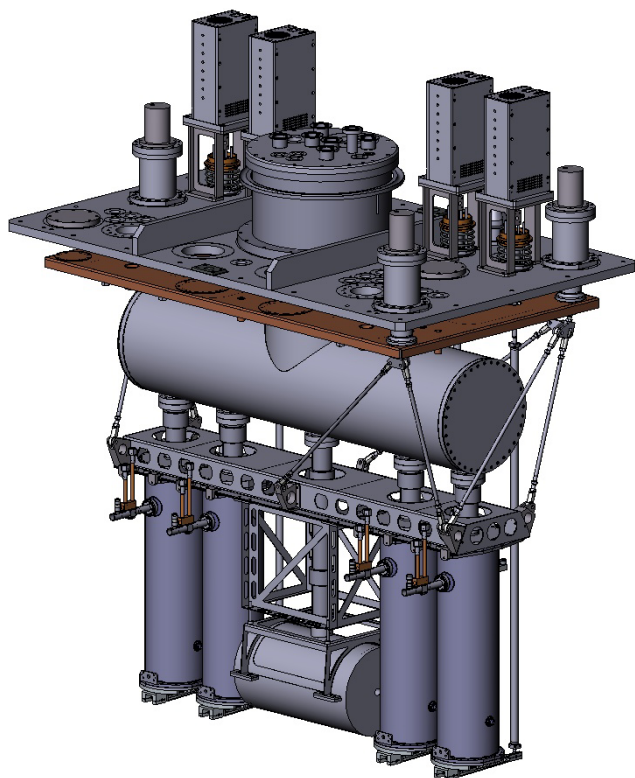


Fig. 296. Cryomodule lid assembly showing internal components.

beam line, and this alignment is also transferred to 3 target posts on the lid since the beam ports will not be visible once the cryomodules are installed in the accelerator vault.

Assembly has progressed to the point where the assembly frame and internal components had been through the cleaning cycle, moved into the class 3 clean room and reassembled on the frame allowing the commencement of alignment. The vacuum tank and thermal shield box had been moved to the class 2 clean room awaiting completion of the lid assembly. The goal is to complete a cryomodule cold alignment investigation in March, 2004.

ISAC-II single cavity tuner development at BC Research

Numerous rf cavity tests were performed using the tuner under superconducting temperatures. Results were very good and well within the required specifications.

ISAC-II four cavity cryostat tuners

Motor and controller parts were purchased for 4 more cavity tuners. The prototype mechanical design was updated to be commensurate with the lessons learned from the BCR tests. The affected design drawings were updated and all components have been fabricated for 4 cavities and are ready to be assembled. A design for the packaging of 4 control amplifiers, along with all support hardware into a standard free standing electrical cabinet, has been established for the ISAC-II clean room 4-cavity test cryostat tuners. All related parts have been purchased and are presently being assembled.

Structural analysis and approvals

As usual, numerous structural analyses of engineered components were performed and shop drawings approved for manufacture. Beyond that, much analysis was done of the structure of the ISAC-II 4-cavity cryostat assembly components in terms of stresses, deflections, thermal behaviour, and vibration/modal analysis.

Engineering – Other

KOPIO

Scintillator extrusion Work continued from the previous year to extrude wider cross section scintillator with more holes in the middle plane. We successfully produced a $\frac{3}{8}$ in. \times 3 in. cross section scintillator with 6 holes in the middle plane compared to a $\frac{1}{2}$ in. \times $1\frac{1}{4}$ in. cross section version containing 3 holes produced last year. Work is continuing to improve the external profile and shape of the holes in the scintillator.



Fig. 297. Scintillator being extruded between the die and the sizer.

Figure 297 shows the scintillator being extruded between the die and the sizer.

Aluminum extrusions As reported in the 2002 Annual Report, an order was placed with a company located in Portland, Oregon, to produce thin walled and tight tolerance aluminum extrusions. The first run looked quite promising. The company had difficulty controlling the flatness tolerances on the base. A straightening jig is being designed to achieve the tight flatness tolerances across the base as well as along the length. The fin thickness and their spacing are within the tolerances.

Structural A finite element program ANSYS was used to analyze the structural strength of the KOPIO preradiator module. Half symmetry was used to analyze one quadrant of the module. The study concluded that the stresses and deflections were low in the structure.

Figure 298 shows a plot of displacements in the half quadrant KOPIO preradiator module.

Other projects

NPDGamma stand The stand structural components and the control system electronics arrived at the LANL neutron science centre in the ER2 area. The stand and controls were assembled and underwent partial testing. During a return visit in September, safety devices were installed on the drive screws along with limit switches and the controls software was updated to accommodate new installations. The prototype control electronics was packaged into a standard cabinet at LANL with

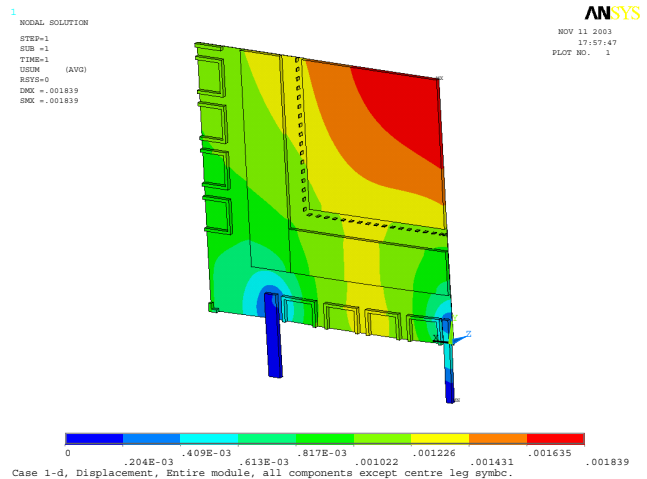


Fig. 298. Plot of displacements in the half quadrant KOPIO preradiator module.

supervision from TRIUMF. Fifty new cesium iodide detector crystals, each weighing 50 lbs, were installed into the detector support module and everything (under full load), remained aligned precisely as required in the specifications.

Engineering – Victoria

Signal feedthrough project

The feedthrough team at the University of Victoria completed their work with the ATLAS feedthroughs at CERN. This included several trips to CERN to assist with the integration of the feedthroughs into the cryostat of the ATLAS detector. The team was responsible for mounting the pedestals, baseplanes, and warm cables, which included the electrical testing for each cable as it was installed.

Hadronic endcap (HEC) module assembly table

There has been continuing support for the manipulation of the second to last HEC module for the ATLAS detector at CERN. During a trip to CERN, TRIUMF staff from the University of Victoria assisted by preparing assembly fixtures and alignment hardware, organizing floor space and equipment storage, as well as other supportive work to carefully move and manipulate the module to its final storage position. There was also some participation in loading the assembly fixture with the final batch of HEC modules.

ISAC target development

Effusion oven The University of Victoria became more involved with ISAC's target development group by researching and designing a high temperature effusion oven capable of reaching 2300°C. This included the development of a graphite filament, construction of a water-cooled vacuum chamber, temperature monitoring thermocouples and radiant heat shielding, as

well as the use of finite element analysis using ANSYS software to confirm the results achieved during testing. This apparatus will be used to test the out-gassing properties of materials at high temperatures for future consideration in target use.

Finned target model Efforts to expand the finite element analysis of the prototype finned target are continuing. Initially, only small sections including one or two fins could be modelled at one time. The model has been expanded to include 45 fins, showing half of the beam tube for the target; however, software limitations were restricting the results of the thermal distribution through these components. Improvements to this analysis are ongoing, and will carry on in 2004.

Heat shield analysis The new design for the ISAC target heat shield needs to have the cooling capacity to remove up to 25 kW of radiant heat being transferred from the target. Calculations were performed to determine the maximum rise in cooling water temperature. This change in water temperature was broken down into increments along the cooling line, and the heat distribution in the heat shield was simulated using Maple software. An iteration to determine a more realistic temperature distribution through the cooling lines is under way and will be compared to a finite element analysis model produced in ANSYS.

ISAC-II – medium-beta accelerator design

In 2002, calculations were done to size the burst disc required for the medium-beta cryomodule helium reservoir and cavities in the case of a vacuum failure and/or solenoid quench. These calculations were adapted for the solenoid test cryostat to confirm the system could safely handle the pressure build up of vapourized helium from a catastrophic event.

In the event of a solenoid quench, the cavities of the medium-beta cryomodule would be subjected to a force causing a bending moment. Calculations were used to show the inner and outer cavity walls could withstand such a force without buckling and causing damage.

T1 and T2 target stations – Be targets

There were questions regarding how much beam current the beryllium targets at the T1 and T2 target stations could be subjected to, and what changes would be necessary to the target design in each case in order for the targets to last two years while being subjected to beam currents as high as 200 μA . Research based on previous calculations for these targets and current operating conditions has begun and will continue in 2004.

Graphite removal

The removal or sale of the excess graphite blocks and plates taking up valuable space at the University of Victoria was completed after considerable effort. Some of the blocks and sheets of graphite had been submerged in salt water for geomagnetism experiments, and were leaching salt. The graphite was sorted into three categories: no obvious salt contamination, minimal or surface only salt contamination, and moderate to significant salt contamination.

Most of the uncontaminated graphite was sold and shipped to the Indiana University Cyclotron Facility (approximately 4.5 tons). The remainder of the uncontaminated graphite, as well as some of the stock with minimal salt contamination, was shipped to TRIUMF for storage (approximately 2 tons).

Engineering – Carleton

ATLAS forward calorimeters (FCAL)

In April, the FCAL 3A module was completed and shipped to CERN, using the reusable shipping crate that carried the 3C module to CERN. Once there, it was tested with 500 V to locate any shorts that shipping might have caused.

The FCAL 3C module was used in a calibration beam test in July and August. After a final cleaning and checking for shorts it was assembled with the FCAL 1C and 2C modules and the Plug3 into its aluminum support structure. As there is only 1.5 mm of clearance between the modules and the tube, this operation took about a week of preparation and alignment.

A detailed heat flow study of the FCAL structure was undertaken to establish an upper limit of heat leakage, into the FCAL through the inner bore, that could be tolerated. This involved complex 3 dimensional FEA models of the heat flow through the various materials, including, in conjunction with the University of Alberta, the convective heat transfer effects of the liquid argon.

Figure 299 shows part of the FCAL assembly.

TPC electronics

A transparent 4-point sensing device was designed and built at Carleton for accurately measuring the surface resistivity of resistively coated films used to increase the accuracy of GEM readout pads. The sensor has spring loaded pins to maintain positive, even contact with the film. The fact that the sensor is transparent allows the operator to use a grid placed beneath the film to get an accurate map of the resistive quality of the film.



Fig. 299. FCAL C end assembly starts.

PLANNING

This year the Planning group was involved in planning, scheduling, coordinating and expediting several sub-projects for ISAC-I (ECR source and upgrades to 8π and β -NMR); ISAC-II (medium-beta cavities, wire position monitor, cryogenics system, high-beta cavities, charge state booster (CSB), HEBT transfer, H-HEBT); planning and coordinating activities for two shutdowns (December 22, 2002–April 15, 2003 and September 18–October 4); ISAC experimental facilities (TIGRESS, TITAN); two step target, actinide target test, and M20Q1,2 refurbishing. The Planning group was also extensively involved in preparing manpower and cash flow estimates for the Five-Year Plan (2005–2010), as well as setting up a new job recording system for the Machine Shop.

Technical details and progress on PERTed activities are described elsewhere in this report under the respective principal group. However, following is a summary of the main projects along with the major milestones achieved.

ISAC

Various plans and PERTs were prepared and updated regularly with manpower estimates and analysis to identify critical areas and resolve any problems. ISAC priorities were evaluated and higher priority was assigned where necessary to optimize the scientific output.

ISAC-I

ECR source ECR design improvements were made after tests with stable beam from the ECR-1 installed on TM 3 in late 2002. Two exit modules were damaged due to high current and absence of proper skimmers. Then skimmers with current limits and cooled collimators were installed, insulators were changed, and the

aperture was reduced from 5 mm to 3 mm. Tests were done first on the test stand, followed by tests with stable beam and then with RIB in April, but still the efficiency and amount of RIB delivered was less than expected. After analyzing the test results, the design was modified and ECR-2 was fabricated and tested extensively on the test stand.

Experimental facilities Several modifications and upgrades were made to 8π and β -NMR during 2003.

ISAC-II

Medium-beta cavities The major milestones achieved included: cavities #1–9 were fabricated, inspected, chemically treated and received at TRIUMF. Cavities #10–20 were fabricated and received at TRIUMF and are expected to be chemically treated by May, 2004. Tuners, coupling loops and amplifiers for the first two cryomodules have been received, with the remaining components expected to arrive early in 2004. The first cryomodule tank was received in July; all the internal components were fabricated and assembled in the tank by early December. A cold alignment was achieved with the wire position monitor before year-end.

Cryogenics system It took much longer to prepare the specifications for the cryogenic system including the distribution system. After receiving the bids in October, it was decided that the distribution system would be designed, procured and installed by TRIUMF with help from outside contractors, to meet budget constraints. A detailed Work Breakdown Structure (WBS) and PERT was developed for this project. The contract for the cold box, compressor/ORS and He ambient vapourizer was awarded in November to Linde. These components will be arriving at TRIUMF in July and September, 2004.

High-beta cavities Preliminary physics specifications for the high-beta systems were done with an aim to complete the conceptual design by July, 2004 and order Nb for all high-beta cavities in April, 2004.

Charge state booster (CSB) The CSB system, matching sections and analyzing magnet were installed. ECR mode and breeding mode were commissioned by the end of November. Tests with the rf cooler will take place in summer, 2004, and optimization will continue until the end of the year, when the CSB will be ready to move to its final location.

HEBT transfer The 4 dipoles were designed and ordered in November and are expected to be received in July, 2004. All 20 quads were received and field mapped by July. Eight steering magnets were assembled and field mapped by December, and will be ready to install by March, 2004. The rebuncher was received at TRIUMF in March, and assembly of the components on to

the rebuncher continued with an aim too be ready to install in the DSC line by July, 2004.

Experimental facilities Work breakdown structures and detailed schedules were developed for two major experimental facilities – TITAN and TIGRESS together with some manpower planning and analysis.

The major components of TITAN included: RFQ cooler, EBIT, Penning trap, and main platform and services to support the components. The plans for TIGRESS included: design and fabrication of prototype substructure for one detector by April, 2004, and test by June, 2004. The summary of the progress and major milestones achieved is covered under the ISAC Planning section.

Shutdown Activities

There were two shutdowns during the year: the winter shutdown (December 22, 2002–April 16, 2003 for BL1A, and March 13 and 27 for proton therapy and ISAC beam production respectively), and a fall mini shutdown (September 18–October 4).

Winter shutdown

BL1A activities started in early January, with the removal of many shielding blocks from the meson hall to get a head start for shutdown work. The planning and coordination of jobs around 1A triplet and T2 became complex and challenging due to high radiation fields and lack of manpower. A total shutdown dose of 186 mSv was distributed among 123 workers.

Major jobs completed by the Remote Handling, Beam Lines, Vacuum and Diagnostics groups in the meson hall included: replacement of leaking 1A triplet along with rerouting of services for better accessibility, removal of some crumbling blocks near 1AM10 and T2 water package and installation of new custom designed shielding blocks (as needed), repairs of M20Q1 water leaks, repair of several BL1A vacuum leaks (1AQ13, M9Q1-T2, M20Q1-B1), M13 jaws and slits MRO, T1 and T2 target and water packages MRO, and repair of 1AQ9 thermal interlocks.

In the cyclotron vault the elevating jack maintenance was completed by mid-January. After that the lid was up for most of February to complete maintenance jobs for probes (extraction probes (2A, 2C), LE2, MRO on both low and high energy probes, slits and periscopes), and engineering physics (MRO on correction plates in Q2, 4 and thermocouples). The RF group completed several jobs that included: voltage probes calibrations and MRO, inspections and cleaning in the centre region, resonator bellows and chore pads (UQ1), installation of new combiner #2, PA tests and tuning, combiner #3, capacitor station #2 upgrade, and MRO work for transmission line pickups. The Vacuum group installed 4 new ion gauges for rf and also

replaced both the inner and outer tank seals (one of the high dose jobs) with the help of volunteers. Some work was also done on 2C to prepare for the removal and reinstallation of STF in the January, 2004 shutdown.

Vault work finished on schedule with the lid down on February 25, main magnet energized on February 28, followed by injection and cyclotron tuning with a beam for proton therapy calibrations on March 13, and beam production for ISAC at ITW on March 27. BL1A beam production was scheduled for April 16.

Fall mini shutdown

This mini shutdown in September was originally scheduled for one week and had to be extended to about 2 weeks because it was decided to raise the lid to replace the water-cooled probe and exchange 2C extraction foils. After 9 days of cool down time and with the south side shadow shields in place, the predicted fields in the area where work had to be done were about 50% higher than last spring. This was confirmed by the radiation surveys done during the shutdown.

Meson hall work started a few days earlier than vault work, when PIF finished running in 1B. The major jobs completed in the meson hall included: repair water leaks at 1A triplet and M9Q5, replace electrical superconducting connectors for M9, repair small air leak at M20 beam blocker, repair water leak in M13 header, upgrade vacuum hardware and install 1A turbo cables. Some work was also done on DB0, target modules MRO, and commissioning of ISAC building services and controls. A total shutdown dose of 28 mSv was distributed among 47 workers.

DESIGN OFFICE

Although the majority of design hours was focused on the ISAC project (58.0% of 16,859), a significant amount of time (26.4%) was devoted to MRO upgrades to the beam line infrastructure, in preparation for future experiments at TRIUMF.

Design of the ISAC-II cryomodule prototype and DSB S-bend HEBT components billed 4,472 hours, equal to approximately 2.4 FTEs. The development of the charge state booster (CSB) to test stand readiness, and the rf cooler prototype for TITAN billed 1,255 hours. The single detector prototype for TIGRESS added 1,063 hours. Upgrades for ISAC target and exit modules, ECR2 for the test stand, low intensity diagnostics, and support for the general ISAC-I experimental program, TUDA, DRAGON, GP2, β -NMR, LTNO and others continued through the year.

TRIUMF's main program MRO upgrades were (a) cyclotron refurbishment: high energy probe replacement prototype, low energy probe cassette re-design, rf transmission line and power switch upgrades, and cyclotron documentation, and (b) beam lines: 1A triplet,

T1/T2 shielding and profile monitor, M9 Q1-2, M9B OMNI spectrometer stand, M11 septum bypass, M13 gate valve and TWIST time expansion chamber, M20 Q1-2 and beam line 2C re-alignment were all visited for experimental upgrade purposes during the year.

External projects received 8.7% of design hours, with most effort concentrated on the MuLan kicker, CERN 66 kV power supplies, SNO glove box and KOPIO.

Photographic and visual art services continue to grow with greater emphasis being given to TRIUMF's image, both within the science community and on the world stage. Publications are more completely processed in house. Instructional aids, models, posters and other materials billed 1,162 hours this year, 60% more than 2002, contributing toward TRIUMF's Outreach Program and corporate presentation.

Network 2D CAD is now available through PC support and SolidWorks 3D modelling software has been adopted as the platform of choice for all TRIUMF users through to the start of the next Five-Year Plan (April, 2005). 90% of the Design Office legacy archive has now been scanned.

MACHINE SHOP

There were several changes in Machine Shop personnel this year. Roland Roper retired after serving as Machine Shop supervisor since 1980. Ivor Yhap is the new supervisor and Andy Hird replaced Ivor as a shift supervisor. Two new machinists were hired, making the present complement 19 technicians and 3 apprentices. One of the new machinists has had considerable experience with CNC machining and the Mastercam software. This experience has already been put to good use with a number of parts being machined using the full capability of the Haas V3 CNC machine with its fourth and fifth axes.

Figure 300 shows an example of the complex components produced at the CNC machining centre.

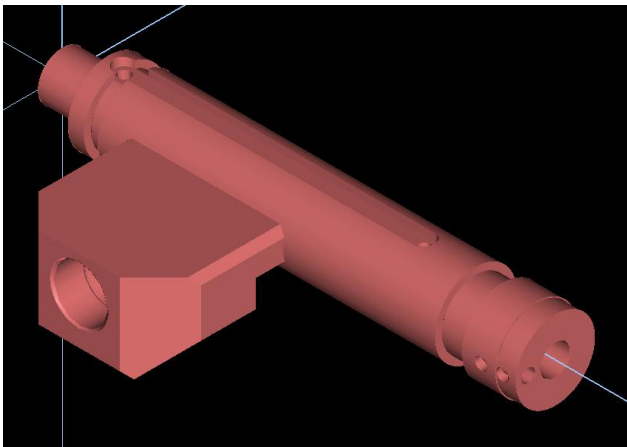


Fig. 300. An LN₂ cooled rf coupler for the SCB cryomodule, machined from a solid piece of copper.

Table XLVII. Machine Shop utilization.

ISAC development	4.1%
Science	26.9%
ISAC operations	14.3%
Nordion	5.1%
ISAC-II	29.8%
Cyclotron	11.5%
Cyclotron refurbishing	2.9%
CERN	0.6%
Affiliated institutions	2.6%
NSERC	0.7%
Site infrastructure	1.1%

The distribution of Machine Shop jobs by TRIUMF divisions and other groups is shown in Table XLVII.

The total value of fabrication work amounted to \$1.68 M this year. The Machine Shop continues to support local industries by sub-contracting out work that is beyond the capacity of the shop, or large volume components that are time sensitive in nature.

BUILDING PROGRAM

Design and management of minor construction projects

The department was involved in lots of small projects around the site. Most of these projects were small renovations and adaptations in the new ISAC-II building. Projects like video conference room and clean room 152 were typical adaptation projects.

Structural design and engineering review

Preliminary structural design was done for the mezzanine in the technical shop of the ISAC-II building. Engineering review was performed for a variety of small structures like lifting bridges, platforms, etc.

Building design review

The Building department did the architectural and structural concept reviews for the new TRIUMF House (see Fig. 301). Based on those reviews, some changes to the original design drawings were done in order to improve the construction.



Fig. 301. The new TRIUMF House.

Construction review

The regular and final construction reviews were done for the new ISAC-II facility. Reviews of minor construction projects managed by the department were also done.

Management of maintenance and repair work

During the course of the year approximately \$108,300 was spent on maintenance and repair work at various TRIUMF buildings and around the site. This included the annual maintenance and repair contract, interior and exterior painting, and upgrades to the parking lot and the parking lot access road.

Management of landscaping work

This year the Building department took over the management of the landscaped areas on site. This work consisted of the annual landscape maintenance contract and some additional landscape projects.

Drawing library maintenance and services

The department provided services of creating new and issuing existing drawings to many in-house clients. It also continued with organizing and updating the site and buildings drawing library.

ELECTRONICS SERVICES

Overview

Electronics Services had a productive year delivering services and products to the majority of the site. Our jobs run from the simplest cable assembly right up to vision based systems measuring wire chambers. Our services include maintenance of 340 PC systems, repairing a wide variety of electronics, assisting experimenters with specialized controllers, manufacturing special modules for groups, and working on CERN projects. A major project this year was installing the entire network communications infrastructure in ISAC-II. Electronics Services also initiated an Electronics Recycling Program that managed to keep approximately 15 tons of electronics garbage out of the normal waste stream.

Site Communications

Site communications was very involved with installation of the ISAC-II data network for the first 7 months of the year, from planning to consulting, pricing, contracting, purchasing, organizing, installing, testing and certifying. Installation consisted of more than 270 cables, comprising over 60,000 feet in length, providing about 500 data outlets. Savings for the site using our own internal manpower for installation was in the order of \$30–60 K. Other work included the consolidation, re-organization and relocation of the data

rack in the chemistry annex after the computing centre move to ISAC-II. There were lots of smaller jobs involving installation and reconfigurations for the RF group, Nordion, M15, 8π , Machine Shop and trailer Ss.

Technical Support

Major work for Technical Support this year was the completion of prototype and final versions of two CAMAC modules for the Controls group. These were DSP based 16-bit ADCs as well as the CAMAC power and diagnostic module. We are now supplying these in dozen lot quantities, which will result in substantial savings for the Controls group as well as vastly improved performance. Another job that was complete was the pair of precision interval gate generator modules built for LTNO. The proton therapy fast shutter system required a few revisions this year, and for TWIST the majority of the documentation was completed. TWIST also required the construction of a PLC based control system for their new TEC gas system. Late in the year a project for the support of the ISAC-II cryo tuner motor system was started.

PC Support/Desktop Services

PC Support, also known as Desktop Services, had a very busy year. PC hardware related tasks increased by 50% to 308 tasks. Software related jobs increased by 18% to 327 tasks, and network related activities decreased by 16% to 139. Although a record of the number of consultations provided by way of phone calls or walk-in requests is not maintained, it is likely similar to the previous year's total of 3000 consultations.

In 2003, virus protection migrated to the Symantec AntiVirus solution. This allows better control of the virus outbreaks and ensures that Windows PCs are receiving adequate protection. The installation base on the TRIUMF site has increased from 229 PCs to 340 PCs. A relocation of one of the offices provided a larger and more efficient working space. A project review process was implemented that keeps the group focused on all the tasks on hand. A number of projects are in progress, one being the Novell server NW01-DO, which is aging and should be updated. A review is under way to improve the reliability of this server. Desktop Services is also investigating a volume mirroring system that will eliminate dependency on our aging and out of warranty tape backup unit.

Electronics Repair Shop

By every measure, this was just an average year, with little activity of any special significance in the Electronics Repair Shop. Most effort was devoted to the repair and/or recalibration of a total of 185 electronic devices, including: 27 monitors/terminals (of which 2 were monochrome and the remaining 25 were

colour), 70 power supplies (comprising 17 NIM devices, 8 CAMAC devices, 34 high-voltage devices, and 11 other devices), 52 nucleonics modules (including 43 NIM units and 9 CAMAC units), 4 items of test equipment, and 32 other miscellaneous items of electronic equipment (mostly various controllers). Some time was also spent repairing the digital readout/controls for some machines in the Machine Shop, refurbishing high output power supplies for KOPIO, being instructed in the maintenance and checkout of the Sairem microwave power supply and source for the ISAC test stand, and the installation of some communications cabling in the Business Office and ISAC-II.

Electronics Shop

The Electronics Shop had a busy year working on a large variety of projects. As opposed to other years, there was no major project or experiment that required months of continuous assembly or cabling. One of the larger projects supported this year was assembling and modifying thyratron bias boards for CERN. For the Central Controls group, a variety of CAMAC modules were manufactured including the new 0946 ADC boards, 0918 power and diagnostics module, and some 0922 I/O gates to replace older units. A half dozen 4-channel visual scalars were manufactured for the Experimental Support group. A number of popular flow-switch units were assembled.

Experimental and Target Technical Support

Most of the year was spent working on the CERN contribution which entailed the assembly and testing of the switch tanks, uniting these with the PFN units, followed by HV testing and a number of modifications. Another job was working on the MuLan kickers for PSI. Site support went to 1AT1 and 1AT2, and the ISAC ITE for which some repairs were also needed in the thermocouple system. Work commenced on the SCRF cryo tuner enclosure and control system.

High Level Software Support

The year included several projects for a variety of groups at TRIUMF. The TIGRESS DAQ system was built using MIDAS and JACQ, and the prototype detector was successfully mapped. This experience helped in creating a DAQ interface to the TWIST TEC gas handling PLC, which was integrated into MIDAS by porting the EPICS Modicon PLC device driver. Some of this work was presented in a talk and poster at the RT2003 conference in Montréal.

For the μ SR group, work continued on solving the M15 separator controls problems, only to be met with a fire in one of the 400 kV power supplies, and a very fast fix with an almost compatible spare. A network based heater controller was integrated into the CAMP

system, and the HiTime motor controller was installed in M15 with a user interface based on JACQ. A new motor driver module was developed for the μ SR cryostat valve controls, and improvements were made to the driver software. A complete rewrite of the magnet survey system was started, to replace the software running on an obsolete DECStation 5000.

Work in ISAC included installation of new device servers for MIDAS systems, changes in the LTNO DAQ system, the new DRAGON ladder target mechanism, and assisting the experimenters on Expt. 920. Further progress was made in constructing the cavity washer for the SCC of ISAC-II. New motor drivers were designed for the slits and jaws in the ISIS beam line and ISAC CSB beam line. Motor controls were installed in the ISAC target conditioning box.

Some work was done in investigating imaging tools for the KOPIO wire chamber inspection system. This involves image capture, analysis and data extraction.

ELECTRONICS DEVELOPMENT

The ISAC control system installation and design accounted for most of the group's effort again this year. A substantial amount of work also went into developing and building specialized modules for TITAN, as well as the fourth revision of the data acquisition board (DAB) for CERN. A member of the group, as part of the quality assurance task force, helped to develop the TRIUMF QA program. Three members of the group attended the International Conference on Accelerator and Large Experimental Physics Control Systems (ICALEPCS) in Gyeongju, Korea. One co-op student was supervised between February and August.

ISAC Support

The group continued to provide all the hardware installation, maintenance and upgrade support for the ISAC control system. An additional 30 CAN-bus modules for power supply control were installed in the CSB. With the development of a new VME 8-channel ADC/1-channel DAC module, the VQSX can be replaced for use with the RPMs potentiometer readback, and for emittance measurements.

The relocation of the SCRF test lab from BC Research to the ISAC-II clean room required the system to be disassembled and reinstalled. In addition to the original equipment, five 2-channel heater control modules were designed, built and installed for the ISAC-II cryomodule in the SCRF.

Several specialized modules were designed for TITAN. Four 8-channel ± 40 Vdc VME power supply modules will set the trap potential. A second VME module will provide 6 channels of up to 500 Vdc for setting the trap extraction potentials. The timing for

controlling the trap and extraction is performed in another VME module. Due to space constraints of the test facility, three rack mount enclosures were built to house the 32 CAN-bus controllers.

A small EPICS/PLC system for a target evaporator was completed.

A test EPICS/PLC system was implemented to monitor an rf amplifier. This system gave us an opportunity to evaluate Modicon's newest I/O modules (Advantys) for ISAC-II.

With assistance from a BCIT co-op student, a module was built for synchronizing the pump laser pulses to the 3 TiSa lasers.

Maintenance activities included repair of malfunctioning components, as well as continued development of procedures and a test facility for TRIUMF built devices. All modules are asstet, recorded and tracked in the new Asset database.

CERN

The digital acquisition board (DAB) entered its fourth revision this year. With CERN's decision to move to VME-64x, considerable modifications were required to support this standard. Additional specifications have also been added to the requirements.

Engineering Support

The group took over the tasks of replacing pressure flow sensors and adding paddle wheel sensors during the rework of T1/T2, when a member of the Electronics Services group fell ill.

The Magnet/Kickers group continued to receive assistance with engineering and prototyping for their PSI kicker. A control card for sequencing the HV stack was designed. Additional control and interlock modules were designed and built for the four rack system. Several iterations of the HV FET module were required, as more knowledge was gained with the system.

Engineering expertise with PLC and EPICS based systems was provided to the Safety group. Technical advice was also supplied to two co-op students with other groups.

Experiment Support

Five high voltage modules along with a test carrier board were designed and built for KOPIO. This module was based on a PSI design.

For the μ SR group, an I- μ SR NIM logic module was designed. This module will replace the equivalent of more than a complete NIM crate of electronics, and will greatly simplify the set-up of these types of experiments. It is a complementary match to the VME based Gate Logic Board that the group developed last year.

The group assisted in the evaluation of a silicon strip detector as part of a ΔE - E telescope for the DRAGON facility.

Secondary Channel Support

The M15 vacuum system was successfully moved into the BL2A PLC system, allowing the M15 beam line to be fully supported by the EPICS based secondary channel control system. The control of the new M13 jaw was incorporated into the existing M13 secondary channel motor controller.

New Hardware Designs

Several new modules were designed and built:

- A second revision of the water flow monitoring module with CAN-bus readout was built and tested. Two modules are currently installed in T2 and the conditioning station.
- A VME based 8-channel programmable gain normalizing module for the NPDGamma experiment at Los Alamos.
- A VME based frequency synthesizer for generating complex modulated, multi-frequency waveforms for the β -NMR group.
- A module to house the MZ104 IOC along with an Ethernet serial converter forming a cohesive PC104 IOC.
- A non-volatile memory enhancement for the new EPICS VME-x86 based IOC (Mariner).
- A HV switch driver module and a HV switch interlock module for the TiSa laser.

Infrastructure

In an effort to facilitate compliance with QA requirements, the group's Web-based REA tracking system was completely redesigned. It now uses the open-source relational database system PostgreSQL. REAs and associated QA documents can be tracked and relevant information is distributed by e-mail. The group's written QA procedures are being updated to comply with the TRIUMF standard operating procedures.

A Linux based firewall was added to protect the group's computer network, especially the fileserver.

The group decided to migrate towards the use of Mentor Graphics Expedition for schematic and PCB layout. The current Protel tools do not handle the iterations required with complex programmable logic devices. This move requires a substantial effort in creating libraries of components which had previously been created over the years for the Protel tool.

CERN COLLABORATION

INTRODUCTION

TRIUMF's collaboration with CERN on producing accelerator components for the Large Hadron Collider (LHC) is another year closer to completion. For the period 1995–2005 the contribution that TRIUMF is coordinating on behalf of Canada is worth \$41.5 million. The highlight of the year was the completion of the largest part of this contribution, the contract with ALSTOM Canada Inc. for the fabrication of 52 twin-aperture quadrupole magnets. The first prototype magnet was delivered to CERN in May, 1998, and the 52nd series magnet was delivered in August, 2003.

The other large contribution consists of components for the LHC injection kicker systems. The five resonant charging power supplies are complete and were acceptance tested this year. Four of the supplies were shipped to CERN in the container that was previously used for shipping the ATLAS calorimeter modules. The fifth supply will remain at TRIUMF for final testing of the pulse forming networks (PFNs).

High voltage testing of the 9 PFNs and the 20 switch tanks was started in 2003, and 5 of the PFNs and 10 of the switch tanks were successfully tested by the year-end. Shipment of the PFNs to CERN will start in March, 2004 and take about a year to complete with the turn-around time of the container.

The other hardware project is the design of the data acquisition boards for the LHC beam pick-up monitors. The third prototype version, DABIII, was delivered to CERN in 2002 for testing. The specification of the fourth and hopefully final version, DABIV, was completed during 2003. This version will be compatible with the newly adopted CERN VME64x standard and requires a new FPGA chip with more memory and increased processing power. At year-end it was in the final stages of design, with 5 prototype modules to be delivered to CERN by May, 2004. Eventually about 1200 of these modules are required and there are still discussions with CERN on how this can best be achieved.

Two beam dynamics efforts continue to be supported. The beam optics and collimation work became a high priority for CERN this year and much effort was made by the LHC collimation project team, including the TRIUMF beam physicist, to develop a final design. New criteria for the collimation scheme, increased space for longer collimators and decreasing the contribution by the collimators to the ring impedance, had to be incorporated into this design. Final designs of the betatron collimation section IR7 and the momentum collimation section IR3 were established by year-end.

The study of beam-beam interactions between the LHC beams at the collision points, which uses a sim-

ulation code developed at TRIUMF, is very computer intensive. This year, use of a small Linux cluster at TRIUMF and a larger system in Edmonton allowed further simulations to be carried out. The plan is to migrate this task to the WestGrid facility in 2004.

More details of the LHC work can be found in the following sections.

BEAM DYNAMICS

Beam Optics and Collimation

During the first half of 2003, exact agreement was demonstrated between the CERN tool for predicting collimation efficiency and the local code (DIMAD-STRUCT). The discrepancy reported in 2002 was attributed to the different treatment of off-momentum halo particles.

Subsequently, some important changes in optics and layout were made in the LHC *betatron* collimation insertion (IR7). In close collaboration with the LHC collimation project and optics team leaders, around 10 solutions for the IR7 were examined, both very old versions (dating back as far as 1998), and more recent lattices (late 2003). The main objectives were: 1) to generate additional space for longer collimators (4 m per secondary, instead of 0.7 m in the old design); and 2) to maximize the β -functions at the collimator jaws and thereby decrease the contribution of collimators to the ring impedance.

The low-impedance requirement represents a conflict with previous requests. A good cleaning efficiency and aperture had to be simultaneously maintained, which led to a severely constrained optimization problem. The code Distribution of Jaws (DJ) was modified so that, for a given optics and collimators, the impedance is computed and minimized along with the usual halo related quantities.

With collimators occupying as much as 40% of the total available space in IR7 (128 m of total 341 m), and in some cases being inserted between two warm quadrupole modules, each new collimator distribution also requires shifts of warm modules (up to 10 m). For each case, the optics rematching was done at TRIUMF, while the (tracking) efficiency was tested at CERN.

As a result, the initial design approach was confirmed. The final IR7 optics chosen (Fig. 302) is very close to the previous LHC version 6.4 and preserves the number of collimators and warm quadrupoles, and the maximum voltage of the power supplies. The new optics provides larger betatron phase advance across the insertion, and the wider domain of phases at intermediate locations makes possible the positioning of collimators at positions of higher $\beta_{x,y}$.

Longitudinal layout

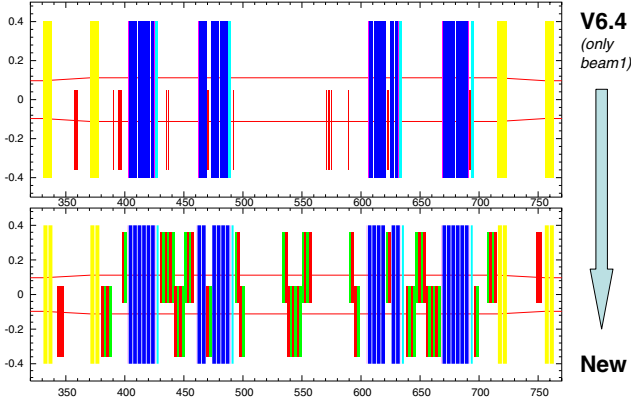


Fig. 302. Layout of the IR7 cleaning insertion. The MQW quadrupoles are shown in dark blue.

In addition, a single revision was made to the *momentum-collimation* insertion (IR3): two of the original six collimators were eliminated and the remaining four secondary collimators were set at new locations and rotation angles computed with DJ.

Coherent Beam-Beam Effects in the LHC

Our study of beam-beam interactions in the LHC seeks to identify potentially unstable coherent modes excited by the electric forces between counter-rotating bunches of protons as the two beams meet and cross in the collision regions. Large-scale multiparticle simulations are a principal tool in this type of investigation and in 2002 our beam-beam simulation code BeamX became one of the first to include a fully 3-dimensional model of the collision process. Of necessity this involved parallelizing the code and finding suitable parallel computing resources.

This year we made extensive use of a small Linux cluster at TRIUMF, and the University of Alberta Physics Department's THOR cluster which offered more advanced communication hardware, in order to debug, optimize, validate, and extend the BeamX code. With the basic longitudinal effects (phase oscillations, density variation, hourglass effect) already in place, we added the treatment of the beam-beam crossing angle, which affects the strength of the beam-beam force and introduces synchro-betatron coupling, resulting in sidebands in the coherent spectrum (Fig. 303).

Since BeamX has several output streams and can produce typically ~ 50 Mbytes of data per run, the logistics of run management and documentation becomes an issue, especially when doing simultaneous runs in Vancouver and Edmonton, and analyzing the results at CERN. To ease this, a working protocol was developed which uses tools such as ssh, rsync, and Matlab, to configure and propagate the simulation runs, and to store, process, and replicate the data.

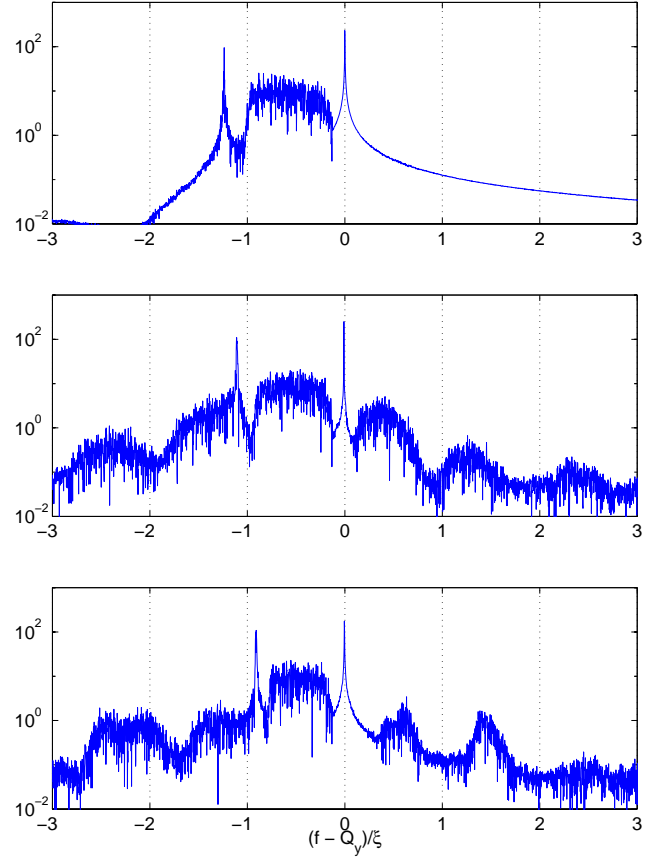


Fig. 303. BeamX: spectra (FFT of beam centroid) for 0, 100, and 300 μr beam-beam crossing angle.

For optimization, the main concern was to minimize interprocess communication bottlenecks and thereby improve the parallel efficiency. The arrangement of master-slave and slave-slave message passing (see Fig. 304) was further generalized to have the least possible dependency on message ordering. This yielded some improvement, but there is still some under-utilization

BeamX Data Flow

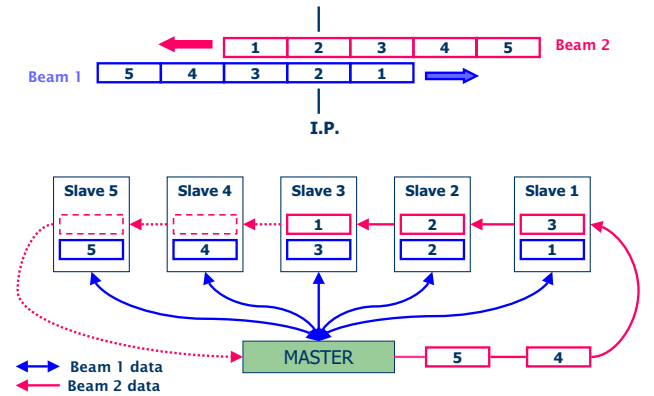


Fig. 304. BeamX: mapping of beam-beam interaction to parallel process and inter-process communication.

of processors due to the large volume of particle coordinate data being transmitted and to unequal load-balancing between processes.

In 2004 we expect to migrate the computing task to the new WestGrid facilities, which include a large multiprocessor shared-memory system that will be an alternative to the message passing approach, given the program's memory-intensive requirements. Evaluating this and other WestGrid platforms will entail further development, profiling and benchmarking exercises. This should yield better knowledge about the program behaviour and about which parallel architecture will best allow us to explore the parameter space of beam-beam collision scenarios contemplated for LHC operation.

CONTROLS AND INSTRUMENTATION

LHC Orbit System Components

The DABIII data acquisition boards delivered and tested at CERN in fall, 2002 were a consolidation of the DABII design with minor hardware modifications. The subsequent request for a VME64x compliant DABIV module with a substantial increase in processing power and memory requirements necessitated the adoption of a new higher density "Stratix" Altera chip set with 10 times the internal memory. Additional module requirements included: JTAG compliant multidrop "scan bridge" interface for module testing, 2×12 -bit look-up tables for beam current transformer (BCT) integrator, and for trajectory data normalization, auxiliary post-mortem memories, VME64x compliant interface and 64-bit data transfers, extra registers for system auto configure, flash memory for power-up configuration, and a new EMC/ESD front panel. After a flurry of activity to define these requirements, work on this project stalled for most of the year due to manpower constraints. Minor progress was made on debugging existing code running in the DABIII and analyzing the VME64x specification to determine additional hardware requirements for the new DABIV module. It is anticipated in 2004 to procure new hardware, redraw module schematics, lay out the new PCB, rewrite embedded control firmware and fabricate 5 prototype modules for delivery to CERN in May. An additional 30 modules will be delivered for beam tests in September.

MAGNET DEVELOPMENT

The largest piece of TRIUMF's contribution to the LHC was completed in August, with delivery of the last of 52 twin-aperture quadrupole magnets to CERN. Seventeen magnets were delivered in 2003. These warm magnets (48 plus 4 spares) will be installed in the two beam cleaning insertions of the LHC, where heating by

lost beam prohibits the use of superconducting coils. The so-called MQW magnets, based on a CERN design, were fabricated by ALSTOM Canada Inc. (Tracy, Quebec) with considerable input and design assistance from TRIUMF and CERN engineers. Their small apertures (46 mm) and high gradient (35 T m) meant that the 3.4 m long modules had to be assembled with unusually high tolerances to achieve the necessary field quality.

A prototype magnet was completed and shipped to CERN in May, 1998 for mechanical and magnetic field measurements. As these measurements showed that the desired field quality had not been achieved, improvements were made in the lamination design, in the punching precision, and in welding the stacks of laminations without distortion. Stronger stacking tables and a separate half-magnet assembly table were also constructed. These changes led to the first series magnet completed in March, 2001, fully meeting specifications. ALSTOM then proceeded to meet and eventually surpass their planned production rate of two magnets per month.

Figure 305 shows the delivery schedule for the 52 magnets relative to the estimated schedule of 2 magnets/month. Figure 306 shows the last delivered

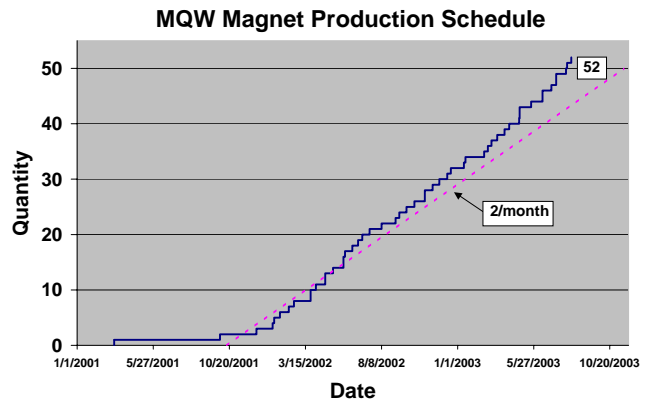


Fig. 305. Delivery schedule for 52 magnets.



Fig. 306. Last delivered magnet with ALSTOM team.

magnet together with the ALSTOM team that produced it. Mechanical measurements were carried out at the factory to qualify the magnets prior to shipping, with detailed magnetic field measurements being made at CERN.

KICKER MAGNETS

In collaboration with CERN, TRIUMF has designed and built all of the resonant charging power supplies (RCPSs), pulse forming networks (PFNs), thyatron switch tanks and dump switch (DS) termination resistors for the CERN LHC injection kicker systems. The kicker magnets and associated terminating resistors are being built at CERN. Each of the two LHC injection kicker magnet systems must produce a kick of 1.3 T m with a flat-top duration variable up to $7.86 \mu\text{s}$, and rise and fall times of less than 900 ns and $3 \mu\text{s}$, respectively. A kicker magnet system consists of four 5Ω transmission line magnets with matching terminating resistors, four 5Ω PFNs and two RCPSs. The combination of ripple and stability in the field from all kicker system components must be less than $\pm 0.5\%$.

RCPS

An RCPS has two parallel outputs to charge two 5Ω PFNs up to 66 kV. The RCPS is designed so that the PFNs can be charged up to 66 kV in less than 1 ms at a repetition rate of 0.2 Hz. Six RCPSs, including the prototype, have been assembled and tested at 66 kV on 2 dummy loads at TRIUMF. The prototype RCPS has been extensively tested at CERN. Representatives from CERN visited TRIUMF in May and carried out successful acceptance tests with 2 of the RCPSs and 2 PFNs. Four of the RCPSs were shipped to CERN and received on December 19. One RCPS remains at TRIUMF in the kicker HV test lab to be used for completion of the HV tests on the PFNs. Figure 307 shows 5 completed RCPSs ready to ship.



Fig. 307. Five RCPSs completed and ready for shipment.

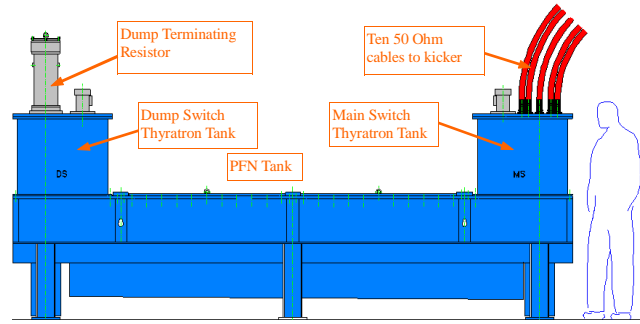


Fig. 308. PFN with thyatron switch tanks, dump switch terminating resistor, and HV cable.

PFN

Each 5Ω PFN is composed of two parallel 10Ω lumped element delay lines; each line consists of a 4.3 m long precision wound coil, with high voltage and high current capacitors and damping resistors in parallel with the coil. There is a thyatron switch tank at each end of the 5Ω PFN (see Fig. 308).

Nine PFNs were built in 2001 and tested at low voltage in 2002. High voltage testing began in 2003. Five PFNs, 10 switch tanks and 5 terminating resistors have been completely HV tested. The high voltage tests on the remaining 4 PFNs will be completed by the end of February, 2004. Figure 309 shows

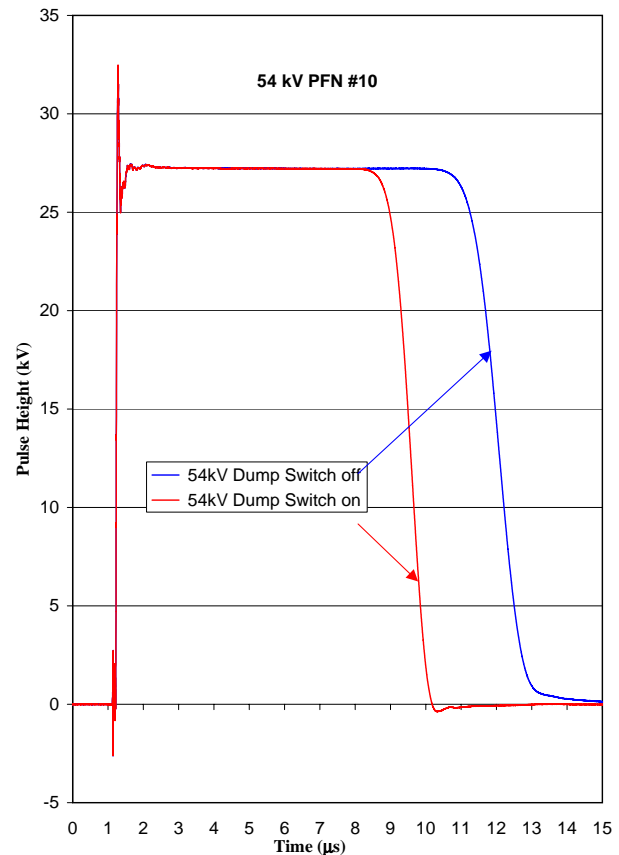


Fig. 309. 27 kV pulses from 54 kV PFN tests with and without triggering the dump switch thyatron.



Fig. 310. 5 PFNs have been tested at high voltage and are ready to ship to CERN.

27 kV pulses obtained from 54 kV PFN tests. The maximum variation in absolute pulse heights in the 5 PFNs tested so far is $\pm 0.08\%$.

Two PFNs with their switch tanks mounted have been assembled with locking bars in place and foam padding installed above the Ω shields and are ready for shipping. Figure 310 shows a photo of the PFNs ready to ship.

Thyratron Switch Tanks

All 20 thyatron switch tanks, which mount on the ends of the PFN tanks, have been completed (Fig. 311). The main switch thyatron will connect to a $5\ \Omega$ transmission line kicker magnet via 10 parallel $50\ \Omega$ coaxial cables, and the kicker magnet output is connected to a $5\ \Omega$ resistive terminator. A $5\ \Omega$ resistive terminator is mounted on top of the DS tank (Fig. 312). Each switch tank contains a bias board that puts a dc bias on each of 2 thyatron grids. TRIUMF has designed, built and bench tested 37 bias boards; 20 of these have been installed in the thyatron switch tanks at TRIUMF, and 14 have been sent to CERN to be used in the MKE (SPS extraction) system. However, when high voltage tests were carried out at CERN and TRIUMF, there was a failure in the bias board at between 25 kV and 30 kV PFN voltage. The failure, which was a voltage to frequency converter integrated circuit, did not prevent operation, but did prevent the read-back of the grid #1 bias voltage via the voltage to frequency converter and a fibre optic link. The bias board “ground” has a 30 kV transient imposed on it with a 30 ns transient time. After many trials and re-arrangements of “ground” circuitry and added filtering, a final successful design was obtained at TRIUMF, such that there have been no further failures in the 10 switch tanks that have been tested at 60 kV.

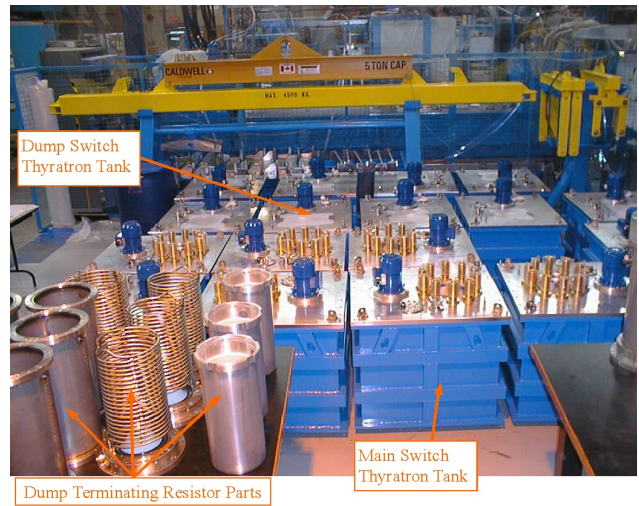


Fig. 311. Thyatron switch tanks assembled.

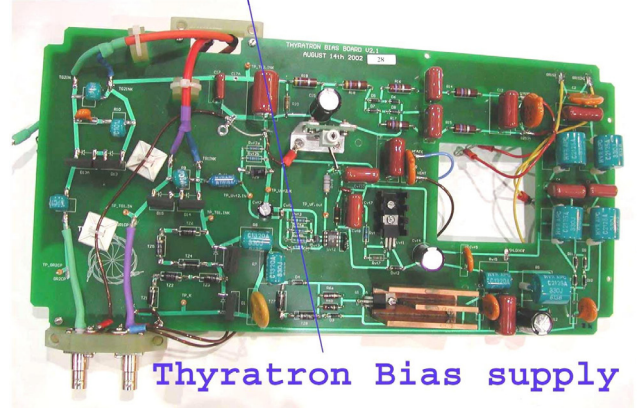
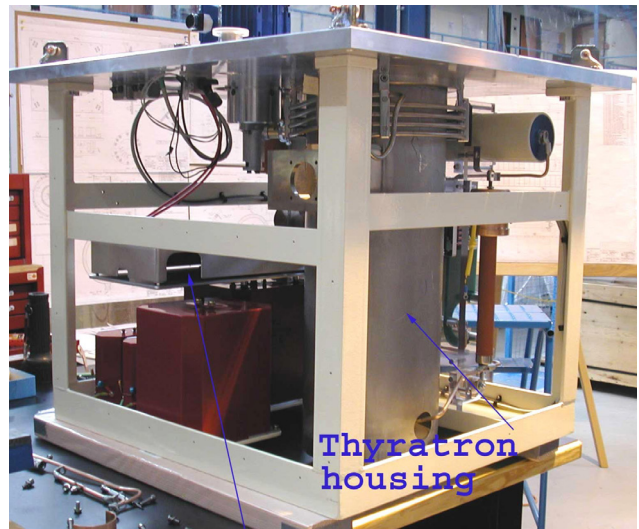


Fig. 312. Modified bias board and internal parts of thyatron switch tank.

Shipping Container

The TRIUMF ATLAS shipping container was generously donated to the Kicker group after the last shipment of the ATLAS detector components from TRIUMF to CERN in 2003. The roof and door of the container have been modified for shipping of kicker components. A new shock absorbing frame was designed and installed in the container. The shock absorbing frame

was designed to allow for shipment of the 4 RCPSs in the first shipment, which left TRIUMF in October, and to allow for shipment of 2 PFNs at a time in subsequent shipments. The turn-around time for the container is approximately 3 months. PFN mounting clamps will be fabricated in early 2004 and the first shipment of 2 PFNs will occur in early March, 2004. The final shipment will be in early March, 2005.

TECHNOLOGY TRANSFER DIVISION

INTRODUCTION

The Technology Transfer Division at TRIUMF is responsible for the commercial interactions for the laboratory. It is composed of a small group dedicated to optimizing the commercialization technologies emanating from TRIUMF research, plus the Applied Technology group that is responsible for the operations of the on-site commercial cyclotrons on behalf of MDS Nordion.

TECHNOLOGY TRANSFER

The mandate of the Division is the pursuit of all financially and technically viable opportunities for commercializing technologies emanating from the research at TRIUMF. This mandate must recognize the preeminence of the scientific research at the laboratory, and proceed in a manner that optimizes the impact on TRIUMF and the Canadian economy while minimizing the impact on scientific activities at the facility.

The current Contribution Agreement between National Research Council (NRC) and TRIUMF includes the requirement for TRIUMF to enhance its impact on the Canadian economy. This impact is measured through the benefits provided to Canadian industry, both through the transfer of TRIUMF's technical knowledge and through its purchasing practices.

APPLIED TECHNOLOGY GROUP

500 MeV Isotope Production Facility

During this year, the 500 MeV irradiation facility received 326.46 mAh. Eight targets were irradiated, six targets delivered to produce $^{82}\text{Sr}/^{82}\text{Rb}$ for MDS Nordion.

CP42 Facility

The total beam delivery for 2003 was 737 mAh. The weekly beam delivery graph is shown in Fig. 313 and the quarterly time evolution of the beam delivery is shown in Fig. 314. The downtime and maintenance statistics are analyzed in Fig. 315 and compared with the TR30-1 and TR30-2.

Work is still proceeding on the CP42 control system upgrade.

TR30-1 Facility

The total beam delivery for 2003 was 3024.5 mAh. The weekly beam delivery graph is shown in Fig. 316 and the quarterly time evolution of the beam delivery is displayed in Fig. 314. The downtime and maintenance statistics are analyzed in Fig. 315.

ATG replaced the north high current target station for palladium production (1B) with the new radiation hard type.

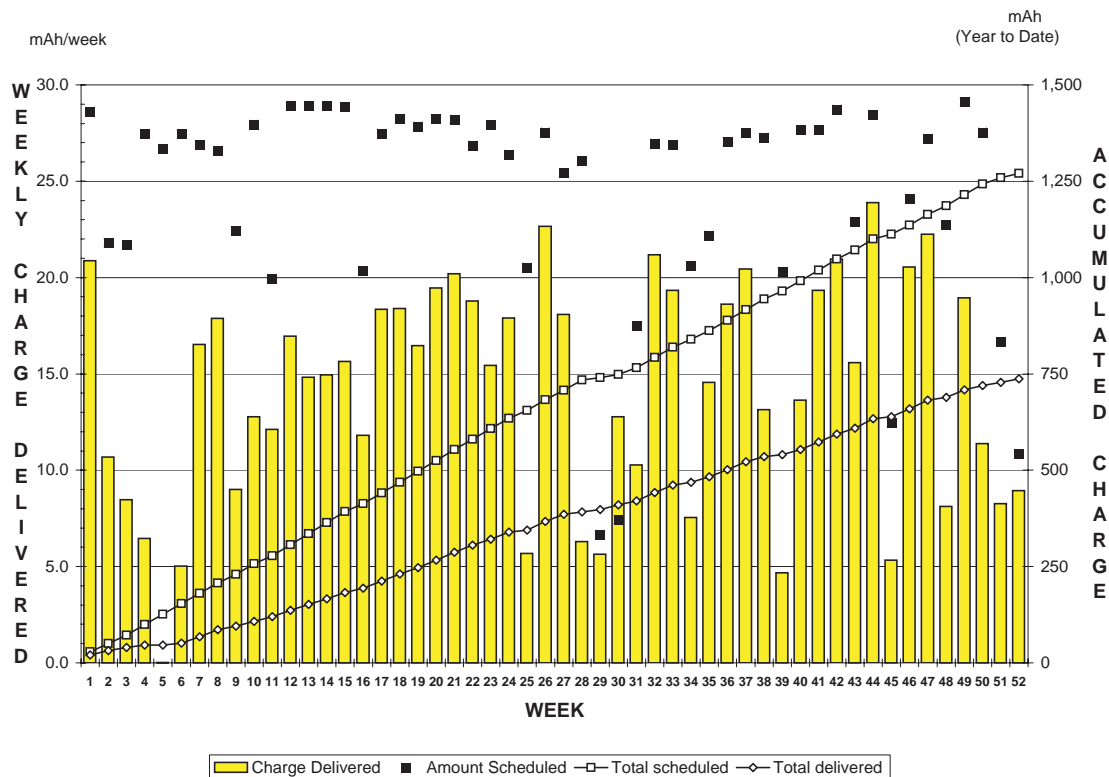


Fig. 313. Weekly beam delivery for the CP42.

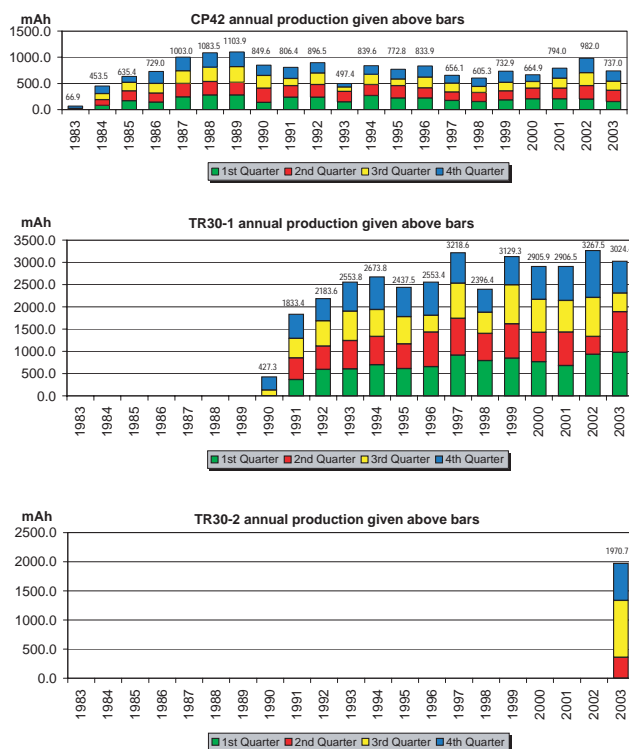


Fig. 314. Quarterly time evolution of the beam delivery for the CP42 (top), TR30-1 (middle) and TR30-2 (bottom).

TR30-2 Facility

A new TR30 industrial cyclotron was installed and commissioned. High beam current irradiations started in June. Two solid target stations and one gas target system are available for medical radioisotope production. Currently, the TR30-2 produces mostly ^{103}Pd at beam currents of up to 500 μA .

The total beam delivery for 2003 was 1970.8 mAh. The weekly beam delivery graph is shown in Fig. 317 and the quarterly time evolution of the beam delivery is displayed in Fig. 314. The downtime and maintenance statistics are analyzed in Fig. 315 and compared with the CP42 and TR30-1.

ATG Development Projects

ATG is working towards a consolidation of the cyclotron control rooms. The CP42 and TR30-1 controls are scheduled to be moved into the TR30-2 control room by the end of 2004.

Improvements to the existing collimators in solid target stations are in progress. The new design uses collimator heads manufactured from a specific high strength tantalum-tungsten alloy.

Collaborations are ongoing with the University of Sherbrooke, Quebec, and the University of Washington Medical Center in Seattle.

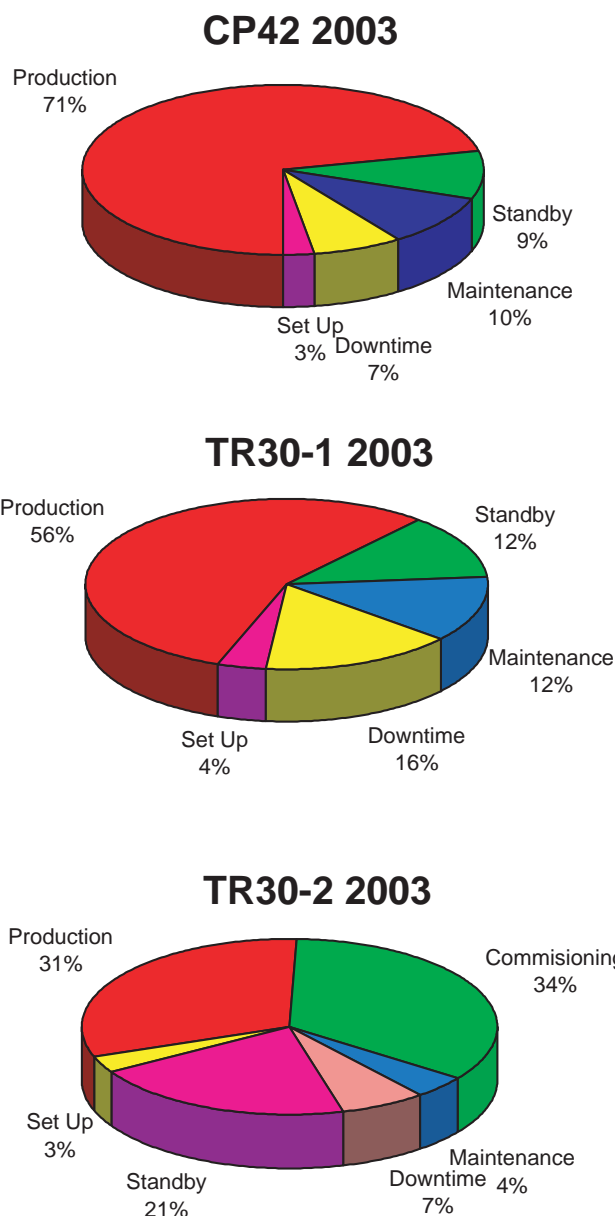


Fig. 315. Breakdown of downtime and maintenance for the CP42 (top), TR30-1 (middle) and the TR30-2 (bottom) during operational hours.

RADIOISOTOPE PROCESSING (MDS NORDION)

During the year 2003, MDS Nordion commissioned a new 30 MeV cyclotron and commenced production operations using it. MDS Nordion now has 3 operating cyclotrons on-site dedicated to isotope production.

The main isotopes produced and shipped in 2003 were iodine-123 used for thyroid imaging and research, palladium-103 used in prostate brachytherapy, and indium-111 used for monoclonal antibody imaging.

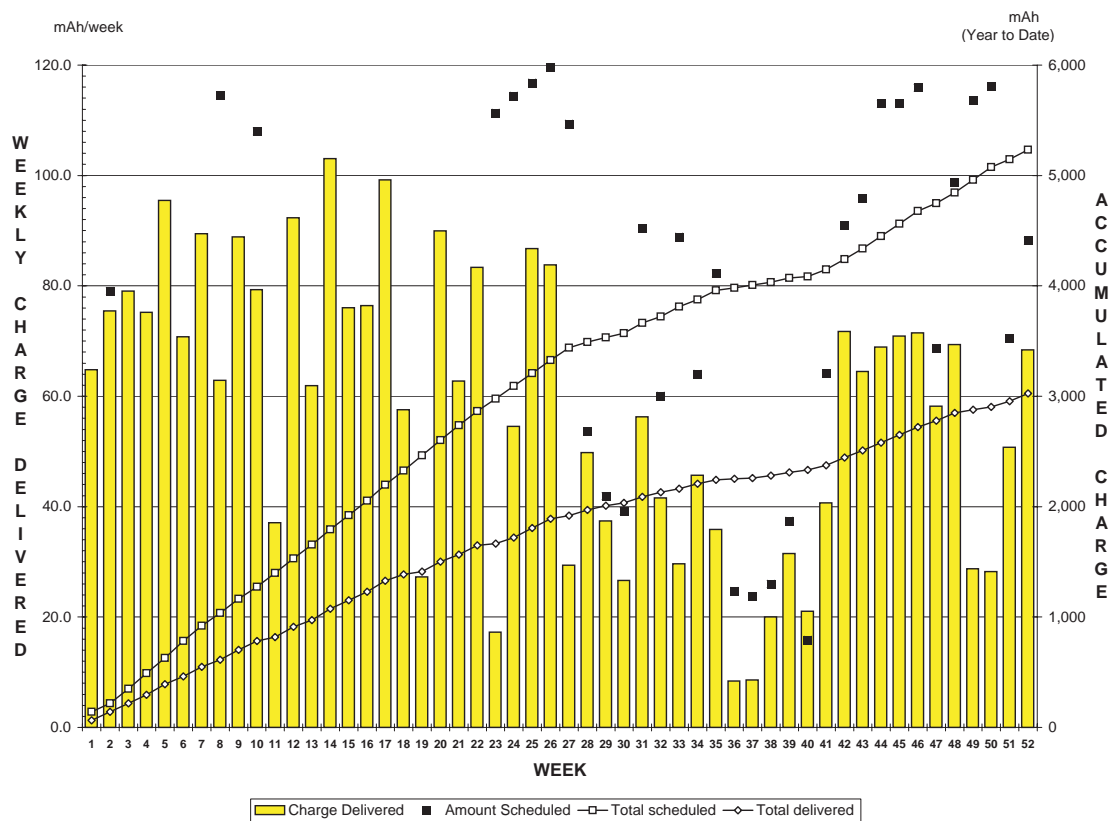


Fig. 316. Weekly beam delivery for the TR30-1.

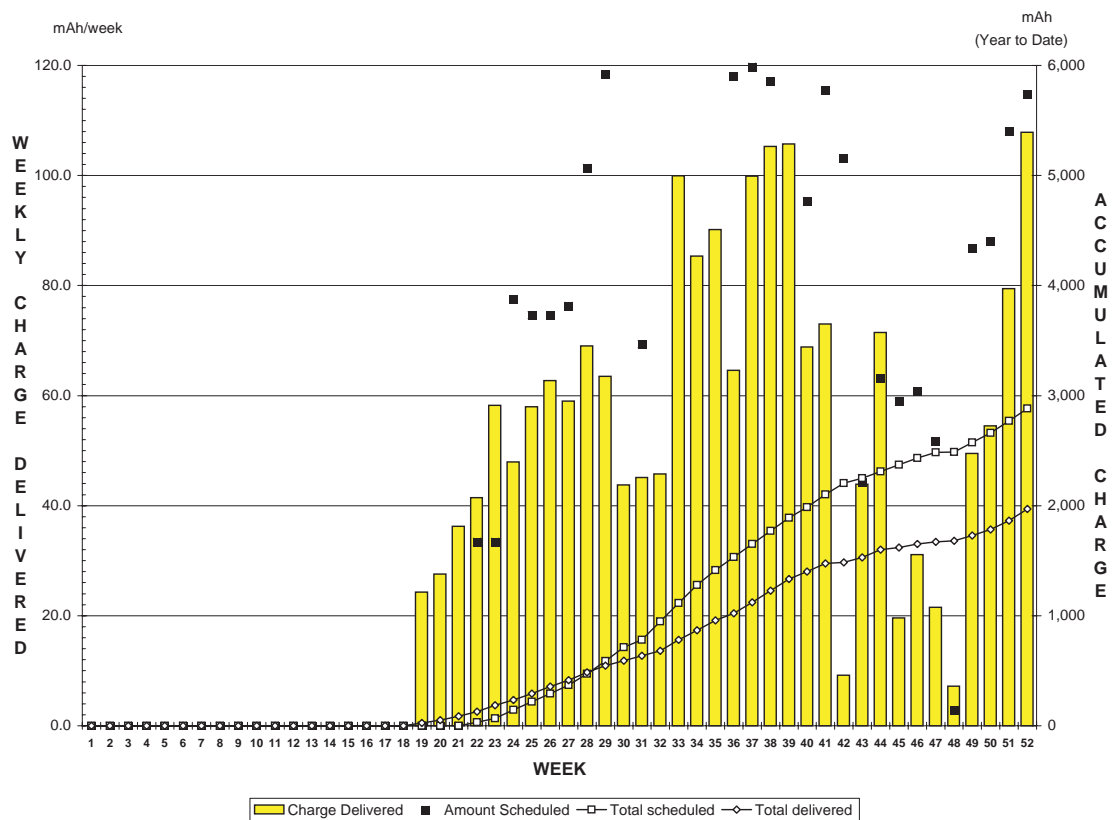


Fig. 317. Weekly beam delivery for the TR30-2.

ADMINISTRATION DIVISION

INTRODUCTION

The Administration Division is made up of Human Resources and Administration, Accounting and Materials Control, Administrative Computing, and Safety. The manager of each group reports to the Director. A summary of Division activities is included in this report.

HUMAN RESOURCES AND ADMINISTRATION

All employees are reviewed for performance on an annual basis. The period covered for Performance Planning and Review coincides with the calendar year.

TRIUMF has a very strong student program and hires on average some 35 summer students per year in addition to approximately 10 university co-op students who are hired each term.

In 2003, TRIUMF established the Researcher Emeritus position. It is intended to mark the past accomplishments of retired researchers and to express TRIUMF's appreciation for the willingness of those persons to continue to be active in research-related activities at TRIUMF.

Both short term and long term visitors are now being tracked. All long-term visitor information is collected, such as their home institution, length of stay, contact person at TRIUMF, radiation badge, and keys issued.

The TRIUMF security card access system is working well with approximately 900 active security cards. The Canadian Nuclear Safety Commission conducted a security audit in September and they were quite satisfied with the security measures that TRIUMF has undertaken. All employees and long-term visitors are required to wear a photo ID card. All short-term visitors, those visitors of less than three weeks, are required to wear a Visitor badge. Security guard coverage continues between 6:00 pm and 6:00 am on working days with twenty-four hour coverage on weekends and statutory holidays. All vehicles accessing the site behind the security fence are required to have a permit.

As a condition of TRIUMF's operating licence, the Canadian Nuclear Safety Commission (CNSC) required TRIUMF to submit a Preliminary Decommissioning Plan (PDP) to the CNSC that would provide an outline of the general process by which the facility could be decommissioned, the approximate schedule for the decommissioning, and an approximate cost for the decommissioning. This PDP was completed in 2003.

The insurance program was renewed with an approximate 25% increase in premiums over the previous

year as a result of market conditions. Third party liability coverage remains at \$50 M. All buildings operated by TRIUMF are owned by the University of British Columbia and insurance coverage for these buildings and contents are covered by the Canadian Universities Reciprocal Insurance Exchange (CURIE).

There are currently five full members and seven associate member universities in the Joint Venture. Effective April 1, the University of Guelph became an associate member. Each full member university has two voting members on the Board of Management. Two additional voting members are appointed by the Board from the private sector. The associate members each retain one non-voting member on the Board.

TRIUMF has an Operating Committee (OPCOM) that is made up of representatives from the full member universities along with representatives from the TRIUMF users community and staff.

TRIUMF must now comply with Federal Treasury Board requirements under a results-based Management and Accountability Framework. The purpose of this framework is to establish a mechanism to help the National Research Council (NRC) and TRIUMF: i) collect performance information related to this initiative; ii) track delivery of commitments and reporting; iii) describe how the success of TRIUMF will be evaluated over time; and iv) provide direction for ongoing and future planning. No Management and Accountability Framework was required to be submitted in 2003 due to the reports submitted by TRIUMF to the NRC in support of TRIUMF's 5 year funding request for the period 2005–2010.

In 2003, TRIUMF entered into a construction agreement with Polygon Construction Management Ltd. for the construction of a new housing facility. The new TRIUMF House will offer modern amenities in a soundproof environment that will ensure visitors to TRIUMF enjoy their home away from home. The project is expected to be completed in late 2004.

ENVIRONMENTAL HEALTH AND SAFETY

Licensing

A licence to commission the new MDS Nordion TR30-2 cyclotron was obtained in early February and an application for routine operation was submitted to the Canadian Nuclear Safety Commission (CNSC) by the end of that month. After a successful commissioning period an amendment to the TRIUMF Operating Licence was issued that includes the TR30-2 as one of the family of accelerators operated by TRIUMF.

A Preliminary Decommissioning Plan was submitted to the CNSC in early February in order to satisfy a

new regulatory requirement. Extensive comments were received from the CNSC in late May and the plan was revised to take account of these comments. The report was then resubmitted in early December. At its November meeting, the TRIUMF Board of Management was charged with obtaining the requisite stakeholder approval and financial guarantees.

A revised set of Quality Assurance documents were also submitted for review to the CNSC in early February. Again detailed comments were returned to TRIUMF by the end of May. The QA documentation was revised accordingly and submitted for internal approval by the TRIUMF Division Heads. In the meantime planning continued for the implementation of the Quality Assurance Program. Phil Jones was appointed as QA manager and an internal assessment team was selected. A workshop on QA Assessment was organized to train the team. The team prepared an internal audit schedule for 2004 with the help of TRIUMF Division Heads. On November 13, an orientation session was held to introduce the program to all TRIUMF supervisory personnel.

The CNSC conducted several inspections of TRIUMF during 2003. The first, in February, focused on the Operator Training Program. The inspection found several positive aspects of the development of the training program. However, they requested that an action plan be submitted to indicate milestones and completion dates for various aspects of the program development. The action plan was put together by Phil Jones, in his capacity as TRIUMF Training Coordinator, and the various operation group training coordinators.

Another CNSC inspection focusing on security was conducted in September. The inspector found that TRIUMF security measures were appropriate to the level of risk.

A third inspection on the topic of emergency preparedness, emission monitoring and waste management was carried out in October. The inspection report included many positive findings but also raised a number of issues regarding documentation of procedures and the requirements for drills and exercises. Several minor technical issues regarding the environmental sampling and effluent monitoring were also identified. TRIUMF must respond to these findings by February, 2004.

Personnel Dosimetry

The collective dose for TRIUMF personnel for the year 2003 was 475.7 mSv as measured by the direct reading dosimeter service. Table XLVIII shows the breakdown of the collective dose by various work groups. The collective dose was somewhat higher than for 2002, largely due to some major tasks such as the

Table XLVIII. Collective dose for TRIUMF personnel by group.

Group	Dose (mSv)	Fraction of total (%)	Median (mSv)
Applied Technology	150.9	31.7	3.8
Remote Handling	50.7	10.7	4.5
500 MeV Operations	40.8	8.6	2.3
Safety Group	30.1	6.3	1.6
RF Group	25.9	5.4	2.7
Vacuum Group	25.3	5.3	3.5
Plant Group	25.2	5.3	0.6
Beam Lines/Probes	19.2	4.0	0.9
Tech Support	17.6	3.7	2.2
Life Sciences	15.8	3.3	0.5
ISAC Operations	10.9	2.3	0.4
Science Division	8.0	1.7	0.06
Outside Contractors	3.4	0.7	0.02
Others	41.9	8.8	—
Total	475.7	100.0	0.6

replacement of the quadrupole triplet downstream of T2 in the high intensity meson beam line. ISAC continues to make a relatively minor direct contribution to the collective dose.

Occupational Health and Safety

All TRIUMF's Occupational Health and Safety Programs continued to run smoothly. The fire alarm system, sprinkler systems and fire extinguishers were all inspected and verified for 2004. The TRIUMF Accident Prevention Committee and the TRIUMF Housekeeping Committee instituted a new system of documenting both safety deficiencies and housekeeping deficiencies on a single form using Novell networking software. This will help manage day-to-day activities more efficiently, allowing organizing the information to best match TRIUMF's operation. A new Injury Reporting System for the First Aid Program is also nearing completion. The new system will help maintain more accurate statistics.

Worker pride at TRIUMF continues to improve in the workplace thanks to all those who help contribute to our Occupational Health and Safety Programs.

Training

The Radiation Safety Course was offered a total of five times in 2003 (January, May, July, September and November) with 52 trainees attending. 96% of the trainees successfully completed the course with an average of 90% on the final exam.

In February the CNSC evaluated the progress of the development of formal operator training programs at TRIUMF. The training was rated as B – Meets Requirements by the evaluators. The inspectors did raise a few action items regarding the training program, and

the program managers, along with the assistance of the training coordinator, submitted an action plan outlining the tasks necessary to complete the development and implementation of the training.

Interlocks and Monitoring

The TR30-2 Access Control System and Radiation Monitoring System were both commissioned early in the year. The Access Control System's functionalities were specified by the Safety Systems Group but the detailed design and construction were completed by outside contractors. The Radiation Monitoring System was purchased from a commercial supplier, then modified to meet the specific requirements of the TR30-2.

A final five safety-critical neutron/gamma detector pairs were installed outside the shielding of the proton hall and a series of Operators' procedures in response to safety-critical detector trips were drafted. A report will be written for each individual trip event. Each report will include an estimate of the maximum radiation field outside shielding (at licensed beam current) had the beam not been tripped off and a record of whether or not that radiation field exceeded 50 mSv/h.

Eight safety-critical detector trips occurred during the year and a report was written for each.

The Safety Systems Group convened Design Reviews of several proposals to develop new systems and expand existing ones. Proposals for review included the interlocking of the ISAC B1 electrical room to the 500 MeV Central Safety System and the interlocking of the ISAC DRAGON experimental area to the Ion Beam Safety System. Both projects are to be completed during the 2004 shutdown.

ADMINISTRATION COMPUTING AND COMMUNICATIONS

Management Information Systems

The MIS systems saw only incremental changes in 2003. The central server, an IBM eServer iSeries, which provides database, directory, application program, Web, and PC file-and-print services for TRIUMF Administration, had both hardware and software updates during the year; aside from increased performance, these updates were largely transparent to users.

Additional databases were implemented to support data-driven Web functions for site announcements, seminar scheduling and notification, and meeting room reservations; this last was integrated via XML with RoomWizard display panels for the ISAC-II meeting rooms.

More information from existing databases was made available to users via the Web, including the abilities to view the status of any project account, to view one's own travel order status, and to view one's own

(and one's subordinates) vacation entitlements.

No major changes were made to the Administration client system configurations (Windows 2000 based PCs).

Public Web Services

A new Web server, www.triumf.info, was installed and made available in 2003. The initial purpose of this server is to provide a better public information Web site, with content addressed more to the outside world than to TRIUMF employees and users; over time, it is intended that this site will become the default site for outsiders to access TRIUMF information.

The new site, which is Linux/Apache based, is largely database-driven, and uses information both in its local MySQL database and in the Administration DB2 database that resides on the Administration iseries server. One feature of this database support is the capability to show randomly selected current headline articles whenever the home page is loaded.

The new Web server is being used to provide additional site support functions, starting with those for the Science Division. In 2003, new interactive Web based tools were implemented to publish beam schedule information, and Web based forms for requesting beam time were under development.

New standardized Web utilities were developed to support conferences that are hosted and managed by TRIUMF. These utilities, which run on the admin.triumf.ca Web server, support conference registration, payment, and email notification functions. Conference Web sites now only need to provide links to these utilities, and no longer require these functions to be re-implemented on their own sites. The first conference to make use of these utilities is the NIC-VIII conference, which will take place in July, 2004.

Telephones

Major changes were made to the site telephone system in 2003. The central switch required expansion to accommodate the new telephone locals in the ISAC-II building; the added capacity allowed for over 200 new locals to be added. The Meridian Mail voicemail system, which was largely unchanged since its original installation in 1995, was completely replaced with new technology, CallPilot. This new version is much more easily managed, and has more capabilities than the old. The conversion was done with negligible impact on users.

TRIUMF OUTREACH PROGRAM

The TRIUMF Outreach Program (TOP) was officially launched in April with generous grants from the Vancouver Foundation and the TRIUMF Technology Transfer Office. These grants will support TOP's

goals of bringing the excitement of subatomic physics research in Canada to as broad a public audience as possible. In 2003, effort was focused on establishing programs for high school teachers and establishing a new High School Fellowship.

High School Teacher Programs

A key component of TOP is to bring high school science teachers to TRIUMF for brief “internships”. Teachers join and participate fully on a running experiment for 3–5 days and, afterwards, the teachers work with TOP to produce resource materials for their classrooms and the general public based on their internship experience. TOP pays travel and housing costs as if the teachers were “visiting scientists”. Three teachers from Victoria, Terrace (see Fig. 318) and Pitt Meadows took part in the program in 2003, with over a dozen more signed up for opportunities in 2004 and beyond. Initial feedback from the program has been very positive, with one teacher writing about his experience in the *Journal for High School Science*.

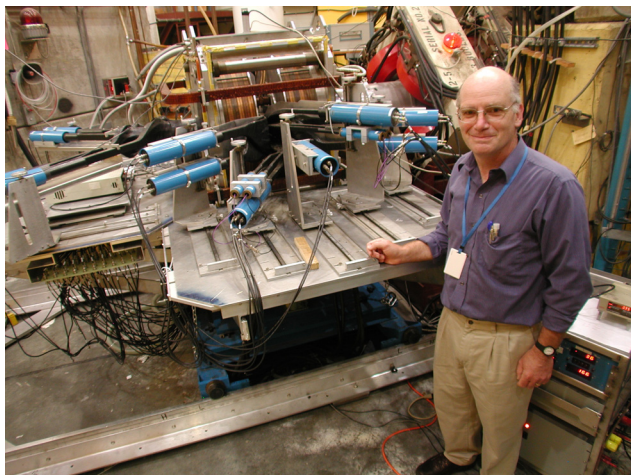


Fig. 318. A visiting high school science teacher from Terrace.

TRIUMF, together with the BC Association of Physics Teachers, hosted a Professional Development Day for high school science teachers in October, 2002 which was deemed an unqualified success. Scheduling conflicts precluded a repeat event in 2003, but it is planned to make the day an annual program starting in October, 2004.

TRIUMF/ISCBC High School Fellowship

In conjunction with the Innovation and Science Council of BC (ISCBC), TRIUMF has instituted a new High School Fellowship program for an outstanding graduating high school student from BC. Top students from across BC will be nominated by their schools, from which the ISCBC will select a short list. TRIUMF will select one winner for the \$3000 fellowship, after which the fellow will spend a six-week summer research experience at TRIUMF. This year's fellowship is considered a pilot project and, if successful, it is hoped to make it an annual program with perhaps more student winners.

Future Directions

In 2004 TOP plans to join the ALTA (Alberta Large-Area Time coincidence Array) cosmic-ray detector in the schools project. This project aims to put scintillator-based cosmic-ray shower detectors on school roofs to be operated by teachers and their students. The detectors are easy to set up and use, and will be interconnected via the Internet with other schools in the project. This project will bring many of the techniques and challenges of running a large-scale physics experiment right into the classroom, providing students with a first-class science education experience. TRIUMF has funding to build several modules, and is working with the University of Alberta in efforts to make each module more affordable.

CONFERENCES, WORKSHOPS AND MEETINGS

WESTERN REGIONAL NUCLEAR AND PARTICLE PHYSICS CONFERENCE

The 2003 Western Regional Nuclear and Particle Physics Conference (WRNPPC) was organized this year by the University of Northern British Columbia on February 14–16 at the Fairmont Chateau Lake Louise in Lake Louise, Alberta. This was the 40th WRNPPC, and the 20th to be held at the Chateau. As before, the conference provided a friendly setting for scientists and graduate students to present their work in nuclear and particle physics, and a forum where a significant portion of the Canadian subatomic physics program was covered by a number of invited speakers who are leading researchers in their respective fields. The talks presented were quite varied and covered topics ranging from low-energy nuclear physics and astrophysics, to intermediate energy hadronic, electromagnetic and electroweak physics, to high energy particle physics, as well as non-accelerator based neutrino physics. The attendance of the conference was quite respectable (47 participants) as was the active participation of graduate students (22). Twenty one institutions were represented, including 9 western Canadian, 6 eastern Canadian, 5 US, and one European.

Highlights of the conference included reports on first or new results from ISAC-I (DRAGON experiments), TRIUMF (TWIST and CSB-E704), Jefferson Lab (nucleon form factors), BaBar (CP violation), and SNO (solar neutrinos). Progress or review talks were also given on ATLAS-LHC, the next linear collider, final results from LEP-II, the new Higgs facility, the parity violation program at Jefferson Lab, and the PICASSO project at SNOLAB, to cite a few examples. In addition, the participants had a chance to hear a presentation on TRIUMF's next five year plan by Dr. Jean-Michel Poutissou, associate director of TRIUMF, and a review talk on the status of neutrino physics by a guest speaker, Dr. Baha Balantekin, chair of the APS Division of Nuclear Physics. Three graduate students, from the University of Guelph, the University of Washington, and Texas A&M University, were chosen for prizes for best talks by graduate students, while all graduate students were subsidized for their accommodation at the Chateau.

By all accounts the conference was a big success and served to emphasize at least two things: the very healthy and dynamic state of subatomic physics in Canada and the importance of carrying on with the WRNPPC tradition (perhaps with a more nationally inclusive character given the increasing participation of our eastern colleagues and students). Finally, the organizers (E. Korkmaz, T. Porcelli, D.

Price and A. Hussein) would like to acknowledge one more time the sponsorship of the offices of the VP-Academic, VP-Research, and Dean of Science and Management at UNBC, the CAP divisions of nuclear and particle physics, and the organizers of the 38th WRNPPC (SFU/TRIUMF). The financial support of these groups was crucial for the success of the conference.

LAKE LOUISE WINTER INSTITUTE

The eighteenth Lake Louise Winter Institute, February 16–22, was a tremendous success. The program for pedagogical talks was a mixture of results from present experiments with their interpretation and a valuable look into the future possibilities for the physics as well as the facilities. The experiments at RHIC yield extremely valuable information about the early times after the Big Bang. New results from B -factories for CP violation and the recent results from microwave data provided a useful window on the development of the universe. Neutrinos provided a tantalizing glimpse of the interior of the sun and the stars. The experiments on nuclear astrophysics yield the mechanism for the production of energy and elements in the stars. The six speakers presented the pedagogical lectures with a coherent picture of the developments in particle physics and cosmology.

The six main speakers along with their topics were:

- M. Baker — Heavy Ion Physics
- J. Ellis — Physics at Future Accelerators
- K. Kowalewski — B Physics and CP violation
- D. Pogosyan — Recent Developments in Cosmology
- H. Schatz — Nuclear Astrophysics
- K. Scholberg — Neutrino Physics

The main talks were complemented by contributed talks from almost all the major experiments in the world. The talks presented new developments in experiments and in theoretical physics.

The outstanding facilities at the Chateau Lake Louise and participants from numerous countries made the Winter Institute a memorable event. The surroundings provided an excellent opportunity for discussions and exchange of ideas.

The Winter Institute is made possible by the financial support of TRIUMF, the Institute of Particle Physics, the Canadian Institute of Theoretical Astrophysics, the University of Alberta conference fund and the Dean, Faculty of Science. The University of Alberta Physics Department provided infrastructure support. Lee Grimard was responsible for many of the details

that made the Winter Institute a great success. The organisers are grateful for all this support.

Organizers: F. Khanna, B. Campbell, M. Vinciter and A. Astbury.

WORKSHOP ON FUNCTIONAL IMAGING IN BASIC BIOMEDICAL RESEARCH THROUGH microPET IMAGING

A two-day workshop, held June 26–27, brought together international and national experts in functional imaging to address the issue of how to validate small animal models of human disease using microPET to achieve quantitative results for assessing physiological function. From this general goal we addressed specific questions that strike at the heart of using animal models of human disease.

1. How to develop a non-invasive imaging method for establishing a predictive assay for cancer treatment using positron emission tomography (PET).
2. Can we establish *in vivo* methods to assess whether we have an effective animal model of the neuropathology of schizophrenia?
3. How can we assess the effectiveness of pro-drugs for the treatment of diabetes using microPET?

The solution to any of these questions would represent a major step forward in using animal models of human disease ultimately leading to the reduction of the morbidity and mortality associated with major diseases (cancer, schizophrenia and diabetes) affecting society today.

The microPET is a positron emission tomographic camera designed specifically for imaging small animals such as mice and rats. The ability to track any molecule that has been appropriately tagged in a live animal means the potential applications of PET technology are vast. Small animal models, particularly genetically engineered mice, are increasingly recognized as powerful tools in cancer research. The potential that could be realized by the use of animal models has not yet been fully realized. Having a window on the functional changes induced by these genetically modified mice increases the power of our understanding of the interplay of these changes on multiple physiological systems. By measuring the effects of interventions in real time, microPET opens a window into such complex areas as brain chemistry function, hormonal regulation of insulin secretion, disruptions in enzymatic pathways, and tumour biology. Since microPET does not require animals to be sacrificed in order to obtain readings, animal behaviour observations can, for the first time, be correlated with physiological markers. Long-term follow-up physiological studies are now possible using the same animals.

The ultimate aim of the workshop was to enable the local researchers to design experiments that will enable them to collect pilot data in as short a time as reasonable so that they can go forward with grant applications for their research projects. Since this program is multidisciplinary by nature the research collaborations will have to contribute to the overall operation of the scanner and support infrastructure. By maintaining a common core, the team can be assured of the highest quality results that are consistent across the individual projects.

While most of the participants of the workshop have research programs that already utilize small animals in their research, there are a number who will not have this experience. There are several participants who serve on the UBC Committee for the Ethical Use of Animals in Research who provided the overview of the requirements and addressed particular questions that arose during the workshop. It was important to make sure that all participants left with a clear understanding of their obligations associated with using animals in research.

SUMMER NUCLEAR INSTITUTE AT TRIUMF – CKM AND MNS: QUARK AND LEPTON MIXINGS

Discovering the mixing matrices for quarks (CKM) and leptons (MNS) is currently an active topic of research both experimentally and theoretically. The goal of this year's Summer Nuclear Institute at TRIUMF (SNIT 2003, July 21 to August 1) was to give the students a background in this important area. In general this series of Institutes is designed to give graduate students an improved understanding of topics surrounding their research area.

The school attracted 39 students (close to the goal of 40 students). As in previous years they came from many different parts of the world: North America, Europe, and Asia. Over a third of the students were working on SNO with the next largest group working at TRIUMF. The 10 invited speakers came from Canada, the United States and Japan. In addition to the lectures, TRIUMF tours were given by Shawn Bishop and Sabine Engel. Attendance at the lectures was consistently high with some TRIUMF staff and Research Associates also attending.

Next year's Summer Nuclear Institute will be held July 5–16, 2004, just prior to the Nuclei in the Cosmos conference and Jens Dilling will be the lead organizer.

Byron Jennings for the organizing committee: Elly Driessen, Akira Konaka, Richard Helmer, Stephen Godfrey, and John Ng.

GEANT4 2003 WORKSHOP

Modern particle physics and nuclear physics experiments, telescopes flown on satellites, scanners in nuclear medicine, all require large-scale, accurate and comprehensive simulations of the particle detectors used in these applications. Over the last eight years, the object-oriented GEANT4 software package has become the tool of choice for many designers. GEANT4 was conceived and is being developed by an international collaboration. It builds on the accumulated experience in Monte Carlo simulations of many physicists and software engineers from around the world. The GEANT4 Workshops and Collaboration Meetings are the most important annual forum for the exchange of information and discussion among the developers. The eighth in a series of meetings which started at TRIUMF in 1996 returned to TRIUMF, September 2–6. The other previous workshops were held at SLAC, USA (97), Niigata University, Japan (98), ESA-ESTEC, The Netherlands (99), LAL Saclay, France (00), Genova University, Italy (01) and CERN, Switzerland (02). As well, this year, a one day Users Workshop was formally added to the program to take advantage of the occasion and bring together developers and some users, particularly from Canada. The workshop further provided the opportunity to motivate a collaboration and coordinate efforts toward future developments. To promote this goal, the program included speakers representing both the developers and the users.

Attendance and participation in the workshop exceeded all expectations. The 53 participants came from Canada (5), the United States (12), Europe (28), Japan (5), and three graduate students with TRIUMF affiliation. All the major HEP experiments which employ GEANT4 as their simulation platform had sent representatives to present their latest results and comment on their experience.

The Associate Director of TRIUMF gave a set of opening remarks, welcoming participants to Vancouver and TRIUMF. He described highlights of the locally based research program and stressed that TRIUMF also plays a key role in providing infrastructure to many Canadian particle/subatomic experiments, including international experiments based elsewhere. He concluded by flashing a transparency pulled from the weather office Web site promising a week of sunshine.

The conference was formatted as four and a half days of plenary sessions in the mornings and after lunch, followed by parallel sessions in the later part of the afternoon. The workshop program also included a tour of the TRIUMF facility and the first ever video conferenced GEANT4 Technical Forum, a new format to facilitate and intensify the communication between the GEANT4 developers and the worldwide commu-

nity of users. The GEANT4 Technical Steering Board also met during the meeting and selected the Laboratori Nazionali del Sud, University of Catania, Italy, as the location of next year's workshop.

The open plenary talks were grouped into eight sessions: Large Experiments – Frameworks/Validation, Collaboration News and Reports, New Kernel/Interactive Framework/Analysis Developments, Software Acceptance and Release Process, Electromagnetic Physics, Hadronic Physics, Special Topics/Interfacing, Closing Plenary Session. Detailed discussions were held in parallel sessions on several of these topics. The last full day was devoted to GEANT4 Applications that brought the latest developments from the user community. One closed plenary session revolved around collaboration internal business. The workshop was complimented by a series of four TRIUMF lunchtime tutorials, beginning with an introduction to GEANT4 (M. Assai), followed by explanations of the electromagnetic physics (M. Maire) and hadronic physics (H.-P. Wellisch) found in GEANT4, and concluding with a presentation of a JAVA based analysis tool (M. Turri) being developed at SLAC.

The first morning of the workshop was devoted to presentations from large HEP experiments: BABAR, ATLAS, CMS, and HARP. This was followed by a presentation from the European Space Agency on several of their future satellite missions, with an emphasis on present achievements and challenges. One presentation of particular relevance described the efforts of the ALICE collaboration to develop a Virtual Monte Carlo with GEANT4 as one specific implementation. One of the primary issues of all the talks was ongoing efforts to validate the simulation results through test beam measurements. The next part of the workshop focused on new developments in GEANT4. Other topics discussed included the physics models described in GEANT4, their present status, and planned extensions. Three presentations described the special topics of how to introduce parallelism in GEANT4 and how to interface external physics packages such as EGS4 and JQMD.

Lively question periods following the talks, and informal discussions, always one of the most rewarding aspects of these meetings, continued during catered lunch and coffee breaks. Additional opportunities for plenty of discussion existed during a reception and conference dinner held in the Peak Chalet at the top of Grouse Mountain in North Vancouver (see Fig. 319).

The TRIUMF auditorium served as an excellent venue for the plenary sessions. Parallel working and discussion sessions were accommodated in the Board Room and the Conference Room. The local organizing committee was formed by P. Gumplinger, F.W. Jones,



Fig. 319. The G4 2003 Workshop participants on the veranda of the Grouse Mountain Peak Chalet where the conference dinner was held.

and E. Driessen. We would like to thank all people who helped to make this workshop efficient and productive, and thus the success it has been. A number of individuals who volunteered their time and efforts for this conference must also be acknowledged. Special thanks go to Corrie Kost, Fred Jones, Hossein Rafighi and Martin Comyn for their patience and extra efforts keeping all of the devices needed in the presentations available and running properly. Elly Driessen was very important during the registration process and budgeting, and in putting together a successful culinary and social program. F.W. Jones put the conference Web pages together.

Detailed information about the meeting, the participants and their e-mail addresses, and electronic versions of all presentations are available on the conference Web pages at <http://www.triumf.ca/geant4-03/>.

FALL 2003 HEPiX/HEPNT MEETING

HEPiX/HEPNT (High Energy Physics in Unix/NT) meetings have been held approximately every 6 months (alternating between Europe and North America) since 1991 (last held at TRIUMF in April, 1996). The meetings bring together UNIX and Windows support staff from the high energy physics community in order to exchange common concerns and establish (or at least discuss) common standards.

There were 76 participants (2 from Japan, 29 from North America, and 45 from Europe) for this meeting held October 20–24 at TRIUMF, unusually large for a North American meeting. The first three days were devoted to general sessions, including site reports from the various represented laboratories. The fourth day was devoted to security topics, and the morning of the fifth day was devoted to brainstorming on mass storage systems, while a parallel session discussed Windows

issues.

Almost all sessions were Webcast in real time and recorded/converted/posted as Real Media files to allow for future replay of the talks (together with the posted Powerpoint or PDF file). A VRVS session, linking TRIUMF, BNL, DESY, CERN, FNAL, IN2P3, and Rutherford, for the mass storage system forum, took place on the final morning of the meeting. In a break with tradition, 2 vendors exhibited their products, and there were talks by commercial vendors – notably Red Hat and Microsoft. The pre-storing of all presentations into a dedicated laptop (pioneered at the GEANT4 workshop the previous month) significantly contributed to both the quality and seamlessness of the presentations. A record number (55) of wireless laptops, serviced by 3 access points, were in use in the auditorium during the meeting.

The need for prompt patches to both the operating kernels and system related utilities was emphasized during the sessions on security.

Details of the meeting can be found at <http://www.triumf.ca/hepixon2003/> with an excellent summary by Alan Silverman of CERN at <http://www.triumf.ca/hepixon2003/pres/24-03/summary/summary.pdf>.



Fig. 320. HEPiX/HEPNT meeting logo.

EMMA WORKSHOP

On December 11–12 a workshop was held to discuss the physics opportunities that would be offered by a recoil mass spectrometer at ISAC-II, dubbed EMMA (ElectroMagnetic Mass Analyzer). The major goals of the workshop were specifying the important physics issues that can be studied with a recoil mass spectrometer and the essential characteristics such a spectrometer would require in order to meet the needs of the ISAC-II experimental community. In addition, a number of individuals were identified whose help in making the scientific case and developing auxiliary detectors and data acquisition systems for the spectrometer will be instrumental.

Among the thirty participants in the workshop were experimenters from Canada, France, Italy, the UK, and the USA. The attendees included the mainly Canadian, British, and American prospective users of EMMA, as well as several scientists involved in the design and operation of similar spectrometers from around the world. Table XLIX lists the invited speakers.

Following an introduction describing the beams that will be provided by ISAC-II, the talks concentrated on three main topics: the properties, limitations, and figures of merit of recoil mass spectrometers in general; classes and specific examples of reactions of interest; and the design parameters of a recoil separator that would allow experimenters to study these reactions most efficiently. The main classes of devices currently in use or under construction were discussed, large acceptance magnetic spectrometers, recoil mass spectrometers that contain both electric and magnetic bending elements, and hybrid devices that seek to combine the features of these classes in a single design in which elements can be turned on or off according to the needs of a specific experiment.

The trade-off between mass resolving power and large energy or angular acceptance, which is due to chromatic and geometric aberrations, was discussed, as was the fact that the purely magnetic and hybrid devices do not produce any physical separation between different masses. This is a real limitation of such spectrometers, in which measurements of the recoil's time of flight through the device and angle in the focal plane are required to achieve even the modest mass resolution of which they are capable. Presentations from those operating and building such devices indicated that the mass resolving power of these spectrometers is inadequate for many if not most of the types of experiments envisioned by those expressing interest in using a recoil spectrometer at ISAC-II.

As a result, the design effort will focus on improving on the designs of combined electric and magnetic recoil mass spectrometers that were built throughout

Table XLIX. Invited EMMA Workshop speakers.

Name	Institution
Jean-Michel Poutissou	TRIUMF
Barry Davids	TRIUMF
Paul Schmor	TRIUMF
Carl Svensson	University of Guelph
Cary Davids	Argonne National Lab
Wilton Catford	University of Surrey
Charles Barton	University of York
Jo Ressler	Yale University
Angelo Cunsolo	LNS Catania
Dan Bardayan	Oak Ridge National Lab
Eddie Paul	University of Liverpool
Herve Savajols	GANIL
Phil Woods	University of Edinburgh
Dave Hutcheon	TRIUMF

the world in the 1980s and 1990s by increasing their angular, energy, and mass acceptance without unacceptable sacrifices in mass resolution and beam suppression. Some modest success along these lines has already been achieved in design studies following the workshop. The current plan calls for a funding proposal based on these design studies to be submitted to NSERC in September, 2004.

TRIUMF USERS' GROUP ANNUAL GENERAL MEETING

The 2003 TRIUMF Users' Group Annual General Meeting was held in the TRIUMF auditorium on Wednesday, December 10. The meeting format was slightly different from previous years in that there was a catered lunch rather than an evening meal, and the agenda was arranged so that the meeting would finish by 6 p.m. Another change was the inclusion of a general physics talk open to all TRIUMF staff. Boye Ahlborn of UBC gave an excellent talk, "Physics for the Birds". The talk was very well attended and there were many favourable comments afterwards. Another important item was the open forum on users' issues. Andrew Daviel Webcast the entire AGM live on streaming video, and Martin Comyn set up a computer so questions from remote viewers could be sent by e-mail. The video files are archived on <http://video.triumf.ca/cgi-bin/archives/TUG2003>. The agenda was as follows:

Welcome	Des Ramsay
State of the Laboratory	Alan Shotter
Science Division Report	Jean-Michel Poutissou
Cyclotron Status	Roger Poirier
ECR Source and	
Charge State Booster	Miguel Olivo
ISAC Status	
and 5 Year Plan	Pierre Bricault

ISAC Accelerators	Bob Laxdal
LADD Facility	Doug Bryman
Open Forum on Users' Issues	Des Ramsay-moderator
Physics for the Birds	Boye Ahlborn <i>UBC</i>
NSERC Subatomic GSC	Dean Karlen
Quality Assurance	Ewart Blackmore
WestGrid for Users	Mike Vetterli
TRIUMF Outreach	Marcello Pavan
New TRIUMF	
Public Web Site	Glenn Jones
TUEC Business Meeting	Des Ramsay

Excerpts from the Meeting

It is clearly not possible to summarize 8 hours of talks and discussion in one paragraph, but here are some brief excerpts to give the flavour.

- 2003 was a good year with 90% efficient beam delivery, ISAC-I producing physics results and the ISAC-II building completed.
- Development of the ISAC ECR ion source is stalled. It works on the bench, but not on-line with the production target. The ISAC schedule had to be re-arranged, as it had been assumed that the ECR source would be ready in the summer.
- CERN activities are proceeding well. 52 LHC quadrupoles and the ATLAS hadronic endcaps had already been delivered.
- A TRIUMF outreach project had been set up, headed by Marcello Pavan. The program is bringing TRIUMF science to the public and to the schools through such initiatives as an internship program for high school teachers.
- The Laboratory for Advanced Detector Development (LADD) had been funded in the amount of \$9.8 million. The facility is headed by Doug Bryman.
- No new appointment had been made yet for the Theory group leader. Three candidates were interviewed for a joint TRIUMF/UBC appointment, but UBC found all three unsuitable.
- MDS Nordion had added a third cyclotron, a TR30, which is now in operation. 45,000 to 50,000 patient doses *per week* are now administered with isotopes from these machines.
- Construction on the new TRIUMF House will begin in 2004. A \$3,000,000 loan had been obtained.
- Many people at TRIUMF had been working on the 2005–2010 five year plan. At the NRC review in September, both a review of activity over the period 1998–2003 and the plan for 2005–2010

were presented. The plan goes to NRC Council at the end of February, 2004. At the time of the AGM there was some political uncertainty due to the new Prime Minister and a shuffle of Cabinet Ministers.

- The Canadian Nuclear Safety Commission (CNSC) had demanded that TRIUMF set up a Quality Assurance (QA) program as a condition for the licence to operate a nuclear facility. A plan had been submitted and was to be implemented by the end of 2003. The users expressed the hope that paralyzing bureaucratic overlay could be avoided.
- The WestGrid computing network was in place. The UBC/TRIUMF Linux farm should be released to users soon. TRIUMF users who want to use “The Grid” should apply for a WestGrid user ID.
- A new TRIUMF Web site, www.triumf.info, had been launched. It was not only intended to be more accessible to the public, but also to make material for TRIUMF users easier to find by being presented in a standardized way.
- A new TRIUMF newsletter had been launched with a fixed deadline and a uniform content.

Open Forum on Users' Issues

An important role of the TRIUMF Users' Group is to provide a link between the TRIUMF users and the TRIUMF management. To this end, an open discussion was scheduled where issues could be raised and solutions to problems suggested. The forum centred around three main issues:

1. A new format for OPCOM – Jean-Michel Poutissou presented a suggested structure in which many different TRIUMF groups, including TUG, would send representatives.
2. A new format for TUEC – Greg Hackman had prepared a suggested model with formalized representation from the various user groups, such as ISAC. In his absence, it was presented by Tracy Porcelli.
3. A better information archive for facts about TRIUMF experiments (publications, people, graduate students, theses, talks, etc.) – Jeff Sonier presented some suggestions for a Web-based on-line software archive.

The discussion was lively with many suggestions from the floor and via e-mail. The session is archived on <http://video.triumf.ca/cgi-bin/archive/TUG2003>. The consensus of the discussion was:

1. OPCOM needs to be changed, as it is not providing useful guidance to the TRIUMF management, but there seemed to be a reluctance to remove the university representation. The new OPCOM positions could be filled by Director's appointment or by election from a slate prepared by a joint TUEC/TRIUMF nominating committee.
2. There seemed to be general opposition to forming several distinct users' groups at TRIUMF. It was not clear how to ensure broad representation on TUEC, although, so far, representation has been pretty even across the various interest groups.
3. Everyone could benefit from better record keeping. TUEC should lobby TRIUMF to produce an on-line archive of papers, talks, beam time, theses, collaborators, and graduate students for *every* experiment. What has to be developed is how to enforce compliance. For most experiments, making reporting a requirement for acceptance of an EEC proposal or beam time request would ensure compliance.

TRIUMF Business Meeting

Election results

There had been an exceptionally good voter turnout, with 40% of the 296 members voting. The

by-laws specify a quorum of 25%, and in past years this had often barely been met. The successful candidates for the vacant positions were Jens Dilling as Chair Elect and Pierre Bricault and Alison Laird as Members for 2004/2005.

TUEC Membership for 2003

W.D. Ramsay	U. Manitoba	<i>Chair</i>
J.E. Sonier	SFU	<i>Chair Elect</i>
G.M. Luke	McMaster U.	<i>Past Chair</i>
G.S. Hackman	TRIUMF	2002/2003
M.M. Pavan	U. Regina/TRIUMF	2002/2003
A.A. Chen	McMaster U.	2003/2004
T.A. Porcelli	U. Northern BC	2003/2004
M. Comyn	TRIUMF	<i>Liaison Officer</i>

Membership review

The end of 2003 marks the tri-annual membership review. This policy was started in 1997. Each member will be asked to reaffirm his or her intention to remain active, and will be removed from the membership list unless membership is reaffirmed.

ORGANIZATION

Board of Management (BOM)

The Board of Management of TRIUMF manages the business of the facility and has equal representation from each of the five member universities. The Board met 3 times during the year. At the end of 2003 the Board comprised:

University of Alberta	Dr. W.J. McDonald Dr. A. Noujaim	Chairman
University of British Columbia	Dr. D. Brooks Dr. B. Turrell	
Carleton University	Dr. R. Carnegie Dr. F. Hamdullahpur	
Simon Fraser University	Dr. M. Plischke Dr. C.H.W. Jones	
University of Victoria	Dr. R. Keeler Dr. M. Taylor	
Private Sector	Ms. G. Gabel Dr. H. Ing	Environmental Sensors Inc. Bubble Technologies Inc.

Towards the end of 1987, Board membership was expanded in anticipation of a broadening of the TRIUMF joint venture to include a more national representation of Canadian universities long associated with the TRIUMF experimental program. The University of Manitoba and Université de Montréal became associate members, and the University of Toronto joined as an observer. At the end of 1988, University of Toronto's status changed from that of observer to associate member. In March, 1989 the University of Regina became an associate member. In December, 1998 Carleton University and Queen's University became associate members. In March, 2000 Carleton University's status changed from that of associate member to full member. In 2001 two private sector positions were added. In October, 2001 McMaster University became an associate member and effective April 1, 2003 the University of Guelph became an associate member. Associate membership at year-end:

Non-voting Associate members:	TBA	University of Guelph
	Dr. W.T.H. van Oers	University of Manitoba
	Dr. A.J. Berlinsky	McMaster University
	Dr. C. Leroy	Université de Montréal
	Dr. A. Hallin	Queen's University
	Dr. K. Bergman	University of Regina
	Dr. R. Orr	University of Toronto
<i>ex officio</i> members:	Dr. W. Davidson	National Research Council
	Dr. P. Sinervo	ACOT
	Dr. A. Shotter	Director, TRIUMF
	Dr. J.-M. Poutissou	Associate Director, TRIUMF
	Mr. J. Hanlon	TRIUMF, Recording Secretary

Administration

Under the directorship of Dr. A. Shotter, TRIUMF personnel were grouped into Divisions, with Division Heads as follows:

Division Head, Science Division	J.-M. Poutissou
Division Head, Accelerator Technology Division	E.W. Blackmore
Division Head, Cyclotron Operations Division	R. Poirier
Division Head, Technology Transfer Division	P.L. Gardner
Division Head, ISAC Division	P.W. Schmor
Division Head, Administration Division	A. Shotter

Operating Committee

The TRIUMF Operating Committee advises the Director and the TRIUMF Board of Management (through the Director) on matters relating to the scientific productivity and direction of the TRIUMF laboratory. The Operating Committee consists of one voting member from each of the five full-member universities, two voting members representing the interests of the Users, and one representing TRIUMF staff. The Associate Director is a non-voting member. The Operating Committee met 5 times in 2003. Members of the committee (alternate members in parentheses) at the end of 2003 were:

Dr. A. Shotter	Chairman	Director	
Dr. J.-M. Poutissou	<i>(ex officio)</i>	Associate Director	
Dr. J. Pinfold		University of Alberta	(Dr. D. Gingrich)
Dr. G. Oakham		Carleton University	(Dr. R. Carnegie)
Dr. J.M. D'Auria		Simon Fraser University	(Dr. P. Percival)
Dr. M. Pospelov		University of Victoria	(Dr. R. Kowalewski)
Dr. D. Bryman		University of British Columbia	(Dr. T. Mattison)
Dr. G.M. Luke		Users	(Dr. J. Sonier)
Dr. S. Yen		Users	(Dr. L. Lee)
Mr. R. Baartman		TRIUMF Employee Group	(Mr. R. Ruegg)
Mr. J. Hanlon	Recording Secretary	TRIUMF	
Dr. W. Davidson	<i>(ex officio)</i>	National Research Council	

Agency Committee on TRIUMF (ACT)

The role of the Agency Committee on TRIUMF is to oversee the Government of Canada's investment in TRIUMF and the economic benefits derived from that investment, with a particular focus on financial and commercialization matters. The Committee provides advice to the Minister of Industry, in conjunction with the reports of the NRC Advisory Committee on TRIUMF on scientific matters. The Agency Committee on TRIUMF usually meets twice a year.

Dr. A.J. Carty	Chairman	President, National Research Council
Dr. T. Brzustowski		President, Natural Sciences and Engineering Research Council
Mr. J.-C. Villiard		Deputy Minister, Industry Canada
Dr. W. Davidson	Secretary	National Research Council

NRC Advisory Committee on TRIUMF (ACOT)

The Advisory Committee on TRIUMF advises the National Research Council on all aspects of the TRIUMF program insofar as they relate to the determination and administration of the federal contribution to TRIUMF. The Committee provides scientific program advice to the Director of TRIUMF. The Committee reports to the National Research Council each year on its findings and recommendations, with particular reference to the arrangement entered into by the National Research Council and TRIUMF under which contribution payments are made, thereby ensuring that TRIUMF utilizes its program in support of its defined role as a national facility and works with all constituencies of the Canadian subatomic physics community to sustain a national program in the field of research, within the context of the funds available.

Dr. P. Sinervo	Chairman	University of Toronto
Dr. W. Davidson	Secretary	National Research Council
Dr. J. Äystö		University of Jyväskylä
Dr. W.J.L. Buyers		National Research Council
Dr. A. Fenster		J.P. Robarts Research Institute
Dr. J. Guigné		Guigné International Ltd.
Dr. G. Kalmus		Rutherford Appleton Laboratory
Dr. W. Nazarewicz		University of Tennessee
Dr. C. Rolfs		Ruhr-Universität Bochum
Dr. J. Siegrist		University of California, Berkeley
Dr. P. Vincett		FairCopy Services Inc.
Dr. D. Karlen	<i>(ex officio)</i>	University of Victoria
Dr. R. Keeler	<i>(ex officio)</i>	University of Victoria
Dr. W.J. McDonald	<i>(ex officio)</i>	University of Alberta
Ms. K. Wilson	<i>(ex officio)</i>	Natural Sciences and Engineering Research Council

TRIUMF Safety Management Committee

Dr. A. Shotter	Director, TRIUMF
Dr. J.-M. Poutissou	Associate Director/Head, Science Division
Dr. E.W. Blackmore	Head, Accelerator Technology Division
Dr. R. Poirier	Head, Cyclotron Operations Division
Mr. P.L. Gardner	Head, Technology Transfer Division
Dr. P.W. Schmor	Head, ISAC Division
Mr. M. Stenning	Head, Operations Group
Mr. D. Preddy	TAPC Chairman
Mr. G. Wood	Industrial Safety Officer/TAPC
Mr. L. Moritz	Head, Environmental Health & Safety
Mr. J. Hanlon	Manager, Human Resources & Administration
Dr. S. Zeisler	Head, Applied Technology Group
Dr. B. Abeysekera	MDS-Nordion
Mrs. K. Gildert	Recording Secretary

Experiments Evaluation Committees (EEC)

In July, 1994 the Experiments Evaluation Committee was formally split into two committees representing subatomic physics and μ SR physics. In 2000 the μ SR Committee changed its name to the Materials Science Committee and in 2003 the name was changed to Molecular and Materials Science Experiments Evaluation Committee. In 2003 these committees comprised:

Subatomic Committee:

Dr. I.S. Towner	Chairman	Queen's University
Dr. J.-M. Poutissou	Associate Director/ (<i>ex officio</i>)	TRIUMF
Dr. B. Jennings	Secretary	TRIUMF
Dr. W. Ramsay	(<i>ex officio</i>)	TUEC Chairman/TRIUMF
Dr. S.J. Freedman		Lawrence Berkeley Laboratory
Dr. B.M. Sherrill		NSCL/Michigan State University
Dr. F.K. Thielemann		Universität Basel
Dr. R.E. Tribble		Texas A&M University

Molecular and Materials Science Committee:

Dr. B. Gaulin	Chairman	McMaster University
Dr. J.-M. Poutissou	Associate Director/ (<i>ex officio</i>)	TRIUMF
Dr. P.W. Percival	Secretary/ (<i>ex officio</i>)	SFU/TRIUMF
Dr. G.M. Luke	(<i>ex officio</i>)	TUEC Past Chairman/McMaster University
Dr. M. Gingras		University of Waterloo
Dr. F. Marsiglio		University of Alberta
Dr. S. Roorda		Université de Montréal
Dr. G.A. Sawatzky		University of British Columbia
Dr. T.W. Swaddle		University of Calgary

Life Sciences Project Evaluation Committee (LSPEC)

Dr. J. Link	Chairman	University of Washington
Dr. J.-M. Poutissou	Associate Director/ (<i>ex officio</i>)	TRIUMF
Dr. L.P. Robertson	Secretary	University of Victoria
Dr. R.F. Dannals		Johns Hopkins PET Center
Dr. S. Houle		PET Centre – CAMH/University of Toronto
Dr. R. Lecomte		Université de Sherbrooke
Dr. A.J.B. McEwan		Cross Cancer Clinic

PUBLICATIONS

This appendix lists publications describing work performed at TRIUMF and also work conducted elsewhere by TRIUMF personnel and TRIUMF users.

Journal Publications

Particle, Nuclear and Atomic Physics

W.M. Snow, W.S. Wilburn, J.D. Bowman, M.B. Leushner, S.I. Penttila, V.R. Pomeroy, D.R. Rich, E.I. Sharapov and V.W. Yuan, *Progress toward a new measurement of the parity violating asymmetry in $\bar{n} + p \rightarrow d + \gamma$* , Nucl. Instrum. Methods **A515**, 563 (2003).

J. Wozniak, A. Adamczak, G.A. Beer, V.M. Bystritsky, M. Filipowicz, M.C. Fujiwara, T.M. Huber, O. Huot, R. Jacot-Guillarmod, P. Kammel, S.K. Kim, P.E. Knowles, A.R. Kunselman, G.M. Marshall, F. Mulhauser, A. Olin, C. Petitjean, T.A. Porcelli, L.A. Schaller, V.A. Stolupin and J. Zmeskal, *Scattering of pu muonic atoms in solid hydrogen*, Phys. Rev. **A68**, 062502 (2003) [nucl-ex/0212005].

H. Imura, M. Miyabe, M. Oba, T. Shibata, N. Shino-hara, Y. Ishida, T. Horiguchi and H.A. Schuessler, *Nuclear moments and isotope shifts of ^{135}La , ^{137}La and ^{138}La by collinear laser spectroscopy*, Phys. Rev. **C68**, 054328 (2003).

A. Toyoda, K. Ishida, K. Shimomura, S.N. Nakamura, Y. Matsuda, W. Higemoto, T. Matsuzaki and K. Nagamine, *New insights in muon-catalyzed dd fusion by using ortho-para controlled solid deuterium*, Phys. Rev. Lett. **90**, 243401 (2003).

C.D. O'Leary, C.E. Svensson, S.G. Frauendorf, D.E. Appelbe, R.A.E. Austin, G.C. Ball, J.A. Cameron, R.M. Clark, M. Cromaz, P. Fallon, D.F. Hodgson, N.S. Kellsall, A.O. Macchiavelli, D. Sarantites, J.C. Waddington, R. Wadsworth, D. Ward, A. Afanasjev and I. Ragnarsson, *Evidence for isovector neutron-proton pairing from high-spin states in ^{74}Rb* , Phys. Rev. **C67**, R021301 (2003).

S. Gu and J.A. Behr, *Off-Raman resonance effects of hyperfine coherences*, Phys. Rev. **A68**, 015804 (2003).

A.R. Berdoz, J. Birchall, J.B. Bland, J.D. Bowman, J.R. Campbell, G.H. Coombes, C.A. Davis, A.A. Green, P.W. Green, A.A. Hamian, R. Helmer, S. Kadantsev, Y. Kuznetsov, L. Lee, C.D.P. Levy, R.E. Mischke, N.T. Okumusoglu, S.A. Page, W.D. Ramsay, S.D. Reitzner, T. Ries, G. Roy, A.M. Sekulovich, J. Soukup, G.M. Stinson, T. Stocki, V. Sum, N.A. Titov, W.T.H. van Oers, R.J. Woo, S. Zadorozny and A.N. Zelenski (E497 collaboration), *Parity violation in proton-proton scattering at 221 MeV*, Phys. Rev. **C68**, 034004 (2003) [TRI-PP-02-18, nucl-ex/0211020].

A.K. Oppen, E. Korkmaz, D.A. Hutcheon, R. Abegg, C.A. Davis, R.W. Finlay, P.W. Green, L.G. Greeniaus, D.V. Jor-

dan, J.A. Niskanen, G.V. O'Rielly, T. Porcelli, S.D. Reitzner, P.L. Walden and S. Yen, *Charge symmetry breaking in $np \rightarrow d\pi^0$* , Phys. Rev. Lett. **91**, 212302 (2003) [nucl-ex/0306027].

B.L. Zhuikov, M.V. Mebel, V.M. Kokhanyuk, A.S. Iljinov, A.Yu. Zyuzin and J.S. Vincent, *Production of high spin isomers in proton induced reactions at 100–500 MeV on ^{181}Ta* , Phys. Rev. **C68**, 054611 (2003).

M.B. Smith, P.M. Walker, G.C. Ball, J.J. Carroll, P.E. Garrett, G. Hackman, R. Propri, F. Sarazin and H.C. Scraggs, *γ -rays emitted in the decay of 31-yr $^{178}\text{Hf}^{m2}$* , Phys. Rev. **C68**, 031302 (2003).

A. Pouladdej, T.P. Gorringe, M.D. Hasinoff, A.J. Larabee, A.J. Noble, C.J. Virtue, D.H. Wright, G. Azuelos and B.C. Robertson, *Photon asymmetry measurement in radiative muon capture on ^{40}Ca* , Phys. Rev. **C68**, 034605 (2003).

A.R. Junghans, E.C. Mohrmann, K.A. Snover, T.D. Steiger, E.G. Adelberger, J.M. Casandjian, H.E. Swanson, L. Buchmann, S.H. Park, A. Zyuzin and A. Laird, *Precise measurement of the $^7\text{Be}(p, \gamma)^8\text{B}$ S -factor*, Phys. Rev. **C68**, 065803 (2003) [nucl-ex/0308003].

A. Piechaczek, E.F. Zganjar, G.C. Ball, B. Bricault, J. D'Auria, J.C. Hardy, D.F. Hodgson, V. Iacob, P. Klages, W.D. Kulp, J.R. Leslie, M. Lipoglavsek, J.A. Macdonald, H.-B. Mak, D.M. Moltz, G. Savard, J. von Schwarzenberg, C.E. Svensson, I.S. Towner and J.L. Wood, *High precision branching ratio measurements for the superallowed β -decay of ^{74}Rb : a prerequisite for exacting tests of the standard model*, Phys. Rev. **C67**, 051305 (2003).

G.J. Hofman, J. Breitschopf, K. Craig, H. Denz, E.F. Gibson, E.L. Mathie, R. Meier, M. Pavan, C. Riedel and R. Tacik, *Analyzing powers for π^-p elastic scattering at 279 MeV*, Phys. Rev. **C68**, 018202 (2003).

J.-M. Poutissou, M. Craddock and J. Gillies, *TRIUMF: the home of Canadian subatomic physics*, CERN Courier **43N1**, 30 (2003).

M. Trinczek, A. Gorelov, D. Melconian, W.P. Alford, D. Asgeirsson, D. Ashery, J.A. Behr, P.G. Bricault, J.M. D'Auria, J. Deutsch, J. Dilling, M. Domsbysky, P. Dubé, S. Eaton, J. Fingler, U. Giesen, S. Gu, O. Häusser, K.P. Jackson, B. Lee, J.H. Schmid, T.J. Stocki, T.B. Swanson and W. Wong, *Novel search for heavy ν mixing from the β^+ decay of ^{38m}K confined in an atom trap*, Phys. Rev. Lett. **90**, 012501 (2003).

S. Gu, J.A. Behr, M.N. Groves and D. Dhat, *Coherent population trapping states with cold atoms in a magnetic field*,

Optics Communications **220**, 365 (2003).

W. Liu *et al.*, *Charge state studies of low energy heavy ions passing through hydrogen and helium gas*, Nucl. Instrum. Methods **A496**, 198 (2003).

S. Bishop, R.E. Azuma, L. Buchmann, A.A. Chen, M.L. Chatterjee, J.M. D'Auria, S. Engel, D. Gigliotti, U. Greife, M. Hernanz, D. Hunter, A. Hussein, D. Hutcheon, C. Jewett, J. Jose, J. King, S. Kubono, A.M. Laird, M. Lamey, R. Lewis, W. Liu, S. Michimasa, A. Olin, D. Ottewell, P.D. Parker, J.G. Rogers, F. Strieder and C. Wrede, $^{21}\text{Na}(p,\gamma)^{22}\text{Mg}$ reaction and oxygen-neon novae, Phys. Rev. Lett. **90**, 162501 (2003), erratum *ibid.* 229902 (2003) [astro-ph/0303285].

G.F. Grinyer, J.C. Waddington, C.E. Svensson, R.A.E. Austin, G.C. Ball, G.S. Hackman, J.M. O'Meara, C. Osborne, F. Sarazin, H.C. Scraggs and H.D.H. Stover, *The half-life of ^{176}Lu* , Phys. Rev. **C67**, 14302 (2003).

B. Aubert *et al.* (BaBar collaboration), *Study of inclusive production of charmonium mesons in B decay*, Phys. Rev. **D67**, 032002 (2003) [SLAC-PUB-9327, BABAR-PUB-02-04, hep-ex/0207097].

B. Aubert *et al.* (BaBar collaboration), *A measurement of the $B^0 \rightarrow J/\psi \pi^+ \pi^-$ branching fraction*, Phys. Rev. Lett. **90**, 091801 (2003) [SLAC-PUB-9261, BABAR-PUB-02-06, hep-ex/0209013].

B. Aubert *et al.* (BaBar collaboration), *Measurement of the branching fraction for inclusive semileptonic B meson decays*, Phys. Rev. **D67**, 031101 (2003) [SLAC-PUB-9306, BABAR-PUB-02-011, hep-ex/0208018].

B. Aubert *et al.* (BaBar collaboration), *Measurement of the CKM matrix element $|V_{ub}|$ with $B \rightarrow \rho \nu$ decays*, Phys. Rev. Lett. **90**, 181801 (2003) [SLAC-PUB-9618, BABAR-PUB-02-015, hep-ex/0301001].

B. Aubert *et al.* (BaBar collaboration), *Measurement of $B^0 \rightarrow D^{(*)+} D^{*-}$ branching fractions and $B^0 \rightarrow D_s^{*+} D^{*-}$ polarization with a partial reconstruction technique*, Phys. Rev. **D67**, 092003 (2003) [SLAC-PUB-9644, BABAR-PUB-03-001, hep-ex/0302015].

B. Aubert *et al.* (BaBar collaboration), *Evidence for $B^+ \rightarrow J/\psi p \bar{\Lambda}$ and search for $B^0 \rightarrow J/\psi p \bar{p}$* , Phys. Rev. Lett. **90**, 231801 (2003) [SLAC-PUB-9690, BABAR-PUB-03-007, hep-ex/0303036].

K. Ackerstaff *et al.* (HERMES collaboration), *Nuclear effects on $R = \sigma_L/\sigma_T$ in deep-inelastic scattering*, Phys. Lett. **B475**, 386 (2002), erratum *ibid.* **B567**, 339 (2003) [DESY-99-150, hep-ex/9910071, DESY-02-092, hep-ex/0210067].

A. Airapetian *et al.* (HERMES collaboration), *Evidence for quark-hadron duality in the proton spin asymmetry A_1* , Phys. Rev. Lett. **90**, 092002 (2003) [DESY-02-137, hep-ex/0209018].

A. Airapetian *et al.* (HERMES collaboration), *The Q^2 -dependence of nuclear transparency for exclusive ρ^0 pro-*

duction, Phys. Rev. Lett. **90**, 052501 (2003) [DESY-02-152, hep-ex/0209072].

A. Airapetian *et al.* (HERMES collaboration), *The Q^2 -dependence of the generalized Gerasimov-Drell-Hearn integral for the deuteron, proton and neutron*, Eur. Phys. J. **C26**, 527 (2003) [DESY-02-172, hep-ex/0210047].

A. Airapetian *et al.* (HERMES collaboration), *Measurement of single-spin azimuthal asymmetries in semi-inclusive electroproduction of pions and kaons on a longitudinally polarised deuterium target*, Phys. Lett. **B562**, 182 (2003) [DESY 02-226, hep-ex/0212039].

A. Airapetian *et al.* (HERMES collaboration), *Double-spin asymmetries in the cross section of diffractive ρ^0 and ϕ production at intermediate energies*, Eur. Phys. J. **C29**, 171 (2003) [DESY-02-230, hep-ex/0302012].

A. Airapetian *et al.* (HERMES collaboration), *Quark fragmentation to π^\pm , π^0 , K^\pm , p and \bar{p} in the nuclear environment*, Phys. Lett. **B577**, 37 (2003) [DESY-03-088, hep-ex/0307023].

V.V. Anisimovsky *et al.* (KEK-PS E246 collaboration), *First measurement of the T-violating muon polarization in the decay $K^+ \rightarrow \mu^+ \nu \gamma$* , Phys. Lett. **B562**, 166 (2003) [hep-ex/0304027].

M.A. Aliev *et al.* (KEK-E470 collaboration), *Measurement of direct photon emission in $K^+ \rightarrow \pi^+ \pi^0 \gamma$ decay using stopped positive kaons*, Phys. Lett. **B554**, 7 (2003) [hep-ex/0212048].

G. Abbiendi *et al.* (OPAL collaboration), *Measurement of the mass of the W boson in e^+e^- collisions using the fully leptonic channel*, Eur. Phys. J. **C26**, 321 (2003) [CERN-EP-2002-022, hep-ex/0203026].

G. Abbiendi *et al.* (OPAL collaboration), *Decay mode independent searches for new scalar bosons with the OPAL detector at LEP*, Eur. Phys. J. **C27**, 311 (2003) [CERN-EP-2002-032, hep-ex/0206022].

G. Abbiendi *et al.* (OPAL collaboration), *Charged particle momentum spectra in e^+e^- annihilation at $\sqrt{s}/2 = 192\text{--}209\text{ GeV}$* , Eur. Phys. J. **C27**, 467 (2003) [CERN-EP-2002-057, hep-ex/0209048].

G. Abbiendi *et al.* (OPAL collaboration), *Search for a low mass CP odd Higgs boson in e^+e^- collisions with the OPAL detector at LEP-2*, Eur. Phys. J. **C27**, 483 (2003) [CERN-EP-2002-058, hep-ex/0209068].

G. Abbiendi *et al.* (OPAL collaboration), *Search for the standard model Higgs boson with the OPAL detector at LEP*, Eur. Phys. J. **C26**, 479 (2003) [CERN-EP-2002-059, hep-ex/0209078].

G. Abbiendi *et al.* (OPAL collaboration), *A measurement of the $\tau^- \rightarrow \mu^- \bar{\nu}_\mu \nu_\tau$* , Phys. Lett. **B551**, 35 (2003) [CERN-EP-2002-085, hep-ex/0211066].

G. Abbiendi *et al.* (OPAL collaboration), *Di-jet production in photon-photon collisions at $\sqrt{s_{ee}}$ from 189 to 209 GeV*, Eur. Phys. J. **C31**, 307 (2003) [CERN-EP-2002-093, hep-ex/0301013].

G. Abbiendi *et al.* (OPAL collaboration), *Bose-Einstein correlations of π^0 pairs from hadronic Z^0 decays*, Phys. Lett. **B559**, 131 (2003) [CERN-EP-2003-005, hep-ex/0302027].

G. Abbiendi *et al.* (OPAL collaboration), *Test of non-commutative QEC in the process $e^+e^- \rightarrow \gamma\gamma$ at LEP*, Phys. Lett. **B568**, 181 (2003) [CERN-EP-2003-010, hep-ex/0303035].

G. Abbiendi *et al.* (OPAL collaboration), *Search for stable and longlived massive charged particles in e^+e^- collisions at $\sqrt{1/2} = 130$ GeV to 209 GeV*, Phys. Lett. **B572**, 8 (2003) [CERN-EP-2003-016, hep-ex/0305031].

G. Abbiendi *et al.* (OPAL collaboration), *Search for pair produced leptiquarks in e^+e^- interactions at $\sqrt{1/2} \simeq 189$ GeV to 209 GeV*, Eur. Phys. J. **C31**, 281 (2003) [CERN-EP-2003-021, hep-ex/0305053].

G. Abbiendi *et al.* (OPAL collaboration), *Measurement of isolated prompt photon production in photon photon collisions at $\sqrt{s_{ee}} = 183$ –209 GeV*, Eur. Phys. J. **C31**, 491 (2003) [CERN-EP-2003-023, hep-ex/0305075].

G. Abbiendi *et al.* (OPAL collaboration), *Measurement of heavy quark forward backward asymmetries and average B mixing using leptons in hadronic Z decays*, Phys. Lett. **B577**, 18 (2003) [CERN-EP-2003-039, hep-ex/0308051].

G. Abbiendi *et al.* (OPAL collaboration), *Search for the single production of doubly charged Higgs bosons and constraints on their couplings from Bhabha scattering*, Phys. Lett. **B577**, 93 (2003) [CERN-EP-2003-041, hep-ex/0308052].

G. Abbiendi *et al.* (OPAL collaboration), *Study of Z pair production and anomalous couplings in e^+e^- collisions at \sqrt{s} between 190 GeV and 209 GeV*, Eur. Phys. J. **C32**, 303 (2003) [CERN-EP-2003-049, hep-ex/0310013].

G.M. Huber *et al.* (TAGX collaboration), *In-medium ρ^0 spectral function study via the ^2H , ^3He , $^{12}\text{C}(\gamma, \pi^+\pi^-)$ reaction*, Phys. Rev. **C68**, 065202 (2003) [nucl-ex/0310011].

Instrumentation/Accelerator Physics/Computing Sciences

D. Hutcheon *et al.*, *The DRAGON facility for nuclear astrophysics at TRIUMF-ISAC: design, construction and operation*, Nucl. Instrum. Methods **A498**, 190 (2003).

C. Johnstone and S. Koscielniak, *FFAGs for rapid acceleration*, Nucl. Instrum. Methods **A503**, 445 (2003).

P. Gumplinger, F. Jones, S. Agostinelli *et al.* (GEANT4 collaboration), *GEANT4 – a simulation toolkit*, Nucl. Instrum. Methods **A506**, 250 (2003).

M. Abe *et al.* (KEK-PS E246 collaboration), *Apparatus for a search for T -violating muon polarization in stopped-kaon decays*, Nucl. Instrum. Methods **A507**, 60 (2003) [INR-1094-2003, KEK-PREPRINT-2002-130, TRI-PP-03-01, hep-ex/0302001].

N.J. Buchanan and D.M. Gingrich, *Proton radiation effects in XC4036XLA field programmable gate arrays*, IEEE Trans. Nucl. Sci. **NS-50**, 263 (2003).

P. Paillet, J.R. Schwank, M.R. Shaneyfelt, V. Ferlet-Cavrois, R.L. Jones, O. Flament and E.W. Blackmore, *Total dose hardness assurance testing using laboratory radiation sources*, IEEE Trans. Nucl. Sci. **50**, 2310 (2003).

Molecular and Materials Science

A. Fukaya, Y. Fudamoto, I.M. Gat, T. Ito, M.I. Larkin, A.T. Savici, Y.J. Uemura, P.P. Kyriakou, G.M. Luke, M.T. Rovers, K.M. Kojima, A. Keren, M. Hanawa and Z. Hiroi, *Muon spin relaxation and susceptibility studies of pure and doped spin 1/2 Kagome-like system $(\text{Cu}_x\text{Zn}_{1-x})_3\text{V}_2\text{O}_7(\text{OH})_{2-2(\text{H}_2\text{O})}$* , Phys. Rev. Lett. **91**, 207603 (2003).

D.R. Harshman, J.D. Dow, W.J. Kossler, D.R. Noakes, C.E. Stronach, A.J. Greer, E. Koster, Z.F. Ren and D.Z. Wang, *Muon spin rotation study of $\text{GdSr}_2\text{Cu}_2\text{RuO}_8$: implications*, Philosophical Magazine **B83**, 2055 (2003).

J. Sugiyama, J.H. Brewer, E.J. Ansaldo, H. Itahara, K. Dohmae, Y. Seno, C. Xia and T. Tani, *Hidden magnetic transitions in thermoelectric layered cobaltite, $[\text{Ca}_2\text{CoO}_3]_{0.62}[\text{CoO}_2]$* , Phys. Rev. **B68**, 134423 (2003).

J. Sugiyama, J.H. Brewer, E.J. Ansaldo, H. Itahara, K. Dohmae, C. Xia, Y. Seno, B. Hitti and T. Tani, *A common behavior of thermoelectric layered cobaltites: incommensurate spin density wave states in $[\text{Ca}_2\text{Co}_{4/3}\text{Cu}_{2/3}\text{O}_4]_{0.62}[\text{CoO}_2]$ and $[\text{Ca}_2\text{CoO}_3]_{0.62}[\text{CoO}_2]$* , J. Phys.: Condensed Matter **15**, 8619 (2003).

P.J.C. King, R.L. Lichti and I. Yonenaga, *Hydrogen behaviour in bulk $\text{Si}_{1-x}\text{Ge}_x$ alloys as modelled by muonium*, Physica **B340-342**, 835 (2003).

J.E. Sonier, K.F. Poon, G.M. Luke, P. Kyriakou, R.I. Miller, R. Liang, C.R. Wiebe, P. Fournier and R.L. Greene, *Superconductivity and field-induced magnetism in $\text{Pr}_{2-x}\text{Ce}_x\text{CuO}_4$ single crystals*, Phys. Rev. Lett. **91**, 147002 (2003).

W. Higemoto, K. Satoh, A. Koda, K. Nishiyama, K. Shimomura, R. Kadono, A. Hanaoka, S. Koiwai, Y. Uwatoko and N. Mori, *μSR study of magnetism of CeRh_2Si_2 under a high pressure*, Physica **B329-333**, 601 (2003).

Y. Aoki, A. Tsuchiya, T. Kanayama, S.R. Saha, H. Sugawara, H. Sato, W. Higemoto, A. Koda, K. Ohishi, K. Nishiyama and R. Kadono, *Time-reversal symmetry-breaking superconductivity in heavy-fermion $\text{PrOs}_4\text{Sb}_{12}$ de-*

- ected by muon-spin relaxation, Phys. Rev. Lett. **91**, 067003 (2003).
- R. Kadono, K. Ohishi, A. Koda, W. Higemoto, K.M. Kojima, S. Kuroshima, M. Fujita and K. Yamada, *Magnetic ground state of $\text{Pr}_{0.89}\text{LaCe}_{0.11}\text{CuO}_{4+\alpha-\delta}$ with varied oxygen depletion probed by muon spin relaxation*, J. Phys. Soc. Jpn. **72**, 2955 (2003).
- K. Ohishi, K. Kakuta, J. Akimitsu, A. Koda, W. Higemoto, R. Kadono, J.E. Sonier, A.N. Price, R.I. Miller, R.F. Kiefl, M. Nohara, H. Suzuki and H. Takagi, *Excess quasiparticles outside the vortex cores in $\text{Y}(\text{Ni}_{1-x}\text{Pt}_x)_2\text{B}_2\text{C}$* , Physica **C388-389**, 197 (2003).
- R. Kadono, W. Higemoto, A. Koda, M.I. Larkin, G.M. Luke, A.T. Savici, Y.J. Uemura, K.M. Kojima, T. Okamoto, T. Kakeshita, S. Uchida, T. Ito and K. Oka, *Large vortex core at low magnetic induction in $\text{La}_{2-x}\text{Sr}_x\text{CuO}_4$ probed by muon spin rotation*, Physica **C388-389**, 631 (2003).
- J. Sugiyama, J.H. Brewer, E.J. Ansaldo, H. Itahara, S. Hirano and T. Tani, μ^+ SR studies on thermoelectric oxides, Physica **B329-333**, 902 (2003).
- J. Sugiyama, H. Itahara, J.H. Brewer, E.J. Ansaldo, T. Motohashi, M. Karppinen and H. Yamauchi, *Static magnetic order $\text{Na}_{0.75}\text{CoO}_2$ detected by muon spin rotation and relaxation*, Phys. Rev. **B67**, 214420 (2003).
- J. van Lierop, H.S. Isaacs, D.H. Ryan, A. Beath and E. McCalla, *Muon spin relaxation study of exchange biased Co/CoO*, Phys. Rev. **B67**, 134430 (2003).
- Y.J. Uemura, *Superfluid density of high- T_c cuprate systems: implication on condensation mechanisms, heterogeneity and phase diagram*, Solid State Comm. **126**, 23 (2003).
- R.I. Miller and R.F. Kiefl, *Magnetism in the cuprates induced by an external magnetic field*, Solid State Comm. **126**, 77 (2003).
- I.M. Gat-Malureanu, A. Fukaya, M.I. Larkin, A.J. Millis, P.L. Russo, A.T. Savici, Y.J. Uemura, P.P. Kyriakou, G.M. Luke, C.R. Wiebe, Y.V. Sushko, R.H. Heffner, D.E. MacLaughlin, D. Andreica and G.M. Kalvius, *Field dependence of muon spin relaxation rate in MnSi* , Phys. Rev. Lett. **90**, 157201 (2003).
- J.A. Chakhalian, R.F. Kiefl, R.I. Miller, J.H. Brewer, S.R. Dunsiger, G.D. Morris, W.A. MacFarlane, J.E. Sonier, S. Eggert, I. Affleck, A. Keren and M. Verdaguer, *Local magnetic susceptibility of the positive muon in the quasi 1D $S = 1/2$ antiferromagnet dichlorobis (pyridine) copper (II)*, Phys. Rev. Lett. **91**, 027202 (2003).
- D.R. Harshman, W.J. Kossler, A.J. Greer, D.R. Noakes, C.E. Stronach, E. Koster, M.K. Wu, F.Z. Chien, J.P. Franck, I. Isaac and J.D. Dow, *Spin-glass behavior, spin-fluctuations and superconductivity in $\text{Sr}_2\text{Y}(\text{Ru}_{1-u}\text{Cu}_u)\text{O}_6$* , Phys. Rev. **B67**, 054509 (2003).
- J. Sugiyama, C. Xia and T. Tani, *Anisotropic magnetic properties of $\text{Ca}_3\text{Co}_4\text{O}_9$; the evidence of a spin density wave transition at 27 K*, Phys. Rev. **B67**, 104410 (2003).
- V.G. Storchak, D.G. Eshchenko, R.L. Lichti and J.H. Brewer, *Weakly bound muonium state in GaP: validity of the effective mass approximation*, Phys. Rev. **B67**, 121201 (2003).
- I. McKenzie, J.-C. Brodovitch, P.W. Percival, T. Ramnial and J.A.C. Clyburne, *The reactions of imidazol-2-ylidenes with the hydrogen atom: a theoretical study and experimental confirmation with muonium*, J. Am. Chem. Soc. **125**, 11565 (2003).
- K. Ghandi, B. Addison-Jones, J.-C. Brodovitch, B. McColum, I. McKenzie and P.W. Percival, *Enolization of acetone in superheated water detected via radical formation*, J. Am. Chem. Soc. **125**, 9594 (2003).
- K. Ghandi and P.W. Percival, *Prediction of rate constants for reactions of the hydroxyl radical in water at high temperatures and pressures*, J. Phys. Chem. **A107**, 3005 (2003).
- J.-C. Brodovitch, B. Addison-Jones, K. Ghandi, I. McKenzie, P.W. Percival and J. Schüth, *Free radicals formed by $\text{H}(\text{Mu})$ addition to fluoranthene*, Can. J. Chem. **81**, 1 (2003).
- D.C. Walker, S. Karolczak, H.A. Gillis and G.B. Porter, *Hot model of muonium formation in liquids*, Can. J. Chem. **81**, 199 (2003).
- D.C. Walker, S. Karolczak, G.B. Porter and H. A. Gillis, *No "delayed" muonium-formation in organic liquids*, J. Chem. Phys. **118**, 3233 (2003).
- S. Karolczak, H.A. Gillis, G.B. Porter and D.C. Walker, *Solvent-dependent rate constants of muonium atom reactions*, Can. J. Chem. **81**, 175 (2003).
- K. Ohishi, T. Muranaka, J. Akimitsu, A. Koda, W. Higemoto and R. Kadono, *Quasiparticle excitations outside the vortex cores in MgB_2 probed by muon spin rotation*, J. Phys. Soc. Jpn. **72**, 29 (2003).
- D.H. Ryan, A.D. Beath, E. McCalla, J. van Lierop and J.M. Cadogan, *Transverse spin freezing in $a-(\text{Fe}_{1-x}\text{Mn}_x)_{78}\text{Si}_8\text{B}_{14}$: a site-frustrated metallic glass*, Phys. Rev. **B67**, 104404 (2003).
- K. Ishida, D.E. MacLaughlin, Ben-Li Young, K. Okamoto, Y. Kawasaki, Y. Kitaoka, G.J. Nieuwenhuys, R.H. Heffner, O.O. Bernal, W. Higemoto, A. Koda, R. Kadono, O. Trovarelli, C. Geibel and F. Steglich, *Low-temperature magnetic order and spin dynamics in YbRh_2Si_2* , Phys. Rev. **B68**, 184401 (2003).
- J.E. Sonier, K.F. Poon, G.M. Luke, P. Kyriakou, R.I. Miller, P. Fournier and R.L. Greene, *Paramagnetic vortex state in $\text{Pr}_{2-x}\text{Ce}_x\text{CuO}_4$ single crystals*, Physica **B329-333**, 685 (2003).

- C.-S. Yu, J. Eisenbarth, A. Runz, K. Weber, S. Zeisler and F. Oberdorfer, *Syntheses of 5-(2-radiohaloethyl)- and 5-(2-radiohalovinyl)-2'-deoxyuridines. Novel types of radio-tracer for monitoring cancer gene therapy with PET*, J. Lab. Comp. Radiopharm. **46**, 421 (2003).
- R.A. Pavan, W.Z. Gelbart and S.K. Zeisler, *Thermal modelling of high current solid targets*, J. Radioanal. Nucl. Chem. **257**, 203 (2003).
- S. Zeisler, R.A. Pavan, J. Orzechowski, R. Langlois, S. Rodrigue and J.E. van Lier, *Production of ^{64}Cu on the Sherbrooke TR-PET cyclotron*, J. Radioanal. Nucl. Chem. **257**, 175 (2003).
- P.L. McGeer, C. Schwab, A. Parent and D.J. Doudet, *Presence of reactive microglia in monkey substantia nigra years after MPTP administration*, Ann. Neurol. **54**, 599 (2003).
- D.J. Doudet and J.E. Holden, *Sequential vs. non-sequential measurement of density and affinity of dopamine D_2 receptors with [^{11}C]raclopride: 1: effect of methamphetamine*, J. Cereb. Blood Flow Metab. **23**, 1489 (2003).
- D.J. Doudet, S. Jivan and J.E. Holden, *In vivo measurement of receptor density and affinity: comparison of the routine sequential method with a non sequential method in studies of dopamine D_2 receptors with [^{11}C]raclopride*, J. Cereb. Blood Flow Metab. **23**, 280 (2003).
- V. Sossi, J.E. Holden, R. de la Fuente-Fernandez, T.J. Ruth and A.J. Stoessl, *The effect of dopamine loss and the metabolite 3-O-methyl-[^{18}F]fluorodopa on the relationship between the ^{18}F -fluorodopa tissue input uptake rate constant K_{occ} and the ^{18}F -fluorodopa plasma input uptake rate constant K_i* , J. Cereb. Blood Flow and Metab. **23**, 301 (2003).
- V. Sossi, *Positron emission tomography (PET) advances in neurological applications*, Nucl. Instrum. Methods **A510**, 107 (2003).
- C.W. Olanow, C.G. Goetz, J.H. Kordower, A.J. Stoessl, V. Sossi, M.F. Brin, K.M. Shannon, G.M. Nauert, D.P. Perl, J. Godbold and T.B. Freeman, *A double-blind controlled trial of bilateral fetal nigral transplantation in Parkinson's disease*, Ann. Neurol. **54**, 403 (2003).
- A. Kumar, S. Mann, V. Sossi, T.J. Ruth, A.J. Stoessl, M. Schulzer and C.S. Lee, *[^{11}C]DTBZ-PET correlates of levodopa responses in asymmetric Parkinson's disease*, Brain, **126**, 2648 (2003).
- A. Kumar, S.N. Silim, M. Okamoto, M.Y. Siddiqi and A.D.M. Glass, *Differential expression of three members of the AMT1 gene family encoding putative high-affinity NH_4^+ transporters in roots of *Oryza sativa* sub species indica*, Plant Cell & Environ. **26**, 907 (2003).
- H.J. Kronzucker, M.Y. Siddiqi, A.D.M. Glass and D.T. Britto, *Root ammonium transport efficiency as a determinant in forest colonization patterns: a hypothesis*, Physiol. Plant **117**, 164 (2003).
- P. Nazoa, J.J. Vidmar, T.J. Tranbarger, K. Mouline, I. Damiani, P. Tillard, D. Zhuo, A.D.M. Glass and B. Touraine, *Regulation of the nitrate transporter gene *At-NRT2.1* in *Arabidopsis thaliana*: responses to nitrate, amino acids and developmental stage*, Plant Mol. Biol. **52**, 689 (2003).
- A.D.M. Glass, *Physiological constraints on nitrogen uptake efficiency*, Critical Reviews in Plant Sciences **22**, 453 (2003).
- M. Okamoto, J.J. Vidmar and A.D.M. Glass, *Regulation of *NRT1* and *NRT2* gene families of *Arabidopsis thaliana*: responses to nitrate provision*, Plant Cell Physiol. **44**, 304 (2003).
- A. Studenov, S. Jivan, K.R. Buckley and M.J. Adam, *Efficient in-loop synthesis of high specific radioactivity [^{11}C]Carfentanil*, J. Lab. Compds. Radiopharm. **46**, 837 (2003).
- T.E. Barnhart, A.K. Converse, K.A. Dabbs, R.J. Nickles, K. Buckley, S. Jivan, T.J. Ruth and A.D. Roberts, *Water-cooled grid support system for high power irradiation with thin target windows*, Appl. Radiat. Isotopes **58**, 21 (2003).
- A.J. Stoessl and R. de la Fuente-Fernandez, *Dopamine receptors in Parkinson's disease: imaging studies*, Advances in Neurol. **91**, 65 (2003).
- R. de la Fuente-Fernandez, A.S. Lim, V. Sossi, M.J. Adam, T.J. Ruth, D.B. Calne, A.J. Stoessl and C.S. Lee, *Age and severity of nigrostriatal damage at onset of Parkinson's disease*, Synapse **47**, 152 (2003).
- H. Dougan, J.I. Weitz, A.R. Stafford, K.D. Gillespie, P. Klement, J.B. Hobbs and D.M. Lyster, *Evaluation of DNA aptamers directed to thrombin as potential imaging agents*, Nucl. Med. and Biol. **30**, 61 (2003).
- A.J. Stoessl, *Agonizing over dopaminergic replacement therapy – lessons from animal models of Parkinson's disease*, Exp. Neurol. **183**, 1(2003).
- A.L. Whone, R.L. Watts, A.J. Stoessl et al., *Slower progression of Parkinson's disease with ropinirole versus levodopa: the REAL-PET study*, Ann. Neurol. **54**, 93 (2003).
- R. de la Fuente-Fernandez, S. Furtado, M. Guttman, Y. Furukawa, C.S. Lee, D.B. Calne, T.J. Ruth, S.J. Kish and A.J. Stoessl, *VMAT2 binding is elevated in dopa-responsive dystonia: visualizing empty vesicles by PET*, Synapse **49**, 20 (2003).

Theoretical Program

- B. Davids and S. Typel, *Electromagnetic dissociation of ^8B and the astrophysical S factor for $^7\text{Be}(p,\gamma)^8\text{B}$* , Phys. Rev. **C68**, 045802 (2003).
- S. Nakamura, T. Sato, S. Ando, T.-S. Park, F. Myhrer, V. Gudkov and K. Kubodera, *Neutrino-deuteron reactions at solar neutrino energies*, Nucl. Phys. **A721**, 549c (2003).

- R.H. Cyburt, B.D. Fields and K.A. Olive, *Primordial nucleosynthesis in light of WMAP*, Phys. Lett. **B567**, 227 (2003) [astro-ph/0302431].
- R.H. Cyburt, J. Ellis, B.D. Fields and K.A. Olive, *Updated nucleosynthesis constraints on unstable relic particles*, Phys. Rev. **D67**, 103521 (2003) [astro-ph/0203240].
- A. Amghar, B. Desplanques and L. Theussl, *Comparison of form factors calculated with different expressions for the boost transformation*, Nucl. Phys. **A714**, 213 (2003) [nucl-th/0202046].
- A. Amghar, B. Desplanques and L. Theussl, *The form factor of the pion in 'point-form' of relativistic dynamics revisited*, Phys. Lett. **B574**, 201 (2003) [hep-ph/0301235].
- C. Barbieri and W.H. Dickhoff, *Extension of the random phase approximation including the self-consistent coupling to two phonon contributions*, Phys. Rev. **C68**, 014311 (2003) [nucl-th/0212025].
- M.A. Doncheski and S. Godfrey, *Resolved photon contributions to Higgs boson production in gamma-gamma collisions*, Phys. Rev. **D67**, 073021 (2003) [TRI-PP-03-02, hep-ph/0105070].
- C.P. Liu, C.H. Hyun and B. Desplanques, *Deuteron anapole moment with heavy mesons*, Phys. Rev. **C68**, 045501 (2003) [nucl-th/0306020].
- F.E. Close and S. Godfrey, *Charmonium hybrid production in exclusive B meson decays*, Phys. Lett. **B574**, 210 (2003) [ADP-03-120-T558, TRI-PP-03-04, OUTP-03-13-P, hep-ph/0305285].
- M.A. Doncheski, S. Godfrey and S. Zhu, *Measurement of $\tan\beta$ in associated tH^\pm production in $\gamma\gamma$ collisions*, Phys. Rev. **D68**, 053001 (2003) [TRI-PP-03-05, ADP-02-121-T559, hep-ph/0306126].
- J. Al-Khalili, C. Barbieri, J. Escher, B.K. Jennings and J.-M. Sparenberg, *Many body approach to proton emission and the role of spectroscopic factors*, Phys. Rev. **C68**, 024314 (2003) [TRI-PP-03-06, nucl-th/0304055].
- C.Q. Geng and C.C. Liu, *Study of $B_s \rightarrow (\eta, \eta', \phi)\ell\bar{\ell}$ decays*, J. Phys. **G29**, 1103 (2003) [hep-ph/0303246].
- C.-H. Chen, C.Q. Geng and I.L. Ho, *Forward backward asymmetry in $K^+ \rightarrow \pi^+\ell^+\ell^-$* , Phys. Rev. **D67**, 074029 (2003) [hep-ph/0302207].
- W.F. Chang and J.N. Ng, *Neutrino masses in 5-D orbifold $SU(5)$ unification models without right handed singlets*, JHEP **0310**, 36 (2003) [hep-ph/0308187].
- C.V. Chang, W.F. Chang and J.N. Ng, *Neutrino masses in a 5-D $SU(3)(W)$ TeV unification model*, Phys. Lett. **B558**, 92 (2003) [hep-ph/0301271].
- R. Allahverdi, B. Dutta and A. Mazumdar, *Sleptogenesis*, Phys. Rev. **D67**, 123515 (2003) [TRI-PP-03-03, hep-ph/0301184].
- M. deMontigny, F.C. Khanna and A.E. Santana, *Lorentz-like covariant equations for non-relativistic fluids*, J. Phys. **A36**, 2009 (2003).
- L.M. Abreu, M. de Montigny, F.C. Khanna and A.E. Santana, *Galilei-covariant path-integral quantization of non-relativistic complex scalar fields*, Annals Phys. **308**, 244 (2003).
- U.T. Yakhshiev, A.W. Thomas and F.C. Khanna, *Meson nucleon vertex form-factors at finite temperature using a soft pion form-factor*, Phys. Rev. **C68**, 048201 (2003) [nucl-th/0304020].
- M. de Montigny, F.C. Khanna and A.E. Santana, *Gauge symmetry in Fokker-Planck dynamics*, Physica **A323**, 327 (2003) [hep-ph/0301197].
- S. Sengupta, F.C. Khanna and S.P. Kim, *Nonequilibrium evolution of correlation functions: a canonical approach*, Phys. Rev. **D68**, 105014 (2003) [hep-ph/0301071].
- M. de Montigny, F.C. Khanna and A.E. Santana, *Nonrelativistic wave equations with gauge fields*, Int. J. Theor. Phys. **42**, 649 (2003).
- D.U. Matrasulov, F.C. Khanna and H. Yusupov, *Spectra of heavy-light mesons*, J. Phys. **G29**, 475 (2003).
- K. Tsushima and F.C. Khanna, *Λ_c^+ and Λ_b hypernuclei*, Phys. Rev. **C67**, 015211 (2003) [nucl-th/0207077].
- C.P. Liu, G. Prézeau and M.J. Ramsey-Musolf, *Hadronic parity violation and inelastic electron deuteron scattering*, Phys. Rev. **C67**, 035501 (2003) [nucl-th/0212041].
- A.K. Dutt-Mazumder, *Omega meson propagation in dense nuclear matter and collective excitations*, Nucl. Phys. **A713**, 119 (2003) [nucl-th/0207070].
- S. Ando, Y.H. Song, T.S. Park, H.W. Fearing and K. Kubodera, *Solar neutrino reactions on deuteron in effective field theory*, Phys. Lett. **B555**, 49 (2003) [USC-NT-02-2, SNUTP-02-014, TRI-PP-02-07, nucl-th/0206001].
- R. Lewis, W. Wilcox and R.M. Woloshyn, *The nucleon's strange electromagnetic and scalar matrix elements*, Phys. Rev. **D67**, 013003 (2003) [BU-HEPP-02-10, TRI-PP-02-15, hep-ph/0210064].
- G. Rupak and X. Kong, *Quartet S-wave $p-d$ scattering in EFT*, Nucl. Phys. **A717**, 73 (2003) [TRI-PP-01-13, nucl-th/0108059].

Journal Publications In Press or Submitted

Particle, Nuclear and Atomic Physics

T. Warner *et al.*, *Diffusion of Xe in Zr, Ta, and Pt* (submitted to Nucl. Instrum. Methods A).

S.R. Nuss-Warren *et al.*, *On-line collection and transfer of radioactive noble gas isotopes* (submitted to Nucl. Instrum. Methods A).

- P.-N. Seo, J.D. Bowman, M. Gericke, J. Long, G.S. Mitchell, S.I. Penttila and W.S. Wilburn, *A measurement of the Flight Path 12 cold moderator brightness at LANSCE* (Nucl. Instrum. Methods, in press).
- G.S. Mitchell, C.S. Blessinger, J.D. Bowman, T.E. Chupp, K.P. Coulter, M. Gericke, G.L. Jones, M.B. Leuschner, H. Nann, S.A. Page, S.I. Penttila, T.B. Smith, W.M. Snow and W.S. Wilburn, *A measurement of parity-violating gamma-ray asymmetries in polarized cold neutron capture on ^{35}Cl , ^{113}Cd , and ^{139}La* (Nucl. Instrum. Methods, in press) [nucl-ex/040109].
- Z. Salman, E.P. Reynard, R.F. Kiefl, W.A. MacFarlane, J. Chakhalian, K.H. Chow, S. Daviel, S. Kreitzman, C.D.P. Levy and R. Poutissou, *Beta-detected nuclear quadrupole resonance with a low energy beam of $^8\text{Li}^+$* (Phys. Rev. B, in press).
- P. Dubé and M. Trinczek, *Hyperfine structure splittings and absorption strengths of molecular iodine transitions near the trapping frequencies of francium* (submitted to J. Optical Society of America B).
- P. Camerini, E. Fragiaco, N. Grion, S. Piano, R. Rui, J. Clark, L. Felawka, E.F. Gibson, G. Hofman, E.L. Mathie, R. Meier, G. Moloney, D. Ottewill, K. Raywood, M.E. Sevier, G.R. Smith and R. Tacik, *General properties of the pion production reaction in nuclear matter* (submitted to Nucl. Phys. A) [nucl-ex/0401018].
- S. Gu and J.A. Behr, *Study of coherent population trapping using off-Raman resonance oscillations* (submitted to Phys. Rev. A).
- A. Airapetian *et al.* [HERMES collaboration], *Measurement of $R = \sigma_L/\sigma_T$ in deep inelastic scattering on nuclei* (submitted to Phys. Lett. B) [DESY-02-091, hep-ex/0210068].
- A. Airapetian *et al.* (HERMES collaboration), *Flavor decomposition of the sea quark helicity distributions in the nucleon from semi-inclusive deep-inelastic scattering* (submitted to Phys. Rev. Lett.) [DESY-03-067, hep-ex/0307064].
- A. Airapetian *et al.* (HERMES collaboration), *Nuclear polarization of molecular hydrogen recombined on a non-metallic surface* (Eur. Phys. J. D, in press) [DESY-03-168].
- A. Airapetian *et al.* (HERMES collaboration), *Evidence for a narrow $|S| = 1$ baryon state at a mass of 1528 MeV in quasi-real photoproduction* (Phys. Lett. B, in press) [DESY-03-213, HERMES-DC-56, hep-ex/0312044].
- W.J. Murray *et al.* (MuScat collaboration), *Status of the MuScat experiment* (J. Phys. G, in press).
- G. Abbiendi *et al.* (OPAL collaboration), *Inclusive analysis of the B quark fragmentation function in Z decays at LEP* (submitted to Eur. Phys. J. C) [CERN-EP-2002-051, hep-ex/0210031].
- G. Abbiendi *et al.* (OPAL collaboration), *Measurement of the cross-section for the process $\gamma\gamma \rightarrow p\bar{p}$ at $\sqrt{s_{ee}} = 183$ – 189 GeV at LEP* (submitted to Eur. Phys. J. C) [CERN-EP-2002-056, hep-ex/0209052].
- G. Abbiendi *et al.* (OPAL collaboration), *Multi-photon production in e^+e^- collisions at $\sqrt{s} = 181$ – 209 GeV* (submitted to Eur. Phys. J.) [CERN-EP-2002-060, hep-ex/0210016].
- G. Abbiendi *et al.* (OPAL collaboration), *Search for nearly mass degenerate charginos and neutralinos at LEP* (submitted to Eur. Phys. J.) [CERN-EP-2002-063, hep-ex/0210043].
- G. Abbiendi *et al.* (OPAL collaboration), *A measurement of semileptonic B decays to narrow orbitally excited charm mesons* (submitted to Eur. Phys. J. C) [CERN-EP-2002-094, hep-ex/0301018].
- G. Abbiendi *et al.* (OPAL collaboration), *Tests of models of color reconnection and a search for glueballs using gluon jets with a rapidity gap* (submitted to Eur. Phys. J. C) [CERN-EP-2003-031, hep-ex/0306021].
- G. Abbiendi *et al.* (OPAL collaboration), *Search for R-parity violating decays of scalar fermions at LEP* (Eur. Phys. J. C, in press) [CERN-EP-2003-036, hep-ex/0310054].
- G. Abbiendi *et al.* (OPAL collaboration), *Search for anomalous production of dilepton events with missing transverse momentum in e^+e^- collisions at $\sqrt{s} = 183$ – 209 GeV* (Eur. Phys. J. C, in press) [CERN-EP-2003-040, hep-ex/0309014].
- G. Abbiendi *et al.* (OPAL collaboration), *Measurement of charged current triple gauge boson couplings using W pairs at LEP* (submitted to Eur. Phys. J. C) [CERN-EP-2003-042, hep-ex/0308067].
- G. Abbiendi *et al.* (OPAL collaboration), *A study of $W^+W^-\gamma$ events at LEP* (submitted to Phys. Lett. B) [CERN-EP-2003-043, hep-ex/0309013].
- G. Abbiendi *et al.* (OPAL collaboration), *A study of charm production in beauty decays with the OPAL detector at LEP* (submitted to Eur. Phys. J. C) [CERN-EP-2003-050, hep-ex/0308050].
- G. Abbiendi *et al.* (OPAL collaboration), *Tests of the standard model and constraints on new physics from measurements of fermion pair production at 189–209 GeV at LEP* (Eur. Phys. J. C, in press) [CERN-EP-2003-053, hep-ex/0309053].
- G. Abbiendi *et al.* (OPAL collaboration), *Experimental studies of unbiased gluon jets from e^+e^- annihilations using the jet boost algorithm* (Phys. Rev. D, in press) [CERN-EP-2003-067, hep-ex/0310048].
- G. Abbiendi *et al.* (OPAL collaboration), *Flavor independent search for Higgs bosons decaying into hadronic final states in e^+e^- collisions at LEP* (submitted to Phys. Lett. B) [CERN-EP-2003-081, hep-ex/0312042].

G. Abbiendi *et al.* (OPAL collaboration), *Measurement of the partial widths of the Z into up and down type quarks* (submitted to Phys. Lett. B) [CERN-EP-2003-082, hep-ex/0312043].

G. Abbiendi *et al.* (OPAL collaboration), *W boson polarization at LEP2* (submitted to Phys. Lett. B) [CERN-EP-2003-088, hep-ex/0312047].

G. Abbiendi *et al.* (OPAL collaboration), *Search for chargino and neutralino production at $\sqrt{s}=192-209$ GeV at LEP* (submitted to Eur. Phys. J. C) [CERN-EP-2003-090, hep-ex/0401026].

S.N. Ahmed *et al.* (SNO collaboration), *Measurement of the total active ^8B solar neutrino flux at the Sudbury Neutrino Observatory with enhanced neutral current sensitivity* (submitted to Phys. Rev. Lett.) [nucl-ex/0309004].

S.N. Ahmed *et al.* (SNO collaboration), *Constraints on nucleon decay via 'invisible' modes from the Sudbury Neutrino Observatory* (submitted to Phys. Rev. Lett.) [hep-ex/0310030].

Instrumentation/Accelerator Physics/Computing Sciences

S. Koscielniak and C. Johnstone, *Mechanisms for non-linear acceleration in FFAGs with fixed rf* (Nucl. Instrum. Methods A, in press).

M.S. Dixit, J. Dubeau, J.-P. Martin and K. Sachs, *Position sensing from charge dispersion in micro-pattern gas detectors with a resistive anode* (Nucl. Instrum. Methods A, in press) [physics/0307152].

Ch. Rauth, Ch. Geppert, R. Horn, J. Lassen, P.G. Bricault and K. Wendt, *First laser ions at an off-line mass separator of the ISAC facility at TRIUMF* (submitted to Nucl. Instrum. Methods B).

J. Baggio, V. Ferlet-Cavrois and O. Flament, *Comparison of SER test methods for commercial SRAMs* (IEEE Trans. Nucl. Sci., in press).

J.R. Schwank, P.E. Dodd, M.R. Shaneyfelt, G.L. Hash, V. Ferlet-Cavrois, P. Paillet and J. Baggio, *Issues for single-event proton testing of ICs* (IEEE Trans. Nucl. Sci., in press).

Y. Tamaki *et al.*, *Upgrade of the level-0 trigger system for BNL-E949* (submitted to IEEE Trans. Nucl. Sci.).

Molecular and Materials Science

K.M. Kojima, J. Yamanobe, H. Eisaki, S. Uchida, Y. Fudamoto, I.M. Gat, M.I. Larkin, A. Savici, Y.J. Uemura, P.P. Kyriakou, M.T. Rovers and G.M. Luke, *Site-dilution in quasi one-dimensional antiferromagnet $\text{Sr}_2(\text{Cu}_{1-x}\text{Pd}_x)\text{O}_3$: reduction of Néel temperature and spatial distribution of ordered moment sizes* (submitted to Phys. Rev. B).

R.F. Kiefl, K. H. Chow, W.A. MacFarlane, C.D.P. Levy and Z. Salman, *Application of low energy spin polarized*

radioactive ion beams in condensed matter research (Nucl. Phys. News, in press).

V.G. Storchak, D.G. Eshchenko, J.H. Brewer, B. Hitti, R.L. Lichti and B.A. Aronzon, *Magnetic freezeout of electrons into muonium atoms in GaAs* (submitted to Phys. Rev. Lett.).

J. Sugiyama, J.H. Brewer, E.J. Ansaldo, B. Hitti, M. Mikami, Y. Mori and T. Sasaki, *Electron correlation in the two-dimensional triangle lattice of Na_xCoO_2* (submitted to Phys. Rev. B).

J. Sugiyama, J.H. Brewer, E.J. Ansaldo, H. Itahara, T. Tani, M. Mikami, Y. Mori, T. Sasaki, S. Hébert and A. Maignan, *Dome-shaped magnetic phase diagram of thermoelectric layered cobaltites* (Phys. Rev. Lett., in press).

D.R. Harshman, W.J. Kossler, X. Wan, A.T. Fiory, A.J. Greer, D.R. Noakes, C.E. Stronach, E. Koster, A. Erb, and J.D. Dow, *Nodeless pairing state in single-crystal $\text{YBa}_2\text{Cu}_3\text{O}_7$* (Phys. Rev. B, in press).

J.J. Pan, D.J. Arseneau, M. Senba and D.G. Fleming, *Gas phase $\text{Mu}+\text{CO}$ termolecular kinetics* (submitted to J. Chem. Phys.).

R. Kadono, W. Higemoto, A. Koda, M.I. Larkin, G.M. Luke, A.T. Savici, Y.J. Uemura, K.M. Kojima, T. Okamoto, T. Kakeshita, S. Uchida, T. Ito, K. Oka, M. Takigawa, M. Ichiooka and K. Machida, *Expansion of vortex cores at low magnetic induction in $\text{La}_{2-x}\text{Sr}_x\text{CuO}_4$* (submitted to Phys. Rev. Lett.).

Y. Fudamoto, I.M. Gat, M.I. Larkin, J. Merrin, B. Nachumi, A.T. Savici, Y.J. Uemura, G.M. Luke, K.M. Kojima, M. Isobe, Y. Ueda, S. Taniguchi and M. Sato, *μSR studies of two-dimensional antiferromagnets CaV_3O_7 and SrV_3O_7* (Physica B, in press).

A.J. Greer, D.R. Harshman, W.J. Kossler, A. Goonewardene, D.L. Williams, E. Koster, W. Kang, R.N. Kleiman and R.C. Haddon, *A μSR study of the $(\text{TMTSF})_2\text{ClO}_4$ system* (submitted to Physica C).

A.D. Beath and D.H. Ryan, *Ordering in the site frustrated Heisenberg ferromagnet revisited* (J. Appl. Phys., in press).

Life Sciences

S.E. Unkles, R. Wang, Y. Wang, A.D.M. Glass, N. Crawford and J.R. Kinghorn, *Nitrate reductase in required for nitrate uptake into fungal but not plant cells* (J. Biol. Chem., in press).

R. Mungur, A.D.M. Glass, D.B. Goodenow and D.A. Lightfoot, *Metabolite fingerprinting in transgenic *Nicotiana tabacum* altered by the *Escherichia coli* glutamate dehydrogenase* (JBB, in press).

A. Rahmi, M. Lenox, A.J. Reader, C. Michel, Z. Burbar, T.J. Ruth and V. Sossi, *Iterative list-mode reconstruction for high resolution research tomographs* (submitted to IEEE).

- A. Rahmim, P. Bloomfield, S. Houle, M. Lenox, C. Michel, K.R. Buckley, T.J. Ruth and V. Sossi, *Motion correction in histogram-mode and list-mode EM reconstruction* (submitted to IEEE Trans. Nucl. Sci.).
- A.R. Studenov, S. Jivan, M.J. Adam, T.J. Ruth and K.R. Buckley, *Studies of the mechanism of the in-loop synthesis of pharmaceuticals* (submitted to Appl. Radiat. Isot.).
- R. de la Fuente-Fernandez, V. Sossi, Z. Huang, S. Furtado, J.-Q. Lu, D.B. Calne, T.J. Ruth and A.J. Stoessl, *Dyskinesias and synaptic dopamine levels in Parkinson's disease: a PET study* (submitted to Brain).
- A. Rahmim, M. Lenox, A.J. Reader, C. Michel, Z. Burbar, T.J. Ruth and V. Sossi, *Weighted iterative list-mode reconstruction with random correction for the high resolution research tomograph* (submitted to Phys. Med. and Biol.).
- E.W.K. Young, D.M. Martinez, J.A. Olson, T. Ruth, V. Sossi, K. Buckley and S. Jivan, *Sedimentation of paper-making fibres* (submitted to Int. J. MultiPhase Flow).
- A. Rahmi, P. Bloomfield, S. Houle, M. Lenox, C. Michel, K.R. Buckley, T.J. Ruth and V. Sossi, *Practically feasible histogram mode and list-mode EM reconstructions with full motion compensation* (submitted to IEEE NS).
- C.S. Lee, M. Schulzer, R. de la Fuente-Fernandez, E. Mak, V. Sossi, T.J. Ruth, D.B. Calne and A.J. Stoessl, *Regional selectivity of progression in Parkinson's disease: implications for pathogenesis* (submitted to Ann. Neurol.).
- V. Sossi, R. de la Fuente-Fernandez, J.E. Holden, M. Schulzer, T.J. Ruth and A.J. Stoessl, *Onset and progression of Parkinsonian symptoms as a manifestation of impaired compensatory mechanisms in the nigrostriatal dopamine pathway* (submitted to Ann. Neurol.).
- D.J. Doudet and J.E. Holden, *[¹¹C]raclopride PET studies of dopamine release by amphetamine: dependence on presynaptic integrity* (Biol. Psychiat., in press).
- D.T. Britto, T.J. Ruth, S. Lapi and H.J. Kronzucker, *Cellular and whole-plant chloride dynamics in barley: insights into chloride-nitrogen interactions and salinity responses* (Planta, in press).
- H. Zaidi and V. Sossi, *Point-counterpoint: correction for image degrading factors is essential for accurate quantification of brain function using PET* (Medical Physics, in press).
- M. Zamburlini, C.S. Lee, J.E. Holden, T.J. Ruth, S. Jivan, M. Adam, C. Williams, J. McKenzie, A.J. Stoessl and V. Sossi, *Methods of analysis of the acetylcholinesterase tracer N[¹¹C]Methylpiperidin-4-yl propionate (PMP): comparison of disease discriminating ability* (submitted to J. Cereb. Blood Flow).
- M.J. Adam, K.R. Buckley, S. Jivan, J. Huser, J. Lu, D. Lyster, R. MacDonald, J. Mercer, S. McQuarrie, J. Wilson and T.J. Ruth, *¹⁸F-FDG production: a comparison of 3 commercial systems and 3 sources of ¹⁸F-fluoride* (submitted to Nucl. Med. Commun.).
- J.E. Holden, V. Sossi, G. Chan, D.J. Doudet, A.J. Stoessl and T.J. Ruth, *Effect of population k2 values in graphical estimation of DV ratios of reversible ligands* (submitted to J. Cereb. Blood Flow).
- A. Kishore, G.L.-Y. Chan, T. Dobko, M. Schulzer, V. Sossi, R. de la Fuente-Fernandez, E. Mak, T.J. Ruth, D.B. Calne and A.J. Stoessl, *Dopamine D1 and D2 receptors and motor complications in idiopathic Parkinsonism: a PET study* (submitted to Brain).
- Z. Huang, R. de la Fuente-Fernandez and A.J. Stoessl, *Etiology of Parkinson's disease* (Can. J. Neurol. Sci., in press).
- D.T. Britto and H.J. Kronzucker, *Can unidirectional influx be measured in higher plants? A mathematical approach using parameters from efflux analysis* (New Phytol., in press).
- M.Y. Siddiqi, H.J. Kronzucker, D.T. Britto and A.D.M. Glass, *Effect of increasing NH₄⁺ on growth of a tomato crop* (J. Plant Nutr. Soil Sci., in press).
- S.E. Unkles, D. Zhou, M.Y. Siddiqi, J.R. Kinghorn and A.D.M. Glass, *Apparent genetic redundancy facilitates ecological plasticity for nitrate transport* (EMBO J., in press).
- R. de la Fuente-Fernandez, S. Furtado, M. Guttman, Y. Furukawa, C.S. Lee, D.B. Calne, T.J. Ruth, S.J. Kish and A.J. Stoessl, *Expression of vesicular monoamine transporter type 2 is not linked to dopamine synthesis: in-vivo evidence from human PET studies* (submitted to Ann. Neurol.).
- C.S. Lee, M. Schulzer, R. de la Fuente-Fernandez, E. Mak, V. Sossi, T.J. Ruth, D.B. Calne and A.J. Stoessl, *Degeneration of dopamine neurons is self-limiting in Parkinson's disease: causation by an event?* (submitted to Science).
- A. Astbury, *Mortality rates for some common cancers in the USA manifest strong geographical effects* [TRI-PP-03-31].

Theoretical Program

- C.Q. Geng, I.-L. Ho and T.H. Wu, *Axial-vector form factors for $K_{l2\gamma}$ and $\pi_{l2\gamma}$ at $\mathcal{O}(p^6)$ in chiral perturbation theory*, (Nucl. Phys. B, in press) [hep-ph/0306165].
- R.H. Cyburt, B.D. Fields and K.A. Olive, *Solar neutrino constraints on the BBN production of Li* (submitted to Phys. Rev. D) [astro-ph/0312629].
- G. Huey, R.H. Cyburt and B.D. Wandelt, *Precision primordial ⁴He measurement with CMB experiments* (Phys. Rev. D, in press) [astro-ph/0307080].
- D. Baye and J.-M. Sparenberg, *Topical review: inverse scattering with supersymmetric quantum mechanics* (submitted to J. Phys. A).

D. Binosi and L. Theussl, *Jaxodraw: A graphical user interface for drawing Feynman diagrams* (submitted to Comp. Phys. Comm.) [hep-ph/0309015].

L. Theussl, S. Noguera and V. Vento, *Generalized parton distributions of the pion in a Bethe-Salpeter approach* (Eur. Phys. J. A, in press) [nucl-th/0211036].

B. Desplanques and L. Theussl, *Form factors in the 'point form' of relativistic quantum mechanics: single and two-particle currents* (Eur. Phys. J. A, in press) [hep-ph/0307028].

D.H. Wilkinson, *Super-allowed Fermi beta-decay: a further visit* (submitted to Nucl. Instrum. Methods) [TRI-PP-03-41].

W.H. Dickhoff and C. Barbieri, *Self-consistent Green's function method for nuclei and nuclear matter* (Prog. Part. Nucl. Phys., in press) [TRI-PP-03-40, nucl-th/0402034].

J.-M. Sparenberg, *On the (non)relation between bound and scattering states in quantum mechanics. Application to $^{12}\text{C} + \alpha$* (Phys. Rev. C, in press) [TRI-PP-03-25, nucl-th/0306053].

D.U. Matrasulov, F.C. Khanna and U.R. Salomov, *Quantum chaos in the heavy quarkonia* (submitted to Phys. Rev. C) [hep-ph/0306214].

D.U. Matrasulov, F.C. Khanna and D.M. Otajanov, *Chao-tization of the periodically driven quarkonia* (submitted to Eur. Phys. J. A) [hep-ph/0306197].

D.U. Matrasulov, F.C. Khanna, U.R. Salomov and A.E. Santana, *Quantum chaos in the Yang-Mills-Higgs system at finite temperature* (submitted to Phys. Rev. D) [hep-ph/0306162].

G. Gour, F.C. Khanna and M. Revzen, *Self adjoint extensions of phase and time operators* (Phys. Rev. A, in press).

R. Allahverdi, C. Bird, S.G. Nibbelink and M. Pospelov, *Cosmological bounds on large extra dimensions from nonthermal production of Kaluza-Klein modes* (Phys. Rev. D, in press) [TRI-PP-03-07, UVIC-TH-05-03, hep-ph/0305010].

T. Gorringer and H.W. Fearing, *Induced pseudoscalar coupling of the proton weak interaction* (Rev. Mod. Phys., in press) [TRI-PP-02-08, nucl-th/0206039].

E. Vogt, *Single neutron halos in the valley of stability* (submitted to Phys. Lett.) [TRI-PP-02-03].

E. Vogt, *Pervasive and extreme neutron halos* (resubmitted to Phys. Rev. C) [TRI-PP-01-23].

W.-F. Chang and J.N. Ng, *Phenomenology of a 5-D orbifold $SU(3)/W$ unification model* (Phys. Rev. D, in press) [hep-ph/0312199].

W.F. Chang and J.N. Ng, *Radiative neutrino masses in 5D $SU(5)$ unification* (submitted to Phys. Rev. D).

J. Escher and B.K. Jennings, *Contemplating a new measure for nuclear shell closures* (Revista Mexicana de Fisica, in press).

Conference Publications

Particle, Nuclear and Atomic Physics

Y. Itow, T. Kajita, K. Kaneyuki, M. Shiozawa, Y. Totsuka, Y. Hayato, T. Ishida, T. Ishii, T. Kobayashi, T. Maruyama, K. Nakamura, Y. Obayashi, Y. Oyama, M. Sakuda, M. Yoshida, S. Aoki, T. Hara, A. Suzuki, A. Ichikawa, T. Nakaya, K. Nishikawa, T. Hasegawa, K. Ishihara, A. Suzuki and A. Konaka, *The JHF-Kamioka neutrino project*, Proc. **3rd Workshop on Neutrino Oscillations and Their Origin (NOON 2001)**, Kashiwa, Japan, December 5–8, 2001, eds. Y. Suzuki *et al.* (World Scientific, Singapore, 2003) p.239 [KEK-REPORT-2001-4, ICRR-REPORT-477-2001-7, TRI-PP-01-05, hep-ex/0106019].

A. Shotter, *ISAC at TRIUMF: status and future*, Proc. **3rd Int. Conf. on Fission and Properties of Neutron-Rich Nuclei, Sanibel Island, FL, November 3–9, 2002**, eds. J.H. Hamilton *et al.* (World Scientific, Singapore, 2003).

H.A. Schuessler, F. Buchinger and H. Iimura, *Laser spectroscopy of short lived rare earth isotopes*, Proc. **17th Int. Conf. on the Application of Accelerators in Research and Industry (CAARI)**, Denton, TX, November 12–16, 2002, eds. J.L. Duggan and I.L. Morgan (AIP Conf. Proc. **680**, Melville, NY, 2003) p.223.

A.A. Chen *et al.*, *Measurement of the $^{21}\text{Na}(p,\gamma)^{22}\text{Mg}$ reaction with the DRAGON facility at TRIUMF-ISAC*, *ibid.* 237.

J. Dilling *et al.* (TITAN collaboration), *The proposed TITAN facility at TRIUMF: a next generation Penning trap mass spectrometer for highly charged ions*, *ibid.*

J.M. D'Auria, J. Thomson and M. Comyn (editors), Proc. **14th Int. Conf. on Electromagnetic Isotope Separators and Techniques Related to Their Applications (EMIS-14)**, Victoria, BC, May 6–10, 2002 (Nucl. Instrum. Methods **B204**, 2003).

A. Shotter, *Advances at ISOL facilities*, *ibid.* 17 [TRI-PP-02-23].

S. Engel *et al.* (DRAGON collaboration), *Commissioning and operation of DRAGON*, *ibid.* 154 [TRI-PP-02-21].

M. Domsbky, P. Bricault, P. Schmor and M. Lane, *ISAC target operation with high proton currents*, *ibid.* 191 [TRI-PP-02-31].

P. Bricault, M. Domsbky, A. Dowling and M. Lane, *High power target developments at ISAC*, *ibid.* 319 [TRI-PP-02-27].

R. Baartman, *Low energy beam transport design optimization for RIBs*, *ibid.* 392 [TRI-PP-02-24].

- R.E. Laxdal, *Acceleration of radioactive ions*, *ibid.* 400 [TRI-PP-02-25].
- S. Engel, L. Buchmann, A. Chen, J.M. D'Auria, D.A. Hutcheon, C.S. Galovich, D. Gigliotti, U. Greife, D. Hunter, A. Hussein, C.C. Jewett, W. Liu, A. Olin, D. Ottewell and J. Rogers, *Testing the ISAC radioactive ion accelerator beam specifications using the $H(^{15}\text{N}, \alpha\gamma)^{12}\text{C}$ reaction*, *ibid.* 416.
- S. Lapi, T.J. Ruth, A. Zyuzin and J.M. D'Auria, *Development of an intense ^{15}O radioactive ion beam using low energy protons*, *ibid.* 444 [TRI-PP-02-32].
- J. Dilling, P. Bricault, M. Smith, H.-J. Kluge *et al.* (TITAN collaboration), *The proposed TITAN facility at ISAC for very precise mass measurements on highly charged short-lived isotopes*, *ibid.* 492 [TRI-PP-02-30].
- J.A. Behr, *Neutral atom traps of radioactives*, *ibid.* 526 [TRI-PP-02-22].
- D. Melconian, D. Ashery, G. Ball, J.A. Behr, P. Bricault, B.A. Brown, M. Dombisky, K.P. Jackson, S. Fostner, A. Gorelov, M.N. Groves, S. Gu, M.R. Pearson, I.S. Towner, M. Trinczek and I. Vollrath, *Measuring isospin mixing in ^{36}Ar using a polarized, neutral atom trap*, *ibid.* 540 [TRI-PP-02-28].
- A.A. Chen *et al.* (DRAGON collaboration), *Results from the development of ionization detection systems for the DRAGON facility*, *ibid.* 614 [TRI-PP-02-20].
- C. Wrede, A. Hussein, J.G. Rogers and J. D'Auria, *A double sided silicon strip detector as a DRAGON end detector*, *ibid.* 619.
- C.E. Svensson, R.A.E. Austin, G.C. Ball, P. Finlay, P.E. Garrett, G.F. Grinyer, G.S. Hackman, C.J. Osborne, F. Sarazin, H.C. Scraggs, M.B. Smith and J.C. Waddington, *Radioactive beam experiments with large gamma-ray detector arrays*, *ibid.* 660.
- D. Gigliotti, J.G. Rogers and A.H. Hussein, *Calibration and simulation of a gamma array for DRAGON at ISAC*, *ibid.* 671 [TRI-PP-02-19].
- R.F. Kiefl, W.A. MacFarlane, P. Amaudruz, D. Arseneau, R. Baartman, T.R. Beal, A. Hatakeyama, B. Hitti, S.R. Kreitzman, C.D.P. Levy, R. Miller, M. Olivo, R. Poutissou, G.D. Morris, S.R. Dunsiger, R. Heffner, K.H. Chow, Y. Hirayama, H. Izumi, C. Bommas, E. Dumont and L.H. Greene, *Low energy spin polarized radioactive beams as a probe of thin films and interfaces*, *ibid.* 682 [TRI-PP-02-29].
- C.D.P. Levy, A. Hatakeyama, Y. Hirayama, R.F. Kiefl, R. Baartman, J.A. Behr, H. Izumi, D. Melconian, G.D. Morris, R. Nussbaumer, M. Olivo, M. Pearson, R. Poutissou and G.W. Wight, *Polarized radioactive beam at ISAC*, *ibid.* 689 [TRI-PP-02-33].
- G.-J. Beyer and T.J. Ruth, *The role of electromagnetic separators in the production of radiotracers for bio-medical research and nuclear medical application*, *ibid.* 694 [TRI-PP-02-26].
- A.B. McDonald *et al.* (SNO collaboration), *Direct evidence for neutrino flavor transformation from neutral-current interactions in SNO*, Proc. **24th Annual Montreal-Rochester-Syracuse-Toronto Conf. on Theoretical Physics (MRST 2002)**, Waterloo, ON, May 15–17, 2002, eds. V. Elias *et al.* (AIP Conf. Proc. **646**, Melville, NY, 2003) p.43.
- J.-M. Poutissou and K. Yoshimura, *Non-neutrino physics working group summary*, Proc. **4th NuFact'02 Workshop (Neutrino Factories based on Muon Storage Rings)**, London, UK, July 1–6, 2002 (J. Phys. **G29**, 2003) p.2005.
- S.H. Park, A.R. Junghans, E.C. Mohrmann, K.A. Snover, T.D. Steiger, E.G. Adelberger, J.M. Cajandian, H.E. Swanson, L. Buchmann, A. Zyuzin and A. Laird, *A new measurement of $^7\text{Be}(p, \gamma)^8\text{B}$ cross section and its astrophysical meaning*, Proc. **7th Int. Symp. on Nuclei in the Cosmos (NIC7)**, Fuji-Yoshida, Japan, July 8–12, 2002, eds. S. Kubono *et al.* (Nucl. Phys. **A718**, 2003) p.113.
- R.E. Azuma, S. Bishop, L. Buchmann, M.L. Chatterjee, A.A. Chen, J.M. D'Auria, T. Davinson, S. Engel, B.R. Fulton, D. Gigliotti, U. Greife, D. Groombridge, D. Hunter, A. Hussein, D. Hutcheon, C. Jewett, J.D. King, N. Khan, S. Kubono, A.M. Laird, M. Lamey, R. Lewis, L. Ling, W. Liu, S. Michimasa, A.S. Murphy, A. Olin, D. Ottewell, P. Parker, J. Pearson, I. Roberts, A. Robinson, J.G. Rogers, G. Roy, C. Ruiz, F. Sarazin, A.C. Shotter, H. Sprenger, F. Strieder, P. Walden, P.J. Woods and C. Wrede, *Results of $^{21}\text{Na} + p$ experiments at ISAC*, *ibid.* 119.
- J.C. Blackmon, D.W. Bardayan, W. Bradfield-Smith, R. Brummit, A.E. Champagne, A.A. Chen, T. Davinson, L. Dessieux, M.W. Guidry, K.I. Hahn, G.M. Hale, W.R. Hix, R.L. Kozub, Z. Ma, P.D. Parker, G. Rajbaidya, R.C. Runkle, C.M. Rowland, A.C. Shotter, M.S. Smith, L.A. Van Wormer, D.W. Visser and P.J. Woods, *The $^{14}\text{O}(\alpha, p)^{17}\text{F}$ reaction rate*, *ibid.* 127.
- S. Bishop, R. Azuma, L. Buchmann, A.A. Chen, M.L. Chatterjee, J.M. D'Auria, S. Engel, D. Gigliotti, U. Greife, D. Hunter, A. Hussein, D. Hutcheon, C. Jewett, J. King, S. Kubono, M. Lamey, R. Lewis, W. Liu, S. Michimasa, A. Olin, D. Ottewell, P.D. Parker, J. Rogers and C. Wrede, *Nuclear astrophysics studies at DRAGON: the $^{21}\text{Na}(p, \gamma)^{22}\text{Mg}$ reaction and oxygen-neon novae*, *ibid.* 263.
- D.A. Hutcheon, S. Bishop, L. Buchmann, M.L. Chatterjee, A.A. Chen, J.M. D'Auria, S. Engel, D. Gigliotti, U. Greife, D. Hunter, A. Hussein, C. Jewett, N. Khan, A. Lamey, W. Liu, A. Olin, D. Ottewell, J.G. Rogers, G. Roy, H. Sprenger and C. Wrede, *The DRAGON facility for nuclear astrophysics at TRIUMF-ISAC*, *ibid.* 515.
- F. Sarazin, L. Buchmann *et al.* (TUDA collaboration), *$(^3\text{He}, p)$ as an alternative to resonant elastic scattering*, *ibid.* 556.
- S. Michimasa, S. Kubono, S.H. Park, T. Teranishi, Y.

Yanagisawa, N. Imai, Zs. Fülöp, X. Liu, T. Minemura, C.C. Yun, J.M. D'Auria and K.P. Jackson, *Study on the $^{21}\text{Na}(p, \gamma)^{22}\text{Mg}$ stellar reaction by the (p, t) reaction*, *ibid.* 581.

B. Aubert *et al.* (BaBar collaboration), *A study of the rare decays $B^0 \rightarrow D_s^{(*)+}\pi^-$ and $B^0 \rightarrow D_s^{(*)-}K^+$* , Proc. **31st Int. Conf. on High Energy Physics (ICHEP 2002)**, Amsterdam, July 24–31, 2002, S. Bentvelsen *et al.* (Nucl. Phys. **B117**, 2003) [SLAC-PUB-9302, BABAR-CONF-02-034, hep-ex/0207053].

B. Aubert *et al.* (BaBar collaboration), *A study of time dependent CP asymmetry in $B^0 \rightarrow J/\psi\pi^0$ decays*, *ibid.* [SLAC-PUB-9298, BABAR-CONF-02-015, hep-ex/0207058].

B. Aubert *et al.* (BaBar collaboration), *A search for the decay $B^0 \rightarrow \pi^0\pi^0$* , *ibid.* [SLAC-PUB-9310, BABAR-CONF-02-32, hep-ex/0207063].

B. Aubert *et al.* (BaBar collaboration), *Measurements of branching fractions and direct CP asymmetries in $\pi^+\pi^0$, $K^+\pi^0$ and $K^0\pi^0 B$ decays*, *ibid.* [SLAC-PUB-9304, BABAR-CONF-02-13, hep-ex/0207065].

B. Aubert *et al.* (BaBar collaboration), *Measurement of the branching fraction for $B^\pm \rightarrow \chi_{e0}K^\pm$* , *ibid.* [SLAC-PUB-9316, BABAR-CONF-02-22, hep-ex/0207066].

B. Aubert *et al.* (BaBar collaboration), *Search for CP violation in $B^0\bar{B}^0$ decays to $\pi^+\pi^-\pi^0$ and $K^\pm\pi^m p\pi^0$ in regions dominated by the ρ^\pm resonance*, *ibid.* [SLAC-PUB-9303, BABAR-CONF-02-033, hep-ex/0207068].

B. Aubert *et al.* (BaBar collaboration), *A search for $B^+ \rightarrow K^+\nu\bar{\nu}$* , *ibid.* [SLAC-PUB-9309, BABAR-CONF-02-027, hep-ex/0207069].

B. Aubert *et al.* (BaBar collaboration), *Measurement of $\sin 2\beta$ in $B^0 \rightarrow \phi K_s^0$* , *ibid.* [SLAC-PUB-9297, BABAR-CONF-02-016, hep-ex/0207070].

B. Aubert *et al.* (BaBar collaboration), *Simultaneous measurement of the B^0 meson lifetime and mixing frequency with $B^0 \rightarrow D^{*-}\ell^+\nu_\ell$ decays*, *ibid.* [SLAC-PUB-9307, BABAR-CONF-02-21, hep-ex/0207071].

B. Aubert *et al.* (BaBar collaboration), *Measurement of time dependent CP asymmetries and the CP odd fraction in the decay $B^0 \rightarrow D^{*+}D^{*-}$* , *ibid.* [SLAC-PUB-9299, BABAR-CONF-02-14, hep-ex/0207072].

B. Aubert *et al.* (BaBar collaboration), *Search for the exclusive radiative decays $B \rightarrow \rho\gamma$ and $B^0 \rightarrow \omega\gamma$* , *ibid.* [SLAC-PUB-9319, BABAR-CONF-02-024, hep-ex/0207073].

B. Aubert *et al.* (BaBar collaboration), *$b \rightarrow s\gamma$ using a sum of exclusive modes*, *ibid.* [SLAC-PUB-9308, BABAR-CONF-02-25, hep-ex/0207074].

B. Aubert *et al.* (BaBar collaboration), *Determination of the branching fraction for inclusive decays $B \rightarrow$*

$X_s\gamma$, *ibid.* [SLAC-PUB-9301, BABAR-CONF-02-026, hep-ex/0207076].

B. Aubert *et al.* (BaBar collaboration), *Measurement of $B^0 \rightarrow D_s^{(*)+}D^{*-}$ branching fractions and polarization in the decay $B^0 \rightarrow D_s^{*+}D^{*-}$ with a partial reconstruction technique*, *ibid.* [SLAC-PUB-9321, BABAR-CONF-02-20, hep-ex/0207079].

B. Aubert *et al.* (BaBar collaboration), *Measurement of the CKM matrix element $|V_{ub}|$ with charmless exclusive semileptonic B meson decays at BABAR*, *ibid.* [SLAC-PUB-9305, BABAR-CONF-02-030, hep-ex/0207080].

B. Aubert *et al.* (BaBar collaboration), *Measurement of the inclusive electron spectrum in charmless semileptonic B decays near the kinematic endpoint*, *ibid.* [SLAC-PUB-9282, BABAR-CONF-02-012, hep-ex/0207081].

B. Aubert *et al.* (BaBar collaboration), *Evidence for the flavor changing neutral current decays $B \rightarrow K\ell^+\ell^-$ and $B \rightarrow K^*\ell^+\ell^-$* , *ibid.* [SLAC-PUB-9323, BABAR-CONF-02-023, hep-ex/0207082].

B. Aubert *et al.* (BaBar collaboration), *Search for decays of B^0 mesons into pairs of leptons*, *ibid.* [SLAC-PUB-9313, BABAR-CONF-02-028, hep-ex/0207083].

B. Aubert *et al.* (BaBar collaboration), *Measurement of the first hadronic spectral moment from semileptonic B decays*, *ibid.* [SLAC-PUB-9314, BABAR-CONF-02-029, hep-ex/0207084].

B. Aubert *et al.* (BaBar collaboration), *Measurement of the $B^0 \rightarrow D^{*-}a_1^+$ branching fraction with partially reconstructed D^** , *ibid.* [SLAC-PUB-9315, BABAR-CONF-02-010, hep-ex/0207085].

B. Aubert *et al.* (BaBar collaboration), *Measurement of the branching fractions for the exclusive decays of B^0 and B^+ to $\bar{D}^{(*)}D^{(*)}K$* , *ibid.* [SLAC-PUB-9322, BABAR-CONF-02-19, hep-ex/0207086].

B. Aubert *et al.* (BaBar collaboration), *Measurement of the branching ratios and CP asymmetries in $B^- \rightarrow D_{(CP)}^0 K^-$ decays*, *ibid.* [SLAC-PUB-9311, BABAR-CONF-02-18, hep-ex/0207087].

B. Aubert *et al.* (BaBar collaboration), *Dalitz plot analysis of D^0 hadronic decays $D^0 \rightarrow K^0 K^- \pi^+$, $D^0 \rightarrow \bar{K}^0 K^+ \pi^-$ and $D^0 \rightarrow \bar{K}^0 K^+ K^-$* , *ibid.* [SLAC-PUB-9320, BABAR-CONF-02-031, hep-ex/0207089].

B. Aubert *et al.* (BaBar collaboration), *Measurement of branching fractions of color suppressed decays of the \bar{B}^0 meson to $D^0\pi^0$, $D^0\eta$, and $D^0\omega$* , *ibid.* [SLAC-PUB-9324, BABAR-CONF-02-17, hep-ex/0207092].

S.I. Penttila, J.D. Bowman, R.D. Carlini, T. Case, T.E. Chupp, K.P. Coulter, S.J. Freedman, T.R. Gentile, M. Gericke, G.L. Greene, B. Hersmann, S. Ishimoto, G.L. Jones, M.B. Leuschner, Y. Masuda, G.S. Mitchell, K. Morimoto, H. Nann, S.A. Page, W.D. Ramsay, E.I. Sharapov, T.B.

- Smith, W.M. Snow, W.S. Wilburn and V.W. Yuan, *A measurement of the parity-violating gamma-ray asymmetry in neutron-proton capture*, Proc. **11th Int. Symp. Capture Gamma-Ray Spectroscopy and Related Topics, Prague, Czech Republic, September 2–6, 2002**, eds. J. Kvasil, P. Cejnar and M. Krťicka (World Scientific, Singapore, 2003) p.604.
- C.A. Miller, *Semi-inclusive deep inelastic scattering*, Proc. **15th Int. Spin Physics Symp. (SPIN 2002), Long Island, NY, September 9–14, 2002**, eds. Y.I. Makdisi *et al.* (AIP Conf. Proc. **675**, 2003) p.23 [DESY-HERMES-02-56].
- W.D. Ramsay, *Parity violation in pp and np experiments*, *ibid.* 196 [TRI-PP-02-16, nucl-ex/0210008].
- P.P.J. Delheij, W.T.H. van Oers, A.N. Zelenski *et al.*, *Spin at U-70: an experiment to measure the analyzing power A_N in very-high- p_t^2 pp elastic scattering at 70 GeV*, *ibid.* 538.
- M. Abe, M. Aliev, V. Anisimovsky, M. Aoki, Y. Asano, T. Baker, M. Blecher, P. Depommier, M. Hasinoff, K. Horie, Y. Igarashi, J. Imazato, A. Ivashkin, M. Khabibullin, A. Khot-jantsev, Yu. Kudenko, Y. Kuno, K.S. Lee, A. Levchenko, Y.-M. Shin, N. Yershov and T. Yokoi, *Further search for T violation in the decay $K^+ \rightarrow \pi^0 \mu^+ \nu$* , Proc. **16th Int. Conf. on Particles and Nuclei (PANIC 02), Osaka, Japan, September 30 – October 4, 2002** (Nucl. Phys. **A721**, 2003) p.445 [hep-ex/0211049].
- J.-M. Poutissou *et al.* (TWIST collaboration), *The TWIST experiment (TRIUMF weak interaction symmetry test)*, *ibid.* 465.
- Y. Masuda, J.D. Bowman, R.D. Carlini, T. Case, T.E. Chupp, K.P. Coulter, S.J. Freedman, T.R. Gentile, M. Gericke, G.L. Greene, F.W. Hersmann, T. Ino, S. Ishimoto, G.L. Jones, M.B. Leuschner, G.S. Mitchell, K. Morimoto, S. Muto, H. Nann, S.A. Page, S.I. Penttila, W.D. Ramsay, E.I. Sharapov, T.B. Smith, W.M. Snow, S.W. Wilburn and Y.W. Yuan, *Parity-violating gamma-ray asymmetry in the neutron-proton capture*, *ibid.* 485.
- T. Numao, T. Awes, S. Berridge, W. Bugg, V. Cianciolo, Y. Davydov, Y. Efremenko, R. Gearhart, Y. Kamyshkov, S. Ovchinnikov, J.-M. Poutissou and G. Young, *π^- absorption in water and light material*, *ibid.* 491.
- R. Meier *et al.* (CHAOS and LEPS collaborations), *Pion-proton scattering at TRIUMF and PSI*, *ibid.*, 649.
- A. Olin, S. Bishop, L. Buchmann, M.L. Chatterjee, A. Chen, J.M. D’Auria, S. Engel, D. Gigliott, U. Griefe, D. Hunter, A. Hussein, D. Hutcheon, C. Jewett, J. King, S. Kubono, M. Lamey, A.M. Laird, R. Lewis, W. Liu, S. Michimasa, D. Ottewell, P. Parker, J. Rogers, F. Strieder and C. Wrede, *Nuclear astrophysics at ISAC with DRAGON: initial studies*, *ibid.* 1019.
- A. Shotter, *Nuclear astrophysics with radioactive beams: a TRIUMF perspective*, Proc. **17th Int. Nuclear Physics Divisional Conf. of the European Physical Society (NPDC-17), Budapest, Hungary, September 30–October 4, 2002** (Nucl. Phys. **A719**, 2003) p.240.
- C.A. Miller, *Nucleon spin physics: experimental status*, **APS Meeting, Philadelphia, PA, April 5–8, 2003**, Proc. Bull. Am. Phys. Soc. **48**, (2), 2003.
- P. Schmor, *Recently commissioned and future RNB facilities*, Proc. **Particle Accelerator Conf. (PAC2003), Portland, OR, May 12–16, 2003** (Piscataway, NJ, IEEE, 2003) p.6 [TRI-PP-03-23].
- R. Assmann, O. Aberle, M. Brugger, L. Bruno, E. Chiaveri, B. Dehning, A. Ferrari, B. Goddard, J.B. Jeanneret, M. Jimenez, V. Kain, M. Lamont, F. Ruggiero, F. Schmidt, P. Sievers, J. Uythoven, V. Vlachoudis, L. Vos, J. Wenninger, I. Baishev and D. Kaltchev, *Designing and building a collimation system for the high-intensity LHC beam*, *ibid.* 45 [TRI-PP-03-17, CERN-LHC-PROJECT-REPORT-640].
- P.G. Bricault, M. Domsbys, P.W. Schmor and A. Dowling, *High power targets for ISOL radioactive ion beams facility*, *ibid.* 439 [TRI-PP-03-10].
- R. Laxdal, G. Clark, G. Dutto, K. Fong, G. Stanford, Z.H. Peng, R. Poirier, W. Rawnsley, T. Ries and I. Sekachev, *The ISAC-II upgrade at TRIUMF – progress and developments*, *ibid.* 601 [TRI-PP-03-20, PAC-2003-ROPA010].
- L. Moritz, J. Drozdoff, G. Dutto, F. Mammarella, M. Mouat and R. Ruegg, *Safety critical monitoring for prompt radiation hazards*, *ibid.* 638 [TRI-PP-03-21].
- L. Ducimetière, N. Garrel, M.J. Barnes and G.D. Wait, *The LHC injection kicker magnet*, *ibid.* 1162 [TRI-PP-03-24].
- I. Bylinsky, Z. Ang, S. Fang, K. Fong, R. Kumaran, J. Lu and R. Poirier, *TRIUMF ISAC RF system improvements after 2 years of operational experience*, *ibid.* 1285 [TRI-PP-03-11, PAC-2003-TPAB040].
- K. Fong, S. Fang, M. Laverty and Q. Zheng, *RF control system for ISAC-II superconducting cavities*, *ibid.* 1404 [TRI-PP-03-14, PAC-2003-TPAB088].
- T. Ries, K. Fong, S. Koscielniak, R.E. Laxdal and G. Stanford, *A mechanical tuner for the ISAC-II quarter wave superconducting acities*, *ibid.* 1488 [TRI-PP-03-22, PAC-2003-TPAG027].
- R. Baartman and Y.-N. Rao, *Investigation of space charge effect in TRIUMF injection beamline*, *ibid.* 1578 [TRI-PP-03-09].
- M.K. Craddock and D. Kaltchev, *Feasibility studies for a radioactive-ion storage ring*, *ibid.* 1581 [TRI-PP-03-12].
- R. Baartman, P. Bricault, I. Bylinsky, M. Domsbys, G. Dutto, R. Laxdal, R. Poirier, Y. Rao, L. Root, R. Ruegg, P. Schmor, M. Stenning and G. Stinson, *The TRIUMF 500 MeV cyclotron: Present operation and intensity upgrade*, *ibid.* 1584 [TRI-PP-03-13, PAC03-TPPE016].
- G. Stinson and P. Bricault, *A proposal for an additional beamline to the TRIUMF ISAC Facility*, *ibid.* 1670 [TRI-PP-03-08, PAC03-TPPE014].

S. Koscielniak *et al.*, *Longitudinal dynamics in an FFAG accelerator under conditions of rapid acceleration and fixed, high rf*, *ibid.* 1831 [TRI-PP-03-18].

F.W. Jones and W. Herr, *Parallel computation of beam-beam interactions including longitudinal motion*, *ibid.* 3404 [TRI-PP-03-15, CERN-AB-2003-019-ABP].

J.S. Berg, S. Kahn, R. Palmer, D. Trbojevic, C. Johnstone, E. Keil, M. Aiba, S. Machida, Y. Mori, T. Ogitsu, C. Ohmori, A. Sessler and S. Koscielniak, *FFAGS for muon acceleration*, *ibid.* 3413 [TRI-PP-03-19].

R. Assmann, M. Brugger, M. Hayes, J.B. Jeanneret, F. Schmidt, I. Baichev and D. Kaltchev, *Tools for predicting cleaning efficiency in the LHC*, *ibid.* 3494 [TRI-PP-03-16, CERN-LHC-PROJECT-REPORT-639].

Instrumentation/Accelerator Physics/Computing Sciences

D. Gray and B. Minato, *Simple "package design" ion chamber monitors for TRIUMF's proton beamlines*, Proc. **10th Beam Instrumentation Workshop (BIW 2002)**, Upton, NY, May 6–9, 2002 (AIP Conf. Proc. **648**, 2003) p.439 [TRI-PP-02-06].

W. Andersson, R.E. Laxdal, I. Sekachev and G. Stanford, *Overview of the cryogenic system for the ISAC-II superconducting linac at TRIUMF*, Proc. **19th Int. Cryogenic Engineering Conf. (ICEC 19)**, Grenoble, France, July 22–26, 2002, eds. G. Gistau Baguer, P. Seyfert (Narosa, New Delhi, 2003) p.47 [TRI-PP-02-34].

C. Kost, S. McDonald, B. Caron and W. Hong, *ATLAS Canada lightpath data transfer trial*, Proc. **iGrid2002**, Amsterdam, Netherlands, September 23–26, 2002 (J. Future Generation of Computer Systems **19**, 2003) p.1051.

L. Moritz, *Radiation safety at ISAC*, Proc. **SAFERIB Workshop at CERN**, Geneva, Switzerland, October 30–November 1, 2002 (CERN-2003-004).

E. Calvo, C. Boccard, D. Cocq, L. Jensen, R. Jones, J.J. Savioz, D. Bishop and G. Waters, *The LHC orbit and trajectory system*, Proc. **6th European Workshop on Beam Diagnostics and Instrumentation for Particle Accelerators (DIPAC 2003)**, Mainz, Germany, May 5–7, 2003 [CERN-AB-2003-057-BDI].

E.W. Blackmore, P.E. Dodd and M.R. Shaneyfelt, *Improved capabilities for proton and neutron irradiations at TRIUMF*, Proc. **IEEE Radiation Effects Data Workshop**, July 21–25, 2003 (IEEE, 2003) p.149.

Molecular and Materials Science

P.W. Percival, *Muonium chemistry*, Pre-conference tutorial on μ SR, Proc. **9th Int. Conf. on Muon Spin Rotation/Relaxation/Resonance (MuSR 2002)**, Williamsburg, VA, June 3–7, 2002 (Physica **B326**, 2003).

D.R. Noakes, R.H. Heffner and P.W. Percival (editors), Proc. **9th Int. Conf. on Muon Spin Rotation/Relaxation/Resonance (MuSR 2002)**, Williamsburg, VA, June 3–7, 2002 (Physica **B326**, 2003).

S. Kreitzman, *An overview of high field/timing resolution and RF/ μ wave μ SR methods*, *ibid.*

J.C. Brodovitch, B. Addison-Jones, K. Ghandi, I.D. McKenzie and P.W. Percival, *^{13}C hyperfine coupling constants of MuC_{70} in solution*, *ibid.*

J.H. Brewer, *More μ^- SR in nuclei with spin*, *ibid.*

K. Ghandi, B. Addison-Jones, J.-C. Brodovitch, S. Kerman, I. McKenzie and P.W. Percival, *Muonium kinetics in sub- and supercritical water*, *ibid.* 55.

V.G. Storchak, D.G. Eshchenko, J.H. Brewer, G.D. Morris, S.P. Cottrell and S.F.J. Cox, *Coherent tunnelling dynamics of muonium in a disordered medium*, *ibid.* 61.

D.J. Arseneau, D.G. Fleming, C.A. Fyfe and M. Senba, *Observation of muonium in zeolites*, *ibid.* 64.

P.W. Percival, J.C. Brodovitch, D.J. Arseneau, M. Senba and D.G. Fleming, *Formation of the muoniated ethyl radical in the gas phase*, *ibid.* 72.

I. McKenzie, J.C. Brodovitch, K. Ghandi, S. Kerman and P.W. Percival, *Formation and spectroscopy of α -muoniated radicals*, *ibid.* 76.

D.G. Eshchenko, V.G. Storchak, J.H. Brewer, S.P. Cottrell, S.F.J. Cox, E. Karlsson and R. Wäppling, *Ionization of a shallow muonium state in a semiconductor*, *ibid.* 120.

R.L. Lichti, *Properties of muonium defect centers in III-V nitrides*, *ibid.* 139.

K.H. Chow, *Isolated positively charged muonium and the analog of hydrogen passivation*, *ibid.* 145.

K.H. Chow, B. Hitti, D.G. Eshchenko, V.G. Storchak, S.R. Kreitzman and J.H. Brewer, *Avoided level crossing measurements of electric field enhanced diamagnetic states in gallium arsenide*, *ibid.* 157.

D.G. Eshchenko, V.G. Storchak, R.L. Lichti and J.H. Brewer, *Short range electron transport in GaAs*, *ibid.* 160.

V.G. Storchak, D.G. Eshchenko, R.L. Lichti and J.H. Brewer, *Weakly bound muonium state in a semiconductor*, *ibid.* 164.

R.L. Lichti, K.H. Chow, E.A. Davis, B. Hitti, Y.G. Celebi and S.F.J. Cox, *Muonium-acceptor interactions in gallium phosphide*, *ibid.* 167.

P.J.C. King, R.L. Lichti and I. Yonenaga, *Muonium behaviour in Czochralski $\text{Si}_{1-x}\text{Ge}_x$ alloys*, *ibid.* 171.

K.L. Hoffman, K.H. Chow, R.F. Kieff, B. Hitti, T.L. Estle and R.L. Lichti, *Frequency shifts and local spin susceptibility of muonium in heavily-doped Si and GaAs*, *ibid.* 175.

B. Hitti and S.R. Kreitzman, *Muonium dynamics in silicon at high temperature*, *ibid.* 178.

- R.F. Kiefl, W.A. MacFarlane, G.D. Morris, P. Amaudruz, D. Arseneau, H. Azumi, R. Baartman, T.R. Beals, J. Behr, C. Bommas, J.H. Brewer, K.H. Chow, E. Dumont, S.R. Dunsiger, S. Daviel, L. Greene, A. Hatakeyama, R.H. Heffner, Y. Hirayama, B. Hitti, S.R. Kreitzman, C.D.P. Levy, R.I. Miller, M. Olivo and R. Poutissou, *Low-energy spin-polarized radioactive beams as a nano-scale probe of matter*, *ibid.* 189.
- T.R. Beals, R.F. Kiefl, W.A. MacFarlane, K.M. Nichol, G.D. Morris, C.D.P. Levy, S.R. Kreitzman, R. Poutissou, S. Daviel, R.A. Baartman and K.H. Chow, *Range straggling of low energy $^8\text{Li}^+$ in thin metallic films using β -NMR*, *ibid.* 205.
- W.A. MacFarlane, G.D. Morris, K.H. Chow, R.A. Baartman, S. Daviel, S.R. Dunsiger, A. Hatakeyama, S.R. Kreitzman, C.D.P. Levy, R.I. Miller, K.M. Nichol, R. Poutissou, E. Dumont, L.H. Greene and R.F. Kiefl, *Quadrupolar split ^8Li β -NMR in SrTiO_3* , *ibid.* 209.
- W.A. MacFarlane, G.D. Morris, T.R. Beals, K.H. Chow, R.A. Baartman, S. Daviel, S.R. Dunsiger, A. Hatakeyama, S.R. Kreitzman, C.D.P. Levy, R.I. Miller, K.M. Nichol, R. Poutissou and R.F. Kiefl, *^8Li β -NMR in thin metal films*, *ibid.* 213.
- D.G. Eshchenko, V.G. Storchak, B. Hitti, S.R. Kreitzman, J.H. Brewer and K.H. Chow, *Radio-frequency μSR experiments in an applied electric field*, *ibid.* 244.
- G.D. Morris and R.H. Heffner, *A method of achieving accurate zero field conditions using muonium*, *ibid.* 252.
- K.H. Chow, R.F. Kiefl, S. Chan, R.I. Miller, P. Amaudruz, R. Poutissou, B. Hitti and D. Arseneau, *MULTI – new detector, new logic, new science*, *ibid.* 279.
- R.I. Miller, R.F. Kiefl, J.H. Brewer, J.C. Chakhalian, S. Dunsiger, A.N. Price, D.A. Bonn, W.H. Hardy, R. Liang and J.E. Sonier, *Penetration depth and core radius μSR measurements in the vortex state near the lower critical field*, *ibid.* 296.
- J.E. Sonier, J.H. Brewer, R.F. Kiefl, R.I. Miller, R.H. Heffner, K.F. Poon, G.D. Morris, W.N. Hardy, R. Liang, D.A. Bonn, J.S. Gardner and C.E. Stronach, *Zero field μSR study of $\text{YBa}_2\text{Cu}_3\text{O}_{6+x}$, $x \geq 0.67$: evidence for charge ordering*, *ibid.* 312.
- K.M. Kojima, S. Uchida, Y. Fudamoto, I.M. Gat, M.I. Larkin, Y.J. Uemura and G.M. Luke, *Superfluid density and volume fraction of static magnetism in stripe-stabilized $\text{La}_{1.85-y}\text{Eu}_y\text{Sr}_{0.15}\text{CuO}_4$* , *ibid.* 316.
- D. Baabe, H.-H. Klauss, D. Mienert, M. Birke, P. Adelmann, B. Hitti, U. Zimmermann, A. Amato and F.J. Litterst, *Inhomogeneous spin order in the magnetic phase of electron-doped high- T_c superconductors*, *ibid.* 338.
- H. Takagiwa, A. Kawano, Y. Mizuta, T. Yamamoto, M. Yamada, K. Ohishi, T. Muranaka, J. Akimitsu, W. Higemoto and R. Kadono, *Magnetic penetration depth of a new boride superconductor Re_3B* , *ibid.* 355.
- K. Ohishi, K. Kakuta, J. Akimitsu, A. Koda, W. Higemoto, R. Kadono, J.E. Sonier, A.N. Price, R.I. Miller, R.F. Kiefl, M. Nohara, H. Suzuki and H. Takagi, *Anomalous quasiparticle excitations in $\text{Y}(\text{Ni}_{1-x}\text{Pt}_x)_2\text{B}_2\text{C}$* , *ibid.* 364.
- G.M. Luke, M.T. Rovers, A. Fukaya, I.M. Gat, M.I. Larkin, A.T. Savici, Y.J. Uemura, K.M. Kojima, P.M. Chaikin, I.J. Lee and M.J. Naughton, *Unconventional superconductivity in $(\text{TMTSF})_2\text{ClO}_4$* , *ibid.* 378.
- D.E. MacLaughlin, M.S. Rose, B.-L. Young, O.O. Bernal, R.H. Heffner, G.D. Morris, K. Ishida, G.J. Nieuwenhuys and J.E. Sonier, *μSR and NMR in f -electron non-Fermi liquid materials*, *ibid.* 381.
- D.E. MacLaughlin, M.S. Rose, B.-L. Young, O.O. Bernal, R.H. Heffner, G.J. Nieuwenhuys, R. Pietri and B. Andraka, *μSR in $\text{Ce}_{1-x}\text{La}_x\text{Al}_3$: anisotropic Kondo effect?*, *ibid.* 387.
- G.D. Morris, R.H. Heffner, J.E. Sonier, D.E. MacLaughlin, O.O. Bernal, G.J. Nieuwenhuys, A.T. Savici, P.G. Pagliuso and J.L. Sarrao, *Magnetism and superconductivity in $\text{CeRh}_{1-x}\text{Ir}_x\text{In}_5$ heavy fermion materials*, *ibid.* 390.
- D.R. Noakes, G.M. Kalvius, H. Nakotte, E. Schreier and R. Wäppling, *μSR magnetic response in UPdSn* , *ibid.* 406.
- D.R. Noakes, G.M. Kalvius, H. Nakotte, E.J. Ansaldo and A.V. Andreev, *$\text{U}_{0.94}\text{Y}_{0.06}\text{CoAl}$: a dilute-moment ferromagnet*, *ibid.* 410.
- J.E. Sonier, R.H. Heffner, G.D. Morris, D.E. MacLaughlin, O.O. Bernal, J. Cooley, J.L. Smith and J.D. Thompson, *μ^+ -Knight shift in the superconducting state of $\text{U}_{1-x}\text{Th}_x\text{Be}_{13}$, $x = 0$ and 0.035 single crystals*, *ibid.* 414.
- J.A. Chakhalian, R.F. Kiefl, R. Miller, S.R. Dunsiger, G. Morris, S. Kreitzman, W.A. MacFarlane, J. Sonier, S. Eggert, I. Affleck and I. Yamada, *Local magnetic susceptibility of the positive muon in the quasi-1D $S = 1/2$ antiferromagnet KCuF_3* , *ibid.* 422.
- D. Mienert, H.-H. Klauss, A. Bosse, D. Baabe, H. Luetkens, M. Birke, F.J. Litterst, B. Büchner, U. Ammerahl, A. Revcolevschi, A. Amato, U. Zimmermann, B. Hitti and S. Kreitzman, *The interplay of charge order and magnetism in the one-dimensional quantum spin system $\text{Sr}_{14}\text{Cu}_{24}\text{O}_{41}$* , *ibid.* 440.
- A. Fukaya, Y. Fudamoto, I.M. Gat, T. Ito, M.I. Larkin, A.T. Savici, Y.J. Uemura, P.P. Kyriakou, G.M. Luke, M. Rovers, H. Kageyama and Y. Ueda, *Spin dynamics in the two-dimensional spin system $\text{SrCu}_2(\text{BO}_3)_2$* , *ibid.* 446.
- D.H. Ryan, J. van Lierop and J.M. Cadogan, *μSR and Mössbauer studies of transverse spin freezing*, *ibid.* 450.
- G.M. Kalvius, D.R. Noakes, R. Wäppling, G. Grosse, W. Schäfer, W. Kockelmann, J.K. Yakinthos and P.A. Kotsonides, *Spin dynamics and spin disorder in frustrated $\text{TbCo}_x\text{Ni}_{1-x}\text{C}_2$* , *ibid.* 465.

G.M. Kalvius, D.R. Noakes, R. Wäppling, E. Schreier, N. Büttgen, A. Krimmel, M. Klemm, S. Horn and A. Loidl, *Magnetic properties of geometrically frustrated $Zn_xLi_{1-x}V_2O_4$* , *ibid.* 470.

S.R. Dunsiger, R.F. Kiefl, J.A. Chakhalian, K.H. Chow, J.S. Gardner, J.E. Greedan, W.A. MacFarlane, R.I. Miller, G.D. Morris, A.N. Price, N.P. Raju and J.E. Sonier, *A comparison of the local magnetic susceptibility in rare earth pyrochlores*, *ibid.* 475.

R.H. Heffner, J.E. Sonier, D.E. MacLaughlin, G.J. Nieuwenhuys, F. Mezei, G. Ehlers, J.F. Mitchell and S.-W. Cheong, *Inhomogeneity in the spin channel of ferromagnetic CMR manganites*, *ibid.* 494.

J. Sugiyama, J.H. Brewer, E.J. Ansaldo, H. Itahara, M. Bayer and T. Tani, *μ SR studies on layered cobalt oxides*, *ibid.* 518.

P.W. Percival, *Closing remarks*, *ibid.*

R.L. Lichti, *Sites and dynamics for muonium in III-V semiconductors*, Proc. **Int. Workshop on Hydrogen in Materials and Vacuum Systems (Hydrogen Workshop 2002)**, Newport News, VA, November 11–13, 2002, eds. G.R. Myneni and S. Ghattopadhyay (AIP Conf. Proc. **671**, 2003) p.55.

D.R. Harshman, W.J. Kossler, X. Wan, A.T. Fiory, A.J. Greer, D.R. Noakes, C.E. Stronach, E. Koster, A. Erb and J.D. Dow, *Verification of nodeless superconductivity pairing in single-crystal $YBa_2Cu_3O_7$* , Proc. **4th Int. Conf. on New Theories, Discoveries, and Applications of Superconductors and Related Materials (New4SC-3)**, San Diego, CA, January 16–21, 2003 (Int. J. Mod. Phys. **B17**, 2003) p.3582.

J.D. Dow and D.R. Harshman, *Locus of high-temperature superconductivity*, *ibid.*

D.E. MacLaughlin, *Critical and glassy dynamics in non-fermi-liquid heavy-fermion metals*, **Am. Phys. Soc. March Meeting**, Austin, TX, March, 2003 (Bull. Am. Phys. Soc. **48**, 2003) p.60.

J. Sugiyama, H. Itahara, J.H. Brewer, E.J. Ansaldo, K. Dohmae, C. Xia, Y. Seno, B. Hitti and T. Tani, *A common behavior of thermoelectric layered cobaltites: incommensurate spin density wave states*, Proc. **Int. Conf. on Thermoelectrics, La Grande-Motte, France, August 17–21, 2003** (IEEE, Piscataway, 2003) p. 215.

Life Sciences

R.L. Watts, C.D. Raiser, N.P. Stover, M.L. Cornfeldt, A.W. Schweikert, R.C. Allen, T. Subramanian, D.J. Doudet, C. Honey and R.A.E. Bakay, *Human retinal pigment epithelial cells attached to gelatin microcarriers: a promising new cell therapy for Parkinson's disease*, Proc. **10th Int. Winter Conf. on Neurodegeneration**, Berlin, Germany, February, 2002 (J. Neural Transm. **65**, 2003) p.1.

G.-J. Beyer and T.J. Ruth, *The role of electromagnetic separators in the production of radiotracers for bio-medical research and nuclear medical application*, Proc. **14th Int. Conf. on Electromagnetic Isotope Separators and Techniques Related to Their Applications (EMIS-14)**, Victoria, BC, May 6–10, 2002 (Nucl. Instrum. Methods **B204**, 2003) p.694 [TRI-PP-02-26].

V. Astakhov, P. Gumplinger, C. Moisan, T.J. Ruth and V. Sossi, *Effect of depth of interaction decoding on resolution in PET: a simulation study*, Proc. **2002 IEEE/Medical Imaging Conf.**, Norfolk, VA, November 13–16, 2002 (IEEE Trans. Med. Imaging **NS50**, 2003) p.1373.

V. Sossi, O. Morin, A. Celler, A. Belzberg, T.D. Rempel and C. Carhart, *PET and SPECT performance evaluation of the Siemens HD3 e.camduet: a 1 in. Na(I) hybrid camera*, *ibid.* 1504.

M. Zamburlini, R. de la Fuente-Fernandez, A.J. Stoessl, T.J. Ruth and V. Sossi, *Impact of different realignment algorithms on the SPM analysis of ^{11}C -raclopride PET studies*, *ibid.*

A.R. Studenov, S. Jivan, M.J. Adam, T.J. Ruth and K.R. Buckley, *Studies of the mechanism of the in-loop synthesis of radiopharmaceuticals*, Proc. **15th Int. Symp. Radiopharmaceutical Chemistry**, Sydney, Australia, August, 2003 (J. Labelled Compds. Radiopharm. **46** Suppl 1, 2003) p.S72.

S. Lu, M.J. Adam, J. Lu and T.R. Ruth, *Simplified synthesis of desmethyl-FLB457 in two steps*, *ibid.* S234.

C.L. Fisher, S.R. Bayly, C.B. Ewart, M.J. Adam and C. Orvig, *Synthesis of rhenium and technetium complexes of glucose derivatives*, *ibid.* S246.

Theoretical Program

D.H. Wilkinson, *Super-allowed fermi beta-decay: CKM unitarity*, Proc. **Fifty Years of Electroweak Physics: A Symposium in Honor of Professor Alberto Sirlin's 70th Birthday**, New York, NY, October 27–28, 2000, eds. A. Sirlin *et al.* (J. Phys. **G29**, 2003), p.189 [TRI-PP-02-14].

A. Astbury, B. Campbell, F.C. Khanna and M. Vinciter (editors), Proc. **Lake Louise Winter Inst. on Fundamental Interactions (LLWI02)**, Lake Louise, AB, February 17–23, 2002 (World Scientific, Singapore, 2003).

D.U. Matrasulov, F.C. Khanna, Kh.Yu. Rakhimov and Kh.T. Butanov, *Spectroscopy of baryons containing two heavy quarks*, *ibid.*

F.C. Khanna and D.U. Matrasulov, *Properties of hadrons in nuclear matter*, Proc. **Joint CCSM/JHF/NITP Workshop on Physics at the Japan Hadron Facility**, Adelaide, Australia, March 14–21, 2002, eds. V. Guzey *et al.* (World Scientific, Singapore, 2003) p.255.

R. Lewis, W. Wilcox and R.M. Woloshyn, *Strange matrix elements of the nucleon*, Proc. **20th Int. Symp. on Lattice**

Field Theory (LATTICE 2002), Cambridge, MA, June 24–29, 2002 (Nucl. Phys. B Proc. Supp. **119**, 2003) p.119 [hep-lat/0208063].

C.S. Kalman, J. McKenna, M. Bozzo, Z. Ligeti, T. Mattison, J. Ng, M.A. Sanchis-Lozano and P. Singer (editors), Proc. 5th Int. Conf. on Hyperons, Charm and Beauty Hadrons (BEACH 2002), Vancouver, BC, June 25–29, 2002 (Nucl. Phys. **115**, 2003).

D.U. Matrasulov, F.C. Khanna, Kh.Yu. Rakhimov and H. Yusupov, *Spectra of heavy flavored hadrons in the relativistic approach*, *ibid.* 195.

T. Numao (for the E787/949 and KOPIO collaborations at BNL), *Status of $K \rightarrow \pi\nu\bar{\nu}$* , *ibid.* 238.

C.-H. Chen, C.Q. Geng and J.N. Ng, *T violation in $A_b \rightarrow A\ell^+\ell^-$ decays*, *ibid.* 263 [hep-ph/0210067].

J. Escher and B.K. Jennings, *A new signature for nuclear shell closures*, Proc. 7th Int. Symp. on Nuclei in the Cosmos (NIC7), Fuji-Yoshida, Japan, July 8–12, 2002, eds. S. Kubono *et al.* (Nucl. Phys. **A718**, 2003) p.694 [TRI-PP-02-12].

L. Theussl, A. Amghar, B. Desplanques and S. Noguera, *Comparison of different boost transformations for the calculation of form factors in relativistic quantum mechanics*, Proc. 18th European Conf. on Few-Body Problems in Physics, Bled, Slovenia, September 8–14, 2002 (Few Body Syst. Suppl. **14**, 2003) p.393 [hep-ph/0301137].

C.-P. Liu, *Nuclear anapole moments and the parity nonconserving nuclear interaction*, Proc. 15th Int. Spin Physics Symp. (SPIN 2002), Long Island, NY, September 9–14, 2002 (AIP Conf. Proc. **675**, 2003) p.262 [nucl-th/0211095].

K. Tsushima and F.C. Khanna, *Properties of charmed and bottom hadrons in nuclear medium: results for Λ_c^+ and Λ_b hypernuclei*, Proc. YITP-RCNP Workshop on Chiral Restoration in Nuclear Medium, Kyoto, Japan, October 7–9, 2002 (Prog. Theor. Phys. Suppl. **149**, 2003) p.160 [nucl-th/0212100].

C. Barbieri and W.H. Dickhoff, *Effects of nuclear fragmentation on single particle and collective motions at low energy*, Proc. 10th Int. Conf. on Nuclear Reaction Mechanisms, Varenna, Italy, June 9–13, 2003, ed. E. Gadioli (Ricerca Scientifica ed Educazione Permanente, Suppl. **122**, 2003), p.89 [TRI-PP-03-26, nucl-th/0307037].

S.-I. Ando, *Solar-neutrino reactions on deuteron in EFT and radiative corrections of neutron beta decay*, Proc. 4th Int. Workshop on Chiral Dynamics (CD2003), Bonn, Germany, September 8–13, 2003, eds. U.-G. Meissner, H.-W. Hammer and A. Wirzba (“Chiral Dynamics: Theory and Experiment (CD2003)”, HSKP-TH-03/23, 2003) [TRI-PP-03-34, hep-ph/0311212].

Conference Presentations

Particle, Nuclear and Atomic Physics

D.S. Armstrong *et al.* (Qweak collaboration), *Qweak: a precision measurement of the proton’s weak charge*, Proc. 8th Conf. on the Intersections of Particle and Nuclear Physics (CIPANP 2003), New York, NY, May 19–24, 2003, ed. Z. Parsa (AIP Conf. Proc., New York, in press) [LA-UR-03-6031, hep-ex/0308049].

C.A. Gagliardi, *TWIST: measuring the space-time structure of muon decay*, *ibid.*

R. Edgecock *et al.* (MuScat collaboration), *The MuScat experiment: status and plans*, Proc. 5th Int. Workshop on Neutrino Factories and Superbeams (NuFact03), New York, NY, June 5–11, 2003 (AIP, in press).

P. Kitching, *TWIST: a precise measurement of muon decay at TRIUMF*, *ibid.*

G.M. Marshall (TWIST collaboration), *First data from the TWIST experiment*, CAP Congress, Charlottetown, June 8–11, 2003.

P.M. Walker, *Nuclear isomers: energy and spin*, *ibid.*

S.A. Page, *Measurement of the parity violating asymmetry in radiative np capture*, *ibid.*

G. Hackman, *A new era of high-resolution gamma-ray spectroscopy at TRIUMF-ISAC*, *ibid.*

W.T.H. van Oers, *Qweak: a search for new physics*, *ibid.*

G. Hackman, *Recent results from the 8π at TRIUMF-ISAC*, Proc. 2003 Gordon Research Conf. on Nuclear Chemistry, New London, NH, June 15–20, 2003.

W.D. Ramsay, *Selected parity violation experiments*, Proc. Advanced Study Inst. on Symmetries and Spin (SPIN-PRAHA-2003), Prague, Czech Republic, July 12–19, 2003 (Czech. J. Phys., in press) [nucl-ex/0401028].

M. Domsbky, P. Bricault and V. Hanemaayer, *Increasing beam currents at the TRIUMF-ISAC facility; techniques and experiences*, Proc. 6th Int. Conf. on Radioactive Nuclear Beams (RNB6), Argonne, IL, September 22–26, 2003 (Nucl. Phys. A, in press) [TRI-PP-03-35].

Y. Hirayama *et al.*, *Structure of ^{11}Be studied in β -delayed neutron- and γ -decay from polarized ^{11}Li* , *ibid.*

C.D.P. Levy, R. Baartman, J.A. Behr, R.F. Kiefl, M. Pearson, R. Poutissou, A. Hatakeyama and Y. Hirayama, *The collinear laser beam line at ISAC*, *ibid.* [TRI-PP-03-36].

D. Hutcheon *et al.* (DRAGON collaboration), *A mechanical tuner and rf drive line system for the ISAC-II study of $^{21}\text{Na}(p,\gamma)^{22}\text{Mg}$ using the DRAGON separator*, *ibid.* [TRI-PP-03-37].

M.B. Smith, P.M. Walker, R.S. Chakrawarthy, R.A.E. Austin, G.C. Ball, J.J. Carroll, E. Cunningham, P. Finlay, P.E. Garrett, G.F. Grinyer, G. Hackman, B. Hyland, K.

Koopmans, W.D. Kulp, J.R. Leslie, A.A. Phillips, R. Propri, P.H. Regan, F. Sarazin, M.A. Schumaker, H.C. Scraggs, T. Shizuma, C.E. Svensson, J. von Schwarzenberg, J.C. Waddington, D. Ward, J.L. Wood, B. Washbrook and E.F. Zganjar, *Studies of high-K isomers at TRIUMF-ISAC*, *ibid.*

K. Minamisono, K. Matsuta, T. Minamisono, C.D.P. Levy, T. Nagatomo, M. Ogura, T. Sumikama, J.A. Behr, K.P. Jackson, H. Fujiwara, M. Mihara and M. Fukuda, *Alignment correlation term in the β -ray angular distribution from spin aligned ^{20}Na* , *ibid.*

K. Minamisono, K. Matsuta, T. Minamisono, C.D.P. Levy, T. Nagatomo, M. Ogura, T. Sumikama, J.A. Behr and K.P. Jackson, *Quadrupole moments of $^{20, 21}\text{Na}$* , *ibid.*

M. Agnello *et al.* (FINUDA collaboration), *First results from the FINUDA experiment at DAF Φ NE*, Proc. **VIII Int. Conf. on Hypernuclear and Strange Particle Physics**, Newport News, VA, October 14–18, 2003 (Nucl. Phys. B Proc. Suppl., in press) LNF-03/23.

J.R. Musser, *TRIUMF weak interaction symmetry test*, Proc. **2003 Fall Meeting of the Division of Nuclear Physics of the American Physical Society**, Tucson, AZ, October 30–November 1, 2003.

A. Gaponenko, *Blind analysis in TWIST*, *ibid.*

Instrumentation/Accelerator Physics/Computing Sciences

P. Bricault, *Laser ion source for the ISAC facility*, Proc. **Int. Conf. on Laser Probing, LAP2002**, Leuven, Belgium, July 7–12, 2002 (Spectrochimica Acta Part B, in press).

G. Dutto, *Recent achievements at TRIUMF*, Proc. **XXXIII European Cyclotron Progress Meeting**, Warsaw, Poland, September 17–21, 2002 (Nukleonika, Poland, in press).

D. Karlen, *GEM-TPC resolution studies*, Proc. **Arlington Linear Collider Workshop**, UTA, January 9–11, 2003.

M.S. Dixit *et al.*, *Position sensing in a gas electron multiplier from charge dispersion on a resistive anode*, *ibid.*

G.D. Wait and M.J. Barnes, *JHF 50 GeV ring combined fast extraction and abort kicker*, Proc. **JHF Neutrino Workshop**, Vancouver, BC, February, 2003.

D. Karlen, *The linear e^+e^- collider*, Proc. **Western Regional Nuclear and Particle Physics Conf. (WRNPPC'03)**, Lake Louise, AB, February 14–16, 2003.

A. Gaponenko, *Introduction to TWIST*, *ibid.*

J.R. Musser, *Extraction of the Michel parameter, ρ , of normal muon decay*, *ibid.*

R.P. MacDonald, *GEANT validation via positrons*, *ibid.*

B. Jamieson, *Event classification with TWIST*, *ibid.*

M.S. Dixit, *An overview of North American R&D in gaseous tracking detectors for the linear collider*, Proc. **Int. Linear Collider Tracking and Muon Conf.**, Amsterdam, Holland, March 31, 2003.

M. Dixit *et al.*, *Carleton update on LC TPC readout studies*, Proc. **4th ECFA/DESY Linear Collider Workshop**, Amsterdam, Holland, April 1–4, 2003.

D. Karlen, *Status of GEM-TPC R&D at Victoria*, *ibid.*

F.W. Jones, *Status of ACCSIM and some simulation issues*, Proc. **XII ICFA Beam Dynamics Mini Workshop on Space Charge Simulation**, Oxford, UK, April 2–4, 2003.

D. Evans, M. Barnes, D. Morris and G. Marshall, *Field mapping the TWIST solenoid with the custom magnet mapper*, Proc. **13th Int. Magnet Measurement Workshop**, Palo Alto, CA, May, 2003.

J.B. Jeanneret *et al.*, *Beam loss and collimation in the LHC*, Proc. **29th ICFA Advanced Beam Dynamics Workshop (HALO'03)**, Montauk, NY, May 19–23, 2003 (AIP, in press).

R. Poutissou, P.-A. Amaudruz, A. Gaponenko, P. Green, K. Olchanski and A. Olin, *The TWIST data acquisition system at TRIUMF*, Proc. **13th IEEE Real Time Conf. on Nuclear and Plasma Sciences**, Montreal, May 20–23, 2003 (IEEE Trans. Nucl. Sci. in press).

M.K. Craddock, *Accelerators at TRIUMF – old roots and new limbs*, Proc. **Symp. Rare Isotopes and Accelerators**, East Lansing, MI, May 22–23, 2003.

D. Karlen, *Development of a time projection chamber with gas electron multipliers*, Proc. **CAP Congress**, Charlotte-town, June 8–11, 2003.

M.J. Barnes and G.D. Wait, *A 25 kV, 75 kHz kicker for measurement of muon lifetime*, Proc. **IEEE Int. Pulsed Power Conf.**, Dallas, TX, June 15–18, 2003 (IEEE, in press) [TRI-PP-03-28].

R.E. Laxdal, Y. Bylinsky, G. Dutto, K. Fong, A.K. Mitra, R. Poirier, W. Rawnsley, T. Ries, I. Sekachev and G. Stanford, *SCRF activities for the ISAC-II upgrade at TRIUMF*, Proc. **11th Workshop on RF Superconductivity (SRF 2003)**, Lübeck/Travemünde, Germany, September 8–12, 2003 [TRI-PP-03-32].

K. Jayamanna, D. Yuan, M. Olivo, R. Baartman, G. Dutto, M. McDonald, A. Mitra, P. Schmor and G. Stanford, *Commissioning the TRIUMF/ISAC ECR source for radioactive ion beams*, Proc. **10th Int. Conf. on Ion Sources**, Dubna, Russia, September 8–13, 2003 (Rev. Sci. Instrum., in press) [TRI-PP-03-42].

K. Fong, R.E. Laxdal, A.K. Mitra, R. Poirier, T. Ries and V. Zviagantsev, *A mechanical tuner and rf drive line system for the ISAC-II quarter wave superconducting cavities*, *ibid.* [TRI-PP-03-33].

A. Mitra, R.E. Laxdal, R. Poirier and K. Fong, *HFSS computation of frequency sensitivity of ISAC-II medium beta superconducting cavities*, *ibid.* [TRI-PP-03-38].

G. Stanford, R.E. Laxdal, C. Marshall, T. Ries and I. Sekatchev, *Design of the medium-beta cryomodule for the ISAC-II superconducting heavy ion accelerator*, Proc. **2003 Cryogenic Engineering Conf. (CEC) and Int. Cryogenic Materials Conf. (ICMC)**, Anchorage, AL, September 22–26, 2003 (AIP, New York, Advances in Cryo. Eng. **49** & **50**, in press) [TRI-PP-03-30].

R. Carnegie *et al.*, *GEM TPC resolution*, Proc. **IEEE Workshop on Micro-Pattern Detectors for Time Projection Chambers**, Portland, OR, October, 2003.

M. Dixit *et al.*, *Charge dispersion studies in MPGDs with a resistive anode*, *ibid.*

M.K. Craddock, *Dependence of path-length spread on FFAG lattice type*, Proc. **FFAG Workshop**, Brookhaven National Laboratory, NY, October 13–17, 2003.

E. Tikhomolov, G. Waters and R. Keitel, *EPICS portable channel access server for multiple applications under Windows*, Proc. **IX Int. Conf. on Accelerator and Large Experimental Physics Control Systems (ICALEPCS2003)**, Gyeongju, South Korea, October 13–17, 2003 (in press).

R. Keitel, J. Richards and E. Tikhomolov, *Upgrade of the ISAC device database from Paradox to PostgreSQL*, *ibid.*

R. Nussbaumer and G. Waters, *Inexpensive IOCs for GPIB support in the TRIUMF/ISAC control system*, *ibid.*

G. Waters, R. Nussbaumer, *TRIUMF/ISAC EPICS IOCs using a PC104 platform*, *ibid.*

E. Tikhomolov, G. Waters, R. Keitel, *EPICS portable channel access server for multiple Windows applications*, *ibid.*

J.J. Pon, E. Klassen, K.S. Lee, M.M. Mouat and P.J. Yogendran, *Preliminary use of PDAs in TRIUMF's central control system*, *ibid.*

K.S. Lee, E.M. Tikhomolov, J.E. Richards, E. Klassen and T. Tateyama, *The TRIUMF secondary beam line control system upgrade using EPICS*, *ibid.*

J.J. Pon, E. Klassen, K.S. Lee, M.M. Mouat and P.J. Yogendran, *Early control system applications using PDAs at TRIUMF*, *ibid.*

D. Karlen, P. Poffenberger, G. Rosenbaum, R. Carnegie, M. Dixit, H. Mes, K. Sachs and J.-P. Martin, *Track resolution measurements for a time projection chamber with gas electron multiplier readout*, Proc. **IEEE Nuclear Science Symp. Medical Imaging Conf. (NSS-MIC)**, Portland, OR, October 19–25, 2003 (Trans. Nucl. Sci., in press).

J.P. Archambault, P. Gumplinger, P. Kitching, A. Konaka, J. McDonald and M. Vincet, *GEANT4 photon readout simulations of plastic scintillating strips with embedded WLS fibers*, *ibid.*

M.J. Barnes, G.D. Wait, Y. Shirakabe and Y. Mori, *Conceptual design of a bipolar kicker magnet for the J-PARC-Kamioka neutrino project*, Proc. **18th Int. Conf. on Magnet Technology (MT18)**, Morioka, Japan, October 20–24, 2003 (IEEE Trans. Applied Superconductivity, in press).

Molecular and Materials Science

J.H. Brewer, *μ^-SR in nuclei with spin*, Proc. **CAP Congress**, Charlottetown, June 8–11, 2003.

K.H. Chow, Z. Salman, R.F. Kiefl, W.A. MacFarlane, C.D.P. Levy, P. Amaudruz, R. Baartman, J. Chakhalian, S. Daviel, Y. Hirayama, A. Hatakeyama, D.J. Arseneau, B. Hitti, S.R. Kreitzman, G.D. Morris, R. Poutissou and E. Raynard, *The new β -NMR facility at TRIUMF and applications in semiconductors*, Proc. **22nd Int. Conf. on Defects in Semiconductors (ICDS-22)**, Aarhus, Denmark, July 28–August 1, 2003 (Physica B, in press).

S.R. Dunsiger, *Persistent spin fluctuations in the geometrically frustrated pyrochlore Gadolinium titanate*, Proc. **Highly Frustrated Magnetism 2003 Conf.**, Grenoble, France, August 2003.

K. Ghandi, D.G. Fleming, D.J. Arseneau and M.D. Bridges, *Studies of free radical and radiation chemistry in sub- and supercritical CO_2* , Proc. **39th IUPAC Congress and 86th Conf. of the Canadian Society for Chemistry**, Ottawa, ON, August 10–15, 2003.

J. Sugiyama, J.H. Brewer, E.J. Ansaldo, H. Itahara, K. Dohmae, Y. Seno, C. Xia and T. Tani, *Successive magnetic transitions in thermoelectric layered cobaltite, $[Ca_2CoO_3]_{0.62}[CoO_2]$* , Proc. **8th IUMRS Int. Conf. on Advanced Materials**, Yokohama, Japan, October, 2003 (Trans. MRS-J, in press).

J. Sugiyama, H. Itahara, J.H. Brewer, E.J. Ansaldo, T. Motohashi, M. Karppinen and H. Yamauchi, *Magnetism in $Na_{0.75}CoO_2$ investigated by μSR* , *ibid.*

Life Sciences

C.S. Lee, B.L. Beattie, T.J. Ruth, V. Sossi, M. Adam, A.J. Stoessl, J. Martzke, I.R. Mackenzie, D. Foti and H. Feldman, *Dopaminergic and cholinergic mechanisms of cognitive and behavioral symptoms in dementia with Lewy bodies and Parkinson's disease with dementia: a double-tracer PET study*, Proc. **55th Annual Meeting of the American Academy of Neurology**, 2003.

S. Savedia-Cayabyab, A. Kumar, V. Sossi, T.J. Ruth, A.J. Stoessl, M. Schulzer and C.S. Lee, *Upregulation of $[^{18}F]$ dopa Ki in the putamen is associated with improvement of motor performance in Parkinson's disease*, *ibid.*

H. van Netten, Z. Wozlek, C.S. Lee, E. Mak, M. Schulzer, V. Sossi, T.J. Ruth and A.J. Stoessl, *Compensatory mechanisms in the dopamine system of patients with dominantly inherited Parkinsonism*, *ibid.*

T.J. Ruth, *Production of radioisotopes for medical applications at RIA*, Proc. **225th ACS National Meeting**, New Orleans, LA, March 23–27, 2003.

T.J. Ruth, *Production of high LET radioisotopes at TRIUMF-ISAC*, *ibid.*

C.S. Lee, B.L. Beattie, T.J. Ruth, V. Sossi, M. Adam, A.J. Stossel, J. Martzke, I.R. Mackenzie, D. Foti and H. Feldman, *Dopaminergic and cholinergic mechanisms of cognitive and behavioural symptoms in dementia with Lewy bodies, and Parkinson's disease with dementia: a double-tracer PET study*, Proc. **55th Annual Meeting American Academy of Neurology**, Honolulu, HI, April, 2003.

C.S. Lee, B.L. Beattie, T.J. Ruth, V. Sossi, M.J. Adam, A.J. Stoessl, D. Christa-Lynn, J. Martzke, I.R. Mackenzie, D. Foti and H. Feldman, *PET correlates of cognitive impairment and hallucinations in Lewy body disorders: comparison with Alzheimer's disease*, Proc. **6th Int. Conf. on Alzheimer's Disease and Parkinson's Disease**, Seville, Spain, May 8–12, 2003.

V. Sossi, R. de la Fuente-Fernandez, J.E. Holden, M. Schulzer, T.J. Ruth and A.J. Stoessl, *Changes in dopamine turnover in the progression of Parkinson's disease as measured by PET*, Proc. **BrainPET 2003**, Calgary, AB, July 2003.

D. Doudet, T.J. Ruth and J.E. Holden, *Increased density and decreased affinity of the dopamine D1 receptors in MPTP-treated rhesus monkeys: In-vivo multiple ligand and concentration receptor assay (MLCRA) studies with [¹¹C]Sch23390*, *ibid.*

K.R. Buckley, S. Jivan, S. Lapi, J. Publicover and T.J. Ruth, *Design considerations for high power gas targets: part II*, Proc. **226th ACS Meeting**, New York, NY, September 2003.

V. Sossi, K.R. Buckley, P. Piccioni, A. Rahmim, M.-L. Camborde, S. Lapi and T.J. Ruth, *Printed sources for positron emission tomography*, Proc. **IEEE Nuclear Science Symp. Medical Imaging Conf. (NSS-MIC)**, Portland, OR, October 19–25, 2003 (IEEE Trans. Nucl. Sci., in press).

Theoretical Program

I.R. Afnan and A.D. Lahiff, *The Bethe-Salpeter equation and the low-energy theorems for πN scattering*, Proc. **Conf. on Quarks and Nuclear Physics (QNP 2002)**, Julich, Germany, June 9–14, 2002, eds. J. Speth, Ch. Elster and Th. Walcher (Eur. Phys. J. A, in press) [nucl-th/0210027].

M. de Montigny, F.C. Khanna and A.E. Santana, *Metric formulation of Galilean invariance in five dimensions*, Proc. **24th Int. Coll. on Group Theoretical Methods in Physics: GROUP – 24 (ICGTMP 2002)**, Paris, France, July 15–20, 2002 (Inst. of Phys., in press).

H. Uys, H.G. Miller and F.C. Khanna, *Generalised statistics and high T_c superconductivity*, Proc. **26th Int. Work-**

shop on Condensed Matter Theories (CMT 26), Luso, Portugal, September 2–7, 2002 (Condensed Matter Theories 18, in press).

M. de Montigny, F.C. Khanna and A.E. Santana, *Physical applications of a five-dimensional metric formulation of Galilean invariance*, Proc. **Workshop on Symmetry in Physics in Memory of Robert T. Sharp**, Montreal, PQ, September 12–14, 2002 (CRM Proc. and Lecture Notes, in press).

A. Astbury, B. Campbell, F.C. Khanna and M. Vincter (editors), Proc. **18th Lake Louise Winter Inst. on Particles and the Universe (LLWI03)**, Lake Louise, AB, February 16–22, 2003.

S. Sengupta, S.P. Kim and F.C. Khanna, *Non-equilibrium evolution equations for correlation functions*, *ibid.*

D. Matrasulov and F.C. Khanna, *Quantum chaos at finite temperature*, *ibid.*

R.H. Cyburt, *Primordial nucleosynthesis in light of WMAP*, Proc. **Great Lakes Cosmology VII Symp.**, Ann Arbor, MI, May 15–18, 2003.

C. Barbieri, L. Lapikas and D. Rohe, *Rescattering contributions to final state interactions in $(e, e'p)$ reactions*, Proc. **2nd Conf. on Nuclear and Particle Physics with CEBAF at JLab (NAPP 2003)**, Dubrovnik, Croatia, May 26–31, 2003 (Croatian Phys. Soc. Fizika B, in press) [TRI-PP-03-29, nucl-th/0309024].

W.T.H. van Oers, *Symmetries and symmetry breaking*, Proc. **17th Int. IUPAP Conf. on Few-Body Problems in Physics (FB 17)**, Durham, NC, June 5–10, 2003 [TRI-PP-03-27, hep-ph/0307285].

B. Desplanques, A. Amghar and L. Theussl, *'Point-form' estimate of the pion form factor revisited*, *ibid.* [hep-ph/0308219].

F. Okiharu and R.M. Woloshyn, *A study of color field distributions in the baryon*, Proc. **21st Int. Symp. on Lattice Field Theory (LATTICE 2003)**, Tsukuba, Ibaraki, Japan, July 15–19, 2003 (Elsevier, Nucl. Phys. B Proc. Suppl., in press) [hep-lat/0310007].

C. Barbieri and L. Lapikas, *Rescattering contributions to final state interactions in $(e, e'p)$ reactions at high (p_m, E_m)* , Proc. **6th Workshop on Electromagnetically Induced Two Hadron Emission**, Pavia, Italy, September 24–27, 2003 [TRI-PP-03-39, nucl-th/0401010].

S. Ando, *Muon capture and solar-neutrino reactions on deuteron in chiral perturbation theory*, Proc. **INT03-3, Theories of Nuclear Forces and Nuclear Systems**, Inst. for Nuclear Theory, Seattle, WA, September 28–December 5, 2003.

D. Rohe and C. Barbieri, *Spectral function at high missing energy and momentum*, Proc. **Int. Workshop on Probing Nucleons and Nuclei Via the (e, e') Reaction**, Grenoble, France, October, 2003.

J.N. Ng, *Neutrino mass models in extra dimensions*, Proc. **2nd Int. Conf. on Flavor Physics (ICFP 2003)**, Seoul, Korea, October 6–11, 2003 [hep-ph/0311352].

R.H. Cyburt, *BBN and the CMB: two great tastes that taste great together*, Proc. **Kingston Theoretical Astrophysics Meeting**, Kingston, ON, November 14–16, 2003.

J.-M. Sparenberg and B. Jennings, *On the practical interest of one-body overlap functions*, Proc. **Int. Symp.: A New Era of Nuclear Structure Physics**, Kurokawa Village, Japan, November 19–22, 2003 (World Scientific, Singapore, in press).

Y. Fujiwara, K. Miyagawa, M. Kohno, Y. Suzuki, D. Baye and J.-M. Sparenberg, *A realistic baryon-baryon interaction in the SU_6 quark model and its applications to few-body systems*, *ibid.*

J.-M. Sparenberg, *Deducing the asymptotic normalization constant of the 2^+ subthreshold state in ^{16}O from $^{12}C + \alpha$ elastic scattering*, Proc. **8th Int. Conf. on Clustering Aspects of Nuclear Structure and Dynamics**, Nara, Japan, November 24–29, 2003 (Nucl. Phys. A, in press).

Y. Hirayama T. Shimoda, H. Izumi, H. Yano, M. Yagi, A. Hatakeyama, C.D.P. Levy, K.P. Jackson and H. Miyatake, *Spectroscopic study of ^{11}Be through β -delayed neutron- and γ -decays of spin-polarized ^{11}Li* , *ibid.*

Y. Fujiwara, K. Miyagawa, M. Kohno, Y. Suzuki, D. Baye and J.-M. Sparenberg, *A consistent 3α and $2\alpha A$ Faddeev calculation using the 2α RGM kernel*, *ibid.*

Y. Fujiwara, K. Miyagawa, M. Kohno, Y. Suzuki, D. Baye and J.-M. Sparenberg, *$2\alpha A$ Faddeev calculation using the quark-model $S = -2$ hyperon hyperon interaction*, *ibid.*

J.-M. Sparenberg, *R-matrix analyses of $^{12}C + \alpha$ elastic scattering phase shifts*, Proc. **20th Meeting between Astrophysicists and Nuclear Physicists**, Brussels, Belgium, December 15–16, 2003.

Technology Transfer

P.L. Gardner, *Mechanisms and initiatives for enabling effective technology transfer*, Proc. **Stimulating Economic Development through the Advancement of Knowledge Based Economies**, Montreal, PQ, March, 2003.

P.L. Gardner, *Transferring technology offshore: Security essentials at a research laboratory*, Proc. **Soc. Research Administrators**, Seattle, WA, March, 2003.

P.L. Gardner, *The best and worst of licensees*, Proc. **Soc. Research Administrators**, Maui, HI, May, 2003.

Books

K. Nagamine, *Introductory muon science* (Cambridge Univ. Press, Cambridge, 2003).

T.J. Ruth, *Criteria for the selection, production, and use of radionuclides for diagnosis and radiotherapy* in *Technetium, Rhenium and other Metals in Chemistry and Nuclear Medicine*, eds. M. Nicolini, U. Mazzi (SG Editorial, Padova, 2003) p. 297.

A.J. Stoessl and S. Furtado, *Positron emission tomography in movement disorders*, in *Positron Emission Tomography: Basic Science and Clinical Practice*, eds. P.E. Valk *et al.* (Springer-Verlag, London, 2003).

J.E. Holden and D.J. Doudet, *PET receptor assay with multiple ligand concentrations: an equilibrium approach* in *Methods in Enzymology: Imaging*, ed. M. Conn (Academic Press, in press).

Theses

M.D. Bridges, *Room-temperature hyperfine coupling constants of the Mu-ethyl and Mu-t-butyl radicals in faujasites* (B.Sc. Hon., Chemistry, University of British Columbia).

T. Warner, *Collection and manipulation of radioactive xenon isotopes: progress towards a radon EDM search at TRIUMF* (B.Sc. Hon., Engineering Physics, Simon Fraser University).

C.J. Osborne, *High-precision measurements of the half-life of ^{26}Na* (M.Sc., Physics, University of Surrey).

K.F. Poon, *μSR studies of the electron-doped high- T_c superconductor $Pr_{2-x}Ce_xCuO_4$* (M.Sc., Physics, Simon Fraser University).

N. Buchanan, *The radiation qualification of a switch capacitor array controller for use in ATLAS* (Ph.D., Physics, University of Alberta).

D. Waller, *A study of charm quark production in beauty quark decays with the OPAL detector at LEP*, (Ph.D., Carleton University).

J. Wendland, *Polarized parton distributions measured at the HERMES experiment* (Ph.D., Physics, Simon Fraser University).

SEMINARS*

The following seminars were presented at TRIUMF this year.

- 09/01 *Precision Spectroscopy of Pionic Hydrogen*, Johannes Zmeskal, Inst. Medium Energy Physics, Vienna.
- 13/01 *QED Theory and Isotope Shifts in Few-Electron Atoms*, Gordon Drake, U. Windsor.
- 17/01 *Pierre Auger Cosmic Ray Observatory*, Gertjan Hofman, TRIUMF.
- 23/01 *The μ SR Technique at TRIUMF: Applications to Superconductivity*, Jeff Sonier, SFU.
- 28/01 *The Present and Future of Big Bang Nucleosynthesis*, Richard Cyburt, U. Illinois.
- 05/02 *REX-ISOLDE: Present Status and Future Plans for the Machine and the Experiments*, Joakim Cederkall, CERN.
- 06/02 *Nucleosynthesis in Shells on Top of Degenerate Cores*, Falk Herwig, U. Victoria.
- 11/02 *Studying Chiral 2N and 3N Forces in Few-Nucleon Systems*, Andreas Nogga, U. Arizona.
- 13/02 *Phenomenology of the Littlest Higgs Model*, Bob McElrath, U. Wisconsin.
- 18/02 *Final-State Phase Information in Heavy Meson Decays*, Cheng Wei Chiang, ANL.
- 20/02 *Nucleosynthesis and Extra-Mixing in Low-Mass Red Giants*, Pavel Denissenkov, U. Victoria/U. St. Petersburg.
- 25/02 *Unquenched QCD with Light Quarks*, Jaebeom Yoo, U. Pittsburgh.
- 26/02 *Shape Coexistence in Neutron-Deficient Lead Nuclei*, George Dracoulis, Australian National U.
- 27/02 *Extraction of the Magnetic Form Factor of the Neutron $G_M^n(Q^2)$ from Inclusive Quasi-Elastic Scattering of Electrons from Light Targets*, Avraham Rinat, Weizmann Inst.
- 04/03 *Desperately Seeking SUSY*, Isabel Trigger, CERN.
- 12/03 *Properties of Nucleons and Their Interaction in the Medium*, Willem Dickhoff, Washington U., St. Louis.
- 13/03 *Magnets for the LHC*, Gijs de Rijk, CERN.
- 14/03 *Can We Trust the Random Phase Approximation?*, Ionel Stetcu, Louisiana State U.
- 17/03 *Recent Rare B Decay Results from the BaBar Experiment*, Steven Robertson, SLAC.
- 31/03 *Virtual Compton Scattering Off the Nucleon*, Stefan Scherer, Johannes-Gutenberg U., Mainz.
- 03/04 *Nuclear Physics and Core-Collapse Supernovae*, Karlheinz Langanke, Aarhus U.
- 04/04 *Fast and Slow Rare Isotope Beams at the NSCL*, Georg Bollen, Michigan State U.
- 07/04 *Parity and Time Reversal Violation in Atoms and Nuclei and Test of the Standard Model*, Victor Flambaum, U. New South Wales.
- 10/04 *Two Examples of Using Nuclear Physics in the Cosmos: Sub-Barrier Fusion and Neutrino-Nucleus Scattering*, Baha Balantekin, U. Wisconsin-Madison.
- 17/04 *Hyperon Semi-Leptonic Decays – An Overview*, Ashkan Alavi, U. Wisconsin-Madison.
- 24/04 *Rare Vector-Vector B Decays: A Laboratory for Strong and Weak Dynamics*, Andrei Gritsan, UC Berkeley.
- 25/04 *Navigating Through Strong Interactions with Heavy Quarks*, Mikhail Voloshin, U. Minnesota.
- 01/05 *MICE – The Muon Ionisation Cooling Experiment*, Rob Edgecock, Rutherford Lab.
- 09/05 *Status Report of the SPIRAL2 Design Study*, Alban Mosnier and Robin Ferdinand, Saclay.
- 14/05 *Recent Nuclear Structure Studies of Neutron-Rich Nuclei Produced by Low-Energy Fission*, Gary Simpson, Institut Laue-Langevin, Grenoble.
- 15/05 *20 Years of PET Chemistry at TRIUMF*, Mike Adam, TRIUMF.
- 22/05 *Prostate Cancer, Pharmaceutical Research and PET*, Emma Guns, VGH/UBC.
- 26/05 *ROOT: A Framework for Data Storage and Analysis*, Rene Brun, CERN.
- 28/05 *Superconducting Linac Developments for the European RIB Facility Projects*, Alberto Facco, LNL-INFN.
- 29/05 *Ups and Downs of Nuclear Isomers*, Phil Walker, U. Surrey/TRIUMF.
- 02/06 *Three Themes for Experiments with Radioactive Beams*, Joakim Cederkall, MPI, Heidelberg/CERN.
- 03/06 *Indirect Measurements for Determining the Production of ^{22}Na and ^{26}Al in Explosive Stellar Burning Sites*, Jac Caggiano, Yale U.
- 04/06 *Indirect Techniques in Experimental Nuclear Astrophysics*, Barry Davids, KVI, Groningen.
- 05/06 *The Charm and Beauty of Lattice QCD*, Aida El-Khadra, U. Illinois.
- 19/06 *LSND and Rare Muon Decays*, Sandip Pakvasa, U. Hawaii.
- 24/06 *Physics with Intense Ultracold Neutrons*, Yasuhiro Masuda, KEK.
- 25/06 *Jet Quenching at RHIC*, Carl Gagliardi, Texas A&M U.
- 02/07 *Accelerator Activities at VECC and in India*, Bikash Sinha, Saha Inst., India.
- 03/07 *Signals of Quark Gluon Plasma – Terrestrial and Cosmological*, Bikash Sinha, Saha Inst., India.
- 10/07 *First Observation of Doubly Charmed Baryons*, Murray Moinester, Tel Aviv U.
- 11/07 *At the Limits of Nuclear Stability: The Observation of Two-Proton Emission*, Bertram Blank, ANL/CEN Bordeaux-Gradignan.

- 18/07 *MINERvA: A High Statistics, Neutrino-Nucleus Scattering Experiment in the NuMI Beam at Fermilab*, Jorge Morfin, Fermilab.
- 24/07 *Status of Neutrino Mixing and Oscillations*, Samoil Bilenky, JINR, Dubna.
- 28/07 *In the Zinc Mine, But Looking Up at the Stars: Neutrino Astronomy at Super-Kamiokande*, Matthew Malek, SUNY.
- 05/08 *Ultraprecise Measurement of the Electronic g-Factor in Hydrogen-Like Oxygen*, Jose Verdu, U. Mainz.
- 08/08 *The HERMES Recoil Detector*, Ralf Kaiser, U. Glasgow.
- 11/08 *g_A , the Lattice and $\pi N \rightarrow \pi\pi N$* , Thomas Hemmert, U. Munich.
- 12/08 *Pentaquark*, Kim Maltman, York U.; Andy Miller and Byron Jennings, TRIUMF.
- 18/08 *Overview and Status of the RIA Project*, Jerry Nolen and Guy Savard, ANL.
- 19/08 *Deconstructing the Charm and Charm-Strange P-Wave Mesons*, Stephen Godfrey, Carleton U.
- 25/08 *LIBO: A CERN-INFN Linac Booster for Proton Therapy at TERA: Rationale, Construction and First Prototype Tests*, Dario Giove, LASA-INFN, Milan.
- 15/09 *First Results from the Salt Phase of the Sudbury Neutrino Observatory*, Alysia Marino, LBNL/UC Berkeley.
- 16/09 *The Penning Trap System of SHIPTRAP*, Günther Sikler, Gesellschaft für Schwerionenforschung, Darmstadt.
- 18/09 *Recent Results from the D0 Experiment*, Brigitte Vachon, Fermilab.
- 22/09 *Highly Excited Nuclear States at Low Laboratory Energies*, Goetz Ruprecht, Technische U., Berlin.
- 03/10 *The $^{21}\text{Na}(p,\gamma)^{22}\text{Mg}$ Reaction from $E_{\text{cm}} = 200$ to 800 keV in Explosive Stellar Events*, Shawn Bishop, SFU.
- 09/10 *Nuclear Spectroscopy Using Radioactive Ion Beams from the HRIBF*, Alfredo Galindo-Uribarri, ORNL.
- 09/10 *Status and Scope of the J-PARC Project in Japan*, Shoji Nagamiya, KEK/JAERI.
- 16/10 *Neutron Electric Dipole Moment*, Richard Mischke, LANL.
- 17/10 *Present Status of Applications of Liquid Xenon Scintillation Detectors*, Tadayoshi Doke, Waseda U.
- 27/10 *Development and Applications of the Gas Electron Multiplier*, Fabio Sauli, CERN.
- 30/10 *Light Baryon Resonances in Constituent Quark Models*, Lukas Theussl, TRIUMF.
- 13/11 *Beautiful Mirrors and Precision Electroweak Data*, Tim Tait, Fermilab.
- 14/11 *Production of Dilepton Events at CDF*, Reda Tafirout, U. Toronto.
- 14/11 *Resonant Bose-Einstein Condensation*, Carl Wieman, U. Colorado.
- 20/11 *$^7\text{Be}(p,\gamma)^8\text{B}$ and Solar Neutrinos*, Kurt Snover, U. Washington.
- 21/11 *Beta-Decay of ^{11}Li* , Fred Sarazin, Colorado School of Mines/TRIUMF.
- 24/11 *Parity Violation in e-p Scattering: The G0 and Qweak Experiments at JLab*, Larry Lee, U. Manitoba.
- 25/11 *Hint of New Physics in $B \rightarrow \phi K_S$* , Alakabha Datta, U. Toronto.
- 26/11 *A Hot Topic with Cool Results – Muon Frictional Cooling*, Raphael Galea, MPI, Munich.
- 01/12 *Very Small Asymmetries and the Weak Interaction*, Gregory Mitchell, LANL.
- 02/12 *Grid Computing for the LHC: A Practical Example*, John White, Helsinki Inst. Physics.
- 04/12 *Secrets of E949*, Joe Mildenberger, TRIUMF.
- 05/12 *Casting Light on Antimatter: Fundamental Physics with Cold Antihydrogen*, Makoto Fujiwara, RIKEN.
- 10/12 *Physics for the Birds*, Boye Ahlborn, UBC.
- 17/12 *Experience with ALPI and PIAVE Resonators*, Anna-Maria Porcellato, LNL-INFN.
- 18/12 *Weak Pion-Nucleon Coupling and Parity Violation in the Radiative Capture of Polarized Cold Neutrons on Hydrogen*, Michael Gericke, Indiana U.

The following ISAC seminars were presented at TRIUMF this year.

- 26/02 *The TRIUMF Neutral Atom Trap Physics Program*, Dan Melconian, TRIUMF.
- 12/03 *Revisiting the $^{12}\text{C} + \alpha$ Theoretical Description*, Jean-Marc Sparenberg, TRIUMF.
- 19/03 *The Heidelberg EBIT (Electron Beam Ion Trap) System, a Device for Breeding High Charge States and Precision Experiments: First Measurements and Tests*, Michael Trinczek, MPI for Nuclear Physics, Heidelberg.
- 26/03 *Reports from the RIA Workshop, Oak Ridge, March 18–22, 2003*, John Behr, Joe Vaz, Helen Scraggs and Fred Sarazin, TRIUMF.
- 09/04 *The DRAGON is Puffing – An Extended Status Report*, Sabine Engel, U. Bochum.
- 23/04 *Meson and Quark Effects in Nuclear Beta Decay of the $A=12$ System and ^{20}Na Beta-Ray Angular Distribution from Oriented Nuclei*, Kei Minamisono, Osaka U./TRIUMF.
- 21/05 *The ISAC Front End: Production of Exotic Nuclei*, Marik Dombsky, TRIUMF.
- 04/06 *The Laser Ion Source System at ISAC*, Jens Lassen, TRIUMF.
- 18/06 *Calibration and Simulation of a Gamma Array for DRAGON*, Dario Gigliotti, UNBC/TRIUMF.
- 02/07 *The Quantum: Still Crazy After All These Years*, Jim Al-Khalili, U. Surrey.
- 06/08 *TIGRESS*, Helen Scraggs, TRIUMF.
- 15/10 *Resonant Elastic Scattering Studies at TUDA*, Chris Ruiz, TRIUMF.
- 12/11 *(α, p) Reactions in Nuclear Astrophysics*, Ernst Rehm, ANL.

- 24/11 *SCEPTAR: The New Scintillating Array for the 8π Spectrometer*, Elizabeth Cunningham, TRIUMF/U. Surrey.
- 24/11 *Enter the DRAGON: Investigating the $^{13}\text{C}(p,\gamma)^{14}\text{N}$ Reaction*, Aaron Bebington, TRIUMF/U. Surrey.
- 03/12 *^{182}Hf , from the Early Solar System to a Possibly Live Supernova Remnant on Earth*, Christof Vockenhuber, U. Vienna.

The following UBC/TRIUMF joint colloquia were presented this year.

- 30/01 *Unstable Nuclei in Cosmic Explosions and in Radioactive Beams on Earth*, Hendrik Schatz, Michigan State U.
- 25/03 *Meson Spectroscopy in the AdS/CFT*, Rob Myers, Perimeter Inst.
- 29/07 *The Decay $K^+ \rightarrow \pi^+ \nu \bar{\nu}$ at BNL E787/E949*, Bipul Bhuyan, Delhi U.

The following lunchtime seminars were presented at TRIUMF this year.

- 20/01 *Report on Neutrino-Nucleus Interactions Conference 2002*, Stan Yen, TRIUMF.
- 28/04 *WestGrid*, Michel Vetterli, SFU.
- 13/05 *Weak Interaction Tests at Low Energies*, Nathal Severijns, K.U. Leuven.
- 16/06 *Building Web-Based Software Applications*, Morgan Burke, TRIUMF.
- 24/07 *VME Standards and CAEN/WIENER Nuclear VME Developments*, Andreas Ruben, WIENER/CAEN USA.
- 02/09 *Introducing GEANT4*, Makoto Asai, SLAC.
- 03/09 *Electromagnetic Physics in GEANT4*, Michel Maire, LN2P3/LAPP.
- 04/09 *Hadronic Physics in GEANT4*, Hans-Peter Wellisch, CERN.
- 05/09 *AIDA/JAS/WIRED: Interactivity and Visualization*, Massimiliano Turri, SLAC.
- 17/11 *Report on the NSS Conference*, P. Amaudruz and P. Gumplinger, TRIUMF.

* All matters concerning TRIUMF seminars should be referred via e-mail to seminar@triumf.ca

The latest listing of TRIUMF seminars can be seen at <http://admin.triumf.ca/netdata/seminars/list>

USERS GROUPS

TRIUMF USERS' GROUP

From the TRIUMF Users' Group Charter:

The TRIUMF Users' Group is an organization of scientists and engineers with special interest in the use of the TRIUMF facility. Its purpose is:

- (a) to provide a formal means for exchange of information relating to the development and use of the facility;
- (b) to advise members of the entire TRIUMF organization of projects and facilities available;
- (c) to provide an entity responsive to the representations of its members for offering advice and counsel to the TRIUMF management on operating policy and facilities.

Membership of the TRIUMF Users' Group (TUG) is open to all scientists and engineers interested in the TRIUMF program. At the end of 2003 the TUG had 310 members from 12 countries.

TRIUMF Users' Executive Committee (TUEC)

The TRIUMF Users' Executive Committee (TUEC) is a committee of elected members whose role is to represent the interests of the TUG to the TRIUMF administration.

Among other things, TUEC maintains the TUG Web site at <http://www.triumf.ca/tug/> where detailed information is available about its membership, that of related committees, and various TUG activities.

TUEC Membership for 2003

W.D. Ramsay	U. Manitoba	<i>Chair</i>
J.E. Sonier	SFU	<i>Chair Elect</i>
G.M. Luke	McMaster U.	<i>Past Chair</i>
G.S. Hackman	TRIUMF	2002/2003
M.M. Pavan	U. Regina/TRIUMF	2002/2003
A.A. Chen	McMaster U.	2003/2004
T.A. Porcelli	U. Northern BC	2003/2004
M. Comyn	TRIUMF	<i>Liaison Officer</i>

J. Dilling was elected as chair elect for 2004.

P. Bricault (TRIUMF) and A. Laird (U. York, UK) were elected as members for 2004/2005.

TUEC nominates two members to represent the Users on the TRIUMF Operating Committee. In 2003 S. Yen (TRIUMF) and L. Lee (U. Manitoba) remained as the on-site member and alternate, respectively, while G.M. Luke (McMaster U.) and J.E. Sonier (SFU) remained as the off-site member and alternate, respectively.

μ SR USERS GROUP

Full details regarding the μ SR Users Group and μ SR facilities can be obtained via the WWW at <http://musr.triumf.ca/>.

EXPERIMENT PROPOSALS

The following lists experiment proposals received up to the end of 2003 (missing numbers cover proposals that have been withdrawn or replaced by later versions, rejected, or combined with another proposal). Experiments 1–699 are omitted from this listing (except for those reporting results in this Annual Report). Please refer to the 1999 Annual Report or see <http://www.triumf.ca/annrep/experiments.html> for a full listing of these earlier experiments. Page numbers are given for those experiments which are included in this Annual Report.

Page

614. TWIST - precise measurement of the ρ , δ and $(\mathcal{P}_\mu\xi)$ parameters in muon decay [active], R. Bayes, Y. Davydov, J. Doornbos, W. Faszer, M.C. Fujiwara, D.R. Gill, R. Henderson, J. Hu, J.A. Macdonald*, G. Marshall, R. Mischke, K. Olchanski, A. Olin, R. Openshaw, T.A. Porcelli, J.-M. Poutissou, R. Poutissou, G. Sheffer, W. Shin (*TRIUMF*), A. Gaponenko, P. Kitching, R.P. MacDonald, M. Quraan, N. Rodning*, J. Schaapman, G.M. Stinson (*U. Alberta*), M. Hasinoff, B. Jamieson (*UBC*), P. Depommier (*U. Montréal*), E.L. Mathie, R. Tacik (*U. Regina*), V. Selivanov, V. Torokhov (*KIAE, Moscow*) C.A. Gagliardi, J.R. Musser, R.E. Tribble, M.A. Vasiliev (*Texas A&M U.*), D.D. Koetke, P. Nord, T.D.S. Stanislaus (*Valparaiso U.*),
700. Measuring cross sections of long-lived radionuclides produced by 200-500 MeV protons in elements found in meteorites and lunar rocks [completed], J. Vincent (*TRIUMF*), J.M. Sisterson (*Harvard U.*), K. Kim (*San Jose State U.*), A.J.T. Jull (*U. Arizona*), M.W. Caffee (*Lawrence Livermore Nat. Lab*), R.C. Reedy (*Los Alamos Nat. Lab*)
702. Measurement of kaon-nucleon elastic scattering at 16 MeV [active], G.A. Beer, P. Knowles, G.R. Mason, A. Olin, L.P. Robertson (*U. Victoria*), P. Amaudruz, D.R. Gill, G. Smith, S. Yen (*TRIUMF*), L. Lee (*U. Manitoba*), G. Tagliente (*UBC*)
703. Study of the decay $\pi^+ \rightarrow e^+ \nu$ phase I – lifetime measurement of the pion [completed], D.A. Bryman, T. Numaou, A. Olin (*TRIUMF*)
704. Charge symmetry breaking in $np \rightarrow d\pi^0$ close to threshold [completed], R. Abegg*, P.W. Green, D.A. Hutcheon (*TRIUMF-U. Alberta*), L.G. Greeniaus (*U. Alberta-TRIUMF*), R.W. Finlay, A.K. Oppen, S.D. Reitzner (*Ohio U.*), E. Korkmaz, T.A. Porcelli (*UNBC*), J.A. Niskanen (*U. Helsinki*), P. Walden (*TRIUMF-UBC*), S. Yen (*TRIUMF*), C.A. Davis (*TRIUMF-U. Manitoba*), D.V. Jordan (*Ohio U.-U. Alberta*), E. Auld (*UBC*)
705. Development of modular gas microstrip chambers as in-target tracking devices for an experiment to detect $\Lambda\Lambda$ hypernuclei at the BNL AGS (BNL885) [completed data-taking], C.A. Davis (*TRIUMF-U. Manitoba*), B. Bassalleck, R. Stotzer (*U. New Mexico*), A.R. Berdoz, A. Biglan, D.S. Carman, G.B. Franklin, P. Khaustov, P. Koran, R. Magahiz, R. McCrady, C.A. Meyer, K. Paschke, B. Quinn, R.A. Schumacher, (*Carnegie-Mellon U.*), J. Birchall, L. Gan, M.R. Landry, L. Lee, S.A. Page, W.D. Ramsay, W.T.H. van Oers (*U. Manitoba*), T. Bürger, H. Fischer, J. Franz, H. Schmitt (*U. Freiburg*), D.E. Alburger, R.E. Chrien, M. May, P.H. Pile, A. Rusek, R. Sawaf, R. Sutter (*Brookhaven Nat. Lab*), A. Ichikawa, K. Imai, Y. Kondo, K. Yamamoto, M. Yosoi (*Kyoto U.*), F. Takeuchi (*Kyoto Sangyo U.*), V.J. Zeps (*U. Kentucky*), P.D. Barnes, F. Merrill (*Los Alamos Nat. Lab*), V.J. Zeps (*U. Kentucky*), T. Iijima (*KEK*), J. Lowe (*U. Birmingham*)
706. μ SR studies of spin fluctuations in CePt_2Sn_2 and other Kondo spin systems [completed], A. Keren, K. Kojima, G.M. Luke, Y.J. Uemura, W.D. Wu (*Columbia U.*), K. Andres, G.M. Kalvius (*Tech. U. Munich*), H. Fujii, G. Nakamoto, T. Takabatake, H. Tanaka (*Hiroshima U.*), M. Ishikawa (*ISSP, U. Tokyo*), B. Andraka (*U. Florida*), D.L. Cox (*Ohio State U.*)
707. μ SR measurements on two-dimensional site-diluted antiferromagnets [active], K. Kojima (*Columbia U.-U. Tokyo*), A. Keren, G.M. Luke, Y.J. Uemura, W.D. Wu (*Columbia U.*), H. Ikeda (*KEK-KENS*), R.J. Birgeneau (*MIT*), K. Nagamine (*U. Tokyo*)
708. The spin relaxation and chemical reactivity of muonium-substituted organic radicals in the gas phase [completed], D.G. Fleming, J.J. Pan, M. Shelley (*UBC*), D.J. Arseneau (*TRIUMF-UBC*), M. Senba (*TRIUMF*), J.C. Brodovitch, P.W. Percival (*SFU*), H. Dilger, E. Roduner (*U. Zürich*), S.F.J. Cox (*Rutherford Appleton Lab*)
709. $^{90,92,94,96}\text{Zr}(n,p)^{90,92,94,96}\text{Y}$ reaction at 200 MeV [completed data-taking], A.G. Ling, P.L. Walden (*TRIUMF*), J. Rapaport (*Ohio U.*), D.A. Cooper, D.L. Prout, E.R. Sugarbaker (*Ohio State U.*), M. Halbert (*Oak Ridge Nat. Lab*), D. Mercer (*U. Colorado*), J. Campbell (*U. Manitoba-TRIUMF*), M. Hartig (*U. Muenster*)
710. Dynamics of muonium in Ge and GaAs [completed], R.L. Lichti (*Texas Tech. U.*), S.F.J. Cox (*Rutherford Appleton Lab*), R.F. Kiehl (*UBC*), K.H. Chow (*Lehigh U.*), T.L. Estle (*Rice U.*), B. Hitti (*TRIUMF*), E.A. Davis (*Leicester U.*), C.R. Schwab (*CNRS, Strasbourg*)

5

712. μ SR study of superconducting spin glasses [completed], V. McMullen, D.R. Noakes, C.E. Stronach (*Virginia State U.*), E.J. Ansaldo (*U. Saskatchewan*), J.H. Brewer (*UBC*), G. Cao, J.E. Crow (*NHMFL*), S. McCall (*Florida State U.-NHMFL*)
713. Muonium chemistry in supercritical water [completed], B. Addison-Jones, J.-C. Brodovitch, K. Ghandi, I. McKenzie, P. Percival (*SFU*), J. Schüth (*U. Bonn*)
714. Atomic PNC in francium: preparations [inactive], J.A. Behr, L. Buchmann, M. Domsbysky, P. Jackson, C.D.P. Levy (*TRIUMF*), J.M. D'Auria, P. Dubé, A. Gorelov, D. Melconian, T. Swanson, M. Trinczek (*SFU*), O. Häusser* (*SFU-TRIUMF*), U. Giesen (*U. Alberta*), I. Kelson, A.I. Yavin (*Tel Aviv U.*), J. Deutsch (*U. Catholique de Louvain*), J. Dilling (*SFU-Heidelberg*)
715. Weak interaction symmetries in β^+ decay of optically trapped $^{37,38\text{m}}\text{K}$ [active], J.M. D'Auria, A. Gorelov, D. Melconian, M. Trinczek (*SFU*), J.A. Behr, P. Bricault, M. Domsbysky, K.P. Jackson, B.K. Jennings (*TRIUMF*), S. Gu, M. Pearson (*UBC*), U. Giesen (*U. Notre Dame*), W.P. Alford (*U. Western Ontario*), J. Deutsch (*U. Catholique de Louvain*), D.A. Ashery, O. Aviv (*Tel Aviv U.*), F. Glück (*U. Mainz*)
716. Complete beta-delayed particle emission study of ^{31}Ar [deferred], J. Cerny, D.M. Moltz, T. Ognibene, M.W. Rowe, R.J. Tighe (*Lawrence Berkeley Lab*), L. Buchmann (*TRIUMF*), J. D'Auria (*SFU*), M. Domsbysky (*SFU-U. Alberta*), G. Roy (*U. Alberta*)
717. Muon hyperfine transition rates in light nuclei [completed], J.H. Brewer, E. Gete, M.C. Fujiwara, J. Lange, D.F. Measday, B.A. Moftah, M.A. Saliba, T. Stocki (*UBC*), T.P. Gorringe (*U. Kentucky*)
718. Superconductivity and magnetism in quaternary boron carbides [completed], A. Keren, G.M. Luke, Y.J. Uemura, W.D. Wu (*Columbia U.*), K. Kojima (*Columbia U.-U. Tokyo*), S. Uchida (*U. Tokyo*)
719. $^4\text{He}(\pi^+, \pi^- pp)$ invariant mass measurement with CHAOS [completed data-taking], P. Amaudruz, L. Felawka, D. Ottewell, G. Smith (*TRIUMF*), E.T. Mathie, R. Tacik, D.M. Yeomans (*U. Regina*), H. Clement, J. Gräter, R. Meier, G.J. Wagner (*U. Tübingen*), J. Clark, M. Sevier (*U. Melbourne*), A. Ambardar, G.J. Hofman, M. Kermani, G. Tagliente (*UBC*), F. Bonutti, P. Camerini, N. Grion, R. Rui (*U. di Trieste*), J. Brack, R. Ristinen (*U. Colorado*), E. Gibson (*California State U., Sacramento*), M. Schepkin (*ITEP Moscow*)
720. Muonium's nucleophilicity [active], G.B. Porter, D.C. Walker (*UBC*), J.M. Stadlbauer* (*Hood Coll.*), K. Venkateswaran (*Hindustan Lever Ltd.*), M.V. Barnabas (*Proctor & Gamble Ltd.*)
721. The delta nucleon reaction in CHAOS [completed data-taking], F. Farzanpay, P. Hong, E.L. Mathie, N. Mobed (*U. Regina*), R. Tacik (*TRIUMF-U. Regina*), P.A. Amaudruz, L. Felawka, R. Meier, D. Ottewell, G.R. Smith (*TRIUMF*), N. Grion (*INFN, Trieste*), P. Camerini, R. Rui (*U. di Trieste*), E. Gibson (*California State U., Sacramento*), G. Hofman, G. Jones, M. Kermani (*UBC*), M.E. Sevier (*U. Melbourne*), J.T. Brack, R.A. Ristinen (*U. Colorado*)
722. Pion initial state interactions in the $^{12}\text{C}(\pi^+, ppp)$ reaction [completed data-taking], T. Mathie, R. Tacik (*U. Regina*), P.A. Amaudruz, L. Felawka, D. Ottewell, K. Raywood, G.R. Smith (*TRIUMF*), M. Kermani, S. McFarland (*UBC*), F. Bonutti, P. Camerini, R. Rui (*U. di Trieste*), N. Grion (*INFN, Trieste*), E.F. Gibson (*California State U., Sacramento*), M. Sevier (*U. Melbourne*), J. Brack, G. Hofman (*U. Colorado*), R. Meier (*U. Tübingen*)
723. Study of pion-nucleus double-scattering reactions [completed data-taking], R. Tacik (*TRIUMF-U. Regina*), T. Mathie (*U. Regina*), P. Amaudruz, L. Felawka, D. Ottewell, K. Raywood, G. Smith (*TRIUMF*), M. Kermani, S. McFarland (*UBC*), F. Bonutti, P. Camerini, R. Rui (*U. di Trieste*), N. Grion (*INFN, Trieste*), J. Brack, G. Hofman (*U. Colorado*), R. Meier (*U. Tübingen*), M. Sevier (*U. Melbourne*), E. Gibson (*California State U. Sacramento*)
724. μ SR measurements on spin ladder systems [completed], A. Keren, G.M. Luke, Y.J. Uemura, W.D. Wu (*Columbia U.*), K. Kojima (*Columbia U.-U. Tokyo*), M. Takano (*Kyoto U.*), K. Nagamine (*U. Tokyo*)
725. Pion double charge exchange reactions on $^3,^4\text{He}$ in the energy range 50–100 MeV [completed], P. Amaudruz, L. Felawka, R. Meier, D. Ottewell, G. Smith (*TRIUMF*), T. Mathie, R. Tacik, M. Yeomans (*U. Regina*), J. Graeter, G. Wagner (*U. Tübingen*), J. Clark, M. Sevier (*U. Melbourne*), G. Hofman, M. Kermani, P. Tagliente (*UBC*), F. Bonutti, P. Camerini, N. Grion, R. Rui (*U. di Trieste*), J. Brack, R. Ristinen (*U. Colorado*), E. Gibson (*California State U., Sacramento*), O. Patarakin (*Kurchatov Inst.*), E. Friedman (*Hebrew U. Jerusalem*)
726. Beta-delayed proton and γ -decay of ^{65}Se , ^{69}Kr and ^{73}Sr [active], D. Anthony, J. D'Auria, M. Trinczek (*SFU*), R.E. Azuma, J.D. King (*U. Toronto*), L. Buchmann, K.P. Jackson, J. Vincent (*TRIUMF*), M. Domsbysky (*SFU-U. Alberta*), U. Giesen (*TRIUMF-U. Alberta*), J. Görres, H. Schatz, M. Wiescher (*U. Notre Dame*), C. Iliadis (*TRIUMF-U. Toronto*), G. Roy (*U. Alberta*)

728. Search for population and de-excitation of low-spin superdeformed states in Po-Hg region via β^+ and α decays [completed data-taking], Y.A. Akovali, M. Brinkman (*Oak Ridge Nat. Lab*), J.M. D'Auria (*TRIUMF-SFU*), J.A. Becker, E.A. Henry (*Lawrence Livermore Nat. Lab*), M. Domsbys (*SFU*), P.F. Mantica (*UNISOR*), W. Nazarewicz (*Joint Inst. for Heavy Ion*), J. Rikowska, N.J. Stone (*Oxford U.*), M.A. Stoyer (*Lawrence Berkeley Nat. Lab*), R.A. Wyss (*MSI, Sweden*)
729. Gamow-Teller and spin-dipole strengths from $^{17,18}\text{O}(n,p)$ [completed data-taking], D.P. Beatty, H.T. Fortune, P.P. Hui, R.B. Ivie, Z.Q. Mao, M.G. McKinzie, D.A. Smith (*U. Pennsylvania*), W.P. Alford (*U. Western Ontario*), K.P. Jackson, A.G. Ling, C.A. Miller, P. Walden, S. Yen (*TRIUMF*)
730. The solar neutrino problem and a new measurement of $^7\text{Be}(p,\gamma)^8\text{B}$ [deferred], R.E. Azuma, J.D. King (*U. Toronto*), P. Bricault, L. Buchmann, T. Ruth, H. Schneider, J. Vincent, S. Zeisler (*TRIUMF*), J. D'Auria, R. Korteling (*SFU*), M. Domsbys (*SFU-U. Alberta*), U. Giesen (*TRIUMF-U. Alberta*), C. Iliadis (*TRIUMF-U. Toronto*), G. Roy (*U. Alberta*), M. Wiescher (*U. Notre Dame*)
731. Investigation of spin-polarized muonium in metallic semiconductors [completed], K.H. Chow, S. Dunsiger, R.F. Kiefl, W.A. MacFarlane, J. Sonier (*UBC*), S.F.J. Cox (*Rutherford Appleton Lab*), E.A. Davis, A. Singh (*Leicester U.*), T.L. Estle, B. Hitti (*Rice U.*), R.L. Lichti (*Texas Tech. U.*), P. Mendels (*Orsay U.*), C. Schwab (*CRN, Strasbourg*)
732. Quantum impurities in one dimensional spin 1/2 chains [completed], I. Affleck, J.H. Brewer, K. Chow, S. Dunsiger, S. Eggert, R.F. Kiefl, A. MacFarlane, J. Sonier (*UBC*), A. Keren, Y.J. Uemura (*Columbia U.*)
733. Probing high T_c superconductor with "paramagnetic" ($\mu^- \text{O}$) system [active], H. Kojima, I. Tanaka, E. Torikai (*Yamanashi U.*), K. Nishiyama (*U. Tokyo*), K. Nagamine (*U. Tokyo-RIKEN*), I. Watanabe (*RIKEN*), T.P. Das (*State U. New York*), S. Maekawa (*Nagoya U.*)
734. Radiative muon capture on nickel isotopes [completed], D.S. Armstrong, P. McKenzie (*Coll. of William & Mary*), G. Azuelos, P. Depommier (*U. de Montréal*), P. Bergbusch, P. Gumplinger, M. Hasinoff, E. Saettler (*UBC*), B. Doyle, T.P. Gorringe, R. Sedlar (*U. Kentucky*), M. Blecher, C. Sigler (*Virginia Polytechnic Inst.*), J.A. MacDonald, J.-M. Poutissou, R. Poutissou, D. Wright (*TRIUMF*)
735. Studies of single layer cuprate superconductors [completed], G.M. Luke, B. Nachumi, Y.J. Uemura (*Columbia U.*), K. Kojima (*Columbia U.-U. Tokyo*), S. Uchida (*U. Tokyo*), R.H. Heffner, L.P. Le (*Los Alamos Nat. Lab*), R. MacLaughlin (*U. California, Riverside*), M.B. Maple (*U. California, San Diego*)
736. Tests of electro-weak theory using ^{14}O beam [deferred], M. Bahtacharya, A. Garcia, R. Rutchi, M. Wayne (*U. Notre Dame*), L. Buchmann (*TRIUMF*), C. Iliadis (*TRIUMF-U. Toronto*), B. Fujikawa (*Lawrence Berkeley Lab*), S.J. Freedman, J. Mortara (*U. California, Berkeley*)
737. Magnetic and superconducting behaviour in selected oxide materials [completed], R.H. Heffner, L.P. Le (*Los Alamos Nat. Lab*), D.E. Maclaughlin (*U. California, Riverside*), G. Luke, B. Nachuma, Y.J. Uemura (*Columbia U.*), K. Kojima (*Columbia U.-U. Tokyo*)
740. Irradiation of silicon tracker components [completed], R. Lipton, L. Spiegel (*Fermilab*), K.F. O'Shaughnessy (*U. California, Santa Cruz*), B. Barnett, J. Cameratta, J. Skarha (*Johns Hopkins U.*), N. Brunner, M. Frautschi, M. Gold, Y. Ling, J. Matthews, S. Seidel (*U. New Mexico*), D. Bortoletto, A. Garfinkel, A. Hardman, K. Hoffman, T. Keaffaber, N.M. Shaw (*Purdue U.*)
741. Beta-delayed proton decay of ^{17}Ne to α -emitting states in ^{16}O [completed], R.E. Azuma, J. Chow, J.D. King, A.C. Morton (*U. Toronto*), L. Buchmann, M. Domsbys (*TRIUMF*), U. Giesen (*U. Notre Dame*), T. Davinson, A.C. Shotton (*U. Edinburgh*), R.N. Boyd (*Ohio State U.*), C. Iliadis (*U. North Carolina*), J. Powell (*U. California, Berkeley*),
742. Scattering of muonic hydrogen isotopes [completed], V.M. Bystritsky, V.A. Stolupin (*JINR*), R. Jacot-Guillarmod, P.E. Knowles, F. Mulhauser (*U. Fribourg*), G.M. Marshall (*TRIUMF*), M. Filipowicz, J. Wozniak (*Fac. Phys., Nucl. Tech., Krakow*), A. Adamczak (*Inst. Nucl. Physics, Krakow*), A.R. Kunselman (*U. Wyoming*), V.E. Markushin, C. Petitjean (*PSI*), T.M. Huber (*Gustavus Adolphus Coll.*), G.A. Beer, M. Maier, A. Olin, T.A. Porcelli (*U. Victoria*), P. Kammel (*U. California, Berkeley*), M.C. Fujiwara (*UBC*), J. Zmeskal (*IMEP Vienna*), S.K. Kim (*Jeonbuk Nat. U.*)
743. Gamow-Teller strength in $^{64,66,68}\text{Zn}$ and $^{63,65}\text{Cu}(n,p)$ [completed data-taking], W.P. Alford (*U. Western Ontario*), D. Beatty, H.T. Fortune, P.P. Hui, R.B. Ivie, Z. Mao, M.G. McKinzie, D.A. Smith (*U. Pennsylvania*), S. Yen (*TRIUMF*)
744. Hadronic weak and electromagnetic form factors via $\pi^- p \rightarrow e^+ e^- n$ [active], P. Gumplinger, M.D. Hasinoff (*UBC*), T.P. Gorringe, M.A. Kovash (*U. Kentucky*), D.H. Wright (*SLAC*), E. Christy (*Hampton U.*), P. Zolnierczuk (*IUCF*)

745. μ^- SR measurements on one-dimensional spin systems [active], K. Kojima (*Columbia U.-U. Tokyo*), K. Nagamine, K. Nishiyama, S. Uchida (*U. Tokyo*), G.M. Luke, B. Nachumi, Y.J. Uemura (*Columbia U.*), I. Affleck, S. Dunsiger, S. Eggert, R.F. Kiefl (*UBC*)
746. Muonium dynamics in Si, Ge and GaAs studied by RF- μ SR and μ W- μ SR [active], S.R. Kreitzman (*TRIUMF*), T.L. Estle, B. Hitti (*Rice U.*), R. Lichti (*Texas Tech. U.*), K. Chow (*UBC*), S.F.J. Cox (*Rutherford Appleton Lab*), E.A. Davis (*Leicester U.*), C. Schwab (*CRN Strasbourg*)
747. μ SR study of re-entrant spin glasses a-FeMn, AuFe, and Fe₇₀Al₃₀ [completed], I.A. Campbell (*U. Paris Sud Orsay*), S. Dunsiger, R.F. Kiefl (*UBC*), M.J.P. Gingras (*TRIUMF*), M. Hennion, I. Mirebeau (*Saclay, LLB*), K. Kojima, G.M. Luke, B. Nachumi, Y.J. Uemura, W.D. Wu (*Columbia U.*)
749. Muonium-substituted free radicals [completed data-taking], B. Addison-Jones, J.C. Brodovitch, K. Ghandi, I. McKenzie, P.W. Percival (*SFU*), J. Schüth (*U. Bonn*)
750. Liquid chemistry μ SR [completed], G.B. Porter, D.C. Walker (*UBC*), J.M. Stadlbauer* (*Hood Coll.*), K. Venkateswaran (*Lever Hindustan Ltd.*), M.V. Barnabas *Procter & Gamble Ltd.*)
751. Tests in preparation for μ SR measurements of off-axis internal magnetic fields in anisotropic superconductors [active], E. Csomortani, W.J. Kossler, X. Wan (*Coll. of William & Mary*), D.R. Harshman (*Physikon Research Inc.*), A. Greer (*Gonzaga U.*), E. Koster, D.L. Williams (*UBC*), C.E. Stronach (*Virginia State U.*)
752. Muonium centres in Si and GaAs [completed], K.H. Chow (*Oxford U.*), S.F.J. Cox (*Rutherford Appleton Lab*), E.A. Davis (*Leicester U.*), S. Dunsiger, R.F. Kiefl, W.A. MacFarlane (*UBC*), T.L. Estle (*Rice U.*), B. Hitti (*TRIUMF*), R.L. Lichti (*Texas Tech. U.*), C. Schwab (*CRN Strasbourg*)
753. Studies of magnetic correlations in planar oxides [completed], K. Kojima (*Columbia U.-U. Tokyo*), M. Larkin, G.M. Luke, J. Merrin, B. Nachumi, Y.J. Uemura (*Columbia U.*), B.J. Sternlieb (*Brookhaven Nat. Lab*), S. Uchida (*U. Tokyo*)
754. A search for the muonium substituted hydroxyl radical [deferred], T.A. Claxton, G. Marston (*Leicester U.*), S.F.J. Cox (*Rutherford Appleton Lab*), D. Arseneau, D. Fleming, M. Senba, P. Wassell (*UBC*), J.-C. Brodovitch, P.W. Percival (*SFU*)
755. Muonium formation in Zn-spinels [deferred], G.M. Kalvius, A. Kratzer, W. Potzel (*Tech. U. Munich*), R. Wäppling (*U. Uppsala*), D.R. Noakes (*Virginia State U.*), S.R. Kreitzman (*TRIUMF*), A. Martin (*U. Jena*), M.K. Krause (*U. Leipzig*)
756. Mu+NO spin relaxation: electron exchange or paramagnetism? [deferred], D.G. Fleming, J.J. Pan, M. Senba, M. Shelley (*UBC*), D.J. Arseneau (*TRIUMF*), E. Roduner (*U. Zürich*)
757. Study of muon dynamics in ferroelectric materials and proton ionic conductors – comparison with proton dynamics [completed], W.K. Dawson, K. Nishiyama, S. Ohira, K. Shimomura (*U. Tokyo*), K. Nagamine (*U. Tokyo-RIKEN*), S. Ikeda (*KEK*), S. Shin (*U. Tokyo-ISSP*), N. Sata (*Tohoku U.*)
758. Electronic structure of muonium and muonium-lithium complexes in graphite and related compounds [completed], J. Brewer, J. Chakhalian, S. Dunsiger, R.F. Kiefl, W.A. MacFarlane, R. Miller, J. Sonier (*UBC*), J. Dahn (*Dalhousie U.*), J. Fischer (*U. Pennsylvania*), B. Hitti, S.R. Kreitzman (*TRIUMF*)
759. Study of the isotropic hyperfine coupling constant of muonium at high temperature and under uniaxial pressure [completed], W.K. Dawson, K. Nishiyama, S. Ohira, K. Shimomura (*U. Tokyo*), K. Nagamine (*U. Tokyo-RIKEN*), T.P. Das (*U. New York, Albany*)
761. Parity violation in $p-p$ scattering at 450 MeV [deferred], J. Birchall, C.A. Davis, L. Lee, S.A. Page, W.D. Ramsay, A.W. Rauf, G. Rutledge, W.T.H. van Oers (*U. Manitoba*), R. Helmer, R. Laxdal, C.D.P. Levy (*TRIUMF*), P.W. Green, G. Roy, G.M. Stinson (*U. Alberta*), N.A. Titov, S. Zadorozhny, A.N. Zelenski (*INR, Moscow*), J.D. Bowman, R.E. Mischke, S. Penttila, W.S. Wilburn (*Los Alamos Nat. Lab*), E. Korkmaz, (*UNBC*), M. Simonius (*ETH Zürich*), J. Bisplinghoff, P.D. Eversheim, F. Hinterberger (*U. Bonn*), W. Kretschmer, G. Morgenroth (*U. Erlangen*), H. Schieck (*U. Cologne*), P. von Rossen (*KFA Jülich*)
762. Gamow-Teller and spin-flip dipole strengths near $A=90$ [completed data-taking], W.P. Alford (*U. Western Ontario*), D.P. Beaty, H.T. Fortune, P.P. Hui, R.B. Ivie, D. Koltenuk, J. Yu (*U. Pennsylvania*), A. Ling, S. Yen (*TRIUMF*), S. El-Kateb (*King Fahd U.*)
763. Muon cooling and acceleration in an undulating crystal channel [deferred], S.A. Bogacz, D.B. Cline, D.A. Sanders (*UCLA*), L.M. Cremaldi, B. Denardo, Q. Jie, D.J. Summers (*U. Mississippi-Oxford*), G.M. Marshall (*TRIUMF*)
764. Calibration of a segmented neutron detector [completed], E. Korkmaz, G. O’Rielly (*UNBC*), D.A. Hutcheon (*TRIUMF*), A.K. Oppen (*U. Alberta*), G. Feldman, N.R. Kolb (*U. Saskatchewan*)

766. The ortho-para transition rate in muonic molecular hydrogen [completed], D.S. Armstrong, J.H.D. Clark, P. King (*Coll. of William & Mary*), T.P. Gorringer, S. Tripathi, P.A. Żohnierczuk (*U. Kentucky*), M.D. Hasinoff, T. Stocki (*UBC*), D.H. Wright (*TRIUMF*)
767. Direct measurement of sticking in muon catalyzed $d - t$ fusion [inactive], J.M. Bailey (*Chester Technology, UK*), G.A. Beer, M. Maier, G.R. Mason, T.A. Porcelli (*U. Victoria*), K.M. Crowe, P. Kammel (*U. California, Berkeley-LBL*), M.C. Fujiwara, E. Gete, T.J. Stocki (*UBC*), T.M. Huber (*Gustavus Adolphus Coll.*), S.K. Kim (*Jeonbuk Nat. U.*), A.R. Kunselman (*U. Wyoming*), G.M. Marshall, A. Olin (*TRIUMF*), C.J. Martoff (*Temple U.*), V.S. Melezhik (*JINR, Dubna*), F. Mulhauser (*U. Fribourg*), C. Petitjean (*PSI*), J. Zmeskal (*IMEP Vienna*)
768. Generalized Fulde-Ferrell-Larkin-Ovchinnikov state in heavy fermion and intermediate valence systems [completed], J. Akimitsu, K. Oishi, T. Muranaka (*Aoyama Gakuin U.*), W. Higemoto, R. Kadono, A. Koda (*KEK-IMSS*), M. Nohara, H. Suzuki, H. Takagi (*U. Tokyo*), R.F. Kiefl, R.I. Miller, A.N. Price (*UBC-TRIUMF*), J.E. Sonier (*SFU*)
769. Effects of uniaxial stress on muonium in semiconductors [completed], K.H. Chow (*Oxford*), B. Hitti (*TRIUMF*), R.F. Kiefl (*UBC*), T.L. Estle (*Rice U.*), R. Lichti (*Texas Tech. U.*)
770. μ SR studies of organic conductors: $(\text{BEDT-TTF})_2\text{-X}$ and $(\text{TMTTF})_2\text{Br}$ [completed], K. Kojima, M. Larkin, G.M. Luke, J. Merrin, B. Nachumi, Y.J. Uemura (*Columbia U.*), P.M. Chaikin (*Princeton U.*), G. Saito (*Kyoto U.*)
771. μ SR studies of geometrically frustrated $S = 1/2$ spin systems [completed], K. Kojima, M. Larkin, G.M. Luke, J. Merrin, B. Nachumi, Y.J. Uemura (*Columbia U.*), M.J.P. Gingras (*TRIUMF*), S. Dunsiger, R.F. Kiefl (*UBC*), D.C. Johnston, S. Kondo (*Iowa State U.*), S. Uchida (*U. Tokyo*), R.J. Cava (*AT&T Bell Labs*)
772. Search for the $\Delta - \Delta$ dibaryon [inactive], R. Abegg*, C.A. Miller, P. Walden, S. Yen (*TRIUMF*), R. Bent (*Indiana U.*), T.Y. Chen, F. Wang, C.H. Ye (*Nanjing U.*), W. Falk (*U. Manitoba*), D. Frekers, M. Hartig (*U. Muenster*), T. Goldman (*Los Alamos Nat. Lab*), M. Heyrat, C.W. Wong (*UCLA*), G. Jones (*UBC*), E. Korkmaz, G. O’Rielly (*UNBC*), C. Rangacharyulu (*U. Saskatchewan*), I. Strakovsky (*Virginia Tech. Inst.*), Z.X. Sun, J.C. Xu (*Inst. Atomic Energy, China*), T. Walton (*Cariboo U. Coll.*)
773. Muon-electron interaction in n -type silicon [completed], D. Arseneau, B. Hitti, S.R. Kreitzman (*TRIUMF*), J.H. Brewer, R.F. Kiefl, G. Morris (*UBC*), K. Chow (*Oxford U.*), S.F.J. Cox (*Rutherford Appleton Lab*), D.G. Eshchenko (*INR, Moscow*), T.L. Estle (*Rice U.*), R. Lichti (*Texas Tech. U.*), V.G. Storchak, (*Kurchatov Inst.*)
774. Muonium dynamics in GaAs studied by rf and μ -wave μ SR [active], B. Hitti, S.R. Kreitzman (*TRIUMF*), T.L. Estle (*Rice U.*), R. Lichti (*Texas Tech. U.*)
775. Electron transport in insulators, semiconductors and magnetic materials [completed], J.H. Brewer, A. Izadi, D.M.C. Liu, K.M. Nichol, S. Sivanandam, A.T. Warkentin (*UBC*), G.D. Morris (*TRIUMF*), V.G. Storchak (*Kurchatov Inst.*), D.G. Eshchenko (*INR, Moscow*), J.D. Brewer (*SFU*)
776. Rare earth materials with disordered spin structures [completed], J.H. Brewer (*UBC*), K. Fukamichi (*Tohoku U.*), G.M. Kalvius (*Tech. U. Munich*), D.R. Noakes, C.E. Stronach (*Virginia State U.*), R. Wäppling (*Uppsala U.*)
777. Vortex state of s -wave superconductors investigated by muon spin rotation [completed], J.C. Chakhalian, K. Chow, R. Miller, A.N. Price (*UBC*), J.H. Brewer, R.F. Kiefl (*UBC-TRIUMF*), G.M. Luke (*McMaster U.*), J.E. Sonier (*SFU*)
778. $\pi^\pm p$ differential cross sections in the Coulomb-nuclear interference region [completed data-taking], P. Amaudruz, D. Ottewell, (*TRIUMF*), P. Camerini, E. Fragiaco, N. Grion, S. Piano, R. Rui (*INFN Trieste-U. Trieste*), K. Babcock, E. Mathie, H. Xu, D.M. Yeomans (*U. Regina*), G. Hofman, M.M. Pavan, K.J. Raywood, R. Tacik (*Regina-TRIUMF*), J. Breitschopf, H. Denz, R. Meier, F. von Wrochem, G. Wagner (*U. Tübingen*), G. Moloney, M. Sevier (*U. Melbourne*), J. Brack, J. Patterson, R. Ristinen (*U. Colorado*), E. Gibson (*California State U., Sacramento*), O. Patarakin (*Kurchatov Inst.*), G. Smith (*Jefferson Lab*)
779. Accelerator mass spectrometry experiments at ISAC [inactive], S. Calvert, A. Glass, R.R. Johnson, T. Petersen (*UBC*), Z. Gelbart, D. Ottewell (*TRIUMF*), R. Schubank (*unaffiliated*), C.S. Wong (*Inst. of Ocean Sciences*), J. Clague (*Geological Survey Canada*), M. Paul (*Hebrew U. Jerusalem*)
780. Deeply bound pionic states through $^{208}\text{Pb}(p, ^3\text{He})^{206}\text{Pb} \otimes \pi^-$ [completed], D. Frekers, W. Garske, K. Grewer, M. Hartig, H. Wörtche (*U. Muenster*), H. Machner (*KFA, Jülich*), D. Hutcheon, P. Walden, S. Yen (*TRIUMF*), A. Oppen (*U. Ohio*)
781. Investigations of the $\pi\pi$ invariant mass distributions of nuclear ($\pi^+, \pi^-\pi^+$) reactions with the CHAOS detector [completed data-taking], J. Clark, G. Moloney, M.E. Sevier (*U. Melbourne*), L. Felawka, G. Hofman, D.F. Ottewell, K. Raywood, G.R. Smith (*TRIUMF*), R. Meier (*U. Tübingen*), P. Camerini, E. Fragiaco, R. Rui (*INFN Trieste-U. Trieste*), N. Grion, S. Piano (*INFN, Trieste*), E.L. Mathie, R. Tacik, (*U. Regina*), E.F. Gibson (*Cal. State U., Sacramento*)

45

88

47

782. Non-fermi-liquid behaviour and other novel phenomena in heavy-fermion alloys [active], D.E. MacLaughlin, L. Shu (*U. California, Riverside*), R.H. Heffner, G.D. Morris (*Los Alamos Nat. Lab*), N.A. Frederick, M.B. Maple, W.M. Yuhasz (*U. California, San Diego*), O.O. Bernal (*Cal. State U., Los Angeles*), J.E. Sonier (*SFU*)
783. Paramagnetic frequency shifts in unconventional superconductors [active], R.H. Heffner, G.D. Morris (*Los Alamos Nat. Lab*), D.E. MacLaughlin (*U. California, Riverside*), G.J. Nieuwenhuys (*U. Leiden*), O.O. Bernal (*Cal. State U., Los Angeles*), J.E. Sonier (*SFU*)
784. μ SR studies of spin singlet states in oxides [active], A. Fukaya, I. Gat, M. Larkin, A. Savici, Y.J. Uemura (*Columbia U.*), T. Ito (*Columbia U.-ETL*), H. Kageyama, K. Ueda, Y. Ueda (*U. Tokyo*), P.P. Kyriakou, G.M. Luke, M.T. Rovers (*McMaster U.*)
785. Pion double charge exchange on ^3He with CHAOS [completed data-taking], R. Tacik (*TRIUMF-U. Regina*), E.L. Mathie, M. Yeomans (*U. Regina*), H. Clement, J. Graeter, R. Meier, J. Petzold, G.J. Wagner (*U. Tübingen*), E. Friedman (*Hebrew U. Jerusalem*), N. Grion (*INFN Trieste*), P. Camerini, E. Fragiaco, R. Rui (*U. Trieste*), L. Felawka, D. Ottewell, K. Raywood, G.R. Smith (*TRIUMF*), G. Hofman, B. Jamieson, G. Tagliente (*UBC*), J. Clark, G. Molony, M.E. Sevier (*U. Melbourne*), E. Gibson (*California State U. Sacramento*), H. Staudenmeyer (*U. Karlsruhe*), S. Filippov, Y. Gavrilov, T. Karavicheva (*Moscow Meson Factory*)
786. Low energy structures in the β -delayed particle decays of ^9C , ^{12}N and ^{17}Ne [completed], N. Bateman (*TRIUMF-SFU-U. Toronto*), L. Buchmann, K.P. Jackson, T. Shoppa (*TRIUMF*), J. Chow, J.D. King, C. Mortin (*U. Toronto*), T. Davison, A. Ostrowski, A. Shotter (*U. Edinburgh*), J. D'Auria (*SFU*), E. Gete, D. Measday (*UBC*), U. Giesen (*U. Alberta*)
788. Nuclear and atomic physics with the CPT spectrometer [inactive], B. Barber, K.S. Sharma (*U. Manitoba*), X. Feng (*U. Manitoba-McGill U.*), F. Buchinger, J. Crawford, S. Gulick, J. Lee, B. Moore (*McGill U.*), E. Hagberg, J. Hardy, V. Koslowsky, G. Savard (*Chalk River Nuclear Lab*)
789. μ SR studies of magnetic fluctuations in hydronium jarosites, model Kagomé antiferromagnets [completed], A. Harrison, A.S. Wills (*U. Edinburgh*), Y. Fudamoto, K. Kojima, M. Larkin, G.M. Luke, J. Merrin, B. Nachumi, Y.J. Uemura (*Columbia U.*), T. Mason (*U. Toronto*)
790. μ SR studies of stripe order in $\text{La}_{1.6-x}\text{Sr}_x\text{Nd}_{0.4}\text{CuO}_4$ modified cuprate superconductors [completed], Y. Fudamoto, K. Kojima, M. Larkin, G.M. Luke, J. Merrin, B. Nachumi, Y.J. Uemura (*Columbia U.*), M. Crawford (*Du Pont*), A. Moodenbaugh (*Brookhaven Nat. Lab*), S. Uchida (*U. Tokyo*)
791. Electronic structure and dynamics of charged muonium and muonium-dopant centers in semiconductors [active], K.H. Chow (*Oxford U.*), R.F. Kiefl (*UBC*), B. Hitti (*TRIUMF*), T.L. Estle (*Rice U.*), R. Lichti (*Texas Tech. U.*), S.F.J. Cox (*Rutherford Appleton Lab*), C. Schwab (*CRN, Strasbourg*)
792. Muonium in III-V semiconductors: identification of states and transitions [completed], K.H. Chow (*Oxford U.*), S.F.J. Cox (*Rutherford Appleton Lab*), B. Hitti (*TRIUMF*), T.L. Estle (*Rice U.*), R.L. Lichti (*Texas Tech. U.*), C. Schwab (*CRN, Strasbourg*)
793. Production of an intense ^{15}O beam for ISAC [completed], J. D'Auria, R. Lange (*SFU*), M. Domsbky, T. Ruth, J. Vincent (*TRIUMF*), K. Carter (*Oak Ridge Nat. Lab*), B. Zhuikov (*INR, Moscow*)
794. μ^+ SR study on the magnetic properties of LaCoO_3 and $\text{La}_{1-x}\text{Sr}_x\text{CoO}_3$ [completed], V.V. Krishnamurthy, I. Watanabe (*RIKEN*), K. Asai, N. Yamada (*U. Electro-communications*), K. Nagamine (*U. Tokyo-RIKEN*)
795. μ SR study on non fermi liquid behaviour [completed], Y. Miyako, Y. Yamamoto (*Osaka U.*), S. Murayama (*Muroran Inst. Tech.*), K. Nagamine (*U. Tokyo*), K. Nishiyama (*U. Tokyo-RIKEN*)
796. μ SR studies in ionic crystals doped with either colour centres or impurity [deferred], Y. Miyake, K. Nagamine, K. Nishiyama, K. Shimomura (*U. Tokyo*), A. Matsusita (*RIKEN*)
797. Magnetic correlations in the ternary equiatomic Ce compounds CeTSn [completed], G. Grosse, G.M. Kalvius A. Kratzer (*Tech. U. Munich*), R. Wäppling (*U. Uppsala*), T. Takabatake (*Hiroshima U.*), D.R. Noakes, C.R. Stronach (*Virginia State U.*), Y. Echizen (*Hiroshima U.*), H. Nakotte (*New Mexico State U.*), H.v. Löhneysen (*U. Karlsruhe*)
798. μ SR studies on the competition of RKKY exchange and Kondo effect in CeT_2X_2 compounds (T=transition metal, X=Si,Ge) [completed], H.-H. Klauss, W. Kopmann, F.J. Litterst, W. Wagener, H. Walf (*Tech. U. Braunschweig*), E. Baggio Saitovitch, M.B. Fontes (*CBPF Rio de Janeiro*), A. Krimmel, A. Loidl (*U. Augsburg*)
799. Hyperfine structure and site determination of $(\mu^- \text{O})$ system in LaSuCuO high T_c superconductors [completed], H. Kojima, I. Tanaka, E. Torikai (*Yamanashi U.*), K. Nishiyama (*U. Tokyo-RIKEN*), K. Nagamine, K. Shimomura (*U. Tokyo*), I. Watanabe (*RIKEN*), T.P. Das (*State U. New York*)
801. Studies of multi-phonon states via β -decay [completed], C.J. Barton, M.A. Caprio, R.F. Casten, N.V. Zamfir (*Yale U.*), D.S. Brenner (*Clark U.*), G.C. Ball, K.P. Jackson (*TRIUMF*)

802. Superdeformation and smooth band termination on and near the $N = Z$ line: Part 1 ^{60}Zn [active], J.A. Cameron, S. Flibotte, D.S. Haslip, J. Nieminen, C. Svensson, J.C. Waddington, J.N. Wilson (*McMaster U.*), G. Ball (*TRIUMF*), A. Galindo-Uribarri, D.C. Radford (*Oak Ridge Nat. Lab*), D. Ward (*Lawrence Berkeley Nat. Lab*)
803. Experimental studies of interaction and properties of neutron-rich nuclei at ISAC [inactive], A.S. Iljinov, A.V. Klyachko, E.S. Konobeevsky, M.V. Morodovskoy, M.A. Prohvatilov, A.I. Reshetin, Yu.V. Ryabov, K.A. Shileev, V.A. Simonov, V.M. Skorkin, S.V. Zuyev (*INR, Moscow*)
804. Muonium in gallium nitride [completed], B.A. Bailey, R.L. Lichti (*Texas Tech. U.*), K.H. Chow (*U. Alberta*), B. Hitti (*TRIUMF*), S.F.J. Cox (*Rutherford Appleton Lab*), E.A. Davis (*Leicester U.*)
805. A study of the $^{13}\text{N}(p, \gamma)^{14}\text{O}$ reaction with a ^{13}N beam [active], R.E. Azuma, J. Chow, J.D. King, A.C. Morton (*U. Toronto*), N. Bateman (*TRIUMF-Toronto*), L. Buchmann, K.P. Jackson, T. Shoppa (*TRIUMF*), J.M. D'Auria (*SFU*), U. Giesen (*SFU-TRIUMF*), G. Roy (*U. Alberta*), W. Galster (*U. Catholique de Louvain*), A.C. Shotter (*U. Edinburgh*), R.N. Boyd (*Ohio State U.*), U. Greife, C. Rolfs, F. Strieder, H.-P. Trautvetter (*Ruhr U. Bochum*)
806. Excitation of high-spin isomeric states and compound nucleus formation by intermediate energy protons and stopped pions [completed data-taking], A.S. Iljinov, V.M. Kokhanyuk, B.L. Zhuikov (*INR, Moscow*), I. Liu, J. Vincent, A.Z. Zyuzin (*TRIUMF*)
808. Spin glass order in magnets frustrated by competing ferro- and antiferromagnetic exchange [completed], G.M. Kalvius, A. Kratzer, E. Schreier (*Techn. U. Munich*), R. Wäppling (*U. Uppsala*), D.R. Noakes (*Virginia State U.*), J. Gal (*Beer Sheva U.*), W. Schäfer (*Bonn U.*)
809. Quantum diffusion of muonium in crystals with orientational degrees of freedom [completed], D. Arseneau, B. Hitti, S.R. Kreitzman (*TRIUMF*), J.H. Brewer, A. Izadi, G.D. Morris (*UBC*), D.G. Eshchenko (*INR, Moscow*), V.G. Storchak (*Kurchatov Inst.*), J.D. Brewer (*SFU*)
810. First direct study of the $^{23}\text{Mg}(p, \gamma)^{24}\text{Al}$ reaction with a recoil mass separator (DRAGON) [active], N.P.T. Bateman, J.M. D'Auria, D. Hunter, R. Korteling (*SFU*), R.N. Boyd (*Ohio State U.*), L. Buchmann, R. Helmer, D. Hutcheon, K.P. Jackson, A. Olin, J. Rogers (*TRIUMF*), U. Giesen, G. Roy (*U. Alberta*), L. Gialanella, U. Greife, C. Rolfs, F. Strieder, H.-P. Trautvetter (*Ruhr U. Bochum*), A. Hussein (*UNBC*), M. Junker (*INFN Gran Sasso*), J.D. King (*U. Toronto*), P.D. Parker (*Yale U.*), A. Shotter (*U. Edinburgh*), M. Wiescher (*U. Notre Dame*)
811. A direct study of the $^{19}\text{Ne}(p, \gamma)^{20}\text{Na}$ reaction with a recoil mass separator (DRAGON) [active], N.P.T. Bateman, J.M. D'Auria, D. Hunter, R. Korteling (*SFU*), R.N. Boyd (*Ohio State U.*), L. Buchmann, R. Helmer, D. Hutcheon, K.P. Jackson, A. Olin, J. Rogers (*TRIUMF*), U. Giesen, G. Roy (*U. Alberta*), L. Gialanella, U. Greife, C. Rolfs, F. Strieder, H.-P. Trautvetter (*Ruhr U. Bochum*), A. Hussein (*UNBC*), M. Junker (*INFN Gran Sasso*), J.D. King (*U. Toronto*), P.D. Parker (*Yale U.*), A. Shotter (*U. Edinburgh*), M. Wiescher (*U. Notre Dame*)
812. Proposed study of the $^8\text{Li}(\alpha, n)^{11}\text{B}$ reaction [active], R.N. Boyd, A. Murphy, L. Sahin, E. Smith, M. Zahar (*Ohio State U.*), L. Buchmann, P. Walden (*TRIUMF*), J.M. D'Auria (*SFU*), J.D. King (*U. Toronto*), M. Nishimura, S. Nishimura, I. Tanihata (*RIKEN*)
813. A study of the $^{15}\text{O}(\alpha, \gamma)^{19}\text{Ne}$ reaction at the astrophysically important energy [active], N.P.T. Bateman, J.M. D'Auria, D. Hunter, R. Korteling (*SFU*), R.N. Boyd (*Ohio State U.*), L. Buchmann, R. Helmer, D. Hutcheon, K.P. Jackson, A. Olin, J. Rogers (*TRIUMF*), U. Giesen, G. Roy (*U. Alberta*), U. Greife, C. Rolfs, F. Strieder, H.-P. Trautvetter (*Ruhr U. Bochum*), A. Hussein (*UNBC*), J.D. King (*U. Toronto*), P.D. Parker (*Yale U.*), A. Shotter (*U. Edinburgh*), M. Wiescher (*U. Notre Dame*)
814. μSR studies of unconventional superconductivity in Sr_2RuO_4 [active], Y. Fudamoto, K.M. Kojima, M. Larkin, G.M. Luke, J. Merrin, B. Nachumi, Y.J. Uemura (*Columbia U.*), Y. Maeno (*Kyoto U.*), R.J. Cava (*Princeton U.*)
815. β -NMR investigation of magnetic multilayers and giant magnetoresistance [active], J. Chakhalian, W.A. MacFarlane, R. Miller, (*UBC*), J.H. Brewer, R.F. Kiefl (*UBC-TRIUMF*), P. Amaudruz, R. Baartman, T.R. Beals, J. Behr, S. Daviel, S.R. Kreitzmann, T. Kuo, C.D.P. Levy, M. Olivo, R. Poutissou, Z. Salman, G.D. Wight (*TRIUMF*) S.R. Dunsiger, R. Heffner, G.D. Morris (*Los Alamos Nat. Lab*), C. Bommas (*U. Bonn*), A. Hatakeyama, Y. Hirayama, T. Shimoda (*Osaka U.*), K.H. Chow (*U. Alberta*), J.E. Elenewski, L.H. Greene (*U. Illinois-Urbana-Champaigne*)
816. Semiconductor quantum wells investigated by β -NMR [active], J.H. Brewer, J.C. Chakhalian, S. Dunsiger, R. Miller, T. Tiedje (*UBC*), M. Gingras (*U. Waterloo*), B. Ittermann (*U. Marburg*), B. Hitti, P. Levy, S.R. Kreitzman, A. Zelenski (*TRIUMF*), R.F. Kiefl (*TRIUMF-UBC*)

817. β -NMR investigation of type II superconductors [active], D. Bonn, J.H. Brewer, J.C. Chakhalian, S. Dunsiger, W. Hardy, R. Liang, R.F. Kiefl, W.A. MacFarlane, R. Miller, J. Sonier (*UBC*), M. Gingras (*U. Waterloo*), R. Heffner (*Los Alamos Nat. Lab*), B. Itterman (*U. Marburg*), B. Hitti, P. Levy, S.R. Kreitzman, A. Zelenski (*TRIUMF*), G.M. Luke (*Columbia U.*), J.W. Brill (*U. Kentucky*)
818. μ^+ SR study of magnetic ordering in the one-dimensional spin-1/2 antiferromagnet copper benzoate [completed], J.C. Chakhalian, S. Dunsiger, R.F. Kiefl, W.A. MacFarlane, R. Miller, J. Sonier (*UBC*), C. Broholm, D.C. Dender, P. Hammar, D. Reich (*Johns-Hopkins U.*), G. Luke, T. Uemura (*Columbia U.*)
819. μ^+ SR studies of the antiferromagnetic instability and metastable state in colossal magnetoresistance system $(\text{Nd}_{1-y}\text{Sm}_y)_{1/2}\text{Sr}_{1/2}\text{MnO}_3$ ($y = 0.875$) [completed], W. Higemoto, I. Watanabe (*RIKEN*), K. Nishiyama (*KEK*), K. Nagamine (*RIKEN-KEK*), A. Asamitsu, H. Kuwahara, Y. Tokura (*JRCAT, U. Tokyo*)
821. Shape coexistence and shape mixing in neutron-deficient platinum isotopes: on-line nuclear orientation studies of the decays of ^{182}Au and ^{186}Au [active], K.S. Krane (*Oregon State U.*), J.L. Wood (*Georgia Inst. Tech.*), J. D'Auria (*SFU*)
822. Effect of disorder on quantum spin liquid state [completed data-taking], W. Higemoto, R. Kadono, A. Koda, K. Ohishi, (*KEK-IMSS*), M. Nohara, H. Takagi, H. Ueda, C. Urano (*U. Tokyo*)
823. Pure fermi decay in medium mass nuclei [active], G.C. Ball, R. Beaton, P. Bricault, G. Hackman, P. Klages, J.A. Macdonald*, E. Vandervoort (*TRIUMF*), D.F. Hodgson (*U. Surrey-TRIUMF*), J. Cerny, D.M. Moltz, J. Powell (*Lawrence Berkeley Lab*), G. Savard (*Argonne Nat. Lab*), J.C. Hardy, V. Iacob (*Texas A&M U.*), S. Bishop, J. D'Auria (*SFU*), J.R. Leslie, H.-B. Mak, I.S. Towner (*Queen's U.*), D. Kulp, J.L. Wood (*Georgia Inst. Tech.*), E.F. Zganjar, A. Piechaczek (*Louisiana State U.*)
824. Measurement of the astrophysical rate of the $^{21}\text{Na}(p,\gamma)^{22}\text{Mg}$ reaction [active], S. Bishop, J.M. D'Auria, D. Hunter, M. Lamey, W. Liu, C. Wrede, (*SFU*), L. Buchmann, D. Hutcheon, A.M. Laird, A. Olin, D. Ottewell, J.G. Rogers (*TRIUMF*), S. Engel, F. Strieder (*Ruhr U.*), D. Gigliotti, A. Hussein (*UNBC*), R. Azuma, J.D. King (*U. Toronto*), R. Lewis, P.D. Parker (*Yale U.*), S. Kubono, S. Michimasa (*U. Tokyo*), M. Chatterjee (*Saha Inst., Calcutta*), U. Greife, C. Jewett (*Colorado School of Mines*), A.A. Chen (*McMaster U.*), M. Hernanz, J. José. *d'Estudis Espacials de Catalunya, Barcelona*)
826. Studies of ultrathin magnetic films with implanted isotopes [active], R. Kiefl, J. Pond, B.G. Turrell (*UBC*), C.A. Davis, P.P.J. Delheij (*TRIUMF*), K.S. Krane, J. Loats, P. Schmelzenbach, C. Stapels (*Oregon State U.*), D. Groh, W. Kumarasiri, P. Mantica (*Michigan State U.*), D. Kulp, J.L. Wood, (*Georgia Inst. Tech.*)
827. Parity violation in ^{182}W [active], J. D'Auria (*TRIUMF-SFU*), C.A. Davis P.P.J. Delheij (*TRIUMF*), R. Kiefl, A. Kotlicki, J. Pond, B. Turrell (*UBC*), K.S. Krane (*Oregon State U.*)
828. Nuclear moments in the mass-100 region [active], K.S. Krane, J. Loats, P. Schmelzenbach, C. Stapels (*Oregon State U.*), D. Kulp, J.L. Wood (*Georgia Inst. Tech.*), C.A. Davis, P.P.J. Delheij (*TRIUMF*), D. Groh, W. Kumarasiri, P. Mantica (*Michigan State U.*), R. Kiefl, J. Pond, B.G. Turrell (*UBC*)
829. Muonium as a hydrogen isotope: reactions in solution [completed], D.P. Chong, G.B. Porter, D.C. Walker (*UBC*), K. Venkateswaran (*Hindustan Lever Ltd.*), H.A. Gillis (*St. Francis Xavier U.*)
830. The hot entropy bubble and the decay of ^9Li [active], N. Bateman (*TRIUMF-SFU-Toronto*), L. Buchmann, K.P. Jackson, S. Karataglidis, T. Shoppa, E. Vogt (*TRIUMF*), J. Chow, J.D. King, C. Mortin (*U. Toronto*), T. Davison, A. Ostrowski, A. Shotter (*U. Edinburgh*), J. D'Auria, U. Giesen (*SFU*), E. Gete, D. Measday (*UBC*)
831. Magnetic properties of $\text{REBa}_2\text{Cu}_3\text{O}_x$ [completed data-taking], D. Andreica, F.N. Gyax, M. Pinkpank, A. Schenck (*ETH Zürich*), B. Hitti (*TRIUMF*), A. Amato (*PSI*), J.H. Brewer (*UBC-TRIUMF*)
832. Study of the non-magnetic-magnetic transition in the $\text{Yb}(\text{Cu}_{1-x}\text{Ni}_x)_2\text{Si}_2$ system [completed data-taking], D. Andreica, F. Gyax, M. Pinkpank, A. Schenck (*ETH Zürich-PSI*), A. Amato (*PSI*), B. Hitti (*TRIUMF*)
833. μ SR studies of doped MnSi and V_{2-y}O_3 : non-fermi-liquid behaviour, spin fluctuations and itinerant magnetism [active], A. Fukaya, I.M. Gat, M. Larkin, A.J. Millis, P.L. Russo, A.T. Savici, Y.J. Uemura (*Columbia U.*), P.P. Kyriakou, G.M. Luke, C.R. Wiebe (*McMaster U.*), Y.V. Sushko (*U. Kentucky*), R.H. Heffner (*Los Alamos Nat. Lab*), D.E. MacLaughlin (*U. California, Riverside*), D. Andreica (*PSI*), M. Kalvius (*Tech. U. Munich*)
834. μ SR study of transverse spin freezing in bond-frustrated magnets [active], A.D. Beath, D.H. Ryan, (*McGill U.*), J.M. Cadogan (*U. New South Wales*), J. van Lierop (*U. Michigan*)
835. μ SR studies of intercalated HfN and Bi2212 superconductors [active], M. Greven, N. Kaneko, (*Stanford U.*), I.M. Gat, M.I. Larkin, P.L. Russo, A. Savici, Y.J. Uemura, emph(Columbia U.), G.M. Luke, G.J. MacDougall, C.R. Wiebe (*McMaster U.*), Y. Ando (*U. Tokyo*)
836. Elasticks [active], R.E. Azuma, J.D. King (*U. Toronto*), G. Ball, L. Buchmann, K.P. Jackson, B. Jennings, S. Karataglidis, E. Vogt (*TRIUMF*), N. Bateman (*TRIUMF-SFU-U. Toronto*), T. Davison, A. Ostrowski, A. Shotter (*U. Edinburgh*), J. D'Auria (*SFU*), W. Galster (*U. Catholique de Louvain*), G. Roy (*U. Alberta*)

48

49

99

837. Pion-induced errors in memory chips [completed], J.T. Brack, G. Hofman, J. Patterson R.J. Peterson, R.A. Ristinen (*U. Colorado*), J.F. Ziegler (*IBM*), M.E. Nelson (*US Naval Academy*), G. Smith (*TRIUMF*)
838. Measurement of the $\pi^-p \rightarrow \gamma\gamma n$ capture mode of pionic hydrogen [completed data-taking], T. Gorringer, M. Kovash, S. Tripathi, P. Żolnierczuk (*U. Kentucky*), D. Armstrong, J. Clark (*Coll. of William & Mary*), M. Hasinoff (*UBC*), D. Healey, D. Wright (*TRIUMF*) 52
839. Thermal test of prototype high power ISAC target [completed], D. Drake, D. Liska, W.L. Talbert, M. Wilson (*Amparo Corp.*), P. Bricault, M. Dombsky, P. Schmor (*TRIUMF*), E. Dalder, C. Landram, K. Sale, D. Slaughter (*Lawrence Livermore Nat. Lab.*), J. Nolen, G. Savard (*Argonne Nat. Lab.*), G. Alton (*Oak Ridge Nat. Lab.*)
840. Muon transfer from excited states of muonic hydrogen with x-ray measurement [active], S. Sakamoto, K. Shimomura (*KEK*), K. Nagamine (*KEK-RIKEN*), K. Ishida, N. Kawamura, Y. Matsuda, T. Matsuzaki, S.N. Nakamura, P. Strasser (*RIKEN*)
841. ISAC beam and target development [active], P. Bricault, M. Dombsky (*TRIUMF*)
842. Muonium-substituted free radicals in sub- and supercritical water [active], J.-C. Brodovitch, S. Kecman, B. McCollum, I. McKenzie, P.W. Percival (*SFU*), B. Addison-Jones (*Douglas College*) 89
843. Quadrupole ordering in dense Kondo system studied by μ LCR [completed data-taking], J. Akimitsu, K. Kakuta, K. Ohishi (*Aoyama Gakuin U.*), W. Higemoto, R. Kadono (*KEK-IMSS*), T. Yokoo (*CREST*)
844. Quantum impurities in one dimensional spin 1/2 chains [completed], I. Affleck, J. Brewer, J. Chakhalian, S. Dunsiger, R.F. Kiefl, R. Miller, A. Price (*UBC*), S. Eggert (*Chalmers U.*), B. Hitti (*TRIUMF*), A.A. Keren (*Israel Inst. Tech.*), W.A. MacFarlane (*U. Paris-Sud*), G. Morris (*UBC-TRIUMF*), Y.J. Uemura (*Columbia U.*), M. Verdager (*CNRS*), I. Yamada (*Chiba U.*)
845. μ SR studies of vortex phases in (Ba,K)BiO₃ [completed], G.M. Luke, M.A. Lumsden (*McMaster U.*), Y. Fudamoto, M.I. Larkin, Y.J. Uemura (*Columbia U.*), K.M. Kojima (*U. Tokyo*), M. Gingras (*U. Waterloo*), I. Jourard, T. Klein, J. Marcus (*U. Grenoble*)
846. Complex order parameter symmetry in YB₂Cu₃O_{7- δ} at low T and high magnetic field [completed], D.A. Bonn, J.H. Brewer, W.N. Hardy, R.F. Kiefl, R.X. Liang, J.-M. Ménard, R.I. Miller (*UBC*), D. Babineau, K.F. Poon, J.E. Sonier (*SFU*), C.E. Stronach (*Virginia State U.*)
847. Electron-doped high- T_c superconductors [active], G.M. Luke, C.R. Wiebe (*McMaster U.*), P. Fournier (*U. Sherbrooke*), F.D. Callaghan, C.V. Kaiser, M. Laulajainen, J.E. Sonier (*SFU*), C.E. Stronach (*Virginia State U.*), R.L. Greene (*U. Maryland*) 91
848. μ SR investigation of the vortex state of YBa₂Cu₃O_{6+x} [completed data-taking], D.A. Bonn, J.C. Chakhalian, K. Chow, W.N. Hardy, R.X. Liang, R. Miller, A.N. Price (*UBC*), J.H. Brewer, R.F. Kiefl (*UBC-TRIUMF*), J. Sonier (*SFU*)
849. Spin structure and magnetic volume fraction of La₂14 systems: revisiting “1/8”, “stripes”, “spin glass”, and “swiss cheese” [completed], K.M. Kojima (*U. Tokyo*), Y. Fudamoto, I.M. Gat, M.I. Larkin, A.T. Savici, Y.J. Uemura (*Columbia U.*), G.M. Luke (*McMaster U.*), M.A. Kastner, Y.S. Lee (*MIT*), R.J. Birgeneau (*MIT-U. Toronto*), K. Yamada (*Kyoto U.*)
850. Effects of dilute (Cu,Zn) substitution in spin gap systems SrCu₂O₃ and CuGeO₃ [completed], Y. Fudamoto, I. Gat, M.I. Larkin, Y.J. Uemura (*Columbia U.*), K.M. Kojima, K. Manabe, K. Uchinokura (*U. Tokyo*), G.M. Luke (*McMaster U.*), M. Azuma, M. Takano (*Kyoto U.*)
851. μ SR in ruthenate and cuprate high- T compounds [active], D.R. Harshman (*Physikon Research Corp.*), M.K. Wu (*Nat. Tsing Hua U.*), F.Z. Chien (*Tamkang U.*), J.D. Dow (*Arizona State U.*), A.J. Greer (*Gonzaga U.*), A. Goonewardene, W.J. Kossler, X. Wan (*Coll. of William & Mary*), E. Koster, D.Ll. Williams (*UBC*), D.R. Noakes, C.E. Stronach (*Virginia State U.*), A.T. Fiory (*New Jersey Inst. Tech.*), A. Erb (*Walther-Meissner-Inst. Tieftemperaturforschung, Garching*), J.P. Franck, I. Issac (*U. Alberta*), Z.F. Ren, D.Z. Wang (*Boston College*), R.N. Kleiman (*Bell Labs*), R.C. Haddon (*U. California, Riverside*), W. Kang (*U. Chicago*) 92
852. Magnetic phases in geometrically frustrated rare earth pyrochlores [active], R. Kiefl (*UBC-TRIUMF*), S. Dunsiger, B.D. Gaulin, (*McMaster U.*), M.J.P. Gingras (*U. Waterloo*), G.D. Morris, J.M. Roper (*Los Alamos Nat. Lab.*), R. Miller (*U. Pennsylvania*), A.N. Price (*U. Erlangen-Nuernberg*), J.S. Gardner (*NIST*), S.T. Bramwell (*U. College London*), K. Chow (*U. Alberta*), J. Chakhalian (*MPI, Stuttgart*) 93
856. μ SR study on CuO [active], W. Higemoto, K. Nishiyama, K. Shimomura (*KEK*), M. Suzuki, S. Tanaka, N. Tsutsumi, X.G. Zheng (*Saga U.*)
857. Investigation of the magnetic properties of the cerium compound probed by negative muon [active], W. Higemoto, K. Nagamine, K. Nishiyama, K. Shimomura (*KEK*), V.V. Krishnamurthy (*RIKEN*)

858. Repolarization of muonic atom in semiconductors by laser optical pumping in solids [active], W. Higemoto, R. Kadono, K. Nagamine, K. Nishiyama K. Shimomura (*KEK*)
859. A search for non-Markovian μ^+ diffusion in solids: μ^+ spectral spin hopping in high transverse field [inactive], G. Alexandrowicz, A. Grayevsky, N. Kaplan, T. Tashma (*Racah Inst. Physics*), A. Schenck (*ETH Zürich*)
860. Mass and charge transport in disordered media: orientational glasses [completed], J.H. Brewer, A. Izadi, D.M.C. Liu, K.M. Nichol, S. Sivanandam, A.T. Warkentin (*UBC*), G.D. Morris (*TRIUMF*), V.G. Storchak (*Kurchatov Inst.*), D.G. Eshchenko (*INR, Moscow*), J.D. Brewer (*SFU*)
862. Polarization observables in the $\bar{p}(\pi^\pm, \pi^+, \pi^\pm)$ reactions: a test of chiral perturbation theory [completed data-taking], K. Craig, G. Hofman, M.M. Pavan, R. Tacik (*Regina-TRIUMF*), E. Mathie (*U. Regina*), J. Breitschopf, H. Denz, R. Meier, G. Wagner (*U. Tübingen*), E. Gibson (*California State U. Sacramento*), C.M. Riedel (*Montana State U. Bozeman*) 54
863. Magnetic dipole moments measurements of $^{75,77,79}\text{Ga}$ using low temperature nuclear orientation and β -NMR [completed data-taking], A.D. Davies, P.F. Mantica, T.J. Mertzimekis (*Michigan State U.*), C.A. Davis, P.P.J. Delheij (*TRIUMF*), B. Turrell (*UBC-TRIUMF*) 54
864. Measurement of the two-photon capture mode of the pionic deuterium atom [completed data-taking], S. Arole, T. Gorringer, C. Nenkov, S. Tripathi, P. Żołnierczuk (*U. Kentucky*), D. Armstrong, J. Clark (*Coll. of William & Mary*), M. Hasinoff (*UBC*), D. Wright (*TRIUMF*) 55
865. Electronic structure and diffusion kinetics of muonium in group III nitrides [active], W. Higemoto, R. Kadono, K. Nishiyama, K. Shimomura (*KEK-IMSS*), M. Mizuta (*NEC Corp.*), M. Saito (*NEC Inf. Syst. Ltd.*) 95
866. $S = 0$ doping to the $1d$ spin chain: comparison between the $S = 1/2$ and $S = 1$ chains [active], I. Eisaki, K.M. Kojima, T. Masuda, S. Uchida, K. Uchinokura (*U. Tokyo*), Y. Fudamoto, I. Gat, M.I. Larkin, Y.J. Uemura (*Columbia U.*), G.M. Luke (*McMaster U.*)
867. μSR studies of magnetic properties of strontium/calcium ruthenates [active], Y. Fudamoto, I. Gat, M. Larkin, A. Savici, Y.J. Uemura (*Columbia U.*), G.M. Luke (*McMaster U.*), K. Kojima (*U. Tokyo*), S. Ikeda, Y. Maeno (*Kyoto U.*)
868. Magnetic correlations in impurity doped one dimensional spin systems [active], D. Baabe, H.-H. Klauss, W. Kopmann, F.J. Litterst, D. Mienert (*Tech. U. Braunschweig*), U. Ammerahl, B. Büchner (*U. Köln*), C. Geibel (*MPI Dresden*)
869. Measurement of the $^1\text{H}(\pi^-, \pi^0)n$ differential cross section at 100–140 MeV/c and forward angles [completed data-taking], S. Arole, T. Gorringer, M. Kovash, S. Tripathi, P. Żołnierczuk (*U. Kentucky*), M. Hasinoff (*UBC*), D. Armstrong (*Coll. of William & Mary*), M. Pavan (*TRIUMF*)
870. Breakout from the hot CNO cycle via the $^{18}\text{Ne}(\alpha, p)^{21}\text{Na}$ reaction [active], T. Davinson, A. Ostrowski, F. Sarazin, A. Shotter, P. Woods (*U. Edinburgh*), L. Buchmann, J. D'Auria (*TRIUMF*), J. Daly, J. Görres, M. Wiescher (*U. Notre Dame*), P. Leleux (*U. Catholique de Louvain*)
871. Meson and quark effects in nuclear β -decay of ^{20}Na [active], H. Fujiwara, M. Fukuda, K. Matsuta, M. Mihara, T. Minamisono, T. Nagatomo, M. Ogura, T. Sumikama (*Osaka U.*), R. Baartman, J. Behr, P. Bricault, M. Dombbsky, K.P. Jackson, P. Levy (*TRIUMF*), R. Kiehl (*UBC*), K. Koshigiri (*Osaka Kyoiku U.*), M. Morita (*Josai Int. U.*), K. Minamisono (*JSPS-TRIUMF*) 56
872. Weak interaction studies with trapped radioactive ions [active], J. Dilling, D. Melconian (*SFU*), G. Savard (*Argonne Nat. Lab-U. Chicago*), G.C. Ball, J.A. Behr, P. Bricault, K.P. Jackson (*TRIUMF*), F. Buchinger, J.E. Crawford, J.K.P. Lee, R.B. Moore (*McGill U.*), K.S. Sharma (*U. Manitoba*)
874. Study of ^{19}Ne α -decay properties related to the hot-CNO breakout reaction $^{15}\text{O}(\alpha, \gamma)^{19}\text{Ne}$ [active], T. Davinson, D. Groombridge, A.M. Laird, A.N. Ostrowski, F. Sarazin, K. Schmidt, A.C. Shotter, P.J. Woods (*U. Edinburgh*), L. Buchmann (*TRIUMF*), S. Cherubini, P. Leleux (*U. Catholique de Louvain*), J. Hinnefeld (*U. South Bend*)
875. Muon scattering in low Z materials for muon cooling studies [active], M. Curtis-Rouse, T.R. Edgecock, M. Ellis, J. Lidbury, W. Murray, P.R. Norton, K.J. Peach (*Rutherford Appleton Lab*), K. Ishida, Y. Matsuda (*RIKEN*), T. McMahon, J.A. Wilson (*U. Birmingham*), G. Barber, A. Jamdagni, K. Long, E. McKigney (*Imp. Coll., London*), W. Allison, S. Holmes (*U. Oxford*), S. Benveniste, D. Cline, Y. Fukui, K. Lee, Y. Pischalnikov (*UCLA*), R. Fernow (*Brookhaven Nat. Lab*), P. Gruber, A. Lombardi (*CERN*), S.N. Nakamura (*U. Tohoku*), G. Marshall (*TRIUMF*), A. Bogacz (*Jefferson Lab*) 61
876. Disordered magnetism near magnetic instabilities in f -electron materials [completed], D.R. Noakes, C.E. Stronach (*Virginia State U.*), G.M. Kalvius (*Tech. U. Munich*), A. Loidl (*Augsburg U.*), H. Nakotte (*New Mexico State U.*), R. Wäppling (*Uppsala U.*), A.V. Andreev (*Charles U.*)

877. μ SR studies of strongly correlated electron systems under a high pressure [active], W. Higemoto, R. Kadono, A. Koda, K. Nishiyama (*KEK-MSL*), K. Satoh (*Saitama U.*), Y. Kitaoka, K. Ishida (*Osaka U.*), K. Nagamine (*RIKEN-KEK-MSL*)
878. μ^+ SR studies on magnetism of layered compounds $\text{Cu}_2(\text{OH})_3\text{X}$ ($\text{X}=\text{Cl}, \text{Br}, \text{I}$) [active], G. Maruta, K. Nishiyama (*KEK-MSL*), S. Takeda (*Gunma U.*)
879. Proton- ^{21}Na elastic scattering at astrophysical energies [completed data-taking], L. Buchmann (*TRIUMF*), T. Davinson, A. Ostrowski, F. Sarazin, A. Shotter, P. Woods (*U. Edinburgh*), R.E. Azuma, J.D. King (*U. Toronto*), A. Chen (*TRIUMF-SFU*), J. Daly, J. Görres, M. Wiescher (*U. Notre Dame*), J. D'Auria (*SFU*), E.S. Konobeevsky, M.V. Mordovskoy, V.A. Simonov, A.V. Stepanov, V.P. Zavarzina (*INR, Moscow*)
880. Ortho-para effect of muon catalyzed fusion in solid deuterium [completed], K. Ishida, Y. Matsuda (*RIKEN*), K. Nagamine, K. Shimomura, A. Toyoda (*KEK*), S.N. Nakamura (*Tohoku U.*) 64
881. Magnetism of Ce-based heavy fermion superconductor [active], W. Higemoto, R. Kadono, A. Koda, K. Ohishi (*KEK-IMSS*), K. Ishida, Y. Kawasaki, Y. Kitaoka (*Osaka U.*), C. Geibel, F. Steglich (*Max-Planck Inst.*)
882. μ SR studies of unconventional superconductivity in an organic superconductor $(\text{TMTSF})_2\text{ClO}_4$ [active], I.M. Gat, M.I. Larkin, A. Savici, Y.J. Uemura (*Columbia U.*), T. Ito (*Columbia U.-ETL*), P. Kyriakou, G.M. Luke, M. Rovers (*McMaster U.*), K.M. Kojima (*U. Tokyo*), P.M. Chaikin, I.J. Lee (*Princeton U.*), M.J. Naughton (*Boston Coll.*)
883. Muonium-substituted methyl and associated free radicals [active], J.-C. Brodovitch, J. Clyburne, S. Kecman, I. McKenzie, P.W. Percival (*SFU*), B. Addison-Jones (*Douglas College*) 96
884. μ SR studies on magnetic ground state of $S = 1/2$ kagomé spin system $\text{Cu}_3\text{V}_2\text{O}_7(\text{OH}) \cdot 2.2\text{H}_2\text{O}$ [active], A. Fukaya, I.M. Gat, M.I. Larkin, A. Savici, Y.J. Uemura (*Columbia U.*), T. Ito (*CERC-AIST*), A. Keren (*Technion-Israel Inst. of Tech.*), P.P. Kyriakou, G.M. Luke, M.T. Rovers (*McMaster U.*), Z. Hiroi (*U. Tokyo*)
885. High-TF line-shape measurement of impurity-doped high- T_c cuprates [active], K.M. Kojima, Y. Kojima, Y. Maeda, T. Okamura, S. Uchida (*U. Tokyo*), I. Gat, T. Itoh, A. Kinkhabwala, M.I. Larkin, Y.J. Uemura (*Columbia U.*), G.M. Luke (*McMaster U.*), S.R. Dunsiger, R.F. Kiefl, R. Miller (*UBC*), J.E. Sonier (*Los Alamos Nat. Lab*)
886. Study of field dependent T_1 relaxation and coexistence of order parameters in the (anti)ferromagnetic ruthenate-cuprate superconductors $\text{RuSr}_2(\text{Gd}, \text{Eu}, \text{Y})\text{Cu}_2\text{O}_8$ [active], C. Bernhard (*Max Planck Inst.*), C. Niedermayer, V. Oehmichen (*U. Konstanz*), E.J. Ansaldo (*U. Saskatoon*), J.L. Tallon (*NZIRD*)
887. Search for broken time reversal symmetry in high temperature superconductors [active], P. Kyriakou, G.M. Luke, M. Rovers (*McMaster U.*), R.H. Heffner (*Los Alamos Nat. Lab*), M.I. Larkin, Y.J. Uemura (*Columbia U.*), J. Sonier (*SFU*), K.M. Kojima (*U. Tokyo*)
888. Test of delayed-muonium model for hydrocarbon liquids [completed], D.C. Walker (*UBC-TRIUMF*), H.A. Gillis (*St. Francis Xavier U.*), G.B. Porter (*UBC*), S. Karolczak (*Politechnika, Poland*)
889. Study of field induced gap in Cu benzoate [active], Y. Ajiro, T. Asano, Y. Inagaki (*Kyushu U.*), H. Nojiri (*Tohoku U.*), W. Higemoto, R. Kadono, A. Koda (*KEK-IMSS*)
890. Anisotropic Kondo effect in $\text{Ce}_{0.8}\text{La}_{0.2}\text{Al}_3$? [completed], D.E. MacLaughlin (*U. California, Riverside*), O.O. Bernal (*Cal. State U., Los Angeles*), R.H. Heffner (*Los Alamos Nat. Lab*), G.M. Luke (*McMaster U.*), G.J. Nieuwenhuys (*U. Leiden*), J.E. Sonier (*SFU*), B. Andraka (*U. Florida*)
891. Superconductivity and magnetism in $\text{Ce}_n\text{T}_m\text{In}_{3n+2m}$ [active], R.H. Heffner, G.D. Morris, J. Sarrao (*Los Alamos Nat. Lab*), J.E. Sonier (*SFU*), D.E. MacLaughlin (*U. California, Riverside*), G.J. Nieuwenhuys (*U. Leiden*), O.O. Bernal (*Cal. State U., Los Angeles*)
892. Resonance ionization spectroscopy of stable and radioactive nuclides at TISOL [deferred] F. Buchinger, J.E. Crawford, S. Gulick, J.K.P. Lee (*McGill U.*), K. Sharma (*U. Manitoba*), J. Pinard (*Lab Aimé Cotton, Orsay*)
893. Hyperfine field of Rb in the ferromagnets Fe, Ni, Co [active], C.A. Davis, P.P.J. Delheij (*TRIUMF*), S. Cottenier (*K.U. Leuven*), H. Haas (*Hahn Meitner Inst.*), K.S. Krane, J. Loats, P. Schmelzenbach, C. Stapels (*Oregon State U.*), R. Kiefl, J. Pond, B. Turrell (*UBC*), D. Kulp, J. Wood (*Georgia Inst. Tech.*), A.D. Davies, D. Groh, P. Mantica, A.C. Morton (*Michigan State U.*) 65
894. Muonium kinetics and free radical formation in solutions of fullerenes [active], B. Addison-Jones (*Douglas College*), J.-C. Brodovitch, S. Kecman, I. McKenzie, P.W. Percival (*SFU*)
895. The vortex structure and magnetism of electron-doped cuprate superconductors [active], K.M. Kojima, S. Uchida (*U. Tokyo*), W. Higemoto, R. Kadono, A. Koda (*KEK*), M. Azuma, M. Fujita, M. Takano, K. Yamada (*Kyoto U.*), K. Ishida, Y. Kawasaki, Y. Kitaoka (*Osaka U.*), M.I. Larkin, Y.J. Uemura (*Columbia U.*) 97

896. Investigation of spin liquid behaviour in chromium and manganese spinels [completed], H. Dabkowska, J. Greedan, P.P. Kyriakou, G.M. Luke, M.T. Rovers (*McMaster U.*), I.M. Gat, M.I. Larkin, A.T. Savici, Y.J. Uemura (*Columbia U.*), K.M. Kojima (*U. Tokyo*)
897. Absolute magnetic penetration depth in the Meissner state of superconductors measured with low frequency beta-NMR [active], D. Bonn, J.H. Brewer, K.H. Chow, W. Hardy, R. Liang, R. Miller, G. Morris (*UBC*), S. Dunsiger, B. Heffner (*Los Alamos Nat. Lab*), R.F. Kiefl (*UBC-TRIUMF*), S. Kreitzman, P. Levy (*TRIUMF*), G. Luke (*McMaster U.*), J. Sonier (*SFU*), C. Stronach (*Virginia State U.*)
898. MULTI development with applications in superconductors and semiconductors [completed], P. Amadruz, D. Arseneau, S. Chan, K.H. Chow, B. Hitti, G. Morris, R. Poutissou (*TRIUMF*), J. Chakhalian, S. Dunsiger, R.F. Kiefl, R. Miller (*UBC*)
900. A determination of the $\alpha + {}^{15}\text{O}$ radiative capture rate by a measurement of the ${}^{15}\text{O}({}^6\text{Li}, d){}^{19}\text{Ne}$ reaction [active], B.R. Fulton, B. Greenhalgh, J. Pearson, D.L. Watson (*U. York*), N.M. Clarke (*U. Birmingham*), T. Davinson, N. Farrington, P. Monroe, C. Ruiz, F. Sarazin, K. Schmidt, A.C. Shotton, P.J. Woods (*U. Edinburgh*), L. Buchmann, P. Walden (*TRIUMF*), J. D'Auria (*SFU*)
902. Muon capture on ${}^{45}\text{Sc}$, ${}^{51}\text{V}$, ${}^{55}\text{Mn}$ and ${}^{59}\text{Co}$ [active], D.F. Measday (*UBC*), T.P. Gorringer (*U. Kentucky*)
903. Spectroscopic study of ${}^{11}\text{Be}$ with polarized ${}^{11}\text{Li}$ beam [active], A. Hatakeyama, Y. Hirayama, H. Izumi, T. Shimoda, M. Yagi, H. Yano (*Osaka U.*), H. Miyatake (*IPNS, KEK*), K.P. Jackson, C.D.P. Levy (*TRIUMF*)
907. Improving $S_{E1}(300)$: the $\beta - \alpha$ branching ratio of ${}^{16}\text{N}$ [deferred] R.E. Azuma, J.D. King (*U. Toronto*), L. Buchmann (*TRIUMF*)
909. Isospin symmetry breaking in superallowed Fermi beta decays [active], C. Andreoiu, P. Finlay, G.F. Grinyer, B.H. Hyland, A.A. Phillips, M. Schumaker, C.E. Svensson, J.J. Valiente-Dobon (*U. Guelph*), R.A.E. Austin, J.A. Cameron, J.C. Waddington (*McMaster U.*), A. Andreyev, G.C. Ball, P. Bricault, G. Hackman, C. Morton, C. Pearson, M.B. Smith (*TRIUMF*), J.C. Hardy, V. Iacob (*Texas A&M U.*), J.R. Leslie (*Queen's U.*), J.L. Woods, W.D. Kulp (*U. Georgia*), P.E. Garrett (*Lawrence Livermore Nat. Lab*), A. Piechaczek, E.F. Zganjar (*Louisiana State U.*), P.M. Walker (*U. Surrey*), F. Sarazin (*U. Colorado*), H.C. Scraggs (*U. Liverpool*), J. von Schwarzenberg (*U. Vienna*)
910. Study of the ground state proton emitter ${}^{73}\text{Rb}$ and implications for the astrophysical rp-process [active], A. Piechaczek, E.F. Zganjar (*Louisiana State U.*), G.C. Ball (*TRIUMF*), J.C. Batchelder (*Oak Ridge Assoc. U.*), D. Kulp, B.D. MacDonald, J.L. Wood (*Georgia Inst. Tech.*)
911. Test of aerogel proto-type detector for $G\theta$ phase II [active], J. Birchall, W. Falk, L. Lee, S. Page, W.D. Ramsay, A. Rauf, G. Rutledge, W.T.H. van Oers (*U. Manitoba*), C. Davis (*TRIUMF*), L. Hannelius, J. Martin (*Caltech*), E. Korkmaz, T. Porcelli (*UNBC*), S. Kox, G. Quemener, R. Tieulent (*ISN Grenoble*), D. Beck (*U. Illinois, Urbana*)
912. Formation, structure, and dynamics of muonium in GaAs studied by EF-ALC-RF $\mu^+\text{SR}$ [active], B. Hitti, S.R. Kreitzman (*TRIUMF*), K.H. Chow (*U. Alberta*), J.H. Brewer (*UBC*), D.G. Eshchenko (*U. Zurich-PSI*), V.G. Storchak (*Kurchatov Inst.*)
913. Photo-induced dynamics and reactivity of spin polarized ${}^8\text{Li}$ in semiconductors [active], K.H. Chow (*U. Alberta*), T. Beals, R.F. Kiefl, R.I. Miller (*UBC*), P. Amadruz, D. Arseneau, S. Daviel, B. Hitti, S.R. Kreitzman, P. Levy, R. Poutissou (*TRIUMF*), R.L. Lichti (*Texas Tech. U.*), G.D. Morris (*Los Alamos Nat. Lab*), C. Bommas (*U. Bonn*)
914. Zero-field μSR in Bi2212 and Bi2201 searching for effects related to the pseudo-gap [active], M. Greven, N. Kaneko, (*Stanford U.*), I.M. Gat, M.I. Larkin, P.L. Russo, A. Savici, Y.J. Uemura, emph(*Columbia U.*), G.M. Luke, G.J. MacDougall, C.R. Wiebe (*McMaster U.*), Y. Ando (*U. Tokyo*)
915. Muonium in semiconductor alloys [completed data-taking], R.L. Lichti (*Texas Tech. U.*), P.J.C. King (*Rutherford Appleton Lab*), I. Yonenaga (*Tohoku U.*)
916. QLCR of diamagnetic states in GaP [completed], R.L. Lichti, W. Nusbaum (*Texas Tech. U.*), K.H. Chow (*U. Alberta*), S.F.J. Cox (*Rutherford Appleton Lab*), B. Hitti (*TRIUMF*)
917. Correlation between magnetism and transport properties of thermoelectric oxides [active], H. Itahara, H. Nozaki, Y. Seno, T. Tani (*Toyota Central R&D Labs Inc.*), E.J. Ansaldo, B. Hitti (*TRIUMF*), H. Hazama (*Nagoya U.*)
918. High field study of La_2CuO_4 based superconductors [active], I.M. Gat, M.I. Larkin, P.L. Russo, A. Savici, Y.J. Uemura (*Columbia U.*), G.M. Luke, G.J. MacDougall, C.R. Wiebe (*McMaster U.*), K.M. Kojima, S.

67

99

100

101

103

- Uchida (*U. Tokyo*), T. Ito (*AIST, Tsukuba*), Y.S. Lee (*Nat. Inst. Standards Technology*), K. Yamada (*Kyoto U.*), M. Greven, M. Kaneko (*Stanford U.*), M.A. Kastner (*MIT*), R.J. Birgeneau (*U. Toronto*), R. Kadono (*KEK*), S. Tajima (*ISTEC*) 105
919. Proton irradiation effects in SOI devices [active], P. Dodd, G. Hash, R. Loemker, J. Schwank, M. Shaneyfelt (*Sandia Nat. Lab*), V. Ferlet-Cavrois, P. Paillet (*CEA*)
920. Nuclear charge radii and moments of short lived neutron deficient Lanthanum isotopes [active], H.A. Schuessler (*Texas A&M U.*), P. Levy (*TRIUMF*), H. Iimura (*Japan Atomic Energy Res. Inst.*), F. Buchinger, J. Crawford, J. Lee (*McGill U.*), R.I. Thompson (*U. Calgary*) 68
921. High-K isomers in neutron-rich $A = 170\text{--}190$ nuclei [active], P.H. Regan (*U. Surrey*), P.M. Walker (*TRIUMF-Surrey*), G.C. Ball, R.S. Chakrawarthy, E. Cunningham, G. Hackman, K. Koopmans, F. Sarazin, H.C. Scraggs, M.B. Smith (*TRIUMF*), P. Finlay, G.F. Grinyer, B. Hyland, A.A. Phillips, M.A. Schumaker, C.E. Svensson (*U. Guelph*), R. Austin, J.C. Waddington, B. Washbrook (*McMaster U.*), E.F. Zganjar (*Louisiana State U.*), J.R. Leslie (*TRIUMF-Queens*), J.J. Carroll, R. Propri (*Youngstown State U.*), P.E. Garrett (*Lawrence Livermore Nat. Lab*), W.D. Kulp, J.L. Wood (*Georgia Inst. Tech.*), T. Shizuma (*JAERI*), J. von Schwarzenberg (*U. Vienna*), D. Ward (*Lawrence Berkeley Nat. Lab*) 69
922. On the production of ^{26}Al in novae: measurement of the $^{25}\text{Al}(p,\gamma)^{26}\text{Si}$ reaction rate [pending], S. Bishop, A.A. Chen, J.M. D'Auria, D. Hunter, M. Lamey, C. Wrede (*SFU*), L. Buchmann, D.A. Hutcheon, K.P. Jackson, A. Olin, J. Rogers (*TRIUMF*), S. Engel (*Ruhr-U. Bochum*), C.S. Galovich (*U. Northern Colorado*), D. Gigliotti, A. Hussein (*UNBC*), U. Greife, C.C. Jewett (*Colorado School of Mines*), J. José (*UPC/IEEC Barcelona*), P.D. Parker (*Yale U.*)
923. Measurement of $^{25}\text{Al} + p$ resonances through elastic scattering [active], A.A. Chen, J.M. D'Auria (*SFU*), L. Buchmann, F. Sarazin, A. Shotter, P. Walden (*TRIUMF*), T. Davinson, A. Murphy, I. Roberts, A. Robinson, C. Ruiz, P. Woods (*U. Edinburgh*), B. Fulton, D. Groombridge, J. Pearson (*U. York*), P.D. Parker (*Yale U.*)
924. The hot CNO cycle and the $^{14}\text{O}(\alpha,p)^{17}\text{F}$ reaction [active], M. Aliotta, T. Davinson, A. Murphy, I. Roberts, A. Robinson, P.J. Woods (*U. Edinburgh*), L. Buchmann, A. Chen, P. Walden (*TRIUMF*), B. Fulton, D. Groombridge, J. Pearson (*U. York*), P. Leleux (*U. Catholique de Louvain*), R. Azuma (*U. Toronto*)
925. Isospin mixing in ^{36}Ar via spin-polarized observables in ^{36}K β^+ decay [active], J.M. D'Auria, D. Melconian (*SFU*), G.C. Ball, J.A. Behr, P. Bricault, M. Dombisky, K.P. Jackson (*TRIUMF*), S. Gu, M. Pearson (*UBC*), W.P. Alford (*U. Western Ontario*), D.A. Ashery, O. Aviv (*Tel Aviv U.*), I.A. Towner (*Queen's U.*), S. Karataglidis (*Los Alamos Nat. Lab*), B.A. Brown (*Michigan State U.*)
926. Measurement of charge radius and β^+ -decay Q-value of laser-trapped ^{74}Rb [active], S. Gu, M. Pearson (*UBC*), J.A. Behr, P. Bricault, M. Dombisky, K.P. Jackson (*TRIUMF*), D. Melconian (*SFU*), D.A. Ashery, O. Aviv (*Tel Aviv U.*)
927. Using $(^3\text{He},p)$: spectroscopy of proton unbound ^{19}Na [active], G.C. Ball, L. Buchmann, G. Hackman, A. Laird, F. Sarazin, A. Shotter, P. Walden (*TRIUMF*), A.A. Chen (*SFU*), T. Davinson, I. Roberts, A. Robinson, C. Ruiz, P. Woods (*U. Edinburgh*), B. Fulton, D. Groombridge, J. Pearson (*U. York*), C.E. Svensson (*U. Guelph*), J. Waddington (*McMaster U.*) 70
928. Level structure of ^{21}Mg : nuclear and astrophysical implications [active], M. Aliotta, T. Davinson, A.St.J. Murphy, A. Robinson, P.J. Woods (*U. Edinburgh*), J.M. D'Auria (*SFU*), R. Azuma (*U. Toronto*), R. Boyd (*Ohio State U.*), L. Buchmann, A. Chen, D. Hutcheon, A. Laird, P. Walden (*TRIUMF*), B. Fulton (*U. York*) 72
929. Octupole deformation and spin-exchange polarization of odd- A radon isotopes: toward radon electric dipole moment measurements at ISAC [active], P. Finlay, B. Hyland, A.A. Phillips, M.A. Schumaker, C.E. Svensson (*U. Guelph*), T.E. Chupp, K.P. Coulter, S.R. Nuss-Warren, E.R. Tardiff (*U. Michigan*), G.C. Ball, J.A. Behr, G.S. Hackman, M.R. Pearson, M.B. Smith (*TRIUMF*), M.E. Hayden, T. Warner (*SFU*) 72
930. Measurement of π^- absorption in water [completed data-taking], T. Awes, V. Cianciolo, G. Young (*Oak Ridge Nat. Lab*), S. Berridge, W. Bugg, Yu. Efremenko, R. Gearhart, Yu. Kamyshkov, S. Ovchinnikov (*U. Tennessee*), Yu. Davydov, T. Numao, J.-M. Poutissou (*TRIUMF*)
931. Magnetic properties of multinuclear, open-shell coordination complexes and polymers probed by μSR [active], F.D. Callaghan, N. Draper, C.V. Kaiser, M. Laulajainen, J. LeFebvre, D.B. Leznoff, C. Shorrock, J.E. Sonier (*SFU*) 105
932. Improving μ^- SR performance [active], J.H. Brewer, D.F. Measday (*UBC*), G.M. Marshall, M.M. Pavan (*TRIUMF*), K. Ghandi (*UBC-TRIUMF*)
933. Effects of nonlocality in superconductors [completed data-taking], R. Miller, R. Kiefl (*UBC-TRIUMF*), S.L. Bud'ko, P. Canfield, V. Kogan (*Iowa State U.*), P. Poon, J.E. Sonier (*SFU*)

934. MuSR study of polymerized C₆₀ [active], A. Fukaya, I.M. Gat, P.L. Russo, A.T. Savici, Y.J. Uemura (*Columbia U.*), P. Kyriakou, G.M. Luke (*McMaster U.*), T. Makarova, B. Sundqvist (*Umea U. Sweden*), V.A. Davydov (*Moscow Inst. High Pressure*), T. Ito (*AIST, Tsukuba*)
935. High pressure study of URu₂Si₂ [active], J. Garrett, P. Kyriakou, G.M. Luke, C. Wiebe (*McMaster U.*), I.M. Gat, A. Savici, Y.J. Uemura (*Columbia U.*), Y. Sushko (*U. Kentucky*), K.M. Kojima (*U. Tokyo*)
936. Magnetic dynamics in spin ice systems [active], S.T. Bramwell, J. Lago (*U. College London*), S.R. Dunsiger (*Los Alamos Nat. Lab*), J.S. Gardner (*NRC*), M.J.P. Gingras (*U. Waterloo*), R. Kiefl (*UBC-TRIUMF*), G.M. Luke (*McMaster U.*)
937. Muonium in hexagonal semiconductors [active], R.L. Lichti (*Texas Tech. U.*), K.H. Chow (*U. Alberta*), S.F.J. Cox (*Rutherford Appleton Lab*), B. Hitti (*TRIUMF*)
938. Muonium formation and ionization in semiconductors and insulators [active], J.H. Brewer, R.F. Kiefl (*UBC*), B. Hitti (*TRIUMF*), R. Lichti (*Texas Tech. U.*), D.G. Eshchenko, E. Morenzoni (*PSI*), V.G. Storchak (*Kurchatov Inst.*), J.D. Brewer (*SFU*), K.H. Chow (*U. Alberta*), S.P. Cottrell, S.F.J. Cox (*Rutherford Appleton Lab*), H. Keller (*U. Zürich*), 107
939. Guest-host interactions and Hfcs of mu-radicals in zeolites [active], M. Bridges, D.G. Fleming, C. Fyfe, G. Patey, A. Wang (*UBC*), D. Arseneau (*TRIUMF*), K. Ghandi (*TRIUMF-UBC*), E. Roduner (*U. Stuttgart*), M. Senba (*Dalhousie U.*) 108
940. Thermoelectrics II: μ SR in layered manganese oxides [completed data-taking], K. Dohmae, H. Itahara, Y. Seno, J. Sugiyama, T. Tani, C. Xia (*Toyota Central R&D Labs Inc.*), J.H. Brewer (*UBC*), E.J. Ansaldo (*U. Saskatchewan*), B. Hitti (*TRIUMF*)
941. Investigation of spin dynamics in geometrically frustrated transition metal oxides [active], J.E. Greedan, G.M. Luke, G. MacDougall, C.R. Wiebe (*McMaster U.*), P. Russo, A. Savici, Y.J. Uemura (*Columbia U.*) 109
942. Magnetic fluctuations near metal insulator transitions in ruthenate pyrochlores [active], N. Curro, S.R. Dunsiger, K.H. Kim (*Los Alamos Nat. Lab*), R.F. Kiefl (*UBC-TRIUMF*), K.H. Chow (*U. Alberta*), M.J.P. Gingras (*U. Waterloo*), W.A. MacFarlane, R.I. Miller (*UBC*), J.E. Sonier (*SFU*), S.W. Cheong, (*Rutgers U.-Lucent Tech.*), N. Hur (*Rutgers U.*), P.C. Hammel (*Ohio State U.*)
943. Muonium and muoniated free radical formation and reactivity in sub- and supercritical carbon dioxide [active], D.J. Arseneau (*TRIUMF*), M. Bridges (*UBC-TRIUMF*), D.G. Fleming, K. Ghandi, G. Patey, A. Wang (*UBC*), M. Pinto (*SFU*) 111
944. Muonium sites and dynamics in silicon carbide [active], R.L. Lichti, W. Nusbaum (*Texas Tech. U.*), K.H. Chow, (*U. Alberta*), E.A. Davis (*U. Leicester*), B. Hitti (*TRIUMF*), S.F.J. Cox (*Rutherford Appleton Lab*) 113
945. Muoniated radicals formed from carbenes and carbene analogues [active], J.-C. Brodovitch, J.A.C. Clyburne, S. Kecman, B. McCollum, I. McKenzie, P.W. Percival (*SFU*)
946. Energy generation and nucleosynthesis in the HotCNO cycles: measurement of the $^{17}\text{F}(p,\gamma)^{18}\text{Ne}$ reaction rate [active], A.A. Chen (*McMaster U.-TRIUMF*), S. Bishop, J.M. D'Auria, M. Lamey, C. Wrede (*SFU*), L. Buchmann, D.A. Hutcheon, A. Olin, D. Ottewell, J. Rogers (*TRIUMF*), S. Engel (*Ruhr-Universität Bochum*), D. Gigliotti, A. Hussein (*UNBC*), U. Greife, C.C. Jewett (*Colorado School of Mines*), J. José (*UPC/IEEC Barcelona*), P.D. Parker (*Yale U.*)
947. Evaluation of the competition between single-step and multi-step γ decay in the $^{12}\text{C}(^{12}\text{C}, \gamma)$ reaction [active], T. Brown, S.P. Fox, B.R. Fulton, D. Groombridge, D.G. Jenkins, J. Pearson, R. Wadsworth, D.L. Watson (*U. York*), L. Buchmann, C. Davis, D. Hutcheon, S. Park, J. Rogers (*TRIUMF*), J.M. D'Auria (*SFU*), U. Greife (*Colorado School of Mines*), M.P. Carpenter, R.V.F. Janssens, T.L. Khoo, C.J. Lister, A.H. Wuosmaa (*Argonne Nat. Lab*), M. Freer (*U. Birmingham*), F. Azaiez, C. Beck, F. Haas, P. Papka, A. Sanchez (*IREs Strasbourg*), C. Andreoiu, M. Chartier, R.-D. Herzberg (*U. Liverpool*) 73
948. Proton radiation effects in silicon-on-insulator and bulk-silicon devices [active], P. Dodd, G. Hash, R. Jones, J. Schwank, M. Shaneyfelt (*Sandia Nat. Labs*), V. Ferlet-Cavroi, C. D'Hose, P. Paillet, J.-E. Sauvestre (*CEA, France*), E. Blackmore (*TRIUMF*) 74
949. μ SR study of magnetic order in high- T_c superconductor under high pressure [active], J. Arai, T. Goko, K. Sato, S. Takeshita (*Tokyo U. of Science*), W. Higemoto, K. Nagamine, K. Nishiyama (*KEK-MSL*) 114
950. High field study of Zn doped/Eu doped/overdoped systems [active], I.M. Gat, M.I. Larkin, P.L. Russo, A. Savici, Y.J. Uemura (*Columbia U.*), G.M. Luke, G.J. MacDougall, C.R. Wiebe (*McMaster U.*), K.M. Kojima, S. Uchida (*U. Tokyo*), T. Ito (*AIST, Tsukuba*), Y.S. Lee (*Nat. Inst. Standards Technology*), K. Yamada (*Kyoto U.*), M. Greven, M. Kaneko (*Stanford U.*), M.A. Kastner (*MIT*), R.J. Birgeneau (*U. Toronto*), R. Kadono (*KEK*), S. Tajima (*ISTEC*) 105

951. Magnetism and flux line lattice structure of oxychloride superconductors [active], W. Higemoto, R. Kadono, A. Koda, K. Ohishi (*KEK-IMSS*), M. Azuma, M. Takano, I. Yamada (*Kyoto U.*), K.M. Kojima (*U. Tokyo*) 115
952. $^{12}\text{C}(\alpha, \gamma)^{16}\text{O}$ at DRAGON [active], C. Barbieri, L. Buchmann, D. Hutcheon, A.M. Laird, A. Olin, M. Pavan, J. Rogers, C. Ruiz, F. Sarazin, J.M. Sparenberg (*TRIUMF*), C.R. Brune (*U. Ohio*), A. Chen (*McMaster U.*), J.M. D'Auria (*SFU*), J. Görres, M. Wiescher (*U. Notre Dame*), U. Greife (*Colorado School of Mines*), A. Hussein (*UNBC*), Z. Li, W. Liu (*Chinese Inst. of Atomic Energy*), A. Murphy (*U. Edinburgh*), S. Woosley (*U. California, Santa Cruz*), H.O. Meyer (*IUCF*) 76
953. Spin dynamics and quantum coherence in molecular magnets [active], Z. Salman (*TRIUMF*), A. MacFarlane, R. Kiefl (*UBC-TRIUMF*), K. Chow (*U. Alberta*), S. Dunsiger (*Los Alamos Nat. Lab*), B. Barbara (*Lab de Magnetisme Louis Néel*) 116
954. Half-lives of long-lived isotopes/chronology and environment [active] R.A.E. Austin, A. Chen, K.A. Koopmans, M. Lee, N. Novo, B. Singh, J.C. Waddington (*McMaster U.*), G.C. Ball, G. Hackman, F. Sarazin, H. Scraggs, M.B. Smith (*TRIUMF*), P.E. Garrett (*Lawrence Livermore Nat. Lab*), G. Grinyer, C.E. Svensson (*U. Guelph*)
955. Probing shell structure with β - and β -n-delayed γ spectroscopy [active], G.C. Ball, P. Bricault, M. Dombsky, G. Hackman, J. MacDonald, F. Sarazin, H. Scraggs, M.B. Smith (*TRIUMF*), G. Grinyer, C.E. Svensson (*U. Guelph*), J.C. Waddington (*McMaster U.*), E. Zganjar (*Louisiana State U.*), W.D. Kulp, J. Wood (*Georgia Inst. Tech.*), P.E. Garrett (*Lawrence Livermore Nat. Lab*), P. Walker (*U. Surrey-TRIUMF*) 77
956. Search for tensor interactions in recoil nucleus singles in decay of polarized ^{80}Rb [active], J.A. Behr, P. Bricault, M. Dombsky, S. Gu, K.P. Jackson, M.R. Pearson (*TRIUMF*), D. Melconian (*SFU*), D. Ashery, O. Aviv (*Tel Aviv U.*)
957. Search for high-spin isomeric states in the vicinity of double-magic $N = Z$ ^{100}Sn [active], G.C. Ball, G.S. Hackman, F. Sarazin, H.C. Scraggs, M.B. Smith (*TRIUMF*), P.M. Walker (*U. Surrey*), C.E. Svensson (*U. Guelph*), J.C. Waddington (*McMaster U.*), E. Zganjar (*Louisiana State U.*), P.E. Garrett (*Lawrence Livermore Nat. Lab*), J.L. Wood (*Georgia Inst. Tech.*)
958. HTF- μ^+ SR lineshapes in overdoped high- T_c superconductors [active], D.A. Bonn, J.H. Brewer, M. Franz, W.N. Hardy, R.F. Kiefl, R.X. Liang, W.A. MacFarlane (*UBC*), F. Callaghan, K.F. Poon, J.E. Sonier (*SFU*), J. Chakhalian, Z. Salman (*TRIUMF*), S. Kim, G.M. Luke (*McMaster U.*), N.N. Kolesnikov (*Russian Acad. of Science*), C.E. Stronach (*Virginia State U.*)
959. New low field integral method for studies of diamagnetic muonium centers in group IV and II-VI semiconductors [active], K.H. Chow, K. Hoffman (*U. Alberta*), B. Hitti (*TRIUMF*), J.M. Gil (*U. Coimbra*), R.F. Kiefl (*UBC*)
960. Hydrogen (Mu) defect level in II-VI chalcogenides [active], H.V. Alberto, J.M. Gil, R.C. Vilao (*U. Coimbra*), K.H. Chow (*U. Alberta*), S.F.J. Cox (*Rutherford Appleton Lab*), B. Hitti (*TRIUMF*), R.L. Lichti (*Texas Tech. U.*) 118
961. $A \geq 62$ super-allowed Fermi β decays: constraining unknown corrections with ^{66}As and ^{70}Br decay [active], P.E. Garrett, W.E. Ormand, A. Schiller (*Lawrence Livermore Nat. Lab*), G.F. Grinyer, C.E. Svensson (*U. Guelph*), R.A.E. Austin, J.C. Waddington (*McMaster U.*), G.C. Ball, G. Hackman, F. Sarazin, H.C. Scraggs, M.B. Smith (*TRIUMF*), J. Allmond, W.D. Kulp, J.L. Wood (*Georgia Inst. Tech.*), A. Piechaczek, E. Zganjar (*Louisiana State U.*)
962. μSR study on $\text{Na}_{0.33}\text{V}_2\text{O}_5$ [active], P.L. Russo, A.T. Savici, Y.J. Uemura (*Columbia U.*), G.M. Luke, C.R. Wiebe (*McMaster U.*), Y. Ueda, T. Yamauchi (*ISSP*)
963. Underdoped/undoped cuprate single crystals [active], D.A. Bonn, J.H. Brewer, W.N. Hardy, R.F. Kiefl, R.X. Liang (*UBC*), F. Callaghan, K.F. Poon, J.E. Sonier (*SFU*), G.M. Luke (*McMaster U.*), R.L. Greene (*Maryland U.*), P. Fournier (*U. Sherbrooke*), C.E. Stronach (*Virginia State U.*), R.I. Miller (*Pennsylvania State U.*)
964. A study of the partial and total cross sections of the $^8\text{Li}(\alpha, n)^{11}\text{B}$ reaction at astrophysically relevant energies [deferred], L. Buchmann, A.C. Shotter, P. Walden (*TRIUMF*), R. Boyd, D. Reitzner (*Ohio State U.*), A.A. Chen (*McMaster U.*), J.M. D'Auria (*SFU*), B. Fulton, A.M. Laird (*U. York*), U. Greife, F. Sarazin (*Colorado School of Mines*), D. Hutcheon (*TRIUMF-U. Alberta*), Z. Li (*Chinese Inst. of Atomic Energy*), A. Murphy (*U. Edinburgh*), S. Nishimura (*RIKEN*), 79
965. Investigation of spin statics and dynamics in the new dipolar spin ice $\text{Ho}_2\text{Ru}_2\text{O}_7$ [active], J.E. Greedan, S.J. Kim, G.M. Luke, G. MacDougall, C.R. Wiebe (*McMaster U.*), M.J.P. Gingras (*U. Waterloo*), P. Russo, A. Savici, Y.J. Uemura (*Columbia U.*) 119
966. High precision mass determination for CVC tests [active], P. Bricault, J. Dilling, J. Vaz (*TRIUMF*), K. Sharma (*U. Manitoba*), M. Trinczek (*MPI-K-TRIUMF*), M. Smith (*UBC-TRIUMF*), F. Buchinger, J. Crawford, J. Lee, R.B. Moore (*McGill U.*)

967. Beta decay branching ratio of ^{21}Na [active], S.J. Freedman (*UC Berkeley-LBNL*), P.A. Vetter (*Lawrence Berkeley Nat. Lab*), A.A. Kwiatkowski, R. Maruyama (*U. California, Berkeley*) 79
968. Ortho-para effect of muon catalyzed fusion in liquid deuterium [active], N. Kawamura, K. Nagamine, A. Toyoda (*KEK*), H. Imao (*U. Tokyo-KEK*), K. Ishida, T. Matsuzaki (*RIKEN*) 80
969. Metamagnetic transitions and quantum critical behavior [active], S.R. Dunsiger, R.H. Heffner, G.D. Morris (*Los Alamos Nat. Lab*), D.E. MacLaughlin (*U. California, Riverside*), O.O. Bernal (*California State U.*), G.J. Nieuwenhuys (*U. Leiden*)
971. Precise measurement of the quadrupole moments of $^{20,21,25}\text{Na}$ [active], R. Baartman, J. Behr, P. Bricault, M. Dombsky, P. Jackson, P. Levy, M. Pearson (*TRIUMF*), M. Fukuda, K. Matsuta, M. Mihara, T. Minamisono, T. Nagatomo, M. Ogura, T. Sumikama (*Osaka U.*), R. Kiefl (*UBC*), K. Koshigiri (*Osaka Kyoiku U.*), K. Minamisono (*JSPS-TRIUMF*), M. Morita (*Josai Int. U.*)
972. Meson and quark effects in the nuclear β decay of ^{20}F [active], R. Baartman, J. Behr, P. Bricault, M. Dombsky, P. Jackson, P. Levy, M. Pearson (*TRIUMF*), M. Fukuda, K. Matsuta, M. Mihara, T. Minamisono, T. Nagatomo, M. Ogura, T. Sumikama (*Osaka U.*), R. Kiefl (*UBC*), K. Koshigiri (*Osaka Kyoiku U.*), K. Minamisono (*JSPS-TRIUMF*), M. Morita (*Josai Int. U.*)
973. Study of coexisting collective phases far from stability: systematic decay spectroscopy of the $N = 90$ isotones [active], J.M. Allmond, W.D. Kulp, III, J.L. Wood (*Georgia Inst. Tech.*), A. Piechaczek, E. Zganjar (*Louisiana State U.*), J. von Schwarzenberg (*U. Vienna*), D.J. Rowe (*U. Toronto*), P.E. Garrett (*Lawrence Livermore Nat. Lab*), K.S. Krane, P. Schmelzenbach (*Oregon State U.*), G.F. Grinyer, C.E. Svensson (*U. Guelph*), R.A.E. Austin, J.C. Waddington (*McMaster U.*), G.C. Ball, G. Hackman, H.C. Scraggs, M.B. Smith (*TRIUMF*)
974. μSR experiments on superconductivity and magnetism in the new layered oxide $\text{Na}_{0.35}\text{CoO}_2 \cdot y\text{H}_2\text{O}$ [active], C.R. Wiebe (*McMaster U.-Columbia U.*), S.J. Kim, G.M. Luke, G. MacDougall (*McMaster U.*), P. Russo, A. Savici, Y.J. Uemura (*Columbia U.*), J.E. Sonier (*SFU*) 120
975. Magnetism and superconductivity in $\text{Na}_x\text{CoO}_2 \cdot y\text{H}_2\text{O}$ and related cobalt oxides [active], W. Higemoto, R. Kadono, A. Koda, K. Ohishi (*KEK-IMSS*), S.R. Saha, H. Sakurai, K. Takada, E. Takayama-Muromachi (*NIMS, Japan*) 122
976. μSR study of strongly correlated electron behavior in filled skutterudite compounds [active], W. Higemoto, R. Kadono, A. Koda, K. Ohishi (*KEK-IMSS*), Y. Aoki, S.R. Saha, H. Sato, H. Sugawara (*Tokyo Metropolitan U.*)
977. Magnetism and superconductivity in spinel oxides [active], W. Higemoto, R. Kadono, A. Koda, K. Ohishi (*KEK-IMSS*), M. Isobe, Y. Ueda (*ISSP U. Tokyo*)
978. Magnetism in organic chiral compounds [active], W. Higemoto, R. Kadono, A. Koda, K. Ohishi (*KEK-IMSS*), H. Imai, K. Inoue (*IMS Okazaki Nat. Res. Inst.*)
979. Magnetism of equiatomic ternary uranium compounds [active], G.M. Kalvius (*Tech. U. Munich*), H. Nakotte (*New Mexico State U.*), D.R. Noakes, C.E. Stronach (*Virginia State U.*), R. Wäppling (*Uppsala U.*)
980. Quantum impurities in spin ladder compounds [active], I. Affleck (*Boston U.*), J. Brewer, R.F. Kiefl, W.A. MacFarlane (*UBC*), J. Chakhalian, Z. Salman (*TRIUMF*), S. Eggert (*Chalmers U.*), K. Kojima (*Tokyo U.*), Y.J. Uemura (*Columbia U.*)
981. Photoinduced magnetism in Prussian blue analogs [active], J. Chakhalian, Z. Salman (*TRIUMF*), R. Kiefl, A. MacFarlane, T. Parolin, D. Wang (*UBC*), K. Chow (*U. Alberta*), D. Leznoff, J. Sonier (*SFU*)
982. μSR study of the superferromagnetic transition in clinoatacamite [active], T. Mori, X.G. Zheng (*Saga U.*), W. Higemoto, K. Nishiyama (*KEK-MSL*)
983. Direct measurement of astrophysical $^{11}\text{C}(p, \gamma)^{12}\text{N}$ reaction at DRAGON [active], Z.H. Li, W.P. Liu (*China Inst. of Atomic Energy*), J.M. D'Auria (*SFU*), L. Buchmann, D. Hutcheon, A. Laird, A. Olin, J. Rogers, C. Ruiz (*TRIUMF*), A.A. Chen (*McMaster U.*), J. Caggiano, A. Parikh, P. Parker (*Yale U.*), X.D. Tang (*Argonne Nat. Lab*)
984. Fast lifetime measurements with the 8π spectrometer and nuclear structure below $N = 82$ [active], J.A. Becker, P.E. Garrett (*Lawrence Livermore Nat. Lab*), H. Mach (*Studsvik*), M. Moszyński (*SINS Swierk*), C. Andreoiu, G.F. Grinyer, A. Phillips, M. Schumaker, C.E. Svensson (*U. Guelph*), R.A.E. Austin, J.C. Waddington (*McMaster U.*), G.C. Ball, R.S. Chakrawarthy, G. Hackman, M.B. Smith (*TRIUMF*), W.D. Kulp, J.L. Wood (*Georgia Inst. Tech.*), E. Zganjar (*Louisiana State U.*), J. von Schwarzenberg (*U. Vienna*), F. Sarazin (*Colorado School of Mines*), J. Ressler (*SFU*), S.W. Yates (*U. Kentucky*), J.R. Leslie (*Queen's U.*)
985. Half-life and branching-ratio measurement of ^{18}Ne superallowed fermi β decay [active], A.N. Andreyev, G.C. Ball, R.S. Chakrawarthy, G. Hackman, M.B. Smith (*TRIUMF*), R.A.E. Austin (*St. Mary's U.*), P.E. Garrett (*Lawrence Livermore Nat. Lab*), J.R. Leslie (*Queen's U.*), R. Sarazin (*Colorado School of Mines*), C.E. Svensson (*U. Guelph*), J.L. Wood (*Georgia Inst. Tech.*), E.F. Zganjar (*Louisiana State U.*)

986. Proton irradiation effects in advanced semiconductor technologies [active], P. Dodd, G. Hash, J. Schwank, M. Shaneyfelt (*Sandia Nat. Lab*), C. D'Hose, V. Ferlet-Cavrois, P. Paillet, J.-E. Sauvestre (*CEA, France*), E. Blackmore (*TRIUMF*)
987. Collinear resonant ionization spectroscopy near proton drip line [deferred], L. Blomeley, F. Buchinger, T. Cocolios, J.E. Crawford, S. Gulick, J.K.P. Lee, R.B. Moore (*McGill U.*), J. Dilling, P. Levy, M. Pearson (*TRIUMF*), G. Gwinner, K. Sharma (*U. Manitoba*), R. Thompson (*U. Calgary*), H. Schuessler (*TAMU, Texas*), J. Billowes, P. Campbell, B.W. Tordoff (*U. Manchester*), F. Ibrahim, F. Le Blanc, J. Sauvage, R. Sifi (*IPN Orsay*), J. Pinard (*LAC Orsay*)
988. Lifetime measurements in the rare-earth neutron-rich region using FEST [active], J.J. Ressler (*Yale U.-SFU*), R.F. Casten, E.A. McCutchan, N.V. Zamfir (*Yale U.*), D.S. Brenner (*Clark U.*), J.M. D'Auria (*SFU*), G. Ball, G. Hackman (*TRIUMF*), P.E. Garrett (*Lawrence Livermore Nat. Lab*), J.L. Wood (*Georgia Inst. Tech.*), R.E.A. Austin, J. Waddington (*McMaster U.*), C. Svensson (*U. Guelph*), E.F. Zganjar (*U. Louisiana*), A.A. Hecht (*Argonne Nat. Lab*)
989. Astrophysical studies using ^{26}Al ground-state and isomeric beams [active], C. Ruiz (*SFU-TRIUMF*), C. Angulo (*CRC Louvain-la-Neuve*), R.E. Azuma, J.D. King (*U. Toronto*), L. Buchmann, J. Caggiano, B. Davids, D.A. Hutcheon, A. Olin, J. Rogers (*TRIUMF*), A. Chen, C. Van Ouellet (*McMaster U.*), J.M. D'Auria (*SFU*), U. Greife, C.C. Jewett, F. Sarazin (*Colorado School of Mines*), A. Hussein, C. Iliadis (*UNBC*), J. Jose (*UPC/IEEC Barcelona*), A.M. Laird (*U. York*), A.S. Murphy (*U. Edinburgh*), P. Parker (*Yale U.*), A. Shotter (*TRIUMF-U. Alberta*)
990. Resonant elastic scattering of isomeric ^{26}Al on protons [active], C. Ruiz (*SFU-TRIUMF*), C. Angulo (*CRC Louvain-la-Neuve*), M. Aliotta, T. Davinson, A.S. Murphy, P.J. Woods (*U. Edinburgh*), R.E. Azuma, J.D. King (*U. Toronto*), L. Buchmann, B. Davids, P. Walden (*TRIUMF*), A. Chen, J. Pearson, C. Van Ouellet (*McMaster U.*), J.M. D'Auria (*SFU*), B.R. Fulton, D. Groombridge, A.M. Laird (*U. York*), F. Sarazin (*Colorado School of Mines*), A. Shotter (*TRIUMF-U. Alberta*)
991. Laser spectroscopic determination of the ^{11}Li charge radius [active], B. Bushaw (*Pacific Northwest Nat. Lab*), A. Dax (*PSI*), G.W.F. Drake (*U. Windsor*), G. Ewald, R. Kirchner, H.-J. Kluge, Th. Kühl (*GSI Darmstadt*), A. Gluzicka (*Warsaw U.*), P. Bricault, J. Dilling, M. Domsbky, J. Lassen, P. Levy, M. Pearson (*TRIUMF*), W. Nörtershäuser, C. Zimmermann (*U. Tübingen*), G. Gwinner (*U. Manitoba*)
992. Lifetime of the 4.033 MeV state in ^{19}Ne [active], G.C. Ball, R.S. Chakrawarthy, B. Davids, G. Hackman, M.B. Smith, P. Walden (*TRIUMF*), J.S. Forster (*U. Montréal*), A.M. Laird (*U. York*), H. Leslie (*Queen's U.*), C. Ruiz (*TRIUMF-SFU*), A. Shotter (*TRIUMF-U. Alberta*)
993. Coulomb excitation of neutron rich beams with TIGRESS and the Si array [active], R.A.E. Austin, A.A. Chen, J.C. Waddington (*McMaster U.*), F. Sarazin (*Colorado School of Mines*), C. Andreoiu, G.F. Grinyer, C.E. Svensson (*U. Guelph*), G.C. Ball, G.S. Hackman, M.B. Smith (*TRIUMF*), T. Drake (*U. Toronto*), P. Garrett (*Lawrence Livermore Nat. Lab*), J.J. Ressler (*SFU*), P.M. Walker (*U. Surrey*)
994. On the rp-process bottleneck at $A = 56$: Coulomb excitation of ^{58}Zn at ISAC-II [active], R.A.E. Austin, A.A. Chen, J.C. Waddington (*McMaster U.*), C. Andreoiu, C.E. Svensson (*U. Guelph*), G.C. Ball, B. Davids, G. Hackman (*TRIUMF*), J.J. Ressler (*SFU*), F. Sarazin (*Colorado School of Mines*)
995. An alternate approach to radioactive beam production for volatile elements: proof-of-principle [active], J.M. D'Auria, S. Lapi (*SFU*), T.J. Ruth (*TRIUMF*)
996. Nova observables – ^{18}F abundance and the $^{18}\text{F}(p,\alpha)^{15}\text{O}$ reaction [active], T. Brown, S. Fox, B. Fulton, D. Groombridge, A.M. Laird (*U. York*), M. Aliotta, P. Davinson, A. Murphy, P. Woods (*U. Edinburgh*), C. Angulo (*CRC Louvain-la-Neuve*), L. Buchmann, B. Davids, C. Ruiz, A. Shotter, P. Walden (*TRIUMF*), J. Jose (*UPC/IEEC Barcelona*), F. Sarazin (*Colorado School of Mines*)
997. μSR study on the magnetic structures in $\text{Cu}_{1-x}\text{Li}_x\text{O}$ [active], T. Mori, X.G. Zheng (*Saga U.*), W. Higemoto, K. Nishiyama (*KEK-MSL*)
998. Muon spin relaxation and dynamic scaling in novel magnetic materials [active], D.E. MacLaughlin (*U. California, Riverside*), S.R. Dunsiger, R.H. Heffner, G.D. Morris, J.L. Sarrao (*Los Alamos Nat. Lab*), J.E. Sonier (*SFU*), O.O. Bernal (*Cal. State U., Los Angeles*), G.J. Nieuwenhuys (*Leiden U.*), G.R. Stewart (*U. Florida*), M.B. Maple (*U. California, San Diego*)
999. Local magnetic properties in Pu and Pu-based alloys [active], B. Chung, M. Fluss (*Lawrence Livermore Nat. Lab*), R. Heffner, J. Lashley, G.D. Morris, J. Sarrao (*Los Alamos Nat. Lab*), D. MacLaughlin (*U. California, Riverside*)

1000. Measurements of the vortex core size in type-II superconductors [active], F.D. Callaghan, C. Kaiser, M. Laulajainen, J.E. Sonier (*SFU*), L. Taillefer (*U. Sherbrooke*), D. Bonn, J.H. Brewer, W.N. Hardy, R.F. Kiefl, R. Liang (*UBC*)
1001. Defect levels and Mu^0 dynamics in III-V semiconductors [active], H.V. Alberto, J.M. Gil, R.C. Vilao (*U. Coimbra*), K.H. Chow (*U. Alberta*), S.F.J. Cox (*Rutherford Appleton Lab*), B. Hitti (*TRIUMF*), R.L. Lichti, D. Stripe (*Texas Tech. U.*)
1002. Knight shift measurements of dynamic spin systems [active], C.R. Wiebe (*McMaster U.-Columbia U.*), S.J. Kim, G.M. Luke, G. MacDougall, J. Rodriguez (*McMaster U.*), P. Russo, A.T. Savici, Y.J. Uemura (*Columbia U.*)
1003. μSR in pure and diluted spin ice pyrochlore systems [active], I.M. Gat, P.L. Russo, A. Savici, Y.J. Uemura (*Columbia U.*), H. Dabkowska, G.M. Luke (*McMaster U.*), C.R. Wiebe (*Columbia U.-McMaster U.*), K. Ishida, Y. Maeno, S. Nakatsuji (*Kyoto U.*), P. Schiffer (*Pennsylvania State U.*), R.J. Cava (*Princeton U.*)
1004. Nuclear hyperfine interactions of the shallow muonium center in GaN [active], K.H. Chow, A.N. MacDonald, B. Schultz (*U. Alberta*), R. Kadono, K. Shimomura (*KEK*), K. Mizuta, K. Ohishi (*NEC Corp.*), R.L. Lichti (*Texas Tech. U.*), B. Hitti (*TRIUMF*), R.F. Kiefl (*UBC*)
1005. Optically induced dynamics and site changes in group IV semiconductors [active], K.H. Chow, A.N. MacDonald, B. Schultz (*U. Alberta*), B. Hitti, Z. Salman (*TRIUMF*), R.F. Kiefl, W.A. MacFarlane (*UBC*)
1006. Magnetic properties of RECrSb_3 ($\text{RE} = \text{La, Gd}$) [active], K.H. Chow, A. Mar, A. Tkachuk (*U. Alberta*), W.A. MacFarlane (*UBC*), B. Hitti, Z. Salman (*TRIUMF*)

*deceased

LIFE SCIENCES PROJECT PROPOSALS

The following lists life sciences project proposals received up to the end of 2003 (missing numbers cover proposals that have been withdrawn or replaced by later versions, rejected, or combined with another proposal). Page numbers are given for those experiments which are included in this Annual Report.

Page

LS0.	PET facilities [active], K.R. Buckley, E.T. Hurtado, P. Piccioni, W. Sievers (<i>TRIUMF</i>), C. English, S. Jivan, S. Shah, C. Williams (<i>UBC-TRIUMF</i>)	125
LS1.	Attenuation maps for quantitative SPECT [completed], <u>A. Celler</u> (<i>UBC-VH&HSC</i>), S. McFarland (<i>UBC</i>), S. Barney, M. Limber (<i>SFU</i>)	
LS2.	Synthesis of ^{18}F -glycosides as potential imaging agents for the study of glycosidase activity in the brain [completed], <u>M.J. Adam</u> (<i>TRIUMF</i>), D. Lyster (<i>VH&HSC</i>), G. Matte (<i>Halifax H.</i>)	
LS3.	Synthesis of radiopharmaceuticals for positron emission tomography [active], M.J. Adam, K.R. Buckley, E.T. Hurtado, J. Huser, <u>S. Jivan</u> , J.-M. Lu, T.J. Ruth (<i>TRIUMF</i>)	126
LS4.	TR13 targets for PET radioisotope production [active], K. Buckley, T. Hurtado, <u>T.J. Ruth</u> , S.K. Zeisler (<i>TRIUMF</i>)	127
LS5.	Production and on-line separation of ^{124}I from enriched tellurium [inactive], W.Z. Gelbart, E.T. Hurtado, <u>T.J. Ruth</u> , N.R. Stevenson, S.K. Zeisler (<i>TRIUMF</i>), R.R. Johnson (<i>UBC</i>)	
LS6.	Bone calcium resorption studies in pre- and peri-menopausal women using accelerator mass spectrometry [completed], R.R. Johnson, A. Priestman, J.C. Prior (<i>UBC</i>), A. Altman, W.Z. Gelbart, V. Sossi (<i>TRIUMF</i>), D. Berkovits, <u>S. Ghelberg</u> , M. Paul (<i>Racah Inst., Hebrew U. Jerusalem</i>), L.M. Shulman (<i>Chaim Sheba Med. Centre</i>), R. Chechik (<i>Weizmann Inst.</i>), E. Venzel (<i>SFU</i>)	
LS7.	PET 3D data quantification and integration into a research clinical environment [completed], K.S. Morrison, T.J. Ruth, V. Sossi, M.W. Stazyk (<i>UBC-TRIUMF</i>), K.R. Buckley (<i>TRIUMF</i>), J.S. Barney (<i>VH&HSC</i>), D. Sirota, B.J. Snow (<i>UBC</i>)	
LS8.	Radiotracers for the physical and biosciences [active], L. Buchmann, <u>T.J. Ruth</u> , S.K. Zeisler (<i>TRIUMF</i>), A.D.M. Glass, R.R. Johnson, M. Lowe, C.E.R. Orvig (<i>UBC</i>), T.F. Budinger (<i>Lawrence Berkeley National Lab</i>)	128
LS10.	Biological evaluation of radiohalogenated DNA aptamers [completed], <u>H. Dougan</u> (<i>TRIUMF</i>), J.B. Hobbs, D.M. Lyster (<i>UBC</i>), J.I. Weitz (<i>McMaster U.</i>)	
LS11.	Development of single photon imaging agents [inactive], <u>D. Lyster</u> (<i>UBC-VH&HSC</i>), L. Alcorn, M. Hampong, T. Lutz, C. Vo (<i>UBC</i>)	
LS12.	A simulation platform for the design of position encoding multicrystal detectors [completed], A. Altman, <u>C. Moisan</u> , <u>J.G. Rogers</u> (<i>TRIUMF</i>), E. Hoskinson, G. Tsang (<i>UBC</i>)	
LS13.	Utility of 2-[F-18]-fluoro-2-deoxy-d-glucose SPECT imaging in the evaluation of patients with solitary pulmonary nodules [completed], A. Celler, D. Lyster, <u>D. Worsley</u> (<i>UBC</i>), M. Adam (<i>TRIUMF</i>)	
LS14.	Production of ^{127}Xe from cesium with 90–110 MeV protons [inactive], D. Pearce, <u>J. Vincent</u> (<i>TRIUMF</i>)	
LS15.	Investigation of frame realignment on the reproducibility of ^{18}F -6-fluorodopa positron emission tomography [inactive], <u>K.S. Morrison</u> , T.J. Ruth (<i>UBC-TRIUMF</i>), B.J. Snow (<i>UBC</i>)	
LS17.	Table-top radiocarbon facility [inactive], W. Gelbart, <u>R.B. Schubank</u> (<i>TRIUMF</i>), E. Venczel (<i>UBC-SFU</i>), S. Calvert, R.R. Johnson, J. Nagel, T. Peterson, V. Sossi (<i>UBC</i>), D.E. Nelson (<i>SFU</i>), J. Prior, K. Schoenholzer, R. Sutton, V. Walker (<i>UBC-VH&HSC</i>), R. Middleton (<i>U. Pennsylvania</i>), M. Paul (<i>Hebrew U. Jerusalem</i>), J. Clague, L. Jackson, J. Lutenauer, D. Templeman-Kluit (<i>Geological Survey of Canada</i>), R.N. McNeely, J.-S. Vincent (<i>GSC Ottawa</i>), V. Barrie (<i>Pacific Geoscience Center</i>), D. Prior, K.R. Robertson, G. Vilks (<i>Bedford Inst. Oceanography</i>), R. Brown, S. Wang (<i>Elemental Research Inc.</i>), J. Vogel (<i>Lawrence Livermore National Lab</i>), A.E. Litherland (<i>U. Toronto</i>), S. Dias, S. Sood (<i>Ontario Hydro</i>), H.R. Andrews, R.M. Brown, R.J. Cornett (<i>AECL</i>), D.B. Carlisle (<i>Environment Canada</i>), J. Carron, A. Kabir, R.C.J. Wilkinson (<i>Canadian Centre for Inland Waters</i>), R. Gephart, P. Molton, D. Robertson (<i>Batelle Pacific Northwest Labs</i>)	
LS18.	Cooperative development of ^{82}Sr -Rb generators for human use in Canada [completed], <u>J. Vincent</u> (<i>TRIUMF</i>), R. Beanlands (<i>U. Ottawa Heart Inst.</i>), B. Bowen (<i>McMaster U.</i>), W. Dickie (<i>Nordion Int.</i>)	
LS19.	An ^{15}O -water generator: a feasibility study [inactive], K.R. Buckley, <u>T.J. Ruth</u> (<i>TRIUMF</i>)	

- LS20. Prototype heat-pipe water target for ^{18}F -production [inactive], K.R. Buckley, E.T. Hurtado, T.J. Ruth (*TRIUMF*), J.W. Lenz (*private consultant*)
- LS21. Aluminum kinetics in plants [inactive], A. Glass, R.R. Johnson, L. Oliveira (*UBC*), K. Buckley, Z. Gelbart (*TRIUMF*), D. Berkovitz, M. Paul (*Hebrew U. Jerusalem*), E. Venczel (*SFU*)
- LS22. Virtual national biomedical tracer facility [inactive], T.J. Ruth, J.S. Vincent (*TRIUMF*), E.J. Peterson, D. Phillips (*Los Alamos National Lab*)
- LS24. Scanning for early detection and staging of breast cancer: a comparative study using FDG PET and MIBI SPECT [inactive], P.F. Cohen, P. Klimo (*Lions Gate H.-UBC*), M. Cackette (*EBCO Industries Ltd.*), J. Whiffen (*JALORN*), V. Sossi (*TRIUMF-UBC*), J. Porter (*Nordion Int.*), R.R. Johnson (*UBC*)
- LS25. 3D PET in human neuroreceptor studies: quantification and reconstruction [completed], K.S. Morrison, T. Oakes, T.J. Ruth, V. Sossi (*UBC-TRIUMF*), K.R. Buckley (*TRIUMF*), M. Krzywinski, M. Schulzer, J. Stoessl (*UBC*)
- LS26. A gaseous planar positron source for routine 3D PET normalization [completed], T. Oakes, T.J. Ruth, V. Sossi (*UBC-TRIUMF*), K. Buckley, S. Jivan, R. MacDonald (*TRIUMF*)
- LS27. The feasibility and efficacy of using 2-(F-18)-fluoro-2-deoxy-D-glucose (18-FDG) to evaluate children with musculoskeletal neoplasm [deferred], R. Anderson, J. Davis, D. Lyster, H.R. Nadel, T.J. Ruth, M. Stilwell, D. Worsley (*UBC*)
- LS28. Evaluation of potentially viable myocardium with dobutamine myocardial SPECT imaging [completed], H. Abbey, A.-Y. Fung, L. Hook, D.M. Lyster, D.F. Worsley (*VH&HSC*), M. Adam, S. Jivan (*TRIUMF*)
- LS29. Production and distribution of FDG for clinical studies [completed], D. Lyster, D. Worsley (*VH&HSC*), P. Cohen (*Lions Gate H.*), H. Nadel (*Children's H.*), M.J. Adam, S. Jivan, T.J. Ruth, V. Sossi (*TRIUMF*)
- LS31. Auger electron emitters for therapy-physics and chemistry [inactive], D. Pearce, T.J. Ruth, J. Vincent, A. Zyuzin (*TRIUMF*), V. Kokhanyuk, V. Kravchuk, B.L. Zhuikov (*INR Moscow*)
- LS32. ^{18}F - H_2^{18}O supply to the University of Alberta [completed], S.A. McQuarrie, J.R. Mercer (*U. Alberta*), A.J.B. McEwan (*CCI*), R.R. Johnson (*UBC-EBCO*), T.J. Ruth (*UBC-TRIUMF*)
- LS33. Evaluation and improvement of a dual head coincidence camera [active], K.S. Morrison, T.J. Ruth, V. Sossi (*UBC-TRIUMF*), M. Krzywinski (*UBC*), P. Cohen (*Lions Gate H.*), P. Klimo (*Lions Gate H.-UBC*), T.K. Lewellen, D.A. Mankoff (*U. Washington*) 129
- LS34. Production of ^{103}Pd [inactive], R.R. Johnson, R. Pavan (*UBC*), M. Cackette, K.L. Erdman (*EBCO Industries Ltd.*), Z. Gelbart (*TRIUMF*)
- LS35. Development of F-18 labelled nitroimidazole PET imaging agents for tissue hypoxia [active], M.J. Adam (*TRIUMF*), K. Skov (*BCCRC-UBC*), S. Evans, C. Koch, A. Kachera (*U. Pennsylvania*), I. Baird, B. James (*UBC*) 129
- LS37. Feasibility of ^{125}Xe implantation as a ^{125}I brachytherapy source [completed], D. Ottewell, T. Ruth, J. Vincent, A. Zyuzin (*TRIUMF*)
- LS38. Dopaminergic tracers kinetic modeling with minimally invasive scanning procedures [completed], G. Chan, M. Krzywinski, T.J. Ruth, V. Sossi (*UBC-TRIUMF*), J. Holden (*U. Wisconsin*), D. Doudet, J. Stoessl (*UBC*)
- LS39. Positron emission profiling (PEP) for pulp and paper fluid dynamic studies [active], M. Martinez, J. Olson (*UBC*), M.J. Adam, K. Buckley, S. Jivan, T.J. Ruth, V. Sossi (*TRIUMF*) 130
- LS40. F-18 FDG cardiac PET scans using a coincidence PET/SPECT camera to assess myocardial viability in patients with fixed abnormalities and low ejection fractions on gated sestamibi stress tests [completed], P.F. Cohen, J. Imrie, K. Woo (*Lions Gate H.*), D. Worsley (*Vancouver General H.*), V. Sossi (*TRIUMF-UBC*), T. Ruth (*UBC-TRIUMF*), R.R. Johnson (*UBC*)
- LS41. Impact of the ADAC coincidence PET camera in the management of selected cancer patients [completed], P.F. Cohen, J. Imrie, K. Woo (*Lions Gate H.*), J. Powe (*Vancouver General H.*), V. Sossi (*TRIUMF-UBC*), T. Ruth (*UBC-TRIUMF*), R.R. Johnson (*UBC*)
- LS42. Configuration modeling and image reconstruction studies on a depth encoding research tomograph [active], T. Ruth, V. Sossi (*UBC-TRIUMF*), V. Astakhov (*UBC*), K. Buckley (*TRIUMF*), S. Houle (*Centre Addiction & Mental Health, Toronto*), C. Moisan (*U. Laval*) 131
- LS43. Positron emission mammography system (PEM) [deferred], K. Buckley, S. Jivan, T.J. Ruth, V. Sossi (*TRIUMF*), M. Stilwell (*B.C. Women's H.*), P. Gordon (*UBC*), H. Nadel (*Children's H.*)
- LS44. Development of a high-speed formation (areal density) measurement system for paper [active], M. Avikainen, S. Heath, M. Martinez, J. Olson (*UBC*), K. Buckley, T.J. Ruth, M. Salomon (*TRIUMF*) 130

- LS45. Modelling genetic risk for ionizing radiation exposure in space [deferred], J.G. de Boer, J. Holcroft, S. Zhang (*U. Victoria*)
- LS46. Modelling of the dopaminergic system in more severely affected PD patients [completed], T.J. Ruth, V. Sossi (*UBC-TRIUMF*), J. Holden (*U. Wisconsin*), R. de la Fuente-Fernandez, D. Doudet, C.S. Lee, M. Schulzer, J. Stoessl (*UBC*)
- LS47. PET imaging of recurrent prostate cancer with 2-F-18-fluoromethy-dimethy-2-hydroxyethylammonia (FCH), [deferred], M. Gleave, D. Lyster, J. Powe, D. Worsley (*Vancouver General H.-UBC*), M. Adam (*TRIUMF*), H. Abbey (*Vancouver General H.*)
- LS48. Anorexia nervosa: autonomic dysfunction, the brain and the heart [completed], A.S. Belzberg, C.L. Birmingham, C. Kerr, G.P. Sexsmith, M. Stilwell (*St. Paul's H.*), M.J. Stock (*St. George's H.*), P. Beumont (*U. Sydney, Aust.*), V. Sossi (*UBC-TRIUMF*)
- LS49. ^{18}F FDG cardiac PET scans using a third generation coincidence camera to assess myocardial viability in patients who are candidates for cardiac transplantation [inactive], A.S. Belzberg, S. Chan, A. Ignaszewski, M. Kiess, G. Sexsmith, M. Stilwell (*St. Paul's H.*), V. Sossi (*TRIUMF-UBC*)
- LS50. Antisense imaging nucleic acids for Parkinson's disease [active], M. Adam, H. Dougan, T.J. Ruth (*TRIUMF*), J.B. Hobbs, D.M. Lyster, J. Stoessl (*UBC*), A.I. Kassir (*Harvard U.*) 131
- LS51. Auger therapy for prostate cancer [active], H. Dougan, T.J. Ruth, J.S. Vincent (*TRIUMF*), C.C. Nelson, P.S. Rennie (*Prostate Centre*), C.M. Ludgate (*UBC-U. Victoria*), D.M. Lyster (*UBC*) 131
- LS52. Comparison of commercial FDG synthesis systems [completed], T.J. Ruth (*UBC/TRIUMF*), M. Adam, K. Buckley, S. Jivan (*TRIUMF*), D. Lyster (*UBC*), R. McDonald (*IPET*)
- LS53. Synthesis of $^{99\text{m}}\text{Tc}$ and $^{186,188}\text{Re}$ sugar derivatives [active], M.J. Adam (*TRIUMF*), C. Orvig (*UBC*), S. Bayly, C. Fisher (*TRIUMF/UBC*), M. Abrams (*AnorMED*) 132
- LS54. Wavelet reconstruction for high resolution three-dimensional positron emission tomography [deferred], C.-H. Chen, A. Rahmin, K. Raywood (*UBC*), T.J. Ruth, V. Sossi (*UBC/TRIUMF*)
- LS55. Detection of metastases in intermediate thickness melanoma with ^{18}F FDG and a coincidence hybrid scanner [inactive], A. Belzberg, G. Sexsmith, M. Stilwell (*St. Paul's H./UBC*), A. Lee (*Surrey Memorial H.*), T.J. Ruth (*UBC/TRIUMF*)
- LS56. Synthesis of radiolabelled nucleotides and oligonucleotides [active], M.J. Adam, H. Dougan, A. Studenov (*TRIUMF*), J. Wilson (*Cross Cancer, Edmonton*), J. Hobbs (*UBC*) 132
- LS57. Quantitative imaging with the Concorde MicroPET [active], A. Rahmin, V. Sossi (*UBC*), K. Raywood, T.J. Ruth (*UBC-TRIUMF*), K. Buckley, P. Piccioni (*TRIUMF*), C. Thompson (*Montreal Neurological Inst.*), S. Lapi (*SFU*) 132
- LS58. Production and distribution of FDG for clinical studies [deferred], D. Lyster (*UBC*), J. Powe, D. Worsley (*VH&HSC*), P. Cohen (*Lions Gate Hospital*), H. Nadel (*Children's Hospital*), M. Stilwell (*BC Women's Hospital*), A. Belzberg (*St. Paul's Hospital*), K. Buckley, T. Hurtado, S. Jivan, P. Piccioni, T.J. Ruth (*TRIUMF*), M. Kovacs (*EBCO Tech.*)
- LS69. In vivo studies on regulation of dopamine turnover using a Parkinson's disease rat model and a microPET [active], D. Doudet, C. Lee, A. Phillips, V. Sossi, E. Vandervoort (*UBC*), M.-L. Camborde, R. Koernelson, S. McCormick (*UBC-TRIUMF*), T.J. Ruth (*TRIUMF*), J. Holden (*U. Wisconsin*) 134
- LS70. Quantification of high resolution brain imaging [active], K. Cheng, A. Rahmin, V. Sossi, E. Vandervoort (*UBC*), S. Blinder, M.-L. Camborde, K. Raywood, T. Ruth (*UBC-TRIUMF*), K. Buckley, P. Picciotto (*TRIUMF*), C. Thompson (*Montreal Neurological Inst.*), S. Lapi (*SFU*) 134